



Pashova, Antoniya (2023) *Investigating the effects of platelet derived growth factor on the microRNA cargo content and function of vascular smooth muscle cell-derived extracellular vesicles*. PhD thesis.

<https://theses.gla.ac.uk/83787/>

Copyright and moral rights for this work are retained by the author

A copy can be downloaded for personal non-commercial research or study, without prior permission or charge

This work cannot be reproduced or quoted extensively from without first obtaining permission from the author

The content must not be changed in any way or sold commercially in any format or medium without the formal permission of the author

When referring to this work, full bibliographic details including the author, title, awarding institution and date of the thesis must be given

Enlighten: Theses

<https://theses.gla.ac.uk/>
research-enlighten@glasgow.ac.uk

Investigating the effects of platelet derived growth factor on the microRNA cargo content and function of vascular smooth muscle cell-derived extracellular vesicles.

Antoniya Pashova

BSc (Hons), MSc

Submitted in fulfilment of the requirements for the degree of Doctor of Philosophy to the School of Cardiovascular and Metabolic Health, University of Glasgow.

Research conducted at the British Heart Foundation Glasgow Cardiovascular Research Centre, School of Cardiovascular and Metabolic Health, College of Medical, Veterinary and Life Sciences, University of Glasgow, UK

March 2023

© Antoniya Pashova 2023

Abstract

Invasive revascularisation procedures such as coronary artery bypass grafting (CABG) and percutaneous coronary intervention (PCI) are used to treat advanced atherosclerosis. The CABG procedure is the most common type of cardiac surgery performed in the UK and the great saphenous vein (SV) remains the most widely used conduit largely due to availability and length. However, recent reports suggest that approximately 50% of all SV grafts fail at 10 years following CABG and the incidence of arterial restenosis, following drug-eluting stent (DES) implantation remains around 10%. Vascular smooth muscle cells (VSMCs) proliferation- and migration- driven neointimal formation post CABG- and/or PCI- induced vascular injury has been considered a major pathological driver of both vein graft disease (VGD) and in-stent restenosis (ISR) ultimately leading to treatment failure.

Accumulating evidence suggests that extracellular vesicles (EVs) play a significant role in intercellular communication in both physiological and pathophysiological conditions, and due to their promising therapeutic potential, EVs are currently being extensively studied as disease mediators and therapeutic delivery vehicles. Understanding the different mechanisms that may be involved in the regulation of VSMC-driven neointimal formation remains an important step towards successfully developing therapeutic strategies that could improve clinical outcomes associated with both CABG and PCI. Therefore, the primary aim of this thesis was to study the effect of VSMC-derived EVs on recipient cell responses with a particular focus on EV-mediated autocrine regulation of VSMC.

Since abnormal signalling mediated by platelet-derived growth factor (PDGF), has been implicated in the development of neointimal formation post vascular injury, prolonged PDGF stimulation of human SV smooth muscle cells (HSVSMCs) was used to model the pathological conditions under which neointimal lesions develop in an *in vitro* setting. Following the optimisation of an EV purification method, EVs were obtained from the conditioned culture media (CCM) of HSVSMCs +/- PDGF stimulation and successfully characterised in terms of size, concentration, protein content and morphological appearance. It was found that while EV size and morphology remained unaltered, PDGF stimulation of HSVSMCs

resulted in increased EV secretion. Further studies determined that PDGF was not packaged into EVs after prolonged PDGF treatment of HSVSMCs.

Next, following small RNA sequencing (RNAseq) analysis, it was found that PDGF stimulation of HSVSMCs induced significant changes in their EV cargo. Six known differentially expressed miRNAs: miR-24-3p, miR-409-3p, miR-21-5p, let-7A-5p, miR-1-3p and miR-224-5p, were found to be significantly upregulated in PDGF EVs compared to control EVs. Four out of six differentially expressed miRNAs (miR-24-3p, miR-224-5p, miR-409-3p and, let-7A-5p) were also successfully validated by qRT-PCR analysis. Gene set enrichment analysis (GSEA) revealed that miR-24-3p and miR-224-5p miRNAs may be involved in the regulation of biological processes such as cell proliferation, migration, and apoptosis - all previously implicated in the development of neointimal formation.

Next, the effects of miR-24-3p or miR-224-5p EVs on HSVSMC proliferation, migration and cell viability were assessed. It was found that, while neither miR-24-3p EVs nor miR-224-5p EVs had any significant effect on PDGF-induced HSVSMC proliferation and cell viability compared to naïve EVs, miR-224-5p EVs significantly inhibited EV-depleted foetal bovine serum (FBS)-induced HSVSMC migration compared to both naïve EVs and miR-24-3p EVs through an unknown mechanism.

Finally, it was found that serum EVs from mice with carotid artery ligation-induced vascular injury do not significantly differ compared to EVs from control mice in terms of size and concentration. However, qRT-PCR analysis of miR-24-3p and miR-224-5p suggested that the expression of both miRNAs was significantly upregulated in serum EVs isolated from injured mice at day 14 and day 5 after surgery respectively compared to control mice.

Overall, these studies provide evidence that prolonged PDGF signalling in HSVSMCs significantly alters the EV population secreted by those cells in terms of concentration of particles released and miRNA expression profile. Additionally, the demonstrated ability of miR-224-5p EVs to suppress HSVSMC migration compared to naïve EVs and miR-24-3p EVs provides valuable insights into an alternative mechanism of EV-mediated regulation of VSMCs with promising potential for future therapeutic studies.

Table of Contents

Investigating the effects of platelet derived growth factor on the microRNA cargo content and function of vascular smooth muscle cell-derived extracellular vesicles.....	1
Abstract	ii
Table of Contents	iv
List of Tables	viii
List of Figures	ix
List of presentations, awards, and publications	xii
Acknowledgements	xiii
Author's Declaration	xv
List of abbreviations and definitions	xvi
Chapter 1 Introduction.....	20
1.1 Coronary artery disease	21
1.2 Treatment of advanced CAD - CABG and PCI	22
1.3 VGD and ISR	23
1.4 Vascular injury and intimal hyperplasia/neointimal formation.....	23
1.4.1 Mechanical injury-associated vascular changes and thrombosis....	24
1.4.2 Intimal hyperplasia/neointimal formation.....	27
1.5 PDGF signalling in VSMCs.....	30
1.5.1 PDGF ligands and PDGF receptors.....	31
1.5.2 PDGF signalling cascades	33
1.5.3 PDGF signalling pathways in the vasculature and beyond - dysregulation and functional effects	36
1.6 MicroRNAs	38
1.6.1 Biogenesis of miRNAs.....	39
1.6.2 Mechanisms of miRNA-mediated gene regulation.....	42
1.6.2.1 MiRNA-mediated gene silencing.....	43
1.6.3 Role and therapeutic potential of miRNAs in vascular remodelling	48
1.6.4 MiRNAs as potential biomarkers	52
1.6.4.1 MiRNAs as potential biomarkers of CAD/atherosclerosis	53
1.6.4.2 MicroRNAs as potential biomarkers of vascular injury.....	54
1.7 Extracellular vesicles	57
1.7.1 Biogenesis and release of exosomes	60
1.7.2 Biogenesis and release of microvesicles.....	63
1.7.3 Uptake of extracellular vesicles.....	64
1.7.4 Extracellular vesicles and their RNA cargo	66
1.7.5 Extracellular vesicle signalling in response to vascular injury.....	67
1.7.6 Improving the therapeutic potential of extracellular vesicles-- bioengineering approaches	73
1.8 Hypotheses and aims	76

Chapter 2	Materials and methods	77
2.1	General laboratory practice	78
2.2	Sourcing of human saphenous vein samples	78
2.3	Cell culture	79
2.3.1	Primary HSVSMC isolation and expansion	79
2.3.2	Primary HSVEC isolation and expansion	81
2.3.3	Sourcing commercially available human primary cells	83
2.3.4	Maintenance of primary cells	83
2.3.5	Cell counting	84
2.3.6	Cryopreservation and recovery of cultured primary cells	84
2.4	Cell work methodology	85
2.4.1	Experimental protocols designed to study the effect of unmodified EVs on activated HSVSMCs	85
2.4.1.1	Cell proliferation studies	85
2.4.1.2	MicroRNA target gene expression studies	86
2.4.2	Experimental protocols designed to study the effect of miRNA loaded EVs on HSVSMCs	88
2.4.2.1	Studies with no EV pre-treatment step	88
2.4.2.2	Studies with an EV pre-treatment step	90
2.4.3	Experimental protocol designed to study the effect of miRNA loaded EVs on HSVECs	90
2.5	Immunofluorescence	92
2.6	Gene expression analysis	93
2.6.1	RNA extraction from cells and EV samples	93
2.6.2	RNA purification	94
2.6.3	On-column DNase digest	95
2.6.4	Reverse transcription polymerase chain reaction (RT-PCR)	96
2.6.4.1	RT-PCR for the detection of miRNA expression levels	96
2.6.4.2	RT-PCR for the detection of mRNA expression levels	97
2.6.5	Real-time quantitative RT-PCR (qRT-PCR)	98
2.6.5.1	Analysis of qRT-PCR	100
2.7	Protein expression analysis	101
2.7.1	Protein extraction	101
2.7.2	Protein quantification	102
2.7.3	Western immunoblotting	103
2.8	Enzyme-linked immunosorbent assay	105
2.9	Functional <i>in vitro</i> assays	109
2.9.1	Cell proliferation assay	109
2.9.2	Cell viability assay	111
2.9.3	Cell migration assays	112
2.9.3.1	Wound scratch method	112
2.9.3.2	The gap closure method	115
2.10	EV-specific protocols and techniques	117
2.10.1	Generation of EVs from HSVSMCs treated with VEH/PDGF	117
2.10.2	Generation of HSVSMC EVs for miRNA overexpression studies	117
2.10.3	EV isolation methods	119
2.10.3.1	EV isolation from CCM samples	119
2.10.3.2	EV isolation from serum samples	121
2.10.4	Nanoparticle tracking analysis	121
2.10.5	Transmission electron microscopy analysis	122
2.10.6	Loading of miRNAs into EVs (optimised protocol)	122
2.11	Next generation sequencing - based profiling of EV-related miRNAs	125

2.12	Bioinformatics	126
2.12.1	Identifying the mature forms of differentially expressed miRNAs	126
2.12.2	Identifying potential ‘true’ miRNA gene targets.....	128
2.12.2.1	Bioinformatics strategy and data gathering.....	128
2.12.2.2	Automation of the bioinformatics data analysis process.....	128
2.12.3	Functional annotation and gene set enrichment analysis	133
2.13	Statistical Analysis	134
Chapter 3 Optimisation of a size exclusion chromatography-based method		
for isolation and characterisation of HSVSMC-derived EVs		
136		
3.1	Introduction	137
3.1.1	Vascular injury and PDGF signalling	137
3.1.2	Extracellular vesicle characterisation: guidelines	137
3.1.3	Isolation of extracellular vesicles	138
3.1.4	Characterisation of VSMC-derived extracellular vesicles	139
3.2	Aims	141
3.3	Methods.....	142
3.3.1	Establishing the EV elution profile specific for CCM samples using qEVsingle SEC column	142
3.3.2	Experimental protocol designed to study the effect of unmodified EVs on proliferation of quiesced HSVSMCs	142
3.4	Results	144
3.4.1	Determining the EV elution profile for CCM samples.....	144
3.4.2	Characterisation of HSVSMC-derived EV populations +/- PDGF stimulation	149
3.4.3	Studying the effect of EVs on proliferation of quiesced HSVSMCs	158
3.5	Discussion.....	160
3.5.1	Study limitations	164
3.6	Summary.....	165
Chapter 4 RNA sequencing and gene enrichment analysis		
166		
4.1	Introduction	167
4.2	Hypotheses and aims	173
4.3	Methodology.....	174
4.3.1	Cell work methodology	174
4.3.2	Workflow	174
4.4	Results	177
4.4.1	Quality control of small RNA sequencing samples	177
4.4.2	Summary of differentially expressed small RNA molecules identified by small RNA sequencing	179
4.4.3	Validation of differentially expressed miRNA between vEVs and pEVs by qRT-PCR.	184
4.4.4	Assessment of miRNA expression levels in HSVSMCs treated with VEH and PDGF	186
4.4.5	Potential ‘true’ miRNA gene targets were identified using basic bioinformatics analysis.	188
4.4.6	Functional annotation and gene set enrichment analysis	192
4.5	Discussion.....	204
4.6	Summary.....	211
Chapter 5 Studying the effect of HSVSMC-derived EVs on recipient cells		
212		
5.1	Introduction	213

5.1.1	MiR-24-3p/miR-224-5p- mediated cellular responses	213
5.1.2	Exogenous loading of miRNAs into extracellular vesicles.....	214
5.1.3	Hypotheses.....	216
5.2	Aims	217
5.3	Methods.....	218
5.3.1	Optimisation of miRNA mimic loading dose.....	218
5.4	Results	222
5.4.1	Studying the effect of EVs on HSVSMCs co-stimulated with PDGF	222
5.4.2	Optimisation of miRNA mimic loading dose.....	228
5.4.3	Characterisation of miRNA mimic loaded HSVSMC-derived EV populations.....	230
5.4.4	Studying the effect of naEVs and miEVs on HSVSMCs	237
5.4.4.1	Effects of naEV/miEV on recipient HSVSMCs.....	237
5.4.4.2	Recipient HSVSMCs pre-treated with naEVs/miEVs	243
5.4.5	Studying the effect of naEVs and miEVs on HSVECs	252
5.5	Discussion.....	254
5.5.1	Study limitations	265
5.6	Summary.....	266
Chapter 6 Validation of miRNA expression profile in a murine model of vascular injury		267
6.1	Introduction	268
6.1.1	Hypothesis	272
6.2	Aims	273
6.3	Methods.....	274
6.3.1	Blood samples collected from mice with vascular injury.....	274
6.3.1.1	Study design.....	274
6.3.2	Blood samples collected from control mice	275
6.3.3	Obtaining serum samples from whole blood.....	275
6.4	Results	277
6.4.1	Characterisation of serum EVs	277
6.4.2	miRNA expression profile in serum EVs.....	281
6.5	Discussion.....	285
6.5.1	Study limitations	291
6.6	Summary.....	292
Chapter 7 General discussion.....		294
7.1	Summary of findings and implications	295
7.2	Future perspectives.....	300
7.3	Concluding remarks	307
7.4	COVID-19 impact and mitigation.....	309
Chapter 8 Appendices		311
8.1	Differentially expressed miRNAs between vEVs and pEVs	312
8.1.1	DESeq2 analysis output	312
8.2	MicroRNA gene targets	313
8.2.1	Hsa-miR-224-5p	313
8.2.2	Hsa-miR-24-3p.....	314
8.2.3	Hsa-miR-409-3p	315
List of References.....		316

List of Tables

Table 2-1 Summary of anthropometric donor patient characteristics.	78
Table 2-2 Details of the different cell culture media used with HSVSMCs.	80
Table 2-3 Details of the different cell culture media used with HSVECs.	82
Table 2-4 Details of the specific seeding density used for each cell culture dish with each cell type.	84
Table 2-5 Details of the reagent volumes used throughout the RNA extraction process.	94
Table 2-6 List of TaqMan® miRNA Assays used throughout this study.	97
Table 2-7 List of human TaqMan® assays used for the detection of mRNA gene expression.	100
Table 2-8 Different primary monoclonal antibodies used throughout this project.	105
Table 2-9 List of keywords used to filter through significantly enriched biological processes.	134
Table 3-1 Other relevant methods for Chapter 3.	144
Table 4-1 Other relevant methods for Chapter 4.	176
Table 4-2 A summary table of all differentially expressed small RNA molecules between control EVs (vEVs) and PDGF EVs (pEVs).	181
Table 4-3 Number of potential ‘true’ miRNA gene targets identified for miR-24-3p, miR-409-3p and miR-224-5p.	190
Table 5-1 Other relevant methods for Chapter 5.	221
Table 6-1 Other relevant methods for Chapter 6.	275
Table 8-1 All significantly differentially expressed genes between pEVs and vEVs.	312
Table 8-2 List of all the identified gene targets for hsa-miR-224-5p which satisfied the pre-defined criteria.	313
Table 8-3 List of all the identified gene targets for hsa-miR-24-3p which satisfied the pre-defined criteria.	314
Table 8-4 List of all the identified gene targets for hsa-miR-409-3p which satisfied the pre-defined criteria.	315

List of Figures

Figure 1-1 Schematic representation of atherosclerotic plaque development within the coronary artery.....	21
Figure 1-2 Schematic representation of neointima formation and accelerated atherosclerosis leading to vein graft failure.	26
Figure 1-3 PDGF-PDGFR-mediated signalling.	35
Figure 1-4 Canonical and non-canonical pathways of miRNA biogenesis.	41
Figure 1-5 Post-transcriptional gene silencing via miRNA-mediated translational repression.	44
Figure 1-6 Post-transcriptional gene silencing via miRNA-mediated mRNA degradation.	47
Figure 1-7 General features of extracellular vesicles.	59
Figure 1-8 Biogenesis of extracellular vesicles.	62
Figure 1-9 Summary of the highlighted miRNAs involved in the regulation of vascular remodelling processes and their effects on different cell types.....	72
Figure 2-1 Schematic representation of the experimental protocols designed to study the effect of unmodified vEVs and pEVs on recipient PDGF-treated HSVSMC.	87
Figure 2-2 Schematic representation of the cell treatment protocol used to study the effects of naEVs/miEVs on HSVSMCs.	89
Figure 2-3 Schematic representation of the cell treatment protocol, involving a 6hr naEV/miEV pre-treatment step, used to study the effects of these EV populations on HSVSMCs.	91
Figure 2-4 Measuring PDGF-BB concentration in HSVSMC vEV and pEV samples by ELISA.	108
Figure 2-5 Quantification of wound closure.....	114
Figure 2-6 Quantification of gap closure.	116
Figure 2-7 Protocols for EV generation from HSVSMCs.	118
Figure 2-8 Schematic representation of the EV isolation protocol for CCM from HSVSMCs.	120
Figure 2-9 Schematic representation of the optimised protocol for loading miRNA mimics into EVs.....	124
Figure 2-10 Identifying the mature forms of differentially expressed miRNAs.	127
Figure 2-11 Identification of potential ‘true’ miRNA gene target interactions.	130
Figure 2-12 A Section of the final binary matrix table.	132
Figure 3-1 Schematic representation of the experimental protocol designed to study HSVSMC proliferation in response to treatment with vEVs and pEVs.	143
Figure 3-2 Determining the EV elution profile specific for CCM samples generated by cells (HSVSMCs) under basal conditions.	146
Figure 3-3 Determining the purity of EV elution fractions specific for CCM samples generated by cells (HSVSMCs) under basal conditions.	148
Figure 3-4 HSVSMCs used for EV generation and other <i>in vitro</i> experiments express α -SMA - a typical SMC marker.	150
Figure 3-5 Characterisation of EV populations secreted by PDGF-treated HSVSMCs (pEVs) and VEH control cells (vEVs) via NTA.	152
Figure 3-6 Characterisation of EV populations secreted by PDGF-treated HSVSMCs (pEVs) and VEH control cells (vEVs) via TEM.	153
Figure 3-7 Analysis of HSVSMC-derived EV protein content by microBCA assay and western immunoblot.....	155
Figure 3-8 Human PDGF detection in different HSVSMC-derived EV samples by ELISA (Assay range: 31.3-2,000 pg/mL).....	157

Figure 3-9 Analysis of quiesced HSVSMC proliferation treated with unmodified HSVSMC vEVs and pEVs.	159
Figure 4-1 Workflow diagram summarising the steps followed to develop a hypothesis.	175
Figure 4-2 Principal component analysis (PCA) plot of the small RNA expression profiles of vEVs and pEVs.	178
Figure 4-3 Volcano plot of differentially expressed genes identified between the pEVs group and control (vEVs) group.	180
Figure 4-4 Heatmap representing the colour-coded difference in expression levels of differentially expressed genes.	182
Figure 4-5 A list of the mature forms of differentially expressed miRNAs.	183
Figure 4-6 Validation of differentially expressed miRNAs in pEVs and vEVs by qRT-PCR.	185
Figure 4-7 MicroRNA expression levels in VEH/PDGF treated HSVSMCs (vEVs and pEVs donor cells respectively).	187
Figure 4-8 Schematic representation of the strategy concept used to identify potential 'true' miRNA gene targets for each miRNA of interest.	189
Figure 4-9 Common miRNA gene targets shared between miR-24-3p, miR-224-5p and miR-409-3p.	191
Figure 4-10 Pathway (KEGG, Panther DB and BIOCARTA) enrichment analysis of potential 'true' miRNA gene targets identified for miR-24-3p.	193
Figure 4-11 Pathway (KEGG, Panther DB and BIOCARTA) enrichment analysis of potential 'true' miRNA gene targets identified for miR-224-5p.	194
Figure 4-12 Pathway (KEGG, Panther DB and BIOCARTA) enrichment analysis of potential 'true' miRNA gene targets identified for miR-409-3p.	195
Figure 4-13 GO term (BP) enrichment analysis of potential 'true' miRNA gene targets identified for miR-24-3p.	197
Figure 4-14 GO term (BP) enrichment analysis of potential 'true' miRNA gene targets identified for miR-224-5p.	198
Figure 4-15 Summary of the most common genes across significantly enriched pathways.	200
Figure 4-16 Summary of the common annotation terms across significantly enriched pathways identified for each miRNA of interest.	202
Figure 4-17 Summary of the common GO annotation terms across significantly enriched biological processes identified for miR-24-3p and miR-224-5p.	203
Figure 4-18 Schematic representation of molecular pathways identified in GSEA as potentially regulated by miR-24-3p and miR-224-5p.	209
Figure 5-1 Optimisation of miRNA mimic loading dose - 'sample preparation' step.	219
Figure 5-2 Optimisation of miRNA mimic loading dose - 'electroporation and EV re-isolation' steps.	220
Figure 5-3 Studying the effect of unmodified EVs on HSVSMC proliferation co-treated with 20ng/mL PDGF and unmodified vEVs/pEVs.	224
Figure 5-4 Analysis of mRNA target gene expression in HSVSMCs co-treated with 20ng/mL PDGF and vEVs/pEVs at 6hr.	226
Figure 5-5 Analysis of mRNA target gene expression in HSVSMCs co-treated with 20ng/mL PDGF and vEVs/pEVs at 24hr.	227
Figure 5-6 Analysis of cel-miR-39 expression levels.	229
Figure 5-7 Characterisation of pre- and post- electroporation EV populations by NTA.	231
Figure 5-8 Characterisation of pre- and post- electroporation EV populations by NTA.	232

Figure 5-9 Assessment of post-electroporation EV morphology by TEM.	233
Figure 5-10 Analysis of the protein content of samples containing post-electroporation EV populations by western immunoblot.	235
Figure 5-11 Analysis of miR-24-3p and miR-224-5p expression levels in electroporated EVs.....	236
Figure 5-12 Assessing the effect of naEVs and miEVs on proliferation of activated recipient HSVSMC at 24hr.	238
Figure 5-13 Assessing the effect of naEVs and miEVs on cell viability of recipient HSVSMCs at 24hr.....	240
Figure 5-14 Analysis of mRNA target gene expression in HSVASMCs co-treated with 20 ng/mL PDGF and naEVs/miEVs (18hr).....	242
Figure 5-15 Assessing the effect of naEVs and miEVs on proliferation (24hr) of activated recipient HSVSMCs pre-treated with naEVs and miEVs.....	244
Figure 5-16 Assessing the effect of naEVs/miEVs on HSVSMC migration at 16hr, 18hr and 20hr (wound scratch assay).	246
Figure 5-17 Studying the effect of naEVs/miEVs on HSVSMC migration at 16hr (gap closure assay).....	248
Figure 5-18 Assessing the effect of naEVs/miEVs on HSVSMC migration at 16hr (gap closure assay).....	249
Figure 5-19 Analysis of mRNA target gene expression in HSVASMCs co-treated with 20 ng/mL PDGF and naEVs/miEVs at 12hr following a 6hr pre-treatment with the same EV populations.....	251
Figure 5-20 Assessing the effect of naEVs and miEVs on cell viability of recipient HSVECs at 4hr.	253
Figure 6-1 Schematic representation of the carotid artery ligation study design as part of which mice blood samples were collected.....	276
Figure 6-2 Characterisation of serum EV populations by NTA (Part 1).....	278
Figure 6-3 Characterisation of serum EV populations by NTA (Part 2).....	279
Figure 6-4 Analysis of mouse serum EV protein content by western immunoblot.	280
Figure 6-5 Assessing miRNA (miR-24-3p and miR-22-5p) expression levels in serum EVs isolated from mice with vascular injury.	282
Figure 6-6 Comparing miRNA (miR-24-3p and miR-22-5p) expression levels in serum EVs isolated from mice with vascular injury and control mice.	284

List of presentations, awards, and publications

- Presentations
 - Poster presentation at the annual meeting of the International Society of Extracellular Vesicles (ISEV) 2022.
 - Poster presentation at the annual meeting of the International Society of Extracellular Vesicles (ISEV) 2021.
 - Flash presentation at the UK Society for Extracellular Vesicles (UKEV) Forum 2020.
- Awards
 - General Travel Grant (Biochemical Society, 2022)
 - Welcome Trust Institutional Strategic Support Fund (ISSF, Dec 2019)
- Publications
 - Pashova, A., Work, LM., Nicklin, SA. (Dec 2020). The role of extracellular vesicles in neointima formation post vascular injury. *Cell Signal* 76:109783. Doi: 10.1016/j.cellsig.2020.109783.
- Published abstracts
 - Pashova, A., Work, LM., Nicklin, SA. (May 2021). Investigating the release of extracellular vesicles from human saphenous vein vascular smooth muscle cells and endothelial cells and their effect on cell proliferation. Abstract number PS03.13.
 - Pashova, A., Work, LM., Nicklin, SA. (May 2022). Exploring the small RNA component of extracellular vesicle populations released from human saphenous vein vascular smooth muscle cells and investigating their effect on cell proliferation. Abstract number: PF05.04.

Acknowledgements

First and foremost, I would like to thank my supervisors, Prof. Stuart Nicklin and Dr Lorraine Work, for their scientific insights and continuous support throughout my PhD in both academic and personal aspect. Thank you for the encouragement, for always appreciating the effort I put into my work and for the moral support through emotionally difficult times during my PhD. I would also like to thank Dr Angela Bradshaw, who was my secondary supervisor at the beginning of my PhD journey. Thank you for being so welcoming and for always being happy to answer my 'rookie' questions. Your smile and positivity made the first few (stressful) months as a new PhD student a lot more enjoyable than anticipated. I would also like to thank the British Heart Foundation (BHF) for their financial support and for funding this project.

Secondly, I would like to thank the Wellcome Institutional Strategic Support Fund for funding the RNA sequencing study, Glasgow Polyomics for carrying out the experiment, and Dr Graham Hamilton for performing the initial analysis of the data. I'd also like to extend my thanks towards Dr John McClure for his statistics advice, Dr Martin McBride for the interesting science discussions and his help and guidance with the RNAseq data, and Margaret Mullin (technician) for her help with obtaining great TEM images.

Next, I'd like to thank all the lab members, past and present, on level 3 and 4, not only for their help but also for being such an enjoyable bunch - I thoroughly enjoyed my time in the lab working alongside all of you. I'd like to specifically thank Jools, Arun, and Rebecca for the precious mouse serum samples and the great lab/office/lunch chats. Thank you to Elaine Friel for her help with the isolation of primary cells from saphenous vein graft tissues which were invaluable part of this project. Special thanks go to Wai and Nicola for taking great care of the lab and for helping me with pretty much everything lab-related, it was comforting to know that you were always there. Special thanks to the lovely Dr Josie, Ryszard, Alex Riddle (PhD buddy), Fiona, Laura, Zaniah and everyone else in the 'big' PhD office (including Tuuli, Sonya, Aisling, Ahmad, Daniel, Talha, Amrita, Laura and Kayley) for their help and all the laughter. Thank you to Tracy McArthur (senior administrator), Dot (PGR administrator),

Jim and Marie (lab assistants), and Steven (security) for their morning smiles and positivity.

I was also very lucky to have made great friends - Eleni, Simon, and Erin, who motivated and helped me throughout my PhD both in the lab and outside work. Thank you for all the emotional support, the long chats, great jokes, and endless laughs. You all deserve special thanks for making my time in Glasgow so much more enjoyable. I will forever be grateful for your friendship.

Finally, and most importantly, I would also want to thank my family - my parents and my husband who have always supported and encouraged me throughout my entire PhD. I'd like to specifically thank my loving husband who had put great effort into understanding my work and helping me in any way possible - most often by proofreading my written work and working late at night alongside me. Thank you for being so patient and kind, for always being there for me, for believing in me (even when I did not), for motivating and encouraging me. Thank you for the incomparable love, care, and support, I wouldn't have been able to do this without you.

Author's Declaration

I declare that this thesis was written entirely by myself, and it is a record of my own work with some exceptions as detailed below.

- Isolations of primary saphenous vein smooth muscle cells and saphenous vein endothelial cells were carried out by Mrs Elaine Friel (School of Cardiovascular and Metabolic Health, University of Glasgow).
- Transmission electron microscopy was carried out by Mrs Margaret Mullin at the Electron Microscopy Facility, University of Glasgow College of MVLS.
- Blood samples from mice were collected on various occasions by Julian Schwartze, Arun Flynn, and Rebecca Rooney (School of Cardiovascular and Metabolic Health, University of Glasgow).
- Next generation sequencing-based small RNA sequencing and analysis were carried out at the Glasgow Polyomics Institute (University of Glasgow, Glasgow, UK).
- Dr Graham Hamilton (Glasgow Polyomics Institute, University of Glasgow, Glasgow, UK) generated the computational RNA sequencing pipeline and used this pipeline to analyse data from the RNA sequencing study.
- Bioinformatics data analysis was automated through PHP scripts by Vassil Kalphov.

This thesis has not been submitted previously for a higher degree. The work included in this thesis was completed at the University of Glasgow Cardiovascular Research Centre in the School of Cardiovascular and Metabolic Health under the supervision of Professor Stuart A. Nicklin and Dr Lorraine M. Work.

Antoniya Pashova

List of abbreviations and definitions

α -SMA	Alpha smooth muscle cell actin
Ab	Antibody
ACS	Acute coronary syndrome
AF(s)	Adventitial fibroblast(s)
AGO	Argonaute
ALIX	Alpha-1,3/1,6-mannosyltransferase (ALG-2)-interacting protein X
ASC(s)	Adipose mesenchymal stem cell(s)
b-FGF	Basic-Fibroblast growth factor
BCL2	B-cell lymphoma 2
BMS	Bare metal stent
BrdU	Bromodeoxyuridine
CABG	Coronary artery bypass grafting
CAD	Coronary artery disease
cAMP	Cyclic adenosine monophosphate
CASMC(s)	Coronary artery smooth muscle cell(s)
CCM	Conditioned culture medium
CCR4-NOT	Carbon catabolite repression 4-negative on TATA-less
CDC42	Cell division control protein 42
COS-7	CV-1 (simian) cell line exhibiting fibroblast morphology
Ct	Cycle threshold
CVD(s)	Cardiovascular disease(s)
DAG	Diacylglycerol
DAPI	4',6-diamidino-2-phenylindole
DCP	De-capping protein
DES	Drug-eluting stent
DGCR8	DiGeorge Syndrome Critical Region 8
DLS	Dynamic light scattering
DPBS	Dulbecco's Phosphate Buffered Saline
DU	Differential ultracentrifugation
ECM	Extracellular matrix
ECs	Endothelial cells
EGR1	Early growth response protein 1
eIF4	cap-binding complex eukaryotic initiation factor 4
ELISA	Enzyme-linked immunosorbent assay
ELK1	ETS Like-1 protein
EndoMT	Endothelial-to-mesenchymal transition
ERK	Extracellular signal-regulated kinase
ESCRT	Endosomal-sorting complex required for transport
ESE	Early-sorting endosome
EV(s)	Extracellular vesicle(s)
F1-9	Fractions 1-9
FBS	Foetal bovine serum
FDR	False discovery rate

FERM2	Fermitin family member 2
GO	Gene ontology
GRB2	Growth factor receptor-bound protein 2
GSEA	Gene set enrichment analysis
GSK3B	Glycogens synthase kinase 3 β
GW182	glycine-tryptophan protein of 182 kDa
HASMC(s)	Human aortic smooth muscle cell(s)
HDL	Low density lipoprotein
HEK293	Human embryonic kidney cells
HSP70	Heat shock protein
HSVEC(s)	Human saphenous vein endothelial cell(s)
HSVSMC(s)	Human saphenous vein smooth muscle cell(s)
HUVECs	Human umbilical vein endothelial cells
HUVSMC(s)	Human umbilical vein smooth muscle cell(s)
ICAM-1	Intercellular adhesion molecule 1
IL	Interleukin
ILVs	Intraluminal vesicles
IMA	Internal mammary artery
IMF	Immunofluorescence
ISR	In-stent restenosis
I κ B α	NF κ B inhibitor α
KEGG	Kyoto encyclopaedia of genes and genomes
KLF4	Kruppel-like factor 4
LAMP2B	Lysosome-associated membrane glycoprotein 2b
LDL	High density lipoprotein
lncRNA	Long non-coding RNA
LRP6	Low-density lipoprotein receptor-related protein 6
LSE	Late-sorting endosome
m7G	7-methylguanosine
MAPK	Mitogen-activated protein kinase
MEK	Mitogen-activated protein kinase
MI	Myocardial infarction
miEVs	EVs exogenously loaded with miRNA mimic via electroporation
miRISC	miRNA-induced silencing complex
miRNAs	MicroRNAs
MISEV	Minimal information for studies of extracellular vesicles
MMP(s)	Matrix metalloproteinase(s)
MREs	miRNA response element
mRNA	Messenger RNA
MSC(s)	Mesenchymal stem cell(s)
MSigDB	The molecular signatures database
mTORC1	Mammalian target of rapamycin complex 1
MVE	Multivesicular endosomes
naEVs	Naïve EVs (electroporated with trehalose only, no nucleic acid)
NF- κ B	Nuclear factor kappa-light-chain-enhancer of activated B cells
NGS	Next generation sequencing

NICE	National Institute for Health and Care Excellence
NO	Nitric oxide
NRAS	Neuroblastoma RAS viral oncogene homolog
NTA	Nanoparticle tracking analysis
Nts	Nucleotides
OCM-1	Ocular choroidal melanoma-1
ox-LDL	Oxidised low-density lipoprotein
PAD	peripheral artery disease
PAEC(s)	Pulmonary artery endothelial cell(s)
PAN	poly(A)-nuclease
PASMC(s)	Pulmonary artery smooth muscle cell(s)
PCI	Percutaneous coronary intervention
PDGF	Platelet-derived growth factor
PDGFR	Platelet-derived growth factor receptor
PKD-1	Phosphoinositide-dependent kinase-1
pEVs	PDGF EVs derived from HSVSMCs treated with 20 ng/mL PDGF-BB
PI3K	Phosphoinositide 3-kinase
PIP2	Phosphatidylinositol (4,5)-bisphosphate
PIP3	Phosphatidylinositol (3,4,5)-trisphosphate
PKC	Protein kinase C
PLC- γ	Phospholipase C- γ
pre-miRNA	Precursor miRNA
pri-miRNA	Primary miRNA
PTEN	Phosphatase and tensin homolog
RA	Radial artery
RAF-1	Proto-oncogene serine/threonine-protein kinase
RAS	Rat sarcoma
RNAseq	RNA sequencing
ROC	Receiver operating characteristic
ROS	Reactive oxygen species
RQ	Relative quantification
RRAS	RAS-related
rRNA	Ribosomal RNA
RT-PCR	Reverse transcription polymerase chain reaction
RTKs	Receptor tyrosine kinases
SDS	Sodium dodecyl sulphate
SEC	Size exclusion chromatography
SEM	Standard error of the mean
SHR	Spontaneously hypertensive rats
SMAD3	Mothers against decapentaplegic homolog 3
SMC(s)	Smooth muscle cell(s)
SNARE	Soluble NSF attachment protein receptor
snoRNA	Small nucleolar RNA
snRNA	Small nuclear RNA
SOS	Son of sevenless
SPRED1	Sprouty-related, EVH1 domain-containing protein 1

STAT3	Signal transducer and activator of transcription 3
SV	Saphenous vein
T2D(M)	Type 2 diabetes (mellitus)
TBS(-T)	TRIS-buffered saline (-Tween 20)
TEM	Transmission electron microscope
TGF- β	Transforming growth factor beta
TNF- α	Tumor necrosis factor α
TRBP	Transactivation response element RNA-binding protein
tRNA	Transfer RNA
TSG101	Tumour susceptibility gene 101
UTR	Untranslated region
VCAM-1	Vascular cell adhesion protein 1
VEGF-A	Vascular endothelial growth factor-A
vEVs	vehicle EVs derived from HSVSMCs treated with vehicle
VGD	Vein graft disease
vRNA	Vault RNA
VSMCs	Vascular smooth muscle cells
VV	Void volume
WB	Western blotting
XPO5	Exportin 5
XRN1	Exoribonuclease 1

Chapter 1 Introduction

1.1 Coronary artery disease

Atherosclerosis is considered the most common cause of coronary artery disease (CAD). It is a progressive and inflammation-driven condition characterised by the process of atheroma (atherosclerotic plaque) formation and thickening of the innermost layer of the artery (arterial intima) resulting in an insufficient supply of oxygen and nutrients to target tissues such as the heart (Figure 1-1) (Falk, 2006; Knuuti et al., 2020; Stary et al., 1995). Common complications of CAD include angina pectoralis, myocardial infarction (MI), cardiac arrhythmias and chronic heart failure (Cassar et al., 2009). The traditional risk factors for developing CAD include age, obesity, smoking, type 2 diabetes mellitus (T2DM), hypertension, dyslipidaemias, and chronic kidney disease (Hajar, 2017). To date, CAD continues to be a leading cause of morbidity and mortality globally, affecting approximately 2.3 million people in the UK (3.5%) (Bhatnagar et al., 2015; Tsao et al., 2022). The treatment options generally depend on the severity of the disease and can be non-invasive and/or invasive. Non-invasive treatments include life-style modifications, such as exercise, healthy diet, smoking cessation, and drug treatments, such as blood pressure- and cholesterol-lowering medication (da Luz et al., 2011). In severe cases of advanced atherosclerotic disease, invasive revascularisation procedures such as percutaneous coronary intervention (PCI) (or angioplasty with a stent) and coronary artery bypass grafting (CABG) are used to restore adequate blood supply (Lawton et al., 2022; Neumann et al., 2019).

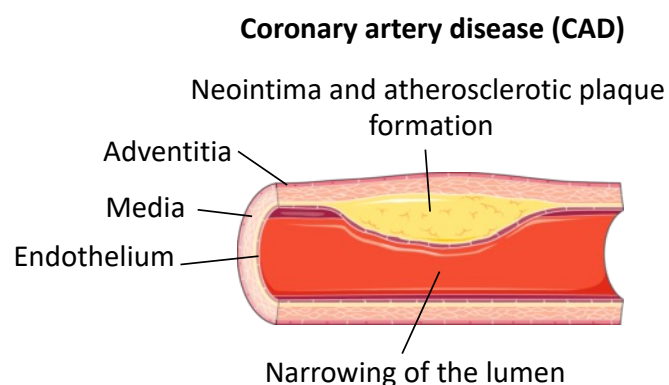


Figure 1-1 Schematic representation of atherosclerotic plaque development within the coronary artery. The coronary artery wall consists of three distinct layers: the innermost layer (tunica intima), the middle layer (tunica media), and the outermost layer (tunica adventitia or externa). Continuous atherosclerotic plaque formation and intimal thickening drives CAD resulting in obstructed blood flow to cardiac tissue (Milutinović et al., 2020). Image taken and adapted from Servier Medical Art (Creative Commons Licence).

1.2 Treatment of advanced CAD – CABG and PCI

CABG is a surgical method which uses the internal mammary artery (IMA), the radial artery (RA) or the great saphenous vein (SV) of the leg to bypass one or more severely occluded coronary arteries (Harris et al., 2013). CABG procedure is the most common type of cardiac surgery performed in the UK (National Institute for Cardiovascular Outcomes Research, 2021) with more than 20,000 CABG procedures performed annually in UK (average over a 15-year period - 2002-2016) (Ohri et al., 2022). CABG surgery remains the standard of care for patients with left main or complex three-vessel CAD (Lawton et al., 2022; Neumann et al., 2019), and the great SV remains the most commonly used conduit for all non-left arterial descending coronary artery cases of CAD (80 - 90% of all patients) (Caliskan et al., 2019). SV grafts are advantageous compared to arterial conduits largely due to their availability and length, which makes them suitable for most patients suffering from multivessel disease, but also because they are easier to harvest, easier to handle when performing anastomoses, not influenced by vasospasm, and do not increase the risk of sternal wound infection (de Vries et al., 2016).

PCI, on the other hand, is a non-surgical technique used to widen narrowed or blocked arteries involving the implantation of a stent such as bare metal stent (BMS) or drug-eluting stent (DES) (Lawton et al., 2022; Neumann et al., 2019; Windecker et al., 2014). The use of DES has been found to be advantageous compared to BMS due to the association of DES with considerably improved safety (reduction in MI/stent thrombosis) and efficacy (reduced target vessel revascularization) profile in the 1st year after implantation (Jensen and Christiansen, 2019; Piccolo et al., 2019). Following the recent guidelines of the National Institute for Health and Care Excellence (NICE), the use of DES is recommended in people with acute coronary syndrome (ACS) undergoing revascularisation by PCI (NICE, 2020). However, despite recent advances in coronary artery interventions, both CABG and PCI are associated with considerably high failure rates arising from the development of vein graft disease (VGD) and in-stent restenosis (ISR), respectively (Buccheri et al., 2016; Caliskan et al., 2019).

1.3 VGD and ISR

Both CABG and PCI interventions have been found to cause vascular injury which results in the development of VGD and ISR, respectively. The development of VGD is characterised by the occurrence of three major pathogenic mechanisms including early thrombosis (Grondin et al., 1974), neointimal lesion formation (Kockx et al., 1996) and accelerated atherosclerosis (Bulkley and Hutchins, 1977), all of which contribute to vein graft failure (Figure 1-2). On the other hand, intimal hyperplasia leading to neointimal formation is considered the main pathological mechanism underlying ISR following PCI with stent implantation (Buccheri et al., 2016; Kim and Dean, 2011; Looser et al., 2016). The introduction of the 'no-touch' technique for SV graft harvesting has improved the patency rate of SV grafts to 83% at 16-year follow-up, a patency rate comparable to IMA grafts (Samano et al., 2015). However, recent reports suggest that between 10-25% of vein grafts fail within 1 year of surgery primarily due to the development of neointimal formation with an overall vein graft patency rate of approximately 40-50% at 10 years follow-up (Caliskan et al., 2019; McKavanagh et al., 2017). In comparison, following the introduction of DES, the incidence of arterial restenosis has been reduced to less than 10% with improvement of both frequency and extent of intimal hyperplasia (Buccheri et al., 2016). Current research efforts are focusing on developing therapeutic strategies to target different stages of VGD and ISR development.

1.4 Vascular injury and intimal hyperplasia/neointimal formation

Intimal hyperplasia is defined as an abnormal accumulation of cells within the innermost layer of an artery or a vein, and it has generally been accepted as the main feature of vascular repair responses following injury. During this process different coagulation and inflammatory factors and cells stimulate proliferation and migration of vascular smooth muscle cells (VSMCs) from the tunica media to the tunica intima (Newby and Zaltsman, 2000). Neointimal lesion formation driven by intimal hyperplasia is a common pathological event observed in diverse proliferative vascular diseases, such as atherosclerosis/CAD, VGD following CABG (Figure 1-2) and arterial restenosis post-PCI (Cizek et al., 2007; Kijani et al., 2017; Newby and Zaltsman, 2000). The pathophysiological mechanisms

underlying the development of both - VGD and ISR, include similar molecular and cellular processes contributing to vessel remodelling and neointimal formation that occur mainly due to induced-vascular injury (Chaabane et al., 2013; de Vries and Quax, 2018; Gaudino et al., 2017; Newby and Zaltsman, 2000). VSMCs have been recognised as major contributors to the development of neointimal formation post vascular injury (in both VGD and ISR) with excessive VSMC proliferation and migration identified as key pathological drivers (Kockx et al., 1992; Marx et al., 2011; Wu et al., 2020; Zou et al., 1998).

1.4.1 Mechanical injury-associated vascular changes and thrombosis

In the case of CABG surgery, early vein graft failure (during the 1st postoperative month) occurs predominantly due to acute thrombosis, secondary to either direct endothelial injury or endothelial activation (Parang and Arora, 2009; Storey, 2011). However, the introduction of the “no touch” technique for harvesting the venous conduit which maintains its endothelium-intact, resulted in increased short- (<12 months) (Tian et al., 2021) and long-term (8.5 years) patency rates comparable to the left internal thoracic artery (Papakonstantinou et al., 2016; Souza et al., 2006). Technical factors such as size mismatch between the graft and the target vessel creating turbulent flow as well as mechanical trauma and manual distention could also lead to acute thrombosis as a result of endothelial layer damage (Parang and Arora, 2009). The venous tissue undergoes a period of ischaemia and reperfusion immediately after harvesting the graft and following engraftment into the arterial circulation, respectively, which leads to significant endothelial cell (EC) damage and subsequently EC activation resulting in a prothrombotic phenotype (Parang and Arora, 2009; Solo et al., 2019; Tsui et al., 2002; Wise and Brophy, 2016). The observed ischaemia/reperfusion injury is aggravated by adverse neutrophil-mediated myocardial inflammation involving the generation of reactive oxygen species (ROS) (Alam et al., 2015; Hausenloy et al., 2007; Vinten-Johansen, 2004). Endothelial denudation results in the exposure of extracellular matrix (ECM) components to the circulation, tissue factor release, and reduction of prostacyclin and nitric oxide (NO) bioavailability, all of which contribute to increased platelet activation, fibrin deposition and ultimately thrombus formation (de Vries and Quax, 2018; Ward et al., 2017). Engraftment in the

arterial circulation triggers vessel remodelling mechanisms involved in the process of arterialisatation (vein adaptation). The venous graft is exposed to augmented pressure, flow and longitudinal and circumferential shear stress which may additionally cause damage to ECs and smooth muscle cells (SMCs) consequently triggering an inflammatory response (Figure 1-2) (Stark et al., 1997; Wadey et al., 2018; Westerband et al., 2001).

Similarly, the mechanical damage induced during PCI with stent implantation also leads to EC damage, platelet activation and thrombus formation along with an inflammatory response (Adriaenssens et al., 2017; Chaabane et al., 2013). Stent implantation induces platelet adhesion, activation, and thrombus formation which demonstrates the mandatory need for an effective anti-platelet therapy for a period of time after the procedure (Gawaz et al., 1996). Technical factors such as stent under-sizing, coronary dissection, postprocedural TIMI flow, and particularly, premature discontinuation of anti-platelet therapy, have all been associated with an increased risk of early stent thrombosis (Tyczyński et al., 2014). Additionally, delayed vessel healing, characterised by persistent fibrin deposition and poorer re-endothelialisation after the deployment of DES, has also been recognised as a major contributing factor to late stent thrombosis (Finn et al., 2007a; Joner et al., 2006) with stent strut coverage reported as an important determinant of thrombosis risk (Finn et al., 2007a). Although, it is important to note, that the implementation of dual anti-platelet therapy has significantly reduced the risk of thrombosis after both CABG surgery and PCI with stent implantation (Généreux et al., 2015; Solo et al., 2019).

Early vessel healing, following venous or arterial injury, has been linked to the early process of re-endothelialisation with proliferating ECs observed during the first two weeks post vein graft and DES implantation in experimental animal models (Finn et al., 2007b; Tseng et al., 2014). Early repairment of the EC monolayer is a crucial disease limiting step in the context of vascular injury. Indeed, increased re-endothelialisation has been correlated with reduced neointimal formation in experimental rat models of vascular injury (Kleinedler et al., 2012; Ren et al., 2020); therefore, highlighting the process of EC monolayer recovery as a valuable therapeutic target in VGD and ISR.

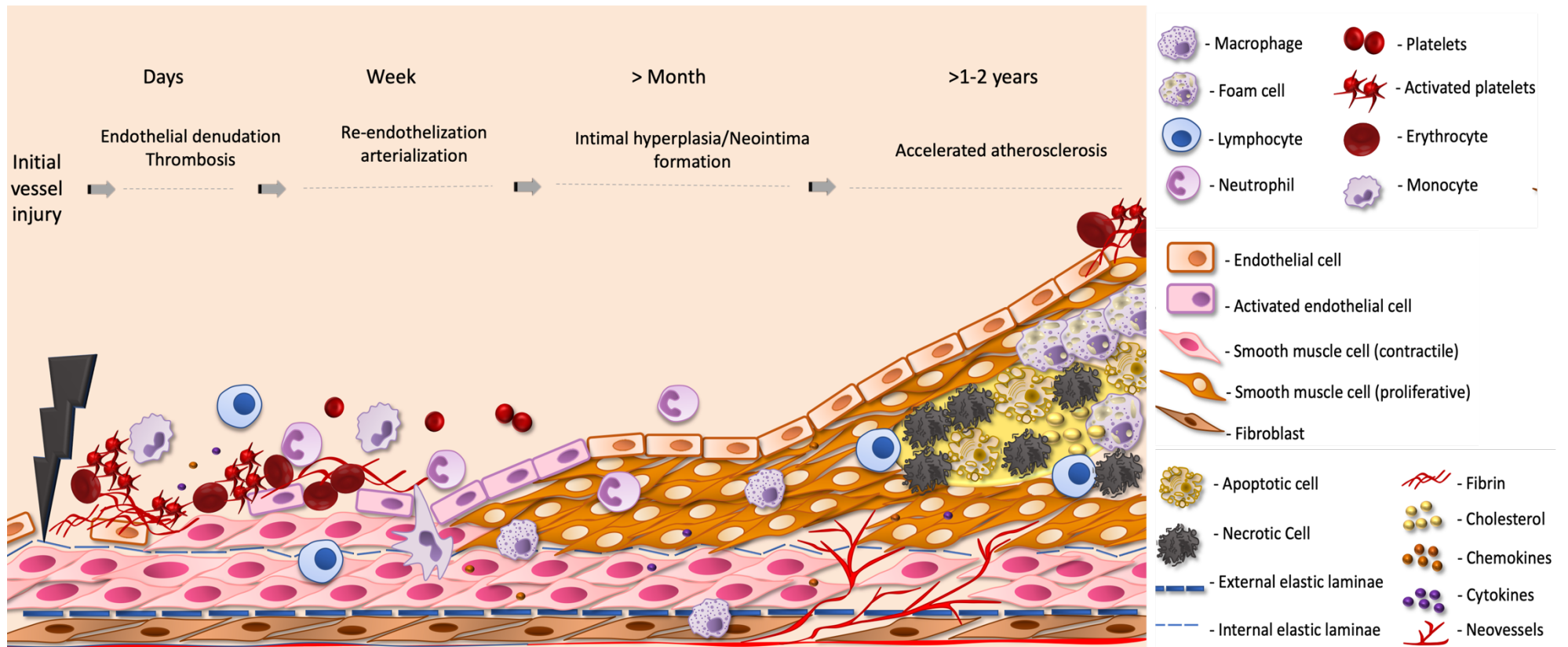


Figure 1-2 Schematic representation of neointima formation and accelerated atherosclerosis leading to vein graft failure. Within hours of vein graft implantation, the endothelial layer becomes damaged due to exposure to increased shear stress leading to fibrin deposition at the site of injury. Circulating inflammatory cells including neutrophils, monocytes, and lymphocytes start to accumulate and infiltrate the intima. Under atherogenic conditions, macrophages within the vessel wall can uptake lipids, thus turning into foam cells. SMCs from the media and adventitial fibroblasts become activated and start migrating towards the intima where they are further stimulated to proliferate by different growth factors and cytokines released by cells in the vessel wall. This process of cell population expansion and ECM deposition results in neointimal formation. Taken and modified from (Pashova et al., 2020).

1.4.2 Intimal hyperplasia/neointimal formation

After the initial phase of endothelial damage and endothelial dysfunction, the next step is the adaptation of the vein to its new arterial environment (arterialisation) which involves the activation and proliferation of VSMCs (Figure 1-2) (Kwei et al., 2004; Owens, 2010; Owens et al., 2006). During this process, the vein graft undergoes structural vessel wall remodelling and intimal thickening, resulting in a more stable intimal layer capable of withstanding the arterial pressure and shear stress. Therefore, moderate intimal hyperplasia within the vein graft is physiological and is required for optimal adaptation/arterialisation and long-term graft patency (de Vries et al., 2016). One of the theories explaining the potential origin of the observed highly proliferative VSMCs within the intima proposes that, under certain conditions, fully matured quiescent 'contractile' VSMCs migrate from the media to the intima where they switch phenotype to a de-differentiated, proliferating 'synthetic' VSMCs (Figure 1-2) (Cooley, 2004; Miano et al., 1993; Wadey et al., 2018). The EC damage and dysfunction trigger abnormal interactions between ECs and VSMCs creating a localised state of inflammation regulated by positive feedback loops, which induce more inflammation, and therefore, more endothelial dysfunction (de Vries and Quax, 2018; Ward et al., 2017). In this pro-inflammatory state observed at the site of injury, activated ECs, platelets, monocytes, and leukocytes secrete various pro-inflammatory mediators including E- and P-selectin, interleukin (IL) -6, IL-8, platelet-derived growth factor (PDGF), transforming growth factor beta 1 (TGF- β 1) and basic fibroblast growth factor (b-FGF), thereby promoting local inflammation and VSMC phenotypic switching, proliferation, migration and ultimately neointimal formation (Figure 1-2) (Barrientos et al., 2008; Christiansen et al., 2004; Goel et al., 2012; Marmur et al., 1992; Sterpetti et al., 1996a; Tsai et al., 2009; Tseng et al., 2014). Even though these mechanisms are important for adaptive vein graft remodelling, pre-clinical studies have demonstrated that TGF- β 1 (Wolff et al., 2006), PDGF (Hu et al., 1999), FGF (Dol-Gleizes et al., 2013), IL-1 β (Li et al., 2014) and tumour necrosis factor α (TNF- α) (Zhang et al., 2004) promote VSMC phenotype switching and vein graft neointimal formation. It has been previously shown that targeting some of those growth factors and/or their receptors (e.g., PDGF, PDGFR, TGF- β 1) *in vivo* negatively affects the development of both venous and

arterial neointimal hyperplasia (Guan et al., 2014; Hu et al., 1999; C. Huang et al., 2017; Sun et al., 2012). Early remodelling of the engrafted vein was found to be predictive of consequent vein graft failure (Gasper et al., 2013), and both *ex vivo* and *in vivo* studies demonstrated that strategies for inhibition of excessive intimal hyperplasia as therapeutic approaches may potentially improve vein graft patency (Longchamp et al., 2014; Moodley et al., 2013).

Vessel recoil is major contributor to arterial restenosis following balloon angioplasty and risks associated with it could virtually be eliminated by the placement of a stent during PCI (Sigwart et al., 1987). However, stent underexpansion during implantation is a procedure-related equivalent of vessel recoil resulting in similar mechanisms of arterial restenosis associated with both types of procedures (Dangas et al., 2010; de Ribamar Costa et al., 2007). Notably, PCI with stent implantation introduces some additional stent-related factors influencing the risk of restenosis (Dangas et al., 2010; de Ribamar Costa et al., 2007). The cascade of events initiated following stent placement during PCI is a very broad concept and many processes have been proposed to be involved. Similar to the mechanisms involved in neointimal formation within the engrafted vein, arterial neointimal hyperplasia is primarily driven by VSMC proliferation and migration and ECM formation (Jukema et al., 2011; Marx et al., 2011). A complex interplay between several cellular and molecular responses, including platelet, leukocyte and EC activation and the secretion of various GFs and pro-inflammatory mediators such as PDGF, TGF- β , IL-1, IL-6, and IL-8, contributes to intimal hyperplasia and the development of restenosis (M. S. Lee et al., 2004). After vessel injury, activated platelets release PDGF and other mitogenic factors that penetrate the vascular wall and trigger medial VSMC proliferation and migration (Forrester et al., 1991; Herring et al., 2014; Welt and Rogers, 2002). Although such wound healing-related reactions are physiological to some extent, in some cases the proliferative response becomes excessive resulting in re-narrowing of the treated vessel. Since VSMCs have been proposed as major drivers of arterial restenosis following injury (Marx et al., 2011), therapeutic approaches involving the inhibition of VSMC proliferation and migration had been successfully utilised to limit the process of intimal hyperplasia and subsequently reducing the rates of arterial restenosis (Liu et al., 2009, 2021; O'Sullivan et al., 2011; Tsai et al., 2009). In clinical settings, a

therapeutic strategy targeting local VSMCs proliferation and migration with DES coated with specific inhibitors of cell proliferation, including plumericin, xanthohumol, paclitaxel, and sirolimus, has been shown to successfully inhibit intimal hyperplasia after PCI both *in vivo* and also in clinical studies (Dibra et al., 2005; Heiss et al., 2016; R. Liu et al., 2017) through potentially different mechanisms of action (Heiss et al., 2016; Kim et al., 2018). Although, the introduction of DES greatly improved PCI as a treatment option for advanced atherosclerotic disease, it has been previously shown that drugs used in this technology could indiscriminately target both ECs and VSMCs leading to severe side effects because of impaired re-endothelialisation, increasing the risk of late thrombosis (Finn et al., 2007a).

Matrix metalloproteinases (MMPs), a group of enzymes with proteolytic activity which could extensively modify the ECM within the vasculature, have also been shown to play a significant role during vascular remodelling and inflammation (Nagase et al., 2006). It has been reported that MMPs, including MMP2 and MMP9 - both capable of degrading collagen and other ECM components, were highly expressed in engrafted veins during structural remodelling (Berceli et al., 2004), and inhibition of MMPs with doxycycline was linked to a significant reduction of intimal hyperplasia *in vitro* and *in vivo* (Lardenoye et al., 2005). MMPs have also been implicated in the pathogenesis of ISR after PCI (Ge et al., 2006; Kusnierova and Pleva, 2017).

Another important aspect of the development of neointimal formation is the immune system which is involved in all phases of VGD (Figure 1-2) and arterial restenosis (de Vries and Quax, 2018; Inoue et al., 2011; Maleknia et al., 2020). Damage of the vessel wall associated with vein graft implantation results in increased selectin-mediated leukocyte adhesion on vascular endothelium and subsequent endothelial dysfunction and vessel wall infiltration (Schlitt et al., 2006; Tseng et al., 2014). Similarly, in the context of injured arteries, neutrophils have been found to infiltrate the vessel wall through the damaged endothelial layer following angioplasty (Welt et al., 2000). Findings indicating that leukocyte activation is increased by coronary stent implantation (Inoue et al., 2000) may help to explain the increased neointimal formation seen in the presence of stent. Indeed, leukocyte depletion in a rabbit model of restenosis

has been linked to reduced neointimal formation in injured arteries (Miller et al., 2001). As known inflammatory mediators, due to their ability to secrete a wide range of pro-inflammatory molecules such as cytokines, GFs and proteases (including MMP2 and MMP9), activated neutrophils have been implicated in the development of diverse vascular pathologies (Leclercq et al., 2007; Packard et al., 2009) including neointimal formation. In the context of the latter, neutrophils adherent to sites of endothelial injury, have been reported to promote VSMC proliferation (Cole et al., 1988). In addition to neutrophils, soon after graft or stent implantation, monocytes start to accumulate in the vessel wall where they become macrophages actively contributing to the inflammatory process by secreting various cytokines and GFs mainly targeting VSMCs (Eslami et al., 2001; Malinska et al., 2013; Rubin et al., 1998). Interestingly, it has been reported that macrophages become the most common type of inflammatory cells present in the vein graft which may be able to serve as an early marker of graft occlusion (Malinska et al., 2013). Furthermore, both direct or indirect inhibition of macrophages, by targeting macrophage activating factors, have been successfully explored as potential strategies in preventing the inflammatory response and VGD (Ewing et al., 2012; Koga et al., 2015; Schepers et al., 2006)

The late stages of vein graft failure and arterial restenosis are characterized by the development of accelerated atherosclerosis (Figure 1-2) and accelerated neoatherosclerosis, respectively (Lardenoye et al., 2002; Otsuka et al., 2014; Yahagi et al., 2016). Hallmark features involve increased oxidised low-density lipoprotein (ox-LDL) retention and subsequent lipid accumulation into the vessel wall (Lardenoye et al., 2002; Yazdani et al., 2012) and accumulation of lipid-loaded foam cells within the neointima, with or without necrotic core formation, calcification or complications of thrombosis (Lardenoye et al., 2002; Romero et al., 2015).

1.5 PDGF signalling in VSMCs

Abnormal PDGF signalling has been implicated in the development of various cardiovascular pathologies including neointimal formation after vascular injury (Hu et al., 1999; M. S. Lee et al., 2004; Raines, 2004). Using different *in vivo* models of vascular injury, it has been possible to study the kinetics of VSMC migration and proliferation following acute injury, and to determine the factors

capable of modulating VSMC accumulation, including the role of PDGF (Ebert et al., 2021; Raines, 2004). Analysis of the time course of PDGF and PDGFR expression following vascular injury demonstrated that the expression of PDGF-A/B and PDGFR- α /B was significantly dysregulated at both the mRNA and protein level with variable expression patterns detected for all factors at different disease stages (Raines, 2004). The dysregulation of PDGF-mediated signalling, leads to a subsequent alteration of multiple downstream pathways controlling VSMC phenotype (Frisantiene et al., 2018). Indeed, the contribution of PDGF to neointimal lesion formation has been successfully demonstrated. It has been shown that inhibition of PDGF signalling (i.e., through a blockade of PDGF ligands or receptors) results in reduction of VSMC proliferation and migration, and ultimately neointimal formation (Ferns et al., 1991; Hu et al., 1999; Jackson et al., 1993; Lewis et al., 2001). Therefore, fully elucidating the role of PDGF-mediated signalling in the context of vascular injury could potentially provide targets for treatment/prevention of VGD/vein graft failure and ISR.

1.5.1 PDGF ligands and PDGF receptors

There are four classical types of PDGF polypeptide chains/subunits, including PDGF-A, PDGF-B, PDGF-C and PDGF-D, encoded by four different genes - *PDGFA*, *PDGFB*, *PDGFC* and *PDGFD* respectively, which can form five distinct PDGF isoforms. Functional PDGF ligands include PDGF-AA, -BB, -CC, and -DD disulphide-linked homodimers and a PDGF-AB heterodimer consisting of both PDGF-A and PDGF-B subunits (reviewed in (Chen et al., 2013)).

Although the α -granules of platelets represent the main storage site for PDGF, various other cell types in addition to platelets have been found to synthesize PDGF including fibroblasts, VSMCs, vascular ECs, and macrophages amongst others (Heldin and Westermark, 1999). The expression of PDGF changes in response to a number of factors. External stimuli such as low oxygen tension (Kourembanas et al., 1997), thrombin (Daniel et al., 1986; Harlan et al., 1986) or stimulation with different cytokines and growth factors, including IL-1 β and TNF- α (Au et al., 2005; Battegay et al., 1995; Peracchia et al., 1991), have been found to increase PDGF synthesis and alter PDGF-mediated signalling. Acting through their transmembrane cell surface receptors, PDGF ligands exert potent mitogenic activity in fibroblasts, SMCs, and other cells of mesenchymal origin

(Hannink and Donoghue, 1989; Heldin and Lennartsson, 2013; Heldin and Westermark, 1999; Kohler and Lipton, 1974; Ross et al., 1974), thus having a critical role in the regulation of embryonic development, especially the formation of vessels and organs (Andrae et al., 2008). In adulthood, however, PDGF expression levels are tightly controlled as PDGF overexpression has been implicated in several pathological conditions, including atherosclerosis, fibroproliferative diseases and various cancers (Östman and Heldin, 2001).

PDGFR- α and PDGFR- β , which belong to the class III receptor tyrosine kinases (RTKs), are transmembrane surface proteins encoded by *PDGFRA* and *PDGFRB* respectively (Chen et al., 2013). The PDGF- α receptor can bind three PDGF isoforms including A, B, and C, but not D, whereas the β receptor can bind only PDGF-B and -D; therefore, PDGF receptor binding can induce the formation of $\alpha\alpha$ -, $\alpha\beta$ -, or $\beta\beta$ -receptor dimers depending on the type of PDGF isoform (Miyazawa et al., 1998; Shim et al., 2010). For example, PDGF-BB is able to bind to both receptors - PDGFR- α and PDGFR- β in both their heterodimer and homodimer forms (Raines, 2004). All RTKs act as signal transducers, relating extracellular signals into the cell (Lemmon and Schlessinger, 2010).

The expression patterns of PDGF receptors are complex and dynamic with relatively low mesenchymal expression of PDGFRs reported *in vivo* which has been found to considerably increase under inflammatory conditions as well as in culture (Heldin and Westermark, 1999; Hoch and Soriano, 2003). There is evidence suggesting that PDGFR- α is expressed in cells of mesenchymal origin with particularly high expression of this receptor reported in lung, skin, and intestine (Andrae et al., 2008; Betsholtz, 2004; Boström et al., 1996). PDGFR- β has been found to be expressed in VSMCs and pericytes (Andrae et al., 2008; Hellström et al., 1999). Notably, variable expression levels of both receptors have also been observed in VSMCs derived from normal and diseased vessels (Raines, 2004). A number of cytokines and growth factors have been reported to affect the expression levels of PDGF receptors in cultured cells including TGF- β , IL-1, b-FGF and TNF- α (Battegay et al., 1990; Gronwald et al., 1989; Paulsson et al., 1993; Schöllmann et al., 1992; Tingstrom et al., 1992). Interestingly, it has been proposed that, in general, soluble mediators, such as serum and cytokines, have relatively small effects on expression levels of PDGFRs, in contrast to other

determinants such as “cell context/environment” (i.e., cell-cell contact, spreading, and attachment of cells) which was found to have markedly stronger, and potentially overriding, effects on receptor expression levels (Barret et al., 1996). Such determinants of “cell context/environment” *in vivo* may be altered during physical trauma (as in dermal wounds or vascular injury) or pathological matrix degradation (as in inflammation) (Barret et al., 1996).

1.5.2 PDGF signalling cascades

Ligand binding induce PDGFR activation and dimerization resulting in receptor autophosphorylation on tyrosine residues within the intercellular cellular tyrosine domain (Rupp et al., 1994), thus providing docking sites for downstream signalling molecules (Kazlauskas and Cooper, 1989). Activation of both PDGFR- α and PDGFR- β mediates a number of well-studied intercellular signalling cascades/pathways including RAS-MAPK (MAPK, mitogen-activated protein kinase), PI3K/AKT (PI3K, phosphoinositide 3-kinase), and PLC- γ (PLC- γ , phospholipase C- γ) – which are known to be involved in the regulation of multiple cellular responses (Andrae et al., 2008) which will be discussed in the next sections. Following PDGFR activation, an extensive cross talk between downstream signalling pathways occurs (Heldin et al., 1998) (Figure 1-3) PDGF signalling is tightly regulated by feedback control mechanisms. The simultaneous presence of stimulatory and inhibitory signals is possible, and the ultimate response depends on the balance between these signals (Heldin et al., 1998).

Following ligand binding, transphosphorylation of PDGFRs activates the RAS/MAPK pathway, the first RAS effector pathway to be identified (Warne et al., 1993), via recruitment of adaptor proteins, containing sequence homology 2 (SH2) domains, such as growth factor receptor-bound protein 2 (GRB2) and SHC-transforming protein 1 (Pawson, 1995; Schlessinger, 2000, 1994) (Figure 1-3). Via its SH3 domain, GRB2 recruits son of sevenless (SOS), a guanine exchange factor (GEF) for RAS, which induces the exchange of guanosine diphosphate (GDP) for nucleotide guanosine triphosphate (GTP) at the cell membrane, thus activating RAS (Schlessinger, 2000). RAF-1 (proto-oncogene serine/threonine-protein kinase) is then recruited to the cell membrane by activated RAS through its switch I domain and by lipid binding (Marais et al., 1995) leading to downstream activation of the MAPK cascade (MEK/ERK, mitogen-activated protein

kinase/extracellular signal-regulated kinase) (Seger and Krebs, 1995). Signalling through the MAPK cascade causes phosphorylation and activation of multiple transcription factors, thus, altering gene expression in the cell leading to multiple cellular responses including cell growth, proliferation, migration and survival (reviewed in (Plotnikov et al., 2011; Seger and Krebs, 1995)).

Activation of PDGF receptors could also engage the PI3K/AKT signalling pathway (Figure 1-3). The class I PI3Ks are predominantly acting in growth factor mediated signalling pathways where activated RTKs, such as PDGFR- α and PDGFR- β , recruit PI3K complexes to the plasma membrane where RAS-dependent activation of PI3K occurs (Castellano and Downward, 2011; Cuesta et al., 2021; Klinghoffer et al., 1996). Activated PI3K could then convert phosphatidylinositol (4,5)-bisphosphate (PIP₂) into phosphatidylinositol (3,4,5)-trisphosphate (PIP₃) at the plasma membrane (Vanhaesebroeck et al., 2010). Acting as a second messenger, PIP₃ propagates the signal by directly binding to proteins with pleckstrin homology domains (Cantley, 2002), such as phosphoinositide-dependent kinase 1 (PDK1) and AKT. Following PIP₃-dependent recruitment of PDK1 and AKT to the plasma membrane, PDK1 phosphorylates and activates AKT (Alessi et al., 1997; Currie et al., 1999). The activation of AKT kinase could then exert both direct and indirect regulatory effects on multiple downstream molecules such as B-cell lymphoma 2 (BCL2) proteins, nuclear factor kappa-light-chain-enhancer of activated B cells (NF- κ B), tuberous sclerosis complex 1/2 (TSC1/2), mammalian target of rapamycin complex 1 (mTORC1), and RAS homolog mTORC1 binding (Rheb) (Cantley, 2002; Duronio, 2008; Engelman et al., 2006). Therefore, stimulation of the PI3K/AKT pathway affects a significant number of intracellular events including cell growth, proliferation, survival, and metabolism (Vanhaesebroeck et al., 2012).

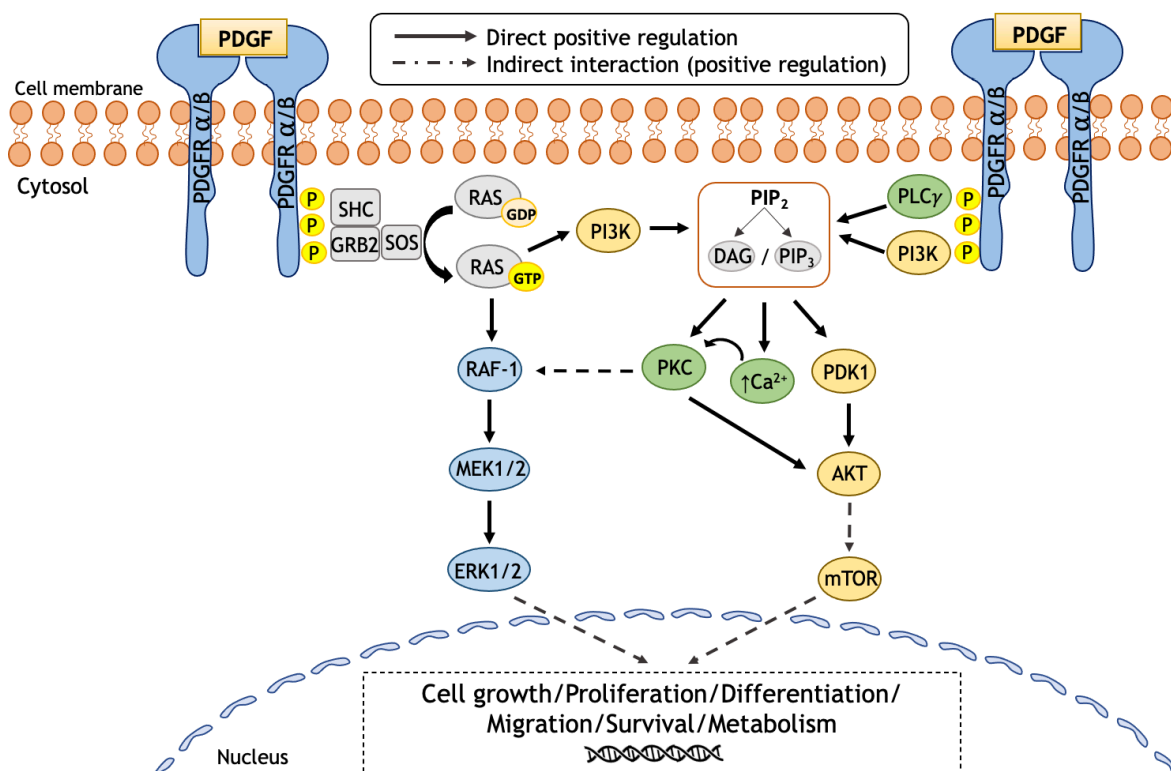


Figure 1-3 PDGF-PDGFR-mediated signalling. Binding of PDGF ligands to their respective PDGFRs causes receptor dimerization and autophosphorylation of the tyrosine residues within their intracellular domains. Activation of PDGFRs may lead to signal transduction via multiple intracellular signalling pathways including RAS/MAPK, PI3K/AKT and PLC- γ engaging various downstream effector molecules. Hydrolytic conversion of RAS-GDP to RAS-GTP leads to activation of PI3K and consequently AKT which is important for the regulation of cell proliferation, survival, and metabolism. Additionally, activated RAS can trigger the MAPK cascade which involves the activation of various kinases such as MEK1/2 and ERK1/2 via RAF-1, resulting in gene target transcription. This pathway is important for cell growth, proliferation, differentiation, and migration. PDGFR activation can also directly interact with PLC- γ , which similar to PI3K, can stimulate the conversion of PIP₂ into DAG and PIP₃, key second messenger molecules involved in the regulation of other effector molecules including PDK1, PKC and intracellular Ca²⁺ levels. PLC- γ signalling is important for cell growth, migration, apoptosis, and proliferation. Abbreviations: PDGF, platelet-derived growth factor; PDGFRA/B, PDGF receptor A/B; GRB2, growth factor receptor-bound protein 2; SHC, SHC-transforming protein 1; SOS, son of sevenless; GDP, guanosine diphosphate; GTP, guanosine triphosphate; PI3K, phosphatidylinositol 3-kinase; PIP₂, phosphatidylinositol (4,5)-bisphosphate; PIP₃, phosphatidylinositol (3,4,5)-trisphosphate; DAG, diacylglycerol; PLC- γ , phospholipase- γ ; RAF-1, proto-oncogene serine/threonine-protein kinase; MEK1/2, mitogen-activated protein kinase 1/2; ERK1/2, extracellular signal-regulated kinase 1/2; PKC, protein kinase C; Ca²⁺, calcium ++; PDK1, phosphoinositide-dependent kinase 1; mTOR, mammalian target of rapamycin;

PDGFR signalling is also implicated in PLC- γ -mediated cellular responses (Figure 1-3). Activated PDGFRs phosphorylate and activate PLC- γ which ultimately catalyses the hydrolysis of PIP₂ to PIP₃ and diacylglycerol (DAG) (Meisenhelder et al., 1989). These second messenger molecules are critical regulators of the activation of protein kinase C (PKC) and the release of Ca²⁺ from intracellular stores (Daniel and Kumjian, 1992) which in turn are responsible for initiating signalling cascades involved in the regulation of cell growth, proliferation, motility and survival (Berridge, 1993; Bill and Vines, 2020; Corbit et al., 2003; Kawakami et al., 2004; Kundra et al., 1994; Li et al., 1999).

1.5.3 PDGF signalling pathways in the vasculature and beyond – dysregulation and functional effects

Although it is well established that PDGF-PDGFR signalling is important during organ development (Andrae et al., 2008), the expression of both PDGFs and PDGFRs are tightly regulated in adulthood. Increased PDGF-PDGFR signalling, except for a short period of time during wound healing (Pierce et al., 1991; Robson et al., 1992), is generally considered abnormal, and is a significant feature observed in several diseases involving excessive cell proliferation, including many types of cancers, inflammation, pulmonary fibrosis and restenosis, injury-related vessel remodelling and also atherosclerosis (Choi et al., 2005; Folestad et al., 2018; He et al., 2015; Heldin and Westermark, 1988; Heldin, 2013; Kardas et al., 2020). Therefore, tight regulation of PDGF-PDGFR signalling is extremely important to prevent the development of the above-mentioned pathological conditions.

Despite that PDGF-PDGFR signalling is generally well regulated (Heldin et al., 1998; Lake et al., 2016), failure of the control mechanisms for PDGF-mediated signalling pathways can occur leading to the development of pathological conditions. Unsurprisingly, PDGFRs and other key downstream mediators, including RAS and PI3K, have been implicated in the regulation of crucial biological processes associated with neointimal formation and modifying the expression levels of the genes encoding these effector molecules have been found to successfully regulate cell proliferation, migration, and apoptosis in various disease settings (as discussed below).

Since PDGF is one of the main regulatory signals that drives mitosis in VSMCs (Shi and Chen, 2014), and its biological effects are initiated through both tyrosine receptors (PDGFR- α and PDGFR- β)(Raines, 2004), dysregulation of any of its receptors could potentially interfere with downstream signalling and consequently PDGF function. For example, increased expression of PDGFR- β following cytomegalovirus infection in VSMCs has been previously associated with a consequent increase in cell proliferation and migration (Zhou et al., 1999). More recently, in the context of vascular restenosis, it was found that direct targeting of PDGFR- β by a microRNA-9 (miR-9) led to decreased expression of *PDGFRB* and subsequent disruption of the downstream (ERK and AKT) signalling cascades mediated by PDGF resulting in inhibition of VSMC proliferation and migration (Ham et al., 2017).

Class I PI3K heterodimers consist of one of four catalytic p110 subunits (p110 α , β , δ or γ) that catalyse the production of PIP₃ and a regulatory subunit p85 α (or its splice variants p55 α and p50 α), p85 β , p55 γ , p101 or p84 (Vanhaesebroeck et al., 2010) which negatively regulate the catalytic subunit by inhibiting both substrate access and kinase activity (Cuesta et al., 2021; Vanhaesebroeck et al., 2010). The class I PI3Ks predominantly act in growth factor mediated signalling pathways where activated RTKs, such as PDGFR- α/β , recruit PI3K complexes to the plasma membrane where RAS-dependent, RTK or GRB2-mediated activation of PI3K can occur relieving the catalytic subunit from inhibition imposed by the regulatory subunit (Castellano and Downward, 2011; Cuesta et al., 2021).

Phosphoinositide-3-kinase regulatory subunit 3 (PIK3R3, or p55 γ) in humans is encoded by the *PIK3R3* gene (Jean and Kiger, 2014). The role of PIK3R3 has been mostly studied in the context of cancer where several studies reported that PIK3R3 positively regulates cancer cell proliferation and tumorigenesis (Soroceanu et al., 2007; Wang et al., 2013a, 2013b; W. Xu et al., 2020; Yoon et al., 2021; Zhou et al., 2012) whereas PIK3R3 knockdown was associated with increased apoptosis in ovarian cancer cells (Zhang et al., 2007). Although the role of PIK3R3 has been extensively studied in cancer, its biological and pathological functions in the cardiovascular system, particularly in the regulation of the fate of VSMCs, have not been widely investigated yet. Interestingly, in contrast to the effects seen in cancer cells, in the context of

neointimal formation and PDGF-mediated cell responses, upregulation of PIK3R3 was reported to inhibit VSMC proliferation *in vitro* and injury-induced arterial neointimal formation *in vivo* through PI3K-independent actions (G. Li et al., 2015). Similarly, N24 peptide, a functional mimetic of PIK3R3/p55 γ , was shown to suppress PDGF-induced VSMC proliferation and migration *in vitro* and balloon injury-induced neointimal formation *in vivo* via a PI3K-independent mechanism which involved activation of the p53-p21 signal cascade (Guo et al., 2015). A more recent study in vascular ECs demonstrated that PIK3R3 was involved in the regulation of EC responses via a PI3K/AKT dependent mechanism where the direct targeting of *PIK3R3* by miR-24-3p was associated with inhibition of EC proliferation and migration, as well as increased EC apoptosis (Y. Xu et al., 2020).

RAS is another crucial signal transduction molecule that can regulate PDGFR-mediated cellular responses through both the regulation of PI3K/AKT signalling pathway and the MAPK cascade which is also involved in the regulation of cell proliferation, migration, and apoptosis (Castellano and Downward, 2011; Roux and Blenis, 2004). In cancer, the role of RAS proteins, including HRAS, NRAS, and KRAS, also known as oncogenes, have been widely studied and implicated in the regulation of various cellular outcomes including cell cycle progression, growth, migration, cytoskeletal changes and apoptosis (Fernández-Medarde and Santos, 2011; Gimple and Wang, 2019). In the context of vascular injury, several studies demonstrated that VSMC proliferation may be regulated by interfering with RAS signalling (Dong et al., 2010; Sedding et al., 2009; Wu et al., 2009). It has been shown that PDGF-induced RAS/MAPK mediated proliferation was attenuated by lercanidipine-dependent reduction of RAS activity (Wu et al., 2009). Similarly, smooth muscle $\alpha 22$ binding to RAS inhibited PDGF-induced RAS-mediated RAS-RAF-MEK-ERK MAPK signalling pathway and consequently VSMC proliferation *in vitro* and neointimal hyperplasia induced by balloon injury *in vivo* (Dong et al., 2010).

1.6 MicroRNAs

MicroRNAs (MiRNAs) are a class of short non-coding RNAs, with an average length of 22 nucleotides, which are known to be important post-transcriptional regulators of gene expression (Makarova et al., 2016). Almost all miRNAs are

transcribed from DNA sequences into primary miRNAs (pri-miRNAs) and processed into precursor miRNAs (pre-miRNAs) and mature miRNAs via the canonical or non-canonical pathways (Figure 1-4). Primarily, miRNAs interact with the 3' untranslated region (UTR) of target messenger RNAs (mRNAs) to suppress gene expression (Ha and Kim, 2014). However, interactions of miRNAs with other regions have also been reported, including the 5' UTR, coding sequence, and gene promoters (Broughton et al., 2016). Since miRNAs were first discovered in 1993 (Lee et al., 1993; Wightman et al., 1993), there are now approximately 2,600 annotated mature miRNAs in the human genome (miRBase v22.1) estimated to regulate over 60% of human genes (Friedman et al., 2009).

1.6.1 Biogenesis of miRNAs

MiRNAs are predominantly processed by the canonical biogenesis pathway (Figure 1-4). In this pathway, RNA polymerase II transcribes miRNA genes producing pri-miRNA stem loop structures (Y. Lee et al., 2004) which are then processed into precursor-miRNAs (pre-miRNAs) by a microprocessor complex, consisting of an RNA binding protein DGCR8 (DiGeorge Syndrome Critical Region 8) and Drosha (a ribonuclease III enzyme) (Denli et al., 2004). The DGCR8 component of the complex recognises the pri-miRNA, while Drosha cleaves the pri-miRNA transcript at the base of the stem loop (Alarcón et al., 2015; Han et al., 2004; Lee et al., 2002) resulting in the formation of a hair-pin structure called a pre-miRNA, which is approximately 70 nucleotides (nts) in length and is characterised by a ~2 nt 3' overhang (Bohnsack et al., 2004; Han et al., 2004). Pre-miRNAs are then exported to the cytoplasm through the nuclear pore complex by the exportin 5 (XPO5)/RanGTP complex (Wang et al., 2011). In the cytoplasm, the pre-miRNA duplex is released from the XPO5/RanGTP complex by hydrolysis of RanGTP to RanGDP before being processed by Rnase III endonuclease Dicer, in complex with transactivation response element RNA-binding protein (TRBP). This processing involves the cleavage of the terminal loop of the pre-miRNA duplex, resulting in the formation of a mature miRNA duplex comprised of two mature miRNA strands, 3p and 5p, the name of which is determined by the directionality of the strands (Chendrimada et al., 2005). TRBP mediates loading of the duplex into Argonaute (AGO) family of proteins (AGO1-4 in humans) - key components of the RNA-induced silencing complex (RISC) (Su et al., 2009). One of the two mature miRNA strands within the duplex is selected

and anchored into the AGO protein, while the other strand is passively unwound from the complex and degraded (Medley et al., 2021). The selection of the strand (5p or 3p) is partially based on the identity of the 5' nucleotide at each strand and the relative thermodynamic stability of the two ends of the miRNA duplex (Medley et al., 2021). A mature RISC complex is formed following the integration of the guide strand into an AGO which directs the miRNA-induced silencing complex (miRISC) to target mRNAs resulting in inhibition of gene expression (Kwak and Tomari, 2012).

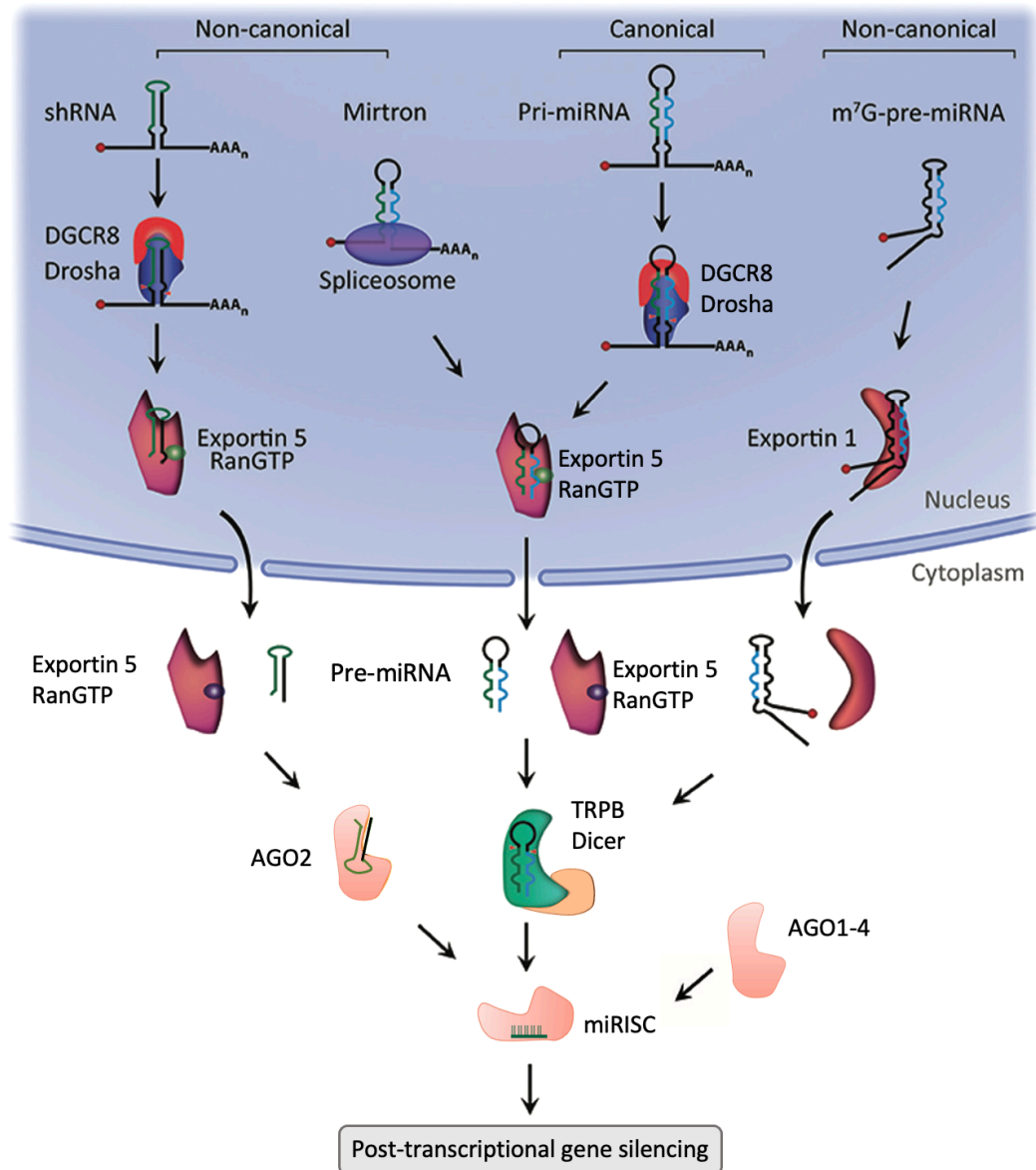


Figure 1-4 Canonical and non-canonical pathways of miRNA biogenesis. The biogenesis of miRNAs via the canonical pathway begins with the generation of pri-miRNA transcript by RNA polymerase II (Y. Lee et al., 2004). A microprocessor complex comprised of DGCR8 and Drosha (Denli et al., 2004) cleaves the pri-miRNA transcript at the base of the stem loop to generate pre-miRNA (Alarcón et al., 2015; Han et al., 2004; Lee et al., 2002). Pre-miRNA is transported out of the nucleus via Exportin 5/RanGTP-dependent manner (Wang et al., 2011). Processing of the free pre-miRNA by Dicer, which is part of a complex with TRBP, produce a mature miRNA duplex which is then loaded into an AGO protein. A single strand, either 5p or 3p, is retained by the AGO proteins forming a mature RISC (miRNA-induced silencing complex (miRISC)) (Chendrimada et al., 2005). The biogenesis of miRNAs via the non-canonical pathways occurs in the absence of either Dicer or Drosha/DGCR8 (Felekis et al., 2010). For instance, shRNAs are first cleaved by DGCR8/Drosha (Yang et al., 2010) and then exported out of the nucleus by Exportin 5/RanGTP where pre-miRNAs are further directly cleaved by AGO proteins (AGO2) in Dicer-independent manner (Cheloufi et al., 2010). Mirtrons (generated by spliceosomes and exported via Exportin 5/RanGTP) (Ruby et al., 2007) and m⁷G-pre-miRNAs (exported via Exportin 1) (M. Xie et al., 2013) are processed in Drosha/DGCR8-independent manner. Once outside the nucleus, both mirtrons and m⁷G-pre-miRNAs are dependent on Dicer to complete their cytoplasmic maturation (Havens et al., 2012; M. Xie et al., 2013). Abbreviations: pri-miRNA, primary miRNA; pre-miRNA, precursor miRNA; shRNA, small hairpin RNA; m⁷G, 7-methylguanosine; DGCR8, DiGeorge syndrome critical region 8; TRBP, transactivation response element RNA-binding protein; AGO, argonaute family of proteins; RISC, RNA-induced silencing complex; miRISC, miRNA-induced silencing complex; shRNA, small hairpin RNA. Figure adapted from (O'Brien et al., 2018) under Creative Commons Attribution License (CC BY 4.0).

The non-canonical miRNA biogenesis pathway utilises different combinations of the components involved in the canonical pathway, and they can be generally categorised as Drosha/DGCR8-independent and Dicer-independent pathways (Figure 1-4). Drosha/DGCR8-independent pathway is known to produce pre-miRNAs called mirtrons, generated from the introns of mRNA during splicing (Ruby et al., 2007), and 7-methylguanosine (m7G)-capped pre-miRNA, pre-miRNAs generated directly by RNA polymerase II transcription (M. Xie et al., 2013). In contrast, in the Dicer-independent pathway, endogenous short hairpin RNA (shRNA) transcripts are processed by Drosha (Yang et al., 2010), followed by AGO2-mediated splicing of the 3p strand within the cytoplasm as the pre-miRNA sequences are of insufficient length to be Dicer-substrates (Cheloufi et al., 2010). Despite differences in the upstream processing of pre-miRNAs, all biogenesis pathways converge at the miRISC to induce post-transcriptional silencing of target genes.

1.6.2 Mechanisms of miRNA-mediated gene regulation

MiRNAs recognise their target mRNAs through Watson-Crick, full or partial complementary, base pairing between the miRNA ‘seed region’ and the mRNA target (Bartel, 2009). It is widely accepted that miRNA binding sites are primarily located within the 3’UTR of target mRNAs and such interactions induce translational repression and mRNA deadenylation and decapping (Huntzinger and Izaurralde, 2011; Ipsaro and Joshua-Tor, 2015). However, alternative miRNA:mRNA interactions can also occur through miRNA binding sites located within other mRNA regions (Xu et al., 2014), such as the 5’ UTR and the coding sequence (CDS region) (Plotnikova et al., 2019), resulting in distinct miRNA functions. While binding of miRNAs to 5’ UTR and coding sequences has been reported to exhibit inhibitory effects on gene expression (Forman et al., 2008; J. Zhang et al., 2018), it has been suggested that binding of miRNAs to promoter regions could have an opposing effect (i.e., activation of transcription) (Dharap et al., 2013). A recent experimental identification of microRNA-binding regions performed by Plotnikova *et al.* suggested that miRNA-binding regions were almost evenly distributed across all types of mRNA regions, including 3’UTR, CDS or 5’UTR, with no enrichment in miRNA-binding sites demonstrated within 3’UTRs (Plotnikova et al., 2019). However, since miRNA:mRNA interactions within the 3’UTR have been predominantly studied, more research focusing on

studying alternative miRNA: mRNA interactions is required to fully understand their functional significance.

1.6.2.1 MiRNA-mediated gene silencing

There are two main mechanisms associated with miRISC function - target recognition mediated by the incorporated guide strand and silencing of the targeted transcript executed by the protein components of the complex (Kawamata and Tomari, 2010). The key components of mammalian miRISC include AGO proteins (AGO1-4) and Argonaute-bound glycine-tryptophan protein of 182 kDa (GW182) (La Rocca and Cavalieri, 2022). Full complementarity base pairing between the miRNA 'seed region' and the miRNA response element (MREs) - sequences located on the target mRNA, leads to cleavage of the target mRNA mediated by catalytically active AGO2 which results in mRNA degradation and gene silencing (Jo et al., 2015). In contrast to AGO2, AGO1, 3 and 4 do not exhibit independent cleavage activity (Su et al., 2009). In the case of partial complementarity base pairing, the recruitment of effector AGO-binding proteins such as the GW182 protein family, which interacts with AGO proteins via an AGO-binding domain, is required to aid the interaction between AGO proteins and downstream components mediating gene silencing in a manner independent of endonucleolytic cleavage (reviewed by (Jonas and Izaurralde, 2015)). In general, when cleavage is not possible, gene silencing post-transcriptionally occurs via two main mechanisms: translational repression (Figure 1-5) and mRNA degradation/decay, which includes deadenylation, decapping, and 5'-to-3' degradation (Jonas and Izaurralde, 2015) (Figure 1-6).

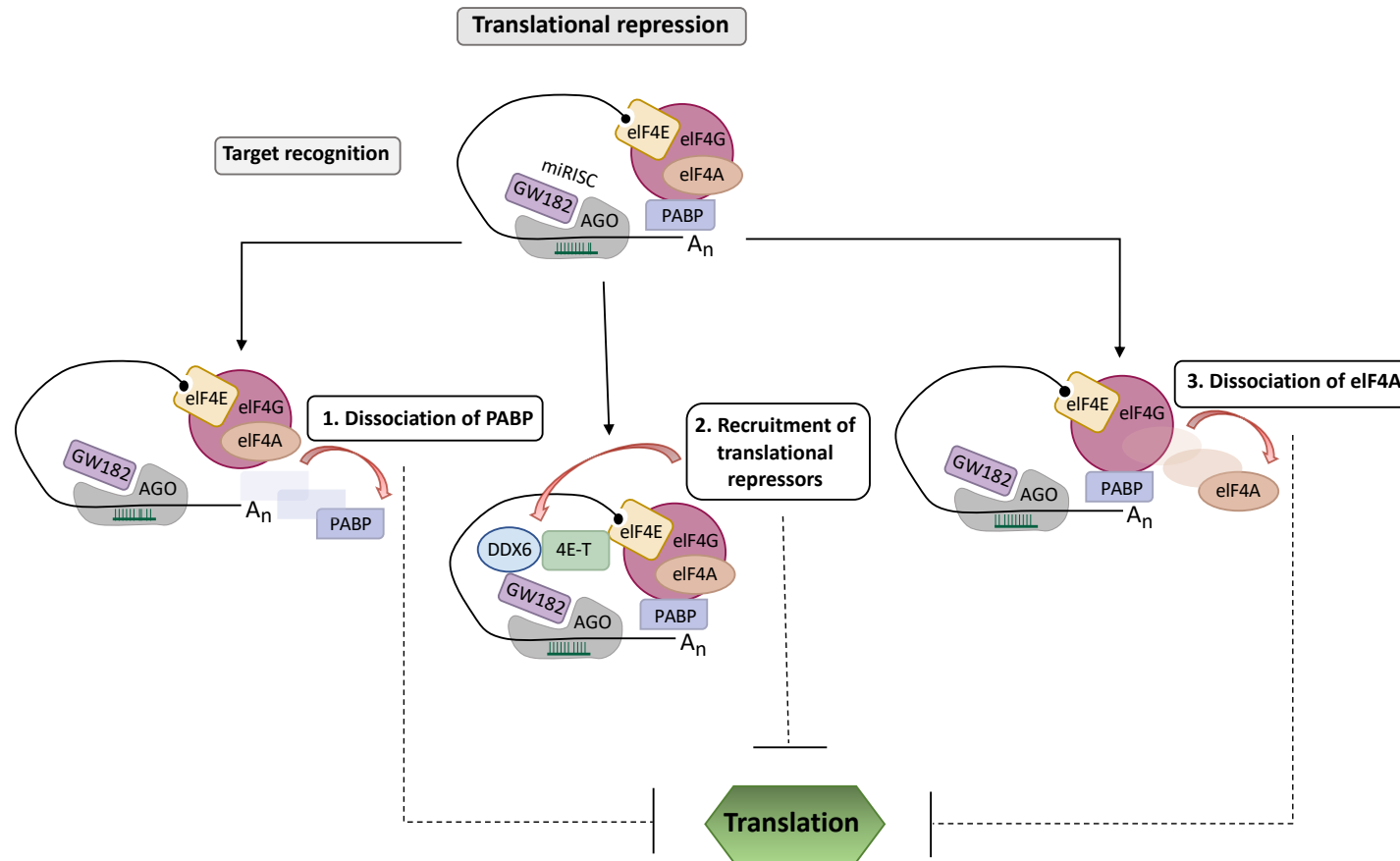


Figure 1-5 Post-transcriptional gene silencing via miRNA-mediated translational repression. Initially, translation is triggered by the recruitment of PABP to the poly(A) tail of mRNAs and recognition of the 5'-cap by the eIF4E which together with the scaffolding protein eIF4G and eIF4A form the eIF4F complex (Gallie, 2014). Following binding of the miRNA-induced silencing complex (miRISC) to the 3' UTR of target mRNAs, translational repression can occur via three main mechanisms: (1) GW182-mediated PABP displacement (Zekri et al., 2013), (2) recruitment of the translational repressors through GW182 including DDX6 and 4E-T (Chen et al., 2014; Mathys et al., 2014; Rouya et al., 2014; Waghray et al., 2015), and (3) dissociation of eIF4A from the cap-binding complex eIF4F (Fukao et al., 2014; Fukaya et al., 2014). Abbreviations: AGO, argonaute family of proteins; miRISC, miRNA-induced silencing complex; eIF4, eukaryotic initiation factor 4; PABP, poly(A)-binding protein; DDX6, DEAD-Box Helicase 6; 4E-T, 4E-Transporter.

In eukaryotes, translation is a complex process which mediates the conversion of mRNA to protein in three distinct steps - initiation, elongation and termination (Jackson et al., 2010), where the initiation step represents the rate-limiting step in the eukaryotic canonical translation (Hinnebusch, 2014; Sonenberg and Hinnebusch, 2009). It has been previously suggested that miRNAs can induce translational repression by interfering with the initiation step of translation (Joerg E. Braun et al., 2012; Eichhorn et al., 2014; Huntzinger and Izaurralde, 2011) (Figure 1-5). Although, the precise mechanisms of miRNA-mediated inhibition of translation remain unclear, three main mechanisms have been proposed, including: (i) GW182-mediated poly(A)-binding protein (PABP) displacement (Zekri et al., 2013) (Figure 1-5), (ii) recruitment of the translational repressors through GW182 (Chen et al., 2014; Mathys et al., 2014; Rouya et al., 2014; Waghray et al., 2015) (Figure 1-5), and (iii) dissociation of eukaryotic initiation factor 4 (eIF4) A from the eIF4F complex (Figure 1-5) (Fukao et al., 2014; Fukaya et al., 2014). However, an *in vitro* ribosomal profiling study, investigating the impact of decreased translational efficiency and destabilization of target mRNAs on changes in mRNA and protein levels, suggested that while translational repression plays a role in gene silencing it is not the primary method of gene silencing (Guo et al., 2010).

In contrast, both genome-wide studies, investigating the effects of miRNAs on mRNA and protein levels, and ribosome profiling experiments, have demonstrated that target mRNA degradation is the primary method accounting for most (66-90%) of the miRNA-mediated gene silencing observed in cultured mammalian cells (Baek et al., 2008; Eichhorn et al., 2014; Guo et al., 2010; Selbach et al., 2008). Increasing evidence suggest that miRNA-induced mRNA degradation is driven by enzymes involved in the cellular 5'-to-3' mRNA decay pathway (Braun et al., 2011; Chekulaeva et al., 2011; Chen et al., 2009; Fabian et al., 2011). In this pathway, target mRNAs first undergo deadenylation, which refers to the removal of the poly(A) tail of mRNAs by poly(A)-specific 3' exonucleases (deadenylases) (Charenton and Graille, 2018) (Figure 1-6). The process is triggered by the action of cytoplasmic deadenylase complexes - poly(A)-nuclease (PAN2-PAN3) and the carbon catabolite repression 4-negative on TATA-less (CCR4-NOT) (Wahle and Winkler, 2013) (Figure 1-6), where the CCR4-NOT complex is the main initiator of miRNA-mediated deadenylation and

mRNA decay (Braun et al., 2011; Chen et al., 2009; Piao et al., 2010). Following deadenylation, target mRNAs can either be directly degraded in 3'-to-5' direction via the recruitment of cytoplasmic RNA exosome - a ribonuclease complex that controls the quantity and quality of RNA transcripts (Kowalinski et al., 2016), or undergo decapping which is the main response to deadenylation (Anderson and Parker, 1998; Behm-Ansmant et al., 2006; Joerg E Braun et al., 2012; Charenton and Graille, 2018) (Figure 1-6). In this process, the mRNA decapping enzyme - de-capping protein 2 (DCP2, the catalytic subunit of decapping complex DCP1/DCP2), catalyses the removal of the 5' m⁷G-cap leading to mRNA degradation via exoribonuclease 1 (XRN1)-mediated 5'-to-3' mRNA decay pathway (Charenton and Graille, 2018) (Figure 1-6).

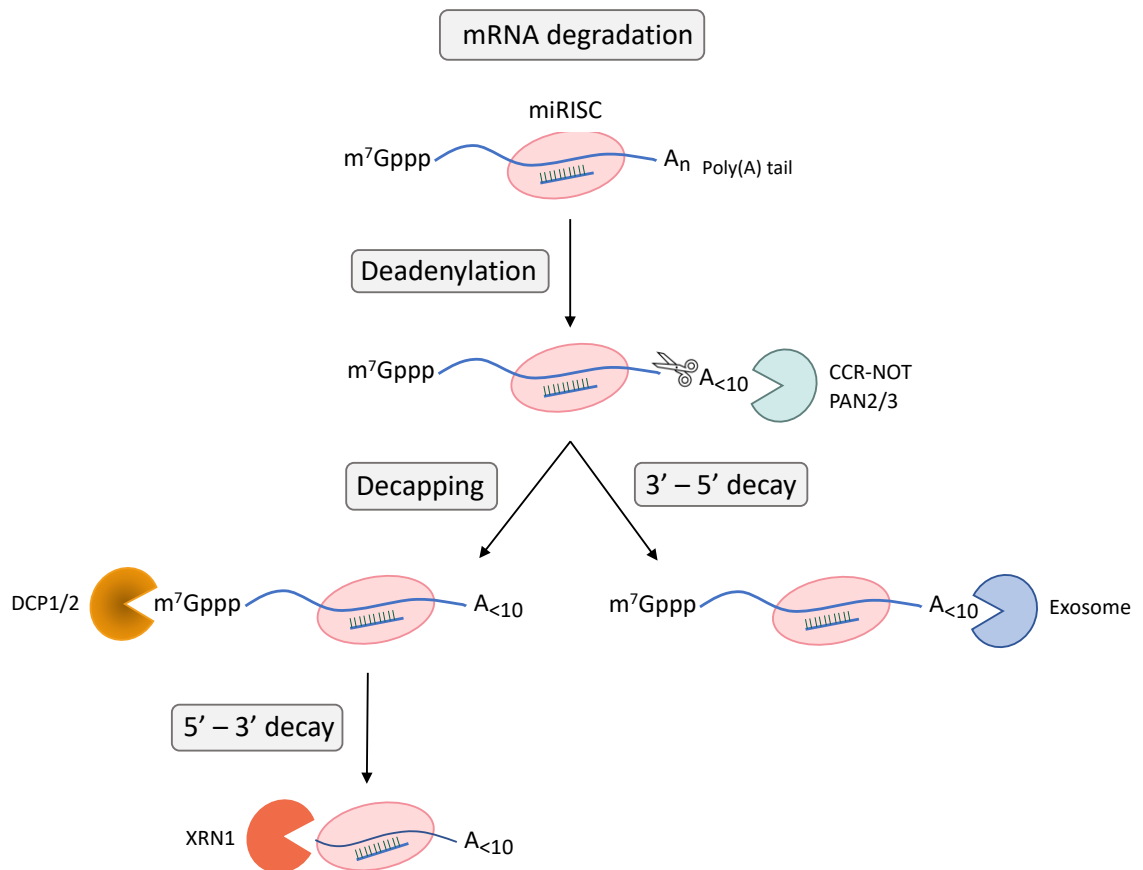


Figure 1-6 Post-transcriptional gene silencing via miRNA-mediated mRNA degradation. The main steps involved in miRNA-mediated mRNA degradation include deadenylation, decapping, and 5'-to-3' decay. Firstly, miRISC binds to the 3' UTR of target mRNAs. Then, target mRNAs undergo deadenylation which refers to the partial or total cleavage of the poly(A) tail triggered by PAN2-PAN3 and CCR4-NOT deadenylase complexes (Charenton and Graille, 2018). Following deadenylation, target mRNAs can be either directly degraded in 3'-to-5' direction by RNA exosome complexes (Anderson and Parker, 1998; Kowalinski et al., 2016) or, more commonly, undergo decapping (Behm-Ansmant et al., 2006; Joerg E Braun et al., 2012; Charenton and Graille, 2018). Decapping refers to the removal of the 5' m⁷G-cap by the decapping enzyme – DCP2. Finally, decapped target mRNAs undergo 5'-to-3' decay via XRN1, leading to mRNA degradation (Charenton and Graille, 2018). Abbreviations: ORF, open reading frame. miRISC, miRNA-induced silencing complex; DCP2, decapping protein 2; XRN1, exoribonuclease 1.

1.6.3 Role and therapeutic potential of miRNAs in vascular remodelling

In addition to their traditional gene regulatory functions intracellularly, miRNAs can also be released from cells and act in a paracrine and endocrine manner regulating the translational activity of target genes in recipient cells. Even though it was initially considered that miRNAs were passively released from dying or injured cells, extensive research findings, from gene expression profiling studies in various disease settings and studies focusing on the characterisation of circulating miRNA, suggest that miRNAs exert biological effects in recipient cells, thus supporting their active role as crucial intercellular communicators (reviewed in (Sohel, 2016)).

Accumulating evidence suggest that miRNAs are significant mediators of vascular remodelling processes in response to different kinds of injury demonstrating their promising therapeutic potential (Gareri et al., 2016; Jamaluddin et al., 2011).

A study by Ji et al. 2007, investigating the role of miR-21 in VSMCs, reported that the miRNA was overexpressed in vascular walls following balloon injury (Ji et al., 2007). In the same study, downregulation of miR-21 inhibited VSMC proliferation and promoted cell apoptosis *in vitro*, and had a significant negative effect on neointimal lesion formation after vascular injury *in vivo* (Ji et al., 2007). The proposed underlying mechanism involved a combination of actions including direct targeting of phosphatase and tensin homolog (*PTEN*) and possibly indirect targeting of *BCL2*, suggesting that miR-21 may exert its effect in VSMCs through the regulation of multiple pathways (Ji et al., 2007). The same miRNA (miR-21) has also been shown to be upregulated in mouse, pig, and human vein graft models of vascular injury (McDonald et al., 2013). In this study, inhibition of miR-21 resulted in target gene de-repression and substantially reduced neointimal formation in a mouse model of vein grafting, demonstrating its considerable therapeutic potential in the prevention of pathological vein graft remodelling (McDonald et al., 2013). It was proposed that the observed effect may be mediated through de-repression of *PTEN*, however, other target genes, including signal transducer and activator of transcription 3 (*STAT3*), *PTEN*, and bone morphogenetic protein receptor type 2 (*BMP2*), were also

found to be re-pressed following anti-miR-21 treatment of human saphenous vein smooth muscle cells (HSVSMCs) suggesting that further mechanistic studies are required to properly investigate the role of these genes in VGD (McDonald et al., 2013).

The upregulation of other miRNAs, including miR-221/222 cluster and miR-424, after vascular injury *in vivo* had been implicated in the regulation of vascular remodelling processes (Liu et al., 2012, 2009; Merlet et al., 2013). The miR-221/222 cluster has been shown to inhibit cell proliferation and migration, while promoting cell apoptosis in both VSMCs, whereas, opposite effects were observed in ECs which were also verified *in vivo* (Liu et al., 2012). Generally, overexpression of miR-221/222 resulted in extensive neointimal growth while their suppression led to 40% reduction of neointima formation (Liu et al., 2012, 2009). The observed effects of the miR-221/222 cluster on vascular remodelling processes in response to injury may be due to a direct inhibition of their target genes, including cyclin-dependent kinase inhibitor 1B (*CDKN1B*) or p27^{Kip1}, cyclin-dependent kinase inhibitor 1C or p57^{Kip2} (*CDKN1C*), and proto-oncogene c-kit (*CD117*) (Liu et al., 2012, 2009). The inconsistent effects resulting from the overexpression of those miRNAs might be due to the observed difference in the expression profile of their target genes between VSMCs and ECs (Liu et al., 2012) suggesting a cell-specific effect.

The expression levels of both miR-143 and miR-145 were found to be downregulated in response to vascular injury and their overexpression has been shown to prevent neointimal hyperplasia (Cheng et al., 2009; Elia et al., 2009). Both miRNAs are believed to cooperatively promote the contractile VSMC phenotype by targeting a network of transcription factors, including KLF4, and ELK1 (Cheng et al., 2009; Cordes et al., 2009; Elia et al., 2009). Similarly, miR-133 and miR-195 have also been shown to modulate VSMC phenotypic switch. Targeting of stimulating protein-1 (*SP1*) by miR-133, resulted in inhibition of VSMC proliferation and migration, and its overexpression promoted cell growth in a rat model of vascular injury (Torella et al., 2011). MiR-195 is thought to be another significant modulator of VSMC phenotype which has been shown to negatively regulate VSMC proliferation and migration, as well as the release of proinflammatory cytokines (e.g., IL-6, IL-8, IL-1 β) (Y. S. Wang et al., 2012a). The

overexpression of miR-195 downregulated the expression of different VSMC regulator molecules, including cell division control protein 42 (*CDC42*), fibroblast growth factor 1, (*FGF1*) and cyclin D1 (*CCD1*) (Liu et al., 2008; Y. S. Wang et al., 2012a), which led to a substantial reduction of neointimal formation in injured carotid arteries (Y. S. Wang et al., 2012a). Notably, the negative regulation of cyclin D1 by miR-195 may be as a result of both - direct *CCD1* targeting or indirect targeting of *CCD1* through *CDC42*, which is upstream of *CCD1* (Y. S. Wang et al., 2012a). Furthermore, the expression levels of miR-16-5p and miR-423 were also found to be downregulated in the context of CABG surgery. For instance, a very recent study by Zhang et al. 2022 reported that miR-16-5p levels were significantly reduced in the vein graft of a rat model over time and in PDGF-treated HSVSMCs compared to the levels detected in the contralateral jugular vein and control cells, respectively (D. Zhang et al., 2022). This aberrant expression of miR-16-5p was linked to increased neointimal thickness and area after CABG and phenotypic switching of HSVSMCs, proposing the inadequate suppression of zyxin (*ZYX*) target gene expression by miR-16-5p as a potential underlying mechanism. Upregulating the expression of miR-16-5p attenuated neointimal formation in vein grafts and inhibited HSVSMC phenotypic switching *in vitro* (D. Zhang et al., 2022). Similarly, decreased miR-423 levels were observed in the plasma of CHD patients following CABG surgery compared to healthy subjects (Ren et al., 2020). Interestingly, in this study, it was found that overexpression of miR-423 suppressed the expression of its target gene - a disintegrin and metalloproteinase with thrombospondin motifs 7 (*ADAMTS7*), resulting in decreased proliferation and migration of human umbilical vein smooth muscle cells (HUVSMCs), in contrast to the observed increase in proliferation and migration of human umbilical vein endothelial cells (HUVECs) *in vitro*. Upregulation of miR-423 also improved re-endothelialisation and attenuated neointimal formation in a rat vein graft model (Ren et al., 2020).

Notably, as major modulators of inflammation and endothelial dysfunction, miR-126, miR-92a and miR-221/222, have also been implicated in the regulation of vascular remodelling processes in response to injury. For instance, miR-126 has been shown to play a role in the regulation of EC inflammatory responses and endothelial dysfunction through inhibition of sprouty-related, EVH1 domain-containing protein 1 (*SPRED1*) and *VCAM-1*, leading to enhanced EGF- and FGF-

mediated angiogenesis and disrupted leukocyte adhesion to ECs (Harris et al., 2008; Wang et al., 2008). MiR-92a is another key EC miRNA, the inhibition of which led to enhanced blood vessel growth and functional recovery of damaged tissue in different *in vivo* models, acting, at least in part, through suppression of the integrin $\alpha 5$ (ITG $\alpha 5$) (Bonauer et al., 2009). In line with these findings, Laconetti et al. 2012 demonstrated that systemic administration of miR-92a significantly improved re-endothelialisation in injured carotid arteries and reduced neointimal formation in an *in vivo* injury model (laconetti et al., 2012).

Additionally, both miR-551b-5p and miR-200c-3p have been implicated in the development of neointimal formation post CABG-induced injury in venous and arterial grafts, respectively (D. Chen et al., 2021; Dong et al., 2017). In their study, Dong et al. 2017 demonstrated that increased miR-551b-5p expression in HUVECs, subjected to mechanical stretch, promoted cell proliferation. In an attempt to investigate the potential underlying mechanism, the authors assessed the expression levels of early growth response protein 1 (EGR1) - one of the identified gene targets through bioinformatics analysis. Through loss- and gain-of-function experiments, it was found that miR-551b-5p potentially positively regulated *EGR1* expression in HUVECs subjected to mechanical stretch; however, this proposed mechanism remains uncertain since following miR-551b-5p overexpression in HUVECs, the expression levels of the miRNA were found to be increased by 793-fold, while EGR1 levels only increased by 1.9-fold (Dong et al., 2017). It is possible that any of the other differentially expressed miRNAs in mechanically injured cells may have contributed to the observed upregulation of EGR1. It has been previously reported that the let-7 family miRNAs downregulated EGR1 expression (Worringer et al., 2014), and in this study, let-7a-5p expression was found to be decreased following mechanical stretch stimulation (Dong et al., 2017), which may have contributed to the slight increase in EGR1 expression compared to the massive upregulation of miR-551b-5p. The studies discussed above collectively suggest that miRNAs are important modulators of vascular remodelling processes in response to injury, demonstrating a great therapeutic potential for targeting pathological neointimal formation.

1.6.4 MiRNAs as potential biomarkers

Following biogenesis, miRNAs are predominantly located intracellularly where they exert their actions, however, they can also be released from cells and, therefore, are found within the extracellular environment including blood or other extracellular fluids such as urine and saliva (Arroyo et al., 2011; Cortez et al., 2011; Weber et al., 2010). In the blood, circulating miRNAs may occur freely, within extracellular vesicles, such as exosomes and microvesicles, or be bound to other molecules such as lipoproteins and extracellular binding protein (AGO2) (Arroyo et al., 2011; Faraldi et al., 2018; Gallo et al., 2012; Seeliger et al., 2014; Sohel, 2016; Yuan et al., 2009).

MiRNAs play a significant regulatory role during development as evident by the observed defects acquired during organogenesis and embryonic lethality in murine models of tissue-specific or germline Dicer knockouts respectively (Bernstein et al., 2003; Park et al., 2010). Furthermore, dysregulation of miRNAs is also linked to the aetiology and/or pathogenesis of different pathological conditions such as cancer, metabolic diseases, viral infections (Hammond, 2015), CAD (Churov et al., 2019) and associated pathologies, including ISR (Varela et al., 2019) and VGD (Błażejowska et al., 2021). In disease settings, miRNAs can have both a causative role, where a particular miRNA could be functioning as an initiator or maintainer of a condition, or be a consequence of a pathology, in which case observed changes in miRNA levels may be due to unregulated secretion from injured/stressed cells, or as a response to a particular insult (Mendell and Olson, 2012). Therefore, by measuring the changes in miRNA expression profiles in an individual at different disease stages (i.e., before, during, and after recovery), it may be possible to identify how miRNAs are behaving in terms of aetiology and pathogenesis. Diagnostic miRNA tests for diseases (e.g., certain cancers) based on the quantification of either a single miRNA or a panel of miRNAs already exist, demonstrating successful proof of concept for the use of miRNA as biomarkers in disease (Bajan and Hutvagner, 2020; Bonneau et al., 2019). Accumulating evidence suggest that certain miRNAs, expressed at local tissue sites, such as atherosclerotic plaques, or in the circulation, may potentially be used to distinguish between individuals with different cardiovascular health statuses (Condorelli et al., 2010; D'Alessandra et al., 2010; Fichtlscherer et al., 2010).

1.6.4.1 MiRNAs as potential biomarkers of CAD/atherosclerosis

Changes in the circulating levels of a number of miRNAs have been associated with CAD. The levels of miR-17, miR-92a, miR-126, miR-145, and miR-155 were found to be significantly lower in patients with CAD compared to healthy individuals (Fichtlscherer et al., 2010). Altered circulating levels of miR-1, miR-133a, miR-499, and miR-663 family associated with AMI has also been reported (Meder et al., 2011; Wang et al., 2010). In addition to using miRNAs as differentiative markers to distinguish between individuals with and without CAD, it has also been proposed that assessment of circulating levels of certain miRNAs may serve as a valuable tool to evaluate vascular disease severity. A study investigating the miRNA expression profile in patients with stable versus unstable carotid plaques, reported that the reduced expression of miR-210, and consequently the increased expression and activity of relevant target genes, resulted in substantial reduction of fibrous cap stability of an atherosclerotic plaque (Eken et al., 2017).

At tissue level, the expression of specific miRNA markers has also been detected at the site of atherosclerotic plaques., Raitoharju et al. 2011, investigated the miRNA expression profiles of human atherosclerotic plaques derived from peripheral arteries (carotid, femoral, and abdominal aorta) in comparison to left internal thoracic arteries, and reported that miR-21, miR-34a, miR-146a, miR-146b-5p, and miR-210 were the most upregulated miRNAs in atherosclerotic plaques in comparison to controls (Raitoharju et al., 2011). In the same study, further analysis revealed that some of the predicted gene targets of these miRNAs were downregulated in the plaque lesions. Following gene set enrichment analysis (GSEA), these miRNAs were linked to the regulation of relevant processes associated with atherosclerosis development such as VSMC proliferation as well as high density lipoprotein (HDL) and low density lipoprotein (LDL) metabolism (Raitoharju et al., 2011). Another human study investigating the expression levels of miRNAs in human atherosclerotic plaques identified a panel of miRNAs (miR-100, miR-127, miR-133a, miRNA-133b, and miR-145) correlated with clinical features of plaque destabilization supporting the prognostic significance of miRNAs for stratifying the risk of vulnerable plaques (Cipollone et al., 2011).

1.6.4.2 MicroRNAs as potential biomarkers of vascular injury

Although symptomatic VGD continues to be a major health problem for a growing number of people due to the impact of an aging population and the persistent increase in the incidence of patients with CABG (Brilakis et al., 2011; Escaned, 2012; Lang et al., 2017), there is still urgent need for establishing novel disease biomarkers that predict CABG surgery outcomes. To date, there is no reliable diagnostic marker, which predicts graft patency, and only a limited number of studies have explored the potential of miRNAs as biomarkers for the development of post-transplant vein restenosis/VGD.

A comprehensive study, using multiple *in vivo* (mouse and porcine vein graft models), *ex vivo* (human SV surplus vein tissue), and *in vitro* (human SV-derived EC and SMCs) models of VGD, investigated the expression of miRNAs in neointimal lesions at different timepoints after surgery (McDonald et al., 2013). In this study, it was found that 21 miRNAs were significantly up-regulated in porcine vein grafts 7- and 28-days post-implantation including miR-21, miR-34a, miR-138, miR-424, miR-142-3p, miR-146b-5p, and miR-449a (McDonald et al., 2013). Interestingly, the finding that miR-21 was dysregulated during neointima formation in the setting of vein graft failure is unsurprising since this miRNA has previously been implicated in SMC and fibroblast proliferation following vascular injury (Ji et al., 2007; F. Wang et al., 2012). Additionally, another more recent study, investigating the miRNA expression profile in rat neointimal lesions of transplanted left external jugular veins compared to control, identified that postoperative neointimal lesions have a significantly dysregulated miRNA expression profile compared to control vessels (Wan et al., 2020), thus, further highlighting a potential role for miRNAs as biomarkers for the development and progression of VGD.

Investigations of circulating miRNAs in patients following CABG surgery identified that the expression of certain miRNAs may be upregulated in response to cardiac and inflammatory injury. For instance, circulating levels of miR-1, a well-known marker of cardiac injury (Jayawardena et al., 2022), were found to be increased in patients with ACS after CABG surgery, however, it did not correlate with cardiac muscle troponin T (cTnT) (Z. Wang et al., 2018), a widely used marker of myocardial damage. Recently, the serum levels of miR-126-3p were also

measured in a cohort of 67 patients who underwent CABG surgery (Mukaihara et al., 2021). It was found that, on day 7 after surgery, miR-126-3p levels in serum were lower in patients with peripheral artery disease (PAD), who suffered from endothelial dysfunction due to atherosclerosis, than in patients without PAD, while the opposite finding was observed for vascular endothelial growth factor A (VEGF-A) levels. VEGF-A is a known positive regulator of VSMC migration and proliferation, thus promoting graft stenosis (Podemska-Jedrzejczak et al., 2018). MiR-126-3p, on the other hand, regulates intracellular VEGF-A signalling by downregulating PIK3R2 and sprouty-related, EVH1 domain-containing protein 1 (SPRED1), which suppresses PIK3 and ERK1/2 pathways and ultimately affects VEGF-A-mediated cellular responses (Yuan et al., 2019). Therefore, it was proposed that this inverse relationship between miR-126-3p levels and VEGF-A levels observed in PAD patients may be associated with potential complications following CABG, such as graft stenosis, however, this relationship needs to be further investigated (Mukaihara et al., 2021). Another recent human study demonstrated the potential of miR-423 as both a novel biomarker and a therapeutic target for vein graft failure, where this cardioprotective miR-423 was found to be downregulated in the plasma of patients with CAD compared with healthy individuals (Ren et al., 2020). Aberrant expression of other miRNAs, including miR-133, miR-199, miR-208, miR-499, in patients undergoing CABG surgery and their potential as biomarkers for CABG surgery-related complications, such as perioperative myocardial infarction, cardiac and inflammatory injury, re-vascularization, heart failure symptoms and stroke, have also been reported (Błażejowska et al., 2021).

To date, only a few studies have assessed the utility of miRNAs as potential ISR biomarkers. One of the pioneer case-control studies, investigating the ability of miRNAs to serve as novel biomarkers for ISR, identified a set of four miRNAs - miR-21, miR-100, miR-143 and miR-145 - as potential candidate ISR markers, where miR-143 and miR-145 demonstrated the highest sensitivity and specificity as suggested by receiver operating characteristic (ROC) curve analysis (He et al., 2014). Interestingly, these findings were consistent with a previously proposed relationship between these four miRNAs and the development of vascular diseases such as neointimal lesion formation (Ji et al., 2007), and the regulation of relevant cellular processes including cell proliferation, migration, and

differentiation (Cordes et al., 2009; Davis et al., 2008; Grundmann et al., 2011; O'Sullivan et al., 2011). Additionally, the same four miRNAs - miR-21, miR-100, miR-143 and miR-145, were also found to be able to distinguish between diffuse vs. focal ISR (He et al., 2014), however, this finding should be interpreted with caution as it was based on additional analyses performed on a fraction of the total sample, thus, potentially introducing bias such as reduced statistical power related to the smaller sample size and/or loss of randomization (i.e. unbalanced cases and controls groups). In their recent study, O'Sullivan et al. 2019 measured plasma miRNA levels in a cohort of CAD patients, with and without ISR, reporting promising results regarding miR-93-5p as a robust independent ISR predictor (O'Sullivan et al., 2019). In this study, it was found that the addition of miR-93-5p levels to a common predictive model considering the main risk factors for ISR e.g., diabetes, stent length and diameter, in combination with the Framingham Heart Study risk factors such as age, sex, active smoking, diabetes, hypertension, and hyperlipidaemia, significantly improved the performance of that model (O'Sullivan et al., 2019). Despite these results being promising, the lack of validation in an independent cohort represents an important weakness of this study to be considered. Recently, it was reported that four miRNAs, miR-19a, miR-126, miR-210, and miR-378, independently associated with decreased restenosis risk in CAD patients who underwent PCI with DES (Dai et al., 2019). ROC curve analysis suggested that these miRNAs as a group had a considerably improved predictive value for restenosis occurrence following PCI in a Chinese population than each miRNA on its own (Dai et al., 2019). Additionally, another recent case-control study proposed that high miRNA-223 serum levels were strongly and positively associated with ISR risk, highlighting the ability of this miRNA to distinguish between ISR and non-ISR patients even after adjusting for common risk factors including age, sex, HDL-C, LDL-C, fasting blood sugar, and statin consumption (Ganjali et al., 2022).

Although, many candidate biomarkers have been investigated and showed considerable potential as biomarkers for various cardiovascular disease pathologies, there are still a number of challenges associated with their use clinically (Gonzalo-Calvo et al., 2022). For instance, despite growing research interest in the area, there is still limited understanding of the roles of miRNAs in different disease settings. Additionally, the lack of standardised methodology,

when it comes to normalising measured values of miRNAs across samples and accounting for natural variation observed in the healthy population, significantly hinders the development of miRNA-based biomarker assays for routine clinical use.

1.7 Extracellular vesicles

Extracellular vesicles (EVs) are membrane cargo carriers secreted by cells under both physiological and pathophysiological conditions (Davidson et al., 2023; Yuana et al., 2013) EVs have the ability to exchange various functional components between cells, including nucleic acids (e.g., RNAs and DNA), lipids and proteins, demonstrating their role as signalling vehicles actively participating in cell-to-cell communication. The generic term ‘extracellular vesicles’ has been introduced relatively recently and is commonly used to refer to all subcategories of membrane vesicles which could be highly heterogeneous varying in size, composition and subcellular origin (Colombo et al., 2014; Teng and Fussenegger, 2021; Willms et al., 2016). Based on the current knowledge of EV biogenesis, they can be broadly categorised into two distinct classes: exosomes and microvesicles (Figure 1-7). Exosomes are generally smaller in size (~40-150nm) compared to microvesicles (~100-1000nm) and there is a considerable overlap in size ranges between the two classes (Davidson et al., 2023)(Figure 1-7A). Although the generation of exosomes and microvesicles within the cell follows distinct pathways, common intracellular mechanisms and components are involved in the biogenesis of both EV types which further complicates the possibility of differentiating between them (Colombo et al., 2014). Therefore, due to their overlapping characteristics in terms of size, morphology, and composition, the development of a more precise nomenclature for EVs has been exceedingly challenging (Gould and Raposo, 2013; Kowal et al., 2016).

In general, exosomes are intraluminal vesicles (ILVs) formed by the inward budding of endosomal membrane, resulting in the formation of multivesicular endosomes (MVEs), with exosomes secreted upon fusion of the outer MVE membrane with the cell surface (Harding et al., 1984; Pan et al., 1985)(Figure 1-7A). On the other hand, microvesicles are released by “donor” cells through the outward budding of the plasma membrane, termed shedding or membrane

budding (Li et al., 2012; Muralidharan-Chari et al., 2009) (Figure 1-7A). It is now known that virtually all cells secrete EVs, and individual cells modify the biogenesis of EVs depending on their physiological state, resulting in the release of EVs, including both exosomes and microvesicles, with a specific composition and cargo signature (Colombo et al., 2014; Doyle and Wang, 2019). Therefore, EVs can be isolated from various different biological fluids, such as conditioned culture medium (CCM), blood, plasma, serum, broncho-alveolar lavage fluid, cerebrospinal fluid, saliva, urine, breast milk and tissues (Admyre et al., 2007; Carnino et al., 2019; Hurwitz et al., 2019; Langevin et al., 2020; Lobb et al., 2015; Martins et al., 2018). However, due to limitations associated with commonly used protocols for EV purification, the isolated EV populations represent mixtures of particles of mostly unknown origin (Willms et al., 2016), thus, limiting the ability to study the role of specific EV types in a comprehensive manner and make direct functional comparisons between EV subtypes (Willms et al., 2018).

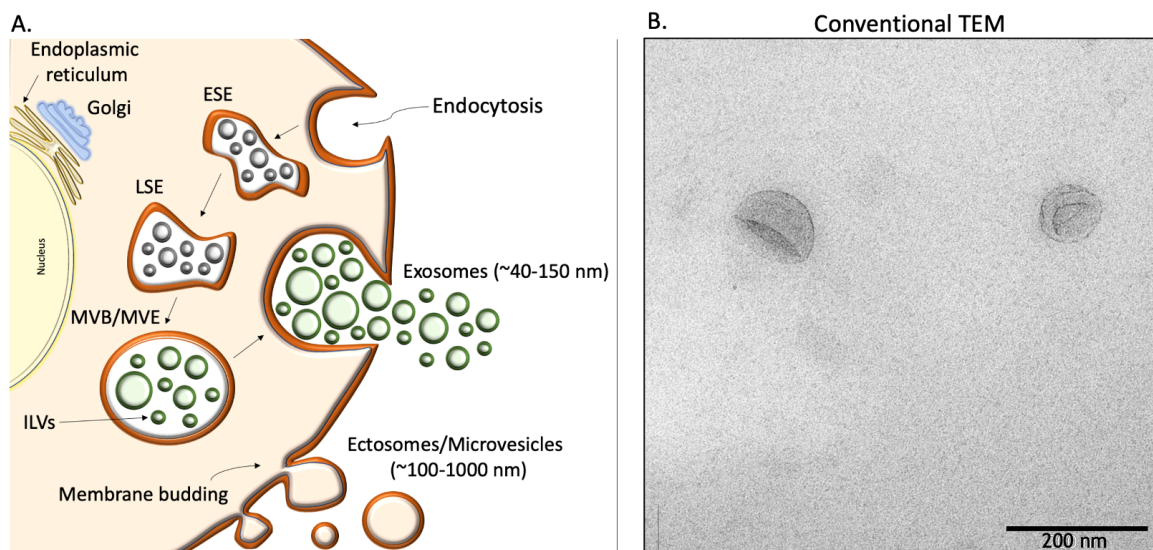


Figure 1-7 General features of extracellular vesicles. (A) Schematic representation of EV size ranges and biogenesis. When EVs are formed through budding of the plasma membrane, they are referred to as microvesicles (~100-1000 nm). In the case when EVs are formed as ILEs within MVEs, which fuse with the plasma membrane to release ILEs in the extracellular space, then they are referred to as exosomes (~40-150 nm). Taken and modified from (Pashova et al., 2020). (B) Visualisation of EVs. EV processing for observation by conventional TEM, causes their shrinkage, leading to an artefactual cup-shaped morphology. Abbreviations: extracellular vesicles, EVs, early-sorting endosome, ESE; late-sorting endosome, LSE; multivesicular body, MVB; multivesicular endosome, MVE; intraluminal vesicles, ILEs; intraluminal vesicles; MVEs, multivesicular endosomes; transmission electron microscopy, TEM;

1.7.1 Biogenesis and release of exosomes

In the process of exosome biogenesis, multiple endosomal structures are formed including early-sorting endosome (ESE) followed by late-sorting endosome (LSE) and finally MVEs containing several ILVs which are ultimately secreted to the extracellular space as exosomes (Colombo et al., 2014; Kalluri and LeBleu, 2020; Mathieu et al., 2019). Additionally, MVEs may also fuse with lysosomal compartments in which case the exosomal cargo becomes destined for degradation (Buschow et al., 2009). Exosomal membrane cargoes reach endosomes via two distinct routes - either through the Golgi apparatus or are directly internalized from the plasma membrane, before being sorted to ILVs during endosome maturation (Klumperman and Raposo, 2014). Sorting of EV cargo on microdomains of the limiting membrane of MVEs, prior to internal budding of the small membrane vesicles (known as ILVs) (Figure 1-8), is an important step in exosome biogenesis.

The components of the endosomal-sorting complex required for transport (ESCRT) system have been shown to be involved in the biogenesis of ILVs. The ESCRT machinery acts in a phased manner wherein all four complexes (ESCRT-0, -I, -II and -III) play a significant role in facilitating MVE formation, vesicle budding, and protein cargo sorting (Figure 1-8) (Adell et al., 2014; Gurunathan et al., 2021; Mathieu et al., 2019; Morvan et al., 2012). Additionally, all four members of the ESCRT machinery are also involved in the clustering of ubiquitylated transmembrane proteins on microdomains, found on the limiting membrane of MVEs, and then budding and fission of these microdomains, delivering the ubiquitinated proteins to the degradation machinery (Gurunathan et al., 2021). The significance of the ESCRT machinery in exosome biogenesis has been demonstrated by the observed altered exosomal protein content and rate of exosome secretion by cancer cells following depletion of specific ESCRT-family members (Colombo et al., 2013). The involvement of other proteins, such as alpha-1,3/1,6-mannosyltransferase interacting protein X (ALIX) and the tumour susceptibility gene 101 (TSG101), in exosome biogenesis has also been reported (Gurunathan et al., 2021; Kowal et al., 2014). For instance, ALIX was found to participate in a parallel, also known as non-canonical, pathway of recruiting ESCRTs for ILV formation and cargo sorting (Baietti et al., 2012), and indeed, inhibition of ALIX resulted in an impaired ability of dendritic or muscle

cells to secrete CD63-enriched exosomes (Colombo et al., 2013; Romancino et al., 2013).

ESCRT-independent processes can also functionally contribute to the biogenesis of exosomes and such mechanisms became evident when studies demonstrated that MVEs, containing ILVs enriched in CD63, were still formed in ESCRT-depleted cells (Stuffers et al., 2009). The generation of ceramide by neutral type II sphingomyelinase-mediated hydrolyses of sphingomyelin was proposed to be involved in an ESCRT-independent mechanism of ILV formation (Trajkovic et al., 2008) where ceramide facilitated the induction of a spontaneous membrane invagination through the generation of membrane subdomains (Goñi and Alonso, 2009). Notably, blocking the activity of neutral sphingomyelinase resulted in the partial inhibition of exosome formation (Trajkovic et al., 2008). Another study found that ceramide could also be metabolized to sphingosine 1-phosphate (S1P) by sphingosine kinase 2 via sphingosine which subsequently activated Gi-coupled S1P receptor on the MVE, an essential mediator of cargo sorting into exosomal ILVs (Figure 1-8) (Kajimoto et al., 2013). Furthermore, members of the tetraspanin family have also been shown to regulate ESCRT-independent endosomal sorting. Some of these proteins, including CD63, CD81, CD82 and CD9, have been implicated in the sorting of various cargoes to exosomes (Buschow et al., 2009; Chairoungdua et al., 2010; van Niel et al., 2011).

The final step of exosome secretion into the extracellular space is the fusion of MVBs with the plasma membrane. Several proteins have been identified as regulators of this process including RAB GTPases, such as RAB11, RAB35 (Abrami et al., 2013), RAB2B, RAB5A, RAB9A, RAB27A and RAB27B (Ostrowski et al., 2010), which act as molecular switches, and soluble NSF attachment protein receptor (SNARE) proteins (Gurunathan et al., 2021). The role of SNARE proteins in membrane fusion, including exocytosis, has been extensively studied and multiple members of the family, including syntaxin 1A (SYX1A), synaptobrevin homolog YKT6 (YKT6) and vesicle associated membrane protein 7 (VAMP7), have been implicated in the regulation of this process (Hessvik and Llorente, 2018). Overall, the mechanism of exosome biogenesis and release may determine the type of exosomal cargo.

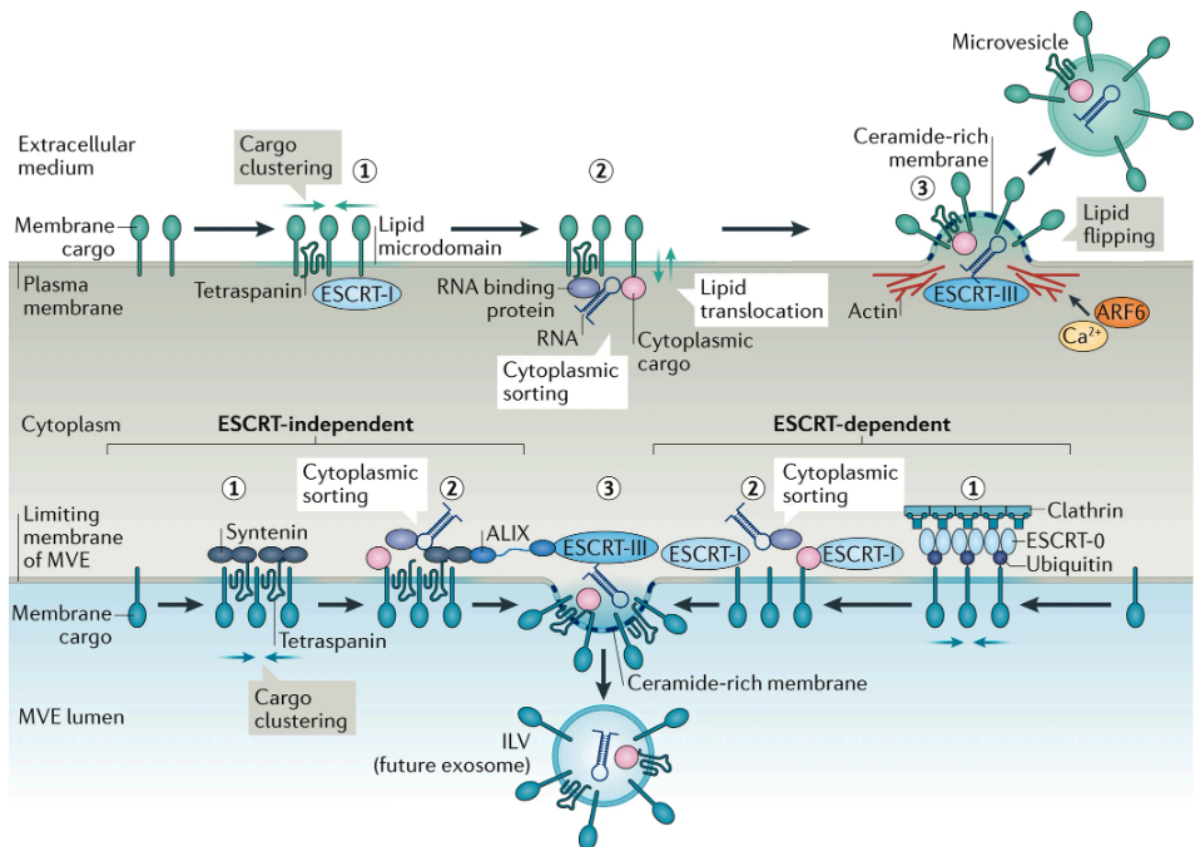


Figure 1-8 Biogenesis of extracellular vesicles. EV biogenesis involves several steps during which different sorting machineries are employed. Initially, lipids and membrane-associated proteins are clustered forming membrane microdomains on the plasma membrane for microvesicles (top) and on the limiting membrane of the MVE for exosomes (bottom) (step 1). These microdomains also contribute to the requirement and sorting of soluble cargo, such as cytosolic protein and RNA molecules, into EVs (Step 2). Finally, the formation of such clustered microdomains, in addition to other machineries, facilitates membrane budding followed by a fission process either at the plasma membrane towards the extracellular medium (for microvesicles) or at the limiting membrane of the MVE towards the lumen of the MVE (for exosomes) (step 3). Generally, mechanisms of exosome biogenesis involve components of the ESCRT system, although to different degrees. For example, ESCRT-III is known to be required for the scission of the ILVs into the MVE lumen, however, both the clustering of cargo and membrane budding can occur through ESCRT-dependent or ESCRT-independent mechanisms. With the exception of the well-described mechanism of microvesicle biogenesis involving the flipping of specific lipid species between the leaflets of the budding membrane, the molecular machineries participating in the different stages of EV biogenesis are partially common between exosomes and microvesicles (including some ESCRT components and the generation of ceramide by sphingomyelinase). Therefore, the identification of the origin of EVs remains a complicated matter and cannot be addressed simply by impairing the function of a given mechanism involved in the biogenesis of both EV types. Abbreviations: MVE, multivesicular endosome; ESCRT, endosomal sorting complex required for transport; ILVs, intraluminal vesicles; ALIX, ALG-2 interacting protein X; ARF6, ADP-ribosylation factor 6. The figure was reproduced with permission from Springer Nature under Licence No: 5440220815991 (van Niel et al., 2018).

1.7.2 Biogenesis and release of microvesicles

The molecular mechanisms of the biogenesis of microvesicles are less well understood compared to exosomes, though a number of cellular events have been implicated in the process, including alterations in lipid and protein composition of the plasma membrane at the site of microvesicle origin, and changes in Ca^{2+} levels (Minciacchi et al., 2015). The latter leads to the recruitment of Ca^{2+} -dependent enzymes, such as scramblase and floppase, which subsequently drive the modification of the plasma membrane in terms of lipid composition where phosphatidylserine (PS) is exposed from the inner leaflet to the outer cell surface (Piccin et al., 2007). Externalization of PS causes physical bending of the plasma membrane and cytoskeleton disruption, thus facilitating the budding of microvesicles (Figure 1-8) (Piccin et al., 2007). In addition to lipids, proteins regulating the cytoskeleton have also been implicated in microvesicle biogenesis. In their study, Li et al. 2012 identified Rho A GTPase along with its downstream targets involved in the regulation of actin dynamics - Rho-associated protein kinase (ROCK) and LIM kinase (LIMK), as important mediators of microvesicle biogenesis in different populations of tumour cells (Li et al., 2012). ADP-ribosylation factor 6 (ARF6), an important regulator of cytoskeleton proteins, has also been reported as a component of the microvesicle biogenesis machinery (Muralidharan-Chari et al., 2009). In their study, Muralidharan-Chari et al. 2009, identified an ARF6-regulated mechanism of microvesicle shedding in tumour cells involving its downstream targets - ERK and myosin light-chain kinase (MLCK), where inhibition of either ARF6 activity or the activity of its targets led to a reduction in microvesicle release (Muralidharan-Chari et al., 2009). Analysis of the microvesicles generated through this mechanism demonstrated an enrichment with specific cargo proteins including major histocompatibility complex - I (MHC-I) and B1-integrin receptors (Muralidharan-Chari et al., 2009).

The release of microvesicles requires their fission from the plasma membrane. In addition to the widely accepted Ca^{2+} -dependent mechanism of microvesicle release (discussed above), other mechanisms, resulting in rearrangement of the plasma membrane, have been identified. In glial cells, an activation of the P2X purinoceptor 7 (P2RX7) is associated with rapid activation of acid sphingomyelinase, translocation of acidic sphingomyelinase to the plasma

membrane, where it generates ceramide, thereby promoting membrane bending and microvesicle release (Bianco et al., 2009). Interestingly, TSG101 and the ATPase vacuolar protein sorting-associated protein (VPS) 4, primarily involved in ESCRT-dependent exosome generation, were reported to engage in the scission and release of a specific type of microvesicles (Nabhan et al., 2012).

Mechanistically, it was shown that an interaction of TSG101 with arrestin domain-containing protein 1 (ARRDC1) through tetrapeptide PSAP leads to relocation of TSG101 from endosomes to the plasma membrane and consequently a VPS4 ATPase-mediated 'pinch-off' of the plasma membrane. As a result microvesicles enriched in TSG101, ARRDC1, and other cellular proteins were released through this mechanism (Nabhan et al., 2012).

1.7.3 Uptake of extracellular vesicles

EV-mediated intercellular communication involves several complex steps, which are not yet very well understood, including, EV docking at the plasma membrane of target/recipient cells, followed by the activation of surface receptors and signalling, vesicle internalization through endocytosis or EV fusion with target cells. The specific targeting of EVs to their recipient cells is, at least in part, determined by the occurrence of specific interactions between proteins present on the surface of EVs and receptors at the plasma membrane of the recipient cells (Chivet et al., 2014; Mallegol et al., 2007; Nolte-'t Hoen et al., 2009). It is important to note that it is also possible the EV producing cell itself could be an acceptor cell participating in EV-mediated autocrine signalling (Matsumoto et al., 2017). Several EV surface molecules, regulating these interactions, have been identified including tetraspanins, integrins, lipids, lectins, heparan sulphate proteoglycans and ECM components (van Niel et al., 2018). For instance, the interaction of EV-associated integrins with cell surface adhesion molecules, such as ICAMs, and extracellular matrix proteins (primarily fibronectin and laminin) present on the surface of recipient cells, have been identified as important mechanisms of EV binding to target cells (Hoshino et al., 2015; Leiss et al., 2008; Purushothaman et al., 2016; Sung et al., 2015). Interestingly, one study reported that heparan sulphate played a dual role in exosome-cell interaction where heparan present on exosomes was found to capture fibronectin, and when present on recipient cells, it acted as a receptor for fibronectin facilitating exosome-mediated signalling (Purushothaman et al.,

2016). Inhibition of heparan sulphate or fibronectin resulted in either markedly reduced exosome-target cell interaction or inhibited fibronectin-mediated exosome signalling in myeloma cells, respectively (Purushothaman et al., 2016). Additionally, a clinical study, revealed that distinct integrin expression patterns on exosomes derived from cancer patients were associated with metastasis within specific organs, including lung and liver, demonstrating that exosomal integrins are important for cell targeting and could be used to predict organ-specific metastasis (Hoshino et al., 2015). Exosomal tetraspanins could also regulate cell targeting where exosome docking and uptake by target cells has been shown to be stimulated by an interaction between tetraspanins, including tetraspanin 8 and CD9, and integrins (Nazarenko et al., 2010; Rana et al., 2012, 2011).

Following their binding to target cells, EVs may be internalized via different mechanisms, including clathrin-mediated or clathrin-independent endocytosis, such as macropinocytosis and phagocytosis (Feng et al., 2010; Nakase et al., 2015; T. Tian et al., 2014a), or through endocytosis involving caveolae and lipids (Kamerkar et al., 2017; Laulagnier et al., 2018; Vargas et al., 2014). One example demonstrating the involvement of lipids, present on recipient cells, in EV internalisation is the disruption of lipid rafts by cholesterol depletion leading to reduced uptake of EVs by target cells (Escrevente et al., 2011). Following EV internalisation mediated by different mechanisms, they enter the endocytic pathway which in most cases leads to lysosomal degradation (Chen et al., 2016; Tian et al., 2010), however, it is also possible for internalised EVs to escape digestion through a mechanism involving back fusion of vesicles with the limiting membrane of the MVE, thereby releasing their contents into the cytoplasm of the recipient cell (Bissig and Gruenberg, 2014).

EVs could also exert their effect by binding to and activating receptors expressed on the surface of recipient cells, thereby inducing EV-mediated signalling cellular responses (Antonyak et al., 2011; Raposo et al., 1996; Zitvogel et al., 1998). One of the early examples demonstrating the ability of EVs to interact with cell surface receptors was a study in dendritic cells (Zitvogel et al., 1998). It was found that tumour-derived EVs expressing MHCs were capable of priming T-cell lymphocytes *in vivo*, resulting in a T-cell-dependent inhibition

of tumour growth in mice (Zitvogel et al., 1998). EV-mediated signalling in recipient cells could also be induced post-EV internalisation, via endocytosis or direct membrane fusion, which leads to the release of their intraluminal cargo in the cytoplasm of acceptor cells. This is an essential mechanism for EV-mediated signalling involving miRNAs and mRNAs, where cargo delivery to the cytoplasm of recipient cells is required to elicit functional responses i.e., modulating gene expression (Skog et al., 2008a; Valadi et al., 2007).

1.7.4 Extracellular vesicles and their RNA cargo

EVs carry a wide range of biological molecules, such as nucleic acids (RNA and DNA), proteins, lipids and metabolites, which may have both metabolic significance and signalling potential (Y. Chen et al., 2021; Mir and Goettsch, 2020; Pathan et al., 2019). There has been substantial research effort toward understanding RNA content within EVs. As a result, several RNA biotypes have been successfully identified in EVs, including mRNA, miRNA, small nucleolar RNA (snoRNA), small nuclear RNA (snRNA), long non-coding RNA (lncRNA), vault RNA (vRNA), Y-RNA, transfer RNA (tRNA) and ribosomal RNA (rRNA), or fragments thereof (Dellar et al., 2022). There are a number of important reasons why EVs containing RNA cargo are believed to have great clinical potential not only as prognostic and diagnostic disease biomarkers but also as therapeutic delivery vehicles. For instance, as membrane vehicles, EVs have been found to protect RNAs from degradation in the extracellular environment (Pua et al., 2019; Shurtleff et al., 2017). Additionally, based on their physical properties, EVs could be separated from other components of different biofluids, and EV preparations could then be concentrated to optimal levels for downstream analysis (Gyuris et al., 2019; F. Liu et al., 2017). Finally, it has been reported that RNAs contained within EVs encode biological state-specific information (Konstantinidou et al., 2016; Murillo et al., 2019; Pua et al., 2019), which, in combination with the idea that EVs participate in intercellular communication by transferring bioactive molecules between cells in a targeted manner without eliciting an immune response (Mathieu et al., 2019; Stahl and Raposo, 2019), demonstrates their great potential in delivering therapeutic RNAs. However, it is still important to consider that the delivery of any given EV-associated RNA molecule is accompanied by the delivery of multiple other, potentially

bioactive, components which may introduce some significant challenges when studying the effects of specific EV RNA cargoes.

Huang et al. 2013 performed a systematic characterisation of the RNA expression profile of human plasma EVs using a RNA sequencing approach (Huang et al., 2013). It was found that miRNAs were the most abundant RNA molecules in EVs accounting for 76.2% of all mappable reads (Huang et al., 2013). Another more recent study, also using RNA sequencing to assess the small RNA expression profile of human serum EVs, reported that 52.1% of small RNAs within circulating EVs were miRNAs (Zhao et al., 2020). This inconsistency between studies may be due to variation between the studied EV populations possibly introduced by the origin of the EV sample (i.e., plasma vs serum EVs). Nevertheless, many recent studies suggested that EV-miRNAs play significant roles in the regulation of various diseases, including cancer and CVD (Chong et al., 2019; Kesidou et al., 2020; Vu et al., 2020), and others successfully demonstrated the clinical potential of EV-associated miRNAs as disease biomarkers (Cheng et al., 2018; X. He et al., 2021; Paterson et al., 2022).

1.7.5 Extracellular vesicle signalling in response to vascular injury

Pathological neointimal formation post vascular injury (i.e., following PCI or CABG) develops progressively over time as a result of complex interaction between several molecular and cellular processes driven by different cell types including vascular ECs, VSMCs, platelets and various inflammatory cells (discussed in Section 1.4). Therefore, understanding the different means of communication between cells is fundamental to successfully develop therapeutic strategies for maintaining vascular health. The key function of EVs in cell-to-cell communication as well as their therapeutic potential in neointimal formation post vascular injury has been studied to some extent, however, the exact role of EVs, and more specifically of VSMC-derived EVs, remains to be fully elucidated.

ECs are critical regulators of vascular homeostasis and consequently vascular health. In addition to being a permeability barrier between the blood and vessel wall, ECs are also important mediators of vascular function, including regulation of VSMC contractility, cell migration, proliferation and apoptosis, and ultimately

vascular remodelling processes (Chien, 2007). As such, disruption of EC homeostasis could lead to endothelial dysfunction, characterised by an inappropriate EC activation and a shift towards a pro-inflammatory state, a hallmark of CVD (Sun et al., 2020). Therefore, EC monolayer repair and restoration of cellular homeostasis post vascular injury represents a crucial step in limiting development of vascular pathologies, including neointimal growth (Evans et al., 2021; Ren et al., 2020; Vanhoutte, 2010), and EC-derived EVs have been shown to be involved in the regulation of various vascular remodelling processes, e.g., cell proliferation and migration (Jansen et al., 2017, 2013). Several miRNAs, including miR-126, miR-146b, miR-625, miR-197 and miR-615, have been found to be highly enriched in ECs (Fish et al., 2008), with miR-126 shown to be involved in the regulation of EC migration, proliferation, cytoskeleton reorganisation, capillary network stability and cell survival (Fish et al., 2008; Qu et al., 2017). In addition to its abundance in ECs, miR-126-3p has also been shown to be highly enriched in EC-derived EVs (Jansen et al., 2017, 2013) which could potentially explain some of the protective effects associated with EC-derived EVs in both ECs and VSMCs. In the context of vascular remodelling, EC-derived EV mediated transfer of miR-126-3p to recipient ECs and VSMCs has been shown to increase EC regeneration and inhibit VSMC migration, proliferation and consequently neointimal formation after vascular injury (Figure 1-9) (Jansen et al., 2017, 2013). The proposed underlying mechanisms involve direct targeting of SPRED1 (Figure 1-9) (Jansen et al., 2013) and by miR-126-3p in ECs and low-density lipoprotein receptor-related protein 6 (LRP6) in VSMCs (Figure 1-9) (Jansen et al., 2017). Interestingly, EC-derived EVs have also been shown to promote VSMC dysfunction in the context of diabetes (Togliatto et al., 2018). EC-derived EVs from individuals with T2D were found to be enriched in membrane bound PDGF resulting in increased VSMC migration and improved apoptotic resistance through a mechanism possibly involving miR-296-5p overexpression and direct targeting of BRI1-associated kinase 1 (BAK1) following EV-mediated PDGF cargo delivery from ECs to VSMCs (Togliatto et al., 2018).

Interestingly, it has been reported that the EVs secreted by quiescent, contractile VSMCs are profoundly different compared to EVs secreted by synthetic, activated VSMCs as suggested by the differentially expressed cargo

proteins between the two EV populations (Comelli et al., 2014). Similarly, the miRNA expression profile of EVs derived from activated VSMCs under PDGF stimulation has been shown to be significantly different compared to VSMCs EVs secreted under normal conditions with 95 highly dysregulated mRNAs (Heo et al., 2020). In the same study, the reduced expression of miR-1246, miR-182, and miR-486 in PDGF VSMC EVs was associated with an increase in EC migration, however, the exact molecular mechanism responsible for this effect remains unclear (Figure 1-9) (Heo et al., 2020).

EVs derived from other cells have also been implicated in vascular remodelling. In peripheral blood, for example, platelet-derived EVs represent the most abundant EV population accounting for around 70-90 % of all circulating EVs (Berckmans et al., 2001; Italiano et al., 2010; Joop et al., 2001), and platelet-derived EVs have been associated with 50-100 times higher coagulation activity in comparison to activated platelets (Sinauridze et al., 2007). In addition to their role in the early stages of vein graft failure where platelets are known to contribute to acute thrombosis (Gaudino et al., 2017), it has also been shown that platelets may contribute to the development of neointima formation after vascular injury (Wang et al., 2005).

Platelet-derived EVs have been found to interact with and modulate the cellular function of both vascular ECs and VSMCs (Nomura et al., 2001; Vajen et al., 2017). The proapoptotic effects of platelet-derived EVs have also been previously demonstrated in vascular ECs where EV-mediated transfer of different miRNAs, including miR-223 and miR-142-3p, to recipient ECs promoted cell apoptosis possibly through the negative regulation of IGF-1 receptor (*IGF-1R*) and BCL2 like 1 (*BCL2L1*), miRNA target genes of miR-223 and miR-142-3p respectively (Figure 1-9) (Bao et al., 2017; Pan et al., 2014). In contrast, when miR-142-3p mimic and inhibitor were both assessed *in vitro*, the authors reported that EC apoptosis appeared to be suppressed (Bao et al., 2017). Further emphasizing the contrasting effects of platelet-derived EVs, platelet-derived EV-mediated transfer of miR-142-3p to ECs led to increased EC proliferation *in vitro* possibly as a result of direct targeting of *BCLAF1* (BCL2-associated transcription factor 1) gene (Figure 1-9) (Bao et al., 2018). This inconsistency between findings may potentially be explained by the fact that a single miRNA is capable

of regulating multiple genes and miR-142-3p has been found to have many apoptosis-related targets including *BCL2L1*, *BCLAF1* and *PRKCA* (Protein Kinase C Alpha) (Bao et al., 2018, 2017). It is also possible that the functional effects of a given miRNA may be cell status dependent. Furthermore, in these studies, platelet-derived EVs were isolated via centrifugation at a relatively low speed of 20,500 g (Bao et al., 2018, 2017) which may have resulted in the isolation of a highly heterogeneous population of EVs (Kowal et al., 2016) potentially containing a wide-range of bioactive molecules with various functions. Further highlighting the potential involvement of platelet-derived EVs in the development of vascular pathologies such as neointima formation, it has been shown that platelet-derived EVs may also directly interact with proliferating VSMCs causing them to switch towards a differentiated quiescent state, inhibiting VSMC proliferation, migration and intimal hyperplasia *in vivo* (Zeng et al., 2019).

Intercellular communication between VSMCs and other cells within the vascular wall including adventitial fibroblasts (aFs), mesenchymal stem cells (MSCs), and macrophages has also been reported (Tong et al., 2018; D. Wang et al., 2019; Z. Wang et al., 2019). EV-mediated cross talk between VSMCs and aFs in vascular remodelling in the context of hypertension was demonstrated where aFs derived from spontaneously hypertensive rats (SHR) were shown to influence VSMC behaviour through EV-mediated transfer of miR-155-5p and angiotensin converting enzyme (ACE) (Figure 1-9) (Ren et al., 2019). Both increased ACE and reduced miR-155-5p in EVs from SHR aFs promoted VSMC proliferation (Ren et al., 2019). Interestingly, an opposite effect of MSC-derived EVs on VSMC proliferation was reported in the context of neointimal formation (D. Wang et al., 2019). MSC-derived EV mediated transfer of miR-125b to recipient VSMC was shown to inhibit VSMC proliferation and migration possibly through inhibition of Myosin 1E (*MYO1E*) expression levels (Figure 1-9) (D. Wang et al., 2019). Another recent study, investigating the communication between macrophages and VSMCs revealed that M1 macrophage-derived EVs could stimulate VSMC proliferation and migration through EV-mediated delivery of miR-222 from M1 macrophages to VSMCs resulting in reduced CDKN1B and CDKN1C protein expression ultimately promoting cell proliferation and migration *in vitro* and neointimal formation *in vivo* (Figure 1-9) (Z. Wang et al., 2019).

The above-mentioned studies clearly demonstrate the importance of EV-mediated intercellular communication in the regulation of vascular pathologies (Figure 1-9). Although most of these studies entailed VSMC communication with other cells within the vessel wall (i.e., ECs and blood cells), in-depth research into autocrine regulation of VSMCs via EV miRNAs is also necessary to better understand the possible underlying mechanisms involved in the regulation of vascular remodelling processes and to fully elucidate the therapeutic potential of EVs in different vascular pathologies, including neointimal formation.

1.7.6 Improving the therapeutic potential of extracellular vesicles— bioengineering approaches

The ability to selectively load therapeutic cargo into EVs and to control their *in vivo* targeting specificity are important factors for the effectiveness of EV-based therapeutic strategies. Based on knowledge of EV biogenesis, secretion, and uptake processes, through various genetic and non-genetic methodologies, bioengineering of EVs with novel functions and properties has proven successful. Currently, commonly used EV engineering methods include cargo loading and target delivery both *in vitro* and *in vivo* (Riazifar et al., 2017; Vader et al., 2016; Wiklander et al., 2019).

Generally, different EV cargo loading approaches could be categorised as endogenous and exogenous. Endogenous EV loading is based on the loading of therapeutics into cells from which the EVs are derived. This approach relies on the endogenous EV loading machinery of the cells which may result in subsequent EV loading with the cargo of interest (Kosaka et al., 2012, 2010; Pan et al., 2012). On the other hand, exogenous EV loading involves loading of therapeutic cargos into EVs after their isolation. For example, one study, using a cell transfection-based approach showed, that transfection of human embryonic kidney cells (HEK293) and COS-7 cells (CV-1 cell line exhibiting fibroblast morphology) with miR-16, -21, -143, -146a, or -155 expressing vectors resulted in successful overexpression of these miRNAs in the cells as well as in the EVs released by those cells (Kosaka et al., 2010). It was also found that the same miRNA-loaded EVs were able to induce gene silencing in recipient COS-7 cells (Kosaka et al., 2010). Alternatively, EV-releasing cells could also be transfected directly with small RNAs (Akao et al., 2011; Zhang et al., 2010). However, the main disadvantage associated with these approaches is that EV RNA incorporation efficiency may depend on the RNA species and/or sequence (Abels and Breakefield, 2016; Batagov et al., 2011; Koppers-Lalic et al., 2014). Other cargo molecules, such as mRNAs and proteins, have also been successfully loaded into EVs using an endogenous approach (Vader et al., 2016).

Exogenous loading of EVs with small RNAs through electroporation, the most commonly used method for exogenous loading of EVs, has also been successfully demonstrated (Alvarez-Erviti et al., 2011; Wahlgren et al., 2012). A very recent

study investigated five different methodologies to load miRNAs into EVs exogenously-- transfection by Exo-Fect or cholesterol-modified miRNA and membrane permeabilization by a detergent (saponin), electroporation or heat shock (de Abreu et al., 2021). It was reported that, transfection of EVs using Exo-Fect was the most efficient method with > 50% transfection efficiency compared with the other methods (de Abreu et al., 2021). Further analysis revealed that this high transfection efficiency was maintained for small EVs isolated from multiple sources including CCM, urine, and foetal bovine serum (FBS). In this study, the main limitation identified associated with the membrane permeabilization methods (electroporation, heat shock and saponin detergent) was miRNA precipitation/aggregation, potentially affecting the transfection efficiency of EVs (de Abreu et al., 2021). Further analysis confirmed that Exo-Fect transfected miR-155 into small EVs was functionally active, demonstrated by the observed inhibition of mCherry expression in the HEK293T reporter line, though, a critical selection of the optimal Exo-Fect concentration for EV loading to avoid cytotoxicity was shown to be extremely important. Nevertheless, since the functional effects of miR-155 loaded EVs through the other EV-modulation methods were not studied, it is possible that methods with lower transfection efficiency than Exo-Fect, such as electroporation, may still prove to be valuable in a given cellular model and/or therapeutic application (de Abreu et al., 2021).

Several studies proposed that systemic administration of exogenous EVs leads to rapid uptake by the mononuclear phagocyte system, therefore, resulting in accumulation in the spleen and liver (Vader et al., 2016). However, in an attempt to address this potential problem associated with EV-based therapeutics, many studies have demonstrated that it is possible to engineer EVs in such a way, that improved targeting to other tissues/specific cell types is achieved. Transfection of EV-donor cells, thus, forcing the expression of targeting moieties fused with EV membrane proteins represents one of the best studied approaches to improve EV targeting properties (Alvarez-Erviti et al., 2011; Wiklander et al., 2015). To achieve improved targeting of EVs to the brain in mice, Alvarez-Erviti et al. 2011, engineered self-derived dendritic cells to express lysosome-associated membrane glycoprotein 2b (LAMP2B), an exosomal membrane protein, fused to brain-specific rabies viral glycoprotein (RVG) peptide-- a neuron specific peptide that binds the acetylcholine receptor

(Alvarez-Erviti et al., 2011). It was found that systemic injection of siRNA loaded EVs successfully targeted the brain in mice as demonstrated by the significant depletion of a specific gene target - decreased β -site amyloid precursor protein cleaving enzyme 1 (*BACE1*) mRNA (by 60%) and protein (by 62%) expression (Alvarez-Erviti et al., 2011). In an attempt to further improve this specific strategy, it was discovered that glycosylation of targeting peptide- LAMP2B fusion protein may protect the peptide against proteolytic degradation, thereby enhancing its targeting performance and increasing EV targeting specificity (Hung and Leonard, 2015).

Together, these studies highlight the possibilities of engineering of EVs to improve EV properties such as enhanced expression of therapeutic cargo and increased specific tissue targeting, which could potentially contribute to developing EV-based therapeutics

1.8 Hypotheses and aims

In this project, an *in vitro* model of the pathological conditions under which neointimal lesions develop following vascular injury was utilised to study the effect of HSVSMC-derived EVs on cell proliferation and migration. Additionally, an *in vivo* model of arterial vascular injury was utilised in a preliminary study of profiling circulating EVs.

It was hypothesised that: (1) the release of EVs from HSVSMCs is altered under pathophysiological conditions; (2) prolonged pathological PDGF signalling in HSVSMC induces changes in the miRNA cargo component of EVs secreted by stimulated cells; (3) unmodified HSVSMC-derived EVs and HSVSMC EVs loaded with specific miRNAs of interest are part of a signalling pathway involved in the autocrine regulation of HSVSMCs.

The main aims were:

- To determine the effects of PDGF treatment on the release of EVs from HSVSMCs, including physical characteristics and cargo through unbiased RNA sequencing (RNAseq), and then to analyse the effect of EVs on the proliferation of recipient HSVSMCs.
- To exogenously load HSVSMC-EVs with miRNAs of interest, to characterise these modified EV populations and then to determine their functional effects on recipient HSVSMCs and human saphenous vein endothelial cells (HSVECs).
- To characterise the circulating EVs from the carotid artery injury mouse model and to investigate their EV miRNA expression profile.

Chapter 2 Materials and methods

2.1 General laboratory practice

Separate laboratory coats were used for cell culture experiments requiring sterile conditions and general laboratory experiments. Nitrile powder-free gloves, safety specs, laminar flow hoods and fume hoods were used where appropriate. All laboratory equipment and consumables required for cell culture experiments were thoroughly disinfected using 70% ethanol (EtOH) prior to introducing them to the laminar flow hood where cells were handled.

2.2 Sourcing of human saphenous vein samples

Surplus SV segments were obtained from patients undergoing CABG procedure at the Golden Jubilee National Hospital in Glasgow (UK) after ethical approval in collaboration with the NHS Greater Glasgow & Clyde Biorepository (REC reference 16/WS/0207; Bio-repository project reference 107). Ethical permission was obtained from the West of Scotland Research Ethics Committee 4 (reference number: 10/S0704/60) and the investigation conformed to the principles outlined in the Declaration of Helsinki. Written informed consent was obtained from each donor patient prior to surgery. Anthropometric patient characteristics of samples used *in vitro* experiments are presented in Table 2-1. Patient samples were used to isolate primary HSVSMCs and HSVECs.

Table 2-1 Summary of anthropometric donor patient characteristics.

Anthropometric parameters	Mean \pm SEM ¹ (N = 10) ²	Range
Male/Female	7/2 (1 unknown)	
Age (years)	55.5 \pm 4.1	41- 79
¹ SEM (Standard error of the mean) ² There was no information regarding age and sex available in the official records kept by the university for one of the donor patients.		

2.3 Cell culture

All tissue culture was performed under sterile conditions in biological safety cabinet class II MSC-Advantage™, Thermo Scientific™, ThermoFisher Scientific, UK) with vertical laminar flow. Cabinets were disinfected before and after use with Chemgene followed by 70% EtOH. Cells were maintained under normal cell culture conditions-- in humidified carbon dioxide (CO₂) incubator (Forma™ Steri-Cycle™ i160, Thermo Scientific) set to 5% CO₂ at 37° C. Details about all types of media used with each cell type can be found in Table 2-2 and Table 2-3.

2.3.1 Primary HSVSMC isolation and expansion

HSVSMCs were isolated by Mrs Elaine Friel (School of Cardiovascular and Metabolic Health, University of Glasgow), following a well-established protocol.

For the isolation of HSVSMCs, venous samples were first transferred to a glass petri dish containing Sylgard resin and immersed in dissection medium. Then, veins were cut open longitudinally using a pair of sterile scissors. A plunger from a 5 mL syringe was used to carefully remove the EC layer. After that, using sterile forceps, the medial layer was gently separated from the vessel wall, transferred to a petri dish containing SMC dissection medium and then chopped into small 1 mm pieces using a tissue chopper (McIlwain, Norwich, UK). All tissue pieces were then transferred into a 50 mL falcon tube to be washed with SMC dissection medium and left to sink to the bottom of the tube before carefully removing the supernatant containing the floating debris. The homogenised tissue was then covered in high-serum growth medium for HSVSMCs (Table 2-2) and transferred to an appropriate number of T-25 cm² (cat.no.: CLS430639, Corning, Sigma-Aldrich) vented cell culture flasks using as little medium as possible. After transferring, the tissue homogenate was smeared onto the bottom of the flask and excess media was removed. The flasks were then left in an incubator at 37° C and 5% CO₂ overnight before adding 5 mL of high-serum HSVSMCs growth media (Table 2-2) the following day. After reaching confluence, cells were transferred to an appropriate number of T-75 cm² vented cell culture flask (cat.no.: CLS430641U, Corning, Sigma-Aldrich) and expanded before being used in different *in vitro* studies. Complete HSVSMCs growth media was used to maintain cells during the cell expansion stage (Table 2-2).

Table 2-2 Details of the different cell culture media used with HSVSMCs. All specialized growth media and supplements were obtained from PromoCell GmbH, Germany

Type of medium	Cell Type	Purpose	Description
Dissection/ Wash medium	HSVSMCs	HSVSMC isolation	<ul style="list-style-type: none"> • 500mL Minimum essential medium (MEM, cat. no.: 11090081, ThermoFisher Scientific) • 25mM HEPES (cat. no.: 75277-39-3, VWR International) • 2mM L-glutamine (cat. no.: 25030081, ThermoFisher Scientific) • 100nM sodium pyruvate (cat. no.: 11360070, ThermoFisher) • 1% (v/v) penicillin-streptomycin 100 units/mL – 100 µg/mL (cat. no.: 15070063, ThermoFisher Scientific)
High-serum growth medium		Initial HSVSMC cultivation post isolation	<ul style="list-style-type: none"> • Smooth Muscle Cell Growth Medium 2: Smooth Muscle Cell Growth Medium 2 Supplement Mix (Cat. No: C-22062, PromoCell) containing: • 2mM L-glutamine • 1% (v/v) penicillin-streptomycin 100 units/mL – 100 µg/mL • additional 10% (v/v) heat inactivated FBS (15% total FBS) (cat. no.: 10500064, Invitrogen, ThermoFisher Scientific)
Complete growth medium		Maintaining cell growth	<ul style="list-style-type: none"> • Smooth Muscle Cell Growth Medium 2: Smooth Muscle Cell Growth Medium 2 Supplement Mix • 1% (v/v) penicillin-streptomycin (100 units/mL – 100 µg/mL)
Low-serum (starvation) medium		Cell quiescence/ Experimental medium	<ul style="list-style-type: none"> • 500mL Dulbecco's Modified Eagle Medium (DMEM, cat.no.: 41966-029, Gibco, ThermoFisher Scientific) • 0.2% (v/v) EV-depleted FBS (cat.no.: A2720803, Gibco, ThermoFisher Scientific) • 1% (v/v) penicillin-streptomycin (100 units/mL – 100 µg/mL)
Cryopreservation medium		Cryopreservation	<ul style="list-style-type: none"> • Smooth Muscle Cell Growth Medium 2: Smooth Muscle Cell Growth Medium 2 Supplement Mix • 1% (v/v) penicillin-streptomycin (100 units/mL – 100 µg/mL) • additional 15% (v/v) heat inactivated FBS • 10% (v/v) dimethyl sulfoxide (DMSO; cat. no.: D/4120/PB08, ThermoFisher Scientific).

2.3.2 Primary HSVEC isolation and expansion

HSVECs were isolated by Mrs Elaine Friel (laboratory technician at the School of Cardiovascular and Metabolic Health, University of Glasgow), following a well-established protocol (described below).

For the isolation of HSVECs, venous samples were first transferred to a sterile petri dish before closing one end of the vein using a sterile clip. The vein was then filled with dissection medium containing 2 mg/mL collagenase type II (Sigma-Aldrich®, Irvine, UK) (Table 2-3) and clipped at the other end to completely seal the collagenase-containing medium within the lumen of the vessel. The double-clipped vein was then placed into a fresh sterile petri dish and incubated for 15 min in the hood at room temperature. Following the incubation, the inside of the vein was washed using dissection medium (Table 2-3) to recover the EC suspension. The same process was repeated one more time with a shorter incubation period (10 min). After the second vein wash, the EC suspension was transferred into a 15 mL falcon tube and spun for 5 min at (750 RCF). After discarding the supernatant, the pellet was then resuspended in 5 mL of high-serum HSVECs growth medium (Table 2-3) and transferred to the appropriate number of T-25 cm² vented cell culture flasks for an overnight incubation at 37° C and 5% CO₂. The medium was changed after cells had attached to the bottom of the flask (24 - 48 hr later). After reaching confluence, cells were transferred to an appropriate number of T-75 cm² vented cell culture flasks and expanded before being used in different *in vitro* studies. Complete HSVECs growth media (Table 2-3) was used to maintain cells during the cell expansion stage.

Table 2-3 Details of the different cell culture media used with HSVECs. All specialized growth media and supplements were obtained from PromoCell GmbH, Germany.

Type of medium	Cell Type	Purpose	Description
Dissection / Wash medium	HSVECs	HSVEC isolation	<ul style="list-style-type: none"> • DMEM, low glucose, GlutaMAX™ Supplement, pyruvate (cat.no.: 21885025, Gibco, ThermoFisher Scientific) • 15mM HEPES • 1% (v/v) penicillin-streptomycin (100units/mL-- 100µg/mL)
High-serum growth medium		Initial HSVEC cultivation post isolation	<ul style="list-style-type: none"> • Endothelial Cell Growth Medium: Endothelial Cell Growth Medium SupplementMix (Cat. No: C-22010, PromoCell) • 1% (v/v) penicillin-streptomycin (100 units/mL-- 100 µg/mL) • additional 10% (v/v) heat inactivated FBS (12% total FBS)
Complete growth medium		Maintaining cell growth/Experimental medium	<ul style="list-style-type: none"> • Endothelial Cell Growth Medium: Endothelial Cell Growth Medium SupplementMix • 1% (v/v) penicillin-streptomycin (100 units/mL-- 100 µg/mL)
Low-serum alternative experimental medium		More basic experimental conditions eliminating contaminating FBS-related EVs	<ul style="list-style-type: none"> • DMEM, low glucose, GlutaMAX™ Supplement, pyruvate • 1% EV-depleted FBS • 1% (v/v) penicillin-streptomycin (100 units/mL-- 100 µg/mL), 2% (v/v) exosome-depleted FBS
Cryopreservation medium		Cryopreservation	<ul style="list-style-type: none"> • Endothelial Cell Growth Medium: Endothelial Cell Growth Medium SupplementMix • 1% (v/v) penicillin-streptomycin (100 units/mL-- 100 µg/mL) • additional 15% (v/v) heat inactivated FBS • 10% (v/v) dimethyl sulfoxide (DMSO; cat. no.: D/4120/PB08, ThermoFisher Scientific)

2.3.3 Sourcing commercially available human primary cells

Cryopreserved HSVECs were obtained from PromoCell (Heidelberg, Germany) and ThermoFisher Scientific (UK) and stored at in the vapour phase of liquid nitrogen prior to use.

2.3.4 Maintenance of primary cells

Cells were maintained in culture using the appropriate cell culture media (see Table 2-2 and Table 2-3) replenishing media every two days. Cells were grown in a monolayer until reaching ~90% confluence when cells were sub-cultivated using a proteolytic enzyme-- 0.05% (1X) trypsin ethylenediamine tetra-acetic acid (trypsin-EDTA; cat.no.: 59427C, Millipore Sigma-Aldrich), to prevent overgrowth. Cells were first washed twice with Dulbecco's Phosphate Buffered Saline, without calcium (Ca^{2+}) or magnesium (Mg^{2+}) (DPBS, cat. no.: 10010023, Gibco, ThermoFisher Scientific) before adding 3 mL trypsin-EDTA to cells and incubating at 37°C for 2-3 min until most adherent cells had detached from the bottom of the flask. Immediately after, 12 mL trypsin-EDTA neutralising medium (DMEM, cat.no.: 21885025, 10% (v/v) heat inactivated FBS, (v/v) penicillin-streptomycin 100 units/mL-- 100 µg/mL) was added to the cells to stop the proteolytic process.

The cell suspension was then transferred to a 50 mL falcon tube and then subjected to centrifugation at 220 RCF for 3 min at room temperature to pellet the cells at the bottom of a sterile falcon tube and to remove the supernatant containing trypsin-EDTA. Supernatant was discarded and the cell pellet was then re-suspended in complete media and transferred to the relevant number of cell culture vessels. Cells were expanded 1:3 until passage (P)4 before being cryopreserved (Whaley et al., 2021) for storage purposes. During the expansion process, cells were maintained in T-75 cm² flasks containing 15 mL of the relevant complete growth media was used (Table 2-2 and Table 2-3). When necessary, manual cell counting using a haemocytometer, was performed to ensure accurate seeding of cells at a specific seeding density depending on the cell culture vessel and/or experimental protocol (Table 2-4). Human HSVMCs and HSVECs used for experiments were within passages 5-7.

Table 2-4 Details of the specific seeding density used for each cell culture dish with each cell type.

Culture vessel:	Seeding density: HSVSMCs	Seeding density: HSVECs
6-well plate	1.5x10 ⁵ cells/mL (2 mL/well)	-
12-well plate	1.5x10 ⁵ cells/mL (1 mL/well)	-
24-well plate	1.5x10 ⁵ cells/mL (500 µL /well)	-
96-well plate	6x10 ⁴ cells/mL (200 µL /well)	1x10 ⁵ cells/ mL (200 µL /well)

2.3.5 Cell counting

Cells were counted using a Bright Light Haematocytometer (Sigma Aldrich) and a light microscope. Ten µL of cell suspension was pipetted under the coverslip onto the grid. The number of cells within the four 1 mm corner squares were counted and then averaged to determine the average number of cells in each 1 mm corner square. This number was multiplied by 10⁴ to estimate the number of cells per mL in the suspension. The calculated concentration (cells/mL) of the cell suspension was used to seed cells at the desired density.

2.3.6 Cryopreservation and recovery of cultured primary cells

Before cryopreservation, cells were washed twice with DPBS and then trypsinised and pelleted through centrifugation as described in Section 2.3.4. The cell pellet was then re-suspended in 1 mL of the relevant complete media (Table 2-2 and Table 2-3). One mL of cell suspension (cells from a confluent T-75 cm² flask) was then aliquoted into a 2 mL cryo-preservation vial (cat. no.: BCS-2502, Brooks Life Sciences) and stored for 24 hr at -80 °C using a freezing container Mr. Frosty™ (Nalgene®, Thermo Scientific™) containing 100% (v/v) isopropanol which provides the steady cooling conditions of a -1 °C /min constant cooling rate required for successful cryopreservation of cells. The next day, cells were transferred to liquid nitrogen for long-term storage.

In preparation for recovery of cryopreserved cells, 15 mL of the relevant complete media was added to the cell culture flasks and warmed to 37 °C in the cell incubator. The vials with cryopreserved cells were transferred to the laboratory on dry ice allowing the thawing process to take place rapidly. Vials were dipped half-way into the water bath containing water at 37 °C for about 1-

2 min for a rapid thawing of the cells. After that, cells were mixed gently using a p1000 Gilson pipette with filter tips and then transferred into a T-75 cm² flask containing the pre-warmed complete media relevant to the cell type. The cell suspension was then gently mixed by tilting the flask allowing the cells to spread evenly over the surface of the flask. After cell attachment to the surface of the flask (usually overnight), the DMSO-containing media was removed and replaced with fresh complete media.

2.4 Cell work methodology

Throughout this project, an *in vitro* model of the pathological conditions under which neointimal lesions develop following vascular injury was utilised. In this model, HSVSMCs were exposed to pathophysiological stimulation with PDGF-BB (Cat. no.: 220-BB, R&D Systems) or treatment with vehicle (VEH) (0.2% bovine serum albumin (BSA) 10 mM acetic acid). PDGF-BB was the pathophysiological stimuli of choice since, as a potent mitogen involved in the regulation of VSMC phenotype, it has been implicated in the development of neointimal formation post vascular injury (Hu et al., 1999; M. S. Lee et al., 2004; Raines, 2004) (discussed in Chapter 1).

2.4.1 Experimental protocols designed to study the effect of unmodified EVs on activated HSVSMCs

The extracellular vesicles used in these studies were generated as described in Section 2.10.1. Briefly, quiesced cells were treated with either 20 ng/mL PDGF or VEH control for 48 hr. At the end of the incubation period, CCM was collected and EVs derived from PDGF stimulated cells (pEVs) and VEH treated cells (vEVs) were isolated as described in Section 2.10.3.1.

2.4.1.1 Cell proliferation studies

The protocols described below were designed to study the effect of unmodified HSVSMCs-derived EVs (vEVs and pEVs) on proliferation of activated recipient HSVSMCs co-treated with PDGF. Cell proliferation was assessed via BrdU incorporation assay (detailed procedure described in Section 2.9.1).

Recipient HSVSMCs were first quiesced for 48 hr, and then cells were co-treated with EVs and 20 ng/mL PDGF (Figure 2-1A). In this study, the effect of two different EV concentrations (C1 = 8.0×10^8 EV particles/mL and C2 = 1.0×10^{10} EV particles/mL) and two different timepoints (6 hr and 24 hr treatment) were assessed. The corresponding number of EV particles used to treat the cells in one well was 8.0×10^7 EV particles and 1.0×10^9 EV particles for C1 and C2 respectively (Figure 2-1A). The BrdU labelling reagent was added at the time of treatment after cells were first quiesced for 48 hr period. All treatments were performed in the relevant quiescence medium for the cell type used.

2.4.1.2 MicroRNA target gene expression studies

The ability of unmodified vEVs and pEVs, containing endogenous concentration of miRNAs, to regulate the cellular expression levels of different miRNA gene targets in HSVSMCs was assessed following the protocol described below.

In this experiment, 1.5×10^5 cells/mL (500 μ L) were seeded onto 24-well plates. HSVSMCs were first quiesced for 48 hr in the relevant quiescence medium before stimulation (Figure 2-1B). Cells were then co-treated with vEVs or pEVs (2.4×10^{10} EVs/mL or 6.0×10^9 EV particles/well) combined with 20 ng/mL PDGF for 6 hr and 24 hr (Figure 2-1B). After the treatments, RNA was purified, and gene target expression levels were assessed as described in sections 2.6.2 and 2.6.5, respectively.

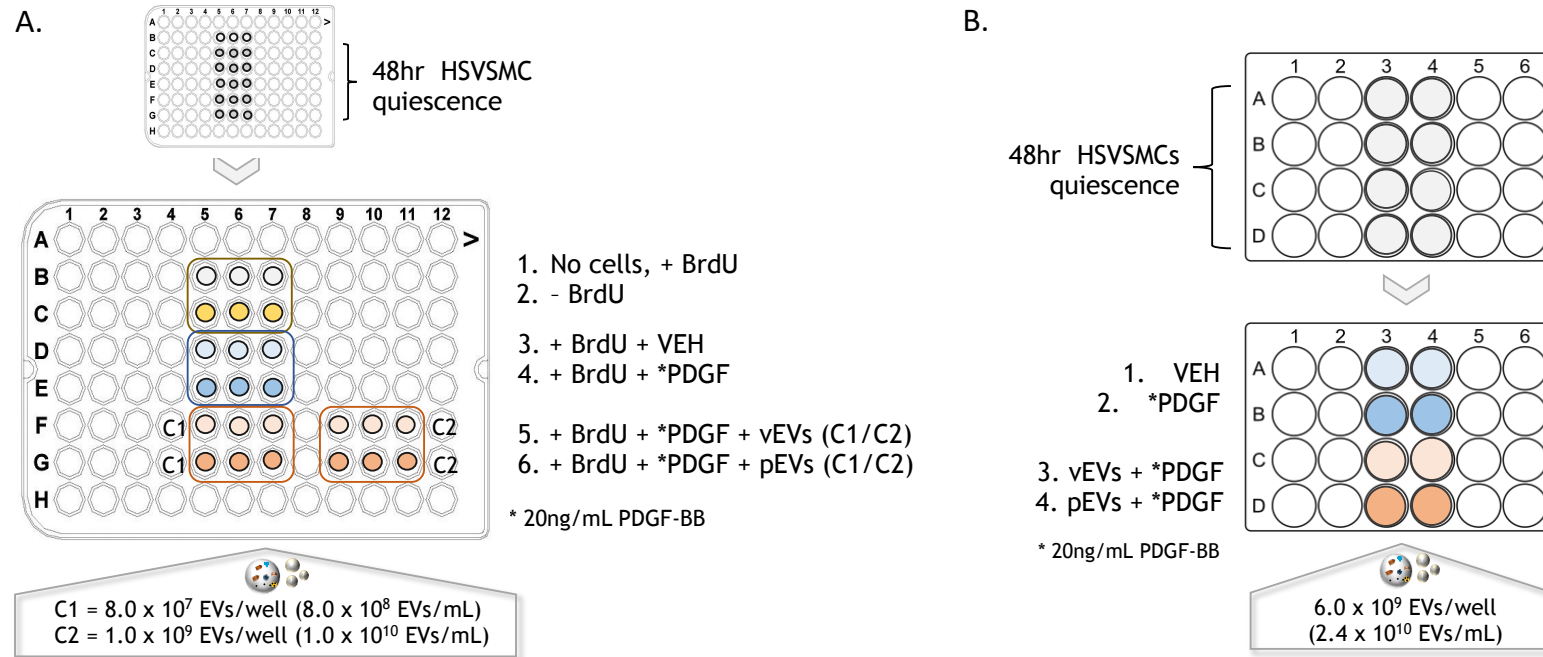


Figure 2-1 Schematic representation of the experimental protocols designed to study the effect of unmodified vEVs and pEVs on recipient PDGF-treated HSVSMC. (A) Experimental protocol followed to study the effect of vEVs and pEVs on proliferation of PDGF-activated HSVSMCs. In this protocol, conditions (1) and (2) were included as background controls; conditions (3) and (4) were included to control for the effect of cell proliferation. (B) Experimental protocol followed to assess the ability of unmodified HSVSMC-derived EVs (vEVs and pEVs) to regulate the expression levels of miRNA gene targets in recipient PDGF-activated HSVSMCs. Quiesced HSVSMCs were co-treated with 20 ng/mL PDGF combined with either vEVs or pEVs (2.4×10^{10} EVs/mL or 6.0×10^9 EV particles/well) and target gene expression was assessed by qRT-PCR.

2.4.2 Experimental protocols designed to study the effect of miRNA loaded EVs on HSVSMCs

The effects of miRNA loaded EVs (miEVs, EVs electroporated with miR-24-3p mimic or miR-224-p5 mimic) on cell proliferation, migration, target gene expression and cell viability were assessed via two different cell treatment protocols. The functional assays used to assess these cellular processes included BrdU incorporation assay for cell proliferation (Section 2.9.1), the wound scratch method and the gap closure method for assessing cell migration (Sections 2.9.3.1 and 2.9.3.2, respectively) and MTT assay for assessing cell viability (Section 2.9.2). The main difference between the two cell treatment protocols was the inclusion or exclusion of a cell preconditioning step where naïve EVs (naEVs) and miRNA loaded EVs (miEVs) were used to pre-treat recipient cells before co-stimulation with 20 ng/mL PDGF or 5% EV-depleted FBS together with naEVs/miEVs. The EVs used in these experiments were generated as described in Section 2.10.2 and miRNA mimics were exogenously loaded into EVs via electroporation (details can be found in Section 2.10.6). The exact EV concentration used in each experiment was dependent on the number of cells seeded on the required cell culture dish. For studies, including cell proliferation assays, where 96-well plates were used, 6.0×10^4 cells/mL (200 μ L) were seeded, and 1.0×10^{10} EVs/mL (1×10^9 EVs/well) were used for treatments. For cell migration studies, 1.5×10^5 cells/mL (500 μ L) were seeded onto 24-well plates and 2.4×10^{10} EVs/mL (6.0×10^9 EV particles/well) were used to treat the cells. When the ability of miEVs to regulate the expression levels of target genes was assessed, 1.5×10^5 cells/mL (500 μ L) were seeded onto 24-well plates and 2.4×10^{10} EVs/mL (6.0×10^9 EV particles/well) were used to treat the cells. RNA was extracted and expression levels of target genes were assessed as described in Section 2.6.2 and Section 2.6.5, respectively.

2.4.2.1 Studies with no EV pre-treatment step

In these experimental setups, HSVSMCs were first quiesced for 48 hr in the relevant quiescence media before stimulation. Cells were then co-treated with naEVs/miEVs combined with 20 ng/mL PDGF for cell proliferation and target gene expression studies (Figure 2-2). When studying the effect of naEVs/miEVs on cell viability, cells were treated with EVs alone (Figure 2-2).

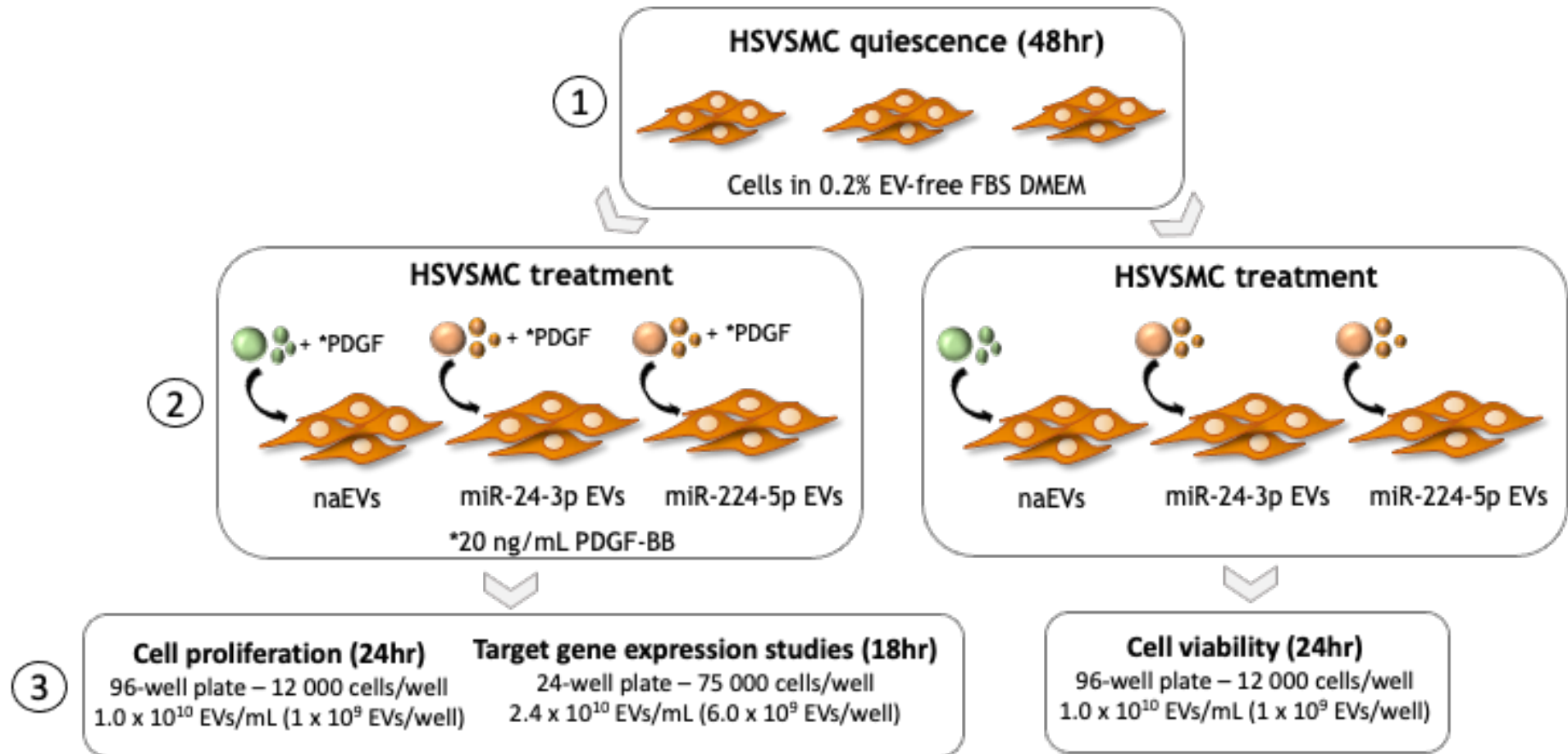


Figure 2-2 Schematic representation of the cell treatment protocol used to study the effects of naEVs/miEVs on HSVSMCs.

Cells were first quiesced for 48 hr before they were co-treated with naEVs/miEVs combined with 20 ng/mL PDGF for cell proliferation and target gene expression studies or treated only with naEVs/miEVs for cell viability studies. The EV concentration used in each experiment was dependent on the number of cells seeded on the cell culture dish used in each experiment. In general, $\sim 8.0 \times 10^4$ EVs/cell were used throughout these experiments.

2.4.2.2 Studies with an EV pre-treatment step

In these experiments, an EV pre-treatment step was included where cells were preconditioned by the addition of EVs - naEVs (naïve EVs) or miEVs (miR-24-3p EVs or miR-224-5p EVs), for 6 hr prior to co-stimulation with naEVs/miEVs combined with 20 ng/mL PDGF, for cell proliferation and target gene expression studies, or 5% EV-depleted FBS for cell migration studies (Figure 2-3).

2.4.3 Experimental protocol designed to study the effect of miRNA loaded EVs on HSVECs

In this experiment, the effects of miEVs (EVs electroporated with miR-24-3p mimic and miR-224-p5 mimic) on cell viability after 4 hr of EV treatment were assessed. HSVECs were seeded in a 96-well plate at seeding density of 1×10^5 cells/mL (200 μ L/well) and 1.0×10^{10} EVs/mL (1×10^9 EVs/well) were used to treat the cells. As HSVECs are very sensitive cells could not withstand the typical starvation conditions used with HSMCs, those cells were not quiesced prior to treatment. Instead, experiments were performed in two different media types - low-serum DMEM medium supplemented with 1% EV-depleted FBS and complete HSVEC medium (Table 2-3). Cell viability was assessed via MTT assay and a detailed protocol describing the procedure can be found in Section 2.9.2.

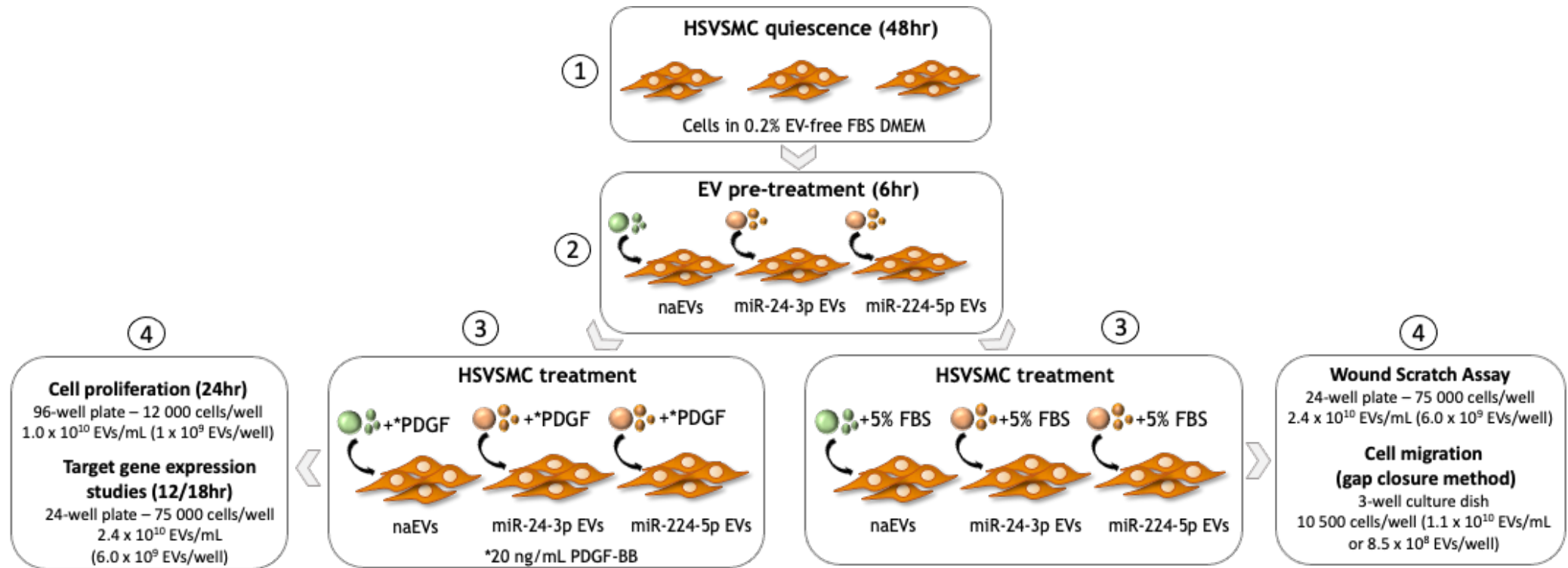


Figure 2-3 Schematic representation of the cell treatment protocol, involving a 6hr naEV/miEV pre-treatment step, used to study the effects of these EV populations on HSVSMCs. In these experiments, cells were again first quiesced for 48 hr. Then, an EV pre-treatment step was introduced where cells were preconditioned by the addition of EVs (naEVs and miEVs) for 6 hr prior to co-stimulation with naEVs/miEVs combined with 20 ng/mL PDGF, for cell proliferation and target gene expression studies, or 5% EV-depleted FBS for cell migrations studies. The EV concentration used in each experiment was dependent on the number of cells seeded on the cell culture dish used. In general, $\sim 8.0 \times 10^4$ EVs/cell were used throughout these experiments.

2.5 Immunofluorescence

HSVSMCs isolated in-house were stained to detect one of the typical smooth muscle cell markers - alpha smooth muscle cell actin (α -SMA). Following the general immunofluorescence (IMF) protocol described below.

HSVSMCS were first seeded in a black sterile 96-well microplate with clear flat bottom (SCREENSTAR, Cat no.: 655866, Greiner Bio-One Ltd) at a seeding density of 5×10^4 cells/mL and left in complete media overnight to recover. The next day, cells were washed once with DPBS and then fixed in 4% (w/v) paraformaldehyde powder (PFA, dissolved in DPBS) for 10 mins at room temperature. Immediately after that, cells were washed 2x5 mins with DPBS (on a slow shaker). After washing, the membrane was permeabilised using 0.1% DPBS-Tween (DPBS-T) solution (Tween® 20, Sigma Aldrich) for 10 mins at room temperature (no shaking). Following this step, cells were washed again 3x5 mins with DPBS at room temperature on a slow shaker. Then, wells were blocked in 1xDPBS-T/1% (v/v) goat serum (Cat. No.: S-1000, Vector Laboratories) for 30 mins at room temperature (no shaking). After blocking, cells were washed once more (1x5 mins with DPBS at room temperature on a slow shaker) before incubating with the appropriate primary antibody (Ab) diluted in 1xDPBS-T/1% (v/v) goat serum. The primary Ab used was rabbit polyclonal IgG Ab to α -SMA (Cat. no: Ab5694, 0.2 mg/mL, 1/200 dilution, Abcam). An appropriate normal rabbit IgG control (Cat.no.: 10500C, 3 mg/mL, Thermo Fisher Scientific) was diluted to the corresponding concentration in 1xDPBS-T/1% (v/v) goat serum to control for non-specific staining. Cells were incubated with anti- α -SMA IgG and control rabbit IgG at 4° C overnight (no shaking).

The next day, cells were first washed 3x5 mins with DPBS at room temperature on a slow shaker and then incubated with the appropriate fluorescent secondary Ab diluted in DPBS-T. The secondary Ab used was goat anti-rabbit IgG Alexa Fluor® 488 (Cat. No.: A-11008, 2 mg/mL, 1/500, Invitrogen, Thermo Fisher Scientific). Cells were incubated with the secondary Ab for 1 hr at room temperature in the dark on a slow shaker. Following this step, cells were washed 3x5 mins with DPBS at room temperature on a slow shaker protected from light before performing a short staining step with 4',6-diamidino-2-phenylindole (DAPI) solution (Cat. No.: D9542, 10 mg/mL, Sigma Aldrich) diluted 1/1000 in DPBS.

Finally, cells were washed again 3x5 mins with DPBS at room temperature on a slow shaker protected from light before adding DPBS to each well for storage at 4°C until ready to image.

The next day, the plastic seal covering the bottom of the plate was removed immediately prior to imaging the cells with Leica DMI8 Inverted Microscope (Leica Microsystems Wetzlar, Germany) and images were acquired using the LASx software (Leica Microsystems Wetzlar, Germany). For each related set of wells (cells from the same patient), laser settings, including exposure time, were guided by imaging negative control samples first to control for non-specific background fluorescence. The rest of the wells were then imaged based on the same microscope settings to allow unbiased comparisons between the negative control wells and wells stained with anti- α -SMA. Scale bar of 100 μ m was imported using the LASx software to all images. Alpha-SMA was detected in cells isolated from SV segments from three different patients.

2.6 Gene expression analysis

2.6.1 RNA extraction from cells and EV samples

Total RNA extraction was performed using the miRNeasy Mini Kit (cat. no.: 217004, Qiagen) in a standard biological safety class II cabinet with vertical laminar flow to prevent exposure to toxic phenol fumes. Manufacturer's instructions were followed throughout this protocol.

Briefly, for adherent cells, cell culture medium was first removed, and cells were washed twice in ice cold sterile DPBS. An appropriate volume of QIAzol Lysis Reagent (provided in the kit) (Table 2-5) was directly added to washed adherent cells or to EVs in DPBS. Adherent cells were gently rubbed away from the surface of the cell culture dish using the rubber end of a sterile 1 mL syringe plunger. The lysed cell suspension was then transferred to a sterile RNase-free 1.5 mL microcentrifuge tube and then stored at -80°C before extracting the RNA. When harvesting RNA from EVs, after the addition of QIAzol to the EV sample, the RNA extraction process was completed without interruption. The rest of the RNA extraction procedure was the same for both cells and EVs.

Table 2-5 Details of the reagent volumes used throughout the RNA extraction process.

QIAzol lysis reagent (μL)	Chloroform (μL)	Approximate volume of upper aqueous phase (μL)	100% Ethanol (μL)
500	100	300	450
750	150	450	675

2.6.2 RNA purification

Cells/EVs lysed in QIAzol were vortexed thoroughly to homogenize the sample and to achieve optimal release of RNA contained in the sample by causing a full disruption of plasma and organelle membranes. The homogenate was then incubated at room temperature for 5 min to promote the dissociation of nucleoprotein complexes.

The appropriate volume of chloroform (Table 2-5) was added to the homogenate, the tubes were mixed vigorously for 15 sec by shaking up and down and then left on the benchtop at room temperature for 2-3 min. After that, tubes were subjected to centrifugation at 12 000 RCF at 4°C for 15 min to separate the samples into 3 phases: a pink organic phase, a white DNA-containing interphase and an upper clear aqueous phase containing the RNA. Using a Gilson pipette with filter tips, the upper aqueous phases were carefully transferred to a new set of RNA-free Eppendorf tubes and 1.5X volume of 100% ethanol was added to each sample (Table 2-5). Following the addition of ethanol, RNA/ethanol samples were mixed thoroughly by pipetting up and down prior to transferring 700 μL of the sample mix to the RNeasy Mini spin columns in collection tubes (provided in the kit). The RNeasy Mini spin columns containing the ethanol/RNA sample were subjected to centrifugation at 10,000 RCF for 30 sec at room temperature allowing the RNA to bind to the silica membrane on the bottom of the spin column. After discarding the flow through, this step was repeated with the remaining sample (up to 700 μL) if necessary. The columns were then washed with two ready-made buffers (provided in the kit) to remove any impurities. Initially, 700 μL of RWT buffer was added to the spin columns which were then subjected to centrifugation at 8 000 RCF for 30 sec at room temperature (only 350 μL of RWT buffer was used for this initial washing step in cases when on-column DNase digest was carried out). The flow through was discarded, and the columns were washed again by adding 500 μL RPE buffer via

centrifugation at 8000 RCF for 30 sec at room temperature. After discarding the flow through, a longer centrifugation step was performed. Five hundred μL RPE buffer was added to the columns again and the columns were then subjected to centrifugation at 8000 RCF for 1 min at room temperature. This longer centrifugation step was required to dry the column membranes, ensuring that no ethanol was carried over during the RNA elution step as ethanol may interfere with downstream analysis. After this step, the spin columns were carefully removed from the collection tubes and placed into a new set of collection tubes which were then subjected to centrifugation at full speed for 1 min. This step was performed to eliminate possible carryover of RPE buffer. Finally, the spin columns were transferred into new 1.5 mL RNA-free Eppendorfs to collect the eluting RNA. After pipetting 30-50 μL RNase-free water (provided in the kit) directly onto the column membranes, the spin columns were left for 1 min at room temperature to allow better hydration of the column membranes. Immediately after, the columns were subjected to centrifugation at 8000 RCF for 1 min to elute the RNA. A second RNA elution step was performed using the first elute and the same collection tube to increase the final RNA concentration. The spin columns were then discarded, and RNA samples were placed on ice. NanoDrop® (ND-1000 spectrophotometer; Thermo Scientific) was used to determine the concentration and quality of each RNA sample and the average of two readings was taken. The ratios of 260nm/280nm and 260nm/230nm were used as indicators of RNA purity providing information about the presence of common RNA contaminants such as protein and phenol respectively. A 260/280 ratio of ≥ 2.0 and a 260/230 ratio between 1.8 - 2.2 generally reflect pure RNA. RNA samples were either directly subjected to complementary cDNA synthesis or stored at -80°C .

2.6.3 On-column DNase digest

Where appropriate, an on-column DNase digest was carried out during RNA isolation. RNase-free DNase (Qiagen, West Sussex, UK) treatment was carried out on RNA isolation samples whenever the aim was to measure mRNA gene expression levels. The purpose of this step was to remove any contaminating DNA and was carried out following the manufacturer's instructions. Three hundred and fifty μL of RWT Buffer was added to the spin column and subjected to centrifugation at 8000 RCF for 15 secs. The flow-through was discarded and

80µL DNase/buffer solution (10 µL DNase + 70 µL Buffer RDD per sample) was added to each column. Samples were incubated for 15 mins at room temperature. Following incubation, 350 µL RWT Buffer was added to each column before centrifugation at 8000 RCF for 15 sec. Finally, the flow through was discarded.

2.6.4 Reverse transcription polymerase chain reaction (RT-PCR)

The reverse transcription reaction was performed for each RNA sample to generate cDNA.

2.6.4.1 RT-PCR for the detection of miRNA expression levels

RT reactions were performed for each miRNA of interest along with a control miRNA. The housekeeping control miRNA measured when studying the expression of miRNAs in cells was RNU48. When studying the expression of miRNAs in EVs, the control miRNA used was *Caenorhabditis elegans* cel-miR-39 (synthetic cel-miR-39, Cat. No.: 4464066, Qiagen). For this purpose, EV samples were first spiked with a known amount of cel-miR-39 (27 pg or 1.95×10^{-3} pmol / sample) prior to purifying the RNA as described in Section 2.6.2. To create cDNA for miRNAs, reverse transcription reactions ($\frac{1}{2}$ reactions = 7.5 µL) were performed in a 96-well plate (cat. no.: E1403-5200, Skirted, Low-Profile, STARLAB) using the TaqMan™ miRNA Reverse Transcription Kit (cat. no.: 4366596, Applied Biosystems by ThermoFisher Scientific). The initial RNA input for EV and cell samples was 2.5 µL and 5 ng respectively. Non-template control (NTC) where nuclease-free water was used instead of RNA sample, was added to the plate for each miRNA mastermix including the control miRNAs (cel-miR-39 and RNU48). A separate mastermix for each miRNA was prepared containing the relevant TaqMan® miRNA RT primer (Table 2-6). To convert the RNA into cDNA, the following reaction constituents and temperature parameters of cycling conditions were used.

Mastermix:	Final concentrations:
dNTPs (100 mM)	1 mM
Multiscribe™ RT enzyme (50 U/μL)	3.33 U/μL
Reverse Transcription Buffer (10X)	1X
RNase Inhibitor (20 U/μL)	0.25 U/μL
2.08μL Nuclease-free water (Qiagen).	N/A
TaqMan® miRNA RT primer (5X)	1X

Multi-Block PCR Thermal Cycler (PTC-225, MJ Research) was used to run the RT-PCR using the following settings:

16 °C for 30 min - primer binding to the RNA template.

42 °C for 30 min - reverse transcription reaction.

85 °C for 5 min - RT enzyme inactivation.

The newly synthesized cDNA samples were stored at -20 °C until next used.

Table 2-6 List of TaqMan® miRNA Assays used throughout this study. All assays were purchased from ThermoFisher Scientific. Provided in this table are details regarding the miRNA's corresponding miRBase/NCBI Identifiers (accession numbers), the Cat. No., and the respective Assay ID as identified by Life Technologies.

TaqMan® miRNA Assay	miRNA	miRBase/NCBI Accession Number	Cat. No. (ThermoFisher Scientific)	Assay ID (Applied Biosystems)
hsa-miR-24	miR-24-3p	MIMAT0000080	4427975	000402
hsa-miR-1	miR-1-3p	MIMAT0000416	4427975	002222
hsa-let-7a	let-7a-5p	MIMAT0000062	4427975	000377
hsa-miR-21	miR-21-5p	MIMAT0004494	4427975	000397
hsa-miR-409-3p	miR-409-3p	MIMAT0001639	4427975	002332
hsa-miR-224-5p	miR-224-5p	MIMAT0000281	4398987	CTFVKZX
cel-miR-39	miR-39-3p	MIMAT0000010	4427975	00200
RNU48	RNU48	NR_002745	4427975	001006

2.6.4.2 RT-PCR for the detection of mRNA expression levels

To create cDNA for protein coding genes, 20 μL reverse transcription reactions were performed in a 96-well plate using the TaqMan Reverse Transcription Reagents. The amount of RNA transcribed was between 200-1000ng and this was kept consistent within experiments. RNA samples were diluted in RNase-free H₂O

directly on the 96-well plate on ice. An NTC was also included for each experiment. A mastermix containing the following components was added to each well:

Mastermix:	Final concentration:
SuperScript™ II buffer (SSII, Invitrogen, 5X)	1X
dNTP Solution mix (NEB, 10 mM)	1 mM
dTT (Invitrogen, 0.1 M)	10 mM
Random Hexamers (Invitrogen, 50 μM)	5 μM
RNasin® Ribonuclease Inhibitor (Promega, 40U/μL)	2 U/μL
Superscript® II RT enzyme (Invitrogen, 200 U/μL)	20 U/μL
1.5μL Nuclease-free water (QIAGEN)	N/A

A Multi-Block PCR Thermal Cycler (PTC-225, MJ Research) was used to run the RT-PCR. Firstly, the RNA was denatured at 70°C for 10 min before adding the mastermix. Upon addition of the mastermix to the wells, the RT-PCR reaction was carried out using the following temperature settings:

- 25°C for 10 min - primer binding to the RNA template.
- 42°C for 60 min - reverse transcription reaction.
- 72°C for 15 min - RT enzyme inactivation.

After completion of the reaction, samples were diluted with 80-180 μL of nuclease-free water, and this was kept consistent within experiments. The newly synthesized cDNA samples were stored at -20°C until next used.

2.6.5 Real-time quantitative RT-PCR (qRT-PCR)

Throughout the studies, relative mRNA expression levels of target genes were determined by TaqMan® qRT-PCR system (Applied Biosystems™) which was used to detect and quantify the expression of different genes in real time. Details about each miRNA and mRNA assay could be found in (Table 2-6) and (Table 2-7), respectively.

The TaqMan® qRT-PCR system uses TaqMan® probes which are labelled with a fluorescent dye (FAM™ or VIC™) at their 5' end. The probes also contain a minor groove binder (MGB) and nonfluorescent quencher (NFQ) at their 3' end. During

the initial stage of the reaction, the temperature is raised denaturing the double-stranded cDNA. In the next step, the lowered reaction temperature allows for primers (forward and reverse) and probe to anneal specifically to their complementary sequences. The synthesis of the new strands by the Taq DNA polymerase starts with the unlabelled primers. When the polymerase reaches a TaqMan probe, it cleaves the probe separating the dye from the quencher, thus, allowing the detection and quantification of the fluorescent dye. If the target sequence is not present and probe annealing does not take place, then the probe remains intact, and the fluorescent signal is not detected as it is inhibited by the quencher. The quencher molecule quenches the fluorescence emitted by the fluorophore when excited by the cyclers light source via a process known as Förster resonance energy transfer (FRET). The accumulation of PCR product can be detected in real time by measuring the increase of fluorescence signal at each amplification cycle with the amount of target amplified being directly proportional to the starting template concentration during the exponential phase of the PCR cycling.

To study the expression of different miRNAs of interest, TaqMan® miRNA probes were used (Table 2-6). Two types of negative controls were also included - NCT RT product and nuclease-free water instead of an RT RNA product. Each reaction contained 2 µL of RT product (or 0.7 µL of RT product for cel-miR-39-3p spike-in detection) and the following components as part of the mastermix:

Mastermix:	Final concentration:
TaqMan® Universal PCR Master Mix II (no UNG) (2X)	1X
TaqMan® miRNA probe (20X)	1X
* 2.5/3.8µL Nuclease-free water	N/A

* When detecting the expression of the spike-in control cel-miR-39-3p, a higher amount of nuclease free water was added to the reaction mixture to make up for the use of lower amount of RT product.

To study the expression of different protein coding genes of interest, TaqMan® mRNA probes were used (Table 2-7). Two types of negative controls were also included - NCT RT product and nuclease-free water. Each reaction contained the following components:

Mastermix:	Final concentration:
TaqMan® Universal PCR Master Mix II (no UNG) (2X)	1X
TaqMan® mRNA probe (20X)	1X
2.5µL Nuclease-free water	N/A

Table 2-7 List of human TaqMan® assays used for the detection of mRNA gene expression.
All assays were purchased from ThermoFisher Scientific.

Gene Name	Gene symbol	TaqMan® Assay ID	Cat. No.
Platelet derived growth factor receptor α	PDGFRA	Hs00998018_m1	4331182
Platelet derived growth factor receptor β	PDGFRB	Hs01019589_m1	4331182
RAS Related	RRAS	Hs00196699_m1	4331182
Neuroblastoma RAS viral oncogene homolog	NRAS	Hs00180035_m1	4331182
Phosphoinositide-3-kinase regulatory subunit 3	PIK3R3	Hs01103591_m1	4331182
Polyubiquitin-c	UBC	Hs00824723_m1	4331182

All reactions were performed in 384-well optical plates (cat. no.: 4309849, Thermo Fisher Scientific) using a QuantStudio 12K Flex Real-Time PCR System (Applied Biosystems by Life Technologies) with temperature parameters of cycling conditions as follows:

Hold stage:

50°C for 2 min (step deleted when amplifying miRNA sequences)

95°C for 10 min - activation

Cycling conditions (x40 cycles):

95°C for 15 sec - denaturation

60°C for 1 min - annealing and extension



2.6.5.1 Analysis of qRT-PCR

In qRT-PCR reactions, the cycle threshold (Ct) is defined as the number of cycles required for the fluorescent signal (amplification curve) to cross the threshold (i.e., exceeds background level) which is set in the linear phase of the reaction. The Ct values are determined in the exponential phase of the reaction and are inversely proportional to the amount of target nucleic acid in the sample (i.e.,

the lower the Ct value the higher the amount of target nucleic acid in the sample).

The expression of miRNAs/mRNA genes of interest were always measured relative to a control miRNA/mRNA gene. In cells, the ‘housekeeper’ controls of choice were RNU48 and UBC when investigating the expression of miRNAs and mRNA genes, respectively. When detecting miRNAs in EV samples, the expression levels of the miRNAs of interest were normalized to that of cel-miR-39 spike-in control.

The data collected was analysed using the $\Delta\Delta Ct$ method (Livak and Schmittgen, 2001). Data normalization was performed by first calculating the mean Ct value of three technical replicates for the same miRNA/mRNA gene. Then, the ΔCt was calculated which is the difference between the Ct value of the miRNA or gene of interest and the Ct of the control miRNA or gene for that sample. Subsequently, the $\Delta\Delta Ct$ was calculated using the following equation:

$$\Delta\Delta Ct = \Delta Ct (\text{treated sample}) - \Delta Ct (\text{control sample})$$

Finally, the fold change in miRNA/mRNA gene expression levels between the treatment group and the control samples was calculated. This is also called relative quantification (RQ) and was calculated using the following equation:

$$RQ = 2^{-\Delta\Delta Ct}$$

This method determines gene expression levels normalized to a control relative to a calibrator selected from within the experiment (i.e., a single sample or a sample group assigned to have relative gene expression level of 1.0).

2.7 Protein expression analysis

2.7.1 Protein extraction

To extract proteins from cells and EVs, samples were prepared on ice using RIPA lysis buffer for whole protein (Pierce™, ThermoFisher Scientific) containing 25 mM Tris HCl (pH 7.6), 150 mM NaCl, 1% NP-40, 1% sodium deoxycholate, 0.1% sodium dodecyl sulphate (SDS). Phosphatase Inhibitor Cocktail (Sigma Life

Science) and Protease Inhibitor Cocktail tablets (cOmplete, Roche Diagnostics) were both added to the buffer prior to use to prevent proteolysis and maintain phosphorylation status of proteins.

Cells were first washed quickly with DPBS before adding 100-700 μL RIPA buffer (depending on the number of cells being lysed) and then scraped off the bottom of the culture dish using a regular cell scraper. Prior to measuring the protein concentration and preparing samples for Western Blotting (WB), all samples were quickly vortexed.

To extract proteins from EVs in preparation for Western Blotting, EV samples were mixed with RIPA lysis buffer in 4:1 ratio. Both cell lysates and EV lysates were vortexed and incubated on ice for 30 min prior to sonication. Samples were sonicated twice for 5 seconds using Ultrasonic Processor (120 watts, 20 kHz, Fisher Scientific) on the following settings: pulse - 30 and amplitude - 50%, and then stored at -20°C . Only for the purpose of measuring EV protein concentration, EV samples were mixed with NaOH (0.2 mM) in 1/20 ratio (no RIPA buffer), then samples were vortexed and left on ice for 30 mins prior to sonication using the same settings as described above.

2.7.2 Protein quantification

Protein concentration in cell lysates and EV lysates was determined in flat bottom 96-well plates using a Pierce™ BCA Protein Assay Kit (cat. no.: 23227, Pierce™, Thermo Scientific™) or Pierce™ Micro BCA™ Protein Assay Kit (ca. no.: 23235 Pierce™, Thermo Scientific™) respectively. The assays were carried out following manufacturer's instructions.

Protein concentration of cell lysates was estimated with reference to a standard curve generated using BSA diluted in DPBS. A new standard curve (25 $\mu\text{g}/\mu\text{L}$ - 2000 $\mu\text{g}/\mu\text{L}$) was prepared for each individual assay. Reagents A and B from the kit were mixed in 50:1 ratio respectively, before being used. Cell lysate samples and standards were first added to the wells of a 96-well plate before the addition of the BCA reagent mixture. After mixing well with the pipette, samples were incubated, protected from light at 37°C for 30 min before reading the absorbance at 560 nm using a Multi Plate Reader Victor™ X3 (Perkin Elmer), or at

562 nm using SpectraMax M2 Spectrophotometer (Molecular Devices). A background control (BC) sample was always included where RIPA buffer alone was mixed with the reaction mixture. Protein concentrations were determined based on the standard curve after subtracting the BC reading from the readings of sample unknowns. Both standards and cell lysate samples were measured in duplicate, and the average was calculated. Analyses were performed using Microsoft® Excel (Version 16.5).

Protein concentration of EV lysates was estimated with reference to a standard curve generated using BSA diluted in NaOH (0.1 mM). A new standard curve (0.5 µg/µL - 200 µg/µL) was prepared for each individual assay. Reagents A, B and C from the kit were mixed in 25:24:1 ratio respectively, before being used. EV lysate samples and standards were first added to the wells of a 96-well plate before the addition of the BCA reagent mixture. After mixing with the pipette, samples were incubated, protected from light at 37°C for 2hr before reading the absorbance at 560 nm using a Multi Plate Reader Victor™ X3 (Perkin Elmer), or at 562 nm using SpectraMax M2 Spectrophotometer (Molecular Devices). Protein concentrations of unknown samples were determined based on the standard curve generated after blank-correcting all standard and unknown sample readings. Both standards and EV lysate samples were measured in duplicate, and the average was calculated. Analyses were performed using Microsoft® Excel (Version 16.50).

2.7.3 Western immunoblotting

Western immunoblotting was used to determine protein expression in qualitative manner. Due to the lack of an established endogenous housekeeping protein to serve as a loading control, EV protein markers were only detected for confirmational purposes when the aim was to characterise an EV population. Details about all antibodies used throughout this project can be found in Table 2.6. Between 10-20 µg of protein was loaded on the gel for positive control samples and 8 µg or 10 µg for EV samples. When detecting the expression of EV protein markers in EV lysates, protein lysates from cells were used as positive controls including lysates from HSVSMCs or HSVECs - depending on the origin of the EVs (HSVSMC lysate was used as a PC when EV-protein markers were detected in serum EVs).

Protein lysates were denatured and prepared for gel electrophoresis in NuPAGE® Lithium Dodecyl Sulphate (LDS, pH 8.5, cat. no.: NP0007 ThermoFisher Scientific) Sample Buffer (4X) containing 988 mM Tris, 2.04 mM EDTA, 8% LDS, 40% Glycerol, 0.88% COOMASSIE® Brilliant Blue G-250, 0.7 mM Phenol red with or without 5mM dithiothreitol (DTT) onto a the 96-well plate. The use of this sample buffer induced negative charge on the proteins which promoted the migration of the proteins through the resolving gel towards the anode. Upon addition of the sample buffer, the 6-well plate containing the protein mixtures was sealed and placed on the MJ Research Tetrad PTC-225 Thermal Cycler to enable denaturation at 95° C for 5 min.

Next, samples were loaded on a 1 mm 12 + 2-well NuPAGE™ 10% Bis-Tris Midi Gel (cat. no.: WG1401BOX, Invitrogen, ThermoFisher Scientific) for separation by electrophoresis (100-120V for 2 - 2:30hr) in 1× NuPAGE® MES SDS Running Buffer (cat. no.: NP002, Novex, Life Technologies). In the first well, 3 µL of pre-stained protein ladder (Chameleon Duo Pre-Stained Protein Ladder, cat. no.: 928-60000, LI-COR Biosciences) was loaded to serve as a molecular weight standard. After separation, proteins were transferred onto a 0.2 µm nitrocellulose membrane (cat. no.: GE10600001, Amersham™, Protran™, GE Healthcare Life Sciences) using a Power Blotter 1-Step™ Transfer Buffer (Invitrogen, ThermoFisher Scientific) and a Power Blotter-Semi-Dry Transfer System (Invitrogen, ThermoFisher, UK) at 25V and 2.5A for 8.5 min. Blocking solution made of 1X TRIS-buffered saline (TBS) pH 7.4 (cat.no.: J60764, Alfa Aesar) and SEA BLOCK blocking (cat. no.: 37527, Thermo Fisher Scientific) in 1:1 ratio was used to block the membranes for 1 hr at room temperature on a slow shaker.

Membranes were then incubated overnight at 4° C on a shaker with different specific primary monoclonal Abs (Table 2-8) prepared in 1X TBS/SEA BLOCK blocking buffer (1:1). Following incubation with primary Abs, membranes were washed three times with 1X TBS with 0.05 % Tween® 20 (cat. no.: P1379, Merck, Sigma-Aldrich) for 5 min. Next, membranes were incubated for 1 hr at room temperature on a slow shaker with the respective fluorescent-dye conjugated secondary Abs. The secondary Abs used were Goat anti-Rabbit IgG Highly Cross-Adsorbed Secondary Antibody (Alexa Fluor® 790, Cat. No.: A11367, 2 mg/mL, 1/15 000, Invitrogen, Thermo Fisher Scientific) and Goat anti-Mouse IgG Highly Cross-Adsorbed Secondary Antibody (Alexa Fluor 790, Cat. No.: A11357, 2

mg/mL, 1/15 000, Invitrogen, Thermo Fisher Scientific). Following incubation with the secondary Ab, membranes were then washed again three times with 1X TBS 0.05% Tween® 20 (TBS-T) for 5 min before signal detection. The membranes were visualised using the LI-COR scanning system (ODYSSEY CLx, LI-COR Biosciences). All immunoblots were visualised using LI-COR ImageStudioLite software (Version 5.2.5).

Table 2-8 Different primary monoclonal antibodies used throughout this project.
Abbreviations: Ab, antibody; UK, United Kingdom, USA, United States of America.

Ab Name:	Monoclonal anti-Annexin A2 (0.391 mg/mL)	Monoclonal anti-Annexin XI (0.2 mg/mL)	Monoclonal anti-CD63 (1 mg/mL), non-reducing conditions	Monoclonal anti-CD81 (0.2 mg/mL)
Host:	Rabbit	Mouse	Mouse	Mouse
Manufacturer and Product no.:	Abcam®, UK (ab189473)	Santa Cruz, USA (sc-46686)	Abcam®, UK (ab59479)	Santa Cruz, USA (sc-166029)
Dilution:	1/5000	1/200	1/2000	1/500

2.8 Enzyme-linked immunosorbent assay

Detection and quantification of human PDGF-BB in EVs was performed by enzyme-linked immunosorbent assay (ELISA) kit (ELISA kit, cat.no.: BMS2071, Invitrogen, ThermoFisher Scientific) with an assay range of 31.3 - 2 000 pg/mL and analytical sensitivity of 4.6 pg/mL. For this experiment, EVs were generated following the protocol described below (Figure 2-4). Three x T-75cm² flasks of confluent (~90%) HSVSMCs were used to generate EVs per condition - VEH (vEVs) and PDGF (pEVs). Cells were first washed with DPBS and then quiesced in the appropriate starvation medium for 48 hr. After that, cells were washed with DPBS again and then treated with either VEH (0.2% BSA 10 mM acetic acid) or human PDGF-BB (20 ng/mL) for 48 hr CCM samples were collected (Figure 2-4). Both CCM samples were clarified and concentrated following the procedure described in Section 2.10.3.1 (steps 1, 2 and 3), except, in this case for the purposes of this experiment, CCM was concentrated up to 500 µL instead of 200 µL. Whenever EVs were isolated throughout this assay protocol, the procedure described in Section 2.10.3.1 (steps 4 and 5) was followed.

The first 3 types of control samples that were prepared to be assayed on the ELISA microplate included pure non-processed 48 hr concentrated CCM samples containing EVs together with VEH (sample 1 - vCCM) or soluble PDGF (sample 2 - pCCM), and also a sample of EVs purified from 100 μ L concentrated CCM containing soluble PDGF (sample 3 - pEVs) (Figure 2-4).

Next, 6 more samples were prepared to be added to the ELISA microplate for all of which EVs were isolated from the same concentrated VEH and PDGF CCM (100 μ L) collected after 48 hr of treatment (3 x vEVs and 3 x pEVs). The first set of two samples were native EV samples (nvEVs and npEVs) and did not undergo any treatment after the first EV isolation. Additionally, the second set of two vEV and pEV samples were subjected to a 1 hr treatment (+37°C) with 500 μ g/mL proteinase K (Roche, Sigma Aldrich, Catalogue No.: 3115879001) dissolved in filtered DPBS. Finally, the last set of two vEV and pEV samples were subjected to the same 1hr treatment (+37°C) but without adding the proteinase K (PK) just DPBS alone (Figure 2-4). The ratio of EV sample to PK/DPBS was 1:1. EV samples were treated with PK, a broad-spectrum serine protease, to help investigate the possibility of EVs carrying PDGF packaged inside them or attached to their surface. To inactivate the enzyme, vEVs +PK, pEVs +PK, vEVs -PK and pEVs - PK were incubated at 60°C for 10 min before EVs from all 6 EV samples (nvEVs, npEVs, vEVs +PK, pEVs +PK, vEVs -PK and pEVs - PK) were re-isolated (Figure 2-4) as described in Section 2.10.3.1 (steps 4 and 5).

Therefore, the following samples were assayed for the presence of human PDGF-BB:

vCCM - 48hr CCM containing VEH

pCCM - 48hr CCM containing soluble PDGF (pre-diluted 1/100)

pEVs - Purified EVs from 48hr CCM sample containing soluble PDGF

nvEVs - Native purified EVs from VEH CCM sample

npEVs - Native purified EVs from PDGF CCM sample

vEVs/-PK - Purified EVs from VEH PDGF CCM **not** treated with PK

pEVs/-PK - Purified EVs from PDGF CCM sample **not** treated with PK

vEVs/+PK - Purified EVs from VEH CCM sample treated with PK

pEVs/+PK - Purified EVs from PDGF CCM sample treated with PK

Before proceeding to the assay test procedure, EVs were lysed by mixing the samples with RIPA (Pierce™, ThermoFisher Scientific) lysis buffer in 4:1 ratio and incubating for 30 min on ice. The ELISA was carried out as per manufacturer's instructions with minor modifications to the protocol concerning the pre-dilution of samples prior to start the test procedure. As very low concentrations of PDGF-BB were expected to be detected in the majority of the samples, only CCM samples containing soluble PDGF (where EVs were not isolated) were pre-diluted with 1X Assay Buffer (1/100).

The microwell strips were washed twice with approximately 400 µL of 1X Wash Buffer before 100 µL of each externally diluted PDGF-BB standard (S1-S7 = 31.3 - 2000 pg/mL) was added to the wells in duplicate. All standards were prepared in 1X Assay Buffer. A BLANK sample containing only 1X Assay Buffer was also included in duplicate. Next, 50 µL of 1X Assay Buffer and 50 µL of each sample was added (in duplicate) to the sample wells. Background Control (BC) samples containing 50 µL of undiluted CCM or prediluted (1/100) CCM mixed with 50 µL of 1X Assay Buffer were also added to the wells in duplicate. Upon the addition of 50 µL of Biotin-Conjugate (1/100 dilution in 1X Assay Buffer) to all wells, the microplate was covered with an adhesive film (provided in the kit) and incubated for 2 hr on a microplate shaker at room temperature.

After the 2 hr incubation, the wells were emptied, and the plate was thoroughly washed six times with 1X Wash Buffer (400 µL/well) before 100 µL of Streptavidin-HRP diluted in 1X Assay Buffer (1/100) was added to the wells. The plate was covered with an adhesive film and incubated for 1 hr on a microplate shaker at room temperature. Next, wells were emptied, and the plate was thoroughly washed again six times with 1X Wash Buffer (400 µL/well). Following the last washing step, 100 µL of Tetramethyl-benzidine (TMB) Substrate Solution (ready-made) was added to each well and the plate was incubated for another 30 min at room temperature protected from sunlight. After the addition of 100 µL ready-made Stop Solution the optical density (OD) was read at 450 nm immediately using a Multi Plate Reader Victor™ X3 (Perkin Elmer).

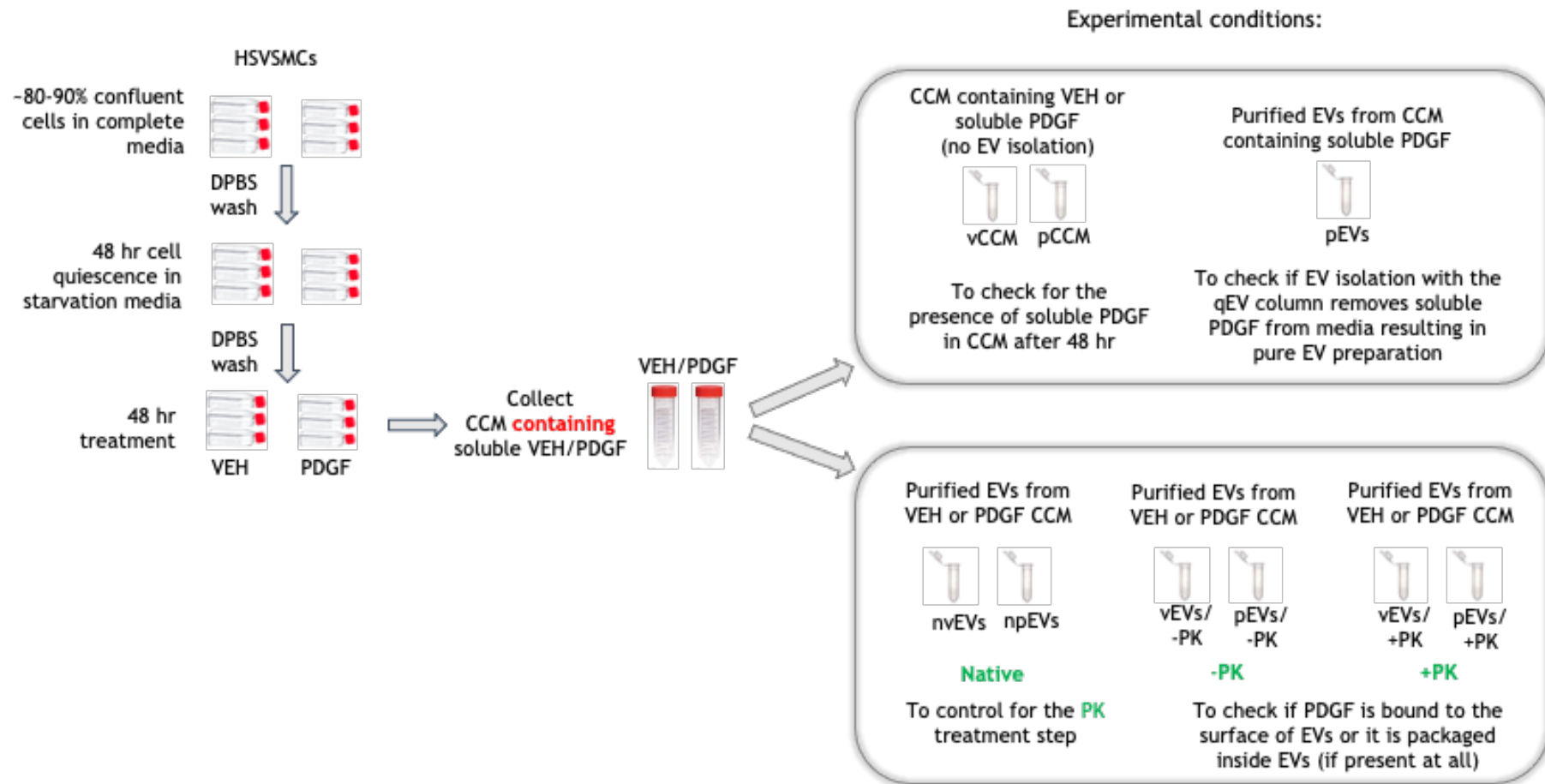


Figure 2-4 Measuring PDGF-BB concentration in HSVSMC vEV and pEV samples by ELISA. Schematic representation of the experimental protocol designed to instigate the presence of PDGF-BB on the surface of EVs or packaged within the EVs secreted by HSVSMCs treated with VEH control or PDGF-BB (20 ng/mL). Abbreviations: CCM, conditioned culture medium; vCCM, VEH CCM; pCCM, PDGF CCM; vEVs, VEH EVs; pEVs, PDGF EVs; nvEVs, Native vEVs; npEVs, native pEVs; PK, proteinase K.

2.9 Functional *in vitro* assays

2.9.1 Cell proliferation assay

The bromodeoxyuridine (BrdU) incorporation assay is a well-established method of assessing cell proliferation. In this assay, actively proliferating cells incorporate the BrdU reagent in their newly synthesised DNA strands. Following partial denaturation of the double stranded DNA, the BrdU signal is detected immunochemically allowing the assessment of the population of cells, which are synthesizing DNA. The intensity of the BrdU signal is directly proportional to the newly synthesised DNA due to cell proliferation.

Throughout this project, BrdU incorporation assay was carried out to assess cell proliferation in various experimental settings which will be discussed in more detail in the relevant chapter-specific methods sections. BrdU assays were always performed on cells seeded on 96-well plates (cell seeding density described in Table 2-4) following the manufacturer's instructions described below. Each experiment was performed in technical triplicates (3 wells/condition). All experiments described here were carried out using the same BrdU Cell Proliferation Kit (cat.no.: 11647229001, Roche, Sigma-Aldrich). To ensure the validity of the assay, background/blank control wells were always included with any of the assay kits. One set of cells (3-wells) was not loaded with BrdU, and another set of 3 wells were left without cells but filled with medium containing BrdU only for background correction.

HSVSMCs were always first quiesced for 48 hr in the relevant quiescent media (Table 2-2) which was also the same medium used with the experimental treatments. If cells were not pre-treated with EVs, BrdU labelling reagent and experimental treatments were added immediately after the 48 hr quiescence period. In the case where an EV pre-treatment step was introduced, HSVSMCs were first pre-treated with EVs for a 6-hr period before BrdU labelling reagent and experimental treatments were added to the cells. The specifics for each experimental design will be described in the relevant chapters.

The BrdU cell proliferation kit manufactured by Roche was used following manufacturer's instructions. Ten μM of BrdU labelling reagent was added to cells

together with experimental treatments (unless otherwise stated) after which the plate was incubated under normal cell culture conditions described in Section 2.3 for a time period specific for each experiment. Depending on the experimental set-up, BrdU was incorporated (1:1000, final volume 100 μL /well) either 6 or 24 hr prior to termination of the experiment. The experimental set up for each experiment designed to assess cell proliferation will be described in detail in the relevant chapter specific method's section. Before proceeding to BrdU label detection, the stimulation media was removed, wells were washed once with DPBS, and the plate was dried at 60°C for 1 hr. The plate was stored in a sealed zip-lock plastic bag at 2° to 8°C for up to a week prior to performing the assay. On the day of the assay, all components of the kit were brought to room temperature prior to starting the assay. Firstly, the experimental wells were fixed, and the DNA denatured during an incubation step with 200 μL FixDenat solution in each well for 30 min at room temperature. Meanwhile, a working solution of anti-BrdU-POD conjugate (POD, peroxidase) was prepared by diluting the anti-BrdU-POD conjugate stock in antibody dilution solution in 1/100 ratio.

Following fixation and denaturation, the FixDenat solution was removed thoroughly by flicking off and tapping the plate. One hundred μL of anti-BrdU-POD working solution was added to each well and the plate was incubated for 1 hr 30 min at room temperature protected from light. After this step, the antibody conjugate was removed by flicking the plate and tapping. The wells were then washed thoroughly three times with 200-300 μL /well 1X washing solution. After the final washing step, the washing solution was removed well by tapping the plate prior to adding 100 μL /well of ready-made substrate solution and incubating for 30 min at room temperature protected from light. Upon the addition of 25 μL of 1 M H_2SO_4 to each well and mixing thoroughly, the absorbance was measured at 450 nm using a Multi Plate Reader Victor™ X3 (Perkin Elmer) or SpectraMax M2 Spectrophotometer (Molecular Devices). If no stop solution was added to the wells, the optical density (OD) was measured at 370 nm on a Multi Plate Reader Victor™ X3 (Perkin Elmer). This step was kept consistent within experiments. The higher the OD reading the higher the BrdU concentration in the sample representing a higher rate of cell proliferation. All

absorbance values were corrected for background intensity by subtracting the mean background from target values.

2.9.2 Cell viability assay

CyQUANT™ MTT Cell Viability Assay (Invitrogen by ThermoFisher Scientific, Cat.no.: V-13154) was used to measure cellular metabolic activity as an indicator of cell viability, proliferation, and cytotoxicity. This is a colorimetric assay based on the conversion of the water soluble MTT (3-(4,5-dimethylthiazol-2-yl)-2,5-diphenyltetrazolium bromide or MTT) to an insoluble purple formazan crystal by metabolically active cells which contain NAD(P)H-dependent oxidoreductase enzymes (Berridge and Tan, 1993; Liu et al., 1997). The insoluble formazan crystals are then solubilised, and the absorbance is measured at 570 nm or the nearest possible wavelength using a multi-well spectrophotometer.

MTT assays were carried out to assess cell viability in various experimental settings which are described in more detail in the relevant chapter-specific methods sections. MTT assays were performed on cells plated on 96-well plates (cell seeding density described in Table 2-4) following the manufacturer's instructions described below. HSVSMCs were always first quiesced for 48 hr in the relevant quiescence media which was also the same medium used with the experimental treatments (Table 2-2 and Table 2-3). HSVECs were not quiesced, instead two different types of experimental media were used to assess cell viability (Table 2-3). Each experiment was performed in technical triplicates (3 wells/condition).

Prior to starting the MTT assay, the necessary reagents were prepared. Twelve μL of MTT stock solution was prepared by adding 1 mL of sterile PBS to one 5 mg vial of MTT (provided in the kit). The solution was mixed by vortexing until completely dissolved. Additionally, 0.1 g/mL SDS-HCl solution was prepared by adding 10 mL of 0.01 M HCl to 1 g of SDS (provided in the kit). The solution was mixed by vortexing until completely dissolved. Cell culture medium was replaced with 100 μL fresh medium and 10 μL of 12 mM MTT stock solution was added to each well before incubating the plate for 4 hr at 37°C in humidified incubator. A negative control was included with each assay where wells containing no cells were incubated with 100 μL fresh medium and 10 μL of 12 mM MTT stock

solution alone. Then, 100 μ L of SDS-HCL solution (0.1 g/mL) was added to each well and mixed thoroughly by pipetting. Upon the addition of the SDS-HCL solution, the plate was incubated for another 4 hr at 37°C in humidified incubator. Each sample was mixed again using a pipette before reading the optical density (OD) at 562 nm immediately using a Multi Plate Reader Victor™ X3 (Perkin Elmer).

2.9.3 Cell migration assays

2.9.3.1 Wound scratch method

In vitro wound scratch assay is usually utilised to quantify cellular migration on two-dimensional (2D) surface over time in response to different treatments. At the start of the procedure, three equally distanced horizontal lines (~5mm apart) were drawn with a thin marker pen on the bottom of each 12-well plate (outside) as shown in Figure 2-5. Cells were then plated in a 12-well cell culture plate (specific cell seeding density in Table 2-4). In this experiment, 2 wells per condition (a total of 4 scratches) were included in the analyses. After plating cells were left to recover overnight in the respective complete media. The next day cells (around ~80-90% confluent) were quiesced for 48 hr in the respective quiescence medium (Table 2-2). Before manually scratching the cells creating two cell-free areas allowing them to migrate, a 6 hr EV pre-treatment step was introduced. Following quiescence, the old medium was replaced with either fresh quiescence medium or quiescence medium containing naïve EVs (naEVs) or miRNA-loaded EVs (miEVs; miR-24-3p EVs or miR-224-5p EVs). MiRNAs were loaded into EVs through electroporation and a detailed protocol of the procedure is described in Section 2.10.6.

Following the pre-treatment step, two scratches were made close to the middle of each well using a 200 μ L pipette tip to create an incision-like gap perpendicular to the horizontal lines drawn on the outside of the wells (Figure 2-5). Next, each well was gently washed once with the respective starvation medium to remove any cell debris. Following this step, different experimental conditions were added to the cells. Cells were cultured in starvation medium alone or medium containing either 5% EV-depleted FBS, naEVs, miR-24-3p EVs, miR-224-5p EVs or a combination of those factors. The scratches in each well

were imaged using EVOS XL Core microscope (Life Technologies) at 10X magnification. The three horizontal lines on the bottom of each well were used as a guide to define three specific areas within each 'wound' for imaging allowing images to be taken at the exact same location for each timepoint (Figure 2-5). The images taken immediately after wounding were recorded as 0 hr timepoint. Following 16 hr, 18 hr and 20 hr treatment, each scratch in each well was then imaged again at the same positions. For each image, representing an area of the scratch, 10 distances between points, along both side edges of the scratch, were measured using the Image J software after setting a horizontal line grid at 10,000 pixels² per point (Figure 2-5). Cell migration was quantified and expressed as average percentage of closure of the scratch area compared to the 0 hr baseline distance.

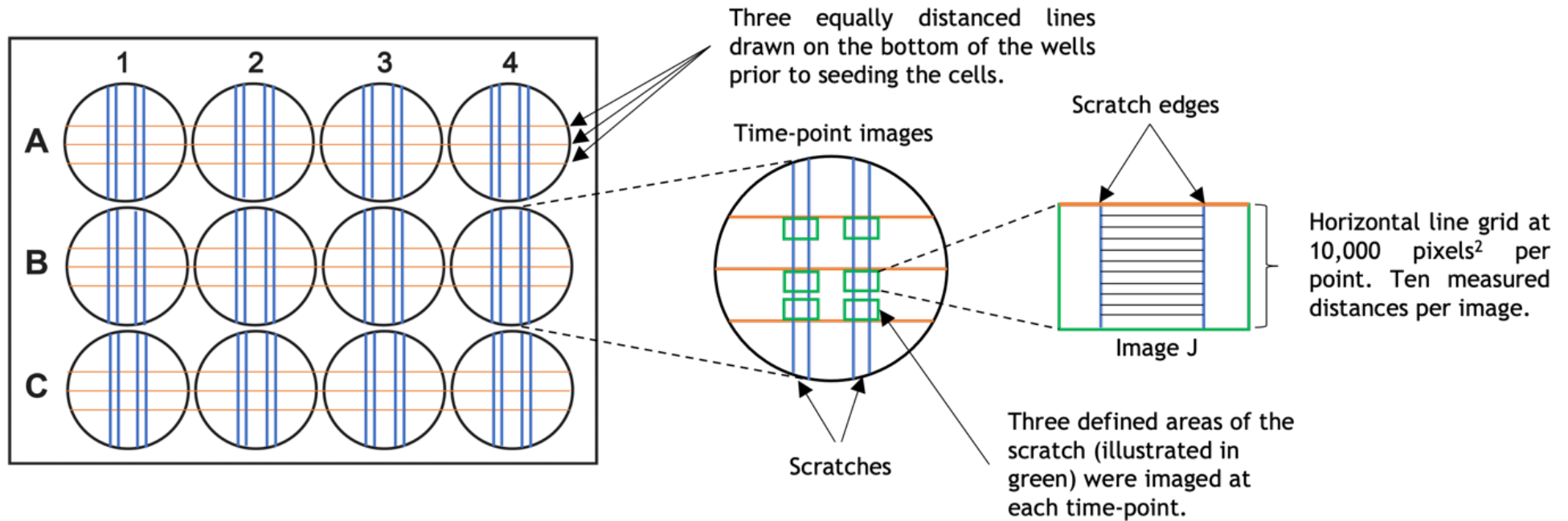
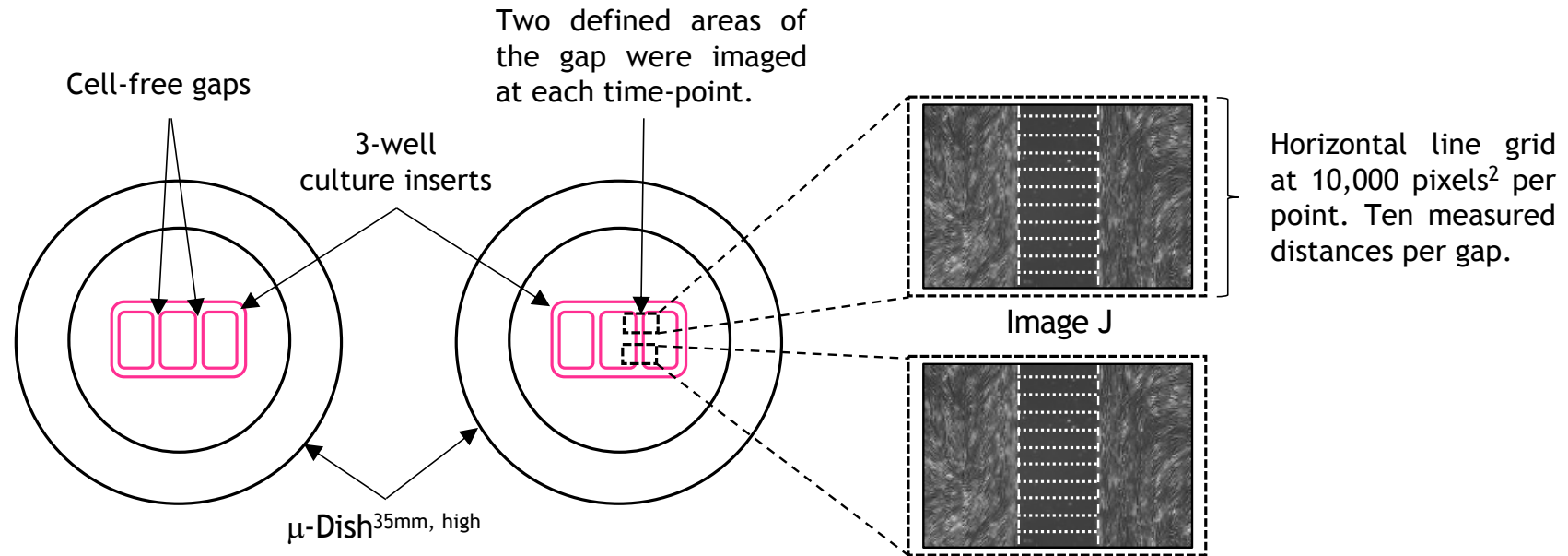


Figure 2-5 Quantification of wound closure. Three equally spaced lines (~5 mm apart) were first drawn on the bottom of the wells (outside) which were then used as guidance to ensure images were always taken at the same three defined areas of the scratch for each timepoint. JPEG files obtained at 10X magnification using an EVOS XL Core microscope were imported into Image J analysis software. The scratch closure was analysed by measuring ten distances between points of the two edges of the scratch for each image after setting a horizontal line grid of 10,000 pixels². Scratch closure at 16 hr, 18 hr and 20 hr were expressed as % closure compared to 0 hr baseline.

2.9.3.2 The gap closure method

In vitro cell migration was also studied in an experimental set up involving no physical injury to the cells. In this assay, a cell-free area was created in a confluent monolayer by physical exclusion. To achieve this, Culture-Insert 3 Well in m-Dish35mm, high (Ibidi, Cat.no.:80366, Thistle Scientific) were used, each containing three distinct wells defining the cells' growth area, thus forming two cell-free gaps with similar width ($500\mu\text{m} \pm 100\mu\text{m}$) (Figure 2-6). Briefly, cells were seeded in the cell culture dishes containing 3-well cell culture insert. Seventy μL of cell suspension (1.5×10^5 cells/ μL) was added to each well allowing the cells to grow in the designated areas only. Cells were left to recover overnight in the respective complete media before quiescing them for 48 hr in the respective media. Each experiment was performed in technical duplicates per condition (a total of 4 cell-free gaps / condition were included in the analyses) (Figure 2-6).

Before removing the insert and allowing the cells to migrate, a 6 hr EV pre-treatment step was introduced. Following quiescence, the old medium was replaced with either fresh quiescence medium or quiescence medium containing naEVs or miEVs (miR-24-3p EVs or miR-224-5p EVs). MicroRNAs were loaded into EVs through electroporation and a detailed protocol of the procedure is described in Section 2.5.6. After this step, the cell culture inserts were removed by using sterile tweezers and cells were washed once with quiescence medium to remove any detached cells and cell debris. Following washing, stimulation medium was added to the cells. During this step, cells were cultured in starvation medium alone or medium containing either 5% EV-depleted FBS, naEVs, miR-24-3p EVs, miR-224-5p EVs or a combination of those factors. Cell-free gaps were imaged at 2 locations (top and bottom of each gap) on the EVOS XL Core microscope (Life Technologies) at 10X magnification. The images taken immediately after removing the cell culture inserts were recorded as 0 hr timepoint. Following a 16 hr stimulation period, the same 2 areas were imaged again. For each image, representing an area of the cell-free gap, 10 distances between points, along both side edges of the gap, were measured using the Image J software after setting a horizontal line grid at $10,000 \text{ pixels}^2$ per point (Figure 2-6). Cell migration was quantified and expressed as average percentage of closure of the cell-free gap area compared to the 0 hr baseline distance.



- 3-well culture-Insert in μ -Dish^{35mm, high}
- two gaps created in each dish
- 2 dishes used / condition
- 4 gaps analysed / condition

Figure 2-6 Quantification of gap closure. Gaps were imaged at the same two locations at 0 hr and 16 hr timepoint JPEG files obtained at 10X magnification using an EVOS XL Core microscope were imported into Image J analysis software. The gap closure was analysed by measuring 10 distances between points of the two edges of the gap for each image after setting a horizontal line grid of 10,000 pixels² per point. Gap closure at 16hr was expressed as % closure compared to 0 hr baseline.

2.10 EV-specific protocols and techniques

2.10.1 Generation of EVs from HSVSMCs treated with VEH/PDGF

In this protocol, 3xT-75cm² flasks of confluent (~90%) HSVSMCs were used to generate EVs per condition - VEH (vEVs) and PDGF (pEVs). Cells were first washed with DPBS and then quiesced in the appropriate starvation medium for 48 hr. Next, the medium was removed, cells were washed with DPBS again and then treated with either VEH (0.2% BSA 10mM acetic acid) or PDGF (20 ng/mL) for another 48 hr before CCM was collected (\approx 45 mL CCM/condition) and EVs were isolated (Figure 2-7A). This protocol was followed to generate EVs from HSVSMCs for the majority of the experiments in this project. An adapted version of this protocol was used for one EV isolation optimisation experiment and description of any modifications to the original protocol can be found in the relevant section.

2.10.2 Generation of HSVSMC EVs for miRNA overexpression studies

In this protocol, confluent (~90%) HSVSMCs in T-75cm² flasks were used to generate EVs for miRNA overexpression studies. Cells were first washed with DPBS and then quiesced in the appropriate starvation medium (Table 2-2) for 48 hr. After that, the medium was removed, cells were washed with DPBS again and fresh quiescent medium was added to the cells for another 48 hr before CCM was collected and EVs were isolated (Figure 2-7B).

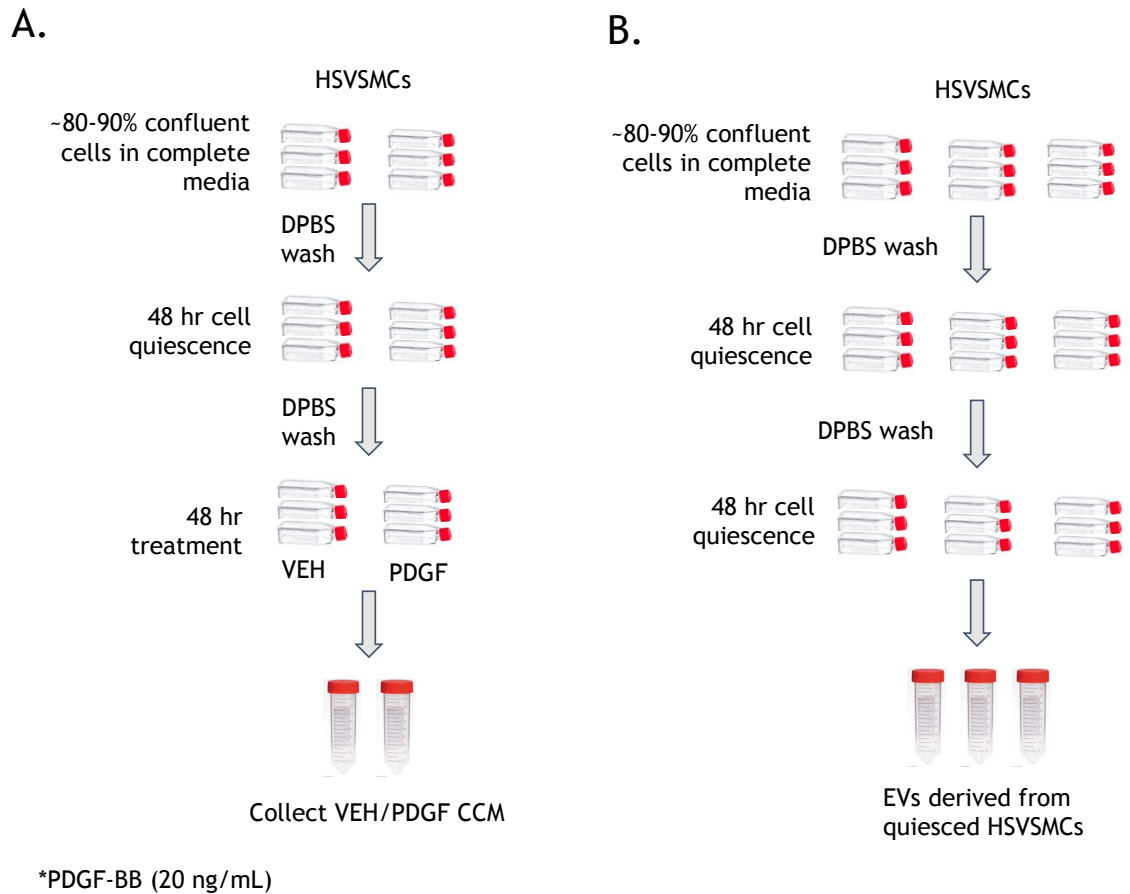


Figure 2-7 Protocols for EV generation from HSVSMCs. Two different HSVSMC- EV generation protocols were utilised and the use of each was experiment-dependent: (A) VEH EVs (vEVs) and PDGF EVs (pEVs); and (B) EVs derived from HSVSMCs under quiescence. Protocol (A) was used to generate EVs used in studies assessing the effect of unmodified EVs in cells, whereas protocol (B) was used to generate EVs for studies assessing the effect of miRNA loaded EVs in cells.

2.10.3 EV isolation methods

2.10.3.1 EV isolation from CCM samples

All CCM EV isolations carried out used size exclusion chromatography (SEC) qEVsingle columns (Izon, New Zealand) fitted onto an automated fraction collector (AFC, Izon, New Zealand) (Figure 2-8). To clarify CCM (\approx 45 mL CCM/condition) from detached cells, contaminating apoptotic bodies, microvesicles and cell debris it was processed as follows: CCM samples were subjected to centrifugation at 300 RCF for 10 min at 4°C (step 1). Supernatant was collected and the centrifugation step was then repeated again at 10,000 RCF for 40 min at 4°C (step 2). Prior to loading 100 μ L of clarified CCM onto the qEVsingle column, it was concentrated using Vivaspin 20 centrifugal concentrator (MWCO 10kDa; Sigma Aldrich) up to 200 μ L which was the lowest achievable volume of concentrate when concentrating 45 mL of CCM (step 3). Then, 100 μ L of EV-concentrated CCM was overlaid on qEVsingle column followed by elution with DPBS (step 4). Two separate EV isolations from 100 μ L of concentrated CCM were carried out per condition and during each isolation 3x200 μ L fractions 1-3 (F1-3) were collected immediately after 1.25 mL of void volume (VV) had passed through the column which was also collected (\sim 1.25 mL). After each isolation, the VV and fractions F1-3 were all pooled (total of \sim 1.85 mL of EV preparation). At the end of the isolation step, both EV preparations per condition were pooled together (2x1.85 mL) and re-concentrated back to 100-200 μ L using Amicon centrifugal concentrator (MWCO 10 kDa; Sigma Aldrich, UK) (step 5). The final volume to which each sample was concentrated was kept consistent within experiments.

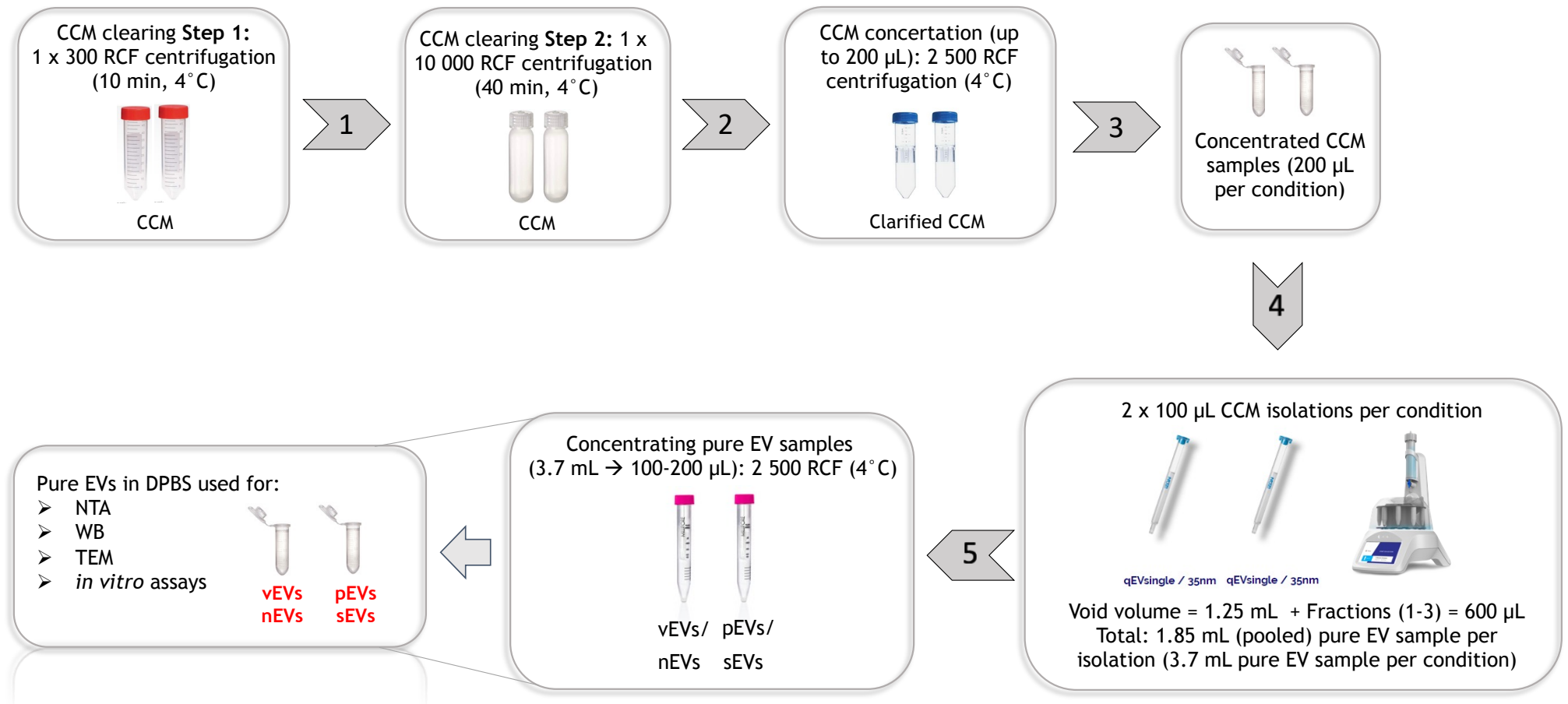


Figure 2-8 Schematic representation of the EV isolation protocol for CCM from HSVSMCs. The diagram summarises the steps involved in the EV process, including CCM clearing steps (1 and 2), CCM concentration step (3), qEV size exclusion chromatography step (4), and the final pure EV sample concentration step (5). Abbreviations: CCM, culture conditioned medium; VEH; vehicle; PDGF, platelet-derived growth factor; vEVs, VEH EVs; pEVs, PDGF EVs; nEVs, non-scratched EC EVs; sEVs, scratched EC EVs; NTA, nanoparticle tracking analysis; WB, western blotting; TEM, transmission electron microscopy.

2.10.3.2 EV isolation from serum samples

Total Exosome Isolation Reagent (Invitrogen, ThermoFisher Scientific) was used to isolate EVs from serum samples. Serum samples were also cleared from dead cells, debris and macroparticles before isolating EVs. All samples were first subjected to centrifugation firstly at 2000 RCF for 30 min at RT and then at 10,000 RCF for 40 min at RT. After the second centrifugation step, the supernatant was carefully transferred to a new Eppendorf tube without disturbing the pellet. The required volume of clarified serum was then transferred to a new tube and the Total Exosome Isolation Reagent (1/5 the volume of clarified serum) was also added to the tube. The mixture was then vortexed until a homogeneous solution with cloudy appearance was achieved. Following a 30 min incubation step at 4 °C, the mixture was subjected to centrifugation again at 10,000 RCF for 30 min at RT. The supernatant was gently removed without disturbing the pelleted EVs at the bottom of the tube. Using a pipette, the pellet was completely re-suspended into an appropriate volume of 1X DPBS (50 µL). The volume of DPBS that was used to re-suspend the pellet, and therefore the final EV volume of the EV preparation, depended on the starting serum volume (e.g., 100 µL of starting serum volume required 25-50 µL DPBS to re-suspend the pellet).

2.10.4 Nanoparticle tracking analysis

EVs were visualised and their size and concentration measured using Nanoparticle Tracking Analysis (NTA). In terms of size (nm), EV populations were characterised by both mean and mode size measurements, representing the average size of EVs and the most frequent EV size within a population, respectively. All samples were diluted in DPBS to a final volume of 1 mL and analysed using a NanoSight LM14 (Malvern Instruments Ltd) equipped with a 532-nm laser and a high-sensitivity sCMOS camera. Samples were introduced manually with a 1 mL syringe directly into the sample chamber which was then placed onto the microscope stage. A laser beam passing through the sample chamber illuminated the particles in solution allowing their visualisation through the microscope oculars. The image was then diverted to the camera and the focus was adjusted using a 20X magnification until a clear image of the particles within the field of view was achieved. Five videos of 60 sec each were captured

for each sample recording the particles moving under Brownian motion. Individual particles were tracked using NanoSight NTA 3.2 software (Malvern Instruments Ltd, UK) at camera level 14-16. For analysis, the following settings were used: screen gain - 10, and detection threshold - 4.

2.10.5 Transmission electron microscopy analysis

To assess EVs' morphology, EVs were visualised on a transmission electron microscope (TEM). Following isolation, EVs in DPBS were mixed with 4% PFA solution in 1:1 ratio. Samples were transported on ice and kept at 4-8 °C until processed. The technique was performed by Mrs Margaret Mullin in the University of Glasgow TEM facility using a JEOL 1200 EX TEM running at 80kV. PFA fixed EVs were processed according to a published protocol (Théry et al., 2006). Tagged Image File Format (TIFF) images were captured on a CANTEGA 2Kx2K camera using Olympus ITEM software.

2.10.6 Loading of miRNAs into EVs (optimised protocol)

The process of electroporation, or electropermeabilization, involves the use of high voltage electric pulses with short duration that cause reversible permeabilization of the EV membranes resulting in the formation of pores which allow small molecules like miRNAs (oligonucleotides) to be inserted into the EVs (Lennaárd et al., 2022; Pomatto et al., 2022). Synthetic miRNAs, hsa-miR-24-3p (cat.no: 4464067/mirVana® miRNA mimic/ ID: MC10737, ThermoFisher Scientific) and hsa-miR-224-5p (cat.no: 4464067/mirVana® miRNA mimic/ ID: MC35019, ThermoFisher Scientific), were exogenously loaded into EVs via electroporation using the Electroporation Cuvettes (Sterile, 1mm electrode, Red Cap; cat. no.: E6-0050, Geneflow) and a Bio-Rad MicroPulser™ Electroporator system. A few hours before the electroporation procedure, the required number of electroporation cuvettes were left in the freezer at -20 °C to cool down, thus, ensuring that the system did not overheat while being used.

Throughout this thesis, in the context of electroporated EVs, miRNA mimics hsa-miR-24-3p and hsa-miR-224-5p are referred to as miR-24-3p and miR-224-5p only without specifying the species (*homo sapiens*) i.e., miEVs - miR-24-3p and miR-224-5p.

Step 1: Sample preparation

The EV concentration was determined by NTA after which the EV preparation was split into 3 equal volume samples - two EV samples receiving different miRNA mimics, miR-24-3p EVs and miR-224-5p-EVs, and one sample receiving no miRNA mimic, including no scramble or no cel-miR-39 (naïve EVs or naEVs). The required amount of miRNA mimic for EV samples was always calculated based on the EV concentration determined by NTA (66 pmol of miRNA mimic was used for 1.0×10^{10} EVs). For each miRNA mimic, the desired amount of mimic was diluted in 50 mM Trehalose (Cat.No.: PHR1344-500MG, Sigma-Aldrich) achieving the same volume as the EV sample. Two of the EV samples were mixed with either one of the miRNA mimic samples (miR-24-3p and miR-224-5p) or with an equal volume of 50 mM Trehalose containing no miRNA mimic (naEVs). Once sample mixtures were ready, they were incubated on wet ice for 45 min (Figure 2-9). Trehalose was used to prevent EV aggregation, ensuring efficient incorporation of miRNAs into the EV particles.

Step 2: Electroporation process

After the incubation step, a maximum of 125 μ L of EV/miRNA mimic sample was added to an electroporation 1 mm electrode sterile cuvette (Geneflow, Cat. No.: E6-0050) and given a 400mV pulse lasting for approximately 3 seconds. Immediately after the electroporation pulse, 875 μ L of ice cold 1% (w/v) sterile BSA (Sigma-Aldrich) was added to the cuvette and mixed carefully with the EV/miRNA mimic sample by pipetting up and down. The sample was then transferred to a falcon tube. If necessary, this process was repeated until all of the EV/miRNA mimic sample was electroporated. Electroporated EV/miRNA mimic sample was left overnight at 4°C. The same process was followed to prepare the naïve EV sample.

The next day, both the miRNA loaded EV (miEV) samples and also the naïve EV (naEV) samples were concentrated to 200 μ L using the Amicon centrifugal concentrator. The EVs were then re-isolated and re-concentrated following the isolation protocol used to isolate EVs from CCM samples (Section 2.5.3.1). Isolated miEVs and naEVs were stored at 4°C until used the next day. EV sample concentration was always measured by NTA prior to carrying out *in vitro* studies.

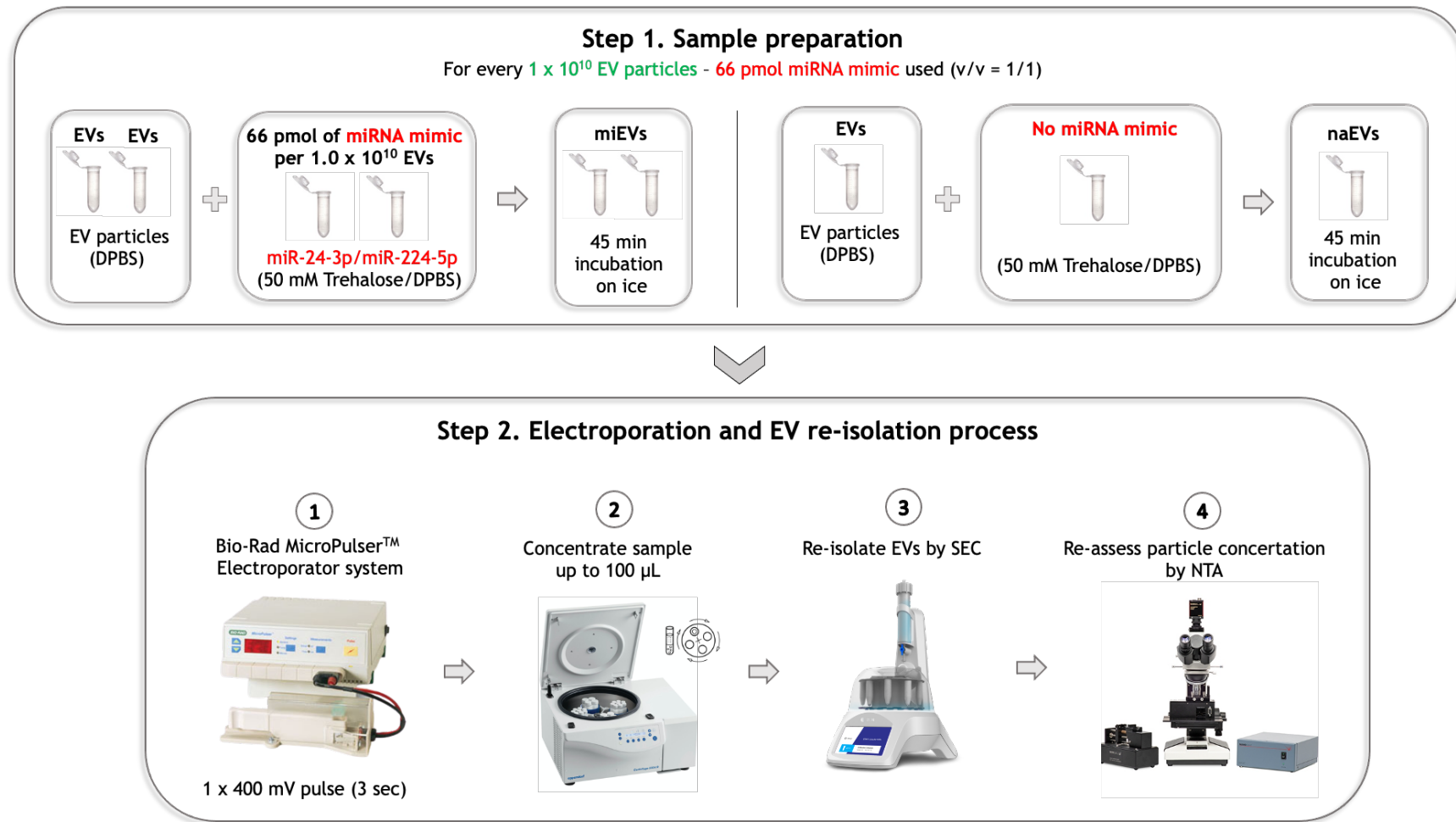


Figure 2-9 Schematic representation of the optimised protocol for loading miRNA mimics into EVs. EV samples were first mixed with miR-24-3p, miR-224-5p in 50 nM Trehalose/DPBS or 50 nM Trehalose/DPBS alone. Sample mixtures were then incubated for 45 min on ice before electroporating miRNA mimics into the EVs. After electroporation, EVs were left overnight in the fridge before re-concentrating the sample to 100 μ L and re-isolating electroporated EVs. Finally, EV sample concentration and EV size were checked by NTA before proceeding to using the EVs for *in vitro* experiment.

2.11 Next generation sequencing – based profiling of EV-related miRNAs

Differential expression analysis of the small RNA component (small RNA sequencing; RNAseq of EVs derived from HSVSMCs under physiological versus pathological conditions) was carried out. EVs used in this study were generated by HSVSMCs as described in Section 2.10.2 and EVs were isolated as described in Section 2.10.3.1. MiRNeasy Mini Kit (Qiagen, Cat No./ID: 217004) was used for the purification of total RNA, including miRNAs, from EVs as described previously (Section 2.6.1 and Section 2.6.2). These samples were then sent for next generation sequencing (NGS)-based small RNA sequencing and analysis in the Glasgow Polyomics facility.

Initial RNAseq data analysis to identify differentially expressed miRNA genes was carried out by Dr Graham Hamilton in the Glasgow Polyomics facility. Briefly, miRNA sequencing libraries were prepared from total RNA using the SMARTer® smRNA-Seq Library Kit for Illumina® (TaKaRa Clontech, Cat No. 635031). Libraries were then sequenced in paired-end mode (2 × 75 bp) on the NextSeq™ 500 platform (Illumina®). Before read mapping, raw sequence reads were trimmed to remove the Qiagen miRNA 3' adapters and poor-quality bases using the command-line tool CutAdap (Martin, 2011). Bases with a Phred score < 15 were trimmed to remove undesired sequences ensuring a good quality genome alignment. Only reads with the adapters present were retained for analysis whereas those without the adapters were discarded. A quality control check on the raw sequence data were performed using FastQC software before and after trimming. The trimmed reads were then aligned to the reference genome (GRCh38, release 79) using an open-source software - Bowtie (version 1.0.0) (Langmead et al., 2009). The number of reads aligning to known small RNAs, as defined by their biotype - snRNA, snoRNA, scaRNA or sRNA, was obtained in 'gtf' file for human (GRCh38, release 79) using bedtools (Quinlan and Hall, 2010). The base mean, log₂ fold change (z-scored), and p-value of <0.05 adjusted for an FDR <5% was determined for comparison of individual small RNA species. The resulting counts for each small RNA specie were recorded in tables which were then used to create a combined counts table for all samples. The combined counts data was then used for input into DESeq2 for differential expression

analysis (Love et al., 2014). Four biological replicates per condition were sequenced.

2.12 Bioinformatics

2.12.1 Identifying the mature forms of differentially expressed miRNAs

The count-based differential expression analysis of RNAseq data was supplied by Glasgow Polyomics in a comma separated values (.csv) format and provided information about the differentially expressed miRNA genes between vEVs (control EVs) and pEVs. An Integrative Genomic Viewer (IGV) software was used to determine exactly which miRNAs, in their mature form, were identified as differentially expressed between the two treatment groups (Figure 2-10). Relevant alignment files (.bam) were visualised using IGV and read sequences mapped to a human reference genome (Genome Reference Consortium h38, GRCh38). As certain target loci within the genome encode for different genes on both the forward and reverse strand, mapped reads were observed for their directionality to infer which gene at the locus was being actively transcribed in the sample. If reads were encoded on the reverse DNA strand, the genomic DNA read sequence was first reverse complemented before transcribing it to the corresponding RNA sequence to generate a sequence which could be cross-referenced to a miRNA database (miRBase) (Figure 2-10A). The miRBase database was used to determine which mature form of each identified miRNA was differentially expressed between vEVs (control EVs) and pEVs. As miRBase curates on the forward strand, it was necessary for all read sequences to be presented in the same orientation to allow direct comparison. If the genomic DNA read sequence mapped directly to the forward DNA strand in IGV, it was not reverse complemented first before generating the corresponding RNA sequence and cross-referencing it to miRBase (Figure 2-10B). The above process of determining the correct mature form of differentially expressed miRNAs was cross-checked by performing a BLAST (Basic Local Alignment Search Tool) search in Ensembl to confirm findings.

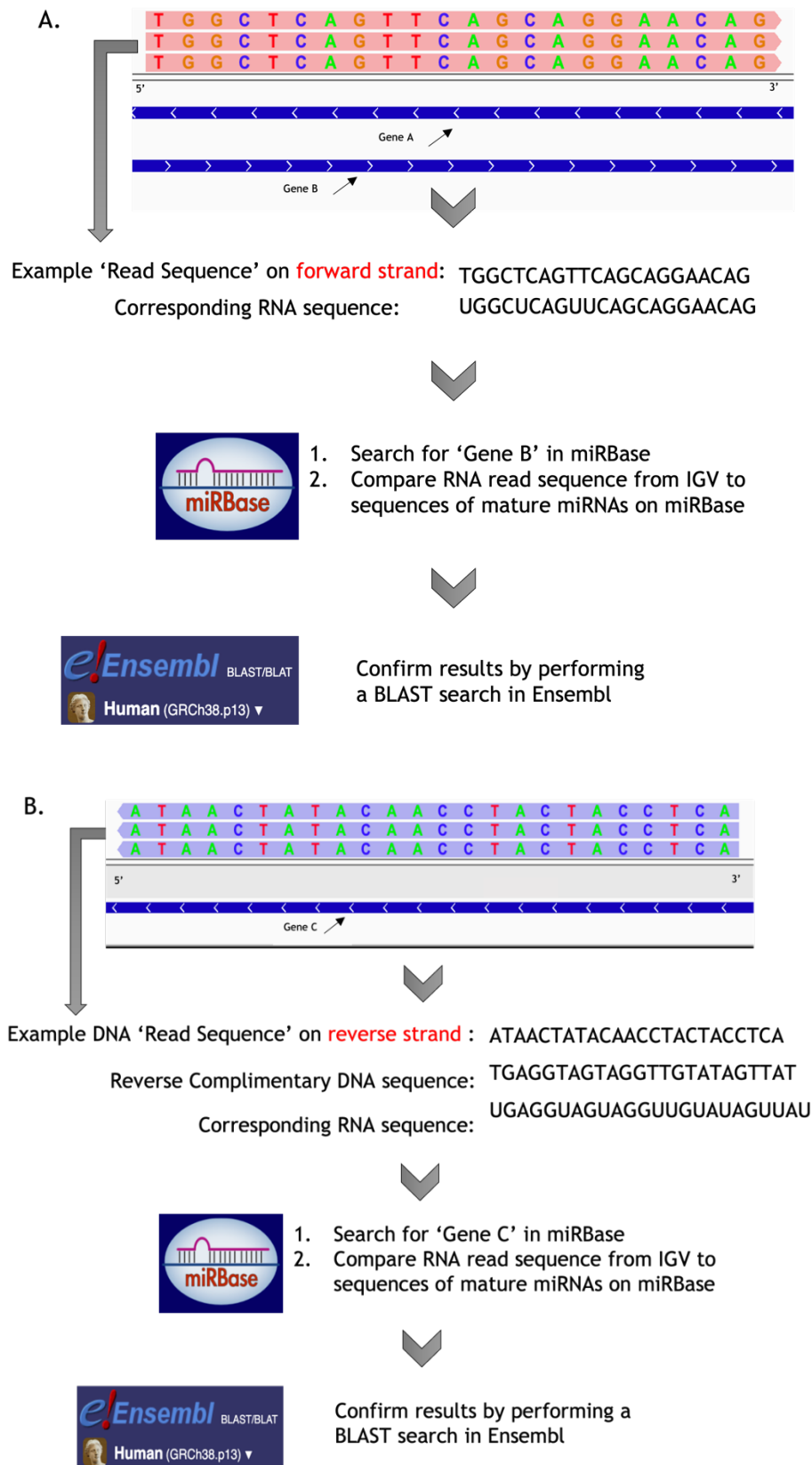


Figure 2-10 Identifying the mature forms of differentially expressed miRNAs. Schematic representation of the workflow followed to identify the mature forms of differentially expressed miRNAs between vEVs (control EVs) and pEVs. Workflow (A) was followed when the DNA read sequence mapped to a gene encoded on the forward DNA strand. Alternatively, workflow (B) was followed when the DNA read sequence mapped to a gene encoded on reverse DNA strand.

2.12.2 Identifying potential ‘true’ miRNA gene targets

2.12.2.1 Bioinformatics strategy and data gathering

Basic bioinformatics analysis was carried out to identify potential ‘true’ miRNA gene targets for all differentially expressed miRNAs, the mature forms of which were identified through analysis described in Section 2.12.1. Firstly, four web applications using twelve different prediction algorithms were used to obtain datasets with predicted miRNA gene targets for each miRNA. While still available, data generated from 9/12 algorithms was accessed through miRWalk 2.0 in Jan-Feb 2021. MicroRNA: mRNA gene interactions in 3’ UTR, 5’ UTR and CDS binding regions were considered during the analysis. Additionally, two curated databases (miRTarBase v8 and DIANATarBase v8) were also used to obtain datasets of experimentally validated miRNA gene target interactions for each miRNA. All datasets were either downloaded directly in CSV format or first downloaded in XLSX format and then converted to CSV.

The concept of the strategy followed to obtain a list of potential ‘true’ miRNA gene targets for each miRNA of interest is described in Chapter 4. Firstly, for each miRNA, a set of predicted gene targets by at least 7 out of all 12 prediction algorithms was created (subset 1). Then, a set of gene targets found in at least one of the two curated databases of experimentally validated miRNA gene targets was also obtained (subset 2) for each miRNA. Finally, an intersection of the two subsets (1 and 2) was used to obtain a final list of potential ‘true’ miRNA gene targets (dataset 3) for each miRNA of interest.

2.12.2.2 Automation of the bioinformatics data analysis process

To allow precise comparisons of datapoints on a large scale in a timely manner while avoiding human error, the above process of data analysis was automated using PHP: hypertext processor (PHP) - a general purpose scripting language. Integrated development environment (IDE) software application PhpStorm 2018.3 was used by Vassil Kalphov to develop and execute PHP scripts which followed the predefined data analysis strategy designed to answer the research question. The raw data was split into structural folders and CSV files according to the source algorithm/database and miRNAs of interest.

In the first step of the automation process, the aim was to produce one file per miRNA in the form of a binary matrix table that used the raw data files (containing the predicted and validated miRNA gene targets) for each miRNA as input (Figure 2-11). For clarity these files were referred to as 'aggregated matrix' files. In this matrix, each row represented a specific gene target. The gene targets included in the matrix were a collection of all unique gene targets that were found in the raw datasets of predicted/validated gene target interactions. The columns indicated whether a specific condition was met for a specific gene target based on the data provided in the source files. The first 12 condition columns corresponded to the 12 prediction algorithms and indicated if a miRNA: gene target interaction was predicted by the algorithm (Figure 2-11). The next two columns corresponded to the two curated databases and indicated if a miRNA: gene target interaction was found in the database (Figure 2-11). Additionally, four more columns were added representing whether a condition related to the other columns was satisfied (Figure 2-11). These additional columns indicated: if the miRNA: gene target interaction was predicted by at least 7 out of 12 prediction algorithms (column Q); if the miRNA gene target was found in at least one of the two curated databases (column R); if the miRNA: gene target interaction was predicted by at least 7 out of 12 algorithms) and was also found in at least one of the two curated databases (column S); and if the miRNA: gene target interaction was predicted by at least one of the 12 prediction algorithms (column T). Therefore, the subsets (1, 2 and 3) described in Figure 2-11 were represented by columns (Q, R and S respectively) in the matrix files produced by the automation script for each miRNA of interest.

	A	B	C	D	E	F	G	H	I	J	K	L	M	N	O	P	Q	R	S	T
1	miRNA	Gene Symbol	miRWalk3.0	miRDB	Microt4	miRanda	mirbridge	miRMap	miRNAMap	Pictar2	PITA	RNA22	RNAhybrid	TargetScan	miRTarBase (validated)	DIANA TarBase (validated)	At Least 7 / 12 Datasets	Validated	At Least 7 / 12 Datasets + validated	At Least 1 Dataset
2	hsa-miR-24-3p	HARS2	1	0	0	0	0	0	0	0	0	1	1	0	0	0	0	0	0	1
3	hsa-miR-24-3p	ZMAT2	1	0	0	0	0	0	1	0	0	1	1	0	1	0	0	1	0	1
4	hsa-miR-24-3p	PCDHA1	1	0	0	0	0	1	0	0	0	0	1	0	0	0	0	0	0	1
5	hsa-miR-24-3p	PCDHA2	1	0	0	0	0	1	0	0	0	0	1	0	0	0	0	0	0	1
6	hsa-miR-24-3p	PCDHA4	1	0	1	1	0	1	0	0	0	1	1	0	0	0	0	0	0	1
7	hsa-miR-24-3p	PCDHA5	1	0	0	0	0	1	0	0	0	0	1	0	0	0	0	0	0	1
8	hsa-miR-24-3p	PCDHA6	1	0	1	0	0	1	0	0	0	1	1	0	0	0	0	0	0	1
9	hsa-miR-24-3p	PCDHA7	1	0	1	1	0	1	0	0	0	1	1	0	0	0	0	0	0	1
10	hsa-miR-24-3p	PCDHA8	1	0	0	0	0	1	0	0	0	1	1	0	0	0	0	0	0	1
11	hsa-miR-24-3p	PCDHA9	1	0	1	1	0	1	0	0	1	1	1	0	0	0	1	0	0	1
12	hsa-miR-24-3p	PCDHA10	1	0	0	0	0	1	0	0	0	1	1	0	0	0	0	0	0	1
13	hsa-miR-24-3p	PCDHA11	1	0	0	0	0	1	0	0	0	1	1	0	0	0	0	0	0	1
14	hsa-miR-24-3p	PCDHA12	1	0	0	0	0	1	0	0	0	0	1	0	0	0	0	0	0	1
15	hsa-miR-24-3p	PCDHAC1	1	0	0	0	0	1	0	0	0	1	1	0	0	0	0	0	0	1
16	hsa-miR-24-3p	PCDHAC2	1	0	0	1	0	1	0	0	0	1	1	0	0	0	0	0	0	1
17	hsa-miR-24-3p	PCDHB1	1	0	0	0	0	0	0	0	0	1	1	0	0	0	0	0	0	1
18	hsa-miR-24-3p	PCDHB2	1	0	0	0	0	0	0	0	0	1	1	0	1	0	0	1	0	1
19	hsa-miR-24-3p	PCDHB3	1	0	0	1	0	1	0	0	1	1	1	0	0	0	0	0	0	1
20	hsa-miR-24-3p	PCDHB4	1	0	0	0	0	0	0	0	0	1	1	0	0	0	0	0	0	1
21	hsa-miR-24-3p	PCDHB5	1	0	0	0	0	0	0	0	0	1	1	0	0	0	0	0	0	1
22	hsa-miR-24-3p	PCDHB6	1	0	1	1	0	1	0	0	1	1	1	0	0	0	1	0	0	1
23	hsa-miR-24-3p	PCDHB7	1	0	0	0	0	0	0	0	0	1	1	0	0	0	0	0	0	1

Figure 2-11 Identification of potential ‘true’ miRNA gene target interactions.

An example of the binary matrix table produced based on which potential ‘true’ miRNA gene target interactions were identified for each miRNA of interest. Columns A and B represent a specific miRNA: gene target interaction. Columns D-N correspond to the 12 prediction algorithms used to predict potential miRNA: gene target interactions. Columns O and P correspond to the curated databases searched for validated miRNA: gene target interactions. Columns Q-T were the additional columns indicating whether a specific condition related to the other columns was satisfied. The above table represents a small Section of the full table generated for miR-24-3p and such tables were produced for each miRNA in separate files. These files were referred to as ‘aggregated matrix’ files.

In the second step, a new binary matrix table file was created through another automation script that used the matrix table files generated at the previous step as input. The resulting file from this step was referred to as 'potential true gene targets matrix' file. The output of the script executed at this step was a single binary matrix (Figure 2-12) in CSV format that contained the previously identified potential 'true' miRNA gene targets for all miRNAs of interest (column S from the 'aggregated matrix' files shown in Figure 2-11). The rows in this matrix represented the set of unique miRNA gene targets (column S from the 'aggregated matrix' files shown in Figure 2-11) for all miRNAs and the columns corresponded to the miRNAs of interest (Figure 2-12). The values ('0' or '1') in the binary matrix indicated if a specific miRNA gene target was identified as potential 'true' gene target (found in column S in the 'aggregated matrix' file) for the corresponding miRNA based on the input files generated at the previous step. The purpose of creating the second binary matrix was to allow the extraction of both: a list of potential 'true' miRNA gene targets for a single miRNA, and also a list of miRNA gene targets common between two or more miRNAs. The CSV file was opened in Microsoft Excel (Version 16.5) and the relevant filters were applied depending on the requirements. After filtration of the data, a list of genes (in official gene name format) satisfying specific requirements was available to extract and work with. A list of common miRNA gene targets between the three miRNAs of interest were identified and the data was visualised using a simple Venn diagram showing the relationship between the miRNAs of interest in terms of shared gene targets.

A	B	C	D	E	F
Gene Symbol	hsa-miR-24-3p	hsa-miR-409-3p	hsa-miR-21-5p	hsa-let-7a-5p	hsa-miR-224-5p
DIAPH1	1	0	0	0	0
RBM27	1	0	0	0	0
PDGFRB	1	0	0	0	0
NDST1	1	0	0	0	0
CCDC69	1	0	0	0	0
G3BP1	1	0	0	0	0
LARP1	1	0	0	0	0
ADAM19	1	0	0	0	0
DUSP16	1	0	0	0	0
CREBL2	1	0	0	0	0
CDKN1B	1	0	0	0	0
SEC11A	1	0	0	0	0
ZNF592	1	0	0	0	0
AKAP13	1	0	0	0	0
ABHD2	1	0	0	0	1
AP3S2	1	0	0	0	0
ZNF710	1	0	0	1	0
HDDC3	1	0	0	0	0
MEF2A	1	0	0	0	0
PDPK1	1	0	0	0	0

Figure 2-12 A Section of the final binary matrix table. 'Potential true gene targets matrix' file was produced based on the data in the 'aggregated matrix' files created in the first step of the automation process. The rows in this table represent all unique potential 'true' miRNA gene targets identified for each miRNA (column S in the 'aggregated matrix' files) following the strategy described in Figure 2-11. The columns in this matrix corresponded to the miRNAs of interest. The binary values indicated whether a target gene was identified as a potential 'true' target for a given miRNA.

2.12.3 Functional annotation and gene set enrichment analysis

Once the 'true gene targets matrix' file was created, a list of potential 'true' miRNA gene targets was extracted for each miRNA of interest. These lists of genes were used as input to perform GSEA using an online functional annotation tool - ToppGene Suite.

ToppGene Suite is a web-based bioinformatics application. It is a powerful enrichment analysis tool utilising multiple biology knowledgebases and different analytical tools to extract biological meaning from large numbers of gene collections. ToppGene was used to interpret the set of genes identified as potential 'true targets' for each miRNA of interest. Gene list functional enrichment analysis was performed based on different annotation sources including the Kyoto Encyclopedia of Genes and Genomes (KEGG), BioCarta, Panther DB, The Molecular Signatures Database (MSigDB) and the biological processes classification category of the Gene Ontology (GO) term system. Benjamini-Hochberg's (B&H) (Benjamini and Hochberg, 1995) multiple testing correction method was used to control the FDR and determine statistical significance ($p_{adj.}/q\text{-value} < 0.05$). Therefore, the resulting output tables contained only annotation terms for which the input gene list was found to be strongly enriched. Next, the output tables containing significantly enriched annotation terms within the biological processes classification category of the GO term system were filtered through keywords (Table 2-9) to allow suitable visualisation of the output data in the form of bar charts.

Table 2-9 List of keywords used to filter through significantly enriched biological processes. The keywords in this table were used to filter through the significantly enriched annotation terms within the biological processes classification category of the GO term system. This step was carried out for both miR-24-3p and miR-224-5p.

Keywords	
'Proliferation' 'Cell growth' 'Cancer' 'Protein kinase' 'Ras protein' 'MAPK' 'AKT' 'TGF-beta' 'Platelet-derived growth factor receptor signalling pathway' 'Smooth muscle cell' 'Shear stress' 'Angiogenesis'	'Division' 'Cell cycle' 'Wounding' 'Cell death' 'Migration' 'Cell motility' 'Locomotion' 'Cytoskeleton' 'Actin' 'Adhesion' 'Apoptosis' 'Apoptotic'

2.13 Statistical Analysis

GraphPad Prism 9.0 software package was used to perform all statistical analyses. For *in vitro* experiments, N numbers represent cells derived from different patients/different biological replicates. The data generated in the form of absorbance values in colorimetric assays (BrdU and MTT) were normalised prior to statistical analysis to reduce the individual error associated with data points and to account for inter-patient cell variability related to cells' response to treatment and the magnitude of absorbance changes. To normalise the data for each individual N, the average of all blank corrected absorbance values generated for one biological replicate across all experimental groups (dataset average) was first calculated. Then, for BrdU assays, the ratio of the blank corrected average value of the technical triplicates for each experimental group within one biological replicate to the calculated dataset average was calculated and plotted. For MTT assays, each blank corrected average value of the technical triplicates for each experimental group within one biological replicate was expressed as percentage of the dataset average before

transforming the values to display the % cell viability relative to untreated cells. Statistical analyses were carried out using untransformed normalised values for both MTT and BrdU experiments. Similarly, for gene expression studies samples were always amplified in technical triplicates and qRT-PCR data were analysed using ΔCt values.

Unless otherwise stated, data are presented as mean \pm standard error of the mean (SEM). Comparisons between multiple groups were made using a repeated measures one-way ANOVA test with Tukey's post-hoc correction unless otherwise stated. *In vitro* experiments were carried out in triplicate and were repeated at least three independent times unless otherwise stated. Where indicated, comparisons between two groups were made using a paired Student's t-test. *In vivo* experimental data was analysed using an ordinary one-way ANOVA test with either Tukey's or Dunnett's post-hoc correction for multiple comparisons depending on the comparisons made. P-values below 0.05 were considered statistically significant. N numbers and relevant statistical tests are detailed in each figure legend.

Chapter 3 Optimisation of a size exclusion chromatography-based method for isolation and characterisation of HSVSMC-derived EVs

3.1 Introduction

3.1.1 Vascular injury and PDGF signalling

Vascular injury stimulates the secretion of growth factors, including PDGF, by different cells associated with the vessel wall. PDGF production induces a phenotypic change in VSMCs through a conversion of their state from a quiescent, “contractile”, to a proliferative, “synthetic” - an event characterized by increased cell proliferation, migration, and ECM secretion (Marmur et al., 1992). In general, phenotypic modulation of VSMCs mediated by PDGF is physiological and it contributes to the maintenance of vascular homeostasis. However, aberrant PDGF signalling has been implicated in vascular remodelling, and subsequently in the development of several vascular pathologies including neointimal formation observed in VGD and ISR, and atherosclerosis (Barst, 2005; Hart and Clowes, 1997; Li et al., 2011; Sterpetti et al., 1996b). The pathogenesis of neointimal formation is characterized by the dysfunctional regulation of major aspects of the vasculature resulting in abnormal proliferation, migration and apoptosis of ECs and VSMCs (Borin et al., 2009; de Vries et al., 2016; Marx et al., 2011; Yahagi et al., 2016). As intercellular communication is essential for not only the maintenance of tissue homeostasis but also for disease development/prevention, understanding the possible means of VSMC self-regulation in the context of vascular injury and pathophysiological PDGF signalling might provide important insights into the development of neointimal formation.

3.1.2 Extracellular vesicle characterisation: guidelines

As interest in the biological functions of EVs is growing exponentially in multiple scientific fields, the need for standardisation in EV research is becoming increasingly important for assuring and improving EV research quality. In 2014, The International Society for Extracellular Vesicles (ISEV) proposed Minimal Information for Studies of Extracellular Vesicles (MISEV) guidelines for the field (Lötvall et al., 2014). Based on evolution of the collective knowledge, the ‘MISEV2014’ guidelines were updated in 2018 (Théry et al., 2018).

The MISEV guidelines were created to promote adherence to minimal experimental requirements for defining extracellular vesicles and their functions

in order to improve the quality of EV research. The main recommended points in these guidelines involved: [1] the detailed reporting of the source material of EVs and isolation methods used; [2] detailed characterisation of the protein content and quantification of EV-enriched proteins in EV preparations. The suggested methods include Western blot, flow cytometry and mass spectrometry. Importantly, according to the 'MISEV2018' guidelines, a single particle characterization is also recommended by two complementary methods such as imaging by electron microscopy, atomic force microscopy, fluorescence microscopy or sizing with NTA or dynamic light scattering (DLS) (Théry et al., 2018). Additionally, recommendations concerning the experimental controls when performing functional analysis were also included, e.g., particles isolated from unconditioned medium, as there is serious concern of contamination if EV purification was not carried out properly (Théry et al., 2018).

3.1.3 Isolation of extracellular vesicles

Previously, the most widely used isolation techniques in EV research were differential ultracentrifugation (DU) and the more specific type of ultracentrifugation - density gradient ultracentrifugation, resulting in purer EV preparations with less co-isolated entities. However, more recently several other methods have been developed based on different EV characteristics including SEC, EVs isolated by precipitation, membrane affinity and protein affinity (Brennan et al., 2020; Doyle and Wang, 2019; Veerman et al., 2021). All of these commonly used EV isolation techniques have both advantages and disadvantages, but first and foremost they all isolate a mixture of the different EV subpopulations including exosomes, microvesicles and sometimes apoptotic bodies (Davidson et al., 2023; Doyle and Wang, 2019). None of the established methods for EV isolation used currently offer a complete separation of pure EVs from the biological fluid. Additionally, studies have suggested that the type of isolation technique could affect not only the co-isolation of different contaminants but also the EV composition itself (Brennan et al., 2020; Veerman et al., 2021) which makes the direct comparison of results from different published studies more difficult. Therefore, determining the definition of 'pure' EV samples and consequently reporting such measure in all EV studies would be greatly beneficial for achieving consistency and reliability when comparing results from different studies. One of the suggested measures of sample purity

was particles-to-protein ratio where a high particles-to-protein ratio ($\sim 3 \times 10^{10}$) was considered a pure EV preparation (Webber and Clayton, 2013). Nonetheless, since there is no perfect method of isolating pure EV populations, the choice of separation method should depend on the biological source of EVs, the downstream analysis or application and the expertise and equipment available in the laboratory.

There are several published studies which compared commonly used EV isolation methods (Brennan et al., 2020; Buschmann et al., 2019; Deville et al., 2021; Jung et al., 2020; Karimi et al., 2018; Serrano-Pertierra et al., 2019; Takov et al., 2019; Tian et al., 2020). A recent study comparing five different EV isolation methods and two different EV sources - plasma and CCM, revealed that the choice of isolation method can significantly affect not only the purity of the EV preparation but also the subcellular origin of isolated EV populations (Veerman et al., 2021). According to this study, for CCM samples the method performed by *Izon 70* column resulted in a relatively pure EV preparation with high concentration of EV particles and EV-related proteins, and a low concentration of non-EV co-isolates which might indicate a pure EV sample (Veerman et al., 2021). Furthermore, it has been proposed that samples of different origin may have different EV elution profiles on the SEC column as suggested by the detected enrichment of a tetraspanin signal in EV-depleted fractions (Takov et al., 2019, 2017; Veerman et al., 2021). Therefore, it is advised that the elution profile of a particular type of EV sample is assessed prior to conducting an experiment using this technique.

3.1.4 Characterisation of VSMC-derived extracellular vesicles

To this date, there are few published studies which have characterised EVs secreted by different types of VSMCs or assessed the effect of PDGF on the EV populations secreted by stimulated VSMCs (Heo et al., 2020; Xu et al., 2019). A recent study investigating whether pulmonary artery SMC-derived EVs exposed to a PDGF signal could regulate pulmonary artery ECs, reported that PDGF EVs and control EVs express similar EV markers including CD63, CD81, CD9 and heat shock protein 70 (HSP70) (Heo et al., 2020). Additionally, according to the NTA analysis the majority of EVs within the secreted EV population by pulmonary artery smooth muscle cells (PASMCs) exhibited a diameter of approximately 100 nm

suggesting that the EVs could be of exosomal origin (Heo et al., 2020). Another study, comparing the proteomes of EV populations secreted by quiescent coronary artery SMCs (CASMCs) versus activated CASMCs proposed that quiescent CASMCs secrete heterogeneous EV populations consisting of apoptotic bodies, microvesicles and exosomes as suggested by TEM analyses and dynamic light scattering analyses (Comelli et al., 2014). Furthermore, the three different EV fractions isolated from quiescent CASMCs were also assessed for the enrichment of protein markers specific for each EV subpopulation. It was shown that TSG101, Flotillin-1 and CD81, protein markers which are widely accepted as markers for microvesicles and exosomes, were detected in the expected EV fractions, whereas they were absent in the fraction containing apoptotic bodies (Comelli et al., 2014). Since none of the studies described above compared in detail the physical characteristics of the EV populations secreted by quiescent VSMCs versus activated VSMCs (as a result of PDGF or EV-depleted FBS stimulation), it still remains unclear whether the two EV populations significantly differ in terms of basic physical characteristics such as size and expression of EV protein markers.

3.2 Aims

- To establish an EV elution profile specific for CCM samples from VSMCs using qEVsingle columns for SEC.
- To characterise EVs derived from HSVSMCs and assess effects of PDGF stimulation on EV release.
- To assess the effect of unmodified EVs purified from HSVSMCs in the absence or presence of PDGF on proliferation of recipient HSVSMCs.

3.3 Methods

3.3.1 Establishing the EV elution profile specific for CCM samples using qEVsingle SEC column

In this study, the EV elution profile specific for HSVSMC-CCM samples using SEC method and an AFC was assessed. One T-75cm² flask of confluent (~90%) HSVSMCs was used to generate EVs under basal conditions (no agonist stimulation). In order to resemble as closely as possible, the usual experimental conditions, cells were first washed with DPBS and then quiesced in the appropriate starvation medium for 48 hr. After that, the medium was removed, and cells were washed again with DPBS before adding fresh starvation medium for another 48 hr to allow EV secretion from cells. At the end of the incubation period, CCM was collected and processed as described in Section 2.10.3.1 with two main differences: (1) CCM (\approx 15mL) was concentrated up to 100 μ L before loading onto the qEVsingle column; and (2) instead of collecting only the first 3 fractions (F1-3) after the void volume, 9 x 200 μ L fractions (F1-9) were collected and were kept separate for individual analysis.

3.3.2 Experimental protocol designed to study the effect of unmodified EVs on proliferation of quiesced HSVSMCs

The EVs used in this study were generated as described in Section 2.10.1. Briefly, quiesced cell were treated with either 20 ng/mL PDGF or VEH control for 48 hr. At the end of the incubation period, CCM was collected and EVs derived from PDGF stimulated cells (pEVs) and VEH treated cells (vEVs) were isolated as described in Section 2.10.3.1.

This protocol was designed to study the effect of unmodified HSVCSMCs-derived EVs (vEVs and pEVs) on proliferation of recipient quiesced HSVSMCs via BrdU incorporation assay. Recipient HSVSMCs were quiesced for 48 hr in the relevant quiescent medium (Table 2-2) before treatment with EVs (1.5×10^{11} EVs/mL or 1.5×10^{10} EVs/well) (Figure 3-1).

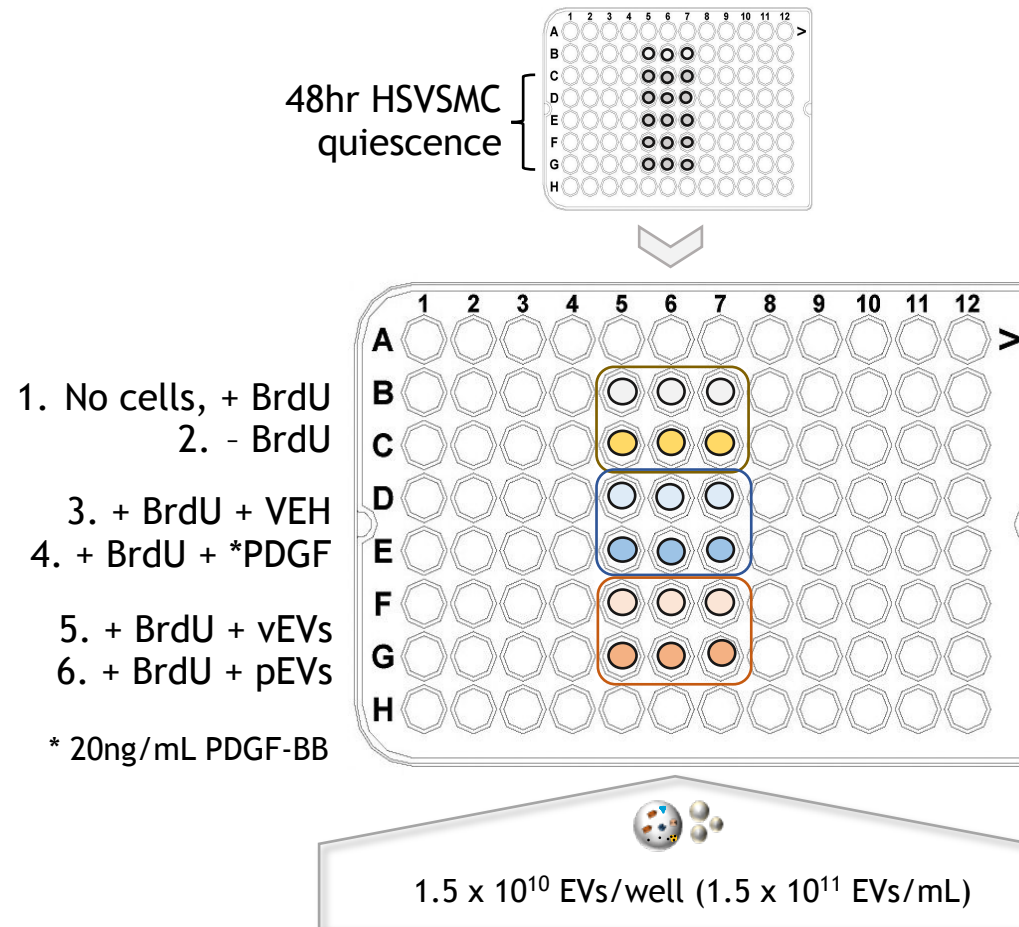


Figure 3-1 Schematic representation of the experimental protocol designed to study HSVSMC proliferation in response to treatment with vEVs and pEVs. Experimental protocol followed to study the effect of vEVs and pEVs (1.5×10^{11} EVs/mL or 1.5×10^{10} EVs/well) on proliferation of quiesced HSVSMCs after 48 hr.

Table 3-1 Other relevant methods for Chapter 3.

EV generation protocols	Section 2.10.1 and Section 2.10.2
EV isolation from CCM	Section 2.10.3.1
EV characterisation	Nanoparticle tracking analysis (Section 2.10.4)
	Protein expression analysis (Section 2.7)
	Transmission electron microscopy (Section 2.10.5)
	Enzyme-linked immunosorbent assay (Section 2.8)
Functional assay	Cell proliferation assay (Section 2.9.1)

3.4 Results

3.4.1 Determining the EV elution profile for CCM samples

The specific EV elution profile for HSVSMC CCM samples was determined since qEVsingle columns' specification sheet only provided guidance for EV isolation from plasma samples. According to the columns' specification sheet, the elution of EVs for a 100 μL plasma sample volume typically peaks at $400 \mu\text{L} \pm 200 \mu\text{L}$ after the EV-free void volume (VV) and the majority of the EVs elute in the first 600 μL following the VV. No EV elution profile data was provided for CCM samples by the manufacturer. In this experiment, EVs were isolated from 100 μL CCM sample by qEVsingle column and 9 x 200 μL EV fractions after the VV were collected separately. EV sample populations were characterised in terms of size and particle concentration by NTA. Protein concentration was assessed via microBCA.

NTA analysis of EV size suggested that the mean and modal particle size of EVs eluting in the first 3 x 200 μL fractions after the VV were all close to or below 150 nm. The mean particle size of VV EVs was found to be significantly larger ($p < 0.01$) than the mean particle size of each of the three post-VV EV fractions

(152.5±2.0nm, 130.7±0.6nm, 130.2±1.2nm and 128.5±3.7nm for VV, F1, F2 and F3 EVs respectively) (Figure 3-2A). No significant difference in modal EV size between VV EVs and F1-3 EVs was detected (109.7±4.9nm, 109.9±2.4nm, 107.2±5.3nm and 107.9±4.4nm for VV, F1, F2 and F3 EVs respectively) (Figure 3-2B). Concentration was also determined in terms of particles/mL (Figure 3-2C). It was found that VV ($1.2 \times 10^{11} \pm 9.3 \times 10^9$ particles/mL), F1 ($1.2 \times 10^{12} \pm 5.0 \times 10^{10}$ particles/mL), and F2 ($1.2 \times 10^{11} \pm 8.2 \times 10^9$ particles/mL) contained a significantly higher concentration of EVs compared to F4 ($1.7 \times 10^{10} \pm 3.1 \times 10^9$ particles/mL). From the NTA data in Figure 3-2C, it is also evident that a significant proportion of the EVs started to elute earlier than F1 during the VV, and EV elution peaked during F1.

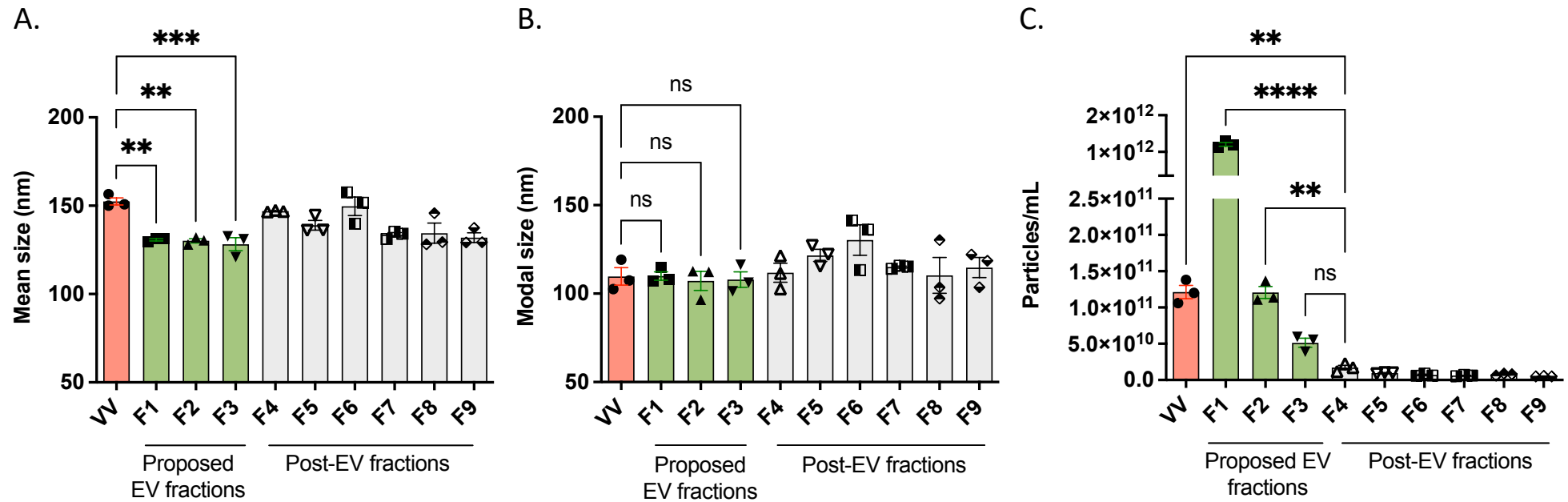
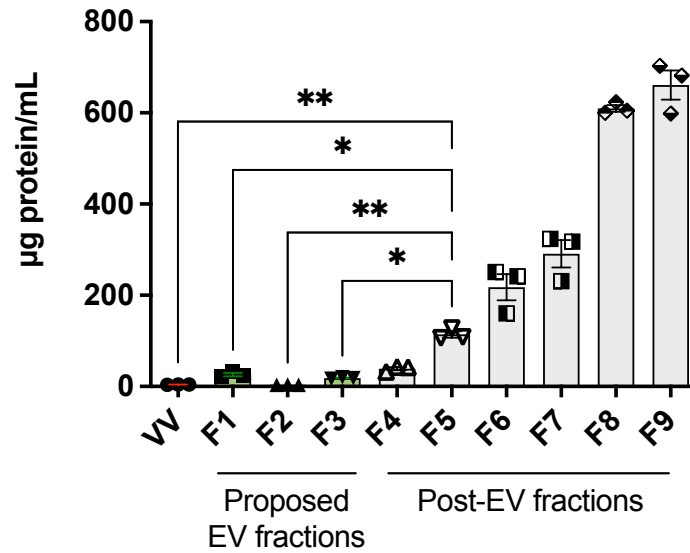


Figure 3-2 Determining the EV elution profile specific for CCM samples generated by cells (HSVSMCs) under basal conditions. (A) NTA data for mean particle size (nm); (B) NTA data for modal particle size (nm); (C) NTA data for mean particle concentration (particles/mL. A one-way ANOVA with a Tukey's correction was performed to compare the means of all groups and a *p-value < 0.05 (*p<0.01 and **p<0.001) was considered statistically significant (N=3). Abbreviations: EVs, extracellular vesicles; NTA, nanoparticle tracking analysis; F, fraction; VV, void volume.

Sample protein concentration ($\mu\text{g}/\text{mL}$) was also determined for each fraction (Figure 3-3A). The amount of protein detected in the VV and the first three fractions (F1-3) did not differ significantly ($3.9\pm 0.3 \mu\text{g}/\text{mL}$, $26.1\pm 3.6 \mu\text{g}/\text{mL}$, $3.7\pm 0.1 \mu\text{g}/\text{mL}$ and $18.5\pm 0.9 \mu\text{g}/\text{mL}$). Significant difference in protein concentration was detected between the first four samples (VV, F1-3) and later fractions starting from F5 (F5: $114.1\pm 6.9 \mu\text{g}/\text{mL}$: vs VV: $3.9\pm 0.3 \mu\text{g}/\text{mL}$, $p<0.01$; vs F1: $26.1\pm 3.6 \mu\text{g}/\text{mL}$, $p<0.05$; vs F2: $3.7\pm 0.1 \mu\text{g}/\text{mL}$, $p<0.01$; and vs F3: $18.5\pm 0.9 \mu\text{g}/\text{mL}$, $p<0.05$)(Figure 3-3A). It was also evident that the protein concentration in the EV fractions continued to increase after F2 through to F9 (Figure 3-3A).

Further analysis of sample purity (Figure 3-3B) determined by the EV particle to protein ratio revealed that the first three fractions including the VV had the highest purity as the mean particle to protein ratio determined for those fractions was above the suggested particle to protein ratio threshold of 3.0×10^{10} ($3.1 \times 10^{10} \pm 3.0 \times 10^9$ particle/protein, $4.7 \times 10^{10} \pm 4.2 \times 10^9$ particle/protein and $3.2 \times 10^{10} \pm 2.3 \times 10^9$ particle/protein for VV, F1 and F3 respectively) (Figure 3-3B). Fraction 3 was found to be less pure as the calculated particle to protein ratio was $2.8 \times 10^9 \pm 2.1 \times 10^8$ which is between 3.0×10^{10} and 1×10^9 . All the other fractions F4-9 were found to be impure as their particle to protein ratios were below the 1×10^9 threshold of purity (Figure 3-3B).

A.



B.

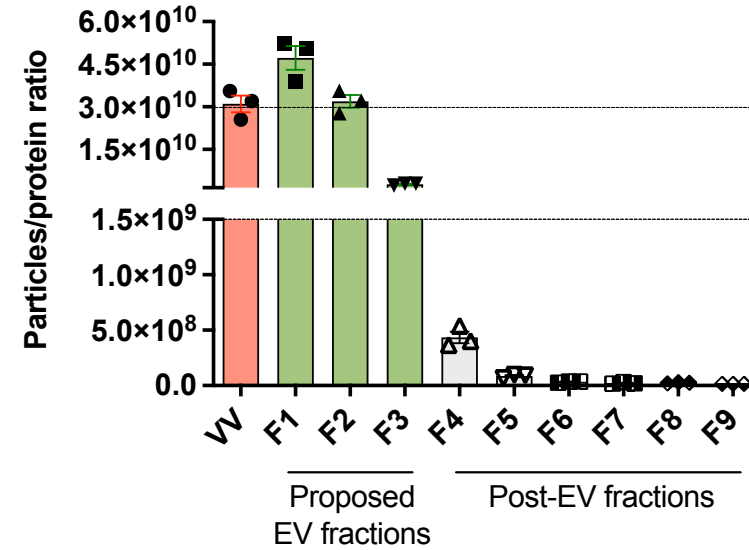


Figure 3-3 Determining the purity of EV elution fractions specific for CCM samples generated by cells (HSVSMCs) under basal conditions. (A) MicroBCA data for protein concentration (µg/mL); (B) Calculated EV particles to protein ratio. A one-way ANOVA with a Tukey's correction was performed to compare the means of all groups and a * p-value < 0.05 was considered statistically significant (N=3). Ratios > 3×10^{10} particles/µg equate to high vesicular purity, whereas ratios below 1.5×10^9 particles/µg were considered impure. Abbreviations: EV, extracellular vesicles; NTA, nanoparticle tracking analysis; F, fraction; VV, void volume.

3.4.2 Characterisation of HSVSMC-derived EV populations +/- PDGF stimulation

As HSVSMCs were the main cell type used in this project and some HSVSMCs were isolated in house following a well-established protocol, successful isolation of SMCs was confirmed by the detection of a typical SMC marker α -SMA (Figure 3-4).

Quiesced HSVSMCs were treated either with 20 ng/mL PDGF or VEH control for 48 hr in 0.2% EV-depleted FBS DMEM. The HSVSMC CCM was collected and EVs were isolated using SEC (Section 2.10.3.1). Both EV sample populations were characterised in terms of size and particle concentration by NTA, and EV morphology was assessed by TEM. EV sample protein concentration was determined by microBCA assay and western immunoblot analysis was carried out to detect specific EV-related protein markers.

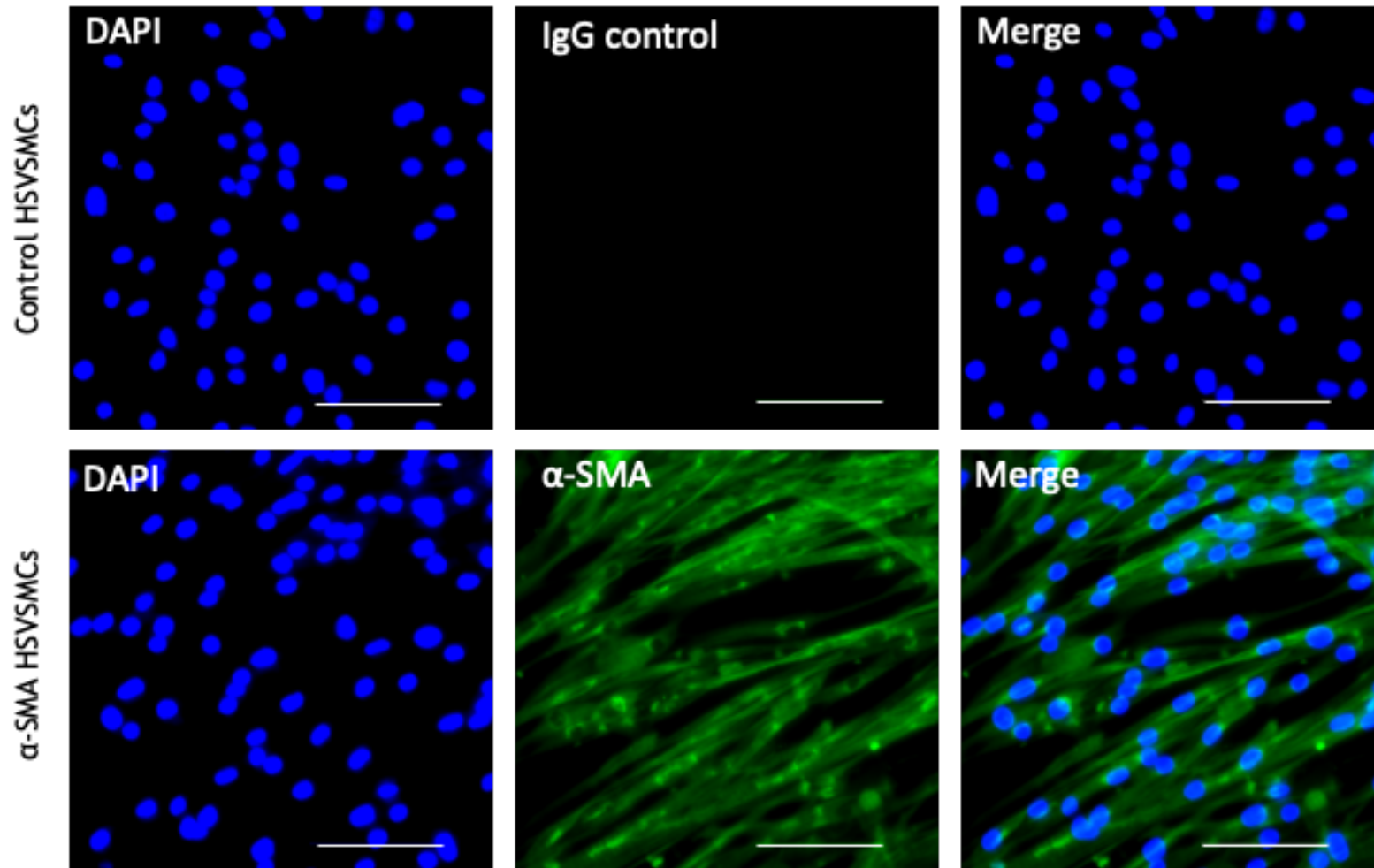


Figure 3-4 HSVSMCs used for EV generation and other *in vitro* experiments express α-SMA – a typical SMC marker. IMF staining was performed to determine the presence of α-SMA (green). DAPI staining (blue) was used to detect nuclei. This figure displays representative images of α-SMA /DAPI-stained HSVSMCs isolated in house following an established protocol for SMC isolation described in detail in Section 2.3.1 (N=3). Images were taken at 40X magnification on Leica DMI8 Inverted Microscope. Scale bar is 100μm.

Both sample populations, pEVs and vEVs, did not significantly differ in terms of size as evidenced by the NTA findings for mean particle size and particle modal size. It was found that vehicle treated HSVSMCs secreted EVs (vEVs) with mean EV size of 130.8 ± 5.4 nm vs. 128.6 ± 4.8 nm for pEVs secreted by HSVSMCs treated with PDGF (N=5, $p > 0.05$) (Figure 3-5A). The EV modal size found for each EV population, vEVs and pEVs, was 117.2 ± 4.2 nm and 107.7 ± 6.3 nm respectively (N = 5, $p > 0.05$) (Figure 3-5B). Representative size distribution peaks (SDP) produced by the NanoSight are shown in (Figure 3-5E). NanoSight NTA analysis of concentration of EVs released from HSVSMCs treated with 20 ng/mL PDGF (pEVs) or vehicle (vEVs) showed that PDGF stimulated cells secreted significantly higher concentration of EV particles per mL than control cells ($1.1 \times 10^{12} \pm 1.7 \times 10^{11}$ and $4.4 \times 10^{11} \pm 2.5 \times 10^{10}$ particles/mL respectively; N=5, $p < 0.01$) (Figure 3-5C). The difference in concentration between the two EV sample populations remained significant following normalization to the number of EVs secreted per cell ($8.2 \times 10^6 \pm 5.6 \times 10^5$ and $1.4 \times 10^7 \pm 2.1 \times 10^6$ particles/cell for vEVs and pEVs respectively, N=5, $p < 0.05$) (Figure 3-5D).

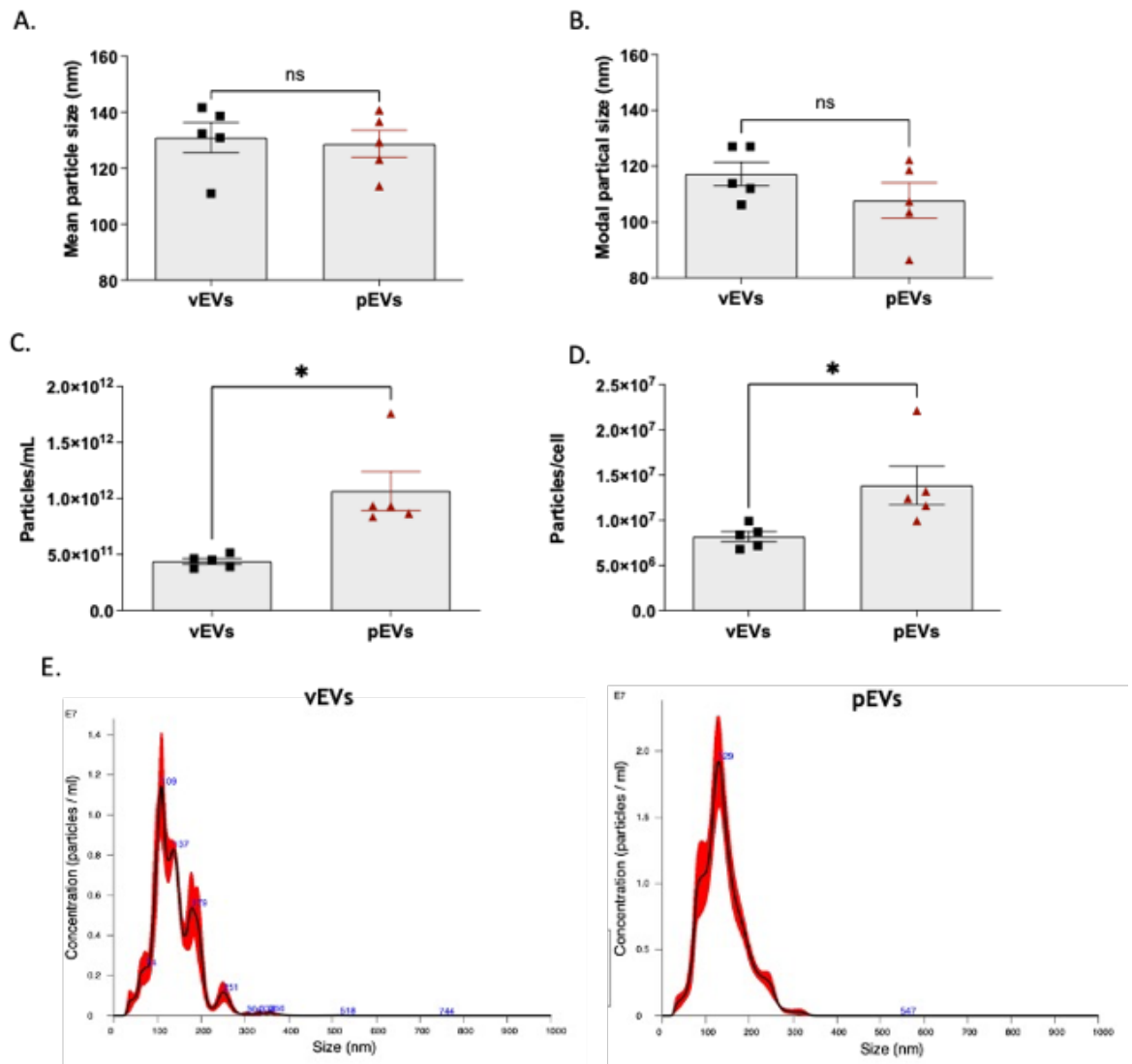


Figure 3-5 Characterisation of EV populations secreted by PDGF-treated HSVMCs (pEVs) and VEH control cells (vEVs) via NTA. (A) NTA data for mean EV particle size; (B) NTA data for modal EV particle size; (C) NTA data for EV particle concentration; (D) Number of EV particles secreted per cell; (E) NTA EV particle size distribution curves; Differences between groups were compared using paired two-sample t-test and a * p-value < 0.05 was considered statistically significant (N=5). Abbreviations: EV, extracellular vesicles; NTA, nanoparticle tracking analysis; PDGF, platelet-derived growth factor; VEH, vehicle; vEVs, vehicle control EVs; pEVs, PDGF EVs;

Assessment of the morphology of EVs in both sample groups by TEM showed the presence of small exosome/extracellular vesicle-like particles (< 200nm) with a typical round or cup-shaped appearance which is usually observed with this type of EM analysis (Figure 3-6).

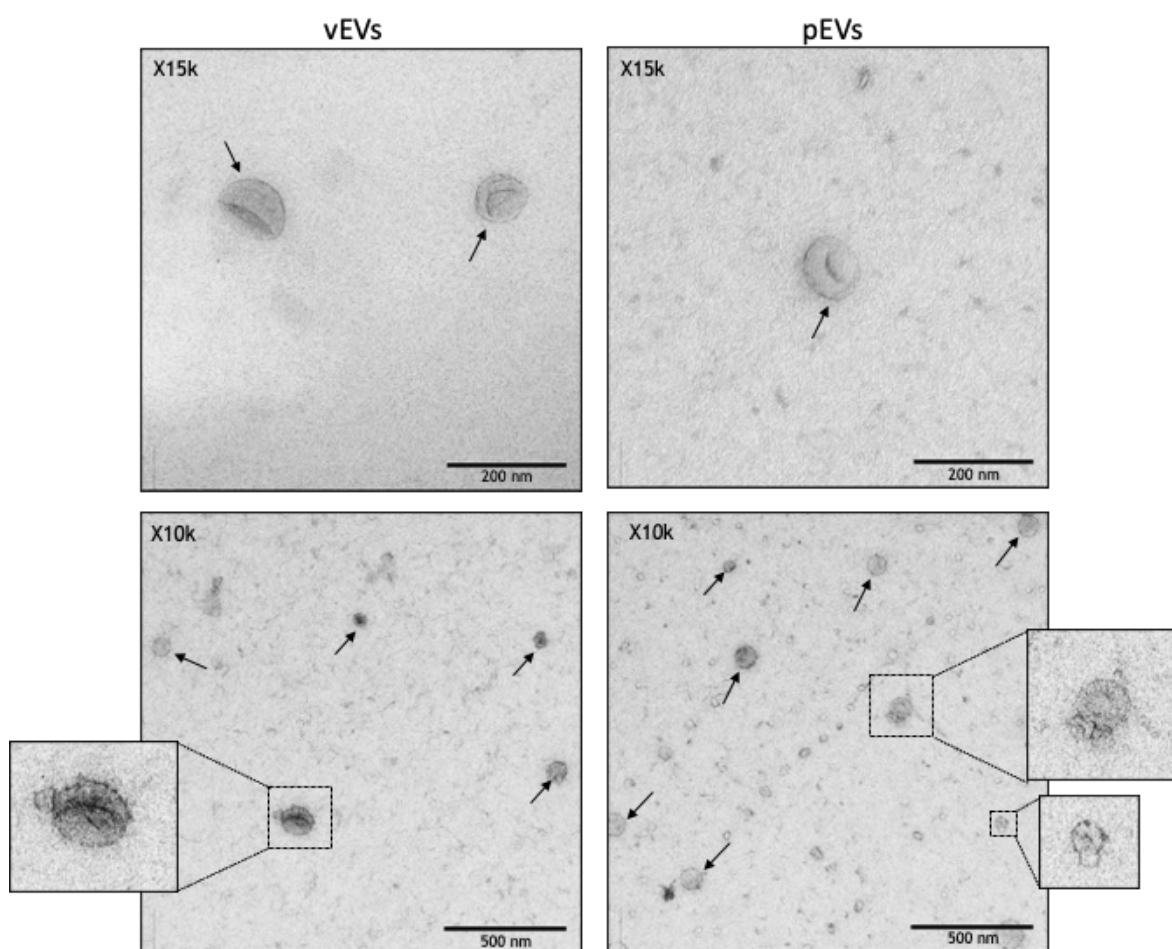


Figure 3-6 Characterisation of EV populations secreted by PDGF-treated HSVSMCs (pEVs) and VEH control cells (vEVs) via TEM. Representative images of EVs derived from VEH control HSVSMCs (vEVs) and PDGF-stimulated HSVSMCs (pEVs). Scale bars: 200nm (top images) and 500nm (bottom images).

Protein concentration was determined by microBCA assay for EVs derived from both HSVSMCs treated pEVs and control vEVs and no significant difference was found between the two groups (Figure 3-7A). The average protein concentration of vEVs was found to be $478.3 \pm 172.7 \mu\text{g/mL}$ vs. $362.4 \pm 80.7 \mu\text{g/mL}$ for pEVs ($N = 4$, $p > 0.05$).

Furthermore, the presence of EVs in both sample groups was confirmed by the detection of different EV-associated protein markers including Annexin A2, Annexin XI, CD81 and CD63 (Figure 3-7B). All four proteins were found to be present in samples of EVs derived from HSVSMCs treated with both PDGF (pEVs) or VEH control (vEVs) ($N=3$). As expected, Annexin XI (predicted molecular weight of 56 kDa) was detected at approximately 55 kDa for all samples, including vEVs and pEVs. The observed double band in the positive control lane for Annexin XI may be due to the detection of an isoform of Annexin XI (Sudo and Hidaka, 1998). For Annexin A2 (predicted molecular weight of 36 kDa) two bands were also detected at the expected region on the blot across all lanes - one above and one below 38 kDa marker. The appearance of the second (top) band may be due to non-specific Ab binding or the detection of an Annexin A2 isoform (Bharadwaj et al., 2013; Gerke and Moss, 2002). Both tetraspanins, CD63 and CD81 were also successfully detected. Although the predicted molecular weight of CD63 is usually around 25 kDa, there are a number of potential glycosylation sites which may affect the migration of the protein and subsequently the appearance of the band on the blot (Metzelaar et al., 1991). CD63 band was smeared between 30-60 kDa which was an expected observation for this protein marker considering the type of samples and EV isolation method used. For CD81 (predicted molecular weight of 26 kDa), a band was consistently detected at approximately 20 kDa in all samples.

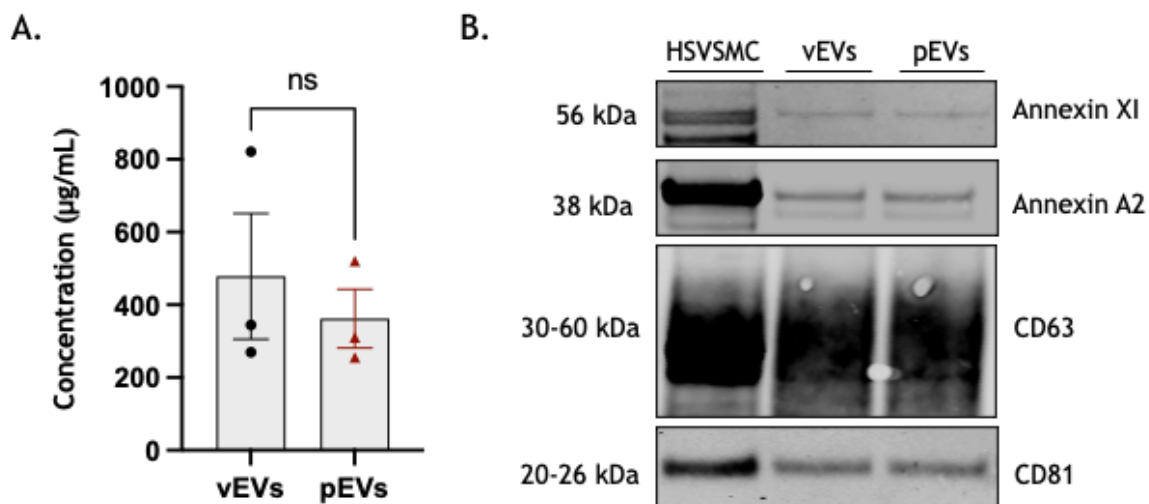


Figure 3-7 Analysis of HSVSMC-derived EV protein content by microBCA assay and western immunoblot. (A) Comparison of protein concentration of EVs released from HSVSMCs +/- PDGF-stimulation (N=3, Paired two-sample t-test). (B) Detection of EV-related protein markers in vEVs, pEVs and control HSVSMC lysate; Annexin XI, Annexin A2, CD63 and CD81. The images shown here are representative images of the markers detected in vEVs and pEVs (N=3 for all markers).

To further explore any potential differences between EVs derived from pEVs and vEVs, a high-sensitivity human PDGF ELISA (assay range: 31.3-2,000 pg/mL) was carried out to determine whether PDGF-treated cells secrete EVs containing or associated with PDGF. With this experiment, it was of interest to explore both: (1) the association of pEVs with PDGF following stimulation of the EV secreting cells; and (2) if associated, explore the location of the peptide in relation to the EV particles i.e., establishing whether PDGF is contained within EVs or attached to the surface of the EVs. A detailed protocol of the experimental design has been described in Section 2.8. The experiment was carried out for two biological replicates on the same ELISA plate, to maximise the use of the plate.

It was found that PDGF was present in the positive control sample confirming the ELISA worked correctly. Additionally, a high concentration of PDGF was detected in pCCM sample (avg. 123,216 pg/mL or 123.2 ng/mL), not in vCCM (Figure 3-8). The pCCM sample was concentrated CCM (from 15 mL to 500 μ L) containing EVs released by PDGF-stimulated HSVSMC prior to EV isolation and purification via SEC and possibly soluble PDGF that was not taken up by the stimulated cells. For comparison, the initial concentration of soluble PDGF used to treat the cells was 20 ng/mL in 15 mL medium (or 600 ng/mL in 500 μ L). After 48 hr stimulation period, when CCM was collected and concentrated down to 500 μ L, the average concentration detected for concentrated CCM containing PDGF (pCCM), as mentioned above, was 124.2 ng/mL which is almost 5 times less than the initial concentration. Although still relatively high concentration of soluble PDGF was present in the medium after 48 hr incubation period, qEV isolation appeared to be sufficient in separating the EVs in the medium from soluble PDGF resulting in pure pEVs free from soluble PDGF (Figure 3-8). The PK treatment was used to determine the possible association of PDGF with EVs either internally or externally, however, since PDGF was not detected in any of the other experimental conditions (vEVs_Native, pEVs_Native, vEVs+/-PK and pEVs+/-PK) (Figure 3-8), it was concluded that PDGF taken up into cells following stimulation was not associated (either internally or externally) with EVs released from those cells.

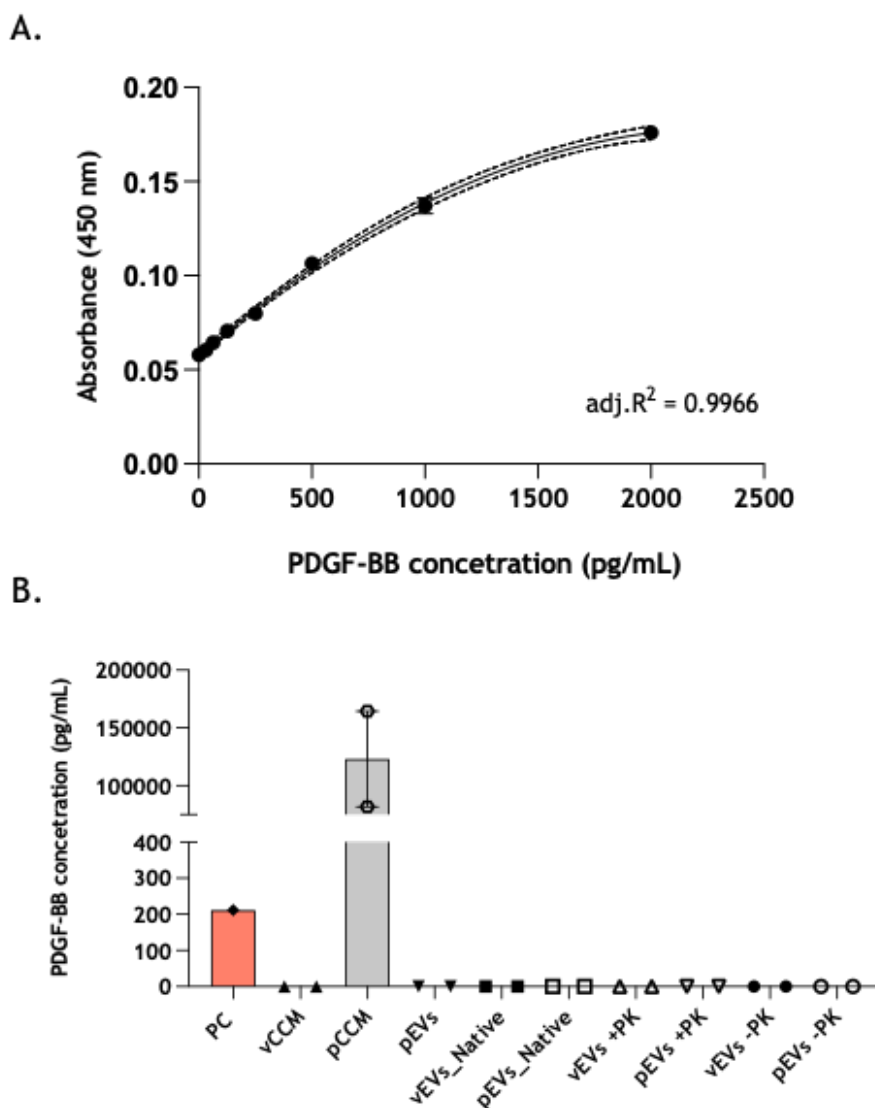


Figure 3-8 Human PDGF detection in different HSVSMC-derived EV samples by ELISA (Assay range: 31.3–2,000 pg/mL). (A) PDGF standard curve. (B) PDGF detection in CCM EV samples (prior to EV isolation) and purified EV samples (post EV isolation) derived from HSVSMCs (N=2). Positive control (PC) - 250 pg/mL human PDGF; vCCM and pCCM – concentrated VEH CCM and PDGFCCM samples respectively; pEVs – isolated PDGF EVs; vEVs_Native and pEVs_Native – isolated EVs from VEH and PDGFCCM respectively; vEVs +PK and pEVs +PK – VEH EVs and PDGF EVs treated with proteinase K; vEVs -PK and pEVs -PK – VEH EVs and PDGF EVs not treated with proteinase K but processed in parallel to vEVs +PK and pEVs +PK samples (N=2).

3.4.3 Studying the effect of EVs on proliferation of quiesced HSVSMCs

After characterising the EV populations secreted from HSVSMCs under normal and PDGF-stimulated conditions, it was of interest to determine whether treatment of HSVSMCs with unmodified pEVs would have any effect on cell proliferation. To do that, quiesced HSVSMCs were either untreated (VEH control), or treated with 20 ng/mL PDGF, control vEVs or pEVs over 48 hr (Section 2.9.1). It was found that compared to untreated VEH control cells, neither pEVs nor vEVs had any effect on proliferation of recipient HSVSMCs (Figure 3-9). There was also no significant difference in proliferation of HSVSMCs treated with vEVs compared to pEVs (Figure 3-9). Significant differences in proliferation of HSVSMCs was only detected between cells treated with VEH compared to PDGF, where in the PDGF group cells proliferated significantly more than cells in the VEH control group ($p < 0.0001$) suggesting that PDGF treatment successfully transformed quiesced HSVSMCs into actively proliferating cells (Figure 3-9).

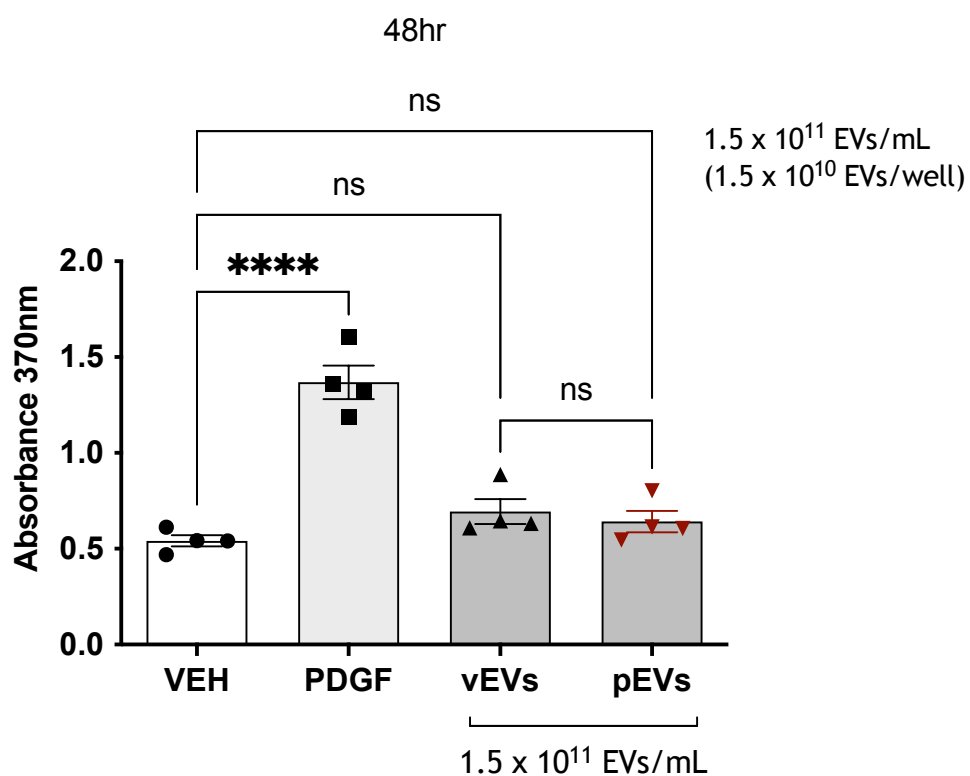


Figure 3-9 Analysis of quiesced HSVSMC proliferation treated with unmodified HSVSMC vEVs and pEVs. In this experiment, 1.5×10^{11} EVs/mL (1.5×10^{10} EVs/well) were used to treat recipient HSVSMCs. Differences between groups were assessed using an RM one-way ANOVA with a Tukey's correction to compare the means of all groups. A p-value < 0.05 (**** $p < 0.0001$) was considered statistically significant (N=4).

3.5 Discussion

In order to successfully be able to study the role of EVs in different biological processes *in vitro*, it was necessary to first optimise and validate an appropriate EV isolation method. There are various different methods currently used for the isolation of EVs from different biological samples including CCM, serum, plasma, saliva and urine (Brennan et al., 2020; Iwai et al., 2016; Markowska et al., 2017; Shtam et al., 2018; Takov et al., 2019).

One of the most widely used methods in the field, also known as the gold standard method, is DU which separates particles based on their volume and physical properties such as size and density. Although it has been labelled as the ‘gold standard’ method for EV isolation, DU has also been associated with a number of shortcomings. A recent quantitative and qualitative comparison of EV populations isolated from serum samples using various commonly used methods for EV isolation, including DU and SEC, suggested that the EV yield along with the efficient depletion of non-EV co-isolates, such as lipoprotein particles and protein contaminants, strongly depend on the type of method used to isolate EVs (Brennan et al., 2020). In this study, DU was associated with lower EV yield, higher protein concentration and consequently lower particle/protein ratio compared to SEC (Brennan et al., 2020). Another study, recently demonstrated that DU is a highly variable technique and significant differences in particle yield and efficiency of EV isolation may occur due to equipment- and operator-dependent technical variability which makes ultracentrifugation-based EV isolation methods less reliable (Torres Crigna et al., 2021). In addition, DU has also been linked to compromised EV integrity (Lobb et al., 2015), which could potentially interfere with future experimental aims such as studies of the functional activity of EVs and their potential as therapeutic vehicles. Therefore, it was decided to explore SEC as an alternative method of EV isolation which appeared to have the potential to overcome some of the problems associated with DU.

SEC method works by separating molecules differing in their hydrodynamic radius and it has been shown to effectively isolate EVs from CCM and also from more complex samples such as plasma and urine where EVs were successfully separated from protein complexes and lipoproteins (Gómez-Valero et al., 2016;

Lozano-Ramos et al., 2015; Veerman et al., 2021; Vogel et al., 2016). According to a recent study, for EV isolation from CCM samples, the SEC method appeared to be one of the most reliable methods resulting in somewhat more pure EV preparation associated with relatively high EV yield and enrichment of EV-related proteins, and a low concentration of non-EV contaminants (Veerman et al., 2021). Importantly, it has been suggested that EV isolation by the SEC method preserves their integrity and biological activity as during filtration EVs move with the fluid (elution buffer) flow under a small differential pressure (Gómez-Valero et al., 2016; Taylor and Shah, 2015). This is, indeed, important when isolated EVs are intended for therapeutic use.

In the first study the specific EV elution profile for CCM samples was assessed where HSVSMC-EVs were isolated from CCM after 48 hr incubation period. According to the qEV column's specification sheet, the elution of EVs for a 100 μL plasma sample volume typically peaks at 400 μL \pm 200 μL after the EV-free VV and the majority of the EVs elute in 600 μL with no data provided specific for CCM samples. The data presented here suggested that for CCM samples, EV elution starts earlier during the VV and peaks during the first 200 μL after the VV suggesting a slight shift of the EV elution profile for CCM samples compared to plasma samples possibly owing to the different qualities (e.g., viscosity) associated with two biological sample types. Nevertheless, the isolated EV populations in the fractions containing the highest particle concentration and the lowest protein concentration, VV and F1-3, appear to consist mainly of small EVs (<150 nm) (van Niel et al., 2018). The purity of all fractions was also assessed by calculating the particle to protein ratio suggesting that along with the proposed EV fractions (F1-3) the VV was also a practical source of purified EVs with an estimated particle to protein ratio above 3×10^{10} for VV, F1 and F2 and above 1×10^9 for F3 indicating an acceptable level of purity for all four fractions (VV, F1-3) (Webber and Clayton, 2013). A possible concern related to the use of particle to protein ratio as a measure of purity is the potential contamination of EV preparations with lipoproteins. For plasma samples, for example, where a large number of plasma particles detected by the NTA are not EVs (Welton et al., 2015), a high particle to protein ratio would not necessarily mean high purity. This is because if a sample consists mainly of lipoprotein particles and a low protein concentration it could still be considered as a pure

EV sample when purity is solely determined based on particle to protein ratio (Takov et al., 2019; Veerman et al., 2021); therefore, this measure alone is not sufficient to determine sample purity when EVs are isolated from plasma. While for certain biological samples particle to protein ratio might be an oversimplified way of assessing sample purity, for CCM samples, where co-isolation of lipoproteins is not a concern, it still might still be a reliable measure of purity.

Following the publication of the MISEV guidelines, more comprehensive EV characterisation by various techniques has become a fundamental requirement for publication in the EV field (Lötvall et al., 2014; Théry et al., 2018). In this study, two HSVSMC-derived EV populations were characterised - vEVs and pEVs. A number of recommended standard methods were used to characterise the EV populations including NTA, WB, TEM, and ELISA. Briefly, it was found that control HSVSMCs compared to PDGF treated HSVSMCs secrete similar EV populations in terms of size, however, cells treated with PDGF secreted significantly more EVs. As recommended by MISEV guidelines, a number of EV-associated protein markers, including both transmembrane and cytosolic proteins, were successfully detected demonstrating the presence of EVs (Théry et al., 2018). Although multiple well-established routine techniques have been used to characterise the EV populations in this study, none of these had the capacity to distinguish between different EV subpopulations accurately and reliably. Examples of such techniques include live imaging where the EV is caught in the act of release (e.g., an image of an EV budding off the plasma membrane or fusion of MVBs with the plasma membrane), however, these are very difficult and elaborate to perform which makes them less suitable for routine use (Théry et al., 2018). Therefore, in this study, isolated vesicles, both from CCM and serum, will always be referred to as 'extracellular vesicles' or 'EVs' instead of assuming the presence of a specific subclass of EVs within a given population.

In this study, it was found that HSVSMCs secrete EVs both under basal conditions as well as under PDGF stimulation which is consistent with the widely accepted notion that all cell types secrete and uptake EVs as a way of communication (Tkach and Théry, 2016; Willms et al., 2018). VSMCs are known to produce a very heterogeneous population of EVs in terms of size including EVs with a size distribution comparable to the one presented in the present study (Comelli et

al., 2014). It has also previously been suggested that the EV population secreted by cells changes under disease conditions or in response to a certain stimulus with studies reporting changes not only in the amount of EVs secreted by cells but also in their content (Auber and Svenningsen, 2022; Freeman et al., 2018; Kharmate et al., 2016; Riches et al., 2014). In this study, it was found that PDGF treatment significantly altered the EV population secreted by HSVSMCs in terms of concentration but not size. Interestingly, a similar change in terms of amount of EV release from adipose mesenchymal stem cells (ASCs) treated with PDGF has been previously reported (Lopatina et al., 2014). It was found that PDGF treatment of ASCs induced a significant increase in EV release compared to control cells and no significant change in mean EV size (Lopatina et al., 2014). Additionally, in the same study, it was also assessed whether ASCs treated with PDGF-released EVs containing PDGF and it was reported that no PDGF was detected in both PDGF-EVs and control EVs as confirmed by western immunoblot analysis (Lopatina et al., 2014). Interestingly, these findings are consistent with the findings in this study suggesting that PDGF is not packaged in EVs after PDGF treatment of HSVSMCs as confirmed by a highly sensitive ELISA. Although, the cell types used in both studies in question are different, it is possible that PDGF may have similar effects on both cell types resulting in the release of EV populations with similar profiles.

Nevertheless, it is important to note that previously it has been proposed that EC- and platelet-derived EVs are enriched in PDGF in patients with cardiovascular diseases (Goetzl et al., 2017; Togliatto et al., 2018). An association between PDGF and both high glucose-cultured EC EVs and circulating CD31 +ve EVs derived from patients with T2DM have been shown, where more specifically CD31 +ve EVs from T2D patients have been demonstrated to carry a membrane-bound PDGF with functional effects (Togliatto et al., 2018). The reason why some cells produce EVs that contain PDGF, and others do not, may be dependent on both the parental cell type as well as the conditions under which EVs are produced.

Preliminary investigation of the potential functional effects of HSVSMCs-derived EVs under pathophysiological conditions suggested that pEVs had no effect on proliferation of recipient quiesced-HSVSMCs compared to control (vEVs). This finding could mean that either pEVs carry no signal capable of interfering with

cell proliferation or the experimental design was not appropriate to assess the potential effect of pEVs on cell proliferation. Although in a different cell type, it has previously been shown that treatment of ASCs with PDGF not only stimulated the secretion of EVs by those cells, but also induced changes in the EV protein composition subsequently enhancing the angiogenic potential of EVs (Lopatina et al., 2014). Additionally, another study investigating the effect of PDGF on EV release by VSMCs, reported that EVs released under normal conditions and PDGF-stimulated conditions have markedly different small RNA expression profile with several dysregulated miRNAs detected within PDGF EVs (Heo et al., 2020). Interestingly, an EV-mediated cross communication between PSMCs and pulmonary artery endothelial cells (PAECs) was also proposed by the authors, where PSMCs-derived PDGF EVs were found to have functional effects on PAECs (Heo et al., 2020). It was demonstrated that certain miRNAs (miR-182, or miR-486, or miR-1246) were able to regulate PDGF-induced EC and VSMC migration but not migration under normal conditions (Heo et al., 2020) further emphasising the importance of the experimental design when assessing functional effects of potential mediators of cellular responses such as miRNAs or EVs. A possible EV-mediated autocrine regulation of VSMCs was not investigated in this study. Therefore, HSVSMC-derived pEVs may still be involved in the regulation of HSVSMC responses, but possibly under certain conditions i.e., pathophysiological rather than physiological conditions.

Based on the findings in the current study that PDGF stimulation of HSVSMCs positively regulates the release of EVs by treated cells in combination with the proposed effect of PDGF on the miRNA cargo component of VSMC EVs with potential functional implications (Heo et al., 2020), it may be beneficial to further explore the effect of HSVSMC EVs generated under PDGF stimulation.

3.5.1 Study limitations

Although EVs isolated from HSVSMCs were characterised via several methods including NTA, TEM, WB and ELISA, the characterisation was limited by a number of factors. For instance, characterisation of EVs via WB and BCA assay were completed with only low N numbers and no negative EV protein marker was detected due to obstacles associated with the optimisation of a specific Ab. Additionally, the ELISA assay was carried out only for two biological replicates

due to both consistent negative findings and budget considerations, therefore, no statistical analyses were carried out for this experiment. To improve the quality of the studies, it would have been beneficial to increase the N numbers where necessary as well as to establish a negative EV marker to fully comply with MISEV guidelines.

3.6 Summary

When isolating EVs from HSVSMC-derived CCM samples by SEC using the commercially available qEV columns by *Izon*, a slight shift of the EV elution profile was observed where EVs started to elute earlier during the VV, and EV elution peaked during the first 200 μ L fraction. It was found that, HSVSMCs secrete EVs under both basal conditions and under PDGF stimulation where PDGF treated HSVSMCs secreted significantly more EVs compared to control cells. The two EV populations did not significantly differ in terms of size, however, the increase in particle release by cells following PDGF stimulation suggest that the EV profile may be different under pathological disease conditions. Initial investigation of the functional effect of pEVs suggested that unmodified HSVSMC-EVs secreted under PDGF stimulation do not have any effect on proliferation of recipient quiesced HSVSMCs.

Chapter 4 RNA sequencing and gene enrichment analysis

4.1 Introduction

Both microarrays and RNAseq methods are used to identify differentially expressed genes in cells and EVs exposed to different experimental conditions (Jenjaroenpun et al., 2013; Rao et al., 2019; Skog et al., 2008b). In contrast to other methods for RNA quantification, such as microarray and qRT-PCR, RNAseq does not rely on a prior hypothesis. Instead, it is an unbiased hypothesis-generating method which has the potential to provide valuable insight into disease mechanisms, thus establishing the basis for a comprehensive research strategy. Unlike microarrays, where gene-specific amplification takes place on a larger scale than qRT-PCR using a selection of pre-defined transcripts/genes, RNAseq performs non-specific RNA selection and reverse transcription on a homogenized sample which provides an unbiased insight into the whole transcriptome of a sample (Rao et al., 2019; Wang et al., 2009a). Such an approach could be helpful in identifying more differentially modulated transcripts compared to microarrays and could lead to the identification of clinically relevant miRNAs which may be suitable therapeutic targets.

A wealth of evidence has been accumulated throughout the years demonstrating a crucial role for miRNAs in different CVD pathologies. A growing number of miRNAs are found to have potential to act as diagnostic and prognostic biomarkers for CVD and/or as novel therapeutic agents (Çakmak and Demir, 2020; Kaur et al., 2020; Romaine et al., 2015; Zhou et al., 2018). The presence of nucleic acids, including mRNAs, miRNAs and lncRNAs, within EVs has been previously confirmed with microarrays and qRT-PCR techniques in a number of reports (Ahadi et al., 2016; Gezer et al., 2014; Lässer et al., 2017; Skog et al., 2008b; Willms et al., 2016; Xiao et al., 2012). A more advanced high-throughput next-generation sequencing method, such as RNAseq, has also been used to more comprehensively study the EV transcriptome further emphasising the potential of EVs as key disease modulators (Baglio et al., 2015; Cheng et al., 2014b; Jenjaroenpun et al., 2013).

Through miRNA expression profiling studies, a number of miRNAs have already been identified and implicated in the development of CVD (Kaur et al., 2020; Romaine et al., 2015). A recent study investigating miRNA-related regulatory mechanisms contributing to atherosclerosis identified several miRNAs, including

miR-21-5p, miR-100-5p, miR-22-3p, miR-34a-5p, and miR-92a-3p, which were significantly upregulated in the main cell types (HUVECs; HAECs, human aortic endothelial cells; HASMCs, human aortic smooth muscle cells, and CD14+ macrophages) associated with disease progression under proatherogenic-stimuli (Moreau et al., 2021). Additionally, treatment of HUVECs with ox-LDL, a well-known proatherogenic stimulus, has led to a largely dysregulated miRNA expression profile in the treated cells where four miRNAs were up-regulated and eleven were downregulated following ox-LDL treatment (Qin et al., 2011). Microarray analysis of HASMCs derived from a mouse model of abdominal aortic aneurysm (AAA) revealed that a total of 15 miRNAs were dysregulated compared to control cells including miR-129-5p which was downregulated in AAA-HASMCs (Zhang et al., 2016). In the same study, miR-129-5p was proposed to be an inhibitor of cell proliferation and inducer of apoptosis in SMCs through regulation of *Wnt5a* (Zhang et al., 2016).

EV cargo represents a diverse selection of bioactive molecules that could either closely reflect the status of the parental cells or could have a distinct molecular fingerprint that only partially reflects the originating cells (Berumen Sánchez et al., 2021; Fontaine et al., 2022; Shihui Fu et al., 2020; Oggero et al., 2019). Therefore, studying EVs released from cells that are damaged, dysfunctional or under stress could provide invaluable information which could improve our understanding of the molecular mechanisms of different diseases and pathological conditions. RNAseq analysis of EVs derived from HUVECs under hyperphosphatemia conditions (HP-EC-EVs) revealed a highly dysregulated miRNA profile in HP-EC-EVs where miR-3182 was found to be significantly upregulated compared to control EVs (Peng et al., 2022). In the context of cancer, miR-3182 has previously been implicated in the regulation of cellular processes such as cell migration, proliferation, and cell survival as well as growth through possible regulation of the mTOR/S6K1 (S6K1, S6 kinase β -1) signalling pathway (Razaviyan et al., 2018). A recent study using a qPCR-based method of microRNA profiling reported that HUVEC- and HUVSMC-derived EVs were enriched in miR-539-5p and miR-582-5p respectively as a result of coculturing both cell types suggesting that EVs might play a role in communication between ECs and SMCs (Fontaine et al., 2022). In the same study, both EV-associated miRNAs, miR-539-5p and miR-582-5p, were implicated in the regulation of HUVEC and HUVSMC proliferation and

migration potentially through targeting various genes such as *AKT1*, tumour protein 53-induced nuclear protein 1 (*TP53INP1*) and programmed cell death protein 6 (*PDCD6*) in ECs and cyclin-dependent kinase 6 (*CDK6*) and *TP53INP1* in SMCs (Fontaine et al., 2022). In the context of vascular remodelling, the miRNA expression profiles of EVs derived from PASMCs under normal and pro-proliferative conditions (PDGF stimulation) were compared by NGS-based small RNAseq and a significant differential expression of several EV miRNAs, including miR-182, miR-486, and miR-1246, was detected (Heo et al., 2020). The aforementioned high throughput NGS-based expression profiling studies enable the detection of changes in RNA expression levels on a global level in a hypothesis-free unbiased manner as opposed to the hypothesis-driven nature of microarrays and qRT-PCR studies. There are not many studies yet that employed this hypothesis-generating method of comprehensively characterising the small RNA component of EVs derived from relevant primary human cells in the context of vascular pathologies.

In addition to quantifying the miRNA expression levels in EVs, exploring potential miRNA - mRNA target interactions and studying their functional role in recipient cells remain crucial steps in elucidating the involvement of EV-associated miRNAs in the regulation of molecular mechanisms associated with different pathological conditions. The widely accepted method of identifying novel miRNA-mRNA interaction is to carry out computational prediction of potential miRNA gene targets followed by experimental validation of these miRNA-mRNA interactions. The two main approaches that underlie the development of miRNA target prediction tools are: algorithms developed based on characteristics of the mRNA sequence and/or based on the miRNA-mRNA interaction, and statistical inference algorithms based on Machine Learning (Riolo et al., 2021). In the former, a number of different features of the miRNA-target complex are usually considered including pairing between the miRNA seed sequence and the mRNAs, thermodynamic stability of the pairing, evolutionary conservation of the target sequence across species, accessibility of the target site, and number of target sites in the same 3'-UTR. Often a combination of these is used in a single tool to compensate for the limitations of each feature alone (Peterson et al., 2014; Riolo et al., 2021). Examples of those prediction tools include miRanda, TargetScan, RNAhybrid, PITA, and PicTar. Machine learning based algorithms, on

the other hand, aim to identify miRNA gene targets based on existing reference miRNA-mRNA interactions with established biological significance (Riolo et al., 2021). Algorithms are “trained” to recognise potential targets by using experimentally verified miRNA-mRNA interactions as positive examples, and artificially created negative examples; therefore, such prediction algorithms are only capable of detecting results similar to the set of examples used in the ‘learning’ process (Parveen et al., 2019). Examples of Machine Learning prediction tools include TargetBoost, DeepMiner, and DIANA-microT-CDS. Not all prediction algorithms have the same specificity and sensitivity and there is no perfect tool which can provide both high sensitivity and high specificity (Kertesz et al., 2007; Krek et al., 2005; Lewis et al., 2005; Miranda et al., 2006). Therefore, obtaining an acceptable balance between sensitivity and specificity by using a combination of tools derived from different prediction assumptions, might be the most effective way of identifying miRNA targets (Oliveira et al., 2017). In addition to prediction algorithms, it is also possible to extract information regarding potential miRNA gene targets using curated databases which contain experimentally validated miRNA-mRNA interactions (Andrés-León et al., 2015). Examples of curated databases include miRTarBase and DIANATarBase.

Once miRNA target genes are identified, the set of genes could then be interpreted by performing functional annotation and GSEA. Enrichment analysis of miRNA targets is a technique used to understand potential miRNA functions. The biological basis of enrichment is that functionally related genes interact forming interaction networks which are part of functional networks or modules (Xu and Wong, 2013). Therefore, it is rational to expect that genes, which are prone to be regulated (e.g., by miRNAs), are enriched in interaction networks, making enrichment-based analysis fundamental to both identifying potential changes to functional networks/modules and understanding underlying functional mechanisms (Xu and Wong, 2013). Following analysis, the potential miRNA functions in different gene regulation networks might be elucidated based on the enrichment of particular functional modules and/or molecular pathways (Lewis et al., 2003; Xu and Wong, 2008).

The main purpose of this type of largescale scanning is to obtain an overall view of the potential functional mechanisms that may be affected as a result of changes that could occur within gene interaction networks due to miRNA gene targeting. From a statistical point of view, one problem related to this type of analysis is to detect the significantly enriched functional categories by comparing the observed number of miRNA gene targets within a specific category with the number of gene targets that might appear in the same category as a result of random selection carried out from the same pool (Xu and Wong, 2013). GSEA tools generally use a list of identified miRNA gene targets (a set of genes) under suitable statistical models (e.g. Fisher's exact test) to detect significantly enriched functional categories (terms) from different annotation databases (Garcia-Moreno and Carmona-Saez, 2020). Gene function annotation can be performed using various annotation sources including databases containing molecular pathway maps such as KEGG and Biocarta, and the GO term system comprising of three different classification categories - biological processes (BP), cellular components (CC), and molecular function (MF) (Ashburner et al., 2000; Kanehisa et al., 2010).

Another common statistical problem in enrichment analysis of miRNA's gene targets is the correction for multiple tests as in this type of analysis many functional categories are considered at the same time (Khatri and Drăghici, 2005). In GSEA, Benjamini-Hochberg false discovery rate (BH-FDR) is one of the most commonly used models for multiple-testing correction as multiple functional categories are assessed at the same time (Khatri and Drăghici, 2005; Xu and Wong, 2013); therefore, it was the method of choice employed in the analysis presented here. With this method, for every 100 significantly enriched (P value < 0.05) annotation terms with a BH-FDR of 5% (P value < 0.05), it means that five of those annotation terms are expected to be falsely enriched (Benjamini and Hochberg, 1995). In contrast, the classic Bonferroni method for multiple-testing correction adjusts the significance threshold by dividing it by the number of tests performed (Tilford and Siemers, 2009). This ensures that the probability of including at least one falsely enriched annotation term is below the corrected P value threshold making this model overly conservative for this type of analysis where some level of false-positive findings can be tolerated. Although the BH-FDR may not be the most accurate multiple testing correction

method for analysis of significantly enriched annotation terms, essentially, it is still a useful approach of filtering and hypothesis generation as confirmational follow-up experiments in laboratory settings are required before making any definitive conclusions.

In the previous chapter, it was found that EVs secreted by PDGF-stimulated HSVSMCs did not significantly differ in terms of size compared to EVs released from control cells, PDGF stimulation significantly increased the secretion of EVs from HSVSMCs which could also be a sign of potential difference between the two EV populations.

4.2 Hypotheses and aims

It was hypothesised that:

- prolonged pathological PDGF signalling in HSVSMC induces changes in the miRNA transcriptome of EVs secreted by stimulated cells.
- differentially expressed EV miRNAs have target genes involved in the regulation of key cellular processes such as cell proliferation, migration, and apoptosis.

The main aims were to:

- identify differentially expressed miRNAs between EVs derived from PDGF-stimulated HSVSMCs (pEVs) and VEH control HSVMSCs (vEVs) using RNA sequencing.
- validate differentially expressed miRNAs in pEVs and vEVs by qRT-PCR.
- identify a list of potential 'true' miRNA gene targets using a bioinformatics approach.
- perform functional annotation and GSEA to study the relationship between differentially expressed EV miRNAs and any potential cellular processes that may be regulated by the miRNAs via their target genes.

4.3 Methodology

4.3.1 Cell work methodology

The extracellular vesicles used in these studies were generated as described in Section 2.10.1. Briefly, quiesced cells were treated with either 20 ng/mL PDGF or VEH for 48 hr. At the end of the incubation period, CCM was collected and EVs derived from PDGF stimulated HSVSMCs cells (pEVs) and VEH treated HSVSMCs (vEVs) were isolated as described in Section 2.10.3.1.

4.3.2 Workflow

The steps included in the process towards developing a hypothesis are summarised in Figure 4-1. After CCM isolation, vEVs and pEVs were sent to Glasgow Polyomics facility for differential expression analysis of the small RNA component (RNAseq) (Figure 4-1). Upon receiving the count-based differential expression analysis providing information about the differentially expressed miRNA genes between vEVs and pEVs an Integrative Genomic Viewer (IGV) software was used to determine the mature forms of the miRNAs of interest (Figure 4-1). Then differentially expressed miRNAs in vEVs vs pEVs were validated by qRT-PCR (Figure 4-1). Following validation, a list of potential miRNA gene targets was obtained for successfully validated miRNAs by qRT-PCR. Finally, functional annotation and GSEA of the identified miRNA gene targets for three miRNAs (miR-24-3p, miR-224-5p and miR-409-3p) were performed for hypothesis generation (Figure 4-1).

Workflow

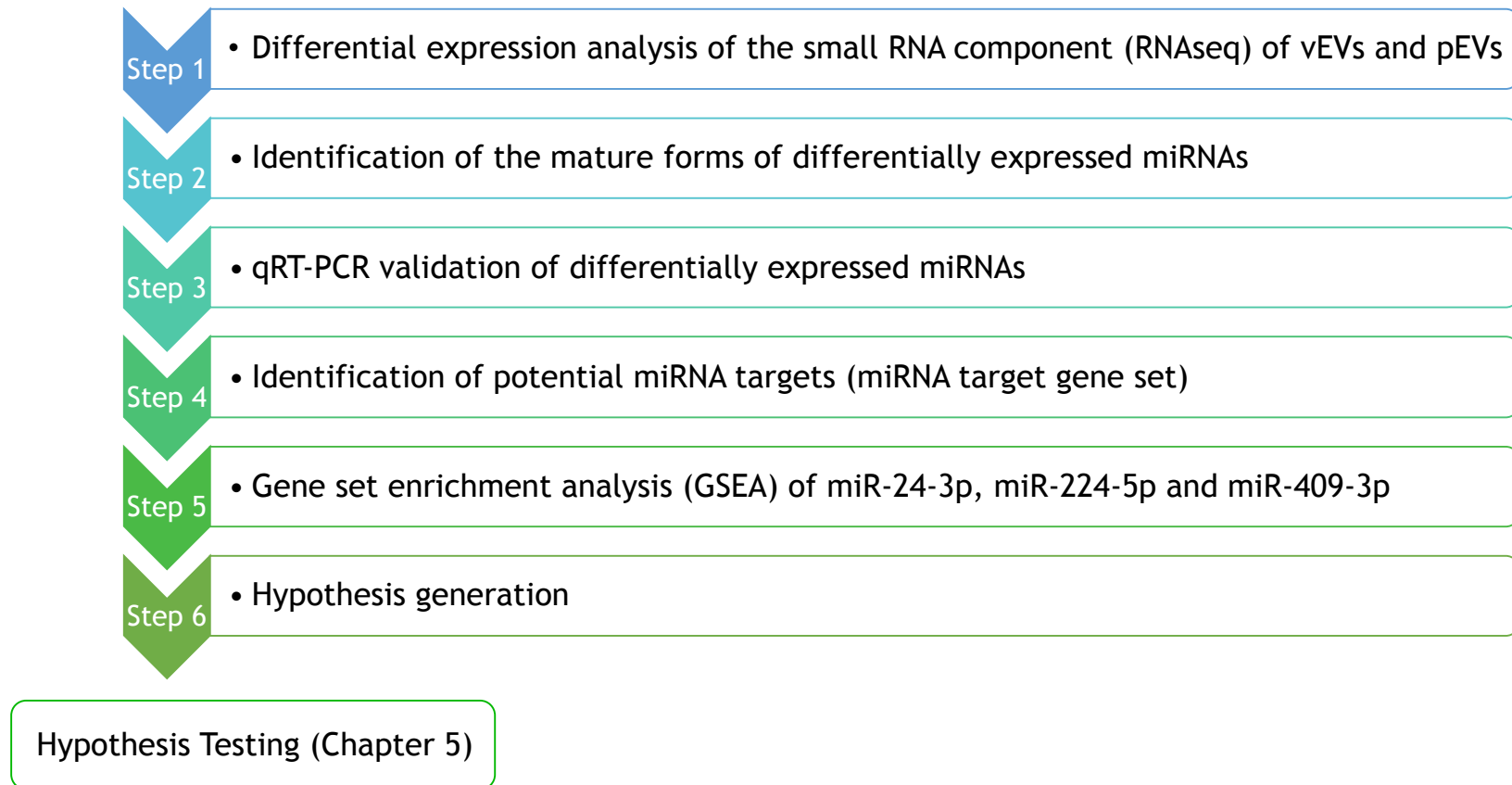


Figure 4-1 Workflow diagram summarising the steps followed to develop a hypothesis. Differentially expressed miRNAs between vEVs and pEVs were first identified by RNAseq analysis and then GSEA were performed for hypothesis generation.

Table 4-1 Other relevant methods for Chapter 4.

EV generation protocols	Section 2.10.1
Measuring of gene expression levels	Sections 2.6
NGS-based profiling of EV-related miRNAs	Section 2.11
Bioinformatics	Section 2.12

4.4 Results

4.4.1 Quality control of small RNA sequencing samples

A principal component analysis (PCA) was carried out to visualise the variance between groups and individual samples based on their small RNA expression profile. It was found that vEVs have markedly different small RNA expression profile when compared to pEVs (Figure 4-2) as suggested by the clear separation of the two sample groups forming two distinct clusters. The observed percentage variance for both clusters (PC1 = 32.4% variance and PC2 20.1% variance) indicate that variation in the small RNA expression profile between vEV and pEV samples was primarily due to treatment differences between VEH control HSVMCs and PDGF-stimulated HSVMCs. Two of the samples in the pEV group (PDGF_1 and PDGF_2) appear to have very similar small RNA expression profiles as evident by their strong overlap in the plot. Overall, all samples in the control (vEVs) group appear to have similar small RNA expression profiles with lower variability compared to samples in the PDGF group (pEVs) as suggested by the improved clustering of all vEV samples (Figure 4-2).

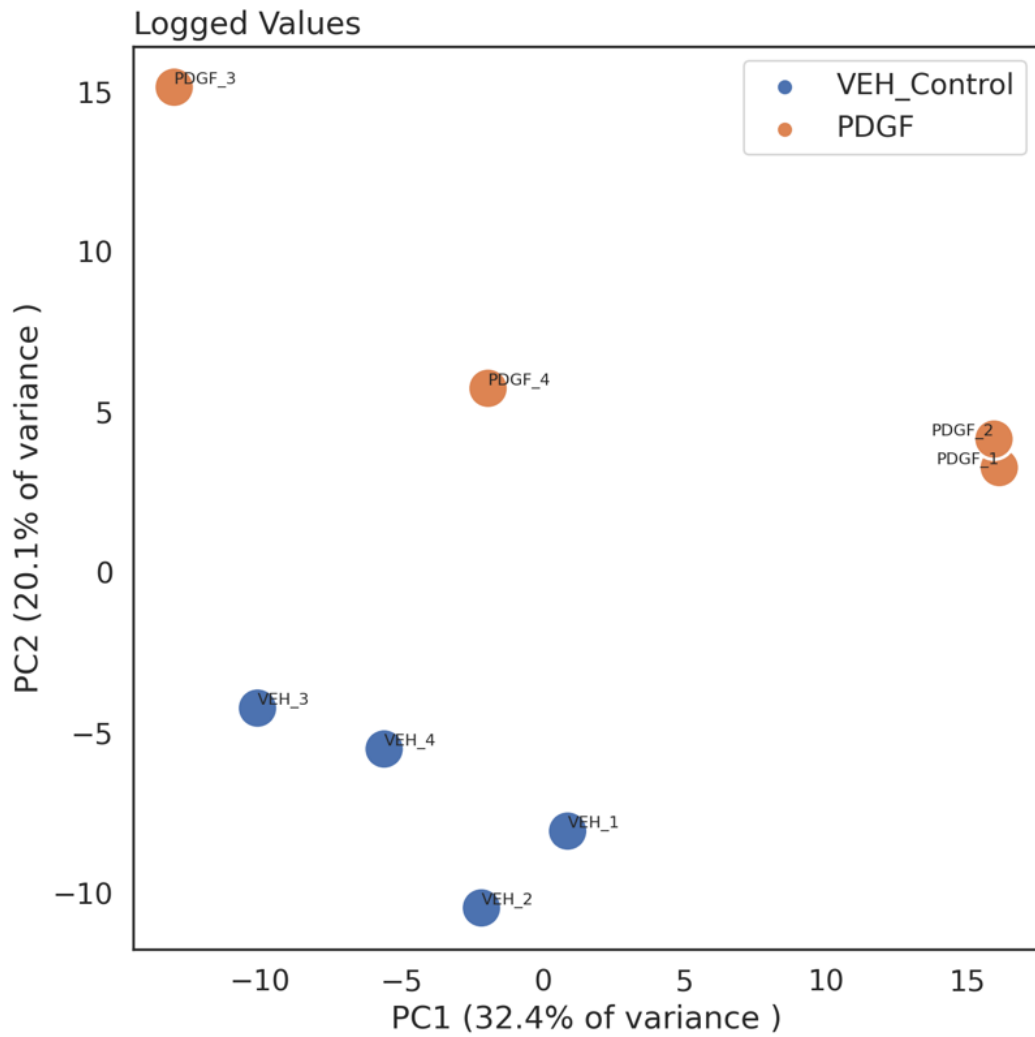


Figure 4-2 Principal component analysis (PCA) plot of the small RNA expression profiles of vEVs and pEVs. Each dot represents a sample, and each colour represents the type of the sample. PC1 and PC2 explain 32.4% and 20.2% (respectively) of the variance in gene expression profiles between vEVs (orange) and pEVs (blue).

4.4.2 Summary of differentially expressed small RNA molecules identified by small RNA sequencing

The small RNA expression profiles of HSVSMC-derived EVs and their changes in response to a long-term (48 hr) PDGF stimulation were investigated by NGS-based small RNA sequencing. RNAseq analysis identified six known differentially expressed miRNAs between pEVs and control EVs (vEVs). For this experiment, the raw data returned by Glasgow Polyomics facility was analysed and visualized using Pad plot (an online tool for RNAseq data analysis developed by Simon Fisher, School of Cardiovascular and Metabolic Health, University of Glasgow) <https://github.com/SimonF92/PadPlot>. As seen in the volcano plot (Figure 4-3) there were 11 significantly differentially expressed small RNA molecules including 7 miRNAs and 4 snRNAs (Table 4-2). Ten of the RNA molecules were upregulated in pEVs and only one snRNA (U6) was downregulated in pEVs compared to control EVs (vEVs) (adjusted p-value of <0.05).

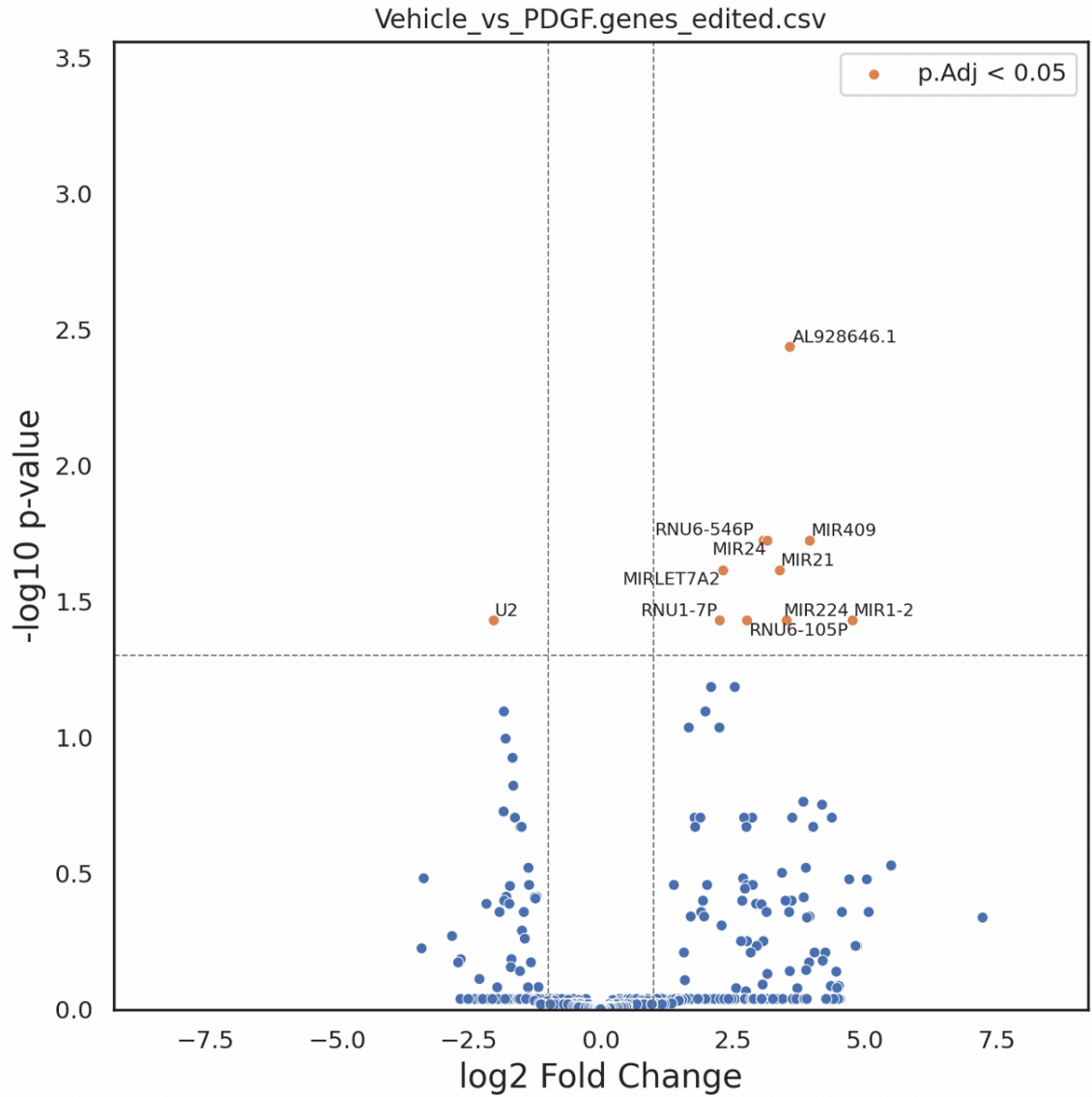


Figure 4-3 Volcano plot of differentially expressed genes identified between the pEVs group and control (vEVs) group. The plot shows statistical significance ($\text{adj.}p < 0.05$) against \log_2 fold-change in expression levels between vEVs and pEVs, demonstrating the most significantly differentially expressed miRNA genes between the two groups – MIR24, MIR409, MIR21, MIRLET7A2, MIR1-2 and MIR224 (all of which upregulated in the PDGF group).

Table 4-2 A summary table of all differentially expressed small RNA molecules between control EVs (vEVs) and PDGF EVs (pEVs).

Differentially expressed small RNAs (external gene name)	P adj.	log2FoldChange (with PDGF-BB treatment)
AL928646.1	0.004	3.58
miR-24	0.019	3.08
miR-409	0.019	3.96
RNU6-546P	0.019	3.16
miR-21	0.024	3.39
miR-let-7A2	0.024	2.32
miR-1-2	0.037	4.77
U2	0.037	-2.03
RNU6-105P	0.037	2.77
miR-224	0.037	3.52
RNU1-7P	0.037	2.25

Further examination (hierarchical clustering) also confirmed that, overall, all differentially expressed miRNAs (miR-24, miR-409, miR-21, miR-let-7A2, miR-1-2 and miR-224) were more highly expressed in pEVs (red coloured boxes) compared to vEVs with apparently less variability present within the VEH group compared to PDGF group as suggested by the uniform presence of yellow colour indicating low gene expression across all vEV samples (Figure 4-4).

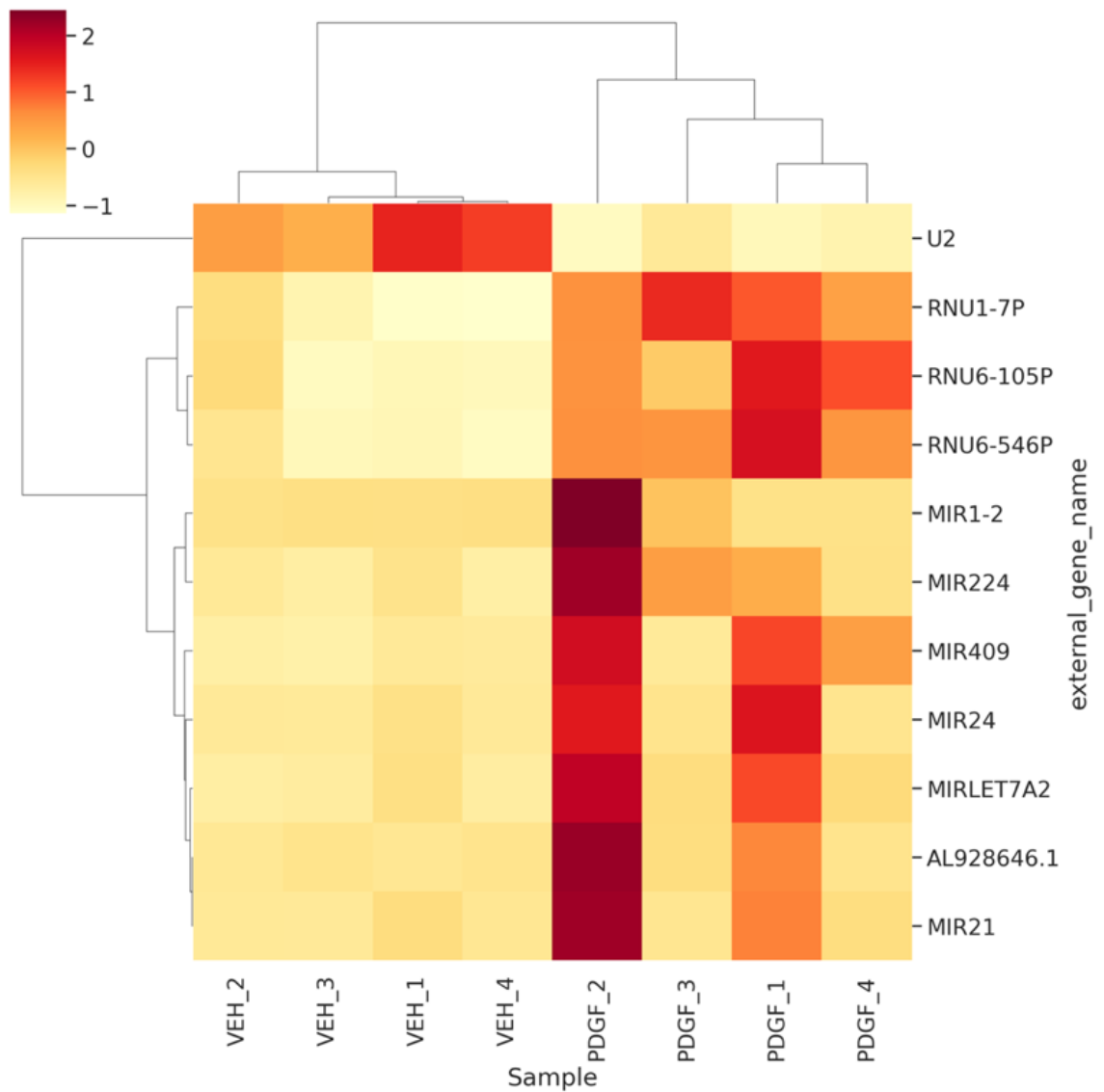


Figure 4-4 Heatmap representing the colour-coded difference in expression levels of differentially expressed genes. Heatmap showing hierarchical cluster analysis of significantly differentially expressed small RNAs between both vEVs (control) and pEVs with expression presented as log₂ fold change (z-scored) (adjusted p-value of <0.05). In this figure, colour intensity is determined by log₂ fold change where 'dark red', positive log₂ fold-change (z score), indicates higher gene expression and 'yellow', negative log₂ fold-change (z score), indicates lower gene expression. Each column represents an EV sample derived from HSVSMCs (N=4, where each N represents cells from a different patient). The EVs for each sample pair – VEH samples (vEVs) and a corresponding PDGF samples (pEVs), come from cells derived from the same patient.

Cross-referencing the genomic DNA read sequences (obtained from the alignment files visualised in IGV) to miRBase led to the identification of the mature form of known differentially expressed miRNA including miR-24-3p, miR-409-3p, miR-21-5p, let-7A-5p, miR-1-3p and miR-224-5p (Figure 4-5). Validation of AL928646.1 miRNA was not attempted at the time as this miRNA appeared to be novel and no information was available regarding its function on miRBase, and annotation databases used for functional annotation and GSEA. While it would have been very interesting to study AL928646.1 as a novel miRNA implicated in PDGF signalling, the lack of background knowledge about this miRNA and the lack of routine production of relevant AL928646.1 detection probes would have hampered the ability to effectively study its functions at the time due to both time- and budget-restrictions. Small nuclear RNAs such as U2, RNU1-7P, RNU6-105P and RNU6-546P were also not studied further as the main aim of these studies was to focus on investigating the role of miRNAs associated with EVs.

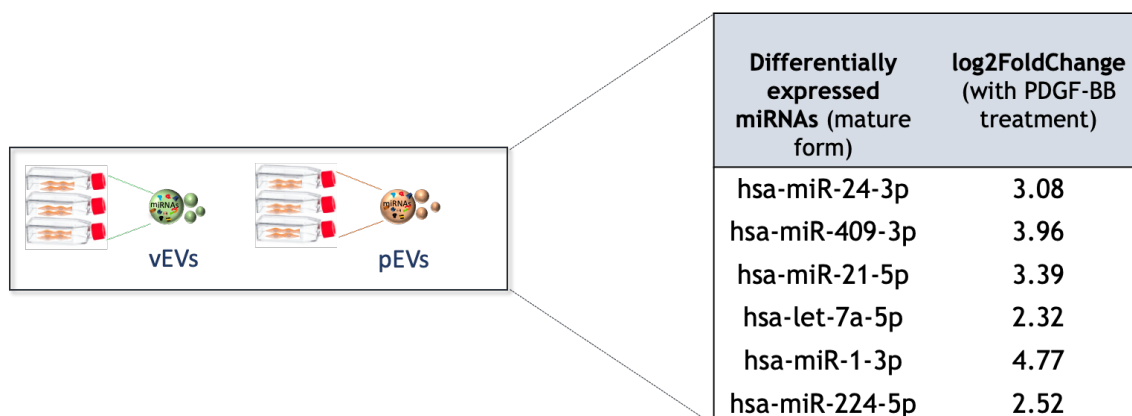


Figure 4-5 A list of the mature forms of differentially expressed miRNAs. There were six known differentially expressed miRNAs identified between vEVs and pEVs and the expression levels of all these miRNAs were upregulated in the EVs after 48 hr PDGF (20 ng/mL) treatment of HSVSMCs.

4.4.3 Validation of differentially expressed miRNA between vEVs and pEVs by qRT-PCR.

RNAseq analysis identified 6 known differentially expressed miRNAs: miR-24-3p, miR-409-3p, miR-21-5p, let-7A-5p, miR-1-3p and miR-224-5p. The next aim was to validate the RNAseq results by qRT-PCR. Out of all 6 miRNAs, 4 miRNAs were found to be significantly upregulated in pEVs compared to control EVs (vEVs) as confirmed by qRT-PCR analysis - miR-24-3p ($RQ_{\text{mean}} \pm \text{SEM}$ vEVs vs pEVs: 2.029 ± 0.150 , $p < 0.01$; Figure 4-6A), miR-224-5p ($RQ_{\text{mean}} \pm \text{SEM}$ vEVs vs pEVs: 3.194 ± 0.072 , $p < 0.05$; Figure 4-6B), miR-409-3p ($RQ_{\text{mean}} \pm \text{SEM}$ vEVs vs pEVs: 2.647 ± 0.391 , $p < 0.05$; Figure 4-6C), and let-7A-5p ($RQ_{\text{mean}} \pm \text{SEM}$ vEVs vs pEVs: 1.507 ± 0.153 , $p < 0.05$; Figure 4-6D), with miR-21-5p ($RQ_{\text{mean}} \pm \text{SEM}$ vEVs vs pEVs: 2.429 ± 0.715 , $p = 0.054$; Figure 4-6E) following the same trend but the difference in expression levels did not reach significance. Additionally, miR-1-3p appeared to be expressed at very low levels as indicated by the high cycle threshold (Ct) values detected for both groups (Figure 4-6F) (mean Ct > 35 for vEVs and pEVs). The Ct values across experimental replicates in each group were also extremely variable, Ct values between 34.706 - 40.000/undetermined and 33.580 - 38.177 were detected for vEVs and pEVs respectively, suggesting very low and inconsistent miRNA expression levels. Additionally, in the DESeq2 output table, a considerable variability between the normalised read counts was present for miR-1-2 across experimental replicates in the PDGF group (Appendix 8.1). A normalised read count of '0' was recorded for two out of four experimental replicates which when cross-validated with IGV also showed '0' reads for these samples. When miRNA levels in EVs were assessed by qRT-PCR, the findings reflected both the DESeq2 output data and the IGV cross-check in both their variability and low expression levels.

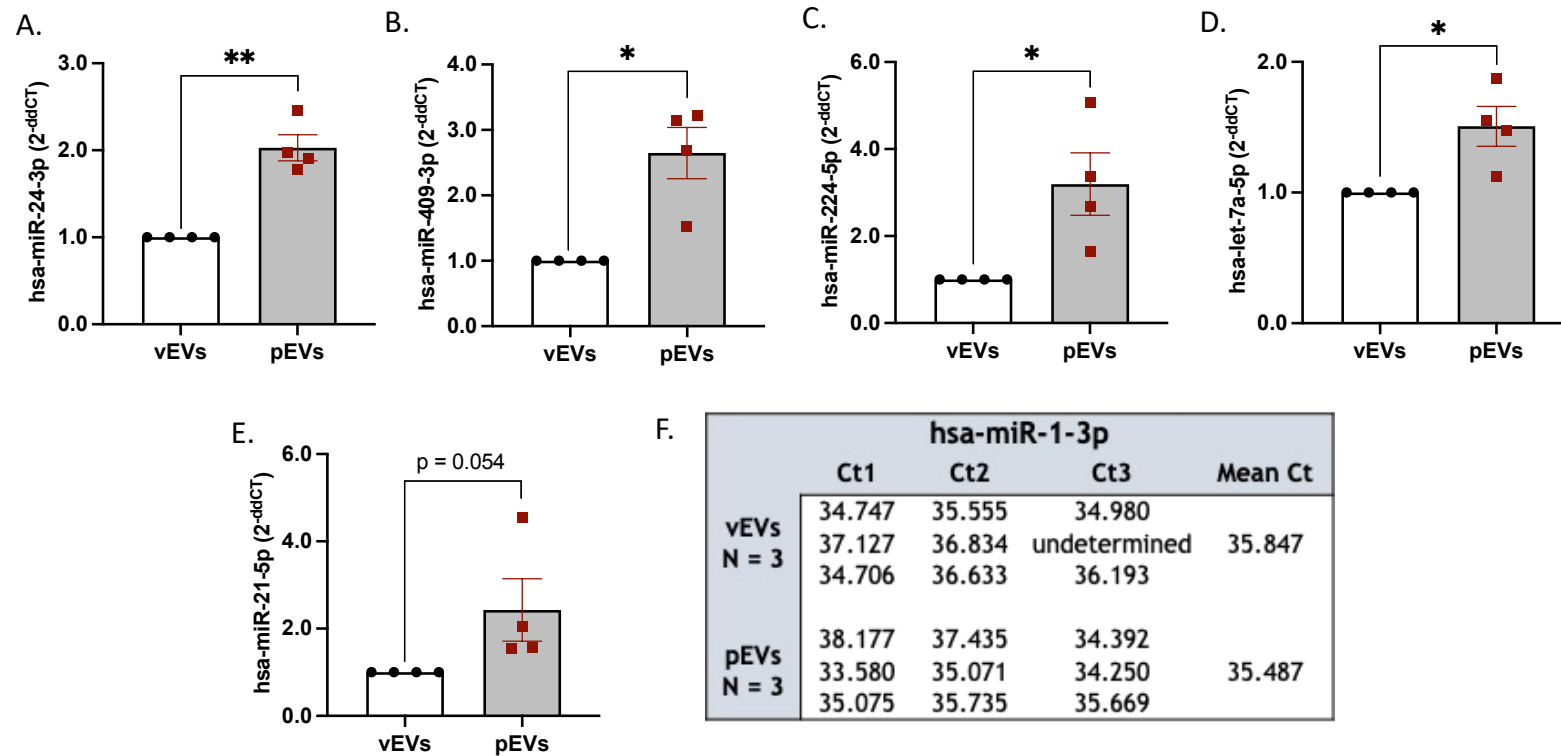


Figure 4-6 Validation of differentially expressed miRNAs in pEVs and vEVs by qRT-PCR. MicroRNA expression levels in vEVs and pEVs were assessed by qRT-PCR: (A) miR-24-3p; (B) miR-224-5p; (C) miR-409-3p, (D) let-7A-5p (E) miR-21-5p. In panel (F) miR-1-3p cycle threshold (Ct) values obtained by qRT-PCR across experimental replicates in both groups (N = 3). The fold change in expression levels for all miRNAs (except has-miR-1-3p) in pEVs was compared to vEVs group and differences between groups were assessed with a paired two-sample t-test; p-values <0.05 (*<0.05) were considered statistically significant (N=4).

4.4.4 Assessment of miRNA expression levels in HSVSMCs treated with VEH and PDGF

The expression levels of each of the upregulated miRNAs in pEVs were also measured directly in HSVSMCs to determine whether PDGF signalling also regulates the expression of miRNAs in the parental cells. Similar to the miRNA expression findings in EVs, the qRT-PCR analysis identified that cellular expression levels of 3 miRNAs, were also significantly upregulated in PDGF-stimulated HSVSMCs compared to VEH control cells including miR-24-3p ($RQ_{\text{mean}} \pm \text{SEM}$ vEVs vs pEVs: 1.138 ± 0.046 , $p < 0.05$; Figure 4-7A), miR-224-5p ($RQ_{\text{mean}} \pm \text{SEM}$ vEVs vs pEVs: 1.627 ± 0.087 , $p < 0.05$; Figure 4-7B), and miR-409-3p ($RQ_{\text{mean}} \pm \text{SEM}$ vEVs vs pEVs: 1.528 ± 0.113 , $p < 0.05$; Figure 4-7C), but not let-7A-5p (Figure 4-7D) or miR-21-5p (Figure 4-7E).

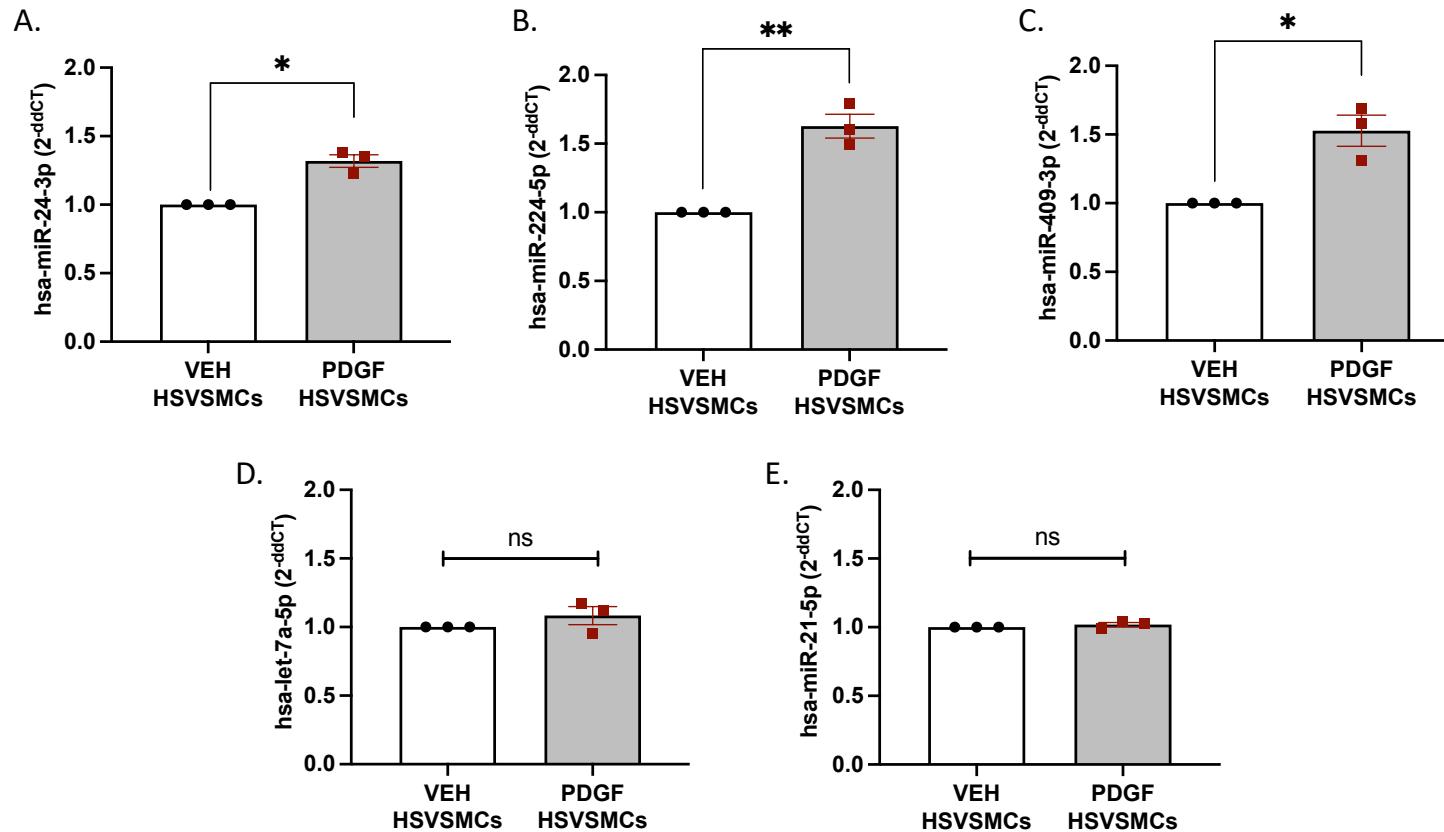


Figure 4-7 MicroRNA expression levels in VEH/PDGF treated HSVSMCs (vEVs and pEVs donor cells respectively). MicroRNA expression levels in vEVs and pEVs were assessed by qRT-PCR: (A) miR-24-3p; (B) miR-224-5p; (C) miR-409-3p, (D) let-7A-5p and (E) miR-21-5p; The relative miRNA expression levels were measured in PDGF HSVSMCs and VEH control HSVSMCs after 48hr incubation period. The fold change in miRNA expression levels was compared to VEH control HSVSMC group and differences between the groups were assessed with a paired two-sample t-test; p-values <0.05 (*<0.05, **<0.01) were considered statistically significant (N=3).

4.4.5 Potential 'true' miRNA gene targets were identified using basic bioinformatics analysis.

Target gene identification of differentially expressed miRNAs was carried out for the 3 most significantly upregulated miRNAs in pEVs - miR-24-3p, miR-409-3p and miR-224-5p, which were also found to be significantly upregulated in the parental cells. The bioinformatics approach of identifying 'true' miRNA gene targets involved the use of both prediction software tools and databases containing validated gene targets. Details of the exact method are summarised in Figure 4-8. Gene targets were considered predicted if predicted by at least 7 out of 12 prediction algorithms. There were 2,128, 1,126 and 1,084 predicted miRNA gene targets for the 3 qRT-PCR validated miRNAs: miR-24-3p, miR-409-3p and miR-224-5p respectively (Table 4-3). Two curated databases (miRTarBase and DianaTarBase) for experimentally validated miRNA gene targets were also used to identify potential 'true' miRNA gene targets. These two curated databases appeared to contain markedly different numbers of experimentally validated miRNA gene targets identified for the three miRNAs of interest - miR-24-3p, miR-409-3p and miR-224-5p (Table 4-3). For example, for miR-24-3p, there were only 855 gene targets identified in miRTarBase as opposed to 1,864 gene targets identified in DIANATarBase. Similarly, for miR-224-5p, there were only 132 gene targets recorded in miRTarBase and 1,810 gene targets found in DIANATarBase. When all predicted gene targets for one miRNA were compared to all gene targets identified in either one of the two curated databases, a list of potential 'true' miRNA gene targets was created which contained only those gene targets that were both predicted (by 7 out of 12 prediction algorithms) and also found in either one of the two curated databases. This led to a considerable reduction of the number of gene targets identified as potentially 'true' for each miRNA - 701, 49 and 288 for miR-24-3p, miR-409-3p and miR-224-5p respectively (Table 4-3).

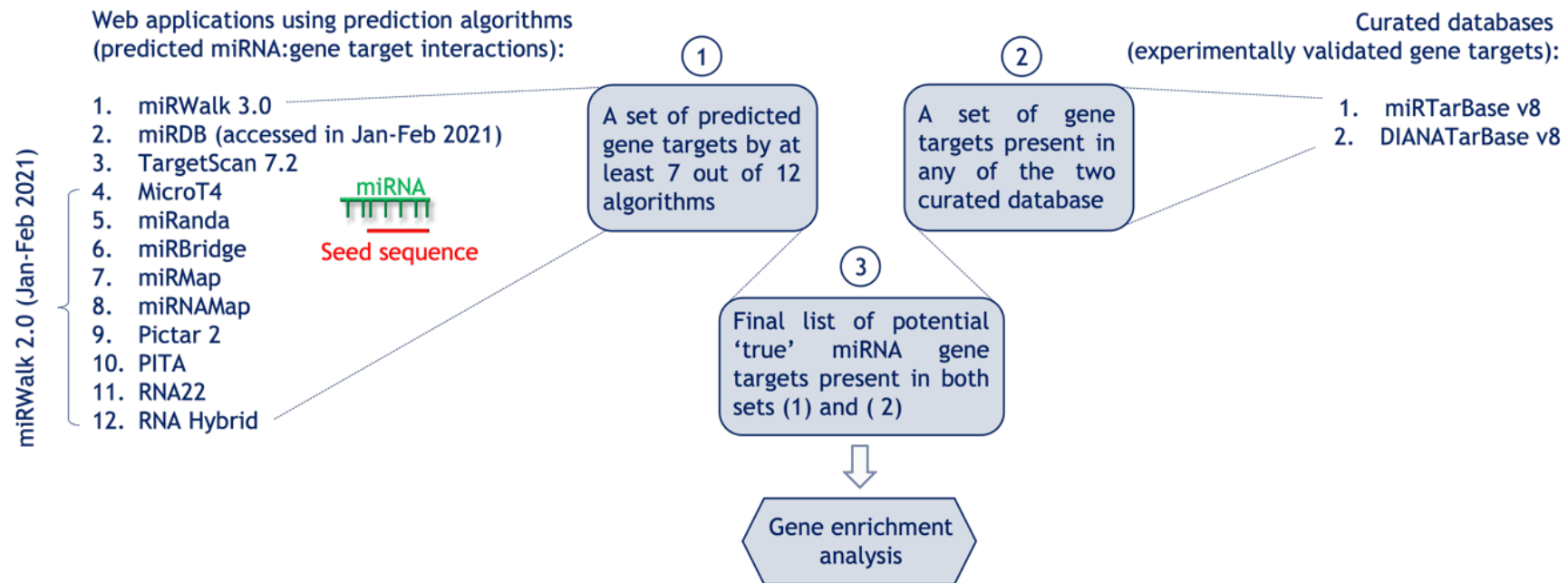


Figure 4-8 Schematic representation of the strategy concept used to identify potential 'true' miRNA gene targets for each miRNA of interest. A dataset of miRNA gene targets predicted by at least 7 out of 12 algorithms was obtained (subset 1). A dataset of gene targets found in at least one of the two curated databases of experimentally validated miRNA gene targets was also obtained (subset 2). An intersection of the two subsets (1 and 2) was used to obtain a final list of potential 'true' miRNA gene targets (subset 3). The process described was repeated on a per miRNA basis.

Table 4-3 Number of potential ‘true’ miRNA gene targets identified for miR-24-3p, miR-409-3p and miR-224-5p.

miRNA	Total predicted target genes across all datasets (12 prediction algorithms)	Validated (MiRTarBase v8)	Validated (DIANATarBase v8)	Predicted by at least 7 (out of 12) algorithms	Predicted by at least 7 algorithms and validated (miRTarBase <u>or</u> DIANATarBase)
hsa-miR-24-3p	20,446	855	1,864	2,128	701
hsa-miR-409-3p	19,984	111	79	1,126	49
hsa-miR-224-5p	19,041	132	1,810	1,084	288

As illustrated by the Venn diagram in Figure 4-9, a total of 41 miRNA gene targets were identified as common between miR-24-3p and miR-224-5p, including *PI3K* regulatory subunit 3 (*PIK3R3*), whereas only 6 and 2 gene targets were common between miR-224-5p and miR-409-3p, and miR-24-3p and 409-3p, respectively. Lists of common gene targets between miRNAs can also be found in Figure 4-9. Other gene targets identified for, for miR-224-5p include *PDGFRA* and *NRAS* (Appendix 8.2.1), and for miR-24-3p include *PDGFRB* and *RRAS* (Appendix 8.2.2).

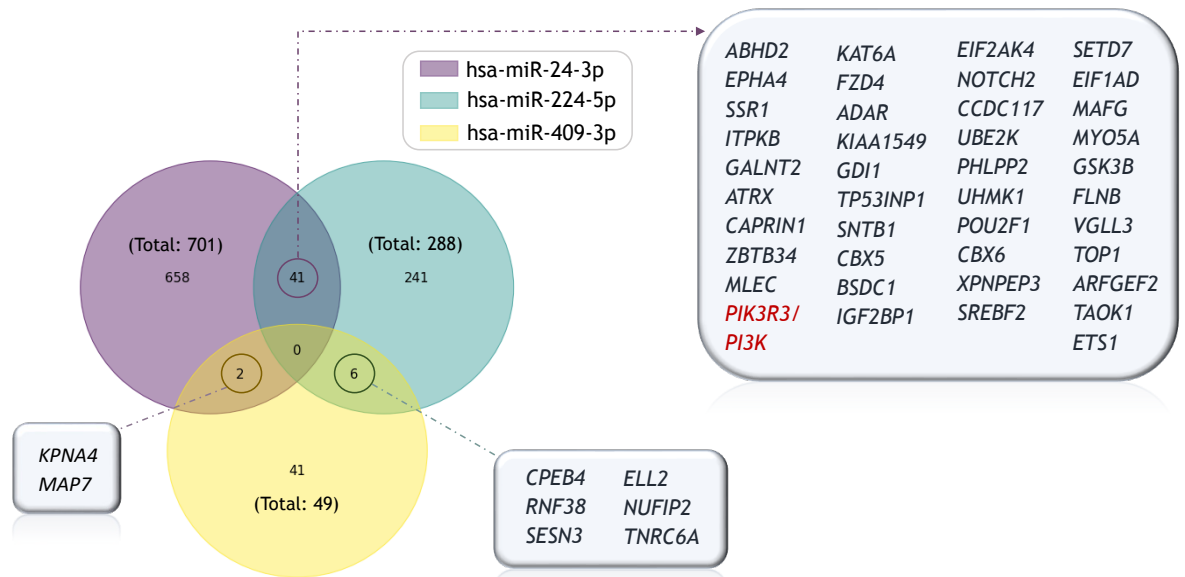


Figure 4-9 Common miRNA gene targets shared between miR-24-3p, miR-224-5p and miR-409-3p. Forty-one gene targets were identified as common between miR-24-3p and miR-224-5p, and 6 and 2 miRNA gene targets identified as common between miR-224-5p and miR-409-3p, and miR-24-3p and miR-409-3p respectively. No miRNA gene targets were identified as common between all three miRNAs.

4.4.6 Functional annotation and gene set enrichment analysis

MicroRNA target gene pathway analysis for miR-24-3p revealed a total of 46 significantly enriched molecular pathways (q-value < 0.05) involved in the regulation of biological processes such as cell proliferation, migration, and cell apoptosis. Some of these pathways included the PDGF signalling pathway, MAPK signalling pathway, Wnt signalling pathway, molecular pathways involved in the regulation of focal adhesion, Forkhead box class O family member proteins (FoxO) signalling pathway, regulation of RAS homolog family member A (RhoA) activity and p53 pathway (Figure 4-10). Pathway analysis for miR-225-5p target genes revealed 53 significantly enriched molecular pathways (q-value < 0.05) (Figure 4-11). Some of those pathways included cancer-related signalling pathways, pathways related to the regulation of actin cytoskeleton, hypoxia and p53, Ras signalling pathway and PI3K/AKT signalling pathway, all of which are also involved in the regulation of biological processes such as cell proliferation, migration, and cell apoptosis (Figure 4-11). Due to the small number of target genes identified for miR-409-3p as potentially true miRNA gene targets (a total of 49 genes), the pathway analysis returned only 3 significantly enriched pathways (q-value < 0.05) (Figure 4-12).

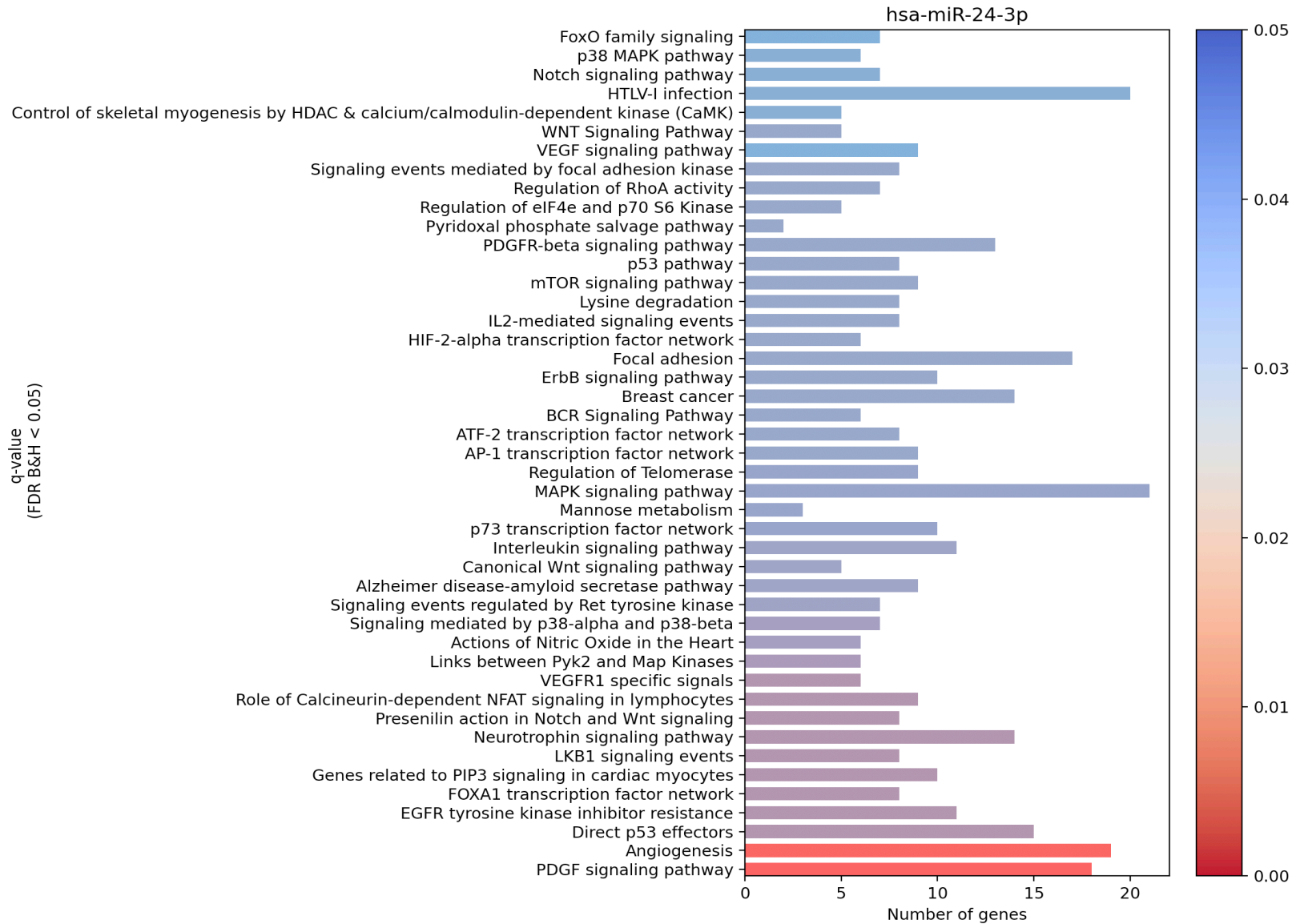


Figure 4-10 Pathway (KEGG, Panther DB and BIOCARTA) enrichment analysis of potential 'true' miRNA gene targets identified for miR-24-3p.

All bar charts illustrate significantly enriched functional categories (terms) for which padj/q-value (BH-FDR) < 0.05. Annotation terms (in this case pathways) are listed on the 'y' axis and the number of genes identified as significantly enriched in each annotation term is shown on the 'x' axis. Annotation terms on the 'y' axis are ordered by significance (q-value for all terms < 0.05) starting from the most significant at the bottom of the chart.

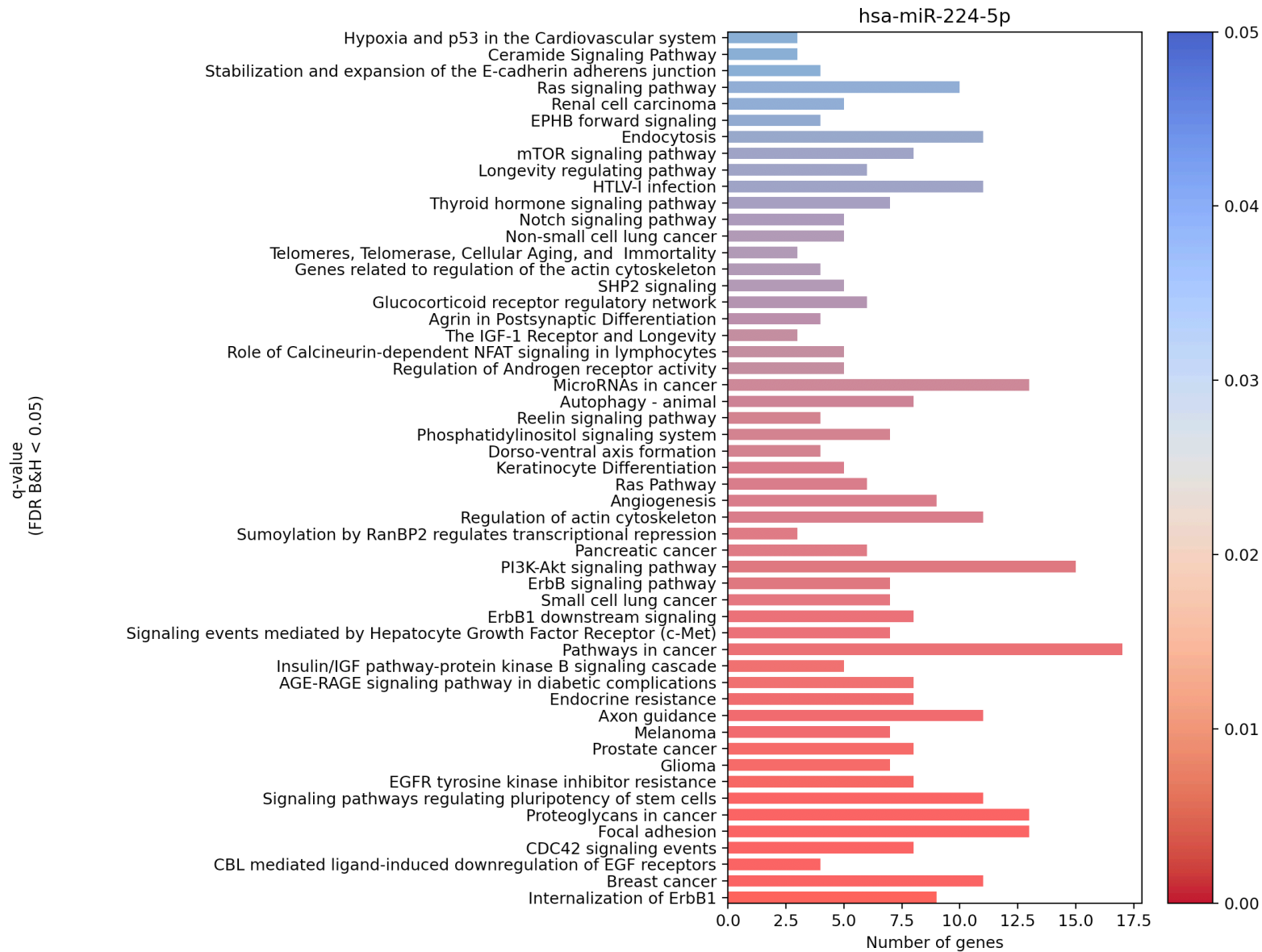


Figure 4-11 Pathway (KEGG, Panther DB and BIOCARTA) enrichment analysis of potential 'true' miRNA gene targets identified for miR-224-5p. All bar charts illustrate significantly enriched functional categories (terms) for which padj/q-value (BH-FDR) < 0.05. Annotation terms (in this case pathways) are listed on the 'y' axis and the number of genes identified as significantly enriched in each annotation term is shown on the 'x' axis. Annotation terms are ordered by significance (q-value for all terms < 0.05) starting from the most significant at the bottom of the chart.

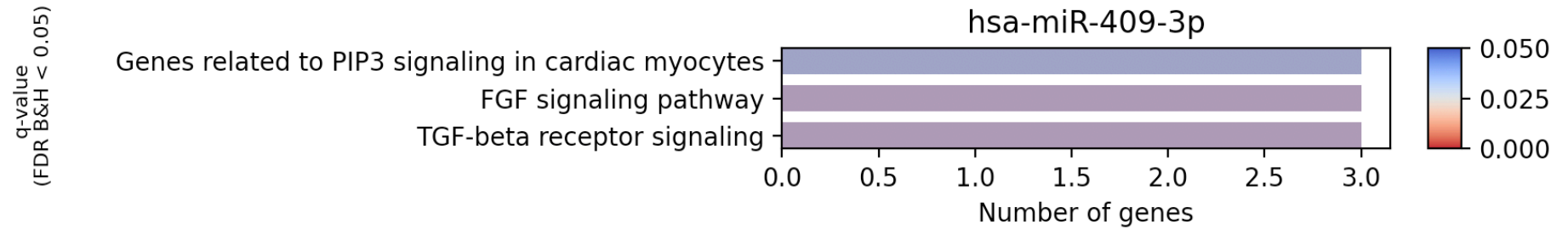


Figure 4-12 Pathway (KEGG, Panther DB and BIOCARTA) enrichment analysis of potential 'true' miRNA gene targets identified for miR-409-3p. All bar charts illustrate significantly enriched functional categories (terms) for which $\text{padj/q-value (BH-FDR)} < 0.05$. Annotation terms (in this case pathways) are listed on the 'y' axis and the number of genes identified as significantly enriched in each annotation term is shown on the 'x' axis.

Further GO (biological processes, BP) term enrichment analysis of miR-24-3p and miR-224-5p gene targets revealed 441 and 418 significantly enriched GO terms/biological processes (q-value < 0.05) respectively (Figure 4-13 and Figure 4-14) while there were no significantly enriched biological processes identified for miR-409-3p gene targets.

Due to the large number of significantly enriched biological processes (q-value < 0.05) identified for miR-24-3p and miR-224-5p target gene sets, the annotation terms for both miRNAs were filtered through keywords to allow suitable visualisation of the output data containing significantly enriched biological processes in the form of bar charts. The keywords used to filter through these files were terms related to cell growth/proliferation/migration/wound healing/cell death/apoptosis, and cancer (Table 2-9) and they were selected based on the findings from the miRNA target gene pathway analysis. It was found that both miR-24-3p and miR-224-5p miRNAs may be involved in the regulation of biological processes relevant to the development of neointimal formation including cell proliferation, migration and apoptosis as suggested by the resulting high number of significantly enriched pathways following targeted filtration aiming to extract annotation terms related to the above-mentioned processes. A total of 58 out of 441 and 50 out of 418 significantly enriched BP terms for miR-24-3p (Figure 4-13) and miR-224-5p (Figure 4-14), respectively, were identified after targeted filtration of all significantly enriched biological processes identified for both miRNAs (Section 2.12.3).

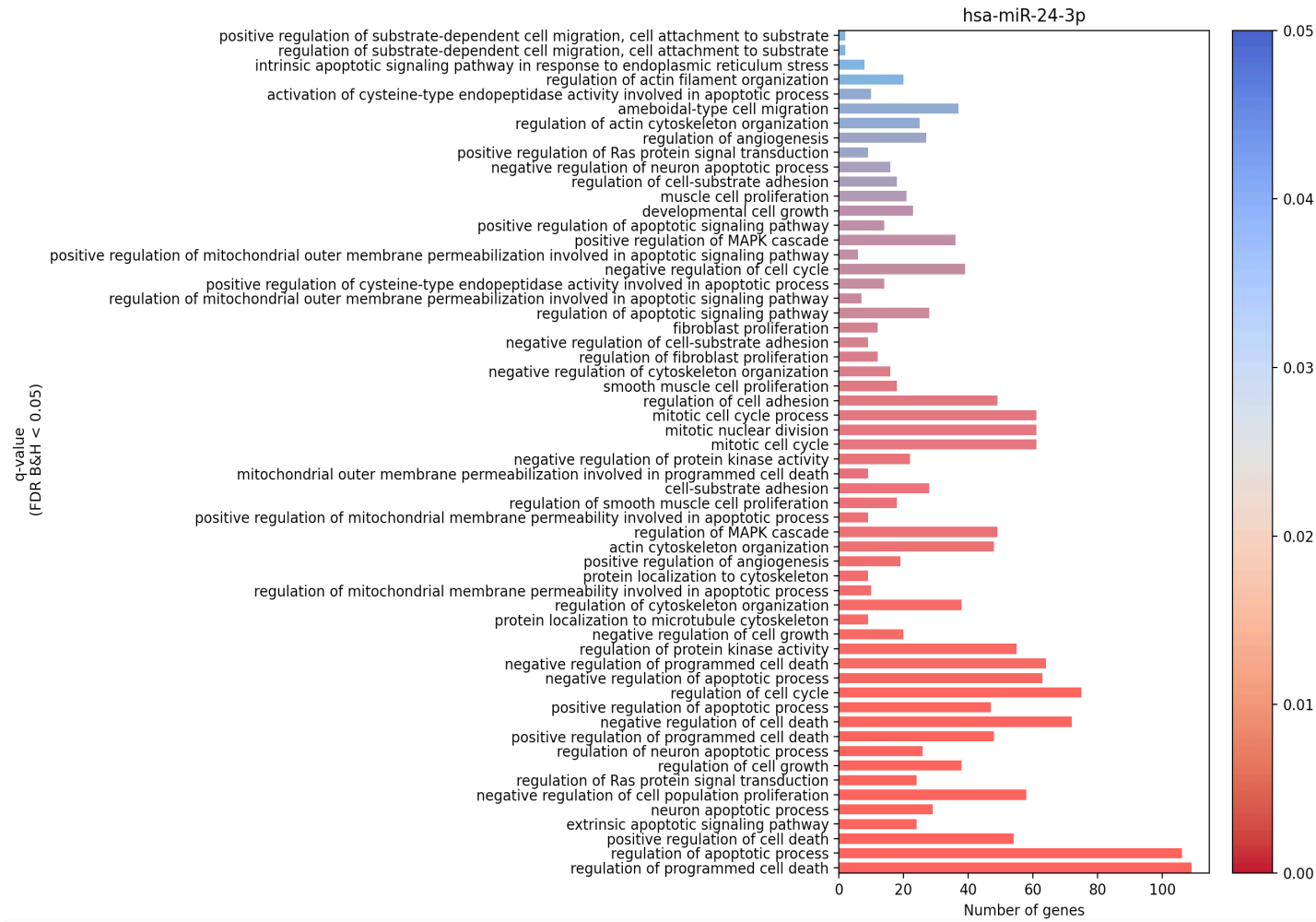


Figure 4-13 GO term (BP) enrichment analysis of potential ‘true’ miRNA gene targets identified for miR-24-3p. All bar charts illustrate significantly enriched BP annotation terms for which BH-FDR <0.05. Annotation terms are listed on the ‘y’ axis and the number of genes identified as significantly enriched in each annotation term is shown on the ‘x’ axis. Annotation terms on the ‘y’ axis are ordered by significance (q-value for all terms <0.05) starting from the most significant at the bottom of the chart. Data presented in this bar chart represents a summary of the filtered significantly enriched BP annotation terms. Keywords used for targeted filtration: ‘Proliferation’, ‘Cell growth’, ‘Cancer’, ‘Protein kinase’, ‘Ras protein’, ‘MAPK’, ‘AKT’, ‘TGF-beta’, ‘Platelet-derived growth factor receptor signalling pathway’, ‘Smooth muscle cell’, ‘Shear stress’, ‘Angiogenesis’, ‘Division’, ‘Cell cycle’, ‘Wounding’, ‘Cell death’, ‘Migration’, ‘Cell motility’, ‘Locomotion’, ‘Cytoskeleton’, ‘Actin’, ‘Adhesion’, ‘Apoptosis’, ‘Apoptotic’

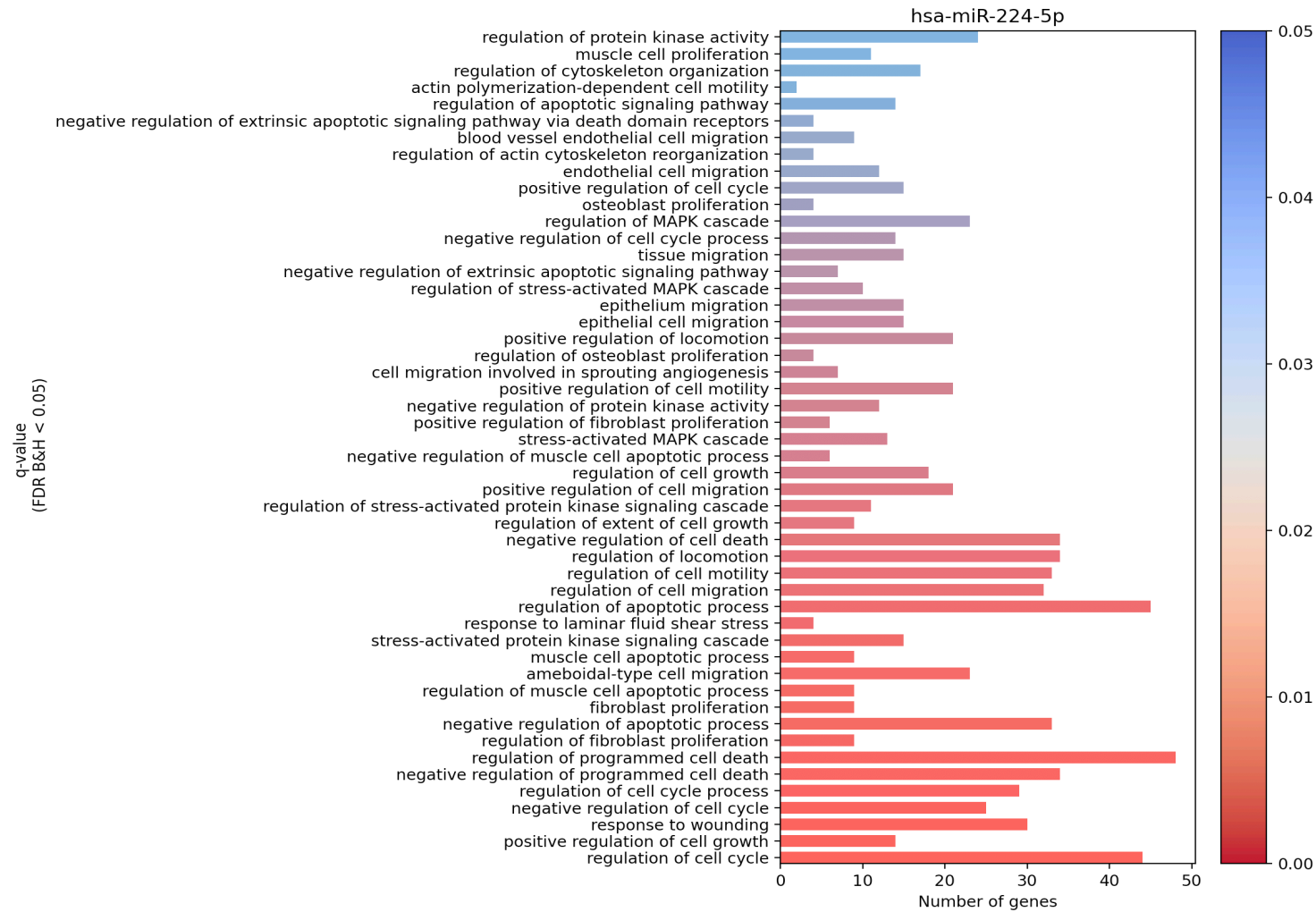


Figure 4-14 GO term (BP) enrichment analysis of potential 'true' miRNA gene targets identified for miR-224-5p. All bar charts illustrate significantly enriched BP annotation terms for which BH-FDR <0.05. Annotation terms are listed on the 'y' axis and the number of genes identified as significantly enriched in each annotation term is shown on the 'x' axis. Annotation terms on the 'y' axis are ordered by significance (q-value for all terms <0.05) starting from the most significant at the bottom of the chart. Data presented in this bar chart represents a summary of the filtered significantly enriched BP annotation terms. Keywords used for targeted filtration: 'Proliferation', 'Cell growth', 'Cancer', 'Protein kinase', 'Ras protein', 'MAPK', 'AKT', 'TGF-beta', 'Platelet-derived growth factor receptor signalling pathway', 'Smooth muscle cell', 'Shear stress', 'Angiogenesis', 'Division', 'Cell cycle', 'Wounding', 'Cell death', 'Migration', 'Cell motility', 'Locomotion', 'Cytoskeleton', 'Actin', 'Adhesion', 'Apoptosis', 'Apoptotic'.

Further analyses revealed the top 20 miRNA gene targets most commonly involved in the regulation of significantly enriched pathways identified for the three miRNAs of interest which are summarised in (Figure 4-15). These include *JUN*, *MAPK14*, glycogens synthase kinase 3 B (*GSK3B*), *PIK3R3*, *PDGFRB* and *eNOS/NOS3* for miR-24-3p (Figure 4-15A); *PIK3R3*, *NRAS*, *MAPK8*, *GSK3B* and *PDGFRA* for miR-224-5p (Figure 4-15B); and tyrosine 3-monooxygenase/tryptophan 5-monooxygenase activation protein epsilon (*WYHAE*) for miR-409-3p (Figure 4-15C). These genes are known to be involved in the regulation of biological processes such as cell proliferation, migration and apoptosis (Figure 4-10, Figure 4-11, and Figure 4-12). *MAPK14*, *PIK3R3* and *PDGFRB* were found to be involved in the regulation of 37.0%, 23.9% and 13.0% of all significantly enriched pathways identified for the miR-24-3p target gene dataset respectively (Figure 4-15A). *PIK3R3*, *NRAS* and *PDGFRA* were found to be involved in the regulation of 56.6%, 54.7% and 26.4% of the significantly enriched pathways identified for the miR-224-5p target gene dataset respectively (Figure 4-15B). *WYHAE* was found to be potentially involved in the regulation of 2 out of 3 significantly enriched pathways identified for the miR-409-3p target gene dataset (Figure 4-15C).

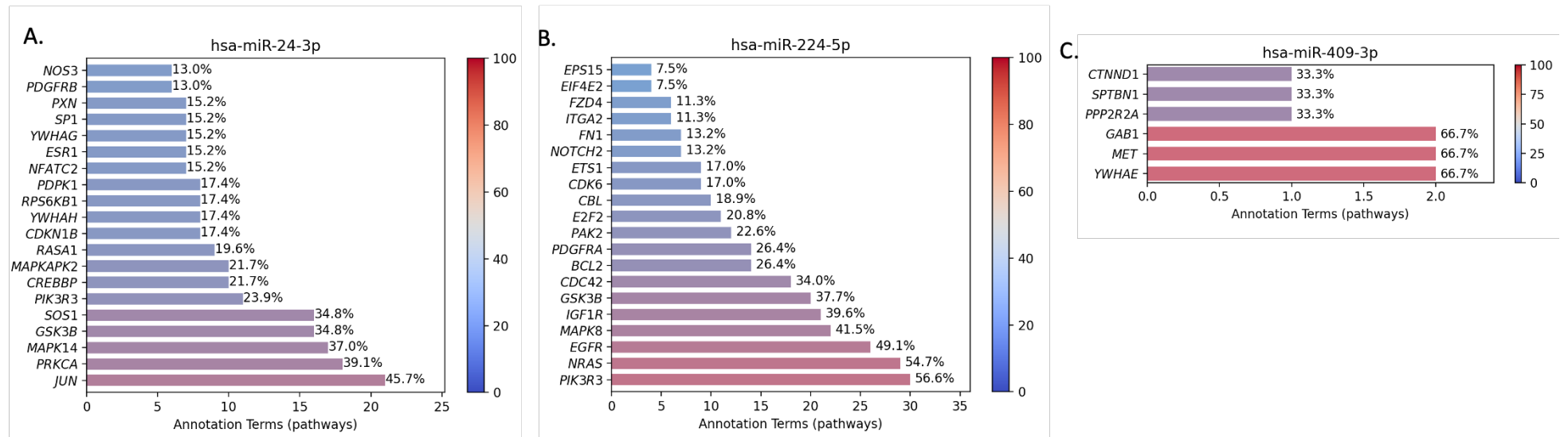


Figure 4-15 Summary of the most common genes across significantly enriched pathways. The most common miRNA target genes identified across significantly enriched pathways: (A) miR-24-3p (top 20 genes); (B) miR-224-5p (top 20 genes); and (C) miR-409-3p. The most common genes found in different functional categories are listed on the 'y' axis and the number significantly enriched annotation terms (pathways) in which each gene was found to be part of is shown on the 'x' axis. Genes on the 'y' axis are ordered by occurrence starting with the most commonly found gene across annotation terms at the bottom of the chart.

Next, it was of interest to assess the potential of two miRNAs working synergistically via the regulation of similar pathways and biological processes. The aim was to find out how many, if any, significantly enriched molecular pathways and biological processes appeared to be regulated by at least two of the miRNAs (miR-24-3p, miR-224-5p and miR-409-3p) via their specific miRNA gene targets. Datasets containing significantly enriched molecular pathways (Figure 4-16) and biological processes (unfiltered and filtered dataset) (Figure 4-17A and Figure 4-17B) identified for all three miRNAs were checked for overlapping annotation terms. It was found that there were no significantly enriched molecular pathways which were found to be common between all three miRNAs (miR-24-3p, miR-224-5p and miR-409-3p) (Figure 4-16). There were 9 common annotation terms, representing significantly enriched molecular pathways, which were shared between miR-24-3p and miR-224-5p including the pathway annotation term 'focal adhesion' (Figure 4-16).

When datasets containing unfiltered significantly enriched biological processes for miR-24-3p and miR-224-5p were checked, it was found that there were 182 (26.9%) common BP annotation terms between the two datasets, suggesting that there were potentially 182 biological processes (out of 676 total for both miRNAs) that may be regulated by both miRNAs via their target genes (Figure 4-17A). For visualisation purposes, the same type of analysis was performed on the filtered datasets containing only significantly enriched annotation BP terms related to cell growth/proliferation/migration/wound healing/cell death/apoptosis, and cancer. When filtered datasets were analysed, it was found that 18.6% of the significantly enriched BP annotation terms across both miRNAs (miR-24-3p and 224-5p) were common between the two (17 out of 91 total for both miRNAs) (Figure 4-17 B). suggesting that at least 17 out of a total of 182 common significantly enriched BP annotation terms identified as shared between both miRNAs (miR-24-3p and 224-5p) were related to proliferation, migration, or cell death (Figure 4-17B).

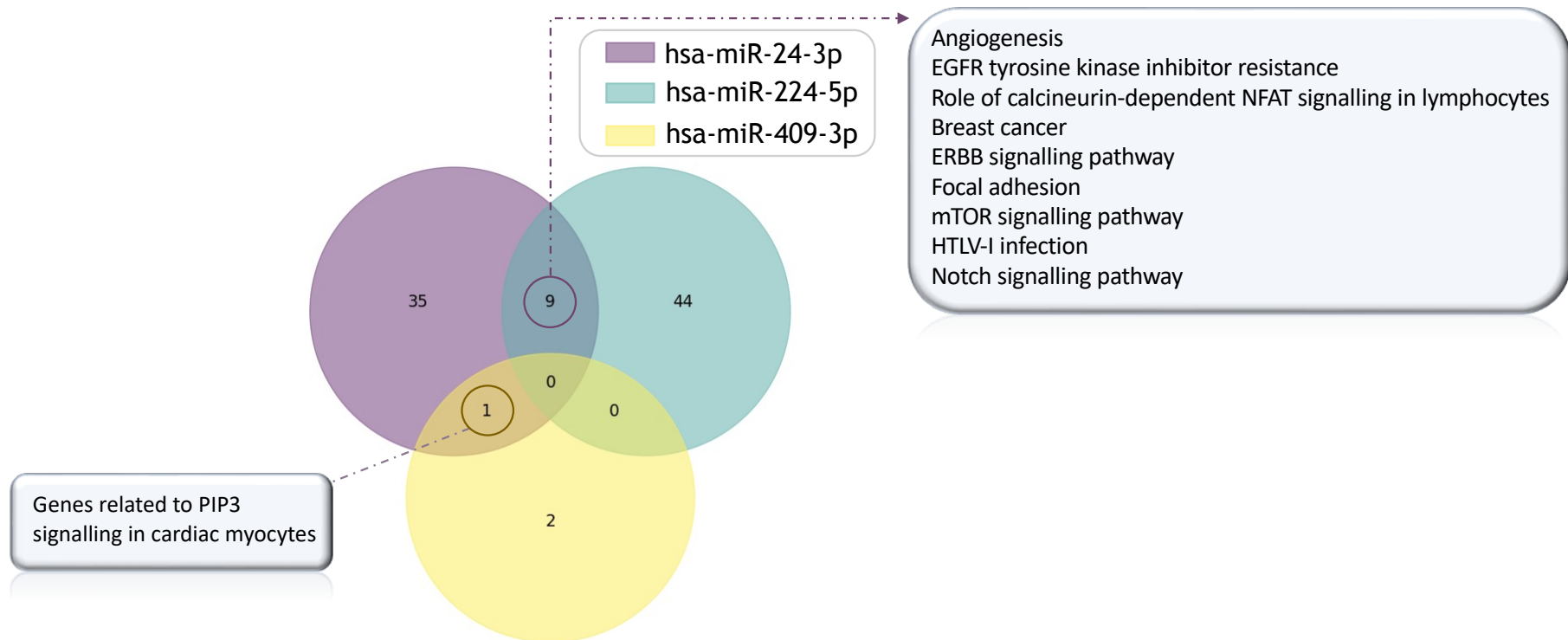


Figure 4-16 Summary of the common annotation terms across significantly enriched pathways identified for each miRNA of interest. Nine annotation terms across all significantly enriched pathways were identified as common between miR-24-3p and miR-224-5p and only one was shared between miR-24-3p and miR-409-3p. No common significantly enriched pathways were identified between miR-224-5p and miR-409-3p as well as between all three miRNAs of interest.

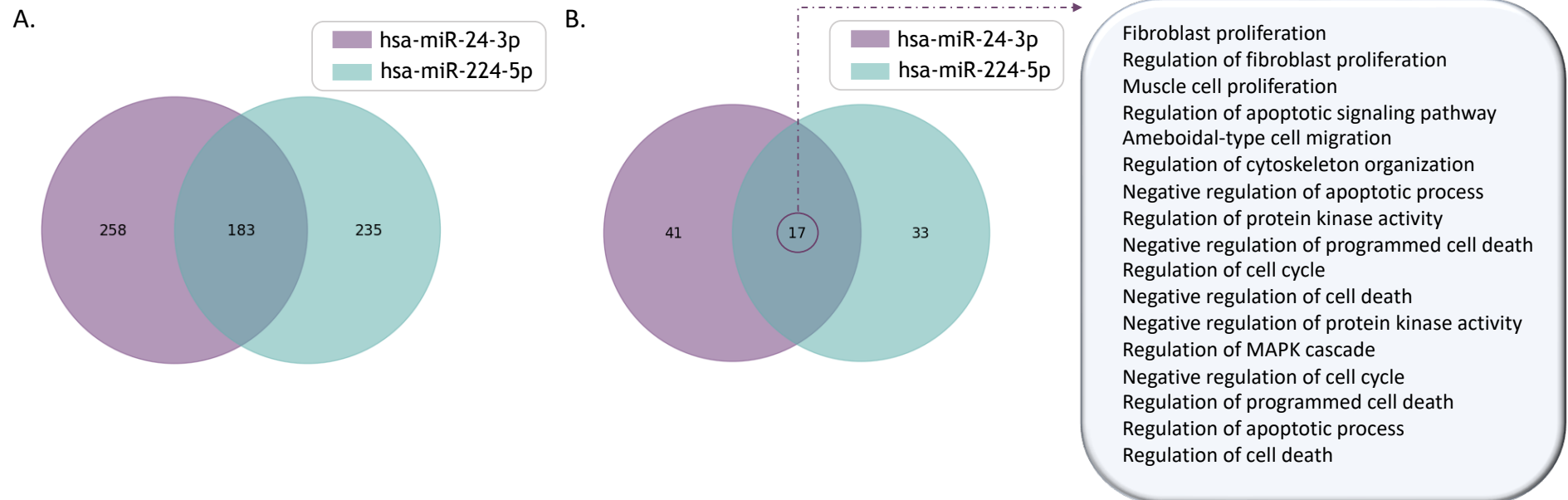


Figure 4-17 Summary of the common GO annotation terms across significantly enriched biological processes identified for miR-24-3p and miR-224-5p. Data analysis was performed on both (A) unfiltered enriched GO BP terms and (B) filtered datasets containing only significantly enriched GO BP terms related to cell growth/proliferation/migration/wound healing/cell death/apoptosis, and cancer. (A) Based on analysis of unfiltered datasets, 183 enriched BP terms were identified as common between miR-24-3p and miR-224-5p. (B) Based on analysis of filtered datasets, 17 enriched BP terms were identified as common between miR-24-3p and miR-224-5p.

4.5 Discussion

Vessel injury leads to an increased production of PDGF by platelets which has been associated with a subsequent phenotypic change in VSMCs through conversion of a mature quiescent 'contractile' VSMC phenotype into a dedifferentiated, proliferating 'synthetic' phenotype (Marmur et al., 1992; Pashova et al., 2020). These induced phenotypic changes in VSMCs are usually characterised by an increase in cell proliferation and migration - hallmark pathological processes in neointimal formation (R. Chakraborty et al., 2021; Chappell et al., 2016; Jawien et al., 1992). In addition to the known regulatory effects that PDGF has on cells, previous reports have demonstrated a potential role of PDGF in the regulation of EV secretion and EV signalling (Heo et al., 2020; Lopatina et al., 2014); however, here the effect of PDGF stimulation on EV release and characteristics from primary vascular cells was investigated.

In this study, it was hypothesised that prolonged pathological PDGF signalling in HSVSMC induces changes in the miRNA transcriptome of EVs secreted by stimulated cells. As EVs are known natural carriers of miRNAs and other small RNA molecules (van Niel et al., 2018), using NGS-based small RNA sequencing, we compared the small RNA expression profile of EVs derived from HSVSMCs under normal and PDGF-stimulated conditions. It was found that PDGF-derived EVs have a markedly different small RNA expression profile compared to control EVs. All differentially expressed miRNAs, including miR-24-3p, miR-409-3p, miR-21-5p, let-7A-5p, miR-1-3p and miR-224-5p, were found to be upregulated in the PDGF EVs and four of those (miR-24-3p, miR-409-3p, let-7A-5p, and miR-224-5p) were successfully validated by qRT-PCR. Further analysis revealed that both miR-24-3p and miR-224-5p miRNAs may be involved in the regulation of biological processes relevant to the development of neointimal formation including cell proliferation, migration, and apoptosis.

Several miRNAs, including miR-19b (Beaumont et al., 2017), miR-145 (Cheng et al., 2009), miR-221, miR-195 (Y. S. Wang et al., 2012b), miR-26a (Tan et al., 2017) have been implicated in the development of vascular stenosis and neointimal hyperplasia. The expression of miR-26a, in particular, has been shown to be tightly regulated by PDGF signalling in VSMCs where downregulation of miR-26a in rat jugular vein VSMCs was associated with a significant increase in

PDGF-induced cell proliferation, whereas an overexpression of miR-26a reduced both the proliferation and migration of rat jugular vein VSMCs (Tan et al., 2017). The expression levels of another two miRNAs, miR-221 and miR-222, were also found to be upregulated by PDGF in VSMCs from rat aorta in a dose-dependent manner (Liu et al., 2009).

Consistent with the findings presented here, it was recently reported that EV miRNA profile is also regulated by PDGF signalling, as demonstrated by the significantly different miRNA expression pattern (41 downregulated miRNAs and 54 miRNAs upregulated by ≥ 2 -fold) observed in EVs derived from PDGF stimulated PASC compared to EVs under normal conditions (Heo et al., 2020). In the same study, only six differentially expressed miRNAs were selected for further investigation and subsequently validated by qRT-PCR. Evidently, the detection of 95 differentially expressed miRNAs in PDGF PASC-derived EVs compared to the 7 differentially expressed miRNAs detected in PDGF HSVSMC EV population described in the present study, suggests that the former EV population exhibits a significantly more dysregulated miRNA expression profile. This substantial difference in miRNA expression profiles may, in part, be explained by the fact that the parental cells were different types of primary VSMCs as well as the fact that the experimental conditions in both studies were considerably different i.e., PASC were stimulated with a higher PDGF concentration (40 ng/mL) for a shorter period (16 hr) (Heo et al., 2020) in contrast to stimulation of HSVSMCs with 20 ng/mL PDGF for 48 hr as described here. It is possible that the response of cells exposed to PDGF stimulation in respect to EV release and miRNA cargo may be variable depending on whether cells are exposed to PDGF acutely or chronically. The expression of miR-26a, for example, has been reported to be closely regulated by PDGF in rat jugular vein VSMCs in a time and dose dependent manner (Tan et al., 2017). Additionally, it has previously been suggested that the EV cargo/miRNA expression profile may change depending on many factors including changes associated with different disease stages (S. He et al., 2021; Vinik et al., 2020). Interestingly, similar to our findings, miR-409 was also one of the significantly upregulated miRNAs in EVs secreted as a result of PASCs stimulation with PDGF (Heo et al., 2020). Another consistent finding between both studies is that the miRNA expression profile of EVs did not fully reflect the miRNA expression profile of parental cells. The

endogenous levels of miR-138, miR-1246, and miR-1260a three of the tightly regulated miRNAs in PDGF EVs, remained unchanged in PDGF-stimulated PSMCs (Heo et al., 2020). In the present study, expression levels of only three of the regulated miRNAs in PDGF-stimulated EVs, miR-24-3p, miR-409-3p, and miR-224-5p, were also found to be significantly upregulated in the parental cells, demonstrating that the EV miRNA expression profile does not always completely reflect the miRNA expression profile of parental cells (Robert et al., 2022) suggesting a designated role of EVs in cell-to-cell communication. These results highlight the importance of understanding the effects of environmental stimuli specifically on EV miRNA expression when studying EV-mediated cell communications. Another study investigating the effect of PDGF signaling on EV release from ASCs presented data further supporting the idea that prolonged PDGF stimulation could have a regulatory effect on EV release and EV cargo profile (Lopatina et al., 2014). PDGF treatment of ASCs was found to not only enhance EV release but also modify the protein content of EVs towards enhanced angiogenic activity as suggested by protein array analysis of 507 proteins (Lopatina et al., 2014).

As an initial step towards understanding the possible mechanisms by which miRNAs could be involved in governing biological processes within HSVSMCs, identification of potential 'true' gene targets of these miRNAs was attempted by using both a computational approach to predicting miRNA gene targets and curated databases of validated gene targets. A number of different prediction algorithms exist, each with a distinct approach to predicting possible miRNA gene targets (Peterson et al., 2014; Riolo et al., 2021). Despite recent advancements in prediction strategies, miRNA target prediction tools are still associated with a considerably high number of false positives due to lack of accuracy and sensitivity (Fridrich et al., 2019; Pinzón et al., 2017). Curated databases on the other hand, contain information about experimentally validated miRNA-gene target interactions (H. Y. Huang et al., 2020; Karagkouni et al., 2018), however, this information is not always up-to-date or accurate due to many challenges including varying quality of evidence between studies and the lack of consistent confirmation of specific interactions across multiple studies (Ji et al., 2015). Therefore, considering the limitations associated with both the use of target prediction algorithms and the sole use of curated

databases to identify miRNA targets, a strategy combining both approaches was employed in order to improve the probability of identifying ‘true’ miRNA targets.

Basic bioinformatics analysis was carried out to find out the potential miRNA gene targets for the three most significantly differentially expressed miRNAs which were also validated by qRT-PCR. As a result, 701, 288 and 49 target genes were identified for miR-24-3p, miR-224-5p and miR-409-3p respectively which satisfied the pre-defined criteria for potential ‘true’ miRNA gene targets. It was found that 41 target genes were common between miR-24-3p and miR-224-5p, including *PIK3R3* - a key enzyme involved in cellular functions such as cell growth, proliferation, migration, and survival (Ghafouri-Fard et al., 2022; Yang et al., 2017), suggesting possible synergistic regulation of individual genes by the two miRNAs (Xu et al., 2011). This is an important finding as it is known that one gene could have multiple binding sites for the same or different miRNAs which may result in multiple miRNAs regulating the expression/repression of target genes in cooperative manner if the binding sites are within optimal range (Enright et al., 2003; Grimson et al., 2007; Saetrom et al., 2007; Watanabe et al., 2005; Wu et al., 2010). Other gene targets identified for miR-24-3p include *PDGFRB*, *MAPK7*, *eNOS/NOS3* and *RRAS*, and for miR-224-5p include *PDGFRA* and *NRAS*.

To understand the biological significance behind the different gene targets identified for miR-24-3p and miR-224-5p, signal pathway and GO term enrichment analysis were performed. It was found that both miRNAs may be involved in the regulation of several molecular pathways, including PDGF, PI3K-AKT, RAS, WNT and MAPK signaling pathways, that are known to control biological processes such as cell proliferation/growth, migration/adhesion, and apoptosis (Azbazdar et al., 2021; Y. He et al., 2021; Zou et al., 2022) - all of which are important for the development of neointimal formation post-vascular injury (de Vries et al., 2016). The following gene targets: *MAPK14*, *PIK3R3*, *PDGFRB*, *eNOS/NOS3* and *PIK3R3*, *MAPK8*, *PDGFRA* were also found to be amongst the top 20 most common genes associated with significantly enriched pathways identified for miR-24-3p and miR-224-5p respectively. Since only 49 miRNA gene targets were identified for miR-409-3p, the GSEA performed for this

miRNA provided only very limited information regarding enrichment of important biological functions and signal pathways that may be regulated by the miRNA. Based on the findings from the GSEA, a diagram summarizing some of the possible mechanisms through which miR-24-3p and miR-224-5p may be involved in the regulation of cellular processes in VSMCs following PDGF stimulation was created (Figure 4-18).

Interestingly, some of the genes identified as potential targets of the miRNAs of interest (miR-24-3p and miR-224-5p in particular) have already been established as key regulators of VSMC proliferation and migration. For instance, the inhibition of both *PDGFRA* and *PDGFRB* in VSMCs has been shown to negatively regulate VSMC proliferation and migration after vascular injury *in vivo* indicating a causal role for activation of PDGFRs and neointimal lesion formation (Myllärniemi et al., 1997). More recently, miR-9 mediated inhibition of *PDGFRA* expression levels led to inhibition of VSMC proliferation and migration after balloon injury (Ham et al., 2017). Amongst the 3 classes of mammalian PI3K, the class 1A PI3K has been recognised as the most important for cellular growth and survival (Vivanco and Sawyers, 2002), and indeed, the involvement of PI3K in the regulation of VSMC migration and proliferation has been previously demonstrated *in vitro* (Cospedal et al., 1999; Liu et al., 2004; Oda et al., 2001). Additionally, MAPK14, a member of the MAPK family, and eNOS, have also been implicated in neointimal formation due to their proposed regulatory effects on VSMC proliferation. A recent study by Wu et al. 2019, found that inhibition of *MAPK14* in human CASMCs led to reduced cell proliferation *in vitro* and neointimal formation *in vivo* (W. Wu et al., 2019). The involvement of eNOS in the regulation of VSMC phenotype has been well established (Jeremy et al., 1999) with many studies demonstrating the ability of NOS enzymes to inhibit VSMC proliferation/migration and neointima formation in balloon injury models (Janssens et al., 1998; Von Der Leyen et al., 1995). Transfection of VSMC to overexpress eNOS was found to suppress VSMC proliferation possibly through a PKA-dependent mechanism (D'Souza et al., 2003). Another more recent study in VSMCs also demonstrated the involvement of eNOS in the regulation of vascular remodelling processes, reporting that urinary trypsin inhibitor inhibits the proliferation, invasion and phenotypic switching of PDGF-stimulated VSMCs via AKT/eNOS/ signalling pathway (C. Huang et al., 2020).

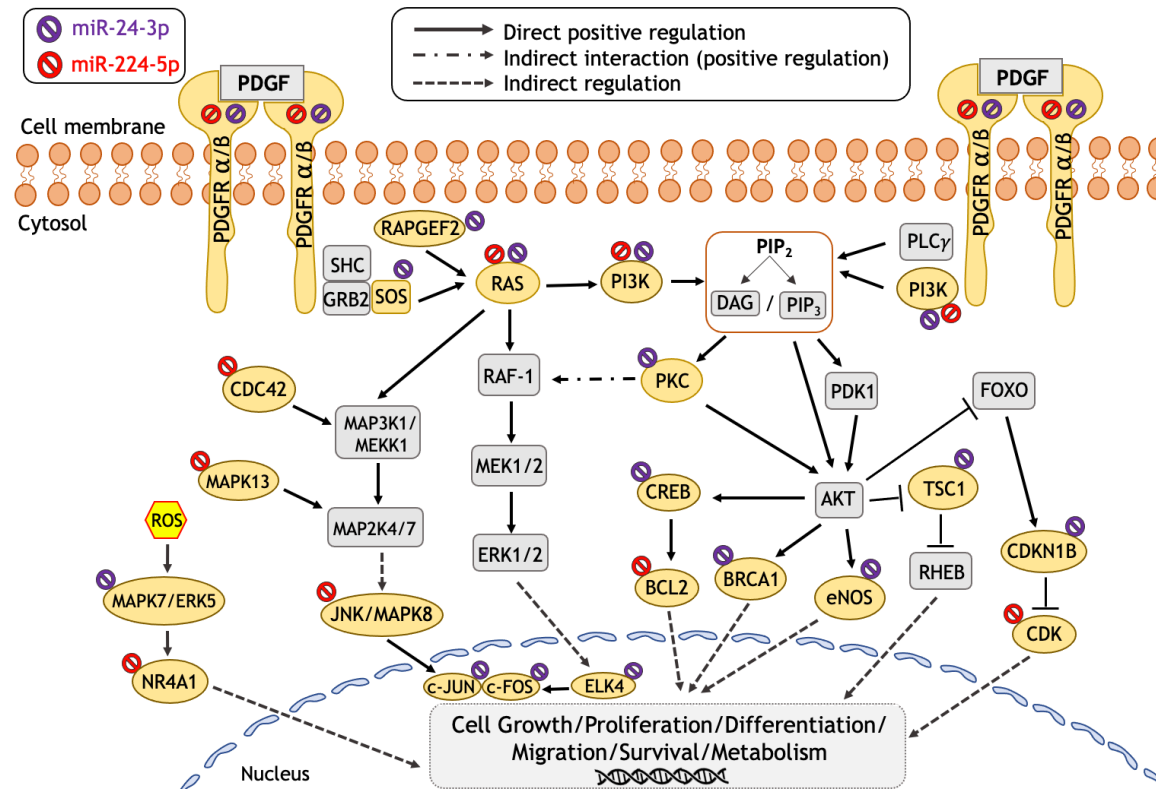


Figure 4-18 Schematic representation of molecular pathways identified in GSEA as potentially regulated by miR-24-3p and miR-224-5p. Abbreviations: PDGF, platelet-derived growth factor; PDGFRA/B, PDGF receptor A/B; GRB2, Growth factor receptor-bound protein 2; PI3K, phosphatidylinositol 3-kinase; SOS, son of sevenless homolog; RAPGEF2, Rap Guanine Nucleotide Exchange Factor 2; RAF-1, rafinose permease-1; MEK1/2, Mitogen-activated protein kinase kinase 1/2; ERK, extracellular signal-regulated kinase; ELK4, ETS Like-4 protein; ROS, reactive oxygen species; MAPK7/ERK5, Mitogen-Activated Protein Kinase 7/ extracellular-signal-regulated kinase 5; NR4A1, Nuclear Receptor Subfamily 4 Group A Member 1; CDC42, Cell division control protein 42 homolog; MAP3K1/MEKK1, Mitogen-activated protein kinase kinase kinase 1; Mitogen-activated protein kinase kinase 4/7, MAPK2/7K4/MEKK4/7; JNK, c-Jun N-terminal kinases; MAP3K13, Mitogen-activated protein kinase kinase kinase 13; PIP₂, Phosphatidylinositol 4,5-bisphosphate; PIP₃, Phosphatidylinositol (3,4,5)-trisphosphate; DAG, diacylglycerol; PDK1, Phosphoinositide-dependent kinase-1; PKB/AKT, Protein kinase B; CREB, cAMP response element binding protein; BCL2, B-cell lymphoma 2; BRCA1, Breast cancer type 1 susceptibility protein 1; eNOS, Endothelial nitric oxide synthase; FOXO, Forkhead box O; CDKN1B, cyclin dependent kinase inhibitor 1B; CDK, Cyclin-dependent kinase;

Consistent with the findings presented here, several lines of evidence from previous studies, primarily in the context of cancer, demonstrated that miR-24-3p and miR-224-5p are both involved in the regulation of cell proliferation and/or migration of cancer cells (Guo et al., 2012; J. Li et al., 2019; Mishra et al., 2009; Peng et al., 2021; Y. Xie et al., 2013), however, their role in vascular remodelling processes after injury has not been fully elucidated.

In cancer, for example, miR-24-3p has been identified as both an anti-proliferative miRNA (Guo et al., 2012; Mishra et al., 2009) and an oncogene (Y. Xie et al., 2013). A recent study, reported that miR-24-3p stimulated the progression of lung carcinoma by increasing cell proliferation and inhibiting cell apoptosis via targeting MAPK7 (Zhou and Yan, 2018). In the context of occlusive arterial disease, miR-24-3p has been shown to inhibit human arterial SMC proliferation and migration by targeting PDGFRB and c-Myc, and promoting human arterial SMC apoptosis (Zhu et al., 2015). In the same study, it was also reported that PDGF stimulation of human arterial SMC resulted in inhibition of miR-24-3p expression which is in contrast with the findings presented here of significantly increased expression levels of miR-24-3p in PDGF-treated human arterial SMC compared to VEH control treated cells. This inconsistency between the two studies could possibly be attributed to differences associated with the experimental conditions and more specifically the PDGF concentration used and the duration of cell stimulation. In the present study, HSVSMCs were stimulated with 20 ng/mL PDGF for 48 hr as opposed to 20 µg/L PDGF for only 24hr stimulation (Zhu et al., 2015) which could mean that after prolonged PDGF-signaling, upregulation of expression of certain miRNAs could be a compensatory mechanism.

Notably, the other two upregulated miRNAs in pEVs, miR-224-5p and miR-409-3p, and their role in the regulation of molecular mechanisms implicated in vascular pathologies, including neointimal formation, has not been investigated yet. However, both miRNAs have been implicated in the regulation of cell proliferation in the context of cancer. Similar to miR-24-3p, miR-224-5p has also been reported to serve as both an anti-proliferative miRNA/tumor suppressor (J. Li et al., 2019) and an oncogene (Fang et al., 2020; Peng et al., 2021; Zhang et al., 2013; L. Zhang et al., 2017) suggesting a possible dual function for this

miRNA (Guglielmi et al., 2020). MiR-224-5p has been demonstrated to successfully inhibit cell proliferation and migration via targeting *PIK3R3* and *AKT3* in ocular choroidal melanoma-1 (OCM-1) cells (J. Li et al., 2019). Conversely, in pancreatic mucinous cystadenocarcinoma cells (MCC), miR-224-5p has been shown to promote the proliferation, migration and invasion of MCC by directly targeting *PTEN* (Peng et al., 2021). Furthermore, silencing of radixin (RDX) and zinc-finger E-box-binding homeobox-1 (ZEB1) by miR-409-3p were also proposed as possible mechanisms of tumor suppression due to reduced cell proliferation and migration (Chen and Dai, 2018; L. Wu et al., 2019).

The findings in the present study along with the studies discussed above collectively support the notion that PDGF is an important messenger molecule capable of inducing changes at a transcriptomic level both in cells and EVs. Therefore, based on the findings in this study, it is reasonable to consider that miR-24-3p and miR-224-5p may be involved in the regulation of VSMC proliferation, migration and/or apoptosis by direct targeting of PDGFRA/B or by targeting other downstream components of the signaling pathway such as *PIK3R3*, or *NRAS/RRAS*.

4.6 Summary

The small RNA content of EVs derived from PDGF stimulated HSVSMCs was found to be significantly different from control EVs. Four out of six differentially expressed miRNAs in pEVs compared to vEVs, miR-24, miR-224, miR-409 and, let-7A-5p, were also successfully validated as significantly upregulated in pEVs by qRT-PCR analysis. GSEA revealed that miR-24-3p and miR-224-5p miRNAs may be involved in the regulation of several molecular pathways, including PDGF, PI3K-AKT, RAS, WNT and MAPK signaling pathways, that are known to control biological processes such as cell proliferation, migration, and apoptosis - all implicated in the development of neointimal formation post-vascular injury. Although there is evidence available supporting the involvement of miR-24-3p and miR-224-5p in the negative regulation of VSMC proliferation and migration, the exact role of EV-mediated delivery of those miRNAs to recipient cells in the setting of vascular injury has not been comprehensively investigated. Further studies are required to determine the potential of EV-associated miR-24-3p and miR-224-5p as therapeutic targets in neointimal formation post vascular injury.

Chapter 5 Studying the effect of HSVSMC-derived EVs on recipient cells

5.1 Introduction

5.1.1 MiR-24-3p/miR-224-5p- mediated cellular responses

EV secreted by HVSVMCs under PDGF stimulation had significantly different small RNA expression profile compared to EVs secreted under normal conditions and miR-24-3p and miR-224-5p were amongst the 6 significantly upregulated miRNAs in pEVs. GSEA revealed that both miRNAs may be involved in the regulation of crucial biological processes associated with neointimal formation, including cell proliferation, migration, and apoptosis (Azbazdar et al., 2021; de Vries et al., 2016; Y. He et al., 2021; Zou et al., 2022), possibly by modifying the expression of some of their target genes such as *PDGFRA/B*, *PIK3R3*, *NRAS* and *RRAS* (Chapter 4).

As previously discussed (Chapter 1), several miRNAs have been identified as key modulators of the process of VSMC phenotypic switching in the context of vascular injury, including miR-17-92, miR-21, miR-23b, miR-125a, miR-133, miR-143, miR-145, miR-146, miR-195, miR-221, miR-222, and miR-424, through regulatory mechanisms involving direct molecular targets such as *PTEN*, *KLF4*, *SMAD3*, *CDC42*, *ELK1*, cyclin D1 (*CCND1*) and *CDKN1C* (Gareri et al., 2016). Similarly, miR-92a, miR-126 and miR-221/222 have also been implicated in the regulation of EC regeneration after vascular injury through mechanisms involving the direct targeting of *SPREAD1*, *VCAM-1*, *KLF4*, *MKK4* and *c-KIT/CD117* (Gareri et al., 2016). While in the context of cancer, both miR-24-3p and miR-224-5p have been reported as potential regulators of cell proliferation and/or migration (Guo et al., 2012; J. Li et al., 2019; Mishra et al., 2009; Peng et al., 2021; Y. Xie et al., 2013), only miR-24-3p has also been implicated in the development of vascular pathologies (J. Yang et al., 2016a; Zhang et al., 2015; Zhu et al., 2015).

A mechanism through which miR-24-3p has been found to negatively regulate VSMC proliferation and migration in the context of diabetes involves direct targeting of high mobility group box-1 (*HMGB1*) (J. Yang et al., 2016a) or proliferation alone possibly through inhibition of WNT4/Dvl-1/ β -catenin signaling pathway by targeting WNT4 (J. Yang et al., 2016b). Interestingly, an inverse correlation between the expression levels of miR-24-3p and WNT4 in the arteries of diabetic rats was reported with significant inhibition of intimal hyperplasia

and ultimately neointimal formation after vessel injury following adenoviral gene transfer of miR-24-3p (J. Yang et al., 2016b). Similar effects of miR-24-3p on suppression of EC proliferation have been reported where miR-24-3p has been found to directly target eNOS resulting in increased expression of specificity protein 1 (SP1) and consequently inhibition of EC proliferation (Zhang et al., 2015). Since eNOS is a well-known EC-specific gene, it has been proposed that miR-24-3p could potentially regulate gene expression in a tissue-specific manner (Zhang et al., 2015). Additionally, serum EV-mediated transfer of miR-24-3p to recipient ECs has been shown to inhibit the process of wound healing by directly targeting PIK3R3 mRNA leading to increased EC apoptosis as well as reduced EC proliferation and migration, and angiogenesis (Y. Xu et al., 2020).

5.1.2 Exogenous loading of miRNAs into extracellular vesicles

Generally, EVs are considered ideal natural nanocarriers for clinical application due to their naturally biocompatible characteristics including their small size allowing penetration into deep tissues (Vader et al., 2016), their somewhat negative zeta potential aiding long circulation (Rupert et al., 2017), as well as their similarity to cell membranes (Hood and Wickline, 2012). Additionally, it has been reported that some EVs exhibit greater ability to escape degradation or clearance by the immune system (Hood, 2016). Indeed, EV-based therapeutics have been successfully utilised both *in vitro* and *in vivo*, with their therapeutic potential also highlighted in clinical settings (Claridge et al., 2021). However, despite that EVs have demonstrated promising clinical application because of their great therapeutic potential, there are still limitations associated with the use of EVs in clinical settings including issues related to low EV recovery rate/scalability and standardisation of EV generation, suboptimal isolation and purification procedures, therapeutic potency assessment, and targeted delivery (Claridge et al., 2021; Tian et al., 2020; Veerman et al., 2021).

Regardless of the disease setting, EV-based therapies generally utilise the functional capacity of EVs to mediate cellular responses in recipient cells through the delivery of various cargoes including siRNAs (Alvarez-Erviti et al., 2011; Shtam et al., 2013), miRNAs (L. Li et al., 2019), proteins (Garaeva et al., 2021) and small drug molecules (Y. Tian et al., 2014). EV therapeutic efficiency could be improved through different bioengineering techniques including

methods for EV content modification such as electroporation (Alvarez-Erviti et al., 2011; Lennaárd et al., 2022). Various small therapeutic molecules have been successfully incorporated as EV cargo leading to an improved potency, increased accumulation in target cells, enhanced drug stability and circulation time, and ultimately decreased IC₅₀ (the half maximal inhibitory concentration) (Luan et al., 2017).

Electroporation is one of the well-studied and commonly used methods for loading small therapeutic molecules into EVs (Lamichhane et al., 2015; Ma et al., 2018; Naseri et al., 2018; Pomatto et al., 2022; Y. Tian et al., 2014; Wahlgren et al., 2012). This method involves the use of high voltage electrical charge creating transient pores on the external EV membrane allowing the permeabilization of the therapeutic molecules into the EVs. Due to the temporal EV membrane interruption that occurs, EVs are usually firstly left to recover under incubation at an appropriate temperature and then washed and re-isolated, removing any non-internalised extracellular therapeutic molecules before using the EVs in functional assays (Alvarez-Erviti et al., 2011). Successful, loading of miRNA mimics or antagomirs (miRNA inhibitors) into EVs via electroporation has been reported in many studies (de Abreu et al., 2021; L. Li et al., 2019; Ma et al., 2018; Naseri et al., 2018). Naseri *et al.*, demonstrated that MSC-derived EVs loaded with anti-miR-142-3p oligonucleotides were able to reduce miR-142-3p and miR-150 expression levels *in vitro* and *in vivo* subsequently resulting in the upregulation of associated tumour suppressor genes including adenomatous polyposis coli protein (*APC*) and P2X purinoceptor 7 (*P2X7R*) in the recipient breast tumour cells (Naseri et al., 2018). The use of electroporation for miRNA loading was also investigated by Ma et al. reporting significant miR-132 overexpression detected by qRT-PCR in electroporated MSC-derived EVs with miR-132 mimic (Ma et al., 2018). HUVEC uptake of electroporated EVs was confirmed by fluorescent microscopy while EV-mediated delivery of functional miR-132 was confirmed by the observed increased miR-132 and decreased target gene (*RASA1*, RAS P21 Protein Activator 1) expression levels by qRT-PCR in recipient HUVECs (Ma et al., 2018). Although there are some potential caveats associated with the use of electroporation for EV cargo modification, such as disturbed structural integrity of the vesicles after electroporation or reduced small RNA loading efficiency due to the formation of

aggregates possibly also impacting the biological activity of the EV cargo (Kooijmans et al., 2013; Lamichhane et al., 2015; Liu and Su, 2019), the above studies suggest that this method could also lead to successful encapsulation of small RNAs in EVs, without affecting EV integrity and function.

5.1.3 Hypotheses

- HSVSMC-derived pEVs, containing up-regulated levels of several miRNAs, could regulate PDGF-induced cell proliferation and the expression of different miRNA target genes in recipient HSVSMCs.
- HSVSMC-derived EVs, containing exogenously overexpressed levels of miR-24-3p and miR-224-5p, are able to regulate HSVSMC and HSVEC responses.

5.2 Aims

- To assess the ability of unmodified vEVs and pEVs to regulate the expression levels of different miRNA gene targets in recipient HSVSMCs.
- To optimise miRNA mimic loading dose electroporated into EVs.
- To characterise EVs derived from HSVSMCs which were exogenously loaded with miRNA mimic (hsa-miR-24-3p and hsa-miR-224-5p) and assess whether the electroporation process had any effect on EV characteristics.
- To investigate the effect of miRNA mimic loaded EVs on proliferation and migration of recipient HSVSMCs.
- To explore the effect of miRNA mimic loaded EVs on recipient cell viability (HSVSMCs and HSVECs).
- To assess the ability of miRNA mimic loaded EVs to regulate the expression levels of different miRNA gene targets in recipient HSVSMCs.

5.3 Methods

5.3.1 Optimisation of miRNA mimic loading dose

First, the amount of miRNA mimic loaded into the EVs during electroporation was optimised. The same number of EV particles was used to treat recipient cells for 24 hr, while exploring EVs' efficiency at transferring varying amounts of miRNA mimic (Figure 5-1). To do that, a cel-miR-39 mimic (was loaded into EVs via electroporation (Section 2.10.6) with changes applicable to the sample preparation step described below. The EV concentration used in this experiment was the higher of the two concentrations explored in a preceding study of cell proliferation ($\approx 8 \times 10^4$ particles/cell) (Figure 5-3).

Prior to sample preparation (Figure 5-1), the concentration of stock EVs in DPBS was determined by NTA, and six equal volume EV samples (59 μ L) were prepared, each containing 2×10^{10} EV particles (samples 1-6). To create cel-miR-39 overexpressing EVs (celEVs) of three different cel-miR-39 mimic concentrations, equal volume samples (59 μ L) containing 66, 133 and 266 pmol of cel-miR-39 mimic were prepared in 50 mM Trehalose/DPBS (samples A-C respectively) and were then mixed with EV samples 1, 2 and 3 (1+A, 2+B, 3+C). Therefore, for every 1×10^{10} EV particles, 33, 66 or 133 pmol of cel-miR-39 mimic was used in the electroporation process respectively. Samples with naïve EVs (naEVs; EV particles which did not receive cel-miR-39 mimic during electroporation) were also prepared and processed. Similarly, to create naEVs, the remaining EV samples (samples 4-6) were mixed with samples D-F respectively, where samples D-F contained 50 mM Trehalose/DPBS only, and no cel-miR-39 mimic. Next, all sample mixtures were incubated on wet ice for 45 min. After incubation, EV samples were electroporated (as described in Section 2.10.6) and re-concentrated back to 100 μ L using Amicon centrifugal concentrator before being re-isolated (as described in Section 2.10.3.1). Electroporated EVs were then re-examined by NTA before adding EVs to recipient cells (Figure 5-2).

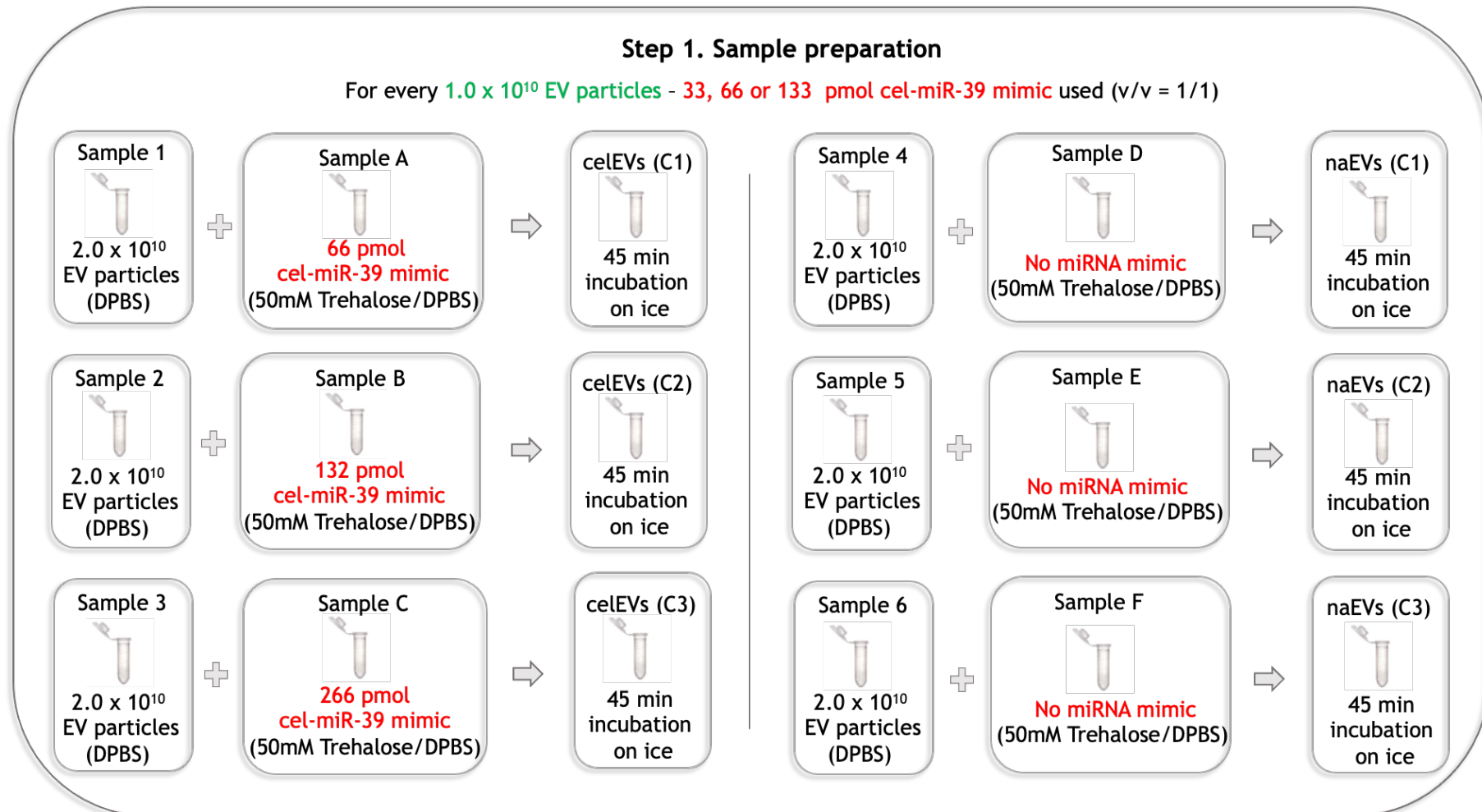


Figure 5-1 Optimisation of miRNA mimic loading dose - 'sample preparation' step. Schematic representation of the 'sample preparation' step followed as part of the optimisation process for miRNA mimic loading dose. EV samples were first mixed with varying amounts of cel-miR-39 mimic in 50 nM Trehalose/DPBS (Sample 1, 2 and 3 + Sample A, B and C respectively) or 50 nM Trehalose/DPBS alone (Sample 4, 5 and 6 with Sample D, E and F respectively). Sample mixtures were then incubated for 45 min on ice before electroporating miRNA mimics into the EVs.

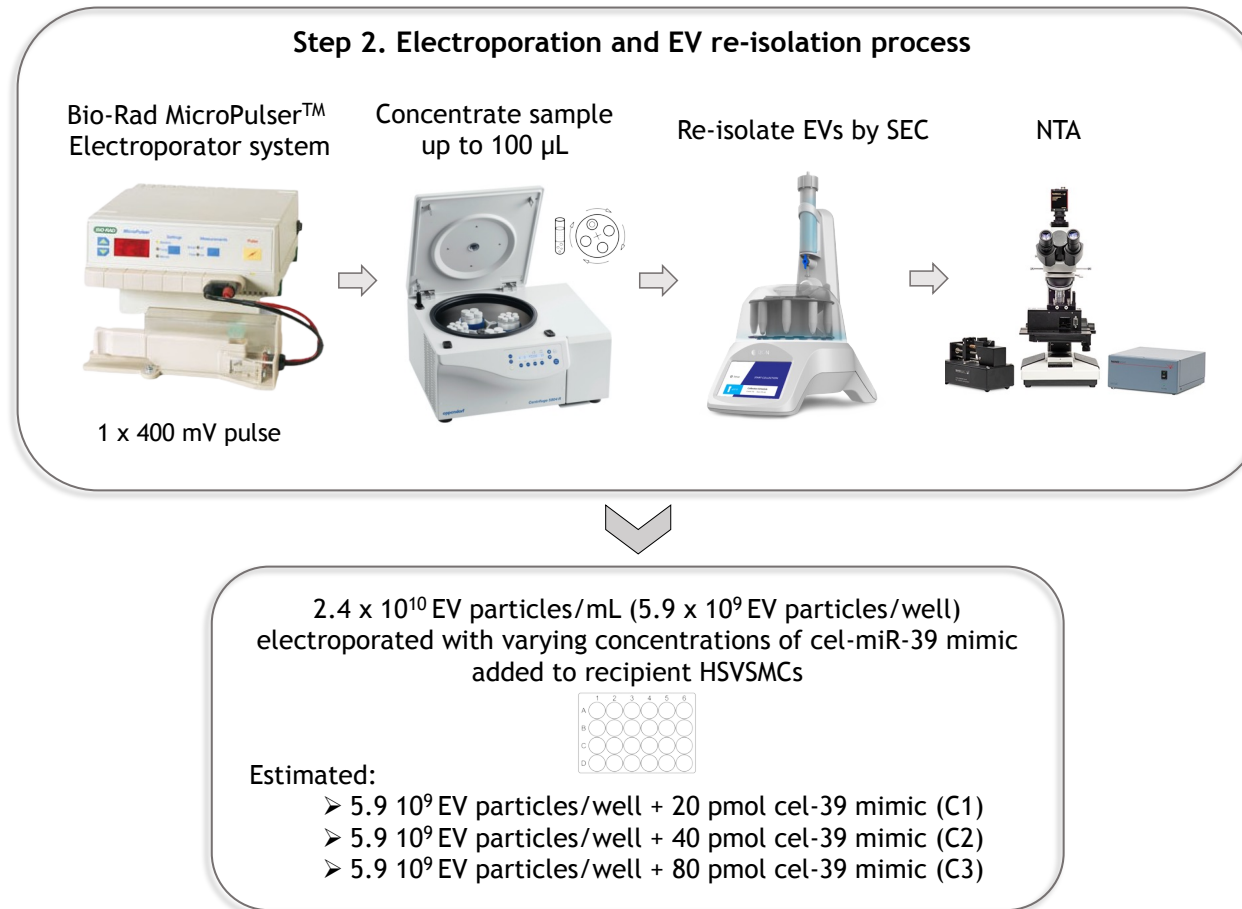


Figure 5-2 Optimisation of miRNA mimic loading dose - 'electroporation and EV re-isolation' steps. Schematic representation of the 'electroporation and EV re-isolation' steps followed as part of the optimisation process for miRNA mimic loading dose. Following incubation, sample mixtures were electroporated and then left to recover overnight in the fridge. The next day, electroporated samples were re-concentrated to 100 µL and EVs were re-isolated (cel-miR-39 EVs, C1, C2 and C3, and naEVs). Finally, EV sample concentration and EV size were checked by NTA before proceeding to using the EVs for *in vitro* experiments.

Table 5-1 Other relevant methods for Chapter 5.

EV generation protocols	Section 2.10.1 and Section 2.10.2
EV isolation from CCM	Section 2.10.3.1
Nanoparticle tracking analysis	Section 2.10.4
Loading of miRNA mimics into EVs	Section 2.10.6
Measuring of gene expression levels	Section 2.6
EV characterisation	Nanoparticle tracking analysis (Section 2.10.4)
	Protein expression analysis (Section 2.7)
	Transmission electron microscopy (Section 2.10.5)
Cell work methodologies	Experimental protocol designed to study the effect of unmodified vEVs and pEVs on activated HSVSMCs (Section 2.4.1)
	Experimental protocols designed to study the effect of miEVs on HSVSMCs (Section 2.4.2)
	Experimental protocol designed to study the effect of miEVs on HSVECs (Section 2.4.3)
Functional assays	Cell proliferation via BrdU incorporation assay (Section 2.9.1)
	Cell viability via MTT assay (Section 2.9.2)
	Cell migration assays (Section 2.9.3)

5.4 Results

5.4.1 Studying the effect of EVs on HSVSMCs co-stimulated with PDGF

In Chapter 3, it was found that unmodified EVs had no significant effect on proliferation of recipient quiesced HSVSMC. Additionally, in Chapter 4 it was also found that several miRNAs (miR-24-3p, miR-224-5p, miR-409-3p, miR-21-5p, let-7a-5p and miR-1-3p) potentially involved in the regulation of PDGF-induced cell proliferation processes via their target genes, were upregulated in pEVs compared to vEVs. Therefore, it was next of interest to determine whether pEVs could affect proliferation of already actively proliferating recipient HSVSMCs following PDGF stimulation.

In this experiment, quiesced HSVSMCs were either untreated (VEH control), treated with 20 ng/mL PDGF alone, or co-treated with 20 ng/mL PDGF and vEVs or pEVs while assessing the effect of two different EV concentrations (C1 = 8.0×10^8 EVs/mL or 8.0×10^7 EVs/well and C2 = 1.0×10^{10} EVs/mL or 1.0×10^9 EVs/well) (Figure 5-3A and B). Initially, absorbance was measured after a treatment period of 6 hr (Figure 5-3A) and then after 24 hr (Figure 5-3B). It was found that, 6 hr treatment was not enough to re-activate quiescent recipient HSVSMCs as evident by the low absorbance (OD < 0.05) detected in all experimental groups including the positive control where cells were treated with 20 ng/mL PDGF alone (Figure 5-3A). When cells were incubated for longer (24 hr), re-activation of cell proliferation was detected as evidenced by an increase in the absorbance detected for all experimental groups including the positive control (OD > 0.5) (Figure 5-3B). After 24 hr of treatment, a tendency towards reduction of cell proliferation was observed when cells were co-treated with 20 ng/mL PDGF and the higher concentration of pEVs (C2) compared to cells treated with 20 ng/mL PDGF alone (with OD values of 0.3 and 0.6) (Figure 5-3B). As this experiment was performed only once (N=1), no statistical tests were carried out and no definitive conclusions were made based on this data. Instead, this experiment was informative, and based on the results obtained it was decided that cell proliferation would be assessed after at least 24 hr treatment and the higher EV concentration (C2 = 1.0×10^{10} EVs/mL or 1.0×10^9 EVs/well) would be used.

Next, quiesced HSVSMCs were untreated (VEH control), treated with 20 ng/mL PDGF alone, or co-treated with 20 ng/mL PDGF and vEVs or pEVs (1.0×10^{10} EVs/mL or 1.0×10^9 EVs/well) for 24 hr and cell proliferation assessed. After 24 hr PDGF-treated cells proliferated significantly more than untreated VEH control cells (Abs: 1.311 ± 0.063 vs 0.326 ± 0.039 respectively; $p < 0.05$) suggesting that PDGF treatment was able to re-activate quiescent cells (Figure 5-3C). Additionally, it was found that compared to cells treated with 20 ng/mL PDGF, neither pEVs or vEVs had any effect on proliferation of recipient HSVSMCs co-treated with PDGF (Figure 5-3C). A tendency towards inhibition of cell proliferation was observed when cells were co-treated with 20 ng/mL PDGF and pEVs compared to vEVs, however, the difference was not statistically significant (Figure 5-3C).

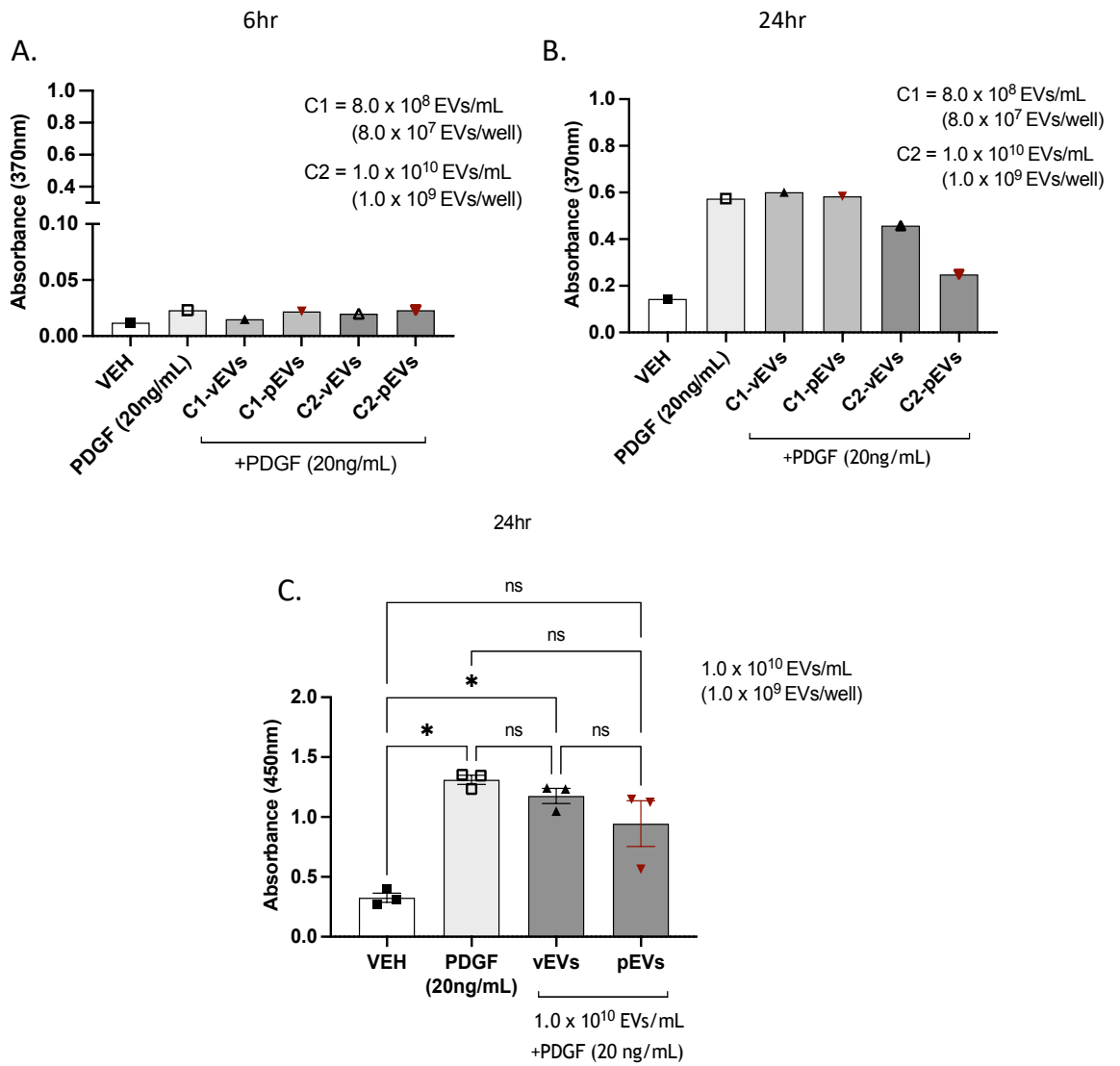


Figure 5-3 Studying the effect of unmodified EVs on HSVSMC proliferation co-treated with 20ng/mL PDGF and unmodified vEVs/pEVs. (A) Assessing the effect of two different EV concentrations on cell proliferation after 6 hr treatment period (N=1); (B) Assessing the effect of two different EV concentrations on cell proliferation after 24 hr treatment period (N=1); (C) Assessing the effect of EVs (1.0×10^{10} EVs/mL / 1.0×10^9 EVs/well) on cell proliferation after 24 hr (N=3). Data are presented as mean \pm SEM where N \geq 3. Differences between groups (when N \geq 3) were assessed using an RM one-way ANOVA with a Tukey's correction to compare the means of all groups. A p-value $<$ 0.05 was considered statistically significant.

Next, whether pEVs could drive any changes in expression levels of target genes in active HSVSMCs was explored. HSVSMCs were either untreated (VEH control), treated with 20ng/mL PDGF alone, or co-treated with 20ng/mL PDGF and vEVs or pEVs (2.4×10^{10} EVs/mL or 6.0×10^9 EVs/well) for 6 or 24 hr before assessing cell proliferation and measuring expression levels of target genes (*PDGFRA*, *PDGFRB*, *PIK3R3*, *NRAS* and *RRAS*) in the recipient cells.

It was noted that the expression of *PDGFRA* appeared to be upregulated in all experimental groups where cells were treated with 20 ng/mL PDGF after 6 hr ($RQ_{\text{mean}} \pm \text{SEM VEH vs 20ng/mL PDGF: } 2.318 \pm 0.142$) compared to untreated VEH control cells (Figure 5-4A). After 24 hr of treatment there was an obvious reduction in the expression levels of *PDGFRA* in these groups to levels comparable to those detected in the untreated VEH cells ($RQ_{\text{mean}} \pm \text{SEM VEH vs 20 ng/mL PDGF: } 1.168 \pm 0.306$) (Figure 5-5A). Additionally, it was observed that 20 ng/mL PDGF treatment did not cause an increase in expression of PDGF signalling pathway-related genes after 6 hr (*PDGFRB* and *RRAS*) or 24 hr (*PDGFRB* and *RRAS*) of treatment (Figure 5-4B and E and Figure 5-5B and E respectively). A slight increase in expression levels of *PIK3R3* and *NRAS* following PDGF stimulation was noted after 6 hr of treatment compared to control cells ($RQ_{\text{mean}} \pm \text{SEM VEH vs 20 ng/mL PDGF: } 1.765 \pm 0.643$ for *PIK3R3* and $RQ_{\text{mean}} \pm \text{SEM VEH vs 20 ng/mL PDGF: } 1.497 \pm 0.296$ for *NRAS* respectively). The observed increase in gene expression levels appeared to be further promoted after 24 hr ($RQ_{\text{mean}} \pm \text{SEM VEH vs 20 ng/mL PDGF: } 2.252 \pm 0.854$ for *PIK3R3* and $RQ_{\text{mean}} \pm \text{SEM VEH vs 20 ng/mL PDGF: } 1.817 \pm 0.033$ for *NRAS* respectively).

When normalised to control untreated VEH cells, there was no difference in the expression levels of any of the analysed genes (*PDGFRA*, *PDGFRB*, *PIK3R3*, *NRAS* and *RRAS*) across all experimental groups (Figure 5-4A-E and Figure 5-5A-E). which was the reason why this experiment was not repeated a third time. No statistical tests were carried out as there were data available from only two experimental replicates.

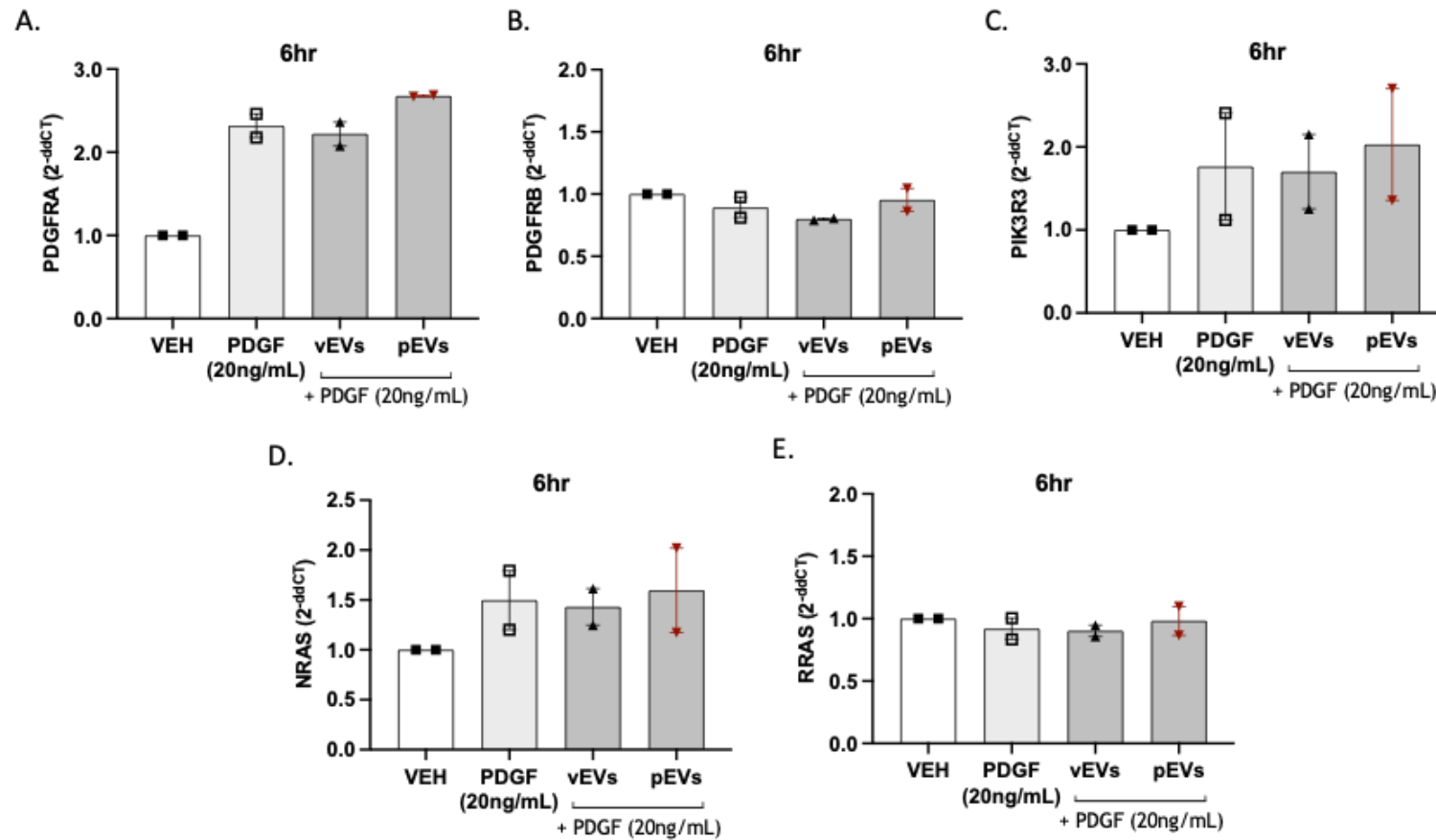


Figure 5-4 Analysis of mRNA target gene expression in HSVSMCs co-treated with 20ng/mL PDGF and vEVs/pEVs at 6hr. Quantitative RT-PCR was performed to determine relative (A) *PDGFRA* (B) *PDGFRB* (C) *PIK3R3* (D) *NRAS* and (E) *RRAS* mRNA expression levels in the indicated experimental groups. The EV concentration used in this experiment was 2.4×10^{10} EVs/mL or 6.0×10^9 EVs/well. Relative target gene expression was normalised to UBC expression to determine dCT values, which were then used to calculate relative quantification (RQ) values (experimental group versus VEH control). Data are presented as RQ_{mean} ± SEM (N=2).

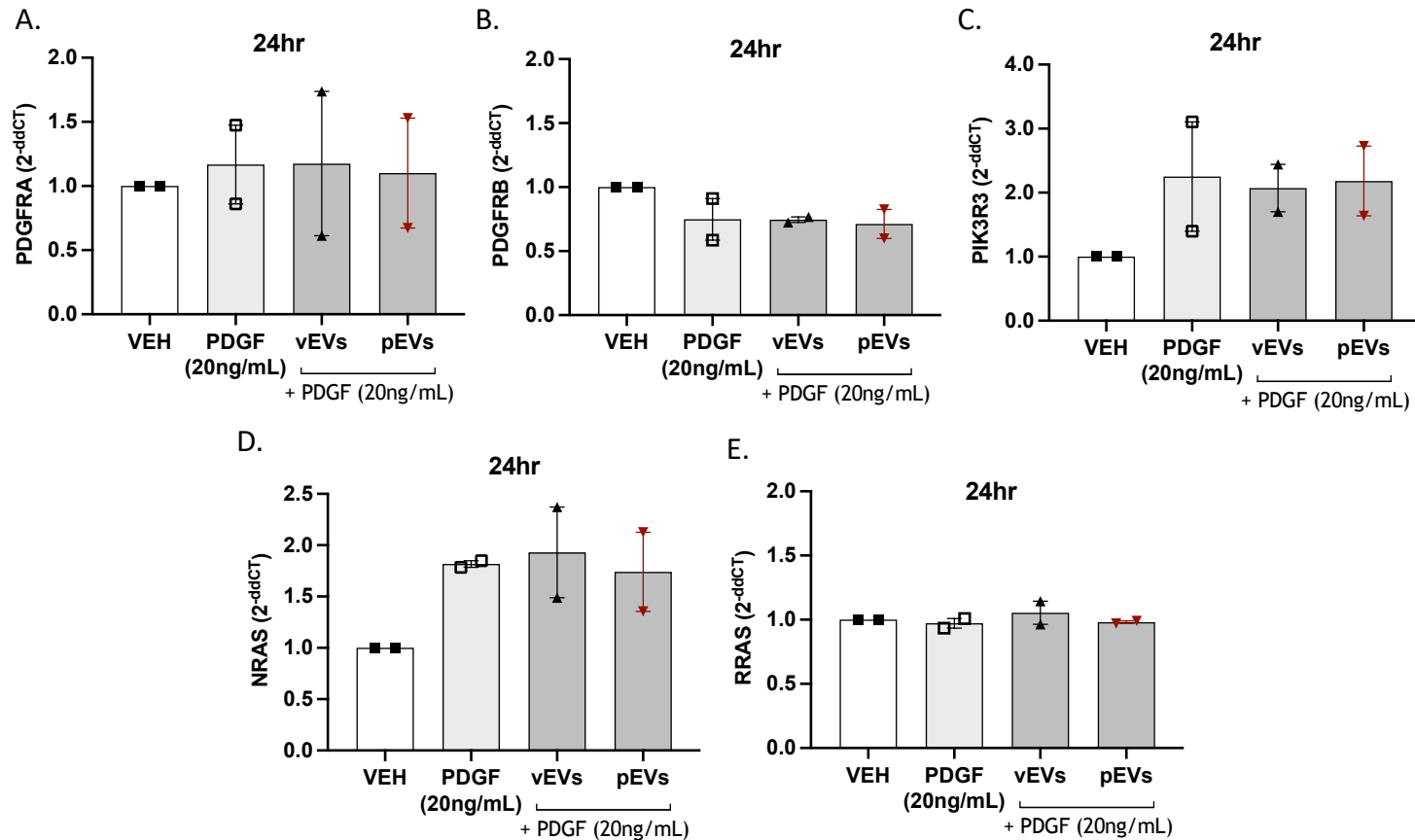


Figure 5-5 Analysis of mRNA target gene expression in HSVSMCs co-treated with 20ng/mL PDGF and vEVs/pEVs at 24hr. Quantitative RT-PCR was performed to determine relative (A) *PDGFRA* (B) *PDGFRB* (C) *PIK3R3* (D) *NRAS* and (E) *RRAS* mRNA expression levels in the indicated experimental groups. The EV concentration used in this experiment was 2.4×10^{10} EVs/mL or 6.0×10^9 EVs/well. Relative target gene expression was normalized to UBC expression to determine ΔCT values, which were then used to calculate relative quantification (RQ) values (experimental group versus VEH control). Data are presented as $RQ_{\text{mean}} \pm \text{SEM}$ (N=2).

5.4.2 Optimisation of miRNA mimic loading dose

Different amounts of synthetic miRNA mimic (cel-miR-39) was loaded into EVs to assess the efficiency of EVs at transferring miRNA mimic into recipient HSVSMCs after 24 hr of treatment. The expression levels of cel-miR-39 mimic was measured by qRT-PCR and it was found that higher concentrations of cel-miR-39 mimic loaded into EVs resulted into higher expression of the miRNA in recipient cells (Figure 5-6). Assuming 100% efficiency of miRNA mimic incorporation into EVs during the electroporation process, when cells were treated with 40 pmol miEVs/well (or 66 pmol mimic for every 1×10^{10} EV particles) the relative expression of cel-miR-39 in recipient cells was around 4 times higher than in the cells treated with EVs containing two times less the amount of mimic - 20 pmol miEVs/well (or 33 pmol mimic for every 1×10^{10} EV particles) (Figure 5-6). A smaller increase in the relative expression of cel-miR-39 in HSVSMCs was observed when the amount of mimic used in the electroporation process was further doubled. When cells were treated with 80 pmol miEVs/well (or 133 pmol mimic for every 1×10^{10} EV particles) the relative expression of cel-miR-39 in recipient cells was less than 1.5 times higher than in the cells treated with EVs containing half the amount of mimic - 40 pmol miEVs/well (or 66 pmol mimic for every 1×10^{10} EV particles).

Based on the results from this optimisation experiment, for every 1×10^{10} EV particles, 66 pmol of miRNA mimic was used in the electroporation process in any further experiments involving miRNA EV loading and delivery to recipient cells. This final protocol, including the optimised version of the sample preparation step, was described in detail in the general methods Section 2.10.6.

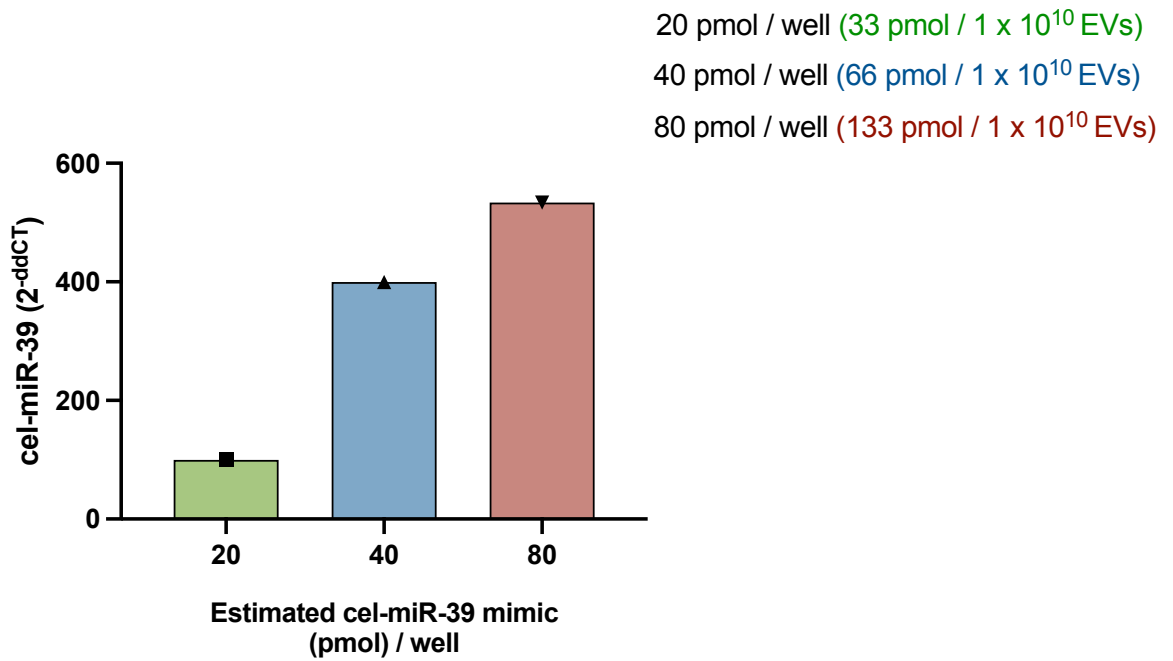


Figure 5-6 Analysis of cel-miR-39 expression levels. The expression levels of cel-miR-39 in recipient HSVSMCs were assessed after 24 hr EV-mediated transfer of varying concentrations of cel-miR-39 mimic. During the electroporation process, varying doses of cel-miR-39 (33, 66 and 133 pmol) were used to electroporate 1×10^{10} EVs. Assuming 100% efficiency of miRNA mimic incorporation into EVs during the electroporation process, 20, 40 and 80 pmol cel-miR-39 mimic was introduced to the recipient cells via electroporated EVs (2.4×10^{10} EV particles/mL or 6×10^9 EV particles/well) (N=1).

5.4.3 Characterisation of miRNA mimic loaded HSVSMC-derived EV populations

Quiesced HSVSMCs were allowed to secrete EVs for 48 hr prior to collecting the CCM and isolating the EVs. Both pre- and post-electroporation EV sample populations were characterised in terms of size by NTA, and EV morphology was assessed by TEM. Western-immunoblot analysis was carried out to detect specific EV-related protein markers. Additionally, miRNA mimic overexpression in electroporated EVs was also assessed by qRT-PCR analysis. Although miR-409-3p was amongst the successfully validated miRNAs by qRT-PCR analysis, complete GSEA were successfully carried out only on the set of target genes identified for miR-24-3p and miR-224-5p, and not for miR-409-3p, due to the small number of potential mRNA targets identified for miR-409-3p (Table 4-3). Therefore, further follow-up experiments were not carried out for miR-409-3p.

NanoSight analysis of EVs showed that there was no significant difference in mean size (nm) between any of the analysed EV populations (Pre-E EVs, pre-electroporation EVs; NaEVs, Naïve EVs; miR-24-3p EVs and miR-224-5p EVs). It was found that, the process of electroporation did not significantly change the mean size of EVs (124.1 ± 3.8 nm and 119.6 ± 3.5 nm for pre-electroporation EVs and naEVs respectively) (Figure 5-7A). Similarly, the incorporation of either of the two synthetic miRNA mimics into EVs did not significantly change the mean size of EVs (119.4 ± 3.5 nm, 120.7 ± 4.0 nm, and 119.5 ± 2.8 nm for post-electroporation naEVs, miR-24-3p EVs and miR-224-5p EVs respectively) (Figure 5-7A). In terms of the modal size of EVs, it was observed that compared to pre-electroporation EVs all post-electroporation EV populations had smaller modal EV sizes (106.5 ± 3.0 nm vs 97.5 ± 4.9 nm, 98.1 ± 5.2 nm, and 93.7 ± 4.8 nm for Pre-E EVs vs naEVs, miR-24-3p EVs, and miR-224-5p EVs respectively) (Figure 5-7A). Interestingly, the post electroporation miR-224-5p EV population had significantly smaller modal EV size compared to Pre-E EVs (106.5 ± 3.0 nm vs 93.7 ± 4.8 , $p < 0.05$). Based on the findings from the NTA of EV modal size, it is evident that the electroporation process may significantly alter the characteristics of the EV population in terms of size (Figure 5-7A); however, the specific incorporation of either one of the two synthetic miRNA mimics did not seem to affect the mean and modal EV size differently (Figure 5-7A and B). Representative SDP produced by the NanoSight are shown in Figure 5-8.

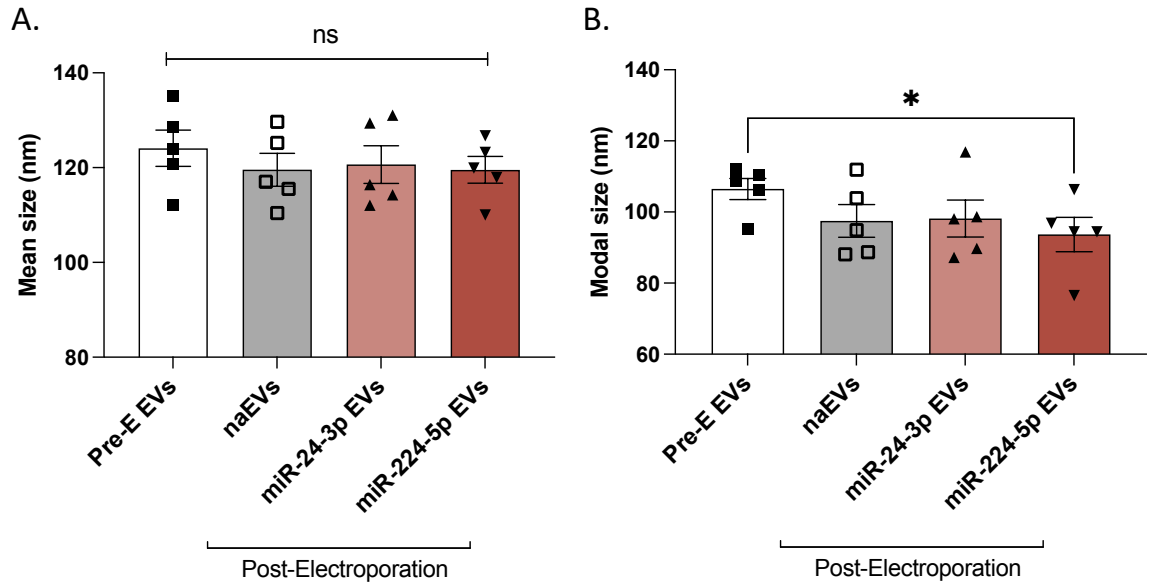


Figure 5-7 Characterisation of pre- and post- electroporation EV populations by NTA. (A) NTA data for mean EV particle size; (B) NTA data for modal EV particle size. Data are presented as Mean \pm SEM (N=5). An RM one-way ANOVA with a Tukey's correction was performed to compare the means of all groups and a *p-value < 0.05 was considered statistically significant. Abbreviations: Pre-E EVs, pre-electroporation EVs, naEVs, Naïve EVs.

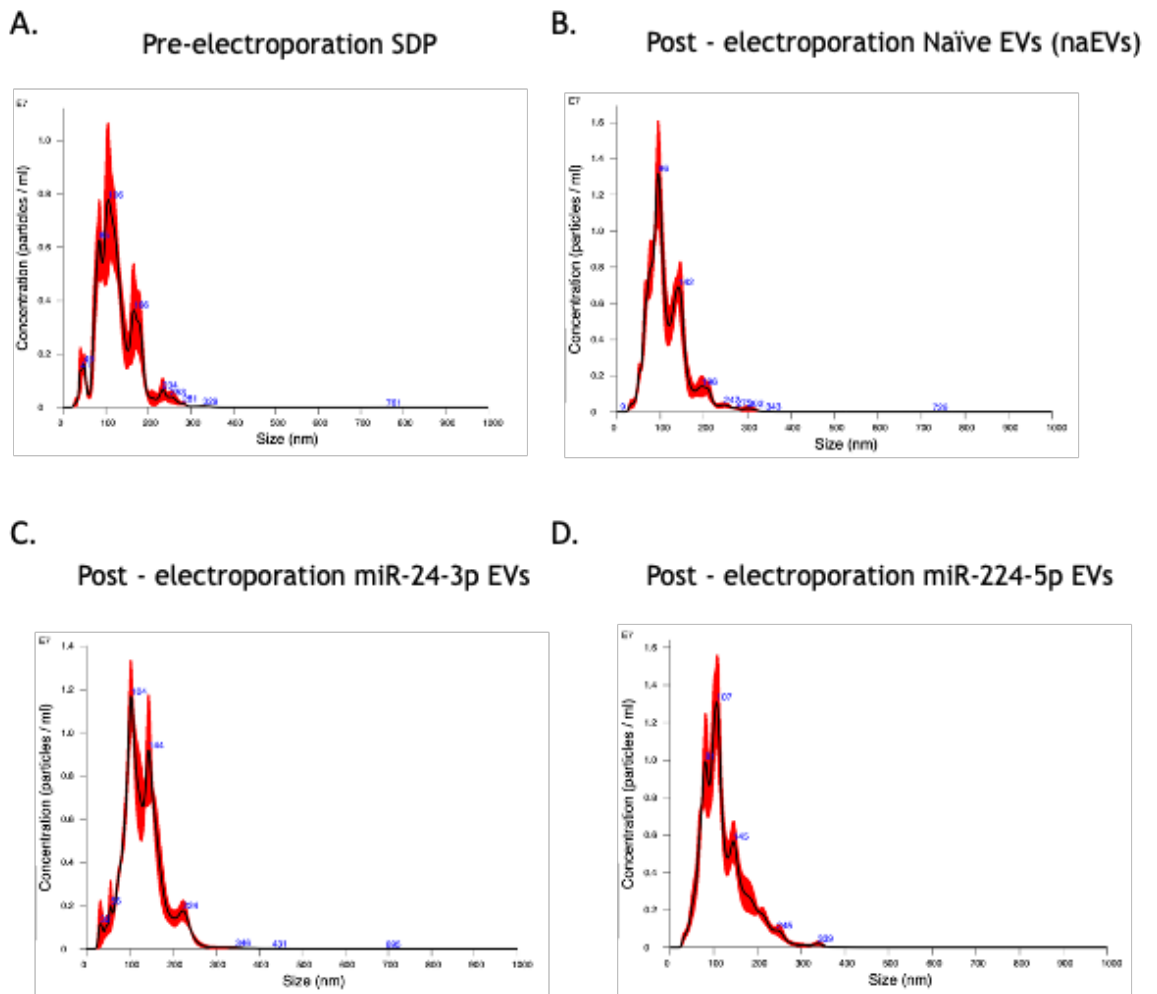


Figure 5-8 Characterisation of pre- and post- electroporation EV populations by NTA. (A) Representative size distribution peak for pre-electroporation EVs; (B) Representative size distribution peak for post-electroporation naïve EVs; (C) Representative size distribution peak for post-electroporation miR-24-3p EVs; (D) Representative size distribution peak for post-electroporation miR-224-5p EVs. Abbreviations: SDP, size distribution peak; Pre-E EVs, pre-electroporation EVs, naïve EVs.

Assessment of the morphology of EVs in all three post-electroporation EV populations groups by TEM revealed the presence of similar vesicle-like structures as the ones identified in the non-electroporated EVs (Figure 5-9). Small exosome/extracellular vesicle-like particles (<200 nm) with a typical round or cup-shaped appearance were observed in all three EV populations - naEVs, miR-24-3p EVs and miR-224-5p EVs (Figure 5-9).

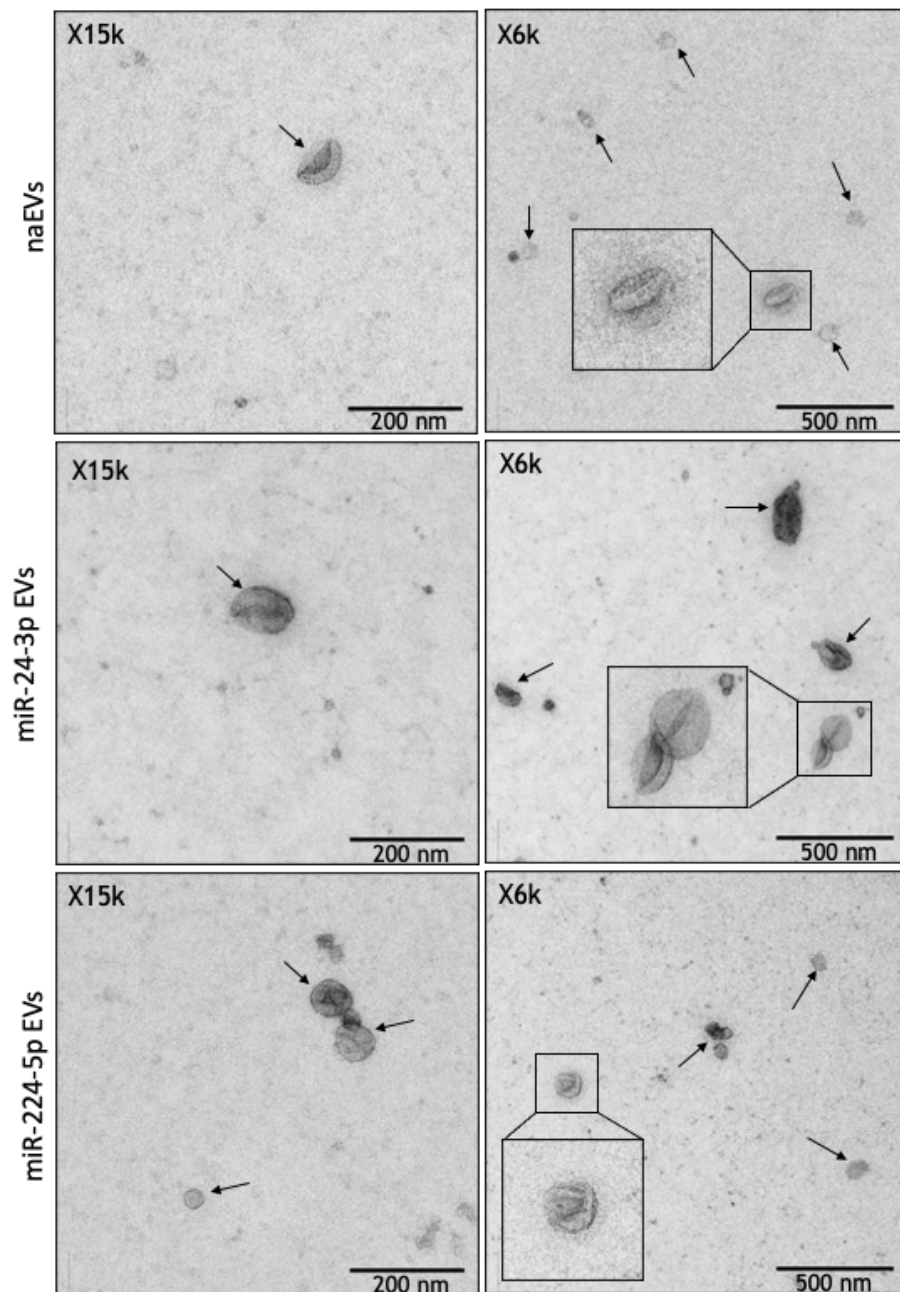


Figure 5-9 Assessment of post-electroporation EV morphology by TEM. Representative images of post-electroporation EVs: naEVs, miR-24-3p EVs and miR-224-5p EVs. Scale bars: 200nm and 500nm.

Furthermore, the presence of EVs post-electroporation of the miRNA mimic was confirmed by the detection of EV-associated protein markers including Annexin A2, Annexin XI, CD81 and CD63 (Figure 5-10). All protein markers were detected in naEVs, miR-24-3p EVs and miR-224-5p EVs. Successful loading of both miRNA mimics in electroporated EVs was assessed by measuring the levels of miR-24-3p and miR-224-5p by qRT-PCR (Figure 5-11). Significantly increased expression of miR-24-3p (Figure 5-11A) and miR-224-5p (Figure 5-11B) was observed in electroporated EVs with a relative miRNA mimic expression of > 5000 higher in both mimic electroporated EVs compared to naEVs ($RQ_{\text{mean}} \pm \text{SEM}$ naEVs vs miR-24-3p EVs: 4343 ± 1610 , $p < 0.01$ and $RQ_{\text{mean}} \pm \text{SEM}$ naEVs vs miR-224-5p EVs: 8950 ± 4634 , $p < 0.01$ respectively). When expression levels of the two miRNA mimics were compared to each other, it was found that there was no significant difference between the two groups, suggesting that both miRNA mimics were electroporated into EVs with a similar efficacy (Figure 5-11C).

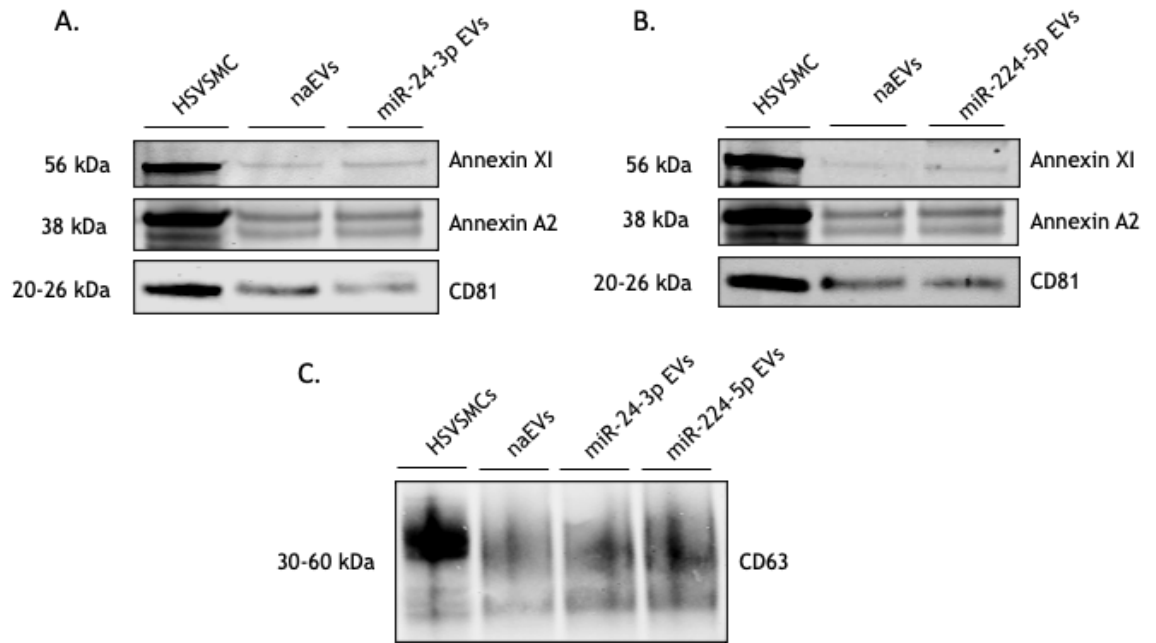


Figure 5-10 Analysis of the protein content of samples containing post-electroporation EV populations by western immunoblot. (A) Detection of Annexin XI, Annexin A2 and CD81 in naEVs, miR-24-3p EVs and control HSVSMC cell lysate; (B) Detection of Annexin XI, Annexin A2 and CD81 in naEVs, miR-224-5p EVs and control HSVSMC cell lysate; (C) Detection of CD63 in naEVs, miR-24-3p EVs, miR-224-5p EVs and control HSVSMC cell lysate (N=3 for all markers).

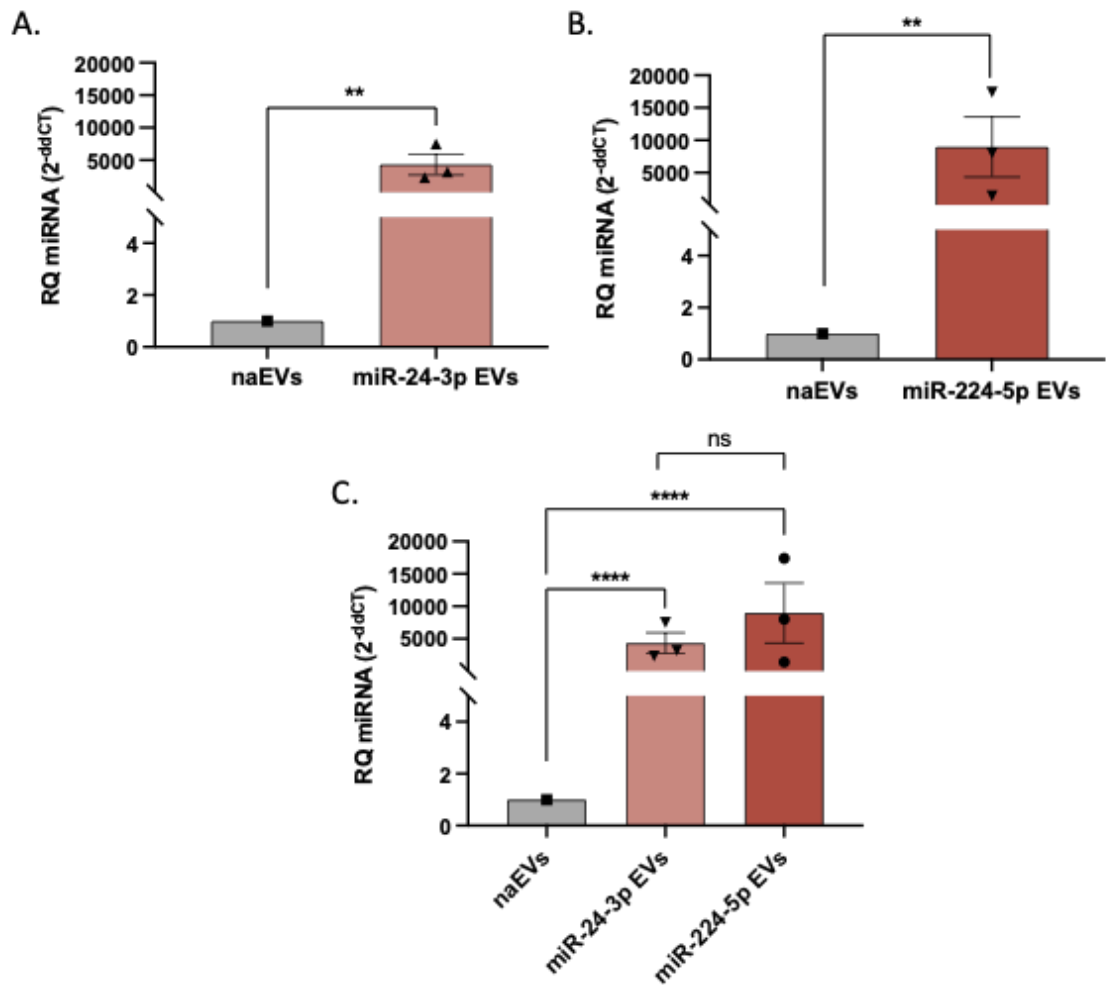


Figure 5-11 Analysis of miR-24-3p and miR-224-5p expression levels in electroporated EVs. Quantitative RT-PCR was performed to determine relative (A) miR-24-3p and (B) miR-224-5p mRNA expression levels in the indicated experimental groups. Relative miRNA gene expression was normalised to cel-miR-39 expression to determine dCT values, which were then used to calculate RQ values (miRNA group versus VEH control group). Data are presented as $RQ_{\text{mean}} \pm \text{SEM}$ (N=3). Differences between groups were assessed with a paired two-sample t-test when only two groups were compared and an Ordinary one-way ANOVA with a Tukey's correction to compare the groups based on dCTs when there were more than two groups. A * p-value < 0.05 was considered statistically significant (**** p < 0.0001, ** p < 0.01).

5.4.4 Studying the effect of naEVs and miEVs on HSVSMCs

Next, it was of interest to explore whether EVs loaded with miR-24-3p or miR-224-5p miRNA would exert any effects on recipient HSVSMCs. MiRNAs were exogenously loaded in EVs via electroporation (detailed protocol in Section 2.10.6) and their effects on cell proliferation, viability, migration, and miRNA target gene expression were analysed.

5.4.4.1 Effects of naEV/miEV on recipient HSVSMCs

To study the effect of naEVs and miEVs (miR-24-3p and miR-224-5p EVs) on cell proliferation, quiesced HSVSMCs were either untreated (VEH control), treated with 20 ng/mL PDGF alone, or co-treated with 20 ng/mL PDGF and 1.0×10^{10} EVs/mL (1.0×10^9 EVs/well) naEVs or miEVs (miR-24-3p EVs and miR-224-5p EVs) for 24 hr. Cell proliferation was assessed and similar to previous observations, PDGF successfully induced cell proliferation in quiescent HSVSMCs (Abs: 0.421 ± 0.097 for VEH vs 1.283 ± 0.013 for 20 ng/mL PDGF alone, $p < 0.05$) (Figure 5-12). Additionally, it was found that compared to cells treated with 20 ng/mL PDGF alone, only miR-224-5p EVs significantly reduced the proliferation of recipient activated HSVSMCs (Abs: 0.992 ± 0.011 vs 1.283 ± 0.013 respectively, $p < 0.0001$) (Figure 5-12). Compared to naEVs, neither miR-24-3p EVs or miR-224-5p EVs had any effect on proliferation of recipient HSVSMCs (Figure 5-12).

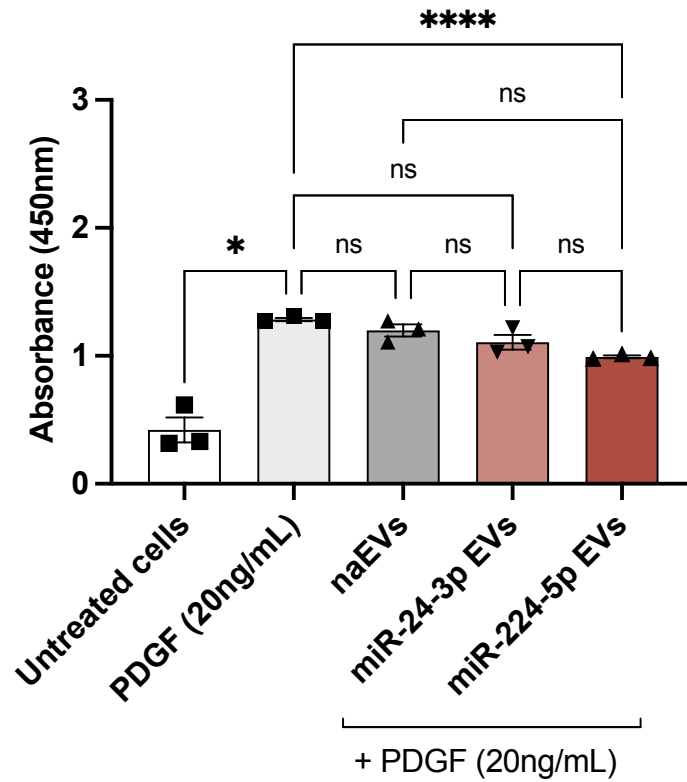


Figure 5-12 Assessing the effect of naEVs and miEVs on proliferation of activated recipient HSVMC at 24hr. In this experiment, the effect of 1.0×10^{10} EVs/mL (1.0×10^9 EVs/well) naEVs/miRNAs (miR-24-3p and miR-224-5p electroporated EVs) on cell proliferation was assessed after 24 hr. Data are presented as Mean \pm SEM (N=3). Differences between groups were analysed using a RM one-way ANOVA with a Tukey's correction to compare the means of all groups and a *p-value < 0.05 was considered statistically significant (****p < 0.0001). Abbreviations: naEVs, Naïve EVs.

To study the effect of naEVs and miEVs (miR-24-3p and miR-224-5p EVs) on cell viability, quiesced HSVSMCs were either untreated, treated with 10% EV-depleted FBS, or treated with 1.0×10^{10} EVs/mL (1.0×10^9 EVs/well) naEVs or miEVs (miR-24-3p EVs and miR-224-5p EVs) for 24 hr. As expected, it was found that compared to untreated cells, cells treated with 10% EV-depleted FBS exhibited ~30% higher viability (relative to untreated cells, 10% EV-depleted FBS: $31.9\% \pm 3.0\%$, $p < 0.01$) (Figure 5-13). Cells treated with naEVs appeared to have similar viability to untreated cells (relative to untreated cells, naEVs: $6.1\% \pm 1.8\%$) (Figure 5-13). There was no significant difference in cell viability between untreated cells compared to any of the EV treatment groups (naEVs, miR-24-3p EVs and miR-224-5p EVs) (Figure 5-13). Additionally, there was also no significant difference in cell viability between cells treated with naEVs and any of the miEVs (miR-24-3p and miR-224-5p EVs) (Figure 5-13).

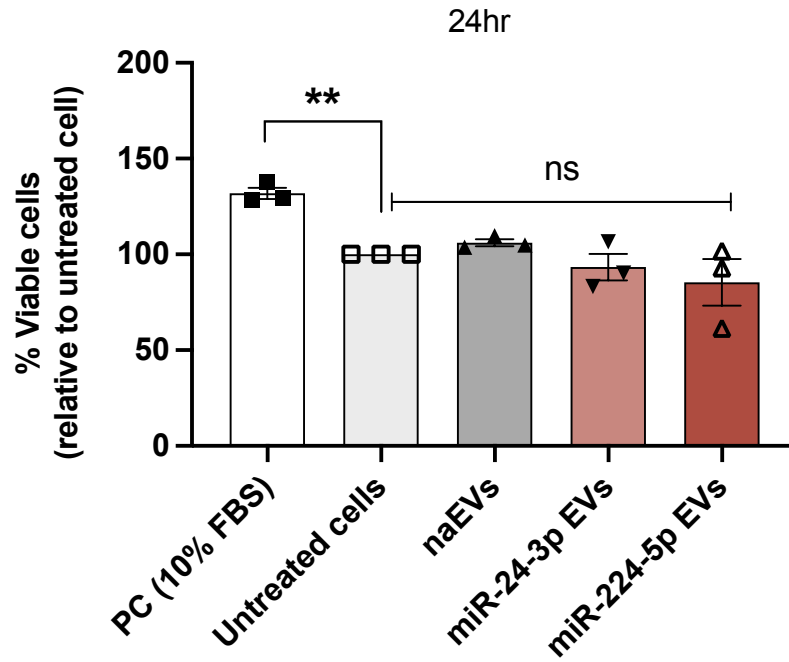


Figure 5-13 Assessing the effect of naEVs and miEVs on cell viability of recipient HSVSMCs at 24hr. In this experiment, the effect of 1.0×10^{10} EVs/mL (1.0×10^9 EVs/well) naEVs/miRNAs (miR-24-3p and miR-224-5p electroporated EVs) on cell viability was assessed after 24hr. Data are presented as Mean \pm SEM (N=3). Differences between groups were analysed using an RM one-way ANOVA with a Tukey's correction to compare the means of all groups and a *p-value < 0.05 was considered statistically significant (**p < 0.01). Abbreviations: naEVs, Naïve EVs.

To evaluate the effect of naEV/miEV (miR-24-3p EVs and miR-224-5p EVs) treatment on expression of miRNA target genes in HSVSMCs, quiesced cells were either untreated (VEH control), treated with 20 ng/mL PDGF alone, or co-treated with 20 ng/mL PDGF and 2.4×10^{10} EVs/mL (1.0×10^9 EVs/well) naEVs or miEVs (miR-24-3p EVs and miR-224-5p EVs) for 18 hr. It was found that the expression of none of the miRNA target genes was significantly altered by PDGF stimulation (Figure 5-14). The expression levels of only one gene (*NRAS*) were increased in cells (albeit not reaching significance) treated with 20 ng/mL PDGF compared to untreated cells ($RQ_{\text{mean}} \pm \text{SEM}$ untreated cells vs 20 ng/mL PDGF: 2.094 ± 0.233 , $p = 0.064$) (Figure 5-14D). The expression levels of *PIK3R3* also appeared to be upregulated in all experimental groups where cells were treated with 20 ng/mL PDGF compared to untreated cells, but the difference was not statistically significant ($RQ_{\text{mean}} \pm \text{SEM}$ untreated cells vs 20ng/mL PDGF EVs: 3.291 ± 0.882 , naEVs: 2.575 ± 0.578 , miR-24-3p EVs: 2.653 ± 0.724 and miR-224-5p EVs: 2.971 ± 1.156) (Figure 5-14E). No statistically significant differences in expression of all measured genes were observed between any of the EV treatment groups (cells co-treated with 20 ng/mL PDGF and naEVs, miR-24-3p EVs or miR-224-5p EVs) compared to cells treated with 20 ng/mL PDGF alone. Furthermore, *PDGFRB*, *RRAS*, *PDGFRA*, *NRAS* and *PIK3R3R* did not appear to be regulated by any of the miEVs (miR-24-3p EVs and miR-224-5p EVs) compared to naEVs Figure 5-14E).

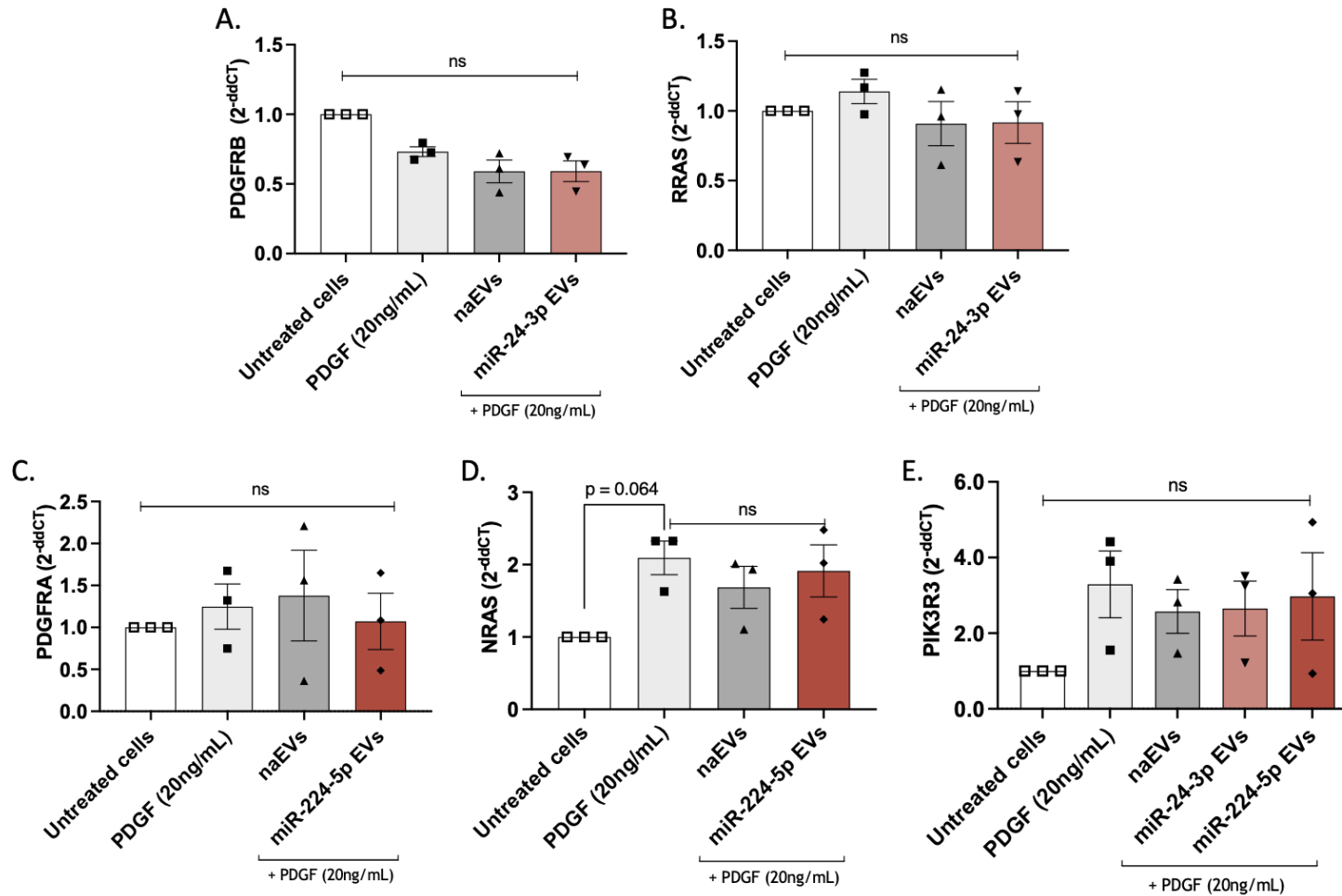


Figure 5-14 Analysis of mRNA target gene expression in HSVASMCs co-treated with 20 ng/mL PDGF and naEVs/miEVs (18hr). The EV concentration used in this experiment was 2.4×10^{10} EVs/mL or 6.0×10^9 EVs/well. Quantitative RT-PCR was performed to determine relative (A) *PDGFRB* (B) *RRAS* (C) *PDGFRA* (D) *NRAS* and (E) *PIK3R3* mRNA expression levels at 18hr. Relative target gene expression was normalised to UBC expression to determine dCT values, which were then used to calculate relative quantification (RQ) values (experimental group versus untreated cells). Data are presented as $RQ_{\text{mean}} \pm \text{SEM}$ (N=3). An RM one-way ANOVA with a Tukey's correction was performed to compare groups based on dCT values. P-value < 0.05 was considered statistically significant.

5.4.4.2 Recipient HSVSMCs pre-treated with naEVs/miEVs

The effect of modified miEVs overexpressing miR-24-3p and miR-224-5p mRNAs on cell proliferation, migration and miRNA target gene expression was further investigated following a different cell treatment protocol involving an EV preconditioning of the recipient cells. In the following experiments, recipient HSVSMCs were first pre-treated with naEVs/miEVs for 6 hr prior to co-treatment with either 20 ng/mL PDGF or 5% EV-depleted FBS depending on the experiment (Figure 2-3 for details).

To study the effect of naEVs and miEVs (miR-24-3p and miR-224-5p EVs) on cell proliferation, quiesced HSVSMCs were first pre-treated with 1.0×10^{10} EVs/mL (1.0×10^9 EVs/well naEVs/miEVs) for 6 hr. Media was then removed, and cells were either left untreated (VEH control), treated with 20 ng/mL PDGF alone, or co-treated with 20 ng/mL PDGF and 1.0×10^{10} EVs/mL (1.0×10^9 EVs/well) naEVs or miEVs (miR-24-3p EVs and miR-224-5p EVs) for 24 hr. Cell proliferation was assessed and 20 ng/mL PDGF was able to induce a significant increase in cell proliferation (Abs: 0.494 ± 0.048 for untreated cells vs 1.197 ± 0.055 for cells treated with 20 ng/mL PDGF, $p < 0.05$) (Figure 5-15). Furthermore, compared to cells treated with 20 ng/mL PDGF, neither naEVs or any of the miEVs (miR-24-3p EVs and miR-224-5p EVs) had any effect on proliferation of recipient HSVSMCs (Abs: 1.197 ± 0.055 for cells treated with 20 ng/mL PDGF vs cells co-treated with 20 ng/mL PDGF and naEVs: 1.140 ± 0.025 , miR-24-3p EVs: 1.168 ± 0.032 , and miR-224-5p EVs: 1.001 ± 0.058) (Figure 5-15). A slight reduction in cell proliferation was observed when cells were co-treated with 20 ng/mL PDGF and miR-224-5p EVs compared to naEVs, however, the difference was not statistically significant (Abs: 1.001 ± 0.058 vs 1.140 ± 0.025 respectively) (Figure 5-15) potentially due to the observed higher variability between biological replicates.

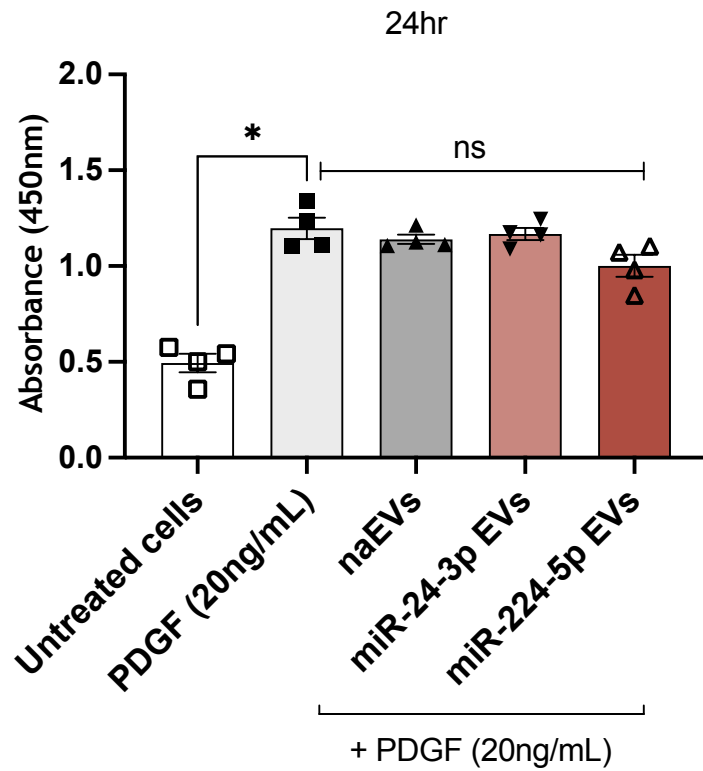


Figure 5-15 Assessing the effect of naEVs and miEVs on proliferation (24hr) of activated recipient HSVSMCs pre-treated with naEVs and miEVs. In this experiment, the effect of 1.0×10^{10} EVs/mL (1.0×10^9 EVs/well) naEVs/miRNAs (miR-24-3p and miR-224-5p electroporated EVs) on previously pre-treated cells with the same EV populations was assessed after 24hr. Data are presented as Mean \pm SEM (N=4). Differences between groups were analysed using an RM one-way ANOVA with a Tukey's correction to compare the means of all groups and a *p-value < 0.05 was considered statistically significant. Abbreviations: naEVs, Naïve EVs.

To further examine the ability of EVs overexpressing miR-24-3p and miR-224-5p miRNAs to regulate biological processes in HSVSMCs, the effect of naEVs/miEVs on cell migration was also studied via two different methods (the classical wound scratch assay and the gap closure assay). In these experiments, quiesced HSVSMCs were pre-treated with 2.4×10^{10} EVs/mL (6.0×10^9 EVs/well naEVs/miEVs) for 6 hr before the addition of PDGF/EV co-treatment using the same EV concentration. Following 6 hr EV preconditioning of cells, the media was removed, and cells were either left untreated, treated with 5% EV-depleted FBS alone, or co-treated with 5% EV-depleted FBS and 2.4×10^{10} EVs/mL (6.0×10^9 EVs/well) naEVs or miEVs (miR-24-3p EVs and miR-224-5p EVs) for 16, 18 and 20 hr.

When cell migration was assessed by the wound scratch assay, untreated control HSVSMCs demonstrated 25.5% (16 hr), 27.7% (18 hr) and 28.7% (20 hr) scratch closure in absence of serum or EV treatment reflecting basal migration (Figure 5-16). Cells treated with 5% EV-depleted FBS migrated significantly more compared to untreated cells after 16 hr (mean scratch closure % \pm SEM., 25.5 ± 1.1 % and 34.3 ± 2.2 % for untreated and 5% EV-depleted FBS treated cells respectively, $P < 0.05$) (Figure 5-16A) and after 18 hr (mean scratch closure % \pm SEM., 27.7 ± 2.7 % vs 38.7 ± 4.0 % for untreated vs 5% EV-depleted FBS treated cells respectively, $P < 0.05$) (Figure 5-16B). No significant difference in cell migration was observed between any of the experimental groups after 20 hr (Figure 5-16C). Interestingly, both the miEVs (miR-24-3p and miR-224-5p) significantly reduced serum-induced scratch closure at 16 hr compared to 5% EV-depleted FBS control (mean scratch closure % \pm SEM., miR-24-3p EVs: 25.6 ± 2.0 % and miR-224-5p EVs: 28.3 ± 1.6 % vs 5% EV-depleted FBS: 34.3 ± 2.2 %, $p < 0.05$) (Figure 5-16A). There was no significant difference in cell migration between naEVs and either miR-24-3p EVs and miR-224-5p EVs at any timepoint (Figure 5-16A-C). Notably, at the later timepoint (18 hr) the difference in cell migration was lost (Figure 5-16B). The findings above suggest that both miRNAs may be having an inhibitory effect on serum-induced cell migration at an earlier timepoint compared to 5% EV-depleted FBS control but not naEVs.

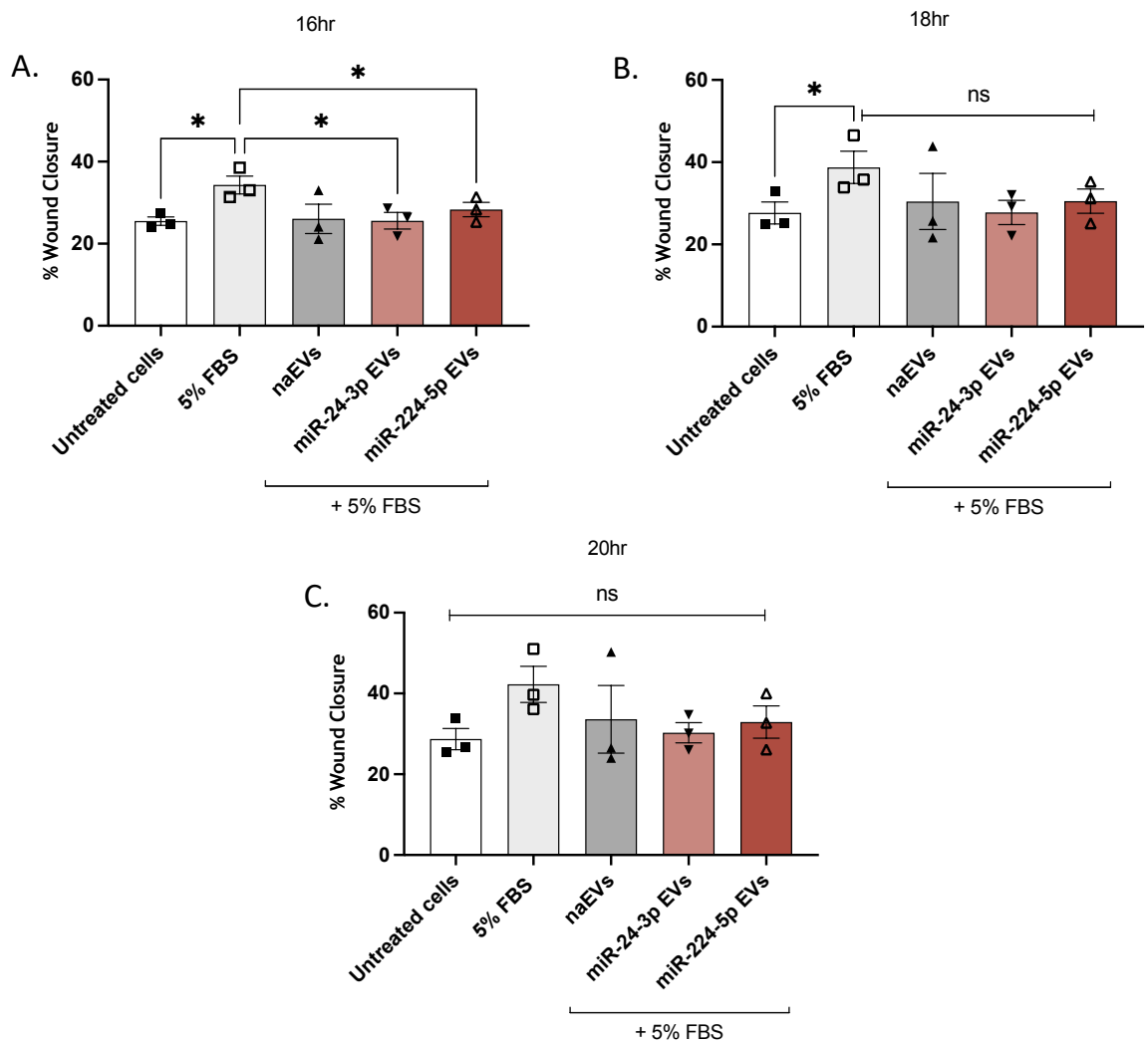


Figure 5-16 Assessing the effect of naEVs/miEVs on HSVSMC migration at 16hr, 18hr and 20hr (wound scratch assay). In this experiment, the effect of 2.4×10^{10} EVs/mL (6.0×10^9 EVs/well) naEVs/miRNAs (miR-24-3p and miR-224-5p EVs) on previously pre-treated cells with the same EV populations was assessed after (A) 16hr, (B) 18hr, and (C) 20hr. Scratches were imaged at 10X magnification. ImageJ software was used to determine scratch closure percentage by measuring distance in pixels. Data are presented as Mean \pm SEM (N=3). Differences between groups were analysed using an RM one-way ANOVA with a Tukey's correction to compare the means of all groups and a *p-value < 0.05 was considered statistically significant. Abbreviations: naEVs, Naïve EVs.

Furthermore, when cell migration was assessed via the gap closure method, similar findings were observed at 16 hr (Figure 5-17 and Figure 5-18). In addition to the previously observed inhibitory effect on serum-induced cell migration of miR-224-5p EVs compared to 5% EV-depleted FBS control (mean gap closure % \pm SEM, 45.6 ± 1.6 % and 55.0 ± 0.7 % respectively, $p < 0.05$) (Figure 5-17 and Figure 5-18), it was also found that miR-224-5p EVs reduced serum-induced cell migration significantly more than each of the other two EV groups - naEVs and miR-24-3p EVs, with observed mean gap closure % \pm SEM of 45.6 ± 1.6 % vs 54.7 ± 1.9 % ($p < 0.01$) and 50.3 ± 1.2 % ($p < 0.05$) for miR-224-5p EVs vs naEVs and miR-24-3p EVs respectively (Figure 5-18). In contrast, although there was a tendency towards negative regulation of cell migration by miR-24-p EVs, no significant difference in serum-induced cell migration was observed between cells treated with miR-24-3p EVs and cells treated with naEVs or 5% EV-depleted FBS control (Figure 5-18). These data further suggests that miR-224-5p EVs may be having an inhibitory effect on serum-induced cell migration.

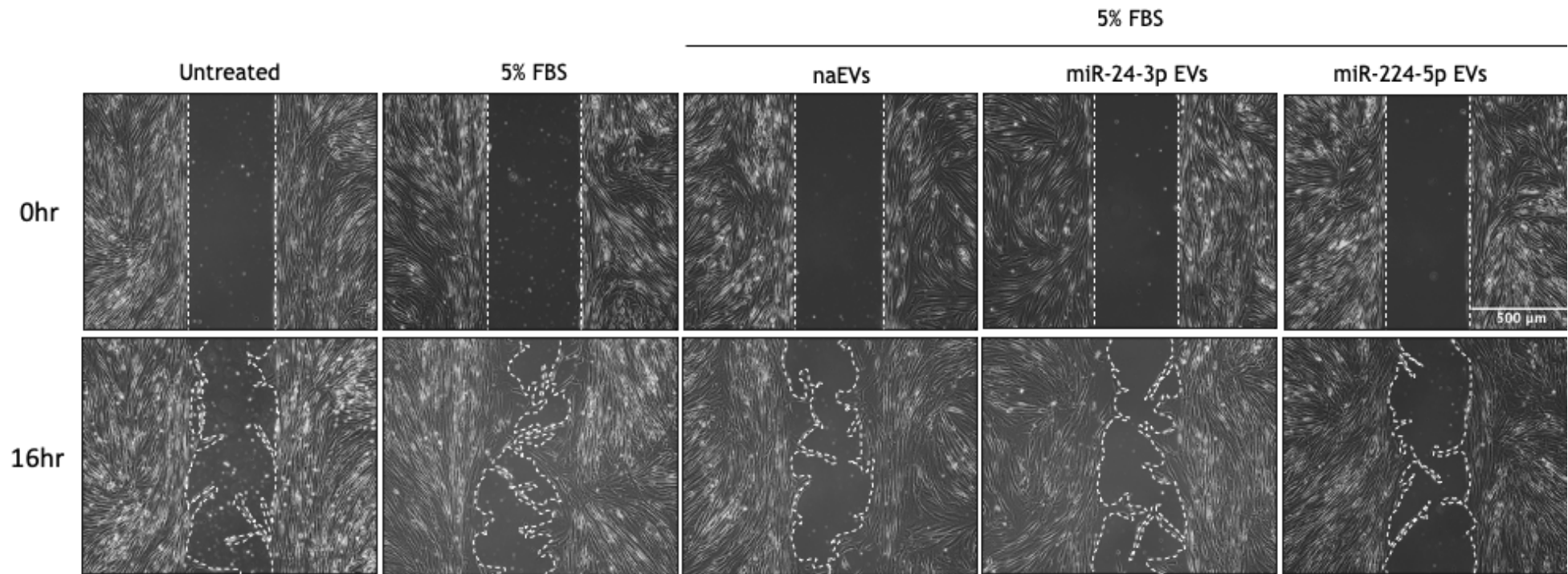


Figure 5-17 Studying the effect of naEVs/miEVs on HSVSMC migration at 16hr (gap closure assay). In this experiment, the effect of 2.4×10^{10} EVs/mL (6.0×10^9 EVs/well) naEVs/miRNAs (miR-24-3p and miR-224-5p EVs) on previously pre-treated (for 6hr) cells with the same EV populations was assessed. After pre-treatment, media was removed and replaced with fresh 0.2% **EV-depleted** FBS (untreated group) or 5% **EV-depleted** FBS containing naEVs, miR-24-3p EVs or miR-224-5p EVs. Gaps between cells were imaged at 10X magnification at 0hr and 16hr (4 technical replicates/group; N=3 biological replicates). White dotted lines indicate gap edges.

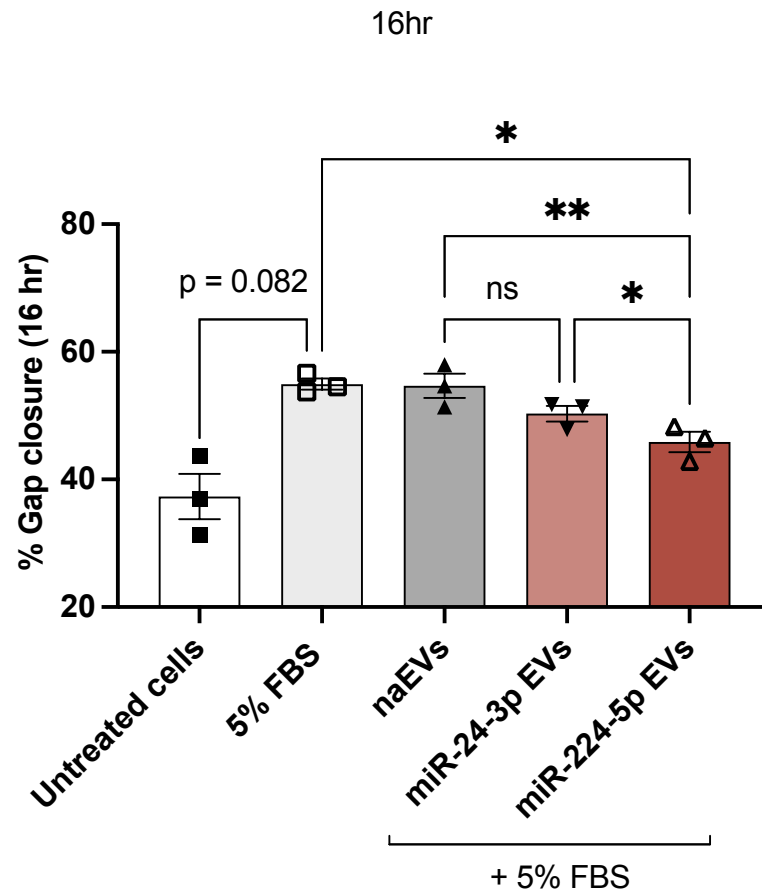


Figure 5-18 Assessing the effect of naEVs/miEVs on HSVSMC migration at 16hr (gap closure assay). In this experiment, the effect of 2.4×10^{10} EVs/mL (6.0×10^9 EVs/well) naEVs/miRNAs (miR-24-3p and miR-224-5p EVs) on previously pre-treated cells with the same EV populations was assessed after 16hr. Gaps between cells were imaged at 10X magnification. ImageJ software was used to determine scratch closure percentage by measuring distance in pixels. Data are presented as Mean \pm SEM (N=3). Differences between groups were analysed using an RM one-way ANOVA with a Tukey's correction to compare the means of all groups and a *p-value < 0.05 was considered statistically significant (** p < 0.01). Abbreviations: naEVs, Naïve EVs.

To further evaluate the ability of naEV/miEV (miR-24-3p EVs and miR-224-5p EVs) to regulate molecular processes in HSVSMCs, the expression of miRNA target genes in HSVSMCs was measured following treatment with EVs. In this experiment, quiesced cells were again pre-conditioned with naEVs/miEVs for 6 hr before treatment. Then, cells were either untreated (VEH control), treated with 20 ng/mL PDGF alone, or co-treated with 20 ng/mL PDGF and 2.4×10^{10} EVs/mL (6.0×10^9 EVs/well) naEVs or miEVs (miR-24-3p EVs and miR-224-5p EVs) for 12 hr. It was found that, similar to previous findings, not all analysed genes were upregulated in response to PDGF treatment (Figure 5-19A, B and C). The expression levels of two genes (*PIK3R3* and *NRAS*) were significantly increased in cells treated with 20 ng/mL PDGF compared to untreated control (RQ_{mean} ± SEM untreated cells vs 20 ng/mL PDGF: 2.186 ± 0.331 , $p < 0.0001$ for *NRAS*; and 20 ng/mL PDGF: 2.303 ± 0.145 , $p < 0.01$ for *PIK3R3* (Figure 5-19D and E respectively).

No statistically significant difference in expression levels of all measured genes was observed between any of the EV treatment groups (cells co-treated with 20 ng/mL PDGF and naEVs, miR-24-3p EVs or miR-224-5p EVs) compared to cells treated with 20 ng/mL PDGF alone. Additionally, PDGFRB, RRAS, PDGFRA, NRAS and PIK3R3 did not appear to be regulated by any of the miEVs (miR-24-3p EVs and miR-224-5p EVs) compared to naEVs (Figure 5-19A-E). A tendency towards inhibition of PDGF-induced upregulation of *NRAS* and *PIK3R3* mRNA expression was observed in cells co-treated with PDGF and either naEV or miEVs (miR-24-3p EVs or miR-224-5p EVs) compared to cells treated with PDGF alone (Figure 5-19D and E respectively) but the difference was not statistically significant.

Additionally, there did not seem to be a difference between the potential inhibitory effect exerted by naEVs vs miR-224-5p EVs for *NRAS* (RQ_{mean} ± SEM naEVs: 1.830 ± 0.229 vs miR-224-5p EVs: 1.895 ± 0.206 (Figure 5-19D) and between naEVs and miR-24-3p EVs or miR-224-5p EVs for *PIK3R3* (RQ_{mean} ± SEM naEVs: 1.834 ± 0.336 vs miR-24-3p: 1.659 ± 0.234 or miR-224-5p EVs: 1.641 ± 0.243) (Figure 5-19E).

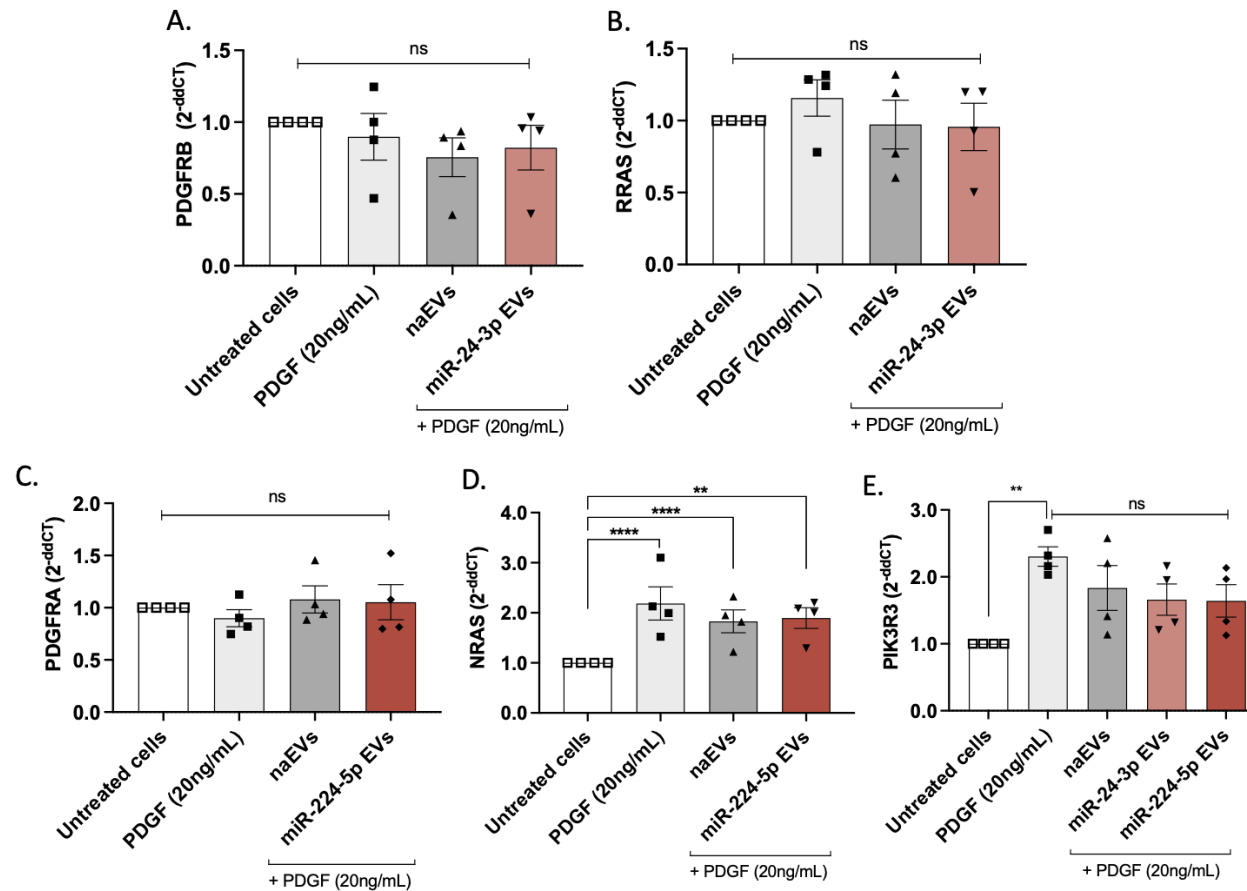


Figure 5-19 Analysis of mRNA target gene expression in HSVASMCs co-treated with 20 ng/mL PDGF and naEVs/miEVs at 12hr following a 6hr pre-treatment with the same EV populations. The EV concentration used in this experiment was 2.4×10^{10} EVs/mL or 6.0×10^9 EVs/well. Quantitative RT-PCR was performed to determine relative (A) *PDGFRB* (B) *RRAS* (C) *PDGFRA* (D) *NRAS* and (E) *PIK3R3* mRNA expression levels at 12hr. Relative target gene expression was normalised to UBC expression to determine dCT values, which were then used to calculate relative quantification (RQ) values (experimental group versus untreated cells). Data are presented as $RQ_{\text{mean}} \pm \text{SEM}$ (N=3). An RM one-way ANOVA with a Tukey's correction was performed to compare groups based on dCT values. P-value < 0.05 was considered statistically significant (**p < 0.01 and ****p < 0.0001).

5.4.5 Studying the effect of naEVs and miEVs on HSVECs

The effect of naEVs and miEVs (miR-24-3p and miR-224-5p EVs) on HSVEC viability was also studied. In this experiment, cells were either untreated, treated with 10% EV-depleted FBS, or treated with 1.0×10^{10} EVs/mL (1.0×10^9 EVs/well) naEVs or miEVs (miR-24-3p EVs and miR-224-5p EVs) for 4 hr (Figure 5-20). Two different types of media both containing serum were used in these experiments due to the inability of ECs to survive in no serum conditions.

As expected, it was found that regardless of the type of medium used in each experiment, HSVECs treated with 10% EV-depleted FBS exhibited increased viability compared to untreated cells (Figure 5-20A and B). Relative to untreated cells, cells treated with 10% EV-depleted FBS demonstrated >35% increased viability ($36.4 \pm 13.4\%$) in 1% EV-depleted FBS DMEM medium (Figure 5-20A), whereas in complete EC medium, the increase in cell viability for cells treated with 10% EV-depleted FBS relative to untreated cells was smaller ($13.8 \pm 3.2\%$) (Figure 5-20B). There was no significant difference in cell viability between different EV treatment groups (naEVs, miR-24-3p EVs and miR-224-5p EVs) compared to untreated cells when either of the two media were used (Figure 5-20A and B). Additionally, there was also no significant difference in cell viability between cells treated with naEVs and cells treated with any of the miEVs (miR-24-3p and miR-224-5p EVs) when either of the two media were used (Figure 5-20A and B). The findings above suggest that neither naEVs or miEVs (miR-24-3p or miR-224-5p) seem to regulate HSVEC survival or growth.

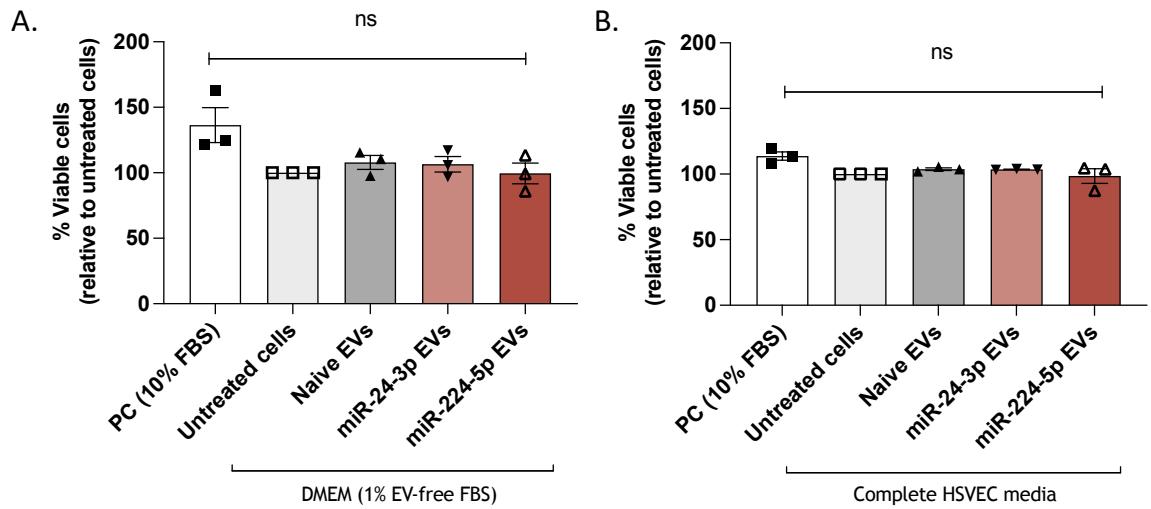


Figure 5-20 Assessing the effect of naEVs and miEVs on cell viability of recipient HSVECs at 4hr. In this experiment, the effect of 1.0×10^{10} EVs/mL (1.0×10^9 EVs/well) naEVs/miRNAs (miR-24-3p and miR-224-5p electroporated EVs) on cell viability was assessed after 4hr. Data are presented as Mean \pm SEM (N=3). Differences between groups were analysed using an RM one-way ANOVA with a Tukey's correction to compare the means of all groups. Abbreviations: naEVs, Naïve EVs.

5.5 Discussion

The results presented in this chapter revealed that unmodified HSVSMC-derived pEVs, containing endogenously upregulated expression of several miRNAs including miR-24-3p and miR-224-5p, did not have any significant effect on proliferation of recipient PDGF-activated HSVSMCs. In terms of use of EVs as a cargo delivery vehicle, it was of interest to investigate the possibility of increasing miR-24-3p and miR-224-5p levels within EVs via exogenous loading for delivery to recipient cells and assessment of potential miRNA-EV mediated cellular responses. Electroporation of EVs with miR-24-3p and miR-224-5p significantly increased the levels of these miRNAs highlighting the potential for this loading method. When the effect of miR-24-3p-EVs or miR-224-5p-EVs on cell proliferation was assessed, it was found that miR-224-5p EVs significantly inhibited the proliferation of PDGF-activated HSVSMCs compared to PDGF control, but not naEVs. Additionally, miR-224-5p EVs were also found to negatively regulate EV-depleted FBS-treated HSVSMC migration compared to both naEVs and EV-depleted FBS control.

There are many possible explanations as to why proliferation of recipient HSVSMCs was not found to be regulated by pEVs (containing upregulated expression of several miRNAs including miR-24-3p and miR-224-5p), including that pEVs may be involved in the regulation of other cellular process rather than cell proliferation or that they may not be involved in the autocrine regulation of HSVSMCs. It is also possible that experimental optimisation was required to establish an optimal EV concentration, experimental time points and conditions. A recent study exploring the effects of PSMCs EVs secreted under PDGF stimulation, found that PDGF EVs had no effect on EC (PAECs) proliferation under basal conditions, but they successfully regulated PDGF-induced EC migration (Heo et al., 2020), supporting the notion that pEVs may be involved in the regulation of cellular processes other than cell proliferation. A comparative proteomic analysis of aortic EC- and VSMC- derived EVs identified several unique proteins specific to either one of the two EV populations as well as many common proteins present in EVs from both ECs and VSMCs (Boyer et al., 2020). Smooth muscle protein 22-alpha/transgelin (SMC-specific marker), matrix GLA protein, and some adhesion molecules (VCAM-1, CD166, and neural cell adhesion molecule 1) were amongst the unique protein markers detected in aortic VSMC

EVs suggesting a potential role for VSMC EVs in autocrine communication (Boyer et al., 2020) which may contribute to the regulation of vascular remodelling processes. Another possible reason as to why a significant difference in cell proliferation was not detected between cells treated with vEVs and pEVs could be the small sample size used in this study (N=3) which may have prevented the detection of significant differences between groups (Columb and Atkinson, 2016). Additionally, it has previously been proposed that EV-mediated biological effects in target cells are concentration-dependent (Tabak et al., 2018), suggesting that the EV concentration may also play a significant role in determining the functional effects of EVs. Therefore, for the experiment discussed here, it is also possible that not enough functional EV cargo (i.e., miRNAs) has been delivered to recipient cells preventing the detection of EV-mediated functional effects i.e., the potential EV-regulation of HSVSMC proliferation. Unfortunately, it is not possible to accurately and reliably compare the EV concentration used in our study to the EV concentrations used in similar published *in vitro* studies as most of the authors employ mass units (μg EV protein) or mass/ concentration ($\mu\text{g}/\text{mL}$) as quantitative measures of EVs which is not an accurate representation of EV concentration (Sverdlov, 2012). The main issue associated to the use of mass units (μg EV protein) to report EV doses used in studies relates to the fact that the protein content in EV samples is not solely representative of EV-proteins and is highly dependent on the EV isolation method due to the possibility of measuring non-EV protein co-isolates such as contaminating proteins and proteins-associated with other non-EV particles such as lipoproteins (Brennan et al., 2020; Ludwig et al., 2019; Ramirez et al., 2018). However, if an approximate comparison was attempted based on the assumption that $1 \mu\text{g}$ EV/exosome protein corresponds to 2×10^9 EVs/exosomes (Sverdlov, 2012), then the EV concentration used in the studies presented in this thesis would be in the lower range of concentrations reported in most published studies (Y. Li et al., 2015; Ramteke et al., 2015; Safdar et al., 2016; T. Tian et al., 2014b; W. Zhang et al., 2018; Y. Zhang et al., 2017).

Since the EV concentration which could have been used for *in vitro* experiments in this project was limited by the fact that EVs were sourced from cultured primary HSVSMCs, exploring multiple (higher) EV concentrations in functional assays was not a practical approach, therefore, an alternative approach was

considered for studying the effect of HSVSMC-derived EV on recipient cells. It was decided that exogenously modifying EVs to overexpress the miRNAs of interest via a commonly used method for EV cargo modulation was a feasible approach to explore the effects of HSVSMC-derived EV-mediated delivery of either miR-24-3p or miR-224-5p to recipient HSVSMCs.

In order to be able to successfully study the role of HSVSMC-derived EVs, overexpressing miR-24-3p or miR-224-5p, it was necessary to first optimise a protocol for exogenous loading of miRNAs into EVs via one of the established methods for EV modification i.e., electroporation. The electroporation protocol used within our research group was developed based on a protocol originally published by El-Andaloussi and colleagues (El-Andaloussi et al., 2012). Initially optimised by Dr. Emily Ord (University of Glasgow) and some further improvements introduced by Miss Rebecca Rooney (University of Glasgow), this protocol was designed for modulating a large number of EVs isolated from plasma/serum samples rather than CCM. Moreover, in this protocol the amount of miRNA mimic used in the EV loading process was determined based on the EV concentration which was estimated by measuring protein concentration in the EV samples instead of using NTA to track individual particles. As protein concentration does not directly and accurately reflect EV concentration, this was the first change introduced in the already established electroporation protocol which, in the current study, was further optimised by assessing different miRNA mimic loading amounts.

Exogenous loading of therapeutic molecules into EVs via electroporation is a highly variable process associated with various factors that can affect protocol efficacy. Nucleic acid aggregation, EV aggregation, nucleic acid and EV sizes have all been reported to reduce transfection efficiency (Johnsen et al., 2016; Kooijmans et al., 2013; Lamichhane et al., 2015; Rankin-Turner et al., 2021) It has previously been shown that different electroporation parameters including voltage intensity and number of pulses can affect the loading of synthetic particles as well as plasma-derived EV particles (Pomatto et al., 2019; Z. Yang et al., 2016). In the current study, different electroporation settings have not been explored as such experiments have previously been performed (personal communication with Rebecca Rooney, University of Glasgow) and the findings from that experiment reflect the electroporation settings used in these studies.

Additionally, a recent study, using Doxorubicin as an exogenous cargo molecule, presented a comprehensive evaluation of the effects of different electroporation parameters, and highlighted that in addition to the well-known contributors to reduced transfection efficiency, drug to EV ratio was also an important parameter that played a role in determining the efficacy of the EV loading process (Lennaárd et al., 2022). In the current study, three different miRNA mimic loading doses were explored in the following EVs to mimic ratios: 1×10^{10} EVs and 33, 66, or 133 pmol mimic, and the observed increase in relative expression of cel-miR-39 in recipient cells reflected the increase in the loading mimic dose. Consistent with our findings, a recent study assessing similar EVs to mimic ratios reported that increasing miRNA mimic loading dose induced a correlated increase in the relative expression of that mimic in recipient cells (Pomatto et al., 2019). For future studies, a ratio of 1×10^{10} EVs to 66 pmol mimic was used since this ratio resulted in potentially the highest transfection efficiency considering the amount of loading mimic dose and the corresponding increase in relative expression of this mimic in recipient cells.

Since modulation of EVs via electroporation could potentially induce changes to the physical characteristics of EVs, due to vesicle aggregation (Johnsen et al., 2016; Rankin-Turner et al., 2021), the EV populations were characterised post electroporation to ensure that they had not been significantly affected post electroporation. Interestingly, while no difference was found between non-electroporated and electroporated EVs in terms of mean size, the modal size of electroporated EVs appeared smaller compared to EVs prior to electroporation. The modal size of EVs electroporated with miR-224-5p specifically was significantly smaller compared to non-electroporated EVs. However, this does not seem to be a miRNA mimic specific effect since the modal EV sizes of all electroporated EVs were smaller than the modal EV size of non-electroporated EVs. Increasing the statistical power by adding more experimental repeats could potentially reveal more significant differences between the other electroporated EV groups and the non-electroporated EVs. While it is possible for nucleic acid and EV aggregates to form following EV electroporation (Johnsen et al., 2016; Kooijmans et al., 2013; Lamichhane et al., 2015), it is not possible to reliably determine whether such aggregates have been formed in electroporated EVs due to the nature of the electroporation protocol. For example, in the event of

aggregates formation following electroporation, a shift in the EV profile is usually observed characterised by an increase in the mean or median size parameters (Johnsen et al., 2016; Pomatto et al., 2019). However, since the mean EV size of electroporated EVs in this study was not changed, the presence of EV aggregates in the electroporated EV samples was considered unlikely.

The use of trehalose during the EV electroporation process has been shown to significantly reduce the formation of EV aggregates (typical size range of 100-500 nm) (Johnsen et al., 2016) suggesting that any changes to the size distribution profile observed in this study may be down to other factors rather than the presence of EV aggregates. For example, the additional EV re-isolation step following electroporation, which aims to separate EVs from any non-EV entities such as contaminating proteins (e.g., bovine serum albumin) from the EV recovery step, may contribute to changes in the EV size distribution profile. The *Izon* SEC column used for EV purification has been shown to more effectively isolate smaller EVs in the range of 50-300nm compared to other methods (Veerman et al., 2021) which may have contributed to a slight shift in the size distribution profile of electroporated EVs following the re-isolation step as suggested by the smaller modal EV size in post-electroporated EV populations. It is also possible that any EV aggregates (>300nm) that might have formed were also cleared during the EV re-isolation step resulting in an electroporated EV population with a similar size distribution profile to the one prior to electroporation. As expected, further comparative analysis revealed that the electroporation process did not seem to alter the morphology and protein content of EVs as suggested by TEM and western immunoblot analysis respectively.

Although, EV size and concentration could be affected by electroporation, it has been previously shown, that such changes may be dependent on the electroporation parameters, such as voltage and pulses capacitance, with higher voltages associated with an increase in EV size primarily due to the formation of EV aggregates (Pomatto et al., 2019). The type of electroporation buffer, is another EV loading parameter that has also been shown to play a crucial role in facilitating efficient EV transfection (Lennaárd et al., 2022). Additionally, it has also been reported that exogenous loading of EVs via electroporation is size-dependent with smaller loading molecules being more efficiently associated with

EVs compared to larger molecules (Lamichhane et al., 2015). Despite all challenges associated with the development of an effective electroporation protocol for EV loading, it has previously been shown that small molecules including miRNAs could effectively be loaded exogenously into EVs via electroporation (Lennaárd et al., 2022; Pomatto et al., 2019). As expected, in this study, successful overexpression of the two miRNAs of interest was also confirmed by qRT-PCR analysis of electroporated EVs demonstrating that both miRNAs were significantly upregulated in the electroporated EVs compared to naïve EVs with no difference in expression levels detected between both miRNAs.

The next part of the studies focused on exploring the effect of HSVSMC EVs exogenously loaded with miR-24-3p or miR-224-5p mimics on cellular responses of recipient cells. Neither naEVs, nor miEVs (miR-24-3p- or miR-224-5p- EVs) were found to affect HSVSMC viability. In terms of regulation of cell proliferation, it was found that miR-224-5p EVs significantly inhibited HSVSMC proliferation compared to PDGF. Additionally, regardless of the experimental protocol (with or without an EV pre-treatment step), no significant difference in proliferation of recipient HSVSMCs was detected between cells treated with naEVs and any of the miEVs (miR-24-3p and miR-224-5p). Although not EV-associated, there is clear evidence in the literature strongly supporting the involvement of miR-24-3p in the regulation of VSMCs proliferation and apoptosis. It has been previously reported that miR-24-3p expression in human PASMC was positively regulated by PDGF, which is in concurrence with our findings, and that the miRNA is a key regulator of VSMCs promoting a switch to the synthetic phenotype (Chan et al., 2010). Additionally, a recent study investigating the role of miR-24-3p in the regulation of VSMCs from human aorta reported that miR-24-3p (possibly EV-associated) was significantly upregulated in whole blood samples of patients with CHD compared to normal controls (Zhang et al., 2020). This is also consistent with our previous finding that miR-24-3p was upregulated in HSVSMC-derived EVs under pathophysiological conditions. In the same study, it was found that miR-24-3p negatively regulated the viability and apoptosis of human aortic VSMCs by targeting BCL-2-like protein 11 (*BCL2L11*), however, the relationship between miRNA-24-3p expression and *BCL2L11* expression in patients with CHD was not analysed (Zhang et al., 2020). In contrast, a study

investigating the role of miR-24-3p in the regulation of VSMC responses, reported that miR-24-3p inhibited PDGF-induced human arterial VSMC proliferation whilst promoting cell apoptosis by directly targeting *PDGFRB* and *MYC* (*c-Myc*) (Zhu et al., 2015). Similarly, in the context of vascular injury and diabetes, miR-24-3p was found to suppress arterial VSMC proliferation by reducing Wnt4 expression (J. Yang et al., 2016b). Taken together, these studies strongly suggest that miR-24-3p is a key regulator of VSMC.

Interestingly, in the present study when the effect of miEVs on cell proliferation was assessed where recipient cells were not preconditioned, it was found that miR-224-3p EVs significantly inhibited cell proliferation of recipient HSVSMCs compared to PDGF control, but not naEV or miR-24-3p EV treatment which also caused a slight, non-significant, reduction in cell proliferation. The observed non-significant effect mediated by naEVs was unexpected, but within our understanding, since naEVs are not empty vesicles and instead they contain potentially bioactive molecules, including endogenous levels of miR-24-3p and miR-224-5p, which may be working together to exert synergistic effects. In previous studies, where the effect of unmodified EVs (containing endogenous levels of miRNAs) on cell proliferation was assessed, similar non-significant effects of vEVs and pEVs compared to PDGF were observed suggesting that bioactive molecules within EVs may be causing some functional effects which, although non-significant, may still contribute to increased variability in cellular responses in recipient cells. Therefore, further optimisation as well as increasing the number of biological replicates to ensure enough power in the study, would be beneficial to observe clearer effects and detect a potentially statistically significant difference in the regulation of cell proliferation between miR-224-5p EVs and naEVs.

There is a wealth of evidence supporting the idea that multiple miRNAs may work in synergism to regulate cellular processes by controlling common genes (Enright et al., 2003; Krek et al., 2005; Raut et al., 2016; Xue et al., 2016) and/or individual genes with functional interconnections (Huang et al., 2016). Notably, it was proposed that miRNAs that tend to control uniformly expressed protein-encoding mRNAs are much more likely to participate in a meaningful miRNA synergy that regulates fundamental biological activities (Chen et al., 2017). Interestingly, miR-24 was considered as one of the more powerful miRNAs

prone to extensive collaboration with other miRNAs within the cardiovascular system due to its relatively high synergy score of 0.6 (synergy score range: 0.2 - 1.2) (Chen et al., 2017). In the same study, miR-21 was also determined as one of the highly powerful miRNAs with a high synergetic potential (synergy score of 1) (Chen et al., 2017), which is an interesting finding considering that miR-21-5p was also one of the 6 significantly upregulated miRNAs in pEVs as suggested by RNAseq. However, it was not one of the selected miRNAs for further analysis as when validating the RNAseq results by qRT-PCR analysis, although the expression of miR-21-5p in pEVs followed the same trend, the difference was not statistically significant compared to vEVs. In previous studies (Chapter 4) multiple common mRNA targets were identified for miR-24-3p and miR-224-5p, including *GSK3B* and *PIK3R3*, genes known to be involved in the regulation of cell migration and proliferation (Flügel et al., 2012; Guo et al., 2015; Sun et al., 2009; Yoon et al., 2021; Zhou et al., 2012). Additionally, several other functionally related gene targets were also identified for both miR-24-3p (*PDGFRB* and *MAPK14*) and miR-224-5p (*PDGFRA* and *MAPK8*). Based on the findings presented here and the studies discussed above, it is not unreasonable to consider the possibility that both miR-24-3p and miR-224-5p may be involved in the regulation of cellular responses in VSMCs in a synergistic manner. Therefore, studying the synergistic potential of certain miRNAs may be an important step for further elucidating miRNA functions in a particular biological system.

In terms of regulation of cell migration following injury to the cells (wound scratch closure assay), in the present study it was found that after 16 hr there was a significant reduction in EV-depleted FBS-induced migration of HSVSMCs treated with miR-24-3p and miR-224-5p EVs compared to EV-depleted 5% FBS control, but not naEVs. After 18 hr and 22 hr the wound appeared to be equivalently closed in all groups suggesting that the effect of the EVs was transient and potentially an additional treatment or treatment with a higher concentration was required to observe prolonged effects. Follow up studies, where HSVSMC migration capacity was assessed by the gap closure method in the absence of cell injury, revealed that miR-224-5p EVs significantly inhibited EV-depleted FBS-induced cell migration compared to 5% EV-depleted FBS control, naEVs and miR-24-3p EVs after 16 hr.

The use of two different cell migration assays helped corroborate the functional effects mediated by miR-224-5p EVs. The observed difference in the results from the two assays may be down to various reasons including that natural variability between primary HSVSMCs considering that cells from different patient donors were used in both experiments. Indeed, isolated primary HSVSMCs are often pre-conditioned by their donors, meaning that certain parameters such as genetic make-up, age, gender and pharmacological treatment may affect the cell biology *in vitro* (Frismantiene et al., 2018). Technical variability associated with the experimental procedure itself could also have an effect on the results, especially when the sample size is small (N=3) (Columb and Atkinson, 2016). For instance, in both assays cell migration is measured based on a change in a cell-free area over time with the main difference between both assays being the method by which the cell-free area was created. The most obvious advantage of using a physical barrier (i.e., silicone insert) for creating a cell-free area over manually scratching the cell monolayer is that the gap sizes are much more reproducible due to reduced variability caused by human error (Ashby and Zijlstra, 2012; Jonkman et al., 2014). Additionally, both methods assess cell migration under somewhat different conditions. While it has been previously reported that both types of wound healing assays (cell scratch-based and cell barrier-based) give similar wound-healing responses (Block et al., 2004; Nikolić et al., 2006; Van Horssen et al., 2006), it is possible that factors associated with the scratch-based method may be influencing the results of the assay. In the scratch-based wound healing assay, cells may be damaged mechanically, causing the release of certain cellular chemicals into the microenvironment and the degree to which cells are damaged cannot be easily controlled (Riahi et al., 2012). Therefore, it has been argued that the physical barrier-based wound healing assay is more advantageous over a scratch-based assay when studying the regulation of different molecular mechanisms and signalling pathways underlying cell migration (Kroening and Goppelt-Struebe, 2010; Riahi et al., 2012).

Nevertheless, the results presented here suggest that miR-224-5p EVs, and possibly miR-24-3p, may be involved in the regulation of HSVSMC migration capacity through an unknown mechanism. While there is some evidence published in the literature supporting the involvement of both miRNAs in the

regulation of cellular migration (J. Li et al., 2019; J. Yang et al., 2016a; Zhu et al., 2015), there are no studies specifically focusing on elucidating the role of miR-24-3p and miR-224-5p associated with EVs in VSMCs. In the context of occlusive arterial disease, it has previously been shown that miR-24-3p negatively regulated human arterial SMC migration by targeting *PDGFRB* and *MYC* (Zhu et al., 2015). Similarly, in the context of diabetes, miR-24-3p has been shown to inhibit primary aortic VSMC migration by downregulating the expression of *HMGB1* (J. Yang et al., 2016a). MiR-224-5p has not been studied in the context of vascular diseases. In cancer, however, there is evidence suggesting that miR-224-5p may exhibit an inhibitory migratory effect on OCM-1 cancer cells by targeting *PIK3R3* and *AKT3* (J. Li et al., 2019). Inconsistent with findings in other cell types, in the present study, neither miR-24-3p nor miR-224-5p were found to have any regulatory effect on the expression levels of any of the assessed target genes in HSVSMCs, including *PDGFRB* (miR-24-3p target) and *PI3KR3* (common target for miR-24-3p and miR-224-5p).

The underlying mechanism responsible for the potential inhibitory effect of miR-224-5p EVs on EV-depleted FBS-stimulated HSVSMC migration remains yet to be elucidated since none of the assessed miRNA gene targets, including *PDGFRB*, *RRAS*, *PDGFRA*, *NRAS* and *PIK3R3*, appeared to be regulated by any of the miEVs (miR-224-5p EVs or miR-24-3p EVs). While it is possible that the observed miR-224-5p effects on cell migration may involve the regulation of other target genes, rather than the ones assessed in the present study, it is certainly worth noting that PDGF treatment did not induce a significant increase in the expression levels of any of the target genes, therefore suggesting that it was not an ideal positive control and that the experimental design may have potentially hindered the ability of assessing the regulatory effects of miR-24-3p and miR-224-5p on target gene expression. Interestingly, it has been previously reported that the expression levels of *PDGFRA* and *PDGFRB* in VSMCs were upregulated in response to treatment with bFGF (Schöllmann et al., 1992) and TGF- β (Battegay et al., 1990), respectively, where TGF- β was also found to have the opposite effect on the expression levels of *PDGFRA* in the same cells (Battegay et al., 1990). However, “cell context/environment” (i.e., cell-cell contact, spreading, and attachment of cells) has been reported as stronger modulators of receptor expression levels compared to soluble mediators (Barret et al., 1996).

Nonetheless, the regulation of other target genes, which were not assessed in the present study, but were identified as potentially true miRNA gene targets in Chapter 4, may have contributed to the observed regulatory effects of HSVSMC miEVs (miR-24-3p and miR-224-5p) on cellular migration of recipient HSVSMCs. Interestingly, the following genes were also identified as potential miRNA gene targets (Chapter 4): *MAPK14* for miR-24-3p, and *MAPK8*, *PIK3C2A*, *SMAD5* for miR-224-5p, all of which previously found to be involved in the regulation of cell migration (Chao et al., 2018; K. Huang et al., 2017; Tiwari et al., 2013; W. Wu et al., 2019). For instance, it has been shown that siRNA-mediated downregulation of *MAPK14* inhibited the proliferation and migration of renal carcinoma cells (Liu et al., 2020). Additionally, in the context of vascular pathologies, *MAPK14* has been implicated in the negative regulation of VSMC contractile phenotype (Long et al., 2013; W. Wu et al., 2019) ultimately promoting neointimal formation following vascular injury (W. Wu et al., 2019). Similarly, suppressed *MAPK8* protein expression following downregulation of myosin phosphatase target subunit 1 (*MYPT1*, a subunit of myosin phosphatase that is capable of regulating smooth muscle contraction) has been reported to negatively influence the migration and invasion renal carcinoma cells (Xie et al., 2022). While the involvement of the above-mentioned genes in the regulation of VSMC migration has not been extensively studied, their proposed role in the regulation of cell motility of other cell types and their known participation in signalling pathways (e.g., p38/MAPK) mediating cellular migration suggest that a link between the post-transcriptional regulation of these genes by miRNAs and the migration of VSMC may be worth investigating further.

The final part of the present studies aimed to elucidate the potential EV-mediated communication between different vascular cell types by assessing the effects of HSVSMC miEVs (miR-24-3p and miR-224-5p EVs) on HSVEC viability. It was found that miEVs had no effect on HSVEC viability as suggested by the results from the MTT assay. Successful EV-mediated cross-talk between VSMCs and ECs has been previously reported in different disease settings (Boyer et al., 2020; Charla et al., 2020; De La Cuesta et al., 2019; Gao et al., 2016; Heo et al., 2020; B. Wang et al., 2021; Y. Wang et al., 2021; Zhang et al., 2021; Zhao et al., 2016), however, the specific effects of PDGF-stimulated VSMC-derived EVs on vascular ECs has not been widely studied. A recent study, investigating the

effect of MSC-derived EVs on human corneal ECs proposed an EV-mediated mechanism through which MSC-EVs protected human corneal ECs by increasing cell survival and decreasing apoptosis (Buono et al., 2021). The proposed underlying mechanism involved MSC EV-mediated transfer of ER stress modulating miRNAs to ECs including miR-21-5p and possibly miR-24-3p (Buono et al., 2021). The regulatory role of miR-21-5p on EC apoptosis was further confirmed in a study where cardiac telocyte EVs were found to inhibit cardiac microvascular EC apoptosis through EV-mediated transfer of miR-21-5p resulting in targeted silencing of cell death inducing p53 target 1 (*CDIP1*) (Liao et al., 2021).

The results presented here along with the reports discussed above highlight the potential involvement of HSVSMC-derived EVs in the autocrine regulation of HSVSMCs through EV-mediated delivery of miRNAs (miR-224-5p and possibly miR-24-3p). Furthermore, the inhibition of HSVSMC migration observed with miR-224-5p EV treatment suggests that EV-transfer of miR-224-5p to recipient HSVSMCs may have protective effects in vascular remodelling processes. However, further studies are required to confirm the causal relationship between the EV-mediated miRNA transfer and the observed regulatory effect on cell migration as well as to elucidate the exact underlying mechanism.

5.5.1 Study limitations

The miRNA loading dose optimisation study was completed only once due to a number of limiting factors including budget and time restrictions. Increasing the N number for this experiment, in addition to exploring other timepoints (e.g., 6 hr and 48 hr) would have been beneficial to allow for more comprehensive analysis of the ability of exogenously loaded EVs to deliver cargo to recipient cells to be made. Loading a non-human miRNA mimic (i.e., cel-miR-39) into EVs (using the same method as the one employed in later studies) to investigate the ability of EVs to transfer cargo into recipient cells was advantageous as the detected levels of the transferred miRNA into recipient cells were not confounded by endogenous expression of that miRNA, however, the successful transfer of biologically active miRNA mimics (miR-24-3p and miR-224-5p) to recipient cells was not confirmed. Therefore, further studies confirming the successful uptake of EVs by recipient cells as well as the biological activity of

transferred miRNAs (i.e., through Luciferase reporter assay) may be useful. Additionally, it would have been beneficial to assess the effect of both miR-24-3p EVs and miR-224-5p EVs on the protein levels of target genes, including *PDGFRB*, *RRAS*, *PDGFRA*, *NRAS* and *PIK3R3*, which would have provided a better understanding of the potential post-transcriptional regulation of these target genes by the EV-miRNAs. Finally, the majority of the *in vitro* experiments presented here were performed with a relatively small sample size (N=3-4) which may have limited interpretation of the results, therefore, increasing the sample size in future experiment could allow more definitive conclusions to be made.

5.6 Summary

Despite the fact that EVs secreted by HSVSMCs under PDGF stimulation (pEVs) had dysregulated miRNA expression profile compared to control EVs, pEVs had no regulatory effect on proliferation of activated HSVSMCs. Similarly, compared to naEVs, miR-24-3p and miR-224-5p electroporated HSVSMC EVs had no effect on proliferation of PDGF-activated HSVSMCs and HSVSMC viability. However, miR-224-5p EVs were found to significantly inhibit PDGF-induced HSVSMC proliferation compared to PDGF control. Interestingly, it was also found that miR-224-5p HSVSMC EVs may be involved in the inhibition of EV-depleted FBS-induced HSVSMC migration compared to naEVs and miR-24-3p EVs through an unknown mechanism as none of the miRNA gene targets assessed appeared to be regulated by either miR-24-3p or miR-224-5p EVs. Finally, when the EV-mediated communication between HSVSMC EVs and ECs was assessed, it was found that compared to naEVs, miR-24-3p and miR-224-5p electroporated HSVSMC EVs had no effect on HSVSMC viability. In conclusion, in the context of vascular remodelling, the present findings suggest that HSVSMC-derived EVs may be involved in the autocrine regulation of HSVSMC responses possibly through an EV-mediated miR-224-5p transfer to recipient cells, however, the related mechanisms remain largely underexplored.

Chapter 6 Validation of miRNA expression profile in a murine model of vascular injury

6.1 Introduction

There are several commonly used vascular injury animal models, including murine models, that exhibit SMC phenotype switch-driven NF, making them suitable *in vivo* models for studying vascular remodelling processes (Ebert et al., 2021). The carotid artery ligation model is a blood cessation model of vascular injury which was first described in 1997 motivated by the aim to study the response of SMCs to injury and ultimately intimal lesion formation (Kumar and Lindner, 1997). The model was developed based on previous findings that changes in blood flow affect the proliferative response of SMCs (Geary et al., 1994; Graham et al., 1992; Kohler et al., 1991) and that vessels have been shown to undergo adaptive compensatory modifications in their lumen size in response to chronic alterations in blood flow (Guyton and Hartley, 1985; Langille and O'Donnell, 1986). During the procedure the common left carotid artery is exposed and ligated near the distal bifurcation causing an immediate cessation of blood flow, while the common right carotid artery remains non-ligated serving as an uninjured control (Kumar and Lindner, 1997). As a result, this model displays SMC-driven neointimal formation with extensive vascular remodelling and a progressive reduction in vessel diameter for 2-4 weeks. In addition to the observed increase in SMC proliferation, leukocytes are also detected within the adventitia close to the developing neointima suggesting an inflammatory component of the injury response (Kumar and Lindner, 1997). A number of studies have been carried out aiming to identify the origin of cells within the neointimal lesion. A study in transgenic SM22- α human diphtheria toxin (DT) receptor mice, showed that DT-mediated depletion of SMC prior to carotid artery ligation surgery significantly reduced the neointimal area revealing VSMC as the primary source of neointimal cells (Yu et al., 2011). Consistent with the above findings, another carotid artery ligation study using SMC lineage-tracing mice found that around 80% of neointimal cells originated from differentiated mature SMCs suggesting that SMC phenotype switching is a crucial pathogenic driver of neointimal formation (Herring et al., 2014). Moreover, a study using the transgenic lineage tracing Myh11-CreERt2/Rosa26-Confetti mice aiming to determine which of the two cellular responses, proliferation or migration, takes place first found that medial SMC proliferation preceded SMC migration to the intima (Chappell et al., 2016).

In addition to the SMC phenotype switching, there are other underlying cellular mechanisms, such as endothelial dysfunction and inflammation, involved in the overall response following carotid artery ligation which also contribute to the development of neointimal lesions thereby recapitulating other pathogenic stimuli of saphenous VGD and to some extent ISR (Costa and Simon, 2005; de Vries et al., 2016; Squadrito et al., 2003; Yahagi et al., 2016; Yamashita et al., 2001). However, the limited mechanical trauma and inflammatory response as well as the largely intact endothelium associated with the ligation model means that this model is not ideal for studying neointimal behaviour in a clinically translatable way (Peterson et al., 2016). On the other hand, the main advantage of the ligation model, i.e., relatively easy surgical procedure associated with relatively high reproducibility due to reduced influence of variables related to the surgical technique, make it suitable for studying cellular responses on a molecular level, such as VSMC dedifferentiation, proliferation, migration, and redifferentiation *in vivo* (Acevedo et al., 2004; Kawasaki et al., 2001; Kraemer, 2002; Kumar and Lindner, 1997; Kuzuya et al., 2003; Morishita et al., 2002; Murakoshi et al., 2002; Rectenwald et al., 2002; Sindermann et al., 2002; Singh et al., 2001). Therefore, the carotid artery ligation model was also considered a suitable *in vivo* model for studying changes in circulating EVs following vascular injury and ultimately the development of SMC-driven neointimal lesions.

The wire injury murine model is another common *in vivo* model of vascular injury (Lindner et al., 1993). Originally, this endovascular dilatation and endothelial denudation model was carried out on the carotid arteries whereas more recently the femoral and iliac arteries have been primarily used. During this procedure, a flexible wire (up to 3 times bigger than the diameter of the vessel) is inserted into the common left carotid artery under rotation or repetitive back and forth movements resulting in complete removal of the endothelium and partial damage to the cells of the medial layer (Lindner et al., 1993; Sata et al., 2016; Takayama et al., 2015). Similar to carotid ligation injury, carotid wire injury is also characterised by increased medial and intimal SMC proliferation, however, the intimal hyperplasia appears more limited occurring only within the endothelium-denuded segments (Lindner et al., 1993). In contrast to ligation injury, femoral wire injury more closely recapitulates human saphenous VGD and ISR since it enables the study of vascular responses

following severe mechanically induced endothelial damage while blood flow is maintained allowing the transmigration of cells from the circulation into the vessel wall (de Vries et al., 2016; Grewe et al., 2000; Morinaga et al., 1985; Sata et al., 2016, 2000). Moreover, in addition to causing SMC phenotypic switching, femoral wire injury has also been associated with induced platelet accumulation and a rapid inflammatory response at the denuded luminal surface which further highlights that this injury model closely resembles the general response to injury that occurs in humans (Roque et al., 2000).

Both injury models described above are associated with several advantages and disadvantages related to technical feasibility and the underlying pathophysiology of the developing neointimal lesions. Overall, in terms of technical feasibility, the ligation injury model is less challenging, hence, it is much more reproducible. Whereas, although more technically challenging, the wire injury model induces cellular response to injury which more closely resembles ISR and VGD (Ebert et al., 2021).

The murine and porcine vein graft models were specifically developed to study the pathophysiological response that occurs during neointimal formation in venous bypass grafts. In the case of mice, either autologous or isogenic vessels of the jugular or inferior vena cava veins are transplanted into the carotid artery via end-to-end anastomosis thus triggering SMC phenotype switching-driven neointimal formation (Zou et al., 1998). Moreover, in this model, it has been found that neointimal cells originate predominantly from the vein graft (Cooley, 2004). In the case of porcine interposition vein graft models, autologous SV or jugular vein grafts are usually anastomosed into the carotid artery as an end-to-end graft (Chen et al., 1994; Lloyd et al., 2001). In this model, increased VSMC proliferation associated with significant remodelling of the vein graft has been observed. Additionally, histologic changes detected within the grafts were found to be strikingly similar to events that occur during wound healing, and the development of neointimal hyperplasia and VGD (O'Brien et al., 1997). While the murine model closely resembles the mechanical characteristics, pathophysiology, and complications of human VGD (Zou et al., 1998), the porcine interposition vein graft model is better because in addition to the above-mentioned advantages associated with the murine model, it also more closely

resembles human anatomical structures (Liu et al., 2018; Swartz and Andreadis, 2013). The murine graft model is also extremely technically challenging which limits its application and reproducibility, and potentially the validity of findings based on this model. Additionally, the specifics of the mouse vascular structures, the exceptionally small vessel sizes along with the known differences in heart rate and blood flow between mice and humans all reduce the clinical relevance of the murine graft model (Cooley, 2016). On the other hand, the use of porcine vein graft models is also limited due to practical considerations associated with the fact that pigs are large animals. Specialised surgical/anaesthesiological expertise, specialised facilities for animal care and equipment are required in addition to a considerably higher cost associated with the maintenance of large animals (Liu et al., 2018; Simon et al., 2015). Nevertheless, both the murine and porcine vein graft models remain valuable *in vivo* tools for studying new therapeutic interventions such as *ex vivo* gene therapy.

Increasing evidence suggests that miRNAs play an essential role in vascular diseases, including saphenous VGD and ISR, not only as disease biomarkers (Emanueli et al., 2016; Meijiao et al., 2014; Mukaihara et al., 2021; Varela et al., 2019) but also as disease mediators (Liu et al., 2021; Qu et al., 2017). For instance, circulating levels of miR-499 (Yao et al., 2014), miR-93-5p (O'Sullivan et al., 2019), and miR-142-5p (Pan et al., 2021) have been reported as potential clinical biomarkers of restenosis capable of predicting the development of graft disease in CABG patients or ISR in stent-implanted patients. Interestingly, exosomal miRNAs (miR-24 and miR-210) compared to miRNAs in whole plasma, were found to be a better predictor of myocardial injury following CABG surgery (Emanueli et al., 2016). Different *in vivo* models of vascular injury have already been successfully utilised to study the role of miRNAs in saphenous VGD and ISR as well as the therapeutic potential of EVs in the context of vascular remodelling processes following injury (Jansen et al., 2013; Liu et al., 2021; Qu et al., 2017). A study by Qu et al. aiming to investigate the role of miR-126-3p in the prevention and treatment of autologous vein graft restenosis in CABG patients found that local overexpression of miR-126-3p improved re-endothelialisation and attenuated neointimal formation in a rat vein graft model using autologous right external jugular vein (Qu et al., 2017). A more recent study using a carotid

artery wire injury mouse model, reported that miR-302a was involved in the regulation of neointimal wire-injury induced vascular remodelling by promoting VSMC proliferation and subsequent neointimal formation (Liu et al., 2021). Moreover, EVs have also been successfully demonstrated to serve as therapeutic cargo delivery vehicles mediating miRNA-transfer to recipient cells *in vivo*. Similar to the findings in the study where miR-126-3p was delivered locally in vein grafts (Qu et al., 2017), EV-mediated delivery of miR-126-3p to carotid artery ECs following systemic EV treatment promoted EC repair in injured mouse carotid arteries (Jansen et al., 2013).

Taken together, the studies highlighted here suggest that vascular injury disease models have successfully been used to study the role of miRNAs in vascular remodelling diseases. Additionally, circulating miRNAs and miRNAs packaged in EVs may be used as potential biomarkers for vascular stenosis in saphenous VGD and ISR following bypass graft surgery or stent implantation respectively.

6.1.1 Hypothesis

- Serum EV characteristics, including EV-miR-24-3p and miR-224-5p expression levels, are altered in mice subjected to vascular injury compared to controls.

6.2 Aims

- To compare the characteristics of serum EVs derived from mice subjected to vascular injury compared to control mice.
- To assess the miR-24-3p and miR-224-5p expression profile in mouse serum EVs.

6.3 Methods

Unfortunately, at the time of this project, no relevant human samples were available to perform potential biomarker studies. Serum samples obtained from mice subjected to carotid artery ligation surgery were the only relevant *in vivo* samples available at the time to study the expression of miR-24-3p and miR-224-5p in circulating EVs in the setting of vascular injury. All animal procedures were carried out by a former PhD student Dr Julian Schwartz and a fellow PhD student Arun Flynn and were approved by the Home Office under the Animals Scientific Procedures Act 1986.

6.3.1 Blood samples collected from mice with vascular injury

The blood samples from mice which had been subjected to carotid artery ligation surgery were a kind donation from Dr Julian Schwartz. Mice for this study (male C57BL/6 mice, 8-10 weeks old) were purchased from Charles River Laboratories (MA, USA). Mice were housed in 12-hr light/dark cycle conditions and fed a standard mouse chow. Following arrival, mice were allowed to acclimatise to their new housing conditions for 2 weeks prior to being subjected to the carotid artery ligation surgery.

The blood samples were collected as part of an *in vivo* carotid artery ligation study performed by Dr Julian Schwartz as authorised by the Home Office under project license number 70/8572, procedure 3. The study did not involve any sham treated control mice as the left carotid artery of the mice was ligated, and the right non-ligated carotid artery was used as a control during analysis. Control blood samples were collected separately as described below (Section 6.3.2).

6.3.1.1 Study design

Detailed description of the study can be found in Dr Julian Schwartz' PhD thesis (Schwartz, 2021). Briefly, in this study, male C57BL/6 mice (10-16 weeks old) were subjected to carotid artery ligation surgery after which mice were separated and housed in individual cages until humane killing and organ/blood harvesting at indicated time points (Figure 6-1). Mice were divided into groups depending on the study endpoint - day 5 after surgery (D5), day 10 after surgery (D10), day 14 after surgery (D14) and day 28 after surgery (D28) (Figure 6-1).

Mice were humanely killed at indicated time points following the Schedule 1 procedure using a CO₂ chamber and the non-aversive tunnelling technique. Death was confirmed by cervical dislocation prior to proceeding to organ/blood harvesting. Blood was collected via right ventricular cardiac puncture.

6.3.2 Blood samples collected from control mice

Control blood samples were collected from age and sex matched control surplus C57BL/6 mice (all males between 8-16 weeks old). Samples were a kind donation from Arun Flynn, a fellow PhD student in our laboratory performing *in vivo* work under a project license number P486284C3 as authorised by the Home Office. Mice were purchased from Envigo (Blackthorn, UK) at 7 weeks of age, and they were housed in the same conditions as the mice in the carotid artery ligation study described above - 12-hr light/dark cycle and a standard mouse chow diet. Control mice were also humanely killed following the Schedule 1 procedure using a CO₂ chamber and the non-aversive tunnelling technique. Death was confirmed by cervical dislocation prior to proceeding to organ/blood harvesting. Blood was collected via right ventricular cardiac puncture.

6.3.3 Obtaining serum samples from whole blood

After collection, blood was placed in serum tubes (cat. no.: 367959, Becton Dickinson, NJ, USA) and centrifuged at 8,000 g and room temperature for 1 min to enable blood phase separation. The upper phase/blood serum was carefully transferred to a sterile 1.5 mL Eppendorf tube which was then stored at -80°C.

Table 6-1 Other relevant methods for Chapter 6.

EV isolation from serum	Section 2.10.3.2
EV characterisation	Nanoparticle tracking analysis (Section 2.10.4)
	Protein expression analysis (Section 2.7)
Measuring of gene expression levels	Section 2.6

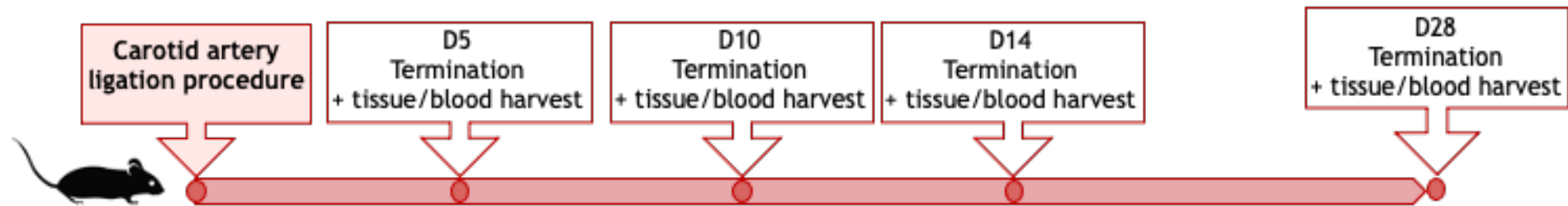


Figure 6-1 Schematic representation of the carotid artery ligation study design as part of which mice blood samples were collected.

Following carotid artery ligation surgery, mice were terminated, and organs/blood were harvested at indicated time points, D5 (N=7), D10 (N=7), D14 (N=7) and D28 (N=3). The study was performed by Dr Julian Schwartze, and the blood samples from this study were kindly donated by him. Abbreviations: D = day after surgery/injury.

6.4 Results

6.4.1 Characterisation of serum EVs

EV sample populations were characterised in terms of size and particle concentration by NTA. EV sample protein concentration was determined by microBCA assay and western immunoblot analysis was carried out to detect specific EV-related protein markers. The aim of this study was to investigate any potential differences in EV characteristics between EVs isolated from control mice and mice with an injured carotid artery.

NTA of serum EVs from control mice and mice with injured left carotid arteries, showed that there was no significant difference in terms of mean particle size (mean size \pm SEM): 88.3 \pm 3.4 nm for CNT EVs, 88.0 \pm 2.5 nm for D5 EVs, 97.4 \pm 7.2 nm for D10 EVs, 89.1 \pm 3.6 nm for D14 EVs and 93.3 \pm 1.7 nm for D28 EVs (Figure 6-2A). Similarly, there was no significant difference in the modal EV size (modal size of 76.0 \pm 2.2 nm for CNT EVs, 73.3 \pm 3.1 nm for D5 EVs, 78.3 \pm 4.2 nm for D10 EVs, 75.1 \pm 3.0 nm for D14 EVs and 78.1 \pm 3.4 nm for D28 EVs) (Figure 6-2B). Additionally, serum EV populations also did not significantly differ in terms of concentration (7.5 \times 10¹² \pm 8.4 \times 10¹¹ EVs/mL, 5.4 \times 10¹² \pm 5.7 \times 10¹¹ EVs/mL, 4.7 \times 10¹² \pm 7.2 \times 10¹¹ EVs/mL, 5.9 \times 10¹² \pm 1.2 \times 10¹² EVs/mL and 5.8 \times 10¹² \pm 8.3 \times 10¹¹ EVs/mL for CNT, D5, D10, D14 and D28 EVs respectively) (Figure 6-2C).

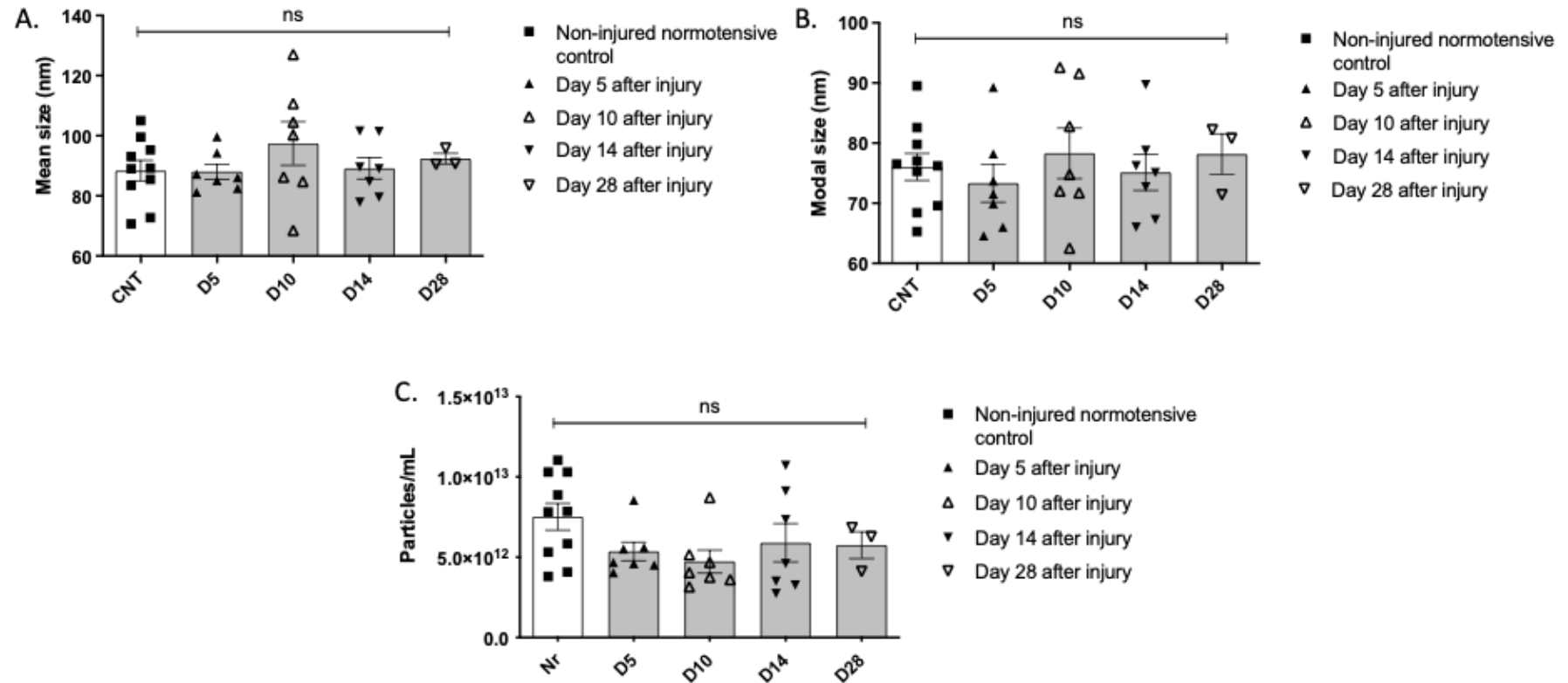


Figure 6-2 Characterisation of serum EV populations by NTA (Part 1). Serum EVs were isolated from CNT mice and mice humanely killed at D5, D10, D14 and D28 after carotid artery ligation surgery. (A) NTA data for mean EV particle size; (B) NTA data for modal EV particle size; (C) NTA data for EV particle concentration; Differences between groups were assessed with a one-way ANOVA with Tukey's correction (CNT EVs: N=10; D5,10 and14 EVs: N=7; and D28: EVs N=3). Abbreviations: NTA, nanoparticle tracking analysis; CNT, control, EVs, extracellular vesicles; D, Day.

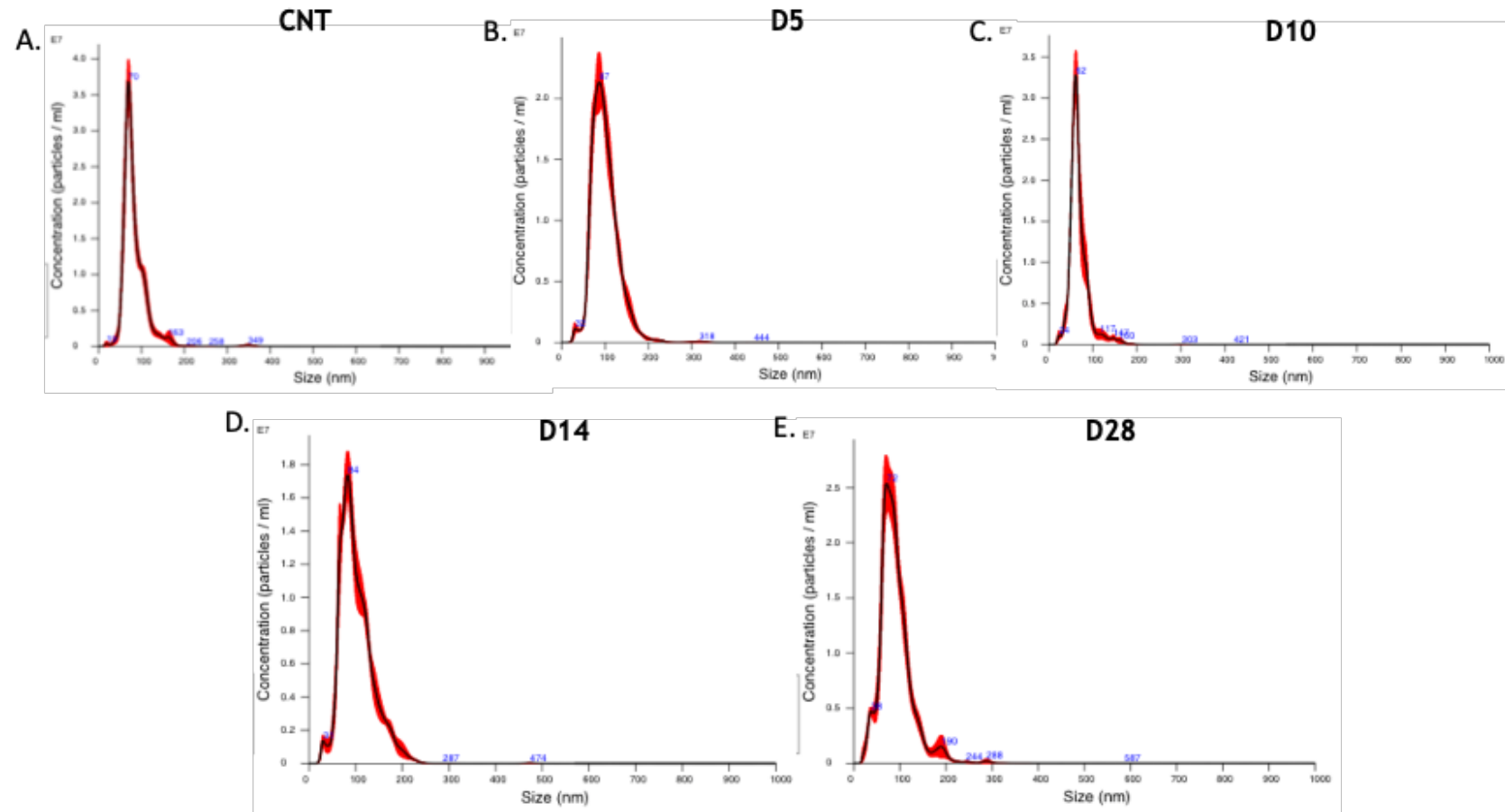


Figure 6-3 Characterisation of serum EV populations by NTA (Part 2). Representative size distribution peaks obtained during NTA of serum EVs isolated from (A) CNT mice and mice terminated at (B) D5 (C) D10 (D) D14 and (E) D28 after carotid artery ligation surgery. Abbreviations: NTA, nanoparticle tracking analysis; CNT, control, EVs, extracellular vesicles; D, Day.

Next, western immunoblot analysis was performed where the presence of EVs in the samples was confirmed by the detection of different EV-associated protein markers including Annexin XI, CD81 and CD63 (Figure 6-4). All protein markers were found to be present in all of the serum EV samples (N=3).

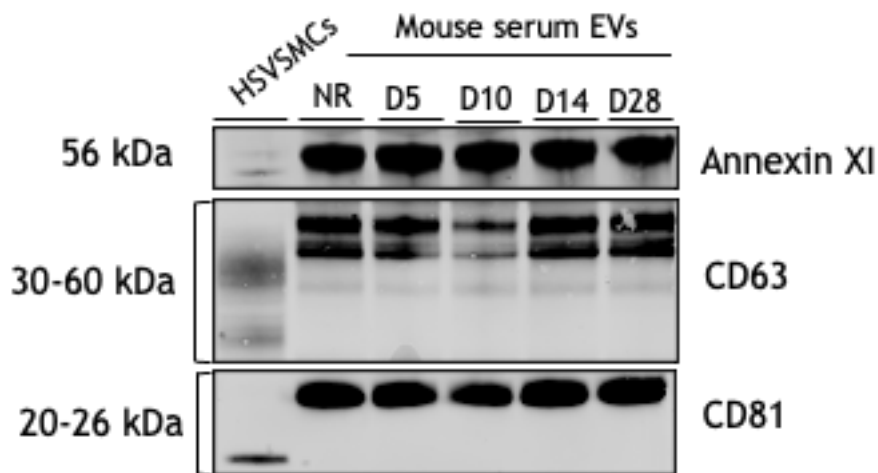


Figure 6-4 Analysis of mouse serum EV protein content by western immunoblot.

EV-related protein markers (Annexin XI, CD63 and CD81) were successfully detected in HSVSMC lysate, CNT, D5, D10, D14 and D28 serum EVs. The images shown here are representative images of the markers detected in serum EVs (N=3 for all markers). Abbreviations: HSVSMCs, human saphenous vein smooth muscle cells; CNT, control, EVs, extracellular vesicles; D, Day.

6.4.2 miRNA expression profile in serum EVs

A number of miRNAs, including miR-21, miR-126-3p and miR-126-5p, have been recognized not only as biomarkers of vascular injury and restenosis but also as therapeutic targets (Mukaihara et al., 2021; Varela et al., 2019). Therefore, it was next of interest to assess miR-24-3p and miR-224-5p expression levels in the serum EVs isolated from injured mice at different timepoints after carotid artery ligation surgery. In the first set of analysis, miR-24-3p and miR-224-5p expression levels in serum EVs from mice humanely killed at D5, D10, D14 and D28 after surgery were compared. Both miRNAs were successfully detected in all experimental groups, however, no statistically significant differences in expression levels of either miRNA were observed (Figure 6-5A and B respectively).

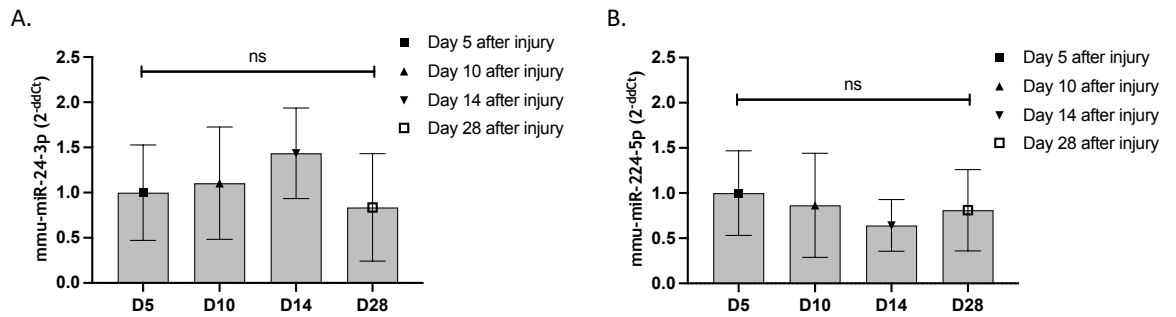


Figure 6-5 Assessing miRNA (miR-24-3p and miR-22-5p) expression levels in serum EVs isolated from mice with vascular injury. MicroRNA expression levels in mice serum EVs were assessed by qRT-PCR. The fold change in expression levels of both (A) miR-24-3p and (B) miR-224-5p in serum EVs isolated from injured mice humanely killed at D5, D10, D14 and D28 were compared (N = 3-10). For these comparisons, differences between groups were assessed based on δC_t values with an Ordinary one-way ANOVA with Tukey's correction <0.05 ($* < 0.05$) were considered statistically significant. Abbreviations: CNT, control, EVs, extracellular vesicles; D, Day.

In the second set of analysis, the expression levels of miR-24-3p and miR-224-5p in serum EVs from mice humanely killed at D5, D10, D14 and D28 after surgery were re-analysed by comparing the previously obtained results for all four timepoints to miR-24-3p and miR-224-5p expression levels in serum EVs isolated from control (CNT) mice. Interestingly, it was found that miR-24-3p and miR-224-5p expression levels in serum EVs isolated from mice at each timepoint (D5, D10, D14 and D28) after injury were generally higher than in control mice (Figure 6-6A and B respectively) and the difference in expression levels between some of the compared groups was statistically significant. For instance, miR-24-3p expression in serum EVs isolated from injured mice at D14 after surgery was significantly upregulated compared to control mice ($RQ_{\text{mean}} \pm \text{SEM.}$, D14 vs CNT: 4.1 ± 0.5 , $p < 0.05$) (Figure 6-6A). Moreover, miR-224-5p expression in serum EVs isolated from injured mice at D5 after surgery was significantly upregulated compared to control mice ($RQ_{\text{mean}} \pm \text{SEM.}$, D5 vs CNT: 4.1 ± 0.47 , $p < 0.05$) (Figure 6-6B). Similar observations were made regarding higher expression levels of miR-224-5p in serum EVs isolated from injured mice at D10 after surgery, however, the difference did not quite reach statistical significance ($RQ_{\text{mean}} \pm \text{SEM.}$, D10 vs CNT: 3.6 ± 0.6) (Figure 6-6B, $p = 0.051$).

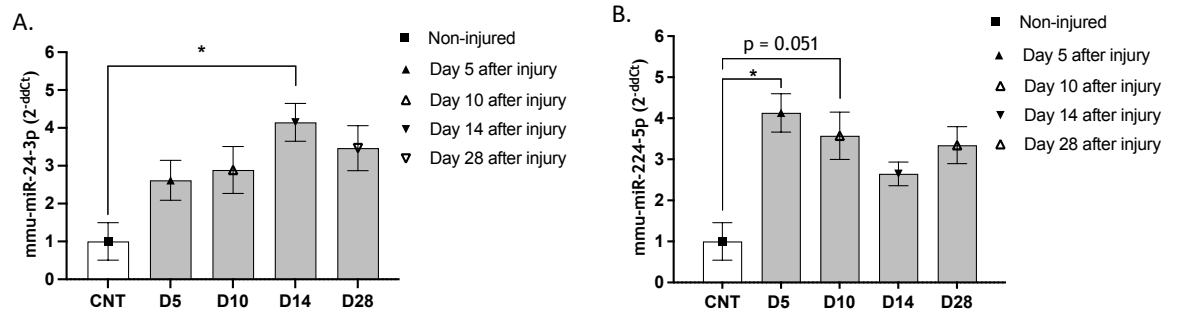


Figure 6-6 Comparing miRNA (miR-24-3p and miR-22-5p) expression levels in serum EVs isolated from mice with vascular injury and control mice. The analysis of miRNA expression levels in mice serum EVs assessed by qRT-PCR was repeated where the fold change in expression levels of both (A) miR-24-3p and (B) miR-224-5p in serum EVs isolated from mice terminated at four different timepoints after carotid artery ligation surgery were compared to serum EVs isolated from non-injured CNT mice (N = 3-10). For these comparisons, differences between groups were assessed based on δ Ct values with a one-way ANOVA with Dunnett's correction <0.05 ($* < 0.05$) were considered statistically significant. Abbreviations: CNT, control, EVs, extracellular vesicles; D, Day.

6.5 Discussion

In this small study, mouse serum EVs were successfully isolated and characterised by NTA and WB. It was found that the physical characteristics of mouse serum EV populations, such as size and concentration, were not affected by the development of carotid artery ligation injury-induced neointimal formation at different stages post-surgery as suggested by NTA. Additionally, the successful isolation of mouse serum EVs was also confirmed by the detection of EV-related protein markers, including Annexin XI, CD63 and CD81, by western immunoblotting. Further qRT-PCR analysis of miR-24-3p and miR-224-5p demonstrated that both miRNAs are present in circulating EVs from mice and suggested that the expression levels of both miR-24-3p and miR-224-5p were significantly upregulated in serum EVs isolated from injured mice at D14 and D5 after surgery, respectively, compared to control mice.

Although most of the studies in the literature, analysing changes in circulating EVs in different disease settings, utilised plasma-derived EVs, it is known that both plasma and serum samples could be utilised to study circulating EVs as EVs may be isolated from either of the two sources (Boulangier et al., 2006; Loyer et al., 2014). At the time of the study, only relevant mouse serum samples were available which could have been used to investigate potential changes in circulating EVs in response to vascular injury *in vivo*, hence only serum derived EVs were utilised in the studies presented in this chapter.

The development of neointimal formation in the injured carotid arteries of the mice, from which serum EVs were isolated in the present study, was confirmed by Dr Julian Schwartz (data not shown). Briefly, in this study, the occurrence of visible structural changes in injured carotid arteries were reported at day 5 after surgery suggesting an early onset of lesion formation. A gradual increase of intimal/media ratio due to increased cell hyperplasia was described between day 5 and day 10 timepoints with a maximal intimal thickening achieved at day 10. In this period (between day 5 and day 10), detected intimal and medial cell proliferation, accompanied by a decrease in SMC α SMA expression, indicated SMC phenotype switching. After day 10, at day 14 and day 28, the intimal/media ratio was found to be unchanged with an observed recovery of α SMA expression in VSMCs at day 28 (Schwartz, 2021). Notably, it was also reported that

neointimal lesions were not observed in some of the injured carotid arteries at day 10 and day 14 after surgery (Schwartz et al., 2021). Since the reason why two 10- and three 14-day-old injured carotid arteries did not display neointimal lesions was not clear, it was important to take these findings into consideration when interpreting the data in the present study.

In contrast to the present findings of no difference in the amount of EVs released into the circulation under disease conditions compared to healthy conditions, it has been commonly suggested that under CVD conditions EV particle release increases (Amabile et al., 2014, 2005; Emanuelli et al., 2016; Frey et al., 2019; Jy et al., 2015; Valencia-Nuñez et al., 2017). Interestingly, however, the findings presented in this study regarding size and protein markers of mouse serum EVs are consistent with previously reported characteristics of mouse serum EVs (Zhao et al., 2020). A recent study in which serum EVs and their RNA contents across different biological species, including mice, were comprehensively characterised, reported that mouse serum EVs are generally smaller than 100 nm within the exosomal size range (Théry et al., 2018), and CD81 and CD63, amongst other EV-related protein markers, were detected in the mouse EV populations (Zhao et al., 2020). The findings in the current study and in the study by Zhao *et al.*, are comparable since both studies used the same strain of adult mice (male C57BL/6), similar precipitation-based EV isolation methods, (ExoQuick solution used by Zhao et al. and Total Exosome Isolation Reagent used in the current study) and similar EV characterisation techniques - NTA and WB analysis.

In the context of myocardial injury following CABG, a study by Emanuelli et al. reported an association between increased plasma levels of EVs (within the exosomal size range) and their miRNA cargo and myocardial injury in patients undergoing CABG surgery (Emanuelli et al., 2016). In the same study, the increased concentration of circulating EVs after CABG was found to positively correlate with the concentration of cardiac troponins (cTns), the “gold standard” surrogate biomarkers of myocardial damage (Tsounis et al., 2013), where the surge in plasma EV concentration was found to precede the increase in plasma cTns levels (Emanuelli et al., 2016). Similarly, plasma EV concentration in patients who developed ISR 1 year after a PCI procedure, and also in rats with

carotid artery balloon injury-induced stenosis, was found to be significantly higher compared to patients without ISR and control animals respectively (Gao et al., 2021). The effect of various cardiovascular and metabolic risk factors on EV release from ECs specifically has also been investigated (Amabile et al., 2014). Amabile *et al.*, reported a positive correlation between higher plasma EC EV (CD144+) levels and cardiometabolic risk factors including hypertension, elevated triglycerides and metabolic syndrome in individuals with no previous history of CVD (Amabile et al., 2014). Similarly, in the context of vascular injury, a study investigating the relationship between plasma EV levels and vascular dysfunction in end-stage renal failure (ESRF) patients, found that increased concentration of circulating plasma EC EVs was tightly associated with endothelial dysfunction and arterial dysfunction in ESRF (Amabile et al., 2005). Another study, investigating the cardioprotective effect of EV miRNAs released in response to episodes of remote ischaemic reperfusion in the left arm, reported that remote ischaemic preconditioning increases serum EV concentrations associated with myocardial protection (Frey et al., 2019) which further emphasises the important roles for EVs released in response to pathological conditions. There are many significant differences, in terms of design, between the studies discussed above and the current study which may potentially, at least in part, explain the inconsistent findings regarding circulating EV levels and CV risk factors including vascular injury. To mention a few, the studies cited above explored human plasma-based EV analysis whereas the present study involved mouse serum-derived EVs. Notably, it has previously been suggested that human and mouse circulating EV populations differ significantly not only in terms of size and concentration but also in terms of EV miRNA cargo content (Zhao et al., 2020), thus, highlighting the importance of considering potential species-specific differences when studying EVs as potential biomarkers.

In 2008, Chen *at al.* reported that human serum contained several stable miRNAs derived from various different tissues throughout the body, the expression profiles of which have demonstrated great potential to serve as novel non-invasive biomarkers for the diagnosis of many diseases (Chen et al., 2008). Since then, the interest in discovering miRNAs with a promising diagnostic value has been increasingly growing with various miRNAs currently recognised as

having great potential as clinical biomarkers for CVD, cancer, metabolic and neurodegenerative diseases (Pogribny, 2018). Prior to the popularity of EV studies, the majority of studies investigating blood miRNA markers were carried out in serum (Chen et al., 2008; Mitchell et al., 2008). However, more recently, not only it has been demonstrated that circulating blood miRNAs are highly enriched in serum EVs (Zhao et al., 2020), but also that serum EV miRNAs could be used as more stable biomarkers with increased sensitivity (Cheng et al., 2014a; Emanuelli et al., 2016; Szabo and Momen-Heravi, 2017). Interestingly, an important advantage of using EV miRNAs as disease biomarkers over non-EV associated extracellular miRNAs is that EVs tend to protect RNA molecules from degradation which could ultimately increase both the sensitivity and specificity of miRNA biomarker assays (Cheng et al., 2014a).

One of the aims of the current study was to validate the previously established (Chapter 4) *in vitro* expression profile of miR-24-3p and miR-224-5p associated with EVs in a vascular injury *in vivo* model. In the present study, qRT-PCR analysis of EV miRNA expression levels showed that both miRNAs were detected in circulating murine EVs and suggested that the expression of miR-24-3p and miR-224-5p in mouse serum EVs may be increased following vascular injury. More specifically it was found that miR-24-3p was significantly upregulated in serum EVs isolated from injured mice at day 14 after surgery compared to EVs from control mice. Similarly, the expression of miR-224-5p was also found to be significantly upregulated in serum EVs isolated from injured mice at day 5 after surgery compared to EVs from control mice. However, as previously outlined, due to the observation that 2 injured carotid arteries at day 10 and 3 injured carotid arteries at day 14 after surgery did not display neointimal lesions, in combination with the limitation that serum from control mice was not collected as part of the original study, it was important to interpret any findings with caution. The absence of lesion formation in some of the 10- and 14-day-old injured arteries, may have hindered the possibility of detecting statistically significant difference in expression levels of miR-24-3p and miR-224-5p in serum EVs from injured mice at day 10 after surgery and control mice. However, since technical tissue handling errors could not have been excluded as a possible reason as to why lesions were not detected in some injured arteries, it was not feasible to exclude those samples from the analysis. Therefore, considering the

above-mentioned limitations, it is possible that both miR-24-3p and miR-224-5p may serve as biomarkers of stenosis following vascular injury, with miR-224-5p possibly playing an active role in the remodelling process when VSMC-phenotypic switching takes place (Kumar and Lindner, 1997).

Despite the high failure rates associated with saphenous VGD following CABG - estimated 50% failure within 5-10 years post-CABG and 20-40% failure within the first year of surgery (Hall and Brilakis, 2019), to date, no reliable diagnostic and prognostic tools have been established to predict outcomes after CABG surgery. Similarly, the development of ISR due to profound neointimal hyperplasia following PCI remains a clinically significant problem with a strong need of identifying useful tools to differentiate and follow-up subjects at risk of developing restenosis. Due to their stability in several biofluids, recent research efforts have demonstrated the potential of blood-based miRNAs as useful non-invasive biomarkers for both ISR and clinical outcomes associated with saphenous VGD (Błażejowska et al., 2021; Varela et al., 2019). Changes in miRNA expression profiles may be triggered by various factors including inflammation (Sonkoly and Pivarcsi, 2009), apoptosis (Jovanovic and Hengartner, 2006; Shirjang et al., 2019), and ischemia/reperfusion injury (Ye et al., 2011), which are all known to occur in the course of CABG and PCI procedures. Several miRNAs have already been recognised as potential biomarkers and therapeutic targets in pathological outcomes following both CABG (e.g., miR-1, miR-126, miR-133, miR-144, miR-195, and miR-320) and PCI (e.g., miR-21, miR-100, miR-145, miR-126 and miR-210) (Błażejowska et al., 2021; Varela et al., 2019).

A recent study, involving 67 patients who underwent CABG surgery, investigated the levels of miR-126 and VEGF-A at different time points (Mukaihara et al., 2021). In their study, Mukaihara et al. found that serum miR-126-3p levels initially increased after CABG, however, after day 3, decreased below preoperative levels and at day 7 serum miR-126-3p levels were found to be lower in patients with PAD, who have atherosclerosis-related systemic endothelial dysfunction, than in patients without it. In parallel, serum VEGF-A levels were also increased 7 days after CABG surgery (Mukaihara et al., 2021). Therefore, since VEGF-A is a known positive regulator of VSMC migration and proliferation leading to graft stenosis (Ferrara, 2009) and miR-126-3p has been previously

shown to modulate VEGF-A signalling by downregulating *PIK3R2* and *SPRED1*, thus suppressing the PIK3 and ERK1/2 pathways (Yuan et al., 2019), it is possible to speculate that low levels of serum miR-126 may lead to increased VEGF-A signalling which may in turn promote neointimal formation and ultimately SV graft failure. In contrast, in another study, it was found that plasma miR-126 concentration was not affected by CABG surgery (Emanueli et al., 2016). Such discrepancies in findings may, at least in part, be explained by the fact that different types of blood samples - serum and plasma, were used to analyse changes in circulating miR-126 levels following CABG surgery. Additionally, Emanueli et al. analysed both miRNA levels in whole plasma and in plasma EVs, and found that plasma EV-associated miRNAs, including miR-24, miR133a/b, and miR-210, were upregulated following CABG and were positively correlated with hs-cTnl indicating their potential as biomarkers for myocardial injury and ischaemia (Emanueli et al., 2016). The finding that miR-24 levels were increased in plasma EVs following CABG but not in whole plasma (Emanueli et al., 2016), was in agreement with the findings presented in this chapter which suggests that the potential of EV-associated miR-24 as a biomarker for saphenous VGD is worth exploring further.

The correlation of circulating levels of various pro-angiogenic miRNAs and the development of ISR following PCI procedure has also been elucidated. In a recent study, Dai et al. reported that plasma levels of miR-19a, miR-126, miR-210, and miR-378 were independently associated with the risk of restenosis in subjects who underwent PCI, and in combination, these four miRNAs showed better predictive value for ISR occurrence in Chinese population than each miRNA individually (Dai et al., 2019). Additionally, another recent study, reported that both increased plasma EV levels and EV-associated miR-501-5p expression were linearly correlated with the development of ISR in PCI patients 1 year after stent implantation (Gao et al., 2021).

Circulating levels of both miR-24-3p and miR-224-5p specifically had previously been demonstrated to have diagnostic and possibly prognostic value in various cancers (Rana et al., 2022; H. Wang et al., 2020; S. Wang et al., 2020; Yang et al., 2020), however, their potential as CVD biomarkers has not been extensively studied yet. In the context of CVD, a study investigating a potential therapeutic

method for myocardial ischemia/reperfusion injury, found that circulating miR-24-3p levels were downregulated in a mouse model of myocardial ischaemia/reperfusion injury (Tan et al., 2018). Another study, focusing on the characterisation of CAD at a molecular level, used plasma samples derived from patients within the PROFLOW cohort (patients with prior type-1 MI) which were differentiated by their coronary flow rate (CFR) ratio, an indicator of endothelial dysfunction and a predictor of the development of major adverse cardiac events (James et al., 2022). Following miRNA profiling of plasma EVs isolated from the two patient groups, James et al. showed that miR-224-5p was inversely related to CFR, therefore, proposing a role for this miRNA as a possible disease biomarker (James et al., 2022). Additionally, a pilot study involving patients with ischemic heart failure with moderately reduced left ventricular ejection fraction (HFmrEF), analysed the serum levels of 84 miRNAs and discovered that several circulating miRNAs, including miR-224-5p, were significantly upregulated in HFmrEF patients compared to healthy volunteers (Kaufmann et al., 2019). However, despite the promising potential of circulating miRNAs as useful non-invasive diagnostic and prognostic tools, their clinical use is still a long way into the future due to the many technical challenges associated with their routine use in a reliable manner (Gonzalo-Calvo et al., 2022) as well as the poor understanding of significant biological questions concerning the natural variations in miRNA levels throughout the day (Heegaard et al., 2016; Rekker et al., 2015).

The results presented here, although of preliminary nature, provide interesting insights into the possible role of EV miRNAs as markers of neointimal formation following vascular injury. However, further research, involving controls and cases collected as part of the same study, is essential in order to be able to make any definitive conclusions. Additionally, in the future it may also be worth exploring if EV associated miR-24-3p and miR-224-5p may have any functional effects on neointimal formation *in vivo*.

6.5.1 Study limitations

In this chapter, EVs were isolated from the serum of injured mice developing neointimal lesions and healthy control mice with the aim to compare the physical characteristics of the isolated EV populations as well as their miRNA

expression profile. Firstly, although NTA and western immunoblot enabled the comparison of EV particle concentration, size, and EV protein content respectively, further characterisation of the morphology of EVs via TEM would also be beneficial to provide a more robust characterisation profile of the EV populations. Secondly, as previously outlined, neointimal lesions were not observed in two 10- and three 14-day old injured carotid arteries (as reported by Dr Julian Schwartz), and since the reason for this observation was not identified and technical errors associated with the tissue handling processing protocol could not have been confirmed, it was not feasible to exclude these samples from the analysis. Finally, in the original study of Dr Julian Schwartz, uninjured control mice were not included for each timepoint since the main aims of the experiment were to do morphometric and proliferation analysis to determine time-dependent neointimal formation and SMC phenotype switching in the left injured carotid arteries. Therefore, as suitable control samples from uninjured mice as part of the original study were not available, in the current study control blood samples were collected on several occasions from healthy age and sex matched C57BL/6 mice). These controls were not optimal potentially introducing unpredictable variables which may have ultimately influenced the results presented here. While the findings in the current study were interpreted with caution considering the significant limitations described above, adding uninjured control mice in carotid artery ligation studies in the future would be important to allow for more accurate and reliable interpretation of findings.

6.6 Summary

EV populations isolated from mice serum following carotid artery ligation-induced vascular injury do not significantly differ compared to EVs from control mice in terms of size and concentration, and the progression of the forming neointimal lesions did not affect those physical characteristics. Additionally, qRT-PCR analysis of miR-24-3p and miR-224-5p suggested that the expression of both miRNAs was significantly upregulated in serum EVs isolated from injured mice at D14 and D5 after surgery respectively compared to control mice. Taken together, these observations highlight a potential difference in the miRNA expression profiles of mouse EVs found in the circulation after vascular injury compared to healthy conditions. Such differences indicate that both miR-24-3p

and miR-224-5p may have diagnostic value and their potential as disease biomarkers may be worth investigating further in the future.

Chapter 7 General discussion

7.1 Summary of findings and implications

Neointimal formation, driven by VSMC proliferation and migration, remains a major pathogenic mechanism associated with CABG- and PCI- induced vascular injury which significantly contributes to increased failure rates of advanced CAD treatments (Chaabane et al., 2013; de Vries and Quax, 2018; Newby and Zaltsman, 2000). Therefore, understanding the mechanisms involved in the regulation of key processes, such as VSMC migration and proliferation, underlying neointimal lesion formation in the setting of vascular injury remains of paramount importance to discovering potential therapeutic targets and successfully developing novel treatments. Growing evidence suggests that EVs play a significant role in the diagnosis and treatment of diseases. Due to their great therapeutic and diagnostic potential, modified EVs are currently being extensively studied as disease mediators and therapeutic delivery vehicles (Y. Zhang et al., 2022). While EV-mediated intercellular communication, including communication of VSMC with other cells within the vessel wall such as ECs and blood cells, has been clearly demonstrated (reviewed in (Pashova et al., 2020)), EV-mediated autocrine regulation of VSMC in the context of vascular injury has not been extensively studied yet. VSMC are important drivers of neointimal formation (Wu et al., 2020) and as such it is important to better understand the possible underlying mechanisms involved in their regulation. The main aims of the work presented in this thesis were to investigate the role of prolonged PDGF signalling on the release of EVs from VSMCs and to study their effect on recipient cell responses with a particular focus on EV-mediated autocrine regulation of VSMC.

Since abnormal PDGF signalling has been implicated in the development of neointimal formation post vascular injury (Raines, 2004), the initial studies presented in Chapter 3 aimed to investigate the effect of prolonged PDGF stimulation on EV release from HSVSMCs. It was found that while EV size and morphology remained unaltered, PDGF stimulation of HSVSMCs resulted in increased EV secretion suggesting potential functional differences between EV populations secreted under basal and pathological disease conditions. This finding is consistent with previous findings that ASCs under PDGF stimulation secrete more EVs compared to control cells with no difference observed in the mean size of EVs (Lopatina et al., 2014). Additionally, however, it has also been

shown that in the context of CVD certain cells, namely ECs and platelets, secrete EVs enriched in PDGF which are functionally active (Goetzl et al., 2017; Togliatto et al., 2018). These findings suggested that PDGF may be involved in the regulation of cellular processes not only directly but also through EV-mediated signalling. Therefore, in Chapter 4, it was of interest to explore whether in addition to the increased EV release, PDGF stimulation of HSVSMCs induced any changes in the content of the EVs that they secreted. Following an unbiased transcriptome-wide analysis of small RNA expression using an NGS-based RNASeq approach, it was discovered that indeed the small RNA expression profile of pEVs was markedly different from that of control EVs. All differentially expressed miRNAs, including miR-24-3p, miR-409-3p, miR-21-5p, let-7A-5p, miR-1-3p and miR-224-5p, were found to be upregulated in pEVs and four of those (miR-24-3p, miR-409-3p, let-7A-5p, and miR-224-5p) were successfully validated by qRT-PCR. In line with the findings presented in this thesis, another study also reported an altered EV miRNA profile (41 downregulated miRNAs and 54 miRNAs upregulated by ≥ 2 -fold) following PSMC treatment with PDGF (Heo et al., 2020).

Currently, miRNAs are being extensively investigated as novel therapeutic targets in a range of diseases, including cancer and various cardiovascular pathologies (Forterre et al., 2020; Zhou et al., 2018), in both preclinical and clinical settings (Bonneau et al., 2019; C. Chakraborty et al., 2021; Gareev et al., 2020). Furthermore, EV miRNA signalling has also been implicated in different disease settings including both cardiovascular disease and cancer (Chong et al., 2019; Di Rocco et al., 2017). Furthermore, it has been demonstrated that specific functional miRNAs are preferentially selected for extracellular transport via EVs facilitating communication between cells of the same type (Montecalvo et al., 2012) or miRNAs could be processed through different pathways within the cell under different conditions (Palma et al., 2012) demonstrating that miRNAs are not randomly secreted in EVs from cells. Taken together these findings suggest that cellular responses governed by PDGF in the context of vascular injury may, at least partially, be further mediated by extracellular signals, i.e., miRNAs specifically packaged in and transported by EVs.

The selection of miRNAs for further follow up through bioinformatic analysis was based on significance of miRNA expression levels detected by qRT-PCR which were also upregulated in pEVs by more than 2-fold. It has been previously shown that miRNA expression levels are positively correlated with their activity (Kozomara et al., 2014), suggesting larger differences in miRNA expression may result in stronger inhibition of target mRNA expression. Such finding encourages the use of fold change cut-off value in gene expression data to select candidate miRNAs for further investigation that are potentially more biologically relevant. However, other evidence suggests that miRNA expression levels are a poor indicator of activity (Kozomara et al., 2014; Plotnikova et al., 2019). Therefore, there is no definitive answer to which strategy would result in selecting the miRNAs with the biggest potential for exerting functional effects in the chosen experimental settings. Although only three miRNAs, miR-24-3p, miR-224-5p and miR-409-3p, met the pre-set criteria for selection for further analysis, it is also possible that both let-7A-5p and miR-21-5p could have been relevant candidates to explore. While all five of those miRNAs have been previously implicated in the regulation of diseases characterised by excessive cell proliferation such as cancer or pulmonary fibrosis (Feng and Tsao, 2016; Mishra et al., 2009; Peng et al., 2021; Shi et al., 2020; L. Wu et al., 2019; Yamada et al., 2013), miR-24-3p and miR-21-5p have also been reported to regulate vascular pathologies such as atherosclerosis and neointimal lesion formation (Ji et al., 2007; Y. Xu et al., 2020; Zhou et al., 2011). MiR-21, in particular, has been very well studied miRNA in the cardiovascular system (Cheng and Zhang, 2010). Due to time and budget constraints, it was not possible to follow up on all differentially expressed miRNAs, hence, a combination of factors including statistical significance, fold difference and disease relevance drove the decision for prioritisation. In future studies, it would be beneficial to explore the potential effects of the other miRNAs as well. Additionally, the possibility of all differentially expressed miRNAs, or a combination of those, working synergistically to exert functional effects on recipient cells, should also not be disregarded when considering the potential regulatory effects of pEVs.

Initially, basic bioinformatics analysis was performed to identify potential mRNA gene targets for miR-24-3p, miR-224-5p and miR-409-3p (Chapter 4), however, further gene set enrichment analyses were successfully carried out only on the

set of target genes identified for miR-24-3p and miR-224-5p (701 and 288 target genes respectively) and not for miR-409-3p (49 gene targets) due to the small number of potential mRNA targets identified for this miRNA. The findings in this chapter suggested that EVs enriched in miR-24-3p and miR-224-5p released following prolonged PDGF signalling in HSVSMCs may potentially be involved in the regulation of biological processes such as cell proliferation, migration and apoptosis, all of which are crucial for the development of neointimal lesions post vascular injury (de Vries et al., 2016). Indeed, in the context of cancer, both miR-24-3p and miR-224-5p have previously been reported to successfully regulate cell proliferation and/or migration through suppression of their target genes, including dihydrofolate reductase (*DHFR*), *PIK3R3* and *AKT3* (J. Li et al., 2019; Mishra et al., 2009). Notably, in the context of vascular pathologies, miR-24-3p has also been shown to inhibit EC proliferation and migration and consequently wound healing by directly targeting *PIK3R3* (Y. Xu et al., 2020). The existence of experimental evidence showing that both miRNAs could successfully regulate cellular proliferation and migration supports the current findings providing insight into understanding the potential regulatory mechanisms that may be involved in the regulation of neointimal formation post vascular injury.

Preliminary findings presented in Chapter 3 suggested that pEVs containing endogenous levels of upregulated miRNAs had no effect on proliferation of recipient quiesced-HSVSMCs compared to control (vEVs). It is possible that the experimental design was not appropriate for assessing the effect of pEVs on HSVSMC proliferation, i.e., the state of recipient cells was not representative of *in vivo* conditions and instead actively proliferating HSVSMCs should have been used or the EV concentration was suboptimal meaning that cells were not exposed to sufficient number of miRNA molecules to exert functional effects. However, since the primary aim was to study the effect of EVs derived from HSVSMCs, CCM was utilised as a source of EVs meaning that exploring very high EV concentrations was not feasible. Therefore, a direct EV content modification approach was employed. To ensure efficient cargo loading, EVs were exogenously loaded with miRNA mimics through electroporation and subsequently (in Chapter 5) the effect of miR-24-3p- or miR-224-5p- loaded EVs, as potential therapeutic targets, was explored in an *in vitro* model of the

pathological conditions under which neointimal lesions develop following vascular injury. It was found that miR-224-5p EVs significantly inhibited PDGF-induced HSVSMC proliferation compared to PDGF control, suggesting a possible contribution of miR-224-5p to the observed inhibitory effect exerted by miR-224-5p loaded EVs. Interestingly, it was also found that miR-224-5p HSVSMC EVs significantly suppressed EV-depleted FBS-induced HSVSMC migration compared to naEVs and miR-24-3p loaded EVs through an unknown mechanism. No previous studies could be identified that have proposed a connection between the levels of miR-224-5p in HSVSMC-EVs and prolonged PDGF signalling or investigated the role of EV-associated miR-224-5p or miR-224-5p alone on VSMCs in the context of vascular injury or in a similar cardiovascular pathology. Although, the findings presented here require further investigation to fully elucidate the effect of miR-224-5p EVs on HSVSMCs, possible underlying mechanisms and ultimately their role in neointimal formation development, these results contribute to the current knowledge within the context of EV miRNAs and their potential effects in the setting of vascular injury. These findings are of particular importance for furthering our understanding of EV-mediated communication between venous VSMCs following CABG-induced injury.

Finally, the work carried out in Chapter 6 focused on exploring whether the levels of miR-24-3p and miR-224-5p in circulating EVs derived from a more clinically relevant *in vivo* model of vascular injury would reflect the findings of upregulated miR-24-3p and miR-224-5p levels in HSVSMC EVs observed in the more simplified *in vitro* model of the pathological conditions under which neointimal formation develops. It was found that miR-24-3p and miR-224-5p expression was significantly upregulated in serum EVs isolated from injured mice at D14 and D5 after surgery respectively compared to control mice. Although this study had limitations associated with it (discussed in detail in Chapter 6), it provided preliminary evidence supporting miR-24-3p and miR-224-5p associated with serum EVs as potential therapeutic targets in neointimal formation following vascular injury and suggesting that both miR-24-3p and miR-224-5p may have diagnostic value. Therefore, both their potential as novel therapeutic targets and disease biomarkers may be worth investigating further in the future. These findings are potentially important as recently it has been shown that blood-based miRNAs, such as miR-1, miR-21, miR-93, miR-126, miR-133 and miR-

145, may be used as non-invasive biomarkers for both ISR and/or clinical outcomes associated with saphenous VGD (Błażejowska et al., 2021; Varela et al., 2019). Considering that there are no established reliable diagnostic and prognostic tools yet for predicting outcomes after CAGB surgery or PCI, there is still unmet need for discovering useful disease biomarkers.

7.2 Future perspectives

Since the primary aim of this thesis was to investigate the role of HSVSMC-EVs on recipient cells it was important to first comprehensively characterise the EV population which would later be used in functional studies. HSVSMC-EVs were characterised by a number of widely used standard methods including NTA, WB and TEM imaging (Lötvald et al., 2014; Théry et al., 2018). In terms of protein content-based EV characterisation, the presence of four EV protein markers from two categories, transmembrane (CD63 and CD81) and cytosolic (Annexin A2 and Annexin XI), were reported. Notably, the most recent MISEV 2018 recommendations suggest that at least one protein of three different categories, including transmembrane, cytosolic and negative protein markers, should be detected to demonstrate the EV nature and the degree of purity of an EV preparation (Théry et al., 2018). Therefore, future studies involving the same EV population would benefit from further analysis of the EV preparation purity by including the detection of a negative protein marker as well. Since EVs used in *in vitro* functional studies were isolated from CCM rather than serum or plasma samples, the co-isolation of lipoprotein particles was not a concern when using the SEC method for EV purification which has been previously associated with increased levels of lipoprotein contamination compared to other EV isolation methods such as DU and polymer-based precipitation (Brennan et al., 2020). Hence, potential lipoprotein contamination was not investigated.

Following the identification of an altered miRNA expression profile in EVs derived from HSVSMCs under prolonged PDGF stimulation, several follow-up studies were designed to assess the effect of two different EV-associated miRNAs (miR-24-3p and miR-224-5p) on recipient cells. To do that, EVs were exogenously loaded with the miRNAs of interest using electroporation. Therefore, the success of all follow-up studies was highly dependent on the efficient loading of the miRNA mimics into EVs and their successful transfer to recipient cells. While

recent efforts have focused on providing standard minimal requirements for conducting basic EV research, no standard reporting guidelines have been established governing the loading of EVs for cargo delivery (Rankin-Turner et al., 2021). The EV loading protocol followed in this thesis was previously optimised by Dr. Emily Ord (University of Glasgow) and Miss Rebecca Rooney (University of Glasgow) and further improved as part of this project by assessing different miRNA mimic loading amounts. Unfortunately, due to considerations related to time and cost limitations this experiment was only carried out once preventing the ability to perform robust analysis to support confident decision-making process regarding EV loading capacity. Although the study was conducted only once, a substantial upregulation of the EV miRNA expression levels was observed with all three tested mimic doses ($RQ > 150$, $N=1$) compared to naEVs. Additionally, studies involving cel-miR-39 mimic, and not the specific miRNAs of interest, were used to assess EV cargo delivery to recipient cells meaning that only data from *in vitro* studies demonstrating a potential biological effect of EVs are available to confirm the successful transfer of biologically active miR-24-3p and miR-224-5p mimics to recipient cells. While the outcomes of these type of studies are valuable and practically support the hypothesis that EVs can be used as delivery vehicles for functional RNA cargoes (Shtam et al., 2013), the lack of fundamental data relating to loading parameters and quantifiable values to validate EV loading make it impossible to accurately and reliably assess their efficiency and also potentially significantly decrease reproducibility (Rankin-Turner et al., 2021). Large variability across the literature has also been observed in terms of several fundamental parameters related to EV loading, including starting material, loading protocols, and estimation and reporting of variables such as EV loading capacity and efficiency, highlighting the lack of established standard practices and the need for standardisation in the methodology and reporting of EV loading parameters (Rankin-Turner et al., 2021).

One of the key challenges hampering EV research studies is the generation of inconsistent batches of EVs, in terms of both purity and physical characteristics (e.g., size and surface markers). Although a myriad of EV separation and analysis methods are being currently developed and used in the field (Théry et al., 2018; Witwer et al., 2013), the lack of appropriate reference materials for accurate

calibration, appropriate data normalization and method development remains a major disadvantage limiting the reproducibility of studies (Geeurickx et al., 2019). In the case of EV loading, this may cause variability associated with the quantification of EVs leading to inaccurate measurement of EV loading ultimately affecting the reproducibility and possible application of research findings (Rankin-Turner et al., 2021). To address the need for appropriate reference material, recombinant EVs (rEVs) with similar physical and biochemical characteristics to native EVs have been recently developed (Geeurickx et al., 2019). These rEVs could be utilised as a suitable trackable biological reference material for the calibration of EV analysis methods (e.g., NTA) ensuring accurate control of the concentration of starting material in various studies including those involving loading of EVs (Geeurickx et al., 2019). Recombinant EVs could also potentially be used to establish standard procedures for the assessment of loading efficiency. The implementation of a calibration step to control EV separation techniques and analysis could potentially reduce the variability implicated in practically all studies involving standard EV measurements such as size and concentration, including EV loading studies. Establishing standard practices and guidelines for EV loading studies would improve reproducibility and increase the probability of translational outcomes.

Additionally, future studies, involving exogenous EV loading via electroporation, would highly benefit from the use of alternative analytical techniques such as Raman spectroscopy, ImageStream flow cytometry and super-resolution microscopy that could improve the accuracy of assessing EV loading (Rankin-Turner et al., 2021). For instance, Raman spectroscopy - a technique utilising scattered light to measure molecule-specific shifts, has already been successfully used to assess the purity of EVs (Gualerzi et al., 2019) and could also be valuable in the assessment of EV loading efficiency. Finally, given that the formation of EV and/or miRNA aggregates during the electroporation process could prevent miRNA functionality (Kooijmans et al., 2013; Lamichhane et al., 2015; Liu and Su, 2019; Pomatto et al., 2019), in addition to NTA providing EV sizing data it could also be beneficial to assess the morphology of loaded-EVs by an imaging technique such as TEM (de Abreu et al., 2021; Pomatto et al., 2019). Such additional studies would help ensure that high quality samples are being

investigated in pre-clinical settings which could ultimately enhance reproducibility in translational research.

In the current study, all *in vitro* experiments were completed with relatively low N numbers (N=3-4) which supports more cautious and balanced interpretation of the results. Unfortunately, due to the COVID-19 pandemic and subsequent lab closure, lab work-related restrictions and cell availability issues, it was not possible to increase the sample size for some of the *in vitro* studies. Therefore, increasing the sample size in future experiments would improve the quality of the data and will allow definitive conclusions to be made.

Furthermore, it would also be valuable to elucidate the underlying mechanism responsible for the observed cellular effects mediated by miR-224-5p EVs. Under the current experimental conditions, none of the assessed mRNA gene targets appeared to be regulated by any of the two EV miRNAs (miR-24-3p or miR-224-5p). In future studies, investigating the potential regulation of other mRNA target genes would also be beneficial. For instance, a number of other genes, which were also identified as potential miRNA gene targets (Chapter 4), have been previously found to be involved in the regulation of cell migration, including *MAPK8*, *PIK3C2A* and *SMAD5* for miR-224-5p (Chao et al., 2018; K. Huang et al., 2017; Tiwari et al., 2013). Additionally, a more comprehensive approach, which is not restricted by the filter of pre-defined selection of mRNA targets, may also be considered when designing studies aiming to elucidate the underlying mechanism of miR-224-5p EV-mediated cellular responses. Messenger RNA sequencing, or mRNAseq, is another NGS-based approach for studying the regulation of genes in an unbiased manner providing a complete view of the coding transcriptome (Roy et al., 2011; Wang et al., 2009b). Such methodology could be employed in future studies to allow for a broader initial screening of the potential miRNA gene targets which may be regulated in response HSVSMC treatment with miR-224-5p EVs. This technology is advantageous over the traditional more targeted approaches such as hybridization-based microarrays, not only because it enables more sensitive and accurate measurement of fold changes in gene expression, but also because it is not subject to gene pre-selection bias (Roy et al., 2011; Wang et al., 2009b). Therefore, in addition to exploring which, if any, miRNA gene targets might be regulated by miR-224-5p

EVs in this particular *in vitro* cell model, mRNA-seq could also provide insights regarding the potential regulation of genes by other bioactive cargo molecules within the EVs. This method is not as widely used as traditional qRT-PCR and microarray assays as there is considerably higher cost associated with it, however, the benefits of RNAseq could indeed outweigh the extra cost.

Although, the results from the target gene expression studies have suggested that PDGFRA, PDGFRB, PIK3R3, NRAS, and RRAS were not likely the mRNA gene targets responsible for the observed miR-224-5p EV-mediated effects detected in recipient cells, it is important to consider that this method of measuring the effect of miRNAs could only detect miRNA-mediated changes by mRNA destabilization. Going forward, it would also be beneficial to assess the expression levels of predicted gene targets of interest at a protein level to enable the detection of potential miRNA-mediated changes by translational inhibition. Such additional investigations will provide further evidence either confirming that the target genes of interest were not responsible for any of the observed miRNA-mediated functional effects or possibly suggesting changes in target protein levels mediated by translational inhibition. Indeed, using a methodology, e.g., western immunoblotting, that measures the protein expression of potential target genes increases the likelihood of detecting miRNA-mediated changes in cells since such methods could identify changes occurring due to either mRNA destabilization or translational inhibition; whereas, if only mRNA levels are measured, changes due to translational inhibition will not be detected (Cloonan, 2015).

In future studies, other commonly used gain- and loss-of-function strategies to probe miRNA functions both *in vitro* and *in vivo* could also be explored. For example, in *in vitro* settings, the opposite effects of EV miRNAs could be assessed by inhibiting the function of miR-24-3p and/or miR-224-5p in recipient cells by using antisense oligonucleotides (antimiRs) delivered via cell transfection or unassisted uptake (Broderick and Zamore, 2011; Stenvang and Kauppinen, 2007; Van Rooij, 2011). Approaching the research questions from multiple angles, i.e., through use of both miRNA mimic and inhibitors, would reduce bias that comes from using a single method while increasing the robustness of the experimental findings. Additionally, it would also be

interesting to explore the possibility of co-loading EVs with miR-24-3p and miR-224-5p and studying their potential combined effect on recipient cells. Such experimental design would also benefit from the use of antimiRs to help elucidate any potential changes driven by either one of the EV miRNAs of interest or both miRNAs working in together. It is also important to note that, since neointimal formation is a common pathological feature of both VGD and arterial ISR (Chaabane et al., 2013; de Vries and Quax, 2018; Gaudino et al., 2017; Newby and Zaltsman, 2000), additional studies utilising clinically relevant arterial cells such as human CASMCs should also be considered. Although the cell type used in the present *in vitro* studies, namely HSVSMCS, is clinically relevant mainly because the cells were derived from human saphenous veins used as CABG conduits, due to existing phenotypic and functional differences between arterial and venous cells (Wong et al., 2004), performing additional studies in arterial cells would broaden the potential application of any valuable findings in the context of neointimal formation post vascular injury.

Going forward, to better understand the clinical significance of the current findings it is important to also investigate the potential protective effects of HSVSMC-derived EVs loaded with miR-224-5p in *in vivo* settings. Although embryonic lethality has been demonstrated in knockout mice lacking key miRNA processing factors, such as Dicer, Drosha and AGO2 (Park et al., 2010), targeted miRNA gene knockouts have been successfully used to study miRNA functions in mice in different disease contexts (Krützfeldt et al., 2005; Prosser et al., 2011; Van Rooij et al., 2008; Zhou et al., 2016). For example, in the context of vascular injury, miR-143/145 double-knockout mice displayed significantly reduced neointima formation following carotid ligation injury (Xin et al., 2009). Another more recent study using both miR-302 heterozygous mice (miR-302^{+/-}) and mice with SMC-specific deletion of miR-302 (miR-302^{SMCKO}) demonstrated that miR-302a accelerates VSMC proliferation and subsequent neointimal formation in carotid artery injury model by directly targeting *PTEN* and consequently activating AKT signalling (Liu et al., 2021). Therefore, in future studies, in addition to studying the effect of systemic delivery of miR-224-5p-loaded EVs using an *in vivo* model of vascular injury, it may be of interest to also explore the functional effects of SMC-specific deletion of miR-224 on neointima formation.

Overall, EVs are considered to have great therapeutic potential not only due to the low immunogenicity associated with the use of autologous EVs (Aslan et al., 2021), but also due to other endogenous properties including ability to protect their cargo content from degradation and to cross biological barriers delivering cargo to recipient cells acting as a therapeutic delivery vehicle that regulates cellular function and phenotype (Claridge et al., 2021). Interestingly, the therapeutic potential of EVs could be improved through bioengineering approaches (Claridge et al., 2021; Shengyang Fu et al., 2020). Not only EVs could be engineered to harbour specific therapeutic cargo molecules (de Abreu et al., 2021) but also their surface epitopes may be modified to improve targeting to recipient cells and tissues *in vivo* thereby increasing the efficiency of cargo delivery while limiting potential side effects (Shengyang Fu et al., 2020). For example, in the context of CVD, an improved targeting ability of EVs to ischemic myocardium has been successfully demonstrated (X. Wang et al., 2018). In this study, using a technology of molecular cloning and lentivirus packaging, membrane protein LAMP2B enriched MSC-derived EVs were modified through LAMP2B fusion with ischemic myocardium-targeting peptide CSTSMLKAC (IMTP). IMTP-engineered EVs were found to specially target ischemic myocardium *in vivo* leading to enhanced EV-mediated therapeutic effects on acute MI (X. Wang et al., 2018). Therefore, assuming a successful confirmation of negative regulation of VSMC migration and/or proliferation mediated by miR-224-5p EVs *in vitro*, it would be highly beneficial to further explore the possible protective effects of these EVs by improving their targeting potential towards desired tissues/cells in pre-clinical settings using a suitable *in vivo* model of vascular injury.

Finally, as preliminary findings from the current work on mouse serum EVs suggested that both EV miRNAs, miR-24-3p and miR-224-5p, are upregulated following carotid artery ligation-induced vascular injury, it would be beneficial to carry out a study which is specifically designed to reliably assess the diagnostic value of both miRNAs and their potential as disease biomarkers in pre-clinical settings. Additional human studies aiming to investigate the miRNA expression profile of circulating EVs in patients who are at risk of developing neointimal formation and ISR following CABG and PCI, respectively, should also be considered. Comparisons between patients and healthy subjects, and comparisons within patients (i.e., pre-, and post- coronary interventions) would

be highly beneficial to assess the potential clinical relevance of the differentially expressed EV miRNAs identified in this thesis.

Overall, EV research has made a great progress since EVs were first described 30 years ago, however, to overcome challenges that can limit the development and use of EV-based clinical applications, additional studies are required to address other fundamental concerns related to EV research in general. Since many factors, including different EV isolation strategies and cell culture conditions, can affect sample purity, EV subtype enrichment and the structural integrity of EVs, further studies are required to define how these factors impact the characteristics of isolated EVs and their fitness for specific applications (Liu et al., 2022). The selection of specific EV population is also a critical aspect in all EV applications and may be influenced by various factors, including the source/origin of EVs, the inherent targeting and regulatory properties of the EVs (since EVs are not empty vesicles and instead they carry several functional molecules capable of inducing various effects), and their ease of production and/or isolation (Liu et al., 2022). Therefore, research efforts should focus on establishing appropriate quality control measures applicable to EV samples, such as assessment of drug release rate and biodegradation, in order to demonstrate both safety and efficacy as required for any medicinal product (Silva et al., 2021). Scale-up studies, aiming to validate that change in isolation volumes do not alter EV characteristics and sample purity, should also be carried out. Finally, future investigations should also aim to explore whether different bioengineering approaches significantly alter the native characteristics of EVs in a way that additional adjustments may be required to reduce their immunogenicity and/or toxicity prior to translation into clinical applications.

7.3 Concluding remarks

In summary, the data presented in this thesis has provided evidence that prolonged pathophysiological PDGF stimulation of VSMCs causes a significant dysregulation of the miRNA expression profile of EVs released from stimulated cells. Six miRNAs, including miR-1-3p, mi-21-5p, miR-24, miR-224, miR-409, let-7A-5p, were found to be significantly upregulated in EVs derived from PDGF treated HSVSMCs compared to control EVs. Here, the EV-mediated autocrine regulation of HSVSMCs was studied using an *in vitro* model of the pathological

conditions under which neointimal lesions develop following vascular injury. The data in this thesis provide evidence of the ability of EVs, exogenously loaded with miR-224-3p, to suppress EV-depleted FBS-induced HSVSMC migration compared to naEVs and miR-24-3p EVs and a possible involvement of miR-224-5p EVs in the negative regulation of proliferation of activated HSVSMCs. Although the exact mechanisms underlying these effects remain unclear and further studies are required to fully elucidate the effects of miR-224-5p EVs on HSVSMCs, to the best of our knowledge, this is the first time miR-224-5p has been implicated in the regulation of HSVSMCs in the context of neointimal formation. Studying the potential effect of miR-224-5p EVs on VSMCs represents a new avenue to explore when investigating future therapeutic strategies for neointimal formation post vascular injury.

7.4 COVID-19 impact and mitigation

The COVID-19 pandemic in general, and more specifically the first full lockdown period (March-July 2020), had a significant negative impact on major research activities related to my project. The full lockdown not only prevented me from conducting more experiments and generating new data during this period, but also introduced a significant delay in receiving results back from the RNA-seq experiment and analysis performed by the Glasgow Polyomics Facility which consequently delayed any follow-up experiments in the laboratory. This negatively affected my experimental work and research project as a whole as I relied on the results from this study, as a hypothesis-generating method, to establish the basis for a focused research strategy for the remainder of my project. During this period of full lockdown, I took the opportunity to analyse all data generated up until that point of my studies. Additionally, I wrote an annual progress review and a literature review on a relevant research topic which was published in the journal of 'Cellular signalling'. While my laboratory-based research activities were greatly disrupted, the lockdown period provided me with the opportunity to focus on writing a high-quality review on a topic relevant to my project.

The initial return to the laboratory followed a shift pattern which resulted in significantly reduced productivity in terms of conducting experiments. Most of my experiments also involved cell culture and all cell work was further hampered by the fact that some tissue culture (TC) hoods from our laboratory were donated to a COVID-19 testing facility. Due to the shift pattern and the limited access to TC hoods for this period there were further delays in collecting data. Furthermore, the disruption of normal training activities severely impacted my training needs at the time. As a result of the imposed COVID-19 regulations in the workplace, I was unable to receive the training required for animal work. More specifically, I could not be trained to perform the carotid artery ligation surgery model required for the in-vivo aspect of my project. The routine supply of patient samples (human SV surplus vein tissue) was also disrupted which led to limited availability of primary HSVSMCs for experimental work.

Finally, significant delays in routine deliveries of supplies, supply shortages, and batch-related variabilities of various consumables such as culture vessels,

centrifugation tubes, filter tubes and functional assay kits, all contributed to technical challenges which additionally hampered the generation of good quality data in a timely manner.

Overall, the COVID-19 pandemic had a significant negative impact on my research work and studies despite the actions taken to mitigate against the disruption.

Chapter 8 Appendices

8.1 Differentially expressed miRNAs between vEVs and pEVs

8.1.1 DESeq2 analysis output

Table 8-1 All significantly differentially expressed genes between pEVs and vEVs. Positive log2 Fold Changes indicates increased expression in high pEVs group. Adjusted p-values indicated Benjamini-Hochberg corrected p-values (DESeq2).

Ensembl ID	log2Fold Change	lfcSE	padj	External Gene Name	Ch	Gene biotype	PDGF_1	PDGF_2	PDGF_3	PDGF_4	VEH_1	VEH_2	VEH_3	VEH_4
ENSG00000275110	3.5817	0.7711	0.0037	AL928646.1	X	miRNA	358.9659	792.0648	75.4524	37.6867	20.2218	12.0078	38.2280	35.2423
ENSG00000284459	3.0822	0.7739	0.0189	MIR24	9	miRNA	286.6562	279.6508	27.4372	25.1245	34.9549	12.6082	11.8932	13.3494
ENSG00000199107	3.9615	0.9979	0.0189	MIR409	14	miRNA	28.4074	36.8402	2.2864	17.5871	2.5999	0.6004	0.0000	2.1359
ENSG00000206718	3.1577	0.8052	0.0189	RNU6-546P	2	snRNA	38.7373	23.4438	22.8644	22.6120	2.3111	7.8051	1.6990	0.5340
ENSG00000284190	3.3923	0.8968	0.0243	MIR21	17	miRNA	211.7641	443.7572	13.7186	42.7116	45.9324	5.4035	3.8228	12.2814
ENSG00000198975	2.3170	0.6134	0.0243	MIRLET7A2	11	miRNA	1035.5779	1443.4670	299.5231	321.5931	266.6391	107.4700	128.2763	119.6104
ENSG00000284453	4.7725	1.3176	0.0371	MIR1-2	18	miRNA	0.0000	58.6094	9.1457	0.0000	0.5778	0.0000	0.8495	1.0679
ENSG00000278591	-2.0312	0.5677	0.0371	U2	17	snRNA	18.0774	15.0710	32.0101	22.6120	113.8200	73.2477	64.9877	104.6591
ENSG00000200779	2.7705	0.7772	0.0371	RNU6-105P	2	snRNA	67.1447	41.8639	25.1508	55.2738	4.0444	19.8129	1.6990	2.6699
ENSG00000284363	3.5217	0.9930	0.0371	MIR224	X	miRNA	15.4949	45.2130	18.2915	5.0249	4.3332	2.4016	0.4248	0.0000
ENSG00000200975	2.2524	0.6380	0.0371	RNU1-7P	1	snRNA	82.6396	66.9822	96.0303	60.2987	7.5110	34.2223	16.5655	6.4077

8.2 MicroRNA gene targets

8.2.1 Hsa-miR-224-5p

Table 8-2 List of all the identified gene targets for hsa-miR-224-5p which satisfied the pre-defined criteria.

hsa-miR-224-5p
ABHD2, EPHA4, SSR1, ITPKB, GALNT2, ATRX, CAPRIN1, ZBTB34, MLEC, PIK3R3, KAT6A, FZD4, ADAR, KIAA1549, GDI1, TP53INP1, SNTB1, CBX5, BSDC1, IGF2BP1, EIF2AK4, NOTCH2, CCDC117, UBE2K, PHLPP2, UHMK1, POU2F1, CBX6, XPNPEP3, SREBF2, SETD7, EIF1AD, MAFG, MYO5A, GSK3B, FLNB, VGLL3, TOP1, ARFGEF2, TAOK1, ETS1, CPEB4, RNF38, SESN3, ELL2, NUFIP2, TNRC6A, HNRNPU, IL6ST, PITHD1, RECK, NFIA, LMBR1, SSFA2, RNF111, ATP2B4, LCOR, BMPR2, ATAD2B, PIK3C2A, MED13, SPIN1, RSF1, PELI1, HIPK3, BCL2, LRP6, SLMAP, CDK6, SPPL3, EIF1AX, IGF1R, ZFYVE26, APPBP2, GGA3, CELF1, PBX3, USP47, CORO1C, CLDN12, EDEM3, KCTD21, MAPK8, UBN2, TMTC3, BRWD1, CBL, DICER1, SMARCC1, NRAS, RANBP2, FAM217B, MAP1B, E2F2, TMC7, CANT1, TMOD2, SERTAD2, MBD2, PHLPP1, FBXO45, SLC25A24, TRIB1, ADAMTS5, NECAP1, ARRDC4, FN1, RIPK1, TMEM14B, TIPARP, PHC3, LAPTM4A, TTC3, STXBP4, MSI2, MTMR4, TRIM37, ENAH, EXOC8, SNX13, API5, UBE2W, HES5, FAT1, IRX2, NPR3, ABCA1, RABGAP1, CDK9, FOSB, ARHGAP35, TMEM9B, IPO7, UNC119B, AACS, EGFR, USP6NL, NEBL, MTPAP, DHX33, SH3KBP1, MAP7D2, DDX3X, IVNS1ABP, DENND1B, ZSWIM5, EFCAB14, DIO1, CACHD1, ELOVL5, HMGCLL1, SLC17A5, TMEM30A, PGM3, EFNA3, SGPL1, ZNF282, TMEM64, AZIN1, OXR1, TMEM65, FAM49B, EFR3A, UBE2D3, PRSS12, B3GALT1, SLC46A3, ITM2B, CPSF6, DCN, SCYL2, DCP2, SMAD5, ANKHD1-EIF4EBP3, CHEK1, DAZAP2, BAZ2A, RNF144B, ZKSCAN8, ZMPSTE24, GPR180, SUPT16H, NBR1, PLCD3, ANKRD40, SERPINE1, NAPEPLD, ATXN7L1, GCC1, ZNF407, EFN3, PFKFB4, WDR6, FANCM, TXNIP, PDGFRA, BMP2K, ERMP1, ARFGEF1, DPP8, DNAJA4, ADAMTSL3, AKAP8, RPA1, ZNF2, RNF149, FHL2, PCMTD2, ZNF81, LHFPL2, EIF4E2, KIAA0232, CDC42, SRSF10, DNAJC8, PIP4K2B, CWC25, CASC3, DPYSL2, XYLT1, TPD52, ZDHHC7, NIT1, TOR1AIP2, CDS2, NCOA6, NPY1R, KDM2A, SOD2, IGF2R, QKI, TBC1D5, ADAM10, XPO1, AFG3L2, PIAS2, HDHD2, IL17RD, KBTBD8, ZNF773, DNM1, ACTR3, MGAT5, RIF1, FKBP5, BRPF3, SDC4, SLC12A5, ATP9A, TNKS2, MGEA5, AHNAK, TBL1XR1, MAP3K13, LPP, PAK2, STIM2, H3F3B, CAST, HOXA5, RRAGC, CSTF2, SEC14L5, EPS15, MGAT4B, AKIRIN1, ACSL4, ITGA2, GPBP1, METAP2, HOXD10, F2RL1, GGNBP2, NR4A1, ZNF207, ID3, KDELR1, EYA4, PEBP1, C12orf49, ATP8B2, FKBP14, IRF2BP2, SOD1, DDX3Y, ARHGEF10, RNF145, MARCH6;

8.2.2 Hsa-miR-24-3p

Table 8-3 List of all the identified gene targets for hsa-miR-24-3p which satisfied the pre-defined criteria.

hsa-miR-24-3p
<p>DIAPH1, RBM27, PDGFRB, NDST1, CCDC69, G3BP1, LARP1, ADAM19, DUSP16, CREBL2, CDKN1B, SEC11A, ZNF592, AKAP13, ABHD2, AP3S2, ZNF710, HDCC3, MEF2A, PDPK1, STRADB, FZD5, IGFBP5, DNAJB2, DNPEP, EPHA4, STK10, BNIP1, STC2, GPRIN1, NSD1, PDLIM7, MAML1, LYRM4, SSR1, CDV3, AMOTL2, PLOD2, TSC22D2, KPNA4, ZCCHC14, ZC3H18, DNMT3A, SLC35F6, SLC5A6, PRKCH, PAPLN, AREL1, YLPM1, TTL5, POMT2, SPTLC2, CALM1, CCDC88C, SMIM7, COLGALT1, UNC13A, DDX49, NCAN, ATP13A1, ZNF507, SPAG9, HLF, CLTC, RPS6KB1, PPM1D, TANC2, DCAF7, LIMD2, PRKCA, HELZ, SLC39A11, SLC9A3R1, KCNK2, LBR, ITPKB, IBA57, GALNT2, NID1, INMT, AVL9, RALA, DBNL, OGDH, PURB, ATRX, TSC22D3, ATG4A, KIAA1210, XIAP, ELF4, RAP2C, HS6ST2, LDHA, CAPRN1, NAT10, CRY2, AMBRA1, ARHGAP1, GBA2, APBA1, TRPM6, UBQLN1, SECISBP2, PHF2, CCDC180, SH3PXD2A, ADD3, VT11A, KNDC1, PTDSS2, RDH10, PEX2, AGRN, ATAD3A, NOL9, H6PD, KIF1B, MTHFR, TMEM51, DNAJC16, FBLIM1, DAP, TRIO, PTBP3, FKBP15, AKNA, TNFSF15, RC3H2, NEK6, MVB12B, ZBTB34, TOR2A, MARK4, BBC3, SPHK2, TEAD2, FCGRT, RCN3, RRAS, NUP62, SLC25A22, DUSP8, CTSD, EIF4G2, ATP2A2, SH2B3, CIT, PXN, MLEC, HIP1R, ABCB9, ATP6V0A2, SCARB1, POM121, YWHAG, RSNB1L, LMTK2, C17orf49, KLF6, NRP1, RASA1, FBLN1, IL17REL, SHROOM2, REPS2, SCML1, SCML2, PDHA1, KLHL15, PDE3A, PTHLH, DDN, KMT2D, LMBR1L, SMARCD1, SLC11A2, LAMC1, RNF2, CDC73, RNPEP, ELF3, KDM5B, BTG2, NUAKE2, ELK4, SLC41A1, MAPKAPK2, PIGR, YOD1, DTL, PIK3R3, RNF11, CC2D1B, JUN, JAK1, LEPR, XPO5, PNRC1, NDUFAF4, BVES, RAB11FIP1, KAT6A, PLAG1, SERPINH1, LRRC32, TSKU, FZD4, FAT3, DENND4B, ADAR, RIT1, SEMA4A, CCT3, MEF2D, NES, ARID5B, MYPN, UNC5B, PSAP, DNAJB12, CREB3L2, KIAA1549, TMEM178B, NOS3, AGAP3, INSIG1, ESYT2, GDI1, G6PD, UBXN2B, TP53INP1, MTDH, ATP6V1C1, DCAF13, TRPS1, SNTB1, PHF20L1, AFF1, PDE11A, TFPI, XPO4, SPATA13, FLT1, SLC7A1, LPAR6, HKR1, SIPA1L3, PAK4, PAF1, MED29, BLVRB, RAB4B, AXL, IRGQ, TOMM40, SRGAP1, DYRK2, IFNG, LRRC10, TMEM19, ATXN7L3B, CDK17, NREP, LOX, IRF1, MATR3, DND1, GTF2B, PRMT6, AHCYL1, WRB, KMT2A, PHLDB1, H2AFX, USP2, ARHGAP32, ZBTB44, KDM5A, SLC4A8, ACVR1B, SP1, CBX5, HNRNPA1, RAB5B, ERBB3, ESYT1, ANKRD52, STAT2, RBMS2, R3HDM2, MBD6, DTX3, CTDSP2, GFOD1, JARID2, MBOAT1, E2F3, PPP1R10, RGMB, SERINC2, MARCKSL1, BSDC1, RBBP4, KIAA1522, GRIK3, YRDC, CITED4, PTPRF, KDM4A, KLF17, KLF12, DOCK9, TMTC4, CHAMP1, ARHGEF40, RAB5C, BRCA1, ATXN7L3, SLC4A1, PLEKHM1, PNPO, IGF2BP1, TMEM92, ACSF2, ABCC3, CUX1, ORAI2, CAV2, CNDP2, ZNF516, MIDN, MOB3A, DOT1L, LMNB2, SLC39A3, SEMA6B, PLIN3, KHSRP, ITPK1, BDKRB2, CEP170B, GABRB3, EIF2AK4, FGF11, ZBTB4, MPDU1, ARHGEF15, GAS7, MED9, LLGL1, ULK2, NLK, ZNF662, LIMD1, ARIH2, BSN, GMPPB, CISH, RAD54L2, BCL2L2, NYNRIN, KHNYN, FBXO34, AP5M1, DCLRE1B, HIPK1, PTGFRN, NOTCH2, SV2A, VPS45, AHP1A, CTSS, POGZ, APBB2, SGCB, GRSF1, EREG, SHROOM3, GRINA, SLC52A2, ARHGAP39, NFIB, TTC39B, MTAP, VCIPI1, SNX1, CSNK1G1, PLEKHO2, MYO9A, ADPGK, NEO1, PML, EDC3, CSK, MPI, SCAMP5, C15orf39, PTPN9, CPT1A, CTXN1, ELAVL1, AP1M2, EPOR, TNPO2, WIZ, GGCX, PTC3, MGAT4A, LONRF2, IL1R1, PRPF6, SCAF4, SON, PDXK, AGPAT3, HIC2, PPM1F, ZNF70, SPECC1L, GUCD1, CCDC117, CDK16, PIM2, OTUD5, KDM5C, HUWE1, FAM120C, ZXDB, ZXDA, SPIN4, ZMYM3, CHIC1, ATXN2L, SH2B1, NFATC2IP, RNF40, FBXL19, PRSS8, NETO2, CHD9, GNAO1, NUDT21, KATNB1, ADAMTS6, GPR55, EFHD1, USP40, PER2, ASB1, BOK, FGFR3, SH3BP2, ADD1, HTT, EVC, UBE2K, SZRD1, ATP13A2, EMC1, LUZP1, MTFR1L, WDTC1, WASF2, EPB41, PHF12, MYO18A, GIT1, AP2B1, ACACA, HNF1B, MLLT6, LASP1, GSDMA, IGFBP4, SOX7, DLC1, POLR3D, CHMP7, BNIP3L, ZNF395, EXTL3, CREBBP, DNAJA3, PMM2, CLEC16A, SNN, LYRM1, GGA2, ZNF704, NDRG4, CMTM3, CMTM4, PDP2, CTCF, RANBP10, ESRP2, SLC7A6, SNTB2, TERF2, CYB5B, EXOSC6, AARS, PHLPP2, BCAR1, USP10, PEA15, NCSTN, DEDD, UHMK1, UCK2, POU2F1, RC3H1, STX6, NIPSNAP1, NF2, DUSP18, PRR14L, YWHAH, CARD10, TRIOBP, SUN2, DNAL4, CBX6, TAB1, XPNPEP3, TOB2, SREBF2, TSPO, TRIB3, SIRPA, CENPB, ENTPD6, PYGB, PLAGL2, KIF3B, PCDH10, SETD7, INPP4B, RAPGEF2, CLCN3, SF1, MEN1, CDC42EP2, EIF1AD, KLC2, TIMP2, TBC1D16, RNF213, NPTX1, MAFG, FASN, TBCD, SASH1, ESR1, ZDHHC14, TTYH3, FOXK1, FBXL18, CYTH3, NUP210, SLC6A6, CMTM6, CTDSPL, RPAP1, MAPKBP1, ZNF106, UBR1, MAP1A, MYO5A, MYO1E, ARHGAP31, GSK3B, LRRC58, GOLGB1, CCDC58, MYLK, HEG1, PLXNA1, HEATR5B, SOS1, EML4, BCL11A, CEP68, GFPT1, PCYOX1, TEX261, PDSS2, SESN1, CD164, PTPRK, MAP7, HIVEP2, CEP76, RNF138, EPG5, RNF165, LIPG, CXXC1, MRO, NEDD4L, CDH7, NEK4, FLNB, MAG11, VGLL3, MBOAT7, IL11, RPL28, EPN1, ZNF264, ZSCAN22, PKN3, FAM78A, SETX, TSC1, MED22, BCL2L11, STEAP3, SAP130, FAM168B, AGPAT1, RGL2, PPAR, MAPK14, TBC1D22B, TFEB, KLHDC3, TRPC4AP, UQCC1, PHF20, DLGAP4, TGIF2, SOGA1, RBL1, TGM2, TOP1, JPH2, TOMM34, STK4, ZMYND8, ARHGEF2, RNF114, TMEM189, MOCS3, NFATC2, ZNF217, FAM210B, PMEPA1, VAPB, TSPAN14, ARHGAP19, MMS19, BZW1, TMEM216, DAGLA, TTC9C, NXF1, NCEH1, ZMAT3, DVL3, MASP1, TNK2, PIGG, PDE6B, TAOX1, C8orf58, GAD1, NCOA5, CNOT6, NFAT5, MRPL4, MAPK7, PPIL6, FURIN, TRAF7, MXI1, BHLHE22, MMP14, ACSL6, PPM1G, FSCN1, S1PR1, NET1, TCERG1, ETS1, KIF1C, C1orf106, B3GNT1, WHSC1, FAM46C, WAPAL, KIAA2018, GIGYF1, CSRN1, KIAA0195, POLR3A, PVRL2, AMFR, RANBP3, PTRF;</p>

8.2.3 Hsa-miR-409-3p

Table 8-4 List of all the identified gene targets for hsa-miR-409-3p which satisfied the pre-defined criteria.

hsa-miR-409-3p
KPNA4, MAP7, NR2F2, CPEB4, FAM193B, MSL2, SEC62, DCAF5, TMED10, ATXN3, MORF4L2, RNF38, YWHAE, ZFHX4, MYO3A, ZEB1, ZFX, SESN3, RDX, SLC26A7, GORASP2, COL5A2, TMPO, MTF2, ATF7, ELL2, MET, BAZ1A, EXOC5, UGT2B17, HSPA13, CAB39, NUFIP2, ATAD5, PPP2R2A, TNRC6A, ELF2, GAB1, FBN1, RASGRP3, SPTBN1, CITED2, GNAL, CTNND1, B4GALT5, SECISBP2L, MAP4K3, MSH6, SLAIN2;

List of References

- Abels, E.R., Breakefield, X.O., 2016. Introduction to Extracellular Vesicles: Biogenesis, RNA Cargo Selection, Content, Release, and Uptake. *Cell. Mol. Neurobiol.* 36, 301-312.
- Abrami, L., Brandi, L., Moayeri, M., Brown, M.J., Krantz, B.A., Leppla, S.H., VanderGoot, F.G., 2013. Hijacking Multivesicular Bodies Enables Long-Term and Exosome-Mediated Long-Distance Action of Anthrax Toxin. *Cell Rep.* 5, 986-996.
- Acevedo, L., Yu, J., Erdjument-Bromage, H., Miao, R.Q., Kim, J.E., Fulton, D., Tempst, P., Strittmatter, S.M., Sessa, W.C., 2004. A new role for Nogo as a regulator of vascular remodeling. *Nat. Med.* 10, 382-388.
- Adell, M.A.Y., Vogel, G.F., Pakdel, M., Müller, M., Lindner, H., Hess, M.W., Teis, D., 2014. Coordinated binding of Vps4 to ESCRT-III drives membrane neck constriction during MVB vesicle formation. *J. Cell Biol.* 205, 33-49.
- Admyre, C., Johansson, S.M., Qazi, K.R., Filén, J.-J., Laheesmaa, R., Norman, M., Neve, E.P.A., Scheynius, A., Gabrielsson, S., 2007. Exosomes with Immune Modulatory Features Are Present in Human Breast Milk. *J. Immunol.* 179, 1969-1978.
- Adriaenssens, T., Joner, M., Godschalk, T.C., Malik, N., Alfonso, F., Xhepa, E., De Cock, D., Komukai, K., Tada, T., Cuesta, J., Sirbu, V., Feldman, L.J., Neumann, F.J., Goodall, A.H., Heestermans, T., Buyschaert, I., Hlinomaz, O., Belmans, A., Desmet, W., Ten Berg, J.M., Gershlick, A.H., Massberg, S., Kastrati, A., Guagliumi, G., Byrne, R.A., 2017. Optical coherence tomography findings in patients with coronary stent thrombosis: A report of the PRESTIGE consortium (prevention of late stent thrombosis by an interdisciplinary global european effort). *Circulation* 136, 1007-1021.
- Ahadi, A., Brennan, S., Kennedy, P.J., Hutvagner, G., Tran, N., 2016. Long non-coding RNAs harboring miRNA seed regions are enriched in prostate cancer exosomes. *Sci. Reports* 2016 61 6, 1-14.
- Akao, Y., Iio, A., Itoh, T., Noguchi, S., Itoh, Y., Ohtsuki, Y., Naoe, T., 2011. Microvesicle-mediated RNA Molecule Delivery System Using Monocytes/Macrophages. *Mol. Ther.* 19, 395-399.
- Alam, S.R., Lewis, S.C., Zamvar, V., Pessotto, R., Dweck, M.R., Krishan, A., Goodman, K., Oatey, K., Harkess, R., Milne, L., Thomas, S., Mills, N.M., Moore, C., Semple, S., Wiedow, O., Stirrat, C., Mirsadraee, S., Newby, D.E., Henriksen, P.A., 2015. Perioperative elafin for ischaemia-reperfusion injury during coronary artery bypass graft surgery: a randomised-controlled trial. *Heart* 101, 1639-1645.
- Alarcón, C.R., Lee, H., Goodarzi, H., Halberg, N., Tavazoie, S.F., 2015. N6-methyladenosine marks primary microRNAs for processing. *Nat.* 2015 5197544 519, 482-485.
- Alessi, D.R., James, S.R., Downes, C.P., Holmes, A.B., Gaffney, P.R.J., Reese, C.B., Cohen, P., 1997. Characterization of a 3-phosphoinositide-dependent protein kinase which phosphorylates and activates protein kinase B α . *Curr. Biol.* 7, 261-269.
- Alvarez-Erviti, L., Seow, Y., Yin, H., Betts, C., Lakhali, S., Wood, M.J.A., 2011. Delivery of siRNA to the mouse brain by systemic injection of targeted exosomes. *Nat. Biotechnol.* 29, 341-345.
- Amabile, N., Cheng, S., Renard, J.M., Larson, M.G., Ghorbani, A., McCabe, E., Griffin, G., Guerin, C., Ho, J.E., Shaw, S.Y., Cohen, K.S., Vasan, R.S., Tedgui, A., Boulanger, C.M., Wang, T.J., 2014. Association of circulating

- endothelial microparticles with cardiometabolic risk factors in the Framingham Heart Study. *Eur. Heart J.* 35, 2972-2979.
- Amabile, N., Guérin, A.P., Leroyer, A., Mallat, Z., Nguyen, C., Boddaert, J., London, G.M., Tedgui, A., Boulanger, C.M., 2005. Circulating endothelial microparticles are associated with vascular dysfunction in patients with end-stage renal failure. *J. Am. Soc. Nephrol.* 16, 3381-3388.
- Anderson, J.S.J., Parker, R., 1998. The 3' to 5' degradation of yeast mRNAs is a general mechanism for mRNA turnover that requires the SK12 DEVH box protein and 3' to 5' exonucleases of the exosome complex. *EMBO J.* 17, 1497-1506.
- Andrae, J., Gallini, R., Betsholtz, C., 2008. Role of platelet-derived growth factors in physiology and medicine. *Genes Dev.* 22, 1276-1312.
- Andrés-León, E., Peña, D.G., Gómez-López, G., Pisano, D.G., 2015. miRGate: a curated database of human, mouse and rat miRNA-mRNA targets. *Database* 2015, 1-9.
- Antonyak, M.A., Li, B., Boroughs, L.K., Johnson, J.L., Druso, J.E., Bryant, K.L., Holowka, D.A., Cerione, R.A., 2011. Cancer cell-derived microvesicles induce transformation by transferring tissue transglutaminase and fibronectin to recipient cells. *Proc. Natl. Acad. Sci. U. S. A.* 108, 4852-4857.
- Arroyo, J.D., Chevillet, J.R., Kroh, E.M., Ruf, I.K., Pritchard, C.C., Gibson, D.F., Mitchell, P.S., Bennett, C.F., Pogosova-Agadjanyan, E.L., Stirewalt, D.L., Tait, J.F., Tewari, M., 2011. Argonaute2 complexes carry a population of circulating microRNAs independent of vesicles in human plasma. *Proc. Natl. Acad. Sci. U. S. A.* 108, 5003-5008.
- Ashburner, M., Ball, C.A., Blake, J.A., Botstein, D., Butler, H., Cherry, J.M., Davis, A.P., Dolinski, K., Dwight, S.S., Eppig, J.T., Harris, M.A., Hill, D.P., Issel-Tarver, L., Kasarskis, A., Lewis, S., Matese, J.C., Richardson, J.E., Ringwald, M., Rubin, G.M., Sherlock, G., 2000. Gene Ontology: tool for the unification of biology. *Nat. Genet.* 25, 25-29.
- Ashby, W.J., Zijlstra, A., 2012. Established and Novel Methods of Interrogating Two-Dimensional Cell Migration. *Integr. Biol. (Camb).* 4, 1338-1350.
- Aslan, C., Kiaie, S.H., Zolbanin, N.M., Lotfinejad, P., Ramezani, R., Kashanchi, F., Jafari, R., 2021. Exosomes for mRNA delivery: a novel biotherapeutic strategy with hurdles and hope. *BMC Biotechnol.* 21, 1-12.
- Au, P.Y.B., Martin, N., Chau, H., Moemeni, B., Chia, M., Liu, F.F., Minden, M., Yeh, W.C., 2005. The oncogene PDGF-B provides a key switch from cell death to survival induced by TNF. *Oncogene* 24, 3196-3205.
- Auber, M., Svenningsen, P., 2022. An estimate of extracellular vesicle secretion rates of human blood cells. *J. Extracell. Biol.* 1.
- Azbazdar, Y., Karabicici, M., Erdal, E., Ozhan, G., 2021. Regulation of Wnt Signaling Pathways at the Plasma Membrane and Their Misregulation in Cancer. *Front. Cell Dev. Biol.* 9.
- Baek, D., Villén, J., Shin, C., Camargo, F.D., Gygi, S.P., Bartel, D.P., 2008. The impact of microRNAs on protein output. *Nature* 455, 64-71.
- Baglio, S.R., Rooijers, K., Koppers-Lalic, D., Verweij, F.J., Pérez Lanzón, M., Zini, N., Naaijken, B., Perut, F., Niessen, H.W.M., Baldini, N., Pegtel, D.M., 2015. Human bone marrow- and adipose-mesenchymal stem cells secrete exosomes enriched in distinctive miRNA and tRNA species. *Stem Cell Res. Ther.* 6, 1-20.
- Baietti, M.F., Zhang, Z., Mortier, E., Melchior, A., Degeest, G., Geeraerts, A., Ivarsson, Y., Depoortere, F., Coomans, C., Vermeiren, E., Zimmermann, P., David, G., 2012. Syndecan-syntenin-ALIX regulates the biogenesis of

- exosomes. *Nat. Cell Biol.* 14, 677-685.
- Bajan, S., Hutvagner, G., 2020. RNA-Based Therapeutics: From Antisense Oligonucleotides to miRNAs. *Cells* 2020, Vol. 9, Page 137 9.
- Bao, H., Chen, Y., Huang, K., Zhuang, F., Bao, M., Han, Y., Chen, X., Shi, Q., Yao, Q., Qi, Y., 2018. Platelet-derived microparticles promote endothelial cell proliferation in hypertension via miR-142-3p. *FASEB J.* 32, 3912-3923.
- Bao, H., Yao, Q.-P., Huang, K., Chen, X.-H., Han, Y., Jiang, Z.-L., Gao, L.-Z., Qi, Y.-X., 2017. Platelet-derived miR-142-3p induces apoptosis of endothelial cells in hypertension. *Cell. Mol. Biol.* 63, 3-9.
- Barret, T.B., Seifert, R.A., Bowen-Pope, D.F., 1996. Regulation of platelet-derived growth factor receptor expression by cell context overrides regulation by cytokines - PubMed. *J. Cell. Physiol.* 169, 126-138.
- Barrientos, S., Stojadinovic, O., Golinko, M.S., Brem, H., Tomic-Canic, M., 2008. Growth factors and cytokines in wound healing. *Wound Repair Regen.* 16, 585-601.
- Barst, R.J., 2005. PDGF signaling in pulmonary arterial hypertension. *J. Clin. Invest.* 115, 2691-2694.
- Bartel, D.P., 2009. MicroRNAs: Target Recognition and Regulatory Functions. *Cell* 136, 215-233.
- Batagov, A.O., Kuznetsov, V.A., Kurochkin, I. V., 2011. Identification of nucleotide patterns enriched in secreted RNAs as putative cis-acting elements targeting them to exosome nano-vesicles. *BMC Genomics* 12.
- Battegay, E.J., Raines, E.W., Colbert, T., Ross, R., 1995. TNF-alpha stimulation of fibroblast proliferation. Dependence on platelet-derived growth factor (PDGF) secretion and alteration of PDGF receptor expression. *J. Immunol.* 154, 6040-6047.
- Battegay, E.J., Raines, E.W., Seifert, R.A., Bowen-Pope, D.F., Ross, R., 1990. TGF-beta induces bimodal proliferation of connective tissue cells via complex control of an autocrine PDGF loop. *Cell* 63, 515-524.
- Beaumont, J., López, B., Ravassa, S., Hermida, N., José, G.S., Gallego, I., Valencia, F., Gómez-Doblas, J.J., De Teresa, E., Díez, J., González, A., 2017. MicroRNA-19b is a potential biomarker of increased myocardial collagen cross-linking in patients with aortic stenosis and heart failure. *Sci. Rep.* 7.
- Behm-Ansmant, I., Rehwinkel, J., Doerks, T., Stark, A., Bork, P., Izaurralde, E., 2006. mRNA degradation by miRNAs and GW182 requires both CCR4:NOT deadenylase and DCP1:DCP2 decapping complexes. *Cold Spring Harb. Lab. Press* 20, 1885-1898.
- Benjamini, Y., Hochberg, Y., 1995. Controlling the False Discovery Rate: A Practical and Powerful Approach to Multiple Testing. *J. R. Stat. Soc. Ser. B* 57, 289-300.
- Berceli, S.A., Jiang, Z., Klingman, N. V., Pfahnl, C.L., Abouhamze, Z.S., Frase, C.D., Schultz, G.S., Ozaki, C.K., 2004. Differential expression and activity of matrix metalloproteinases during flow-modulated vein graft remodeling. *J. Vasc. Surg.* 39, 1084-1090.
- Berckmans, R.J., Nieuwland, R., Böing, A.N., Romijn, F.P.H.T.M., Hack, C.E., Sturk, A., 2001. Cell-derived microparticles circulate in healthy humans and support low grade thrombin generation. *Thromb. Haemost.* 85, 639-646.
- Bernstein, E., Kim, S.Y., Carmell, M.A., Murchison, E.P., Alcorn, H., Li, M.Z., Mills, A.A., Elledge, S.J., Anderson, K. V., Hannon, G.J., 2003. Dicer is essential for mouse development. *Nat. Genet.* 2003 353 35, 215-217.
- Berridge, M.J., 1993. Inositol trisphosphate and calcium signalling. *Nat. Publ.*

- Gr. 361, 315-325.
- Berridge, M. V., Tan, A.S., 1993. Characterization of the Cellular Reduction of 3-(4,5-dimethylthiazol-2-yl)-2,5-diphenyltetrazolium bromide (MTT): Subcellular Localization, Substrate Dependence, and Involvement of Mitochondrial Electron Transport in MTT Reduction. *Arch. Biochem. Biophys.* 303, 474-482.
- Berumen Sánchez, G., Bunn, K.E., Pua, H.H., Rafat, M., 2021. Extracellular vesicles: mediators of intercellular communication in tissue injury and disease. *Cell Commun. Signal.* 2021 191 19, 1-18.
- Betsholtz, C., 2004. Insight into the physiological functions of PDGF through genetic studies in mice. *Cytokine Growth Factor Rev.* 15, 215-228.
- Bharadwaj, A., Bydoun, M., Holloway, R., Waisman, D., 2013. Annexin A2 Heterotetramer: Structure and Function. *Int. J. Mol. Sci.* 2013, Vol. 14, Pages 6259-6305 14, 6259-6305.
- Bhatnagar, P., Wickramasinghe, K., Williams, J., Rayner, M., Townsend, N., 2015. The epidemiology of cardiovascular disease in the UK 2014. *Heart* 101, 1182-1189.
- Bianco, F., Perrotta, C., Novellino, L., Francolini, M., Riganti, L., Menna, E., Saglietti, L., Schuchman, E.H., Furlan, R., Clementi, E., Matteoli, M., Verderio, C., 2009. Acid sphingomyelinase activity triggers microparticle release from glial cells. *EMBO J.* 28, 1043-1054.
- Bill, C.A., Vines, C.M., 2020. Phospholipase C. *Adv. Exp. Med. Biol.* 1131, 215-242.
- Bissig, C., Gruenberg, J., 2014. ALIX and the multivesicular endosome: ALIX in Wonderland. *Trends Cell Biol.* 24, 19-25.
- Błażejowska, E., Urbanowicz, T., Gąsecka, A., Ołasińska-Wiśniewska, A., Jaguszewski, M.J., Targoński, R., Szarpak, Ł., Filipiak, K.J., Perek, B., Jemielity, M., 2021. Diagnostic and Prognostic Value of miRNAs after Coronary Artery Bypass Grafting: A Review. *Biology (Basel)*. 10.
- Block, E.R., Matela, A.R., SundarRaj, N., Iszkula, E.R., Klarlund, J.K., 2004. Wounding Induces Motility in Sheets of Corneal Epithelial Cells through Loss of Spatial Constraints. *J. Biol. Chem.* 279, 24307-24312.
- Bohnsack, M.T., Czaplinski, K., Görlich, D., 2004. Exportin 5 is a RanGTP-dependent dsRNA-binding protein that mediates nuclear export of pre-miRNAs. *RNA* 10, 185-191.
- Bonauer, A., Carmona, G., Iwasaki, M., Mione, M., Koyanagi, M., Fischer, A., Burchfield, J., Fox, H., Doebele, C., Ohtani, K., Chavakis, E., Potente, M., Tjwa, M., Urbich, C., Zeiher, A.M., Dimmeler, S., 2009. MicroRNA-92a controls angiogenesis and functional recovery of ischemic tissues in Mice. *Science (80-)*. 324, 1710-1713.
- Bonneau, E., Neveu, B., Kostantin, E., Tsongalis, G.J., De Guire, V., 2019. How close are miRNAs from clinical practice? A perspective on the diagnostic and therapeutic market. *EJIFCC* 30, 114-127.
- Borin, T.F., Miyakawa, A.A., Cardoso, L., De Figueiredo Borges, L., Gonçalves, G.A., Krieger, J.E., 2009. Apoptosis, cell proliferation and modulation of cyclin-dependent kinase inhibitor p21cip1 in vascular remodelling during vein arterialization in the rat. *Int. J. Exp. Pathol.* 90, 328-337.
- Boström, H., Willetts, K., Pekny, M., Levéen, P., Lindahl, P., Hedstrand, H., Pekna, M., Hellström, M., Gebre-Medhin, S., Schalling, M., Nilsson, M., Kurland, S., Törnell, J., Heath, J.K., Betsholtz, C., 1996. PDGF-A signaling is a critical event in lung alveolar myofibroblast development and alveogenesis. *Cell* 85, 863-873.

- Boulanger, C.M., Amabile, N., Tedgui, A., 2006. Circulating Microparticles. *Hypertension* 48, 180-186.
- Boyer, M.J., Kimura, Y., Akiyama, T., Baggett, A.Y., Preston, K.J., Scalia, R., Eguchi, S., Rizzo, V., 2020. Endothelial cell-derived extracellular vesicles alter vascular smooth muscle cell phenotype through high-mobility group box proteins. *J. Extracell. Vesicles* 9.
- Braun, J.E., Huntzinger, E., Fauser, M., Izaurralde, E., 2011. GW182 proteins directly recruit cytoplasmic deadenylase complexes to miRNA targets. *Mol. Cell* 44, 120-133.
- Braun, Joerg E., Huntzinger, E., Izaurralde, E., 2012. A Molecular Link between miRISCs and Deadenylases Provides New Insight into the Mechanism of Gene Silencing by MicroRNAs. *Cold Spring Harb. Perspect. Biol.* 4.
- Braun, Joerg E, Truffault, V., Boland, A., Huntzinger, E., Chang, C.-T., Haas, G., Weichenrieder, O., Coles, M., Izaurralde, E., 2012. A direct interaction between DCP1 and XRN1 couples mRNA decapping to 5' exonucleolytic degradation. *Nat. Struct. Mol. Biol.* 19, 1324-1331.
- Brennan, K., Martin, K., FitzGerald, S.P., O'Sullivan, J., Wu, Y., Blanco, A., Richardson, C., Mc Gee, M.M., 2020. A comparison of methods for the isolation and separation of extracellular vesicles from protein and lipid particles in human serum. *Sci. Rep.* 10.
- Brilakis, E.S., Rao, S. V., Banerjee, S., Goldman, S., Shunk, K.A., Holmes, D.R., Honeycutt, E., Roe, M.T., 2011. Percutaneous coronary intervention in native arteries versus bypass grafts in prior coronary artery bypass grafting patients: a report from the National Cardiovascular Data Registry. *JACC. Cardiovasc. Interv.* 4, 844-850.
- Broderick, J.A., Zamore, P.D., 2011. MicroRNA therapeutics. *Gene Ther.* 18, 1104-1110.
- Broughton, J.P., Lovci, M.T., Huang, J.L., Yeo, G.W., Pasquinelli, A.E., 2016. Pairing beyond the Seed Supports MicroRNA Targeting Specificity. *Mol. Cell* 64, 320-333.
- Buccheri, D., Piraino, D., Andolina, G., Cortese, B., 2016. Understanding and managing in-stent restenosis: a review of clinical data, from pathogenesis to treatment. *J. Thorac. Dis.* 8, 1150-1162.
- Bulkley, B.H., Hutchins, G.M., 1977. Accelerated "atherosclerosis". A morphologic study of 97 saphenous vein coronary artery bypass grafts. *Circulation* 55, 163-169.
- Buono, L., Scalabrin, S., De Iuliis, M., Tanzi, A., Grange, C., Tapparo, M., Nuzzi, R., Bussolati, B., 2021. Mesenchymal stem cell-derived extracellular vesicles protect human corneal endothelial cells from endoplasmic reticulum stress-mediated apoptosis. *Int. J. Mol. Sci.* 22.
- Buschmann, D., Kirchner, B., Hermann, S., Märte, M., Wurmser, C., Brandes, F., Kotschote, S., Bonin, M., Steinlein, O.K., Pfaffl, M.W., Schelling, G., Reithmair, M., 2019. Evaluation of serum extracellular vesicle isolation methods for profiling miRNAs by Next-Generation Sequencing. *J. Extracell. Vesicles* 8.
- Buschow, S.I., Nolte-'t Hoen, E.N.M., van Niel, G., Pols, M.S., ten Broeke, T., Lauwen, M., Ossendorp, F., Melief, C.J.M., Raposo, G., Wubbolts, R., Wauben, M.H.M., Stoorvogel, W., 2009. MHC II in dendritic cells is targeted to lysosomes or T cell-induced exosomes via distinct multivesicular body pathways. *Traffic* 10, 1528-1542.
- Çakmak, H.A., Demir, M., 2020. MicroRNA and Cardiovascular Diseases. *Balkan Med. J.* 37, 60.

- Caliskan, E., de Souza, D.R., Böning, A., Liakopoulos, O.J., Choi, Y.H., Pepper, J., Gibson, C.M., Perrault, L.P., Wolf, R.K., Kim, K.B., Emmert, M.Y., 2019. Saphenous vein grafts in contemporary coronary artery bypass graft surgery. *Nat. Rev. Cardiol.* 2019 173 17, 155-169.
- Cantley, L.C., 2002. The Phosphoinositide 3-Kinase Pathway. *Science* (80-.). 296, 1655-1657.
- Carnino, J.M., Lee, H., Jin, Y., 2019. Isolation and characterization of extracellular vesicles from Broncho-alveolar lavage fluid: a review and comparison of different methods. *Respir. Res.* 20.
- Cassar, A., Holmes, D.R., Rihal, C.S., Gersh, B.J., 2009. Chronic Coronary Artery Disease: Diagnosis and Management. *Mayo Clin. Proc.* 84, 1130-1146.
- Castellano, E., Downward, J., 2011. RAS Interaction with PI3K: More Than Just Another Effector Pathway. *Genes and Cancer* 2, 261-274.
- Chaabane, C., Otsuka, F., Virmani, R., Bochaton-Piallat, M.L., 2013. Biological responses in stented arteries. *Cardiovasc. Res.* 99, 353-363.
- Chairoungdua, A., Smith, D.L., Pochard, P., Hull, M., Caplan, M.J., 2010. Exosome release of β -catenin: a novel mechanism that antagonizes Wnt signaling. *J. Cell Biol.* 190, 1079-1091.
- Chakraborty, C., Sharma, A.R., Sharma, G., Lee, S.S., 2021. Therapeutic advances of miRNAs: A preclinical and clinical update. *J. Adv. Res.* 28, 127-138.
- Chakraborty, R., Chatterjee, P., Dave, J.M., Ostriker, A.C., Greif, D.M., Rzcudlo, E.M., Martin, K.A., 2021. Targeting smooth muscle cell phenotypic switching in vascular disease. *JVS-Vascular Sci.* 2, 79-94.
- Chan, M.C., Hilyard, A.C., Wu, C., Davis, B.N., Hill, N.S., Lal, A., Lieberman, J., Lagna, G., Hata, A., 2010. Molecular basis for antagonism between PDGF and the TGF β family of signalling pathways by control of miR-24 expression. *EMBO J.* 29, 559-573.
- Chao, L.-M., Sun, W., Chen, H., Liu, B.-Y., Li, P.-F., Zhao, D.-W., 2018. MicroRNA-31 inhibits osteosarcoma cell proliferation, migration and invasion by targeting PIK3C2A. *Eur. Rev. Med. Pharmacol. Sci.* 22, 7205-7213.
- Chappell, J., Harman, J.L., Narasimhan, V.M., Yu, H., Foote, K., Simons, B.D., Bennett, M.R., Jørgensen, H.F., 2016. Extensive Proliferation of a Subset of Differentiated, yet Plastic, Medial Vascular Smooth Muscle Cells Contributes to Neointimal Formation in Mouse Injury and Atherosclerosis Models. *Circ. Res.* 119, 1313-1323.
- Charenton, C., Graille, M., 2018. mRNA decapping: finding the right structures. *Philos. Trans. R. Soc. B Biol. Sci.* 373.
- Charla, E., Mercer, J., Maffia, P., Nicklin, S.A., 2020. Extracellular vesicle signalling in atherosclerosis. *Cell. Physiol. Biochem.* 75.
- Chekulaeva, M., Mathys, H., Zipprich, J.T., Attig, J., Colic, M., Parker, R., Filipowicz, W., 2011. miRNA repression involves GW182-mediated recruitment of CCR4-NOT through conserved W-containing motifs. *Nat. Struct. Mol. Biol.* 18, 1218-1226.
- Cheloufi, S., Dos Santos, C.O., Chong, M.M.W., Hannon, G.J., 2010. A dicer-independent miRNA biogenesis pathway that requires Ago catalysis. *Nat.* 2010 4657298 465, 584-589.
- Chen, C.-Y.A., Zheng, D., Xia, Z., Shyu, A.-B., 2009. Ago-TNRC6 triggers microRNA-mediated decay by promoting two deadenylation steps. *Nat. Struct. Mol. Biol.* 16, 1160-1166.
- Chen, D., Zhang, C., Chen, J., Yang, M., Afzal, T.A., An, W., Maguire, E.M., He, S., Luo, J., Wang, X., Zhao, Y., Wu, Q., Xiao, Q., 2021. miRNA-200c-3p

- promotes endothelial to mesenchymal transition and neointimal hyperplasia in artery bypass grafts. *J. Pathol.* 253, 209-224.
- Chen, H., Dai, J., 2018. miR-409-3p suppresses the proliferation, invasion and migration of tongue squamous cell carcinoma via targeting RDX. *Oncol. Lett.* 16, 543-551.
- Chen, P.H., Chen, X., He, X., 2013. Platelet-derived growth factors and their receptors: structural and functional perspectives. *Biochim. Biophys. Acta* 1834, 2176-2186.
- Chen, S.J., Wilson, J.M., Muller, D.W.M., 1994. Adenovirus-mediated gene transfer of soluble vascular cell adhesion molecule to porcine interposition vein grafts. *Circulation* 89, 1922-1928.
- Chen, W., Wen, X., Latzel, M., Heilmann, M., Yang, J., Dai, X., Huang, S., Shrestha, S., Patterson, R., Christiansen, S., Conibeer, G., 2016. Nanoscale Characterization of Carrier Dynamic and Surface Passivation in InGaN/GaN Multiple Quantum Wells on GaN Nanorods. *ACS Appl. Mater. Interfaces* 8, 31887-31893.
- Chen, X., Ba, Y., Ma, L., Cai, X., Yin, Y., Wang, K., Guo, J., Zhang, Yujing, Chen, J., Guo, X., Li, Q., Li, X., Wang, W., Zhang, Yan, Wang, Jin, Jiang, X., Xiang, Y., Xu, C., Zheng, P., Zhang, Juanbin, Li, R., Zhang, H., Shang, X., Gong, T., Ning, G., Wang, Jun, Zen, K., Zhang, Junfeng, Zhang, C.Y., 2008. Characterization of microRNAs in serum: a novel class of biomarkers for diagnosis of cancer and other diseases. *Cell Res.* 2008 1810 18, 997-1006.
- Chen, X., Zhao, W., Yuan, Y., Bai, Y., Sun, Y., Zhu, W., Du, Z., 2017. MicroRNAs tend to synergistically control expression of genes encoding extensively-expressed proteins in humans. *PeerJ* 5.
- Chen, Y., Boland, A., Kuzuoğlu-Öztürk, D., Bawankar, P., Loh, B., Chang, C. Te, Weichenrieder, O., Izaurralde, E., 2014. A DDX6-CNOT1 complex and W-binding pockets in CNOT9 reveal direct links between miRNA target recognition and silencing. *Mol. Cell* 54, 737-750.
- Chen, Y., Zhao, Y., Yin, Y., Jia, X., Mao, L., 2021. Mechanism of cargo sorting into small extracellular vesicles. *Bioengineered* 12, 8186-8201.
- Chendrimada, T.P., Gregory, R.I., Kumaraswamy, E., Norman, J., Cooch, N., Nishikura, K., Shiekhattar, R., 2005. TRBP recruits the Dicer complex to Ago2 for microRNA processing and gene silencing. *Nature* 436, 740-744.
- Cheng, H.L., Fu, C.Y., Kuo, W.C., Chen, Y.W., Chen, Y.S., Lee, Y.M., Li, K.H., Chen, C., Ma, H.P., Huang, P.C., Wang, Y.L., Lee, G. Bin, 2018. Detecting miRNA biomarkers from extracellular vesicles for cardiovascular disease with a microfluidic system. *Lab Chip* 18, 2917-2925.
- Cheng, L., Sharples, R.A., Scicluna, B.J., Hill, A.F., 2014a. Exosomes provide a protective and enriched source of miRNA for biomarker profiling compared to intracellular and cell-free blood. *J. Extracell. vesicles* 3.
- Cheng, L., Sun, X., Scicluna, B.J., Coleman, B.M., Hill, A.F., 2014b. Characterization and deep sequencing analysis of exosomal and non-exosomal miRNA in human urine. *Kidney Int.* 86, 433-444.
- Cheng, Y., Liu, X., Yang, J., Lin, Y., Xu, D.Z., Lu, Q., Deitch, E.A., Huo, Y., Delphin, E.S., Zhang, C., 2009. MicroRNA-145, a Novel Smooth Muscle Cell Phenotypic Marker and Modulator, Controls Vascular Neointimal Lesion Formation. *Circ. Res.* 105, 158-166.
- Cheng, Y., Zhang, C., 2010. MicroRNA-21 in Cardiovascular Disease. *J. Cardiovasc. Transl. Res.* 3, 251-255.
- Chien, S., 2007. Mechanotransduction and endothelial cell homeostasis: The wisdom of the cell. *Am. J. Physiol. - Hear. Circ. Physiol.* 292, H1209-24.

- Chivet, M., Javalet, C., Laulagnier, K., Blot, B., Hemming, F.J., Sadoul, R., 2014. Exosomes secreted by cortical neurons upon glutamatergic synapse activation specifically interact with neurons. *J. Extracell. vesicles* 3.
- Choi, M.H., Lee, I.K., Kim, G.W., Kim, B.U., Han, Y.H., Yu, D.Y., Park, H.S., Kim, K.Y., Lee, J.S., Choi, C., Bae, Y.S., Lee, B.I., Rhee, S.G., Kang, S.W., 2005. Regulation of PDGF signalling and vascular remodelling by peroxiredoxin II. *Nature* 435, 347-353.
- Chong, S.Y., Lee, C.K., Huang, C., Ou, Y.H., Charles, C.J., Richards, A.M., Neupane, Y.R., Pavon, M.V., Zharkova, O., Pastorin, G., Wang, J.W., 2019. Extracellular Vesicles in Cardiovascular Diseases: Alternative Biomarker Sources, Therapeutic Agents, and Drug Delivery Carriers. *Int. J. Mol. Sci.* 20.
- Christiansen, J.F., Hartwig, D., Bechtel, J.F.M., Klü, H., Sievers, H.-H., Bartels, C., 2004. Diseased Vein Grafts Express Elevated Inflammatory Cytokine Levels Compared With Atherosclerotic Coronary Arteries. *Ann. Thorac. Surg.* 77, 1575-1579.
- Churov, A., Summerhill, V., Grechko, A., Orekhova, V., Orekhov, A., 2019. MicroRNAs as Potential Biomarkers in Atherosclerosis. *Int. J. Mol. Sci.* 20.
- Cipollone, F., Felicioni, L., Sarzani, R., Uchino, S., Spigonardo, F., Mandolini, C., Malatesta, S., Bucci, M., Mammarella, C., Santovito, D., De Lutiis, F., Marchetti, A., Mezzetti, A., Buttitta, F., 2011. A Unique MicroRNA Signature Associated With Plaque Instability in Humans. *Stroke* 42, 2556-2563.
- Cizek, S.M., Bedri, S., Talusan, P., Silva, N., Lee, H., Stone, J.R., 2007. Risk factors for atherosclerosis and the development of preatherosclerotic intimal hyperplasia. *Cardiovasc. Pathol.* 16, 344-350.
- Claridge, B., Lozano, J., Poh, Q.H., Greening, D.W., 2021. Development of Extracellular Vesicle Therapeutics: Challenges, Considerations, and Opportunities. *Front. Cell Dev. Biol.* 9.
- Cloonan, N., 2015. Re-thinking miRNA-mRNA interactions: Intertwining issues confound target discovery. *BioEssays* 37, 379-388.
- Cole, C.W., Makhoul, R.G., McCann, R.L., O'Malley, M.K., Hagen, P.O., 1988. A neutrophil derived factor(s) stimulates [³H]thymidine incorporation by vascular smooth muscle cells in vitro. *Clin. Investig. Med.* 11, 62-7.
- Colombo, M., Moita, C., Van Niel, G., Kowal, J., Vigneron, J., Benaroch, P., Manel, N., Moita, L.F., Théry, C., Raposo, G., 2013. Analysis of ESCRT functions in exosome biogenesis, composition and secretion highlights the heterogeneity of extracellular vesicles. *J. Cell Sci.* 126, 5553-5565.
- Colombo, M., Raposo, G., Théry, C., 2014. Biogenesis, Secretion, and Intercellular Interactions of Exosomes and Other Extracellular Vesicles. *Annu. Rev. Cell Dev. Biol.* 30, 255-289.
- Columb, M.O., Atkinson, M.S., 2016. Statistical analysis: sample size and power estimations. *BJA Educ.* 16, 159-161.
- Comelli, L., Rocchiccioli, S., Smirni, S., Salvetti, A., Signore, G., Citti, L., Trivella, M.G., Cecchetti, A., 2014. Characterization of secreted vesicles from vascular smooth muscle cells. *Mol. Biosyst.* 10, 1146-1152.
- Condorelli, G., Latronico, M.V.G., Dorn, G.W., 2010. microRNAs in heart disease: putative novel therapeutic targets? *Eur. Heart J.* 31, 649-658.
- Cooley, B.C., 2016. Murine models of vein grafting. *Mouse Model. Vasc. Dis.* 143-155.
- Cooley, B.C., 2004. Murine model of neointimal formation and stenosis in vein grafts. *Arterioscler. Thromb. Vasc. Biol.* 24, 1180-1185.
- Corbit, K.C., Trakul, N., Eves, E.M., Diaz, B., Marshall, M., Rosner, M.R., 2003. Activation of Raf-1 signaling by protein kinase C through a mechanism

- involving Raf kinase inhibitory protein. *J. Biol. Chem.* 278, 13061-13068.
- Cordes, K.R., Sheehy, N.T., White, M.P., Berry, E.C., Morton, S.U., Muth, A.N., Lee, T.H., Miano, J.M., Ivey, K.N., Srivastava, D., 2009. miR-145 and miR-143 regulate smooth muscle cell fate and plasticity. *Nat.* 2009 4607256 460, 705-710.
- Cortez, M.A., Bueso-Ramos, C., Ferdin, J., Lopez-Berestein, G., Sood, A.K., Calin, G.A., 2011. MicroRNAs in body fluids—the mix of hormones and biomarkers. *Nat. Rev. Clin. Oncol.* 2011 88 8, 467-477.
- Cospedal, R., Abedi, H., Zachary, I., 1999. Platelet-derived growth factor-BB (PDGF-BB) regulation of migration and focal adhesion kinase phosphorylation in rabbit aortic vascular smooth muscle cells: roles of phosphatidylinositol 3-kinase and mitogen-activated protein kinases. *Cardiovasc. Res.* 41, 708-721.
- Costa, M.A., Simon, D.I., 2005. Molecular Basis of Restenosis and Drug-Eluting Stents. *Circulation* 111, 2257-2273.
- Cuesta, C., Arévalo-Alameda, C., Castellano, E., 2021. The Importance of Being PI3K in the RAS Signaling Network. *Genes (Basel).* 12.
- Currie, R.A., Walker, K.S., Gray, A., Deak, M., Casamayor, A., Downes, C.P., Cohen, P., Alessi, D.R., Lucocq, J., 1999. Role of phosphatidylinositol 3,4,5-trisphosphate in regulating the activity and localization of 3-phosphoinositide-dependent protein kinase-1. *Biochem. J.* 337, 575-583.
- D'Alessandra, Y., Devanna, P., Limana, F., Straino, S., Di Carlo, A., Brambilla, P.G., Rubino, M., Carena, M.C., Spazzafumo, L., De Simone, M., Micheli, B., Biglioli, P., Achilli, F., Martelli, F., Maggiolini, S., Marenzi, G., Pompilio, G., Capogrossi, M.C., 2010. Circulating microRNAs are new and sensitive biomarkers of myocardial infarction. *Eur. Heart J.* 31, 2765-2773.
- D'Souza, F.M., Sparks, R.L., Chen, H., Kadowitz, P.J., Jeter, J.R., 2003. Mechanism of eNOS gene transfer inhibition of vascular smooth muscle cell proliferation. *Am. J. Physiol. Cell Physiol.* 284.
- da Luz, P., Nishiyama, M., Chagas, A.C.P., 2011. Drugs and lifestyle for the treatment and prevention of coronary artery disease: comparative analysis of the scientific basis. *Brazilian J. Med. Biol. Res.* 44, 973-991.
- Dai, R., Liu, Y., Zhou, Y., Xiong, X., Zhou, Wei, Li, W., Zhou, Wenping, Chen, M., 2019. Potential of circulating pro-angiogenic microRNA expressions as biomarkers for rapid angiographic stenotic progression and restenosis risks in coronary artery disease patients underwent percutaneous coronary intervention. *J. Clin. Lab. Anal.* 34.
- Dangas, G.D., Claessen, B.E., Caixeta, A., Sanidas, E.A., Mintz, G.S., Mehran, R., 2010. In-stent restenosis in the drug-eluting stent era. *J. Am. Coll. Cardiol.* 56, 1897-1907.
- Daniel, T. O., Kumjian, D.A., 1992. Platelet-derived growth factor receptors and phospholipase C activation. *Kidney Int.* 41, 575-580.
- Daniel, T.O., Gibbs, V.C., Milfay, D.F., Garovoy, M.R., Williams, L.T., 1986. Thrombin stimulates c-sis gene expression in microvascular endothelial cells. *J. Biol. Chem.* 261, 9579-9582.
- Davidson, S.M., Boulanger, C.M., Aikawa, E., Badimon, L., Barile, L., Binder, C.J., Brisson, A., Buzas, E., Emanuelli, C., Jansen, F., Katsur, M., Lacroix, R., Lim, S.K., Mackman, N., Mayr, M., Menasché, P., Nieuwland, R., Sahoo, S., Takov, K., Thum, T., Vader, P., Wauben, M.H.M., Witwer, K., Sluijter, J.P.G., 2023. Methods for the identification and characterization of extracellular vesicles in cardiovascular studies: from exosomes to microvesicles. *Cardiovasc. Res.* 119, 45-63.
- Davis, B.N., Hilyard, A.C., Lagna, G., Hata, A., 2008. SMAD proteins control

- DROSHA-mediated microRNA maturation. *Nat.* 2008 4547200 454, 56-61.
- de Abreu, R.C., Ramos, C. V., Becher, C., Lino, M., Jesus, C., da Costa Martins, P.A., Martins, P.A.T., Moreno, M.J., Fernandes, H., Ferreira, L., 2021. Exogenous loading of miRNAs into small extracellular vesicles. *J. Extracell. Vesicles* 10.
- De La Cuesta, F., Passalacqua, I., Rodor, J., Bhushan, R., Denby, L., Baker, A.H., 2019. Extracellular vesicle cross-Talk between pulmonary artery smooth muscle cells and endothelium during excessive TGF- β signalling: Implications for PAH vascular remodelling. *Cell Commun. Signal.* 17, 1-16.
- de Ribamar Costa, J., Mintz, G.S., Carlier, S.G., Fujii, K., Sano, K., Kimura, M., Tanaka, K., Costa, R.A., Lui, J., Na, Y., Castellanos, C., Biro, S., Moussa, I., Stone, G.W., Moses, J.W., Leon, M.B., 2007. Intravascular ultrasound assessment of drug-eluting stent expansion. *Am. Heart J.* 153, 297-303.
- de Vries, M.R., Quax, P.H.A., 2018. Inflammation in Vein Graft Disease. *Front. Cardiovasc. Med.* 5.
- de Vries, M.R., Simons, K.H., Jukema, J.W., Braun, J., Quax, P.H.A., 2016. Vein graft failure: from pathophysiology to clinical outcomes. *Nat. Rev. Cardiol.* 13, 451-470.
- Dellar, E.R., Hill, C., Melling, G.E., Carter, D.R., Alberto Baena-Lopez, L., Elizabeth Dellar, C.R., 2022. Unpacking extracellular vesicles: RNA cargo loading and function. *J. Extracell. Biol.* 1.
- Denli, A.M., Tops, B.B.J., Plasterk, R.H.A., Ketting, R.F., Hannon, G.J., 2004. Processing of primary microRNAs by the Microprocessor complex. *Nat.* 2004 4327014 432, 231-235.
- Deville, S., Berckmans, P., Van Hoof, R., Lambrichts, I., Salvati, A., Nelissen, I., 2021. Comparison of extracellular vesicle isolation and storage methods using high-sensitivity flow cytometry. *PLoS One* 16.
- Dharap, A., Pokrzywa, C., Murali, S., Pandi, G., Vemuganti, R., 2013. MicroRNA miR-324-3p Induces Promoter-Mediated Expression of RelA Gene. *PLoS One* 8.
- Di Rocco, G., Baldari, S., Toietta, G., 2017. Exosomes and other extracellular vesicles-mediated microRNA delivery for cancer therapy. *Transl. Cancer Res.* 6, 1321-1330.
- Dibra, A., Kastrati, A., Mehilli, J., Pache, J., Schühlen, H., Von Beckerath, N., Ulm, K., Wessely, R., Dirschinger, J., Schömig, A., 2005. Paclitaxel-eluting or sirolimus-eluting stents to prevent restenosis in diabetic patients. *N. Engl. J. Med.* 353, 663-670.
- Dol-Gleizes, F., Delesque-Touchard, N., Marès, A.M., Nestor, A.L., Schaeffer, P., Bono, F., 2013. A New Synthetic FGF Receptor Antagonist Inhibits Arteriosclerosis in a Mouse Vein Graft Model and Atherosclerosis in Apolipoprotein E-Deficient Mice. *PLoS One* 8.
- Dong, L.H., Wen, J.K., Liu, G., McNutt, M.A., Miao, S.B., Gao, R., Zheng, B., Zhang, H., Han, M., 2010. Blockade of the ras-extracellular signal-regulated kinase 1/2 pathway is involved in smooth muscle 22α -mediated suppression of vascular smooth muscle cell proliferation and neointima hyperplasia. *Arterioscler. Thromb. Vasc. Biol.* 30, 683-691.
- Dong, R., Zhang, K., Wang, Y.L., Zhang, F., Cao, J., Zheng, J.B., Zhang, H.J., 2017. MiR-551b-5p Contributes to Pathogenesis of Vein Graft Failure via Upregulating Early Growth Response-1 Expression. *Chin. Med. J. (Engl.)* 130, 1578-1585.
- Doyle, L.M., Wang, M.Z., 2019. Overview of Extracellular Vesicles, Their Origin, Composition, Purpose, and Methods for Exosome Isolation and Analysis. *Cells*

8.

- Duronio, V., 2008. The life of a cell: apoptosis regulation by the PI3K/PKB pathway. *Biochem. J.* 415, 333-344.
- Ebert, M.L.A., Schmidt, V.F., Pfaff, L., von Thaden, A., Kimm, M.A., Wildgruber, M., 2021. Animal Models of Neointimal Hyperplasia and Restenosis: Species-Specific Differences and Implications for Translational Research. *Basic to Transl. Sci.* 6, 900-917.
- Eichhorn, S.W., Guo, H., McGeary, S.E., Rodriguez-Mias, R.A., Shin, C., Baek, D., Hsu, S. hao, Ghoshal, K., Villén, J., Bartel, D.P., 2014. mRNA Destabilization Is the Dominant Effect of Mammalian MicroRNAs by the Time Substantial Repression Ensues. *Mol. Cell* 56, 104-115.
- Eken, S.M., Jin, H., Chernogubova, E., Li, Y., Simon, N., Sun, C., Korzunowicz, G., Busch, A., Bäcklund, A., Österholm, C., Razuvaev, A., Renné, T., Eckstein, H.H., Pelisek, J., Eriksson, P., González Díez, M., Perisic Matic, L., Schellinger, I.N., Raaz, U., Leeper, N.J., Hansson, G.K., Paulsson-Berne, G., Hedin, U., Maegdefessel, L., 2017. MicroRNA-210 enhances fibrous cap stability in advanced atherosclerotic lesions. *Circ. Res.* 120, 633-644.
- El-Andaloussi, S., Lee, Y., Lakhali-Littleton, S., Li, J., Seow, Y., Gardiner, C., Alvarez-Erviti, L., Sargent, I.L., Wood, M.J.A., 2012. Exosome-mediated delivery of siRNA in vitro and in vivo. *Nat. Protoc.* 2012 7, 2112-2126.
- Elia, L., Quintavalle, M., Zhang, J., Contu, R., Cossu, L., Latronico, M.V.G., Peterson, K.L., Indolfi, C., Catalucci, D., Chen, J., Courtneidge, S.A., Condorelli, G., 2009. The knockout of miR-143 and -145 alters smooth muscle cell maintenance and vascular homeostasis in mice: correlates with human disease. *Cell Death Differ.* 2009 16, 1590-1598.
- Emanueli, C., Shearn, A.I.U., Laftah, A., Fiorentino, F., Reeves, B.C., Beltrami, C., Mumford, A., Clayton, A., Gurney, M., Shantikumar, S., Angelini, G.D., 2016. Coronary Artery-Bypass-Graft Surgery Increases the Plasma Concentration of Exosomes Carrying a Cargo of Cardiac MicroRNAs: An Example of Exosome Trafficking Out of the Human Heart with Potential for Cardiac Biomarker Discovery. *PLoS One* 11.
- Engelman, J.A., Luo, J., Cantley, L.C., 2006. The evolution of phosphatidylinositol 3-kinases as regulators of growth and metabolism. *Nat. Rev. Genet.* 2006 7, 606-619.
- Enright, A.J., John, B., Gaul, U., Tuschl, T., Sander, C., Marks, D.S., 2003. MicroRNA targets in *Drosophila*. *Genome Biol.* 5.
- Escaned, J., 2012. Secondary revascularization after CABG surgery. *Nat. Rev. Cardiol.* 2012 9, 540-549.
- Escrevente, C., Keller, S., Altevogt, P., Costa, J., 2011. Interaction and uptake of exosomes by ovarian cancer cells. *BMC Cancer* 11.
- Eslami, M.H., Gangadharan, S.P., Belkin, M., Donaldson, M.C., Whittemore, A.D., Conte, M.S., 2001. Monocyte adhesion to human vein grafts: A marker for occult intraoperative injury? *J. Vasc. Surg.* 34, 923-929.
- Evans, C.E., Iruela-Arispe, M.L., Zhao, Y.Y., 2021. Mechanisms of Endothelial Regeneration and Vascular Repair and Their Application to Regenerative Medicine. *Am. J. Pathol.* 191, 52-65.
- Ewing, M.M., Karper, J.C., Sampietro, M.L., de Vries, M.R., Pettersson, K., Jukema, J.W., Quax, P.H.A., 2012. Annexin A5 prevents post-interventional accelerated atherosclerosis development in a dose-dependent fashion in mice. *Atherosclerosis* 221, 333-340.
- Fabian, M.R., Cieplak, M.K., Frank, F., Morita, M., Green, J., Srikumar, T., Nagar, B., Yamamoto, T., Raught, B., Duchaine, T.F., Sonenberg, N., 2011.

- miRNA-mediated deadenylation is orchestrated by GW182 through two conserved motifs that interact with CCR4-NOT. *Nat. Struct. Mol. Biol.* 18, 1211-1217.
- Falk, E., 2006. Pathogenesis of Atherosclerosis. *J. Am. Coll. Cardiol.* 47, 7-12.
- Fang, X., Dong, Y., Yang, R., Wei, L., 2020. LINC00619 restricts gastric cancer progression by preventing microRNA-224-5p-mediated inhibition of OPCML. *Arch. Biochem. Biophys.* 689.
- Faraldi, M., Gomasasca, M., Banfi, G., Lombardi, G., 2018. Free Circulating miRNAs Measurement in Clinical Settings: The Still Unsolved Issue of the Normalization. *Adv. Clin. Chem.* 87, 113-139.
- Felekis, K., Touvana, E., Stefanou, C., Deltas, C., 2010. MicroRNAs: A newly described class of encoded molecules that play a role in health and disease. *Hippokratia* 14, 236-240.
- Feng, D., Zhao, W.L., Ye, Y.Y., Bai, X.C., Liu, R.Q., Chang, L.F., Zhou, Q., Sui, S.F., 2010. Cellular internalization of exosomes occurs through phagocytosis. *Traffic* 11, 675-687.
- Feng, Y.H., Tsao, C.J., 2016. Emerging role of microRNA-21 in cancer. *Biomed. Reports* 5, 395-402.
- Fernández-Medarde, A., Santos, E., 2011. Ras in Cancer and Developmental Diseases. *Genes Cancer* 2, 344-358.
- Ferns, G.A.A., Raines, E.W., Sprugel, K.H., Motani, A.S., Reidy, M.A., Ross, R., 1991. Inhibition of Neointimal Smooth Muscle Accumulation After Angioplasty by an Antibody to PDGF. *Science* (80-.). 253, 1129-1132.
- Ferrara, N., 2009. Vascular endothelial growth factor. *Arterioscler. Thromb. Vasc. Biol.* 29, 789-791.
- Fichtlscherer, S., De Rosa, S., Fox, H., Schwietz, T., Fischer, A., Liebetrau, C., Weber, M., Hamm, C.W., Röxe, T., Müller-Ardogan, M., Bonauer, A., Zeiher, A.M., Dimmeler, S., 2010. Circulating MicroRNAs in Patients With Coronary Artery Disease. *Circ. Res.* 107, 677-684.
- Finn, A. V., Joner, M., Nakazawa, G., Kolodgie, F., Newell, J., John, M.C., Gold, H.K., Virmani, R., 2007a. Pathological Correlates of Late Drug-Eluting Stent Thrombosis. *Circulation* 115, 2435-2441.
- Finn, A. V., Nakazawa, G., Joner, M., Kolodgie, F.D., Mont, E.K., Gold, H.K., Virmani, R., 2007b. Vascular Responses to Drug Eluting Stents. *Arterioscler. Thromb. Vasc. Biol.* 27, 1500-1510.
- Fish, J.E., Santoro, M.M., Morton, S.U., Yu, S., Yeh, R.F., Wythe, J.D., Ivey, K.N., Bruneau, B.G., Stainier, D.Y.R., Srivastava, D., 2008. miR-126 Regulates Angiogenic Signaling and Vascular Integrity. *Dev. Cell* 15, 272-284.
- Flügel, D., Görlach, A., Kietzmann, T., 2012. GSK-3 β regulates cell growth, migration, and angiogenesis via Fbw7 and USP28-dependent degradation of HIF-1 α . *Blood* 119, 1292-1301.
- Folestad, E., Kunath, A., Wågsäter, D., 2018. PDGF-C and PDGF-D signaling in vascular diseases and animal models. *Mol. Aspects Med.* 62.
- Fontaine, M., Herkenne, S., Ek, O., Paquot, A., Boeckx, A., Paques, C., Nivelles, O., Thiry, M., Struman, I., 2022. Extracellular vesicles mediate communication between endothelial and vascular smooth muscle cells. *Int. J. Mol. Sci.* 23.
- Forman, J.J., Legesse-Miller, A., Collier, H.A., 2008. A search for conserved sequences in coding regions reveals that the let-7 microRNA targets Dicer within its coding sequence. *Proc. Natl. Acad. Sci. U. S. A.* 105, 14879-14884.
- Forrester, J.S., Fishbein, M., Helfant, R., Fagin, J., 1991. A paradigm for restenosis based on cell biology: clues for the development of new

- preventive therapies. *J. Am. Coll. Cardiol.* 17, 758-769.
- Forterre, A., Komuro, H., Aminova, S., Harada, M., 2020. A Comprehensive Review of Cancer MicroRNA Therapeutic Delivery Strategies. *Cancers (Basel)*. 12, 1-21.
- Freeman, D.W., Noren Hooten, N., Eitan, E., Green, J., Mode, N.A., Bodogai, M., Zhang, Y., Lehrmann, E., Zonderman, A.B., Biragyn, A., Egan, J., Becker, K.G., Mattson, M.P., Ejiogu, N., Evans, M.K., 2018. Altered extracellular vesicle concentration, cargo, and function in diabetes. *Diabetes* 67, 2377-2388.
- Frey, U.H., Klaassen, M., Ochsenfarth, C., Murke, F., Thielmann, M., Kottenberg, E., Kleinbongard, P., Klenke, S., Engler, A., Heusch, G., Giebel, B., Peters, J., 2019. Remote ischaemic preconditioning increases serum extracellular vesicle concentrations with altered micro-RNA signature in CABG patients. *Acta Anaesthesiol. Scand.* 63, 483-492.
- Fridrich, A., Hazan, Y., Moran, Y., 2019. Too Many False Targets for MicroRNAs: Challenges and Pitfalls in Prediction of miRNA Targets and Their Gene Ontology in Model and Non-model Organisms. *BioEssays* 41, 1-11.
- Friedman, R.C., Farh, K.K.H., Burge, C.B., Bartel, D.P., 2009. Most mammalian mRNAs are conserved targets of microRNAs. *Genome Res.* 19, 92-105.
- Frismantiene, A., Philippova, M., Erne, P., Resink, T.J., 2018. Smooth muscle cell-driven vascular diseases and molecular mechanisms of VSMC plasticity. *Cell. Signal.* 52, 48-64.
- Fu, Shengyang, Wang, Y., Xia, X., Zheng, J.C., 2020. Exosome engineering: Current progress in cargo loading and targeted delivery. *NanoImpact* 20.
- Fu, Shihui, Zhang, Y., Li, Y., Luo, L., Zhao, Y., Yao, Y., 2020. Extracellular vesicles in cardiovascular diseases. *Cell Death Discov.* 6, 1-9.
- Fukao, A., Mishima, Y., Takizawa, N., Oka, S., Imataka, H., Pelletier, J., Sonenberg, N., Thoma, C., Fujiwara, T., 2014. MicroRNAs trigger dissociation of eIF4A1 and eIF4AII from target mRNAs in humans. *Mol. Cell* 56, 79-89.
- Fukaya, T., Iwakawa, H. oki, Tomari, Y., 2014. MicroRNAs block assembly of eIF4F translation initiation complex in *Drosophila*. *Mol. Cell* 56, 67-78.
- Gallie, D.R., 2014. The role of the poly(A) binding protein in the assembly of the Cap-binding complex during translation initiation in plants. *Translation* 2, e959378.
- Gallo, A., Tandon, M., Alevizos, I., Illei, G.G., 2012. The Majority of MicroRNAs Detectable in Serum and Saliva Is Concentrated in Exosomes. *PLoS One* 7.
- Gámez-Valero, A., Monguió-Tortajada, M., Carreras-Planella, L., Franquesa, M., Beyer, K., Borràs, F.E., 2016. Size-Exclusion Chromatography-based isolation minimally alters Extracellular Vesicles' characteristics compared to precipitating agents. *Sci. Rep.* 6.
- Ganjali, S., Aghaee-Bakhtiari, S.H., Reiner, Ž., Sahebkar, A., 2022. Differential Expression of miRNA-223 in Coronary In-Stent Restenosis. *J. Clin. Med.* 2022, Vol. 11, Page 849 11.
- Gao, X.-F., Wang, Z.-M., Chen, A.-Q., Wang, F., Luo, S., Gu, Y., Kong, X.-Q., Zuo, G.-F., Jiang, X.-M., Ding, G.-W., Chen, Y., Ge, Z., Zhang, J.-J., Chen, S.-L., 2021. Plasma Small Extracellular Vesicle-Carried miRNA-501. *Oxid. Med. Cell. Longev.* 2021.
- Gao, Y., Chen, T., Raj, J.U., 2016. Endothelial and smooth muscle cell interactions in the pathobiology of pulmonary hypertension. *Am. J. Respir. Cell Mol. Biol.* 54, 451-460.
- Garaeva, L., Kamyschinsky, R., Kil, Y., Varfolomeeva, E., Verlov, N., Komarova,

- E., Garmay, Y., Landa, S., Burdakov, V., Myasnikov, A., Vinnikov, I.A., Margulis, B., Guzhova, I., Kagansky, A., Konevega, A.L., Shtam, T., 2021. Delivery of functional exogenous proteins by plant-derived vesicles to human cells in vitro. *Sci. Rep.* 11, 1-12.
- Garcia-Moreno, A., Carmona-Saez, P., 2020. Computational methods and software tools for functional analysis of miRNA data. *Biomolecules* 10, 1-16.
- Gareev, I., Beylerli, O., Yang, G., Sun, J., Pavlov, V., Izmailov, A., Shi, H., Zhao, S., 2020. The current state of MiRNAs as biomarkers and therapeutic tools. *Clin. Exp. Med.* 20, 349-359.
- Gareri, C., De Rosa, S., Indolfi, C., 2016. MicroRNAs for restenosis and thrombosis after vascular injury. *Circ. Res.* 118, 1170-1184.
- Gasper, W.J., Owens, C.D., Kim, J.M., Hills, N., Belkin, M., Creager, M.A., Conte, M.S., 2013. Thirty-day vein remodeling is predictive of midterm graft patency after lower extremity bypass. *J. Vasc. Surg.* 57, 9-18.
- Gaudino, M., Antoniades, C., Benedetto, U., Deb, S., Franco, A. Di, Giammarco, G. Di, Fremes, S., Glineur, D., Grau, J., He, G.-W., Marinelli, D., Ohmes, L.B., Patrono, C., Puskas, J., Tranbaugh, R., Girardi, L.N., Taggart, D.P., 2017. Mechanisms, Consequences, and Prevention of Coronary Graft Failure. *Circulation* 136, 1749-1764.
- Gawaz, M., Neumann, F.J., Ott, I., May, A., Schömig, A., 1996. Platelet activation and coronary stent implantation: Effect of antithrombotic therapy. *Circulation* 94, 279-285.
- Ge, J., Shen, C., Liang, C., Chen, L., Qian, J., Chen, H., 2006. Elevated matrix metalloproteinase expression after stent implantation is associated with restenosis. *Int. J. Cardiol.* 112, 85-90.
- Geary, R.L., Kohler, T.R., Vergel, S., Kirkman, T.R., Clowes, A.W., 1994. Time course of flow-induced smooth muscle cell proliferation and intimal thickening in endothelialized baboon vascular grafts. *Circ. Res.* 74, 14-23.
- Geurickx, E., Tulkens, J., Dhondt, B., Van Deun, J., Lippens, L., Vergauwen, G., Heyrman, E., De Sutter, D., Gevaert, K., Impens, F., Miinalainen, I., Van Bockstal, P.J., De Beer, T., Wauben, M.H.M., Nolte-'t-Hoen, E.N.M., Bloch, K., Swinnen, J. V., van der Pol, E., Nieuwland, R., Braems, G., Callewaert, N., Mestdagh, P., Vandesompele, J., Denys, H., Eyckerman, S., De Wever, O., Hendrix, A., 2019. The generation and use of recombinant extracellular vesicles as biological reference material. *Nat. Commun.* 2019 101 10, 1-12.
- Généreux, P., Rutledge, D.R., Palmerini, T., Caixeta, A., Kedhi, E., Hermiller, J.B., Wang, J., Krucoff, M.W., Jones-McMeans, J., Sudhir, K., Simonton, C.A., Serruys, P.W., Stone, G.W., 2015. Stent Thrombosis and Dual Antiplatelet Therapy Interruption with Everolimus-Eluting Stents: Insights from the Xience v Coronary Stent System Trials. *Circ. Cardiovasc. Interv.* 8.
- Gerke, V., Moss, S.E., 2002. Annexins: From structure to function. *Physiol. Rev.* 82, 331-371.
- Gezer, U., Özgür, E., Cetinkaya, M., Isin, M., Dalay, N., 2014. Long non-coding RNAs with low expression levels in cells are enriched in secreted exosomes. *Cell Biol. Int.* 38, 1076-1079.
- Ghafouri-Fard, S., Noie Alamdari, A., Noee Alamdari, Y., Abak, A., Hussen, B.M., Taheri, M., Jamali, E., 2022. Role of PI3K/AKT pathway in squamous cell carcinoma with an especial focus on head and neck cancers. *Cancer Cell Int.* 2022 221 22, 1-27.
- Gimple, R.C., Wang, X., 2019. RAS: Striking at the Core of the Oncogenic Circuitry. *Front. Oncol.* 9.
- Goel, S.A., Guo, L.W., Liu, B., Kent, K.C., 2012. Mechanisms of post-

- intervention arterial remodelling. *Cardiovasc. Res.* 96, 363-371.
- Goetzl, E.J., Schwartz, J.B., Mustapic, M., Lobach, I. V., Daneman, R., Abner, E.L., Jicha, G.A., 2017. Altered cargo proteins of human plasma endothelial cell-derived exosomes in atherosclerotic cerebrovascular disease. *FASEB J.* 31.
- Goñi, F.M., Alonso, A., 2009. Effects of ceramide and other simple sphingolipids on membrane lateral structure. *Biochim. Biophys. Acta* 1788, 169-177.
- Gonzalo-Calvo, D., Pérez-Boza, J., Curado, J., Devaux, Y., 2022. Challenges of microRNA-based biomarkers in clinical application for cardiovascular diseases. *Clin. Transl. Med.* 12, e585.
- Gould, S.J., Raposo, G., 2013. As we wait: coping with an imperfect nomenclature for extracellular vesicles. *J. Extracell. Vesicles* 2.
- Graham, L.M., Bassiouny, H.S., White, S.S., Glagov, S.S., Choi, E.S., Giddens, D.P., 1992. Anastomotic intimal hyperplasia: mechanical injury or flow induced. *J. Vasc. Surg.* 15, 708-717.
- Grewe, P.H., Deneke, T., Machraoui, A., Barmeyer, J., Müller, K.M., 2000. Acute and chronic tissue response to coronary stent implantation: pathologic findings in human specimen. *J. Am. Coll. Cardiol.* 35, 157-163.
- Grimson, A., Kai-How Farh, K., Johnston, W.K., Garrett-Engele, P., Lim, L.P., Bartel, D.P., 2007. MicroRNA Targeting Specificity in Mammals: Determinants beyond Seed Pairing. *Mol. Cell* 27, 91-105.
- Grondin, C.M., Lesperance, J., Bourassa, M.G., 1974. Serial angiographic evaluation in 60 consecutive patients with aorto-coronary artery vein grafts 2 weeks, 1 year, and 3 years after operation. *J. Thorac. Cardiovasc. Surg.* 67, 1-6.
- Gronwald, R.G.K., Seifert, R.A., Bowen-Pope, D.F., 1989. Differential regulation of expression of two platelet-derived growth factor receptor subunits by transforming growth factor- β . *J. Biol. Chem.* 264, 8120-8125.
- Grundmann, S., Hans, F.P., Kinniry, S., Heinke, J., Helbing, T., Bluhm, F., Sluijter, J.P.G., Hofer, I., Pasterkamp, G., Bode, C., Moser, M., 2011. MicroRNA-100 Regulates Neovascularization by Suppression of Mammalian Target of Rapamycin in Endothelial and Vascular Smooth Muscle Cells. *Circulation* 123, 999-1009.
- Gualerzi, A., Kooijmans, S.A.A., Niada, S., Picciolini, S., Brini, A.T., Camussi, G., Bedoni, M., 2019. Raman spectroscopy as a quick tool to assess purity of extracellular vesicle preparations and predict their functionality. *J. Extracell. Vesicles* 8.
- Guan, S., Tang, Q., Liu, W., Zhu, R., Li, B., 2014. Nobiletin inhibits PDGF-BB-induced vascular smooth muscle cell proliferation and migration and attenuates neointimal hyperplasia in a rat carotid artery injury model. *Drug Dev. Res.* 75, 489-496.
- Guglielmi, L., Nardella, M., Musa, C., Cifola, I., Porru, M., Cardinali, B., Iannetti, I., Di Pietro, C., Bolasco, G., Palmieri, V., Vilaro, L., Panini, N., Bonaventura, F., Papi, M., Scavizzi, F., Raspa, M., Leonetti, C., Falcone, G., Felsani, A., D'agnano, I., 2020. Circulating miRNAs in Small Extracellular Vesicles Secreted by a Human Melanoma Xenograft in Mouse Brains. *Cancers* 2020 12.
- Guo, H., Ingolia, N.T., Weissman, J.S., Bartel, D.P., 2010. Mammalian microRNAs predominantly act to decrease target mRNA levels. *Nature* 466, 835-841.
- Guo, J., Xie, N., Li, G., Zhang, Y., Lv, F., Guo, S., Feng, Y., Cao, C.-M., Xiao, R.-P., 2015. p55y functional mimetic peptide N24 blocks vascular

- proliferative disorders. *J. Mol. Med.* 93, 1107-1118.
- Guo, Y., Fu, W., Chen, H., Shang, C., Zhong, M., 2012. miR-24 functions as a tumor suppressor in Hep2 laryngeal carcinoma cells partly through down-regulation of the S100A8 protein. *Oncol. Rep.* 27, 1097-1103.
- Gurunathan, S., Kang, M.H., Qasim, M., Khan, K., Kim, J.H., 2021. Biogenesis, membrane trafficking, functions, and next generation nanotherapeutics medicine of extracellular vesicles. *Int. J. Nanomedicine* 16, 3357-3383.
- Guyton, J.R., Hartley, C.J., 1985. Flow restriction of one carotid artery in juvenile rats inhibits growth of arterial diameter. *Am. J. Physiol.* 248, 540-546.
- Gyuris, A., Navarrete-Perea, J., Jo, A., Cristea, S., Zhou, S., Fraser, K., Wei, Z., Krichevsky, A.M., Weissleder, R., Lee, H., Gygi, S.P., Charest, A., 2019. Physical and Molecular Landscapes of Mouse Glioma Extracellular Vesicles Define Heterogeneity. *Cell Rep.* 27, 3972-3987.
- Ha, M., Kim, V.N., 2014. Regulation of microRNA biogenesis. *Nat. Rev. Mol. Cell Biol.* 2014 15, 509-524.
- Hajar, R., 2017. Risk Factors for Coronary Artery Disease: Historical Perspectives. *Heart Views* 18, 109-114.
- Hall, A.B., Brilakis, E.S., 2019. Saphenous vein graft failure: seeing the bigger picture. *J. Thorac. Dis.* 1, S1441-S1444.
- Ham, O., Lee, S.Y., Song, B.W., Lee, C.Y., Lee, J., Seo, H.H., Kim, S.W., Lim, S., Kim, I.K., Lee, S., Hwang, K.C., 2017. Small molecule-mediated induction of miR-9 suppressed vascular smooth muscle cell proliferation and neointima formation after balloon injury. *Oncotarget* 8, 93360-93372.
- Hammond, S.M., 2015. An overview of microRNAs. *Adv. Drug Deliv. Rev.* 87, 3-14.
- Han, J., Lee, Y., Yeom, K.H., Kim, Y.K., Jin, H., Kim, V.N., 2004. The Drosha-DGCR8 complex in primary microRNA processing. *Genes Dev.* 18, 3016-3027.
- Hannink, M., Donoghue, D.J., 1989. Structure and function of platelet-derived growth factor (PDGF) and related proteins. *Biochim. Biophys. Acta - Rev. Cancer* 989.
- Harding, C., Heuser, J., Stahl, P., 1984. Endocytosis and intracellular processing of transferrin and colloidal gold-transferrin in rat reticulocytes: demonstration of a pathway for receptor shedding. *Eur. J. Cell Biol.* 324, 256-263.
- Harlan, J.M., Thompson, P.J., Ross, R.R., Bowen-Pope, D.F., 1986. Alpha-thrombin induces release of platelet-derived growth factor-like molecule(s) by cultured human endothelial cells. *J. Cell Biol.* 103, 1129-1133.
- Harris, R., Croce, B., Tian, D.H., 2013. Coronary artery bypass grafting. *Ann. Cardiothorac. Surg.* 2.
- Harris, T.A., Yamakuchi, M., Ferlito, M., Mendell, J.T., Lowenstein, C.J., 2008. MicroRNA-126 regulates endothelial expression of vascular cell adhesion molecule 1. *Proc. Natl. Acad. Sci. U. S. A.* 105, 1516-1521.
- Hart, C.E., Clowes, A.W., 1997. Platelet-Derived Growth Factor and Arterial Response to Injury. *Circulation* 95, 555-556.
- Hausenloy, D.J., Mwamure, P.K., Venugopal, V., Harris, J., Barnard, M., Grundy, E., Ashley, E., Vichare, S., Di Salvo, C., Kolvekar, S., Hayward, M., Keogh, B., MacAllister, R.J., Yellon, D.M., 2007. Effect of remote ischaemic preconditioning on myocardial injury in patients undergoing coronary artery bypass graft surgery: a randomised controlled trial. *Lancet* 370, 575-579.
- Havens, M.A., Reich, A.A., Duelli, D.M., Hastings, M.L., 2012. Biogenesis of mammalian microRNAs by a non-canonical processing pathway. *Nucleic*

- Acids Res. 40, 4626-4640.
- He, C., Medley, S.C., Hu, T., Hinsdale, M.E., Lupu, F., Virmani, R., Olson, L.E., 2015. PDGFRB signalling regulates local inflammation and synergizes with hypercholesterolaemia to promote atherosclerosis. *Nat. Commun.* 2015 61 6, 1-14.
- He, M., Gong, Y., Shi, J., Pan, Z., Zou, H., Sun, D., Tu, X., Tan, X., Li, J., Li, W., Liu, B., Xue, J., Sheng, L., Xiu, C., Yang, N., Xue, H., Ding, X., Yu, C., Li, Y., 2014. Plasma MicroRNAs as Potential Noninvasive Biomarkers for In-Stent Restenosis. *PLoS One* 9.
- He, S., Huang, L., Shao, C., Nie, T., Xia, L., Cui, B., Lu, F., Zhu, L., Chen, B., Yang, Q., 2021. Several miRNAs derived from serum extracellular vesicles are potential biomarkers for early diagnosis and progression of Parkinson's disease. *Transl. Neurodegener.* 10, 1-12.
- He, X., Park, S., Chen, Y., Lee, H., 2021. Extracellular Vesicle-Associated miRNAs as a Biomarker for Lung Cancer in Liquid Biopsy. *Front. Mol. Biosci.* 8.
- He, Y., Sun, M.M., Zhang, G.G., Yang, J., Chen, K.S., Xu, W.W., Li, B., 2021. Targeting PI3K/Akt signal transduction for cancer therapy. *Signal Transduct. Target. Ther.* 2021 61 6, 1-17.
- Heegaard, N.H.H., Carlsen, A.L., Lilje, B., Ng, K.L., Rønne, M.E., Jørgensen, H.L., Sennels, H., Fahrenkrug, J., 2016. Diurnal Variations of Human Circulating Cell-Free Micro-RNA. *PLoS One* 11.
- Heiss, E.H., Liu, R., Waltenberger, B., Khan, S., Schachner, D., Kollmann, P., Zimmermann, K., Cabaravdic, M., Uhrin, P., Stuppner, H., Breuss, J.M., Atanasov, A.G., Dirsch, V.M., 2016. Plumericin inhibits proliferation of vascular smooth muscle cells by blocking STAT3 signaling via S-glutathionylation. *Sci. Rep.* 6, 20771.
- Heldin, C.-H., Westermark, B., 1988. Role of Platelet-Derived Growth Factor in Vivo. *Mol. Cell. Biol. Wound Repair* 249-273.
- Heldin, C.H., 2013. Targeting the PDGF signaling pathway in tumor treatment. *Cell Commun. Signal.* 11.
- Heldin, C.H., Lennartsson, J., 2013. Structural and Functional Properties of Platelet-Derived Growth Factor and Stem Cell Factor Receptors. *Cold Spring Harb. Perspect. Biol.* 5, 9100-9101.
- Heldin, C.H., Östman, A., Rönstrand, L., 1998. Signal transduction via platelet-derived growth factor receptors. *Biochim. Biophys. Acta - Rev. Cancer* 1378, 79-113.
- Heldin, C.H., Westermark, B., 1999. Mechanism of action and in vivo role of platelet-derived growth factor. *Physiol. Rev.* 79, 1283-1316.
- Hellström, M., Kalén, M., Lindahl, P., Abramsson, A., Betsholtz, C., 1999. Role of PDGF-B and PDGFR-beta in recruitment of vascular smooth muscle cells and pericytes during embryonic blood vessel formation in the mouse. *Development* 126, 3047-3055.
- Heo, J., Yang, H.C., Rhee, W.J., Kang, H., 2020. Vascular Smooth Muscle Cell-Derived Exosomal MicroRNAs Regulate Endothelial Cell Migration Under PDGF Stimulation. *Cells* 9, 1-16.
- Herring, B.P., Hoggatt, A.M., Burlak, C., Offermanns, S., 2014. Previously differentiated medial vascular smooth muscle cells contribute to neointima formation following vascular injury. *Vasc. Cell* 6.
- Hessvik, N.P., Llorente, A., 2018. Current knowledge on exosome biogenesis and release. *Cell. Mol. Life Sci.* 75, 193-208.
- Hinnebusch, A.G., 2014. The Scanning Mechanism of Eukaryotic Translation

- Initiation. *Annu. Rev. Biochem.* 83, 779-812.
- Hoch, R. V., Soriano, P., 2003. Roles of PDGF in animal development. *Development* 130, 4769-4784.
- Hood, J.L., 2016. Post isolation modification of exosomes for nanomedicine applications. *Nanomedicine* 11, 1745-1756.
- Hood, J.L., Wickline, S.A., 2012. A systematic approach to exosome-based translational nanomedicine. *Wiley Interdiscip. Rev. Nanomedicine Nanobiotechnology* 4, 458-467.
- Hoshino, A., Costa-Silva, B., Shen, T.L., Rodrigues, G., Hashimoto, A., Tesic Mark, M., Molina, H., Kohsaka, S., Di Giannatale, A., Ceder, S., Singh, S., Williams, C., Soplop, N., Uryu, K., Pharmed, L., King, T., Bojmar, L., Davies, A.E., Ararso, Y., Zhang, T., Zhang, H., Hernandez, J., Weiss, J.M., Dumont-Cole, V.D., Kramer, K., Wexler, L.H., Narendran, A., Schwartz, G.K., Healey, J.H., Sandstrom, P., Jørgen Labori, K., Kure, E.H., Grandgenett, P.M., Hollingsworth, M.A., De Sousa, M., Kaur, S., Jain, M., Mallya, K., Batra, S.K., Jarnagin, W.R., Brady, M.S., Fodstad, O., Muller, V., Pantel, K., Minn, A.J., Bissell, M.J., Garcia, B.A., Kang, Y., Rajasekhar, V.K., Ghajar, C.M., Matei, I., Peinado, H., Bromberg, J., Lyden, D., 2015. Tumour exosome integrins determine organotropic metastasis. *Nature* 527, 329-335.
- Hu, Y., Zou, Y., Dietrich, H., Wick, G., Xu, Q., 1999. Inhibition of Neointima Hyperplasia of Mouse Vein Grafts by Locally Applied Suramin. *Circulation* 100, 861-868.
- Huang, C., Huang, W., Wang, R., He, Y., 2020. Ulinastatin Inhibits the Proliferation, Invasion and Phenotypic Switching of PDGF-BB-Induced VSMCs via Akt/eNOS/NO/cGMP Signaling Pathway. *Drug Des. Devel. Ther.* 14, 5505-5514.
- Huang, C., Mei, H., Zhou, M., Zheng, X., 2017. A novel PDGF receptor inhibitor-eluting stent attenuates in-stent neointima formation in a rabbit carotid model. *Mol. Med. Rep.* 15, 21-28.
- Huang, H.Y., Lin, Y.C.D., Li, J., Huang, K.Y., Shrestha, S., Hong, H.C., Tang, Y., Chen, Y.G., Jin, C.N., Yu, Y., Xu, J.T., Li, Y.M., Cai, X.X., Zhou, Z.Y., Chen, X.H., Pei, Y.Y., Hu, L., Su, J.J., Cui, S.D., Wang, F., Xie, Y.Y., Ding, S.Y., Luo, M.F., Chou, C.H., Chang, N.W., Chen, K.W., Cheng, Y.H., Wan, X.H., Hsu, W.L., Lee, T.Y., Wei, F.X., Huang, H. Da, 2020. MiRTarBase 2020: Updates to the experimentally validated microRNA-target interaction database. *Nucleic Acids Res.* 48, D148-D154.
- Huang, K., Bao, H., Yan, Z.Q., Wang, L., Zhang, P., Yao, Q.P., Shi, Q., Chen, X.H., Wang, K.X., Shen, B.R., Qi, Y.X., Jiang, Z.L., 2017. MicroRNA-33 protects against neointimal hyperplasia induced by arterial mechanical stretch in the grafted vein. *Cardiovasc. Res.* 113, 488-497.
- Huang, W., Tian, S.S., Hang, P.Z., Sun, C., Guo, J., Du, Z.M., 2016. Combination of microRNA-21 and microRNA-146a Attenuates Cardiac Dysfunction and Apoptosis During Acute Myocardial Infarction in Mice. *Mol. Ther. - Nucleic Acids* 5.
- Huang, X., Yuan, T., Tschannen, M., Sun, Z., Jacob, H., Du, M., Liang, Meihua, Dittmar, R.L., Liu, Y., Liang, Mingyu, Kohli, M., Thibodeau, S.N., Boardman, L., Wang, L., 2013. Characterization of human plasma-derived exosomal RNAs by deep sequencing. *BMC Genomics* 14, 1-14.
- Hung, M.E., Leonard, J.N., 2015. Stabilization of exosome-targeting peptides via engineered glycosylation. *J. Biol. Chem.* 290, 8166-8172.
- Huntzinger, E., Izaurralde, E., 2011. Gene silencing by microRNAs: contributions of translational repression and mRNA decay. *Nat. Rev. Genet.* 12, 99-110.

- Hurwitz, S.N., Olcese, J.M., Meckes, D.G., 2019. Extraction of extracellular vesicles from whole tissue. *J. Vis. Exp.*
- Iaconetti, C., Polimeni, A., Sorrentino, S., Sabatino, J., Pironti, G., Esposito, G., Curcio, A., Indolfi, C., 2012. Inhibition of miR-92a increases endothelial proliferation and migration in vitro as well as reduces neointimal proliferation in vivo after vascular injury. *Basic Res. Cardiol.* 107, 1-14.
- Inoue, T., Croce, K., Morooka, T., Sakuma, M., Node, K., Simon, D.I., 2011. Vascular inflammation and repair: Implications for re-endothelialization, restenosis, and stent thrombosis. *JACC Cardiovasc. Interv.* 4, 1057-1066.
- Inoue, T., Sohma, R., Miyazaki, T., Iwasaki, Y., Yaguchi, I., Morooka, S., 2000. Comparison of activation process of platelets and neutrophils after coronary stent implantation versus balloon angioplasty for stable angina pectoris. *Am. J. Cardiol.* 86, 1057-1062.
- Ipsaro, J.J., Joshua-Tor, L., 2015. From guide to target: molecular insights into eukaryotic RNA-interference machinery. *Nat. Struct. Mol. Biol.* 22, 20-28.
- Italiano, J.E., Mairuhu, A.T., Flaumenhaft, R., 2010. Clinical Relevance of Microparticles from Platelets and Megakaryocytes. *Curr. Opin. Hematol.* 17, 578-584.
- Iwai, K., Minamisawa, T., Suga, K., Yajima, Y., Shiba, K., 2016. Isolation of human salivary extracellular vesicles by iodixanol density gradient ultracentrifugation and their characterizations. *J. Extracell. Vesicles* 5.
- Jackson, C.L., Raines, E.W., Ross, R., Reidy, M.A., 1993. Role of endogenous platelet-derived growth factor in arterial smooth muscle cell migration after balloon catheter injury. *Arterioscler. Thromb. A J. Vasc. Biol.* 13, 1218-1226.
- Jackson, R.J., Hellen, C.U.T., Pestova, T. V., 2010. The mechanism of eukaryotic translation initiation and principles of its regulation. *Nat. Rev. Mol. Cell Biol.* 11, 113-127.
- Jamaluddin, M.S., Weakley, S.M., Zhang, L., Kougias, P., Lin, P.H., Yao, Q., Chen, C., 2011. miRNAs: roles and clinical applications in vascular disease. *Expert Rev. Mol. Diagn.* 11, 79-89.
- James, K., Bryl-Gorecka, P., Olde, B., Gidlof, O., Tornngren, K., Erlinge, D., 2022. Increased expression of miR-224-5p in circulating extracellular vesicles of patients with reduced coronary flow reserve. *BMC Cardiovasc. Disord.* 22.
- Jansen, F., Stumpf, T., Proebsting, S., Franklin, B.S., Wenzel, D., Pfeifer, P., Flender, A., Schmitz, T., Yang, X., Fleischmann, B.K., Nickenig, G., Werner, N., 2017. Intercellular transfer of miR-126-3p by endothelial microparticles reduces vascular smooth muscle cell proliferation and limits neointima formation by inhibiting LRP6. *J. Mol. Cell. Cardiol.* 104, 43-52.
- Jansen, F., Yang, X., Hoelscher, M., Cattelan, A., Schmitz, T., Proebsting, S., Wenzel, D., Vosen, S., Franklin, B.S., Fleischmann, B.K., Nickenig, G., Werner, N., 2013. Endothelial Microparticle-Mediated Transfer of MicroRNA-126 Promotes Vascular Endothelial Cell Repair via SPRED1 and Is Abrogated in Glucose-Damaged Endothelial Microparticles. *Circulation* 128, 2026-2038.
- Janssens, S., Flaherty, D., Nong, Z., Varenne, O., Van Pelt, N., Haustermans, C., Zoldhelyi, P., Gerard, R., Collen, D., Nabel, E., 1998. Human Endothelial Nitric Oxide Synthase Gene Transfer Inhibits Vascular Smooth Muscle Cell Proliferation and Neointima Formation After Balloon Injury in Rats. *Circulation* 97, 1274-1281.
- Jawien, A., Bowen-Pope, D.F., Lindner, V., Schwartz, S.M., Clowes, A.W., 1992. Platelet-derived growth factor promotes smooth muscle migration and

- intimal thickening in a rat model of balloon angioplasty. *J. Clin. Invest.* 89, 507-511.
- Jayawardena, E., Medzikovic, L., Ruffenach, G., Eghbali, M., 2022. Role of miRNA-1 and miRNA-21 in Acute Myocardial Ischemia-Reperfusion Injury and Their Potential as Therapeutic Strategy. *Int. J. Mol. Sci.* 23.
- Jean, S., Kiger, A.A., 2014. Classes of phosphoinositide 3-kinases at a glance. *J. Cell Sci.* 127, 923-928.
- Jenjaroenpun, P., Kremenska, Y., Nair, V.M., Kremensky, M., Joseph, B., Kurochkin, I. V., 2013. Characterization of RNA in exosomes secreted by human breast cancer cell lines using next-generation sequencing. *PeerJ* 1, e201.
- Jensen, L.O., Christiansen, E.H., 2019. Are drug-eluting stents safer than bare-metal stents? *Lancet* 393, 2472-2474.
- Jeremy, J.Y., Rowe, D., Emsley, A.M., Newby, A.C., 1999. Nitric oxide and the proliferation of vascular smooth muscle cells. *Cardiovasc. Res.* 43, 580-594.
- Ji, R., Cheng, Y., Yue, J., Yang, J., Liu, X., Chen, H., Dean, D.B., Zhang, C., 2007. MicroRNA Expression Signature and Antisense-Mediated Depletion Reveal an Essential Role of MicroRNA in Vascular Neointimal Lesion Formation. *Circ. Res.* 100, 1579-1588.
- Ji, Y., Lee, D., Kim, V., Muth, D., Witwer, K.W., 2015. Validated MicroRNA Target Databases: an Evaluation. *Drug Dev. Res.* 389-396.
- Jo, M.H., Shin, S., Jung, S.R., Kim, E., Song, J.J., Hohng, S., 2015. Human Argonaute 2 Has Diverse Reaction Pathways on Target RNAs. *Mol. Cell* 59, 117-124.
- Johnsen, K.B., Gudbergsson, J.M., Skov, M.N., Christiansen, G., Gurevich, L., Moos, T., Duroux, M., 2016. Evaluation of electroporation-induced adverse effects on adipose-derived stem cell exosomes. *Cytotechnology* 68, 2125-2138.
- Jonas, S., Izaurralde, E., 2015. Towards a molecular understanding of microRNA-mediated gene silencing. *Nat. Rev. Genet.* 16, 421-433.
- Joner, M., Finn, A. V., Farb, A., Mont, E.K., Kolodgie, F.D., Ladich, E., Kutys, R., Skorija, K., Gold, H.K., Virmani, R., 2006. Pathology of Drug-Eluting Stents in Humans. Delayed Healing and Late Thrombotic Risk. *J. Am. Coll. Cardiol.* 48, 193-202.
- Jonkman, J.E.N., Cathcart, J.A., Xu, F., Bartolini, M.E., Amon, J.E., Stevens, K.M., Colarusso, P., 2014. An introduction to the wound healing assay using live-cell microscopy. *Cell Adh. Migr.* 8, 440-451.
- Joop, K., Berckmans, R.J., Nieuwland, R., Berkhout, J., Romijn, F.P.H.T.M., Hack, C.E., Sturk, A., 2001. Microparticles from patients with multiple organ dysfunction syndrome and sepsis support coagulation through multiple mechanisms. *Thromb. Haemost.* 85, 810-820.
- Jovanovic, M., Hengartner, M.O., 2006. miRNAs and apoptosis: RNAs to die for. *Oncogene* 2006 2546 25, 6176-6187.
- Jukema, J W, Verschuren, J J W, Ahmed, T A N, Jukema, J Wouter, Verschuren, Jeffrey J W, Ahmed, Tarek A N, Quax, P.H.A., 2011. Restenosis after PCI. Part 1: pathophysiology and risk factors. *Nat. Rev. Cardiol.* 2011 91 9, 53-62.
- Jung, H.H., Kim, J.Y., Lim, J.E., Im, Y.H., 2020. Cytokine profiling in serum-derived exosomes isolated by different methods. *Sci. Rep.* 10.
- Jy, W., Gómez-Marín, O., Salerno, T.A., Panos, A.L., Williams, D., Horstman, L.L., Ahn, Y.S., 2015. Presurgical levels of circulating cell-derived microparticles discriminate between patients with and without transfusion

- in coronary artery bypass graft surgery. *J. Thorac. Cardiovasc. Surg.* 149, 305-311.
- Kajimoto, T., Okada, T., Miya, S., Zhang, L., Nakamura, S.I., 2013. Ongoing activation of sphingosine 1-phosphate receptors mediates maturation of exosomal multivesicular endosomes. *Nat. Commun.* 4.
- Kalluri, R., LeBleu, V.S., 2020. The biology, function, and biomedical applications of exosomes. *Science* (80-.). 367, eaau6977.
- Kamerkar, S., Lebleu, V.S., Sugimoto, H., Yang, S., Ruivo, C.F., Melo, S.A., Lee, J.J., Kalluri, R., 2017. Exosomes facilitate therapeutic targeting of oncogenic KRAS in pancreatic cancer. *Nature* 546, 498-503.
- Kanehisa, M., Goto, S., Furumichi, M., Tanabe, M., Hirakawa, M., 2010. KEGG for representation and analysis of molecular networks involving diseases and drugs. *Nucleic Acids Res.* 38, 355-360.
- Karagkouni, D., Paraskevopoulou, M.D., Chatzopoulos, S., Vlachos, I.S., Tastsoglou, S., Kanellos, I., Papadimitriou, D., Kavakiotis, I., Maniou, S., Skoufos, G., Vergoulis, T., Dalamagas, T., Hatzigeorgiou, A.G., 2018. DIANA-TarBase v8: A decade-long collection of experimentally supported miRNA-gene interactions. *Nucleic Acids Res.* 46, D239-D245.
- Kardas, G., Daszyńska-Kardas, A., Marynowski, M., Brząkalska, O., Kuna, P., Panek, M., 2020. Role of Platelet-Derived Growth Factor (PDGF) in Asthma as an Immunoregulatory Factor Mediating Airway Remodeling and Possible Pharmacological Target. *Front. Pharmacol.* 11.
- Karimi, N., Cvjetkovic, A., Jang, S.C., Crescitelli, R., Hosseinpour Feizi, M.A., Nieuwland, R., Lötvall, J., Lässer, C., 2018. Detailed analysis of the plasma extracellular vesicle proteome after separation from lipoproteins. *Cell. Mol. Life Sci.* 75.
- Kaufmann, D., Daniłowicz-Szymanowicz, L., Sakowicz-Burkiewicz, M., Szwoch, M., Pawełczyk, T., Raczak, G., 2019. Expression profile of circulating microRNAs in patients with ischemic heart failure with moderately reduced left ventricular ejection fraction - pilot study. *Eur. J. Transl. Clin. Med.* 1, 53-57.
- Kaur, A., Mackin, S.T., Schlosser, K., Wong, F.L., Elharram, M., Delles, C., Stewart, D.J., Dayan, N., Landry, T., Pilote, L., 2020. Systematic review of microRNA biomarkers in acute coronary syndrome and stable coronary artery disease. *Cardiovasc. Res.* 116, 1113-1124.
- Kawakami, Y., Nishimoto, H., Kitaura, J., Maeda-Yamamoto, M., Kato, R.M., Littman, D.R., Rawlings, D.J., Kawakami, T., 2004. Protein kinase C beta11 regulates Akt phosphorylation on Ser-473 in a cell type- and stimulus-specific fashion. *J. Biol. Chem.* 279, 47720-47725.
- Kawamata, T., Tomari, Y., 2010. Making RISC. *Trends Biochem. Sci.* 35, 368-376.
- Kawasaki, T., Dewerchin, M., Lijnen, H.R., Vreys, I., Vermylen, J., Hoylaerts, M.F., 2001. Mouse Carotid Artery Ligation Induces Platelet-Leukocyte-Dependent Luminal Fibrin, Required for Neointima Development. *Circ. Res.* 88, 159-166.
- Kazlauskas, A., Cooper, J.A., 1989. Autophosphorylation of the PDGF receptor in the kinase insert region regulates interactions with cell proteins. *Cell* 58, 1121-1133.
- Kertesz, M., Iovino, N., Unnerstall, U., Gaul, U., Segal, E., 2007. The role of site accessibility in microRNA target recognition. *Nat. Genet.* 2007 3910 39, 1278-1284.
- Kesidou, D., da Costa Martins, P.A., de Windt, L.J., Brittan, M., Beqqali, A., Baker, A.H., 2020. Extracellular Vesicle miRNAs in the Promotion of Cardiac

- Neovascularisation. *Front. Physiol.* 11.
- Kharmate, G., Hosseini-Beheshti, E., Caradec, J., Chin, M.Y., Tomlinson Guns, E.S., 2016. Correction: Epidermal Growth Factor Receptor in Prostate Cancer Derived Exosomes. *PLoS One* 11.
- Khatri, P., Drăghici, S., 2005. Ontological analysis of gene expression data: current tools, limitations, and open problems. *Bioinformatics* 21, 3587-3595.
- Kijani, S., Maria V Azquez, A., Levin, M., Bor En, J., Fogelstrand, P., 2017. Intimal hyperplasia induced by vascular intervention causes lipoprotein retention and accelerated atherosclerosis. *Physiol Rep* 5.
- Kim, M.S., Dean, L.S., 2011. In-Stent Restenosis. *Cardiovasc. Ther.* 29, 190-198.
- Kim, Y., Park, J.K., Seo, J.H., Ryu, H.S., Lim, K.S., Jeong, M.H., Kang, D.H., Kang, S.W., 2018. A rapamycin derivative, biolimus, preferentially activates autophagy in vascular smooth muscle cells. *Sci. Reports* 2018 8, 1-13.
- Kleinedler, J.J., Foley, J.D., Orchard, E.A., Dugas, T.R., 2012. Novel nanocomposite stent coating releasing resveratrol and quercetin reduces neointimal hyperplasia and promotes re-endothelialization. *J. Control. Release* 159, 27-33.
- Klinghoffer, R.A., Duckworth, B., Valius, M., Cantley, L., Kazlauskas, A., 1996. Platelet-derived growth factor-dependent activation of phosphatidylinositol 3-kinase is regulated by receptor binding of SH2-domain-containing proteins which influence Ras activity. *Mol. Cell. Biol.* 16, 5905-5914.
- Klumperman, J., Raposo, G., 2014. The complex ultrastructure of the endolysosomal system. *Cold Spring Harb. Perspect. Biol.* 6.
- Knuuti, J., Wijns, W., Achenbach, S., Agewall, S., Barbato, E., Bax, J.J., Capodanno, D., Cuisset, T., Deaton, C., Dickstein, K., Edvardsen, T., Escaned, J., Funck-Brentano, C., Gersh, B.J., Gilard, M., Hasdai, D., Hatala, R., Mahfoud, F., Masip, J., Muneretto, C., Prescott, E., Saraste, A., Storey, R.F., Svitil, P., Valgimigli, M., Windecker, S., Aboyans, V., Baigent, C., Collet, J.P., Dean, V., Delgado, V., Fitzsimons, D., Gale, C.P., Grobbee, D.E., Halvorsen, S., Hindricks, G., Iung, B., Juni, P., Katus, H.A., Landmesser, U., Leclercq, C., Lettino, M., Lewis, B.S., Merkely, B., Mueller, C., Petersen, S., Petronio, A.S., Richter, D.J., Roffi, M., Shlyakhto, E., Simpson, I.A., Sousa-Uva, M., Touyz, R.M., Benkhedda, S., Metzler, B., Sujayeva, V., Cosyns, B., Kusljagic, Z., Velchev, V., Panayi, G., Kala, P., Haahr-Pedersen, S.A., Kabil, H., Ainla, T., Kaukonen, T., Cayla, G., Pagava, Z., Woehrle, J., Kanakakis, J., Toth, K., Gudnason, T., Peace, A., Aronson, D., Riccio, C., Elezi, S., Mirrakhimov, E., Hansone, S., Sarkis, A., Babarskiene, R., Beissel, J., Cassar Maempel, A.J., Revenco, V., de Grooth, G.J., Pejkov, H., Juliebø, V., Lipiec, P., Santos, J., Chioncel, O., Duplyakov, D., Bertelli, L., Dikic, A.D., Studencan, M., Bunc, M., Alfonso, F., Back, M., Zellweger, M., Addad, F., Yildirim, A., Sirenko, Y., Clapp, B., 2020. 2019 ESC guidelines for the diagnosis and management of chronic coronary syndromes. *Eur. Heart J.* 41, 407-477.
- Kockx, M.M., Cambier, B.A., Bortier, H.E., De Meyer, G.R., Van Cauwelaert, P.A., 1992. The modulation of smooth muscle cell phenotype is an early event in human aorto-coronary saphenous vein grafts. *Virchows Arch. A. Pathol. Anat. Histopathol.* 420, 155-162.
- Kockx, M.M., De Meyer, G.R.Y., Bortier, H., De Meyere, N., Muhring, J., Bakker, A., Jacob, W., Van Vaeck, L., Herman, A., 1996. Luminal Foam Cell Accumulation Is Associated With Smooth Muscle Cell Death in the Intimal Thickening of Human Saphenous Vein Grafts. *Circulation* 94, 1255-1262.
- Koga, J.I., Nakano, T., Dahlman, J.E., Figueiredo, J.L., Zhang, H., Decano, J.,

- Khan, O.F., Niida, T., Iwata, H., Aster, J.C., Yagita, H., Anderson, D.G., Keith Ozaki, C., Aikawa, M., 2015. Macrophage Notch ligand Delta-like 4 promotes vein graft lesion development: implications for the treatment of vein graft failure. *Arterioscler. Thromb. Vasc. Biol.* 35, 2343-2353.
- Kohler, N., Lipton, A., 1974. Platelets as a source of fibroblast growth-promoting activity. *Exp. Cell Res.* 87, 297-301.
- Kohler, T.R., Kirkman, T.R., Kraiss, L.W., Zierler, B.K., Clowes, A.W., 1991. Increased blood flow inhibits neointimal hyperplasia in endothelialized vascular grafts. *Circ. Res.* 69, 1557-1565.
- Konstantinidou, A., Mougios, V., Sidossis, L.S., 2016. Acute Exercise Alters the Levels of Human Saliva miRNAs Involved in Lipid Metabolism. *Int. J. Sports Med.* 37, 584-588.
- Kooijmans, S.A.A., Stremersch, S., Braeckmans, K., De Smedt, S.C., Hendrix, A., Wood, M.J.A., Schiffelers, R.M., Raemdonck, K., Vader, P., 2013. Electroporation-induced siRNA precipitation obscures the efficiency of siRNA loading into extracellular vesicles. *J. Control. Release* 172, 229-238.
- Koppers-Lalic, D., Hackenberg, M., Bijnsdorp, I. V., van Eijndhoven, M.A.J., Sadek, P., Sie, D., Zini, N., Middeldorp, J.M., Ylstra, B., de Menezes, R.X., Würdinger, T., Meijer, G.A., Pegtel, D.M., 2014. Nontemplated nucleotide additions distinguish the small RNA composition in cells from exosomes. *Cell Rep.* 8, 1649-1658.
- Kosaka, N., Iguchi, H., Yoshioka, Y., Hagiwara, K., Takeshita, F., Ochiya, T., 2012. Competitive interactions of cancer cells and normal cells via secretory microRNAs. *J. Biol. Chem.* 287, 1397-1405.
- Kosaka, N., Iguchi, H., Yoshioka, Y., Takeshita, F., Matsuki, Y., Ochiya, T., 2010. Secretory Mechanisms and Intercellular Transfer of MicroRNAs in Living Cells. *J. Biol. Chem.* 285, 17442-17452.
- Kourembanas, S., Morita, T., Liu, Y., Christou, H., 1997. Mechanisms by which oxygen regulates gene expression and cell-cell interaction in the vasculature. *Kidney Int.* 51, 438-443.
- Kowal, J., Arras, G., Colombo, M., Jouve, M., Morath, J.P., Primdal-Bengtson, B., Dingli, F., Loew, D., Tkach, M., Théry, C., 2016. Proteomic comparison defines novel markers to characterize heterogeneous populations of extracellular vesicle subtypes. *Proc. Natl. Acad. Sci. U. S. A.* 113, 968-977.
- Kowal, J., Tkach, M., Théry, C., 2014. Biogenesis and secretion of exosomes. *Curr. Opin. Cell Biol.* 29, 116-125.
- Kowalinski, E., Kögel, A., Ebert, J., Reichelt, P., Stegmann, E., Habermann, B., Conti, E., 2016. Structure of a Cytoplasmic 11-Subunit RNA Exosome Complex. *Mol. Cell* 63, 125-134.
- Kozomara, A., Hunt, S., Ninova, M., Griffiths-Jones, S., Ronshaugen, M., 2014. Target Repression Induced by Endogenous microRNAs: Large Differences, Small Effects. *Small Eff. PLoS ONE* 9.
- Kraemer, R., 2002. Reduced apoptosis and increased lesion development in the flow-restricted carotid artery of p75(NTR)-null mutant mice. *Circ. Res.* 91, 494-500.
- Krek, A., Grün, D., Poy, M.N., Wolf, R., Rosenberg, L., Epstein, E.J., MacMenamin, P., Da Piedade, I., Gunsalus, K.C., Stoffel, M., Rajewsky, N., 2005. Combinatorial microRNA target predictions. *Nat. Genet.* 37, 495-500.
- Kroening, S., Goppelt-Struebe, M., 2010. Analysis of matrix-dependent cell migration with a barrier migration assay. *Sci. Signal.* 3.
- Krützfeldt, J., Rajewsky, N., Braich, R., Rajeev, K.G., Tuschl, T., Manoharan, M., Stoffel, M., 2005. Silencing of microRNAs in vivo with 'antagomirs.' *Nat.*

- 2005 4387068 438, 685-689.
- Kumar, A., Lindner, V., 1997. Remodeling with neointima formation in the mouse carotid artery after cessation of blood flow. *Arterioscler. Thromb. Vasc. Biol.* 17, 2238-2244.
- Kundra, V., Escobedo, J.A., Kazlauskas, A., Kim, H.K., Rhee, S.G., Williams, L.T., Zetter, B.R., 1994. Regulation of chemotaxis by the platelet-derived growth factor receptor-beta. *Nature* 367, 474-476.
- Kusnierova, P., Pleva, L., 2017. Matrix Metalloproteinases MMP-3 and MMP-9 as Predictors of In-Stent Restenosis, in: *The Role of Matrix Metalloproteinase in Human Body Pathologies*. InTech, pp. 57-69.
- Kuzuya, M., Kanda, S., Sasaki, T., Tamaya-Mori, N., Cheng, X.W., Itoh, T., Itohara, S., Iguchi, A., 2003. Deficiency of gelatinase a suppresses smooth muscle cell invasion and development of experimental intimal hyperplasia. *Circulation* 108, 1375-1381.
- Kwak, P.B., Tomari, Y., 2012. The N domain of Argonaute drives duplex unwinding during RISC assembly. *Nat. Struct. Mol. Biol.* 2012 192 19, 145-151.
- Kwei, S., Stavrakis, G., Takahas, M., Taylor, G., Folkman, M.J., Gimbrone, M.A., García-Cardena, G., 2004. Early Adaptive Responses of the Vascular Wall during Venous Arterialization in Mice. *Am. J. Pathol.* 164, 81-89.
- La Rocca, G., Cavalieri, V., 2022. Roles of the Core Components of the Mammalian miRISC in Chromatin Biology. *Genes (Basel)*. 13.
- Lake, D., Corrêa, S.A.L., Müller, J., 2016. Negative feedback regulation of the ERK1/2 MAPK pathway. *Cell. Mol. Life Sci.* 73, 4397-4413.
- Lamichhane, T.N., Raiker, R.S., Jay, S.M., 2015. Exogenous DNA Loading into Extracellular Vesicles via Electroporation is Size-Dependent and Enables Limited Gene Delivery. *Mol. Pharm.* 12, 3650-3657.
- Lang, I.M., Badr-Eslam, R., Greenlaw, N., Young, R., Steg, P.G., 2017. Management and clinical outcome of stable coronary artery disease in Austria: Results from 5 years of the CLARIFY registry. *Wien. Klin. Wochenschr.* 129, 879-892.
- Langevin, S.M., Kuhnell, D., Biesiada, J., Zhang, X., Medvedovic, M., Talaska, G.G., Burns, K.A., Kasper, S., 2020. Comparability of the small RNA secretome across human biofluids concomitantly collected from healthy adults. *PLoS One* 15.
- Langille, B.L., O'Donnell, F., 1986. Reductions in arterial diameter produced by chronic decreases in blood flow are endothelium-dependent. *Science* 231, 405-407.
- Langmead, B., Trapnell, C., Pop, M., Salzberg, S.L., 2009. Ultrafast and memory-efficient alignment of short DNA sequences to the human genome. *Genome Biol.* 10, 25.1-25.10.
- Lardenoye, J.H.P., de Vries, M.R., Deckers, M., van Lent, N., Hanemaaijer, R., van Bockel, J.H., Quax, P.H.A., 2005. Inhibition of intimal hyperplasia by the tetracycline derived mmp inhibitor doxycycline in vein graft disease in vitro and in vivo. *EuroIntervention* 1, 236-243.
- Lardenoye, J.H.P., de Vries, M.R., Löwik, C.W.G.M., Xu, Q., Dhore, C.R., Cleutjens, J.P.M., van Hinsbergh, V.W.M., van Bockel, J.H., Quax, P.H.A., 2002. Accelerated Atherosclerosis and Calcification in Vein Grafts. *Circ. Res.* 91, 577-584.
- Lässer, C., Shelke, G.V., Yeri, A., Kim, D.K., Crescitelli, R., Raimondo, S., Sjöstrand, M., Ghosh, Y.S., Van Keuren Jensen, K., Lötval, J., 2017. Two distinct extracellular RNA signatures released by a single cell type identified

- by microarray and next-generation sequencing. *RNA Biol.* 14, 58-72.
- Laulagnier, K., Javalet, C., Hemming, F.J., Chivet, M., Lachenal, G., Blot, B., Chatellard, C., Sadoul, R., 2018. Amyloid precursor protein products concentrate in a subset of exosomes specifically endocytosed by neurons. *Cell. Mol. Life Sci.* 75, 757-773.
- Lawton, J.S., Tamis-Holland, J.E., Bangalore, S., Bates, E.R., Beckie, T.M., Bischoff, J.M., Bittl, J.A., Cohen, M.G., DiMaio, J.M., Don, C.W., Fremes, S.E., Gaudino, M.F., Goldberger, Z.D., Grant, M.C., Jaswal, J.B., Kurlansky, P.A., Mehran, R., Metkus, T.S., Nnacheta, L.C., Rao, S. V., Sellke, F.W., Sharma, G., Yong, C.M., Zwischenberger, B.A., 2022. 2021 ACC/AHA/SCAI Guideline for Coronary Artery Revascularization: A Report of the American College of Cardiology/American Heart Association Joint Committee on Clinical Practice Guidelines. *J. Am. Coll. Cardiol.* 79, 21-129.
- Leclercq, A., Houard, X., Philippe, M., Ollivier, V., Sebbag, U., Meilhac, O., Michel, J.-B., 2007. Involvement of intraplaque hemorrhage in atherothrombosis evolution via neutrophil protease enrichment. *J. Leukoc. Biol.* 82, 1420-1429.
- Lee, M.S., David, E.M., Makkar, R.R., Wilentz, J.R., 2004. Molecular and cellular basis of restenosis after percutaneous coronary intervention: The intertwining roles of platelets, leukocytes, and the coagulation-fibrinolysis system. *J. Pathol.* 203, 861-870.
- Lee, R.C., Feinbaum, R.L., Ambrost, V., 1993. The *C. elegans* Heterochronic Gene *lin-4* Encodes Small RNAs with Antisense Complementarity to *lin-14*. *Cell* 75, 843-854.
- Lee, Y., Jeon, K., Lee, J.T., Kim, S., Kim, V.N., 2002. MicroRNA maturation: stepwise processing and subcellular localization. *EMBO J.* 21, 4663-4670.
- Lee, Y., Kim, M., Han, J., Yeom, K.H., Lee, S., Baek, S.H., Kim, V.N., 2004. MicroRNA genes are transcribed by RNA polymerase II. *EMBO J.* 23, 4051-4060.
- Leiss, M., Beckmann, K., Girós, A., Costell, M., Fässler, R., 2008. The role of integrin binding sites in fibronectin matrix assembly in vivo. *Curr. Opin. Cell Biol.* 20, 502-507.
- Lemmon, M.A., Schlessinger, J., 2010. Cell signaling by receptor-tyrosine kinases. *Cell* 141, 1117-1134.
- Lennaárd, A.J., Mamand, D.R., Wiklander, R.J., Andaloussi, S.E.L., Wiklander, O.P.B., 2022. Optimised electroporation for loading of extracellular vesicles with doxorubicin. *Pharmaceutics* 14.
- Lewis, B.P., Burge, C.B., Bartel, D.P., 2005. Conserved seed pairing, often flanked by adenosines, indicates that thousands of human genes are microRNA targets. *Cell* 120, 15-20.
- Lewis, B.P., Shih, I.H., Jones-Rhoades, M.W., Bartel, D.P., Burge, C.B., 2003. Prediction of Mammalian MicroRNA Targets. *Cell* 115, 787-798.
- Lewis, C.D., Olson, N.E., Raines, E.W., Reidy, M.A., Jackson, C.L., 2001. Modulation of smooth muscle proliferation in rat carotid artery by platelet-derived mediators and fibroblast growth factor-2. *Platelets* 12, 352-358.
- Li, B., Antonyak, M.A., Zhang, J., Cerione, R.A., 2012. RhoA triggers a specific signaling pathway that generates transforming microvesicles in cancer cells. *Oncogene* 31, 4740-4749.
- Li, G., Xie, N., Yao, Y., Zhang, Y., Guo, J., Feng, Y., Lv, F., Xiao, R.P., Cao, C.M., 2015. Identification of PI3K regulatory subunit p55 γ as a novel inhibitor of vascular smooth muscle cell proliferation and neointimal formation. *Cardiovasc. Res.* 105, 75-85.

- Li, J., Liu, X., Li, C., Wang, W., 2019. miR-224-5p inhibits proliferation, migration, and invasion by targeting PIK3R3/AKT3 in uveal melanoma. *J. Cell. Biochem.* 120, 12412-12421.
- Li, L., Blumenthal, D.K., Terry, C.M., He, Y., Carlson, M.L., Cheung, A.K., 2011. PDGF-Induced Proliferation in Human Arterial and Venous Smooth Muscle Cells: Molecular Basis for Differential Effects of PDGF Isoforms. *J. Cell. Biochem.* 112, 289-298.
- Li, L., Lu, S., Liang, X., Cao, B., Wang, S., Jiang, J., Luo, H., He, S., Lang, J., Zhu, G., 2019. $\gamma\delta$ TDEs: An Efficient Delivery System for miR-138 with Anti-tumoral and Immunostimulatory Roles on Oral Squamous Cell Carcinoma. *Mol. Ther. Nucleic Acids* 14, 101-113.
- Li, P., Li, Y.L., Li, Z.Y., Wu, Y.N., Zhang, C.C., Xi, A., Wang, C.X., Shi, H.T., Hui, M.Z., Xie, B., Ahmed, M., Du, J., 2014. Cross talk between vascular smooth muscle cells and monocytes through interleukin-1 β /interleukin-18 signaling promotes vein graft thickening. *Arterioscler. Thromb. Vasc. Biol.* 34, 2001-2011.
- Li, W., Zhang, J., Flechner, L., Hyun, T., Yam, A., Franke, T.F., Pierce, J.H., 1999. Protein kinase C- α overexpression stimulates Akt activity and suppresses apoptosis induced by interleukin 3 withdrawal. *Oncogene* 1999 1847 18, 6564-6572.
- Li, Y., Shen, Z., Yu, X.Y., 2015. Transport of microRNAs via exosomes. *Nat. Rev. Cardiol.* 2015 124 12, 198-198.
- Liao, Z., Chen, Y., Duan, C., Zhu, K., Huang, R., Zhao, H., Hintze, M., Pu, Q., Yuan, Z., Lv, L., Chen, H., Lai, B., Feng, S., Qi, X., Cai, D., 2021. Cardiac telocytes inhibit cardiac microvascular endothelial cell apoptosis through exosomal miRNA-21-5p-targeted cdip1 silencing to improve angiogenesis following myocardial infarction. *Theranostics* 11, 268-291.
- Lindner, V., Fingerle, J., Reidy, M.A., 1993. Mouse model of arterial injury. *Circ. Res.* 73, 792-796.
- Liu, B., Itoh, H., Louie, O., Kubota, K., Kent, K.C., 2004. The role of phospholipase C and phosphatidylinositol 3-kinase in vascular smooth muscle cell migration and proliferation. *J. Surg. Res.* 120, 256-265.
- Liu, C., Su, C., 2019. Design strategies and application progress of therapeutic exosomes. *Theranostics* 9, 1015-1028.
- Liu, F., Vermesh, O., Mani, V., Ge, T.J., Madsen, S.J., Sabour, A., Hsu, E.C., Gowrishankar, G., Kanada, M., Jokerst, J. V., Sierra, R.G., Chang, E., Lau, K., Sridhar, K., Bermudez, A., Pitteri, S.J., Stoyanova, T., Sinclair, R., Nair, V.S., Gambhir, S.S., Demirci, U., 2017. The Exosome Total Isolation Chip. *ACS Nano* 11, 10712-10723.
- Liu, J., Yu, X., Yu, H., Liu, B., Zhang, Z., Kong, C., Li, Z., 2020. Knockdown of MAPK14 inhibits the proliferation and migration of clear cell renal cell carcinoma by downregulating the expression of CDC25B. *Cancer Med.* 9, 1183-1195.
- Liu, Q., Fu, H., Sun, F., Zhang, H., Tie, Y., Zhu, J., Xing, R., Sun, Z., Zheng, X., 2008. miR-16 family induces cell cycle arrest by regulating multiple cell cycle genes. *Nucleic Acids Res.* 36, 5391-5404.
- Liu, R., Heiss, E.H., Schachner, D., Jiang, B., Liu, W., Breuss, J.M., Dirsch, V.M., Atanasov, A.G., 2017. Xanthohumol Blocks Proliferation and Migration of Vascular Smooth Muscle Cells in Vitro and Reduces Neointima Formation in Vivo. *J. Nat. Prod.* 80, 2146-2150.
- Liu, R.H., Ong, C.S., Fukunishi, T., Ong, K., Hibino, N., 2018. Review of Vascular Graft Studies in Large Animal Models. *Tissue Eng. Part B. Rev.* 24, 133-142.

- Liu, S., Wu, X., Chandra, S., Lyon, C., Ning, B., jiang, L., Fan, J., Hu, T.Y., 2022. Extracellular vesicles: Emerging tools as therapeutic agent carriers. *Acta Pharm. Sin. B* 12, 3822-3842.
- Liu, X., Cheng, Y., Yang, J., Xu, L., Zhang, C., 2012. Cell-specific effects of miR-221/222 in vessels: Molecular mechanism and therapeutic application. *J. Mol. Cell. Cardiol.* 52, 245-255.
- Liu, X., Cheng, Y., Zhang, S., Lin, Y., Yang, J., Zhang, C., 2009. A Necessary Role of miR-221 and miR-222 in Vascular Smooth Muscle Cell Proliferation and Neointimal Hyperplasia. *Circ. Res.* 104, 476-486.
- Liu, Y., Liu, X., Zhou, J., Liang, S., 2021. MicroRNA-302a promotes neointimal formation following carotid artery injury in mice by targeting PHLPP2 thus increasing Akt signaling. *Acta Pharmacol. Sin.* 42, 550-559.
- Liu, Y., Peterson, D.A., Kimura, H., Schubert, D., 1997. Mechanism of Cellular 3-(4,5-Dimethylthiazol-2-yl)-2,5-Diphenyltetrazolium Bromide (MTT) Reduction.
- Livak, K.J., Schmittgen, T.D., 2001. Analysis of Relative Gene Expression Data Using Real-Time Quantitative PCR and the $2^{-\Delta\Delta CT}$ Method. *Methods* 25, 402-408.
- Lloyd, C.T., George, S.J., Angelini, G.D., Newby, A.C., Baker, A.H., 2001. A Pig Model of Vein Graft Disease Applications for Potential Gene Therapies. *Methods Mol. Med.* 52, 233-243.
- Lobb, R.J., Becker, M., Wen Wen, S., Wong, C.S.F., Wiegmans, A.P., Leimgruber, A., Möller, A., 2015. Optimized exosome isolation protocol for cell culture supernatant and human plasma. *J. Extracell. Vesicles* 4.
- Long, X., Cowan, S.L., Miano, J.M., 2013. Mitogen-activated protein kinase 14 is a novel negative regulatory switch for the vascular smooth muscle cell contractile gene program. *Arterioscler. Thromb. Vasc. Biol.* 33, 378-386.
- Longchamp, A., Alonso, F., Dubuis, C., Allagnat, F., Berard, X., Meda, P., Saucy, F., Corpataux, J.M., Sébastien Déglise, Haefliger, J.A., 2014. The use of external mesh reinforcement to reduce intimal hyperplasia and preserve the structure of human saphenous veins. *Biomaterials* 35, 2588-2599.
- Looser, P.M., Kim, L.K., Feldman, D.N., 2016. In-stent restenosis: Pathophysiology and treatment. *Curr. Treat. Options Cardiovasc. Med.* 18.
- Lopatina, T., Bruno, S., Tetta, C., Kalinina, N., Porta, M., Camussi, G., 2014. Platelet-derived growth factor regulates the secretion of extracellular vesicles by adipose mesenchymal stem cells and enhances their angiogenic potential. *Cell Commun. Signal.* 12.
- Lötvall, J., Hill, A.F., Hochberg, F., Buzás, E.I., Di Vizio, D., Gardiner, C., Song Gho, Y., Kurochkin, I. V, Mathivanan, S., Quesenberry, P., Sahoo, S., Tahara, H., Wauben, M.H., Witwer, K.W., Théry, C., 2014. Minimal experimental requirements for definition of extracellular vesicles and their functions: a position statement from the International Society for Extracellular Vesicles Minimal experimental requirements for definiti. *J. Extracell. Vesicles* 3.
- Love, M.I., Huber, W., Anders, S., 2014. Moderated estimation of fold change and dispersion for RNA-seq data with DESeq2. *Genome Biol.* 15.
- Loyer, X., Vion, A.C., Tedgui, A., Boulanger, C.M., 2014. Microvesicles as Cell-Cell Messengers in Cardiovascular Diseases. *Circ. Res.* 114, 345-353.
- Lozano-Ramos, I., Bancu, I., Oliveira-Tercero, A., Armengol, M.P., Menezes-Neto, A., Portillo, H.A. Del, Lauzurica-Valdemoros, R., Borràs, F.E., 2015. Size-exclusion chromatography-based enrichment of extracellular vesicles from urine samples. *J. Extracell. Vesicles* 4.

- Luan, X., Sansanaphongpricha, K., Myers, I., Chen, H., Yuan, H., Sun, D., 2017. Engineering exosomes as refined biological nanoplatforms for drug delivery. *Nat. Publ. Gr.* 38, 754-763.
- Ludwig, N., Whiteside, T.L., Reichert, T.E., 2019. Challenges in Exosome Isolation and Analysis in Health and Disease. *Int. J. Mol. Sci.* 20.
- Ma, T., Chen, Yueqiu, Chen, Yihuan, Meng, Q., Sun, J., Shao, L., Yu, Y., Huang, H., Hu, Y., Yang, Z., Yang, J., Shen, Z., 2018. MicroRNA-132, Delivered by Mesenchymal Stem Cell-Derived Exosomes, Promote Angiogenesis in Myocardial Infarction. *Stem Cells Int.* 2018.
- Makarova, J.A., Shkurnikov, M.U., Wicklein, D., Lange, T., Samatov, T.R., Turchinovich, A.A., Tonevitsky, A.G., 2016. Intracellular and extracellular microRNA: An update on localization and biological role. *Prog. Histochem. Cytochem.* 51, 33-49.
- Maleknia, M., Ansari, N., Haybar, H., Maniati, M., Saki, N., 2020. Inflammatory Growth Factors and In-Stent Restenosis: Effect of Cytokines and Growth Factors. *SN Compr. Clin. Med.* 2, 397-407.
- Malinska, A., Perek, B., Buczkowski, P., Kowalska, K., Ostalska-Nowicka, D., Witkiewicz, W., Nowicki, M., 2013. CD68 expression in aortocoronary saphenous vein bypass grafts. *Histochem. Cell Biol.* 140, 183-188.
- Mallegol, J., Van Niel, G., Lebreton, C., Lepelletier, Y., Candalh, C., Dugave, C., Heath, J.K., Raposo, G., Cerf-Bensussan, N., Heyman, M., 2007. T84-intestinal epithelial exosomes bear MHC class II/peptide complexes potentiating antigen presentation by dendritic cells. *Gastroenterology* 132, 1866-1876.
- Marais, R., Light, Y., Paterson, H.F., Marshall, C.J., 1995. Ras recruits Raf-1 to the plasma membrane for activation by tyrosine phosphorylation. *EMBO J.* 14, 3136-3145.
- Markowska, A., Pendergrast, R.S., Pendergrast, J.S., Pendergrast, P.S., 2017. A novel method for the isolation of extracellular vesicles and RNA from urine. *J. Circ. biomarkers* 6.
- Marmur, J.D., Poon, M., Rossikhina, M., Taubman, M.B., 1992. Induction of PDGF-responsive genes in vascular smooth muscle. Implications for the early response to vessel injury. *Circulation* 86.
- Martin, M., 2011. Cutadapt removes adapter sequences from high-throughput sequencing reads. *EMBnet J* 17, 10-12.
- Martins, T.S., Catita, J., Rosa, I.M., Da Cruz e Silva, O.A.B., Henriques, A.G., 2018. Exosome isolation from distinct biofluids using precipitation and column-based approaches. *PLoS One* 13.
- Marx, S.O., Totary-Jain, H., Marks, A.R., 2011. Vascular Smooth Muscle Cell Proliferation in Restenosis. *Circ. Cardiovasc. Interv.* 4, 104-111.
- Mathieu, M., Martin-Jaular, L., Lavieu, G., Théry, C., 2019. Specificities of secretion and uptake of exosomes and other extracellular vesicles for cell-to-cell communication. *Nat. Cell Biol.* 2019 211 21, 9-17.
- Mathys, H., Basquin, J.Ô., Ozgur, S., Czarnocki-Cieciura, M., Bonneau, F., Aartse, A., Dziembowski, A., Nowotny, M., Conti, E., Filipowicz, W., 2014. Structural and biochemical insights to the role of the CCR4-NOT complex and DDX6 ATPase in microRNA repression. *Mol. Cell* 54, 751-765.
- Matsumoto, A., Takahashi, Y., Nishikawa, M., Sano, K., Morishita, M., Charoenviriyakul, C., Saji, H., Takakura, Y., 2017. Accelerated growth of B16BL6 tumor in mice through efficient uptake of their own exosomes by B16BL6 cells. *Cancer Sci.* 108, 1803-1810.
- McDonald, R.A., White, K.M., Wu, J., Cooley, B.C., Robertson, K.E., Halliday,

- C.A., McClure, J.D., Francis, S., Lu, R., Kennedy, S., George, S.J., Wan, S., Van Rooij, E., Baker, A.H., 2013. miRNA-21 is dysregulated in response to vein grafting in multiple models and genetic ablation in mice attenuates neointima formation. *Eur. Heart J.* 34, 1636-1643.
- McKavanagh, P., Yanagawa, B., Zawadowski, G., Cheema, A., 2017. Management and Prevention of Saphenous Vein Graft Failure: A Review. *Cardiol. Ther.* 6, 203-223.
- Meder, B., Keller, A., Vogel, B., Haas, J., Sedaghat-Hamedani, F., Kayvanpour, E., Just, S., Borries, A., Rudloff, J., Leidinger, P., Meese, E., Katus, H.A., Rottbauer, W., 2011. MicroRNA signatures in total peripheral blood as novel biomarkers for acute myocardial infarction. *Basic Res. Cardiol.* 106, 13-23.
- Medley, J.C., Panzade, G., Zinovyeva, A.Y., 2021. microRNA strand selection: Unwinding the rules. *Wiley Interdiscip. Rev. RNA* 12, 1-22.
- Meijiao, H., Yongtai, G., Jing, S., Zhenwei, P., Hui, Z., Danghui, S., Xin, T., Xiangyang, T., Jianqiang, L., Weimin, L., Bin, L., Jingyi, X., Li, S., Chunhong, X., Ning, Y., Hongjie, X., Xue, D., Chengyuan, Y., Yue, L., 2014. Plasma microRNAs as potential noninvasive biomarkers for in-stent restenosis. *PLoS One* 9.
- Meisenhelder, J., Suh, P.-G., Rhee, S.G., Hunter, T., 1989. Phospholipase C- γ Is a Substrate for the PDGF and EGF Receptor Protein-Tyrosine Kinases In Vivo and In Vitro. *Cell* 57, 1109-1122.
- Mendell, J.T., Olson, E.N., 2012. MicroRNAs in Stress Signaling and Human Disease. *Cell* 148, 1172-1187.
- Merlet, E., Atassi, F., Motiani, R.K., Mougnot, N., Jacquet, A., Nadaud, S., Capiod, T., Trebak, M., Lompré, A.M., Marchand, A., 2013. miR-424/322 regulates vascular smooth muscle cell phenotype and neointimal formation in the rat. *Cardiovasc. Res.* 98, 458-468.
- Metzelaar, M.J., Wijngaard, P.L., Petersll, P.J., Sixma, J.J., Karel NieuwenhuisS, H., CleversB, H.C., 1991. CD63 antigen. A novel lysosomal membrane glycoprotein, cloned by a screening procedure for intracellular antigens in eukaryotic cells. *J. Biol. Chem.* 266, 3239-3245.
- Miano, J.M., Vlastic, N., Tota, R.R., Stemerman, M.B., 1993. Localization of Fos and Jun proteins in rat aortic smooth muscle cells after vascular injury. *Am. J. Pathol.* 142, 715-724.
- Miller, A.M., McPhaden, A.R., Wadsworth, R.M., Wainwright, C.L., 2001. Inhibition by leukocyte depletion of neointima formation after balloon angioplasty in a rabbit model of restenosis. *Cardiovasc. Res.* 49, 838-850.
- Milutinović, A., Šuput, D., Zorc-Pleskovič, R., 2020. Pathogenesis of atherosclerosis in the tunica intima, media, and adventitia of coronary arteries: An updated review. *Bosn. J. Basic Med. Sci.* 20, 21-30.
- Minciacchi, V.R., Freeman, M.R., Di Vizio, D., 2015. Extracellular vesicles in cancer: exosomes, microvesicles and the emerging role of large oncosomes. *Semin. Cell Dev. Biol.* 40, 41-51.
- Mir, B., Goettsch, C., 2020. Extracellular Vesicles as Delivery Vehicles of Specific Cellular Cargo. *Cells* 9.
- Miranda, K.C., Huynh, T., Tay, Y., Ang, Y.S., Tam, W.L., Thomson, A.M., Lim, B., Rigoutsos, I., 2006. A pattern-based method for the identification of MicroRNA binding sites and their corresponding heteroduplexes. *Cell* 126, 1203-1217.
- Mishra, Prasad J., Song, B., Mishra, Pravin J., Wang, Y., Humeniuk, R., Banerjee, D., Merlino, G., Ju, J., Bertino, J.R., 2009. Mir-24 tumor suppressor activity is regulated independent of p53 and through a target site

- polymorphism. *PLoS One* 4.
- Mitchell, P.S., Parkin, R.K., Kroh, E.M., Fritz, B.R., Wyman, S.K., Pogosova-Agadjanyan, E.L., Peterson, A., Noteboom, J., O'Briant, K.C., Allen, A., Lin, D.W., Urban, N., Drescher, C.W., Knudsen, B.S., Stirewalt, D.L., Gentleman, R., Vessella, R.L., Nelson, P.S., Martin, D.B., Tewari, M., 2008. Circulating microRNAs as stable blood-based markers for cancer detection. *Proc. Natl. Acad. Sci. U. S. A.* 105, 10513-10518.
- Miyazawa, K., Bäckström, G., Leppänen, O., Persson, C., Wernstedt, C., Hellman, U., Heldin, C.H., Östman, A., 1998. Role of immunoglobulin-like domains 2-4 of the platelet-derived growth factor alpha-receptor in ligand-receptor complex assembly. *J. Biol. Chem.* 273, 25495-25502.
- Montecalvo, A., Larregina, A.T., Shufesky, W.J., Stolz, D.B., Sullivan, M.L.G., Karlsson, J.M., Baty, C.J., Gibson, G.A., Erdos, G., Wang, Z., Milosevic, J., Tkacheva, O.A., Divito, S.J., Jordan, R., Lyons-Weiler, J., Watkins, S.C., Morelli, A.E., 2012. Mechanism of transfer of functional microRNAs between mouse dendritic cells via exosomes. *Blood* 119, 756-766.
- Moodley, L., Franz, T., Human, P., Wolf, M.F., Bezuidenhout, D., Scherman, J., Zilla, P., Barnard, C., 2013. Protective constriction of coronary vein grafts with knitted nitinol. *Eur. J. Cardio-Thoracic Surg.* 44, 64-71.
- Moreau, P.R., Tomas Bosch, V., Bouvy-Liivrand, M., Öunap, K., Örd, T., Pulkkinen, H.H., Pölönen, P., Heinäniemi, M., Ylä-Herttua, S., Laakkonen, J.P., Linna-Kuosmanen, S., Kaikkonen, M.U., 2021. Profiling of Primary and Mature miRNA Expression in Atherosclerosis-Associated Cell Types. *Arterioscler. Thromb. Vasc. Biol.* 41.
- Morinaga, K., Okadome, K., Kuroki, M., Miyazaki, T., Muto, Y., Inokuchi, K., 1985. Effect of wall shear stress on intimal thickening of arterially transplanted autogenous veins in dogs. *J. Vasc. Surg.* 2, 430-433.
- Morishita, T., Tsutsui, M., Shimokawa, H., Horiuchi, M., Tanimoto, A., Suda, O., Tasaki, H., Huang, P.L., Sasaguri, Y., Yanagihara, N., Nakashima, Y., 2002. Vasculoprotective roles of neuronal nitric oxide synthase. *FASEB J.* 16.
- Morvan, J., Rinaldi, B., Friant, S., 2012. Pkh1/2-dependent phosphorylation of Vps27 regulates ESCRT-I recruitment to endosomes. *Mol. Biol. Cell* 23, 4054-4064.
- Mukaihara, K., Yamakuchi, M., Kanda, H., Shigehisa, Y., Arata, K., Matsumoto, K., Takenouchi, K., Oyama, Y., Koriyama, T., Hashiguchi, T., Imoto, Y., 2021. Evaluation of VEGF-A in platelet and microRNA-126 in serum after coronary artery bypass grafting. *Heart Vessels* 36, 1635-1645.
- Murakoshi, N., Miyauchi, T., Kakinuma, Y., Ohuchi, T., Goto, K., Yanagisawa, M., Yamaguchi, I., 2002. Vascular endothelin-B receptor system in vivo plays a favorable inhibitory role in vascular remodeling after injury revealed by endothelin-B receptor-knockout mice. *Circulation* 106, 1991-1998.
- Muralidharan-Chari, V., Clancy, J., Plou, C., Romao, M., Chavrier, P., Raposo, G., D'Souza-Schorey, C., 2009. ARF6-regulated shedding of tumor-cell derived plasma membrane microvesicles. *Curr. Biol.* 19, 1875-1885.
- Murillo, O.D., Thistlethwaite, W., Rozowsky, J., Subramanian, S.L., Lucero, R., Shah, N., Jackson, A.R., Srinivasan, S., Chung, A., Laurent, C.D., Kitchen, R.R., Galeev, T., Warrell, J., Diao, J.A., Welsh, J.A., Hanspers, K., Riutta, A., Burgstaller-Muehlbacher, S., Shah, R. V., Yeri, A., Jenkins, L.M., Ahsen, M.E., Cordon-Cardo, C., Dogra, N., Gifford, S.M., Smith, J.T., Stolovitzky, G., Tewari, A.K., Wunsch, B.H., Yadav, K.K., Danielson, K.M., Filant, J., Moeller, C., Nejad, P., Paul, A., Simonson, B., Wong, D.K., Zhang, X., Balaj, L., Gandhi, R., Sood, A.K., Alexander, R.P., Wang, L., Wu, C., Wong,

- D.T.W., Galas, D.J., Van Keuren-Jensen, K., Patel, T., Jones, J.C., Das, S., Cheung, K.H., Pico, A.R., Su, A.I., Raffai, R.L., Laurent, L.C., Roth, M.E., Gerstein, M.B., Milosavljevic, A., 2019. exRNA Atlas Analysis Reveals Distinct Extracellular RNA Cargo Types and Their Carriers Present across Human Biofluids. *Cell* 177, 463-477.
- Myllärniemi, M., Calderon, L., Lemström, K., Buchdunger, E., Häyry, P., 1997. Inhibition of platelet-derived growth factor receptor tyrosine kinase inhibits vascular smooth muscle cell migration and proliferation. *FASEB J.* 11, 1119-1126.
- Nabhan, J.F., Hu, R., Oh, R.S., Cohen, S.N., Lu, Q., 2012. Formation and release of arrestin domain-containing protein 1-mediated microvesicles (ARMMs) at plasma membrane by recruitment of TSG101 protein. *Proc. Natl. Acad. Sci. U. S. A.* 109, 4146-4151.
- Nagase, H., Visse, R., Murphy, G., 2006. Structure and function of matrix metalloproteinases and TIMPs. *Cardiovasc. Res.* 69, 562-573.
- Nakase, I., Kobayashi, N.B., Takatani-Nakase, T., Yoshida, T., 2015. Active macropinocytosis induction by stimulation of epidermal growth factor receptor and oncogenic Ras expression potentiates cellular uptake efficacy of exosomes. *Sci. Rep.* 5.
- Naseri, Z., Oskuee, R.K., Jaafari, M.R., Moghadam, M.F., 2018. Exosome-mediated delivery of functionally active mirNa-142-3p inhibitor reduces tumorigenicity of breast cancer in vitro and in vivo. *Int. J. Nanomedicine* 13, 7727-7747.
- National Institute for Cardiovascular Outcomes Research, 2021. National Cardiac Audit Programme: National Adult Cardiac Surgery Audit (NACSA). 2021 Summary Report.
- Nazarenko, I., Rana, S., Baumann, A., McAlear, J., Hellwig, A., Trendelenburg, M., Lochnit, G., Preissner, K.T., Zöller, M., 2010. Cell surface tetraspanin Tspan8 contributes to molecular pathways of exosome-induced endothelial cell activation. *Cancer Res.* 70, 1668-1678.
- Neumann, F.-J., Sousa-Uva, M., Ahlsson, A., Alfonso, F., Banning, A.P., Benedetto, U., Byrne, R.A., Collet, J.-P., Falk, V., Head, S.J., Jüni, P., Kastrati, A., Koller, A., Kristensen, S.D., Niebauer, J., Richter, D.J., Seferović, P.M., Sibbing, D., Stefanini, G.G., Windecker, S., Yadav, R., Zembala, M.O., Wijns, W., Glineur, D., Aboyans, V., Achenbach, S., Agewall, S., Andreotti, F., Barbato, E., Baumbach, A., Brophy, J., Bueno, H., Calvert, P.A., Capodanno, D., Davierwala, P.M., Delgado, V., Dudek, D., Freemantle, N., Funck-Brentano, C., Gaemperli, O., Gielen, S., Gilard, M., Gorenek, B., Haasenritter, J., Haude, M., Ibanez, B., Jung, B., Jeppsson, A., Katritsis, D., Knuuti, J., Kolh, P., Leite-Moreira, A., Lund, L.H., Maisano, F., Mehilli, J., Metzler, B., Montalescot, G., Pagano, D., Petronio, A.S., Piepoli, M.F., Popescu, B.A., Sádaba, R., Shlyakhto, E., Silber, S., Simpson, I.A., Sparv, D., Tavilla, G., Thiele, H., Tousek, P., Van Belle, E., Vranckx, P., Witkowski, A., Zamorano, J.L., Roffi, M., Windecker, S., Aboyans, V., Agewall, S., Barbato, E., Bueno, H., Coca, A., Collet, J.-P., Coman, I.M., Dean, V., Delgado, V., Fitzsimons, D., Gaemperli, O., Hindricks, G., Jung, B., Jüni, P., Katus, H.A., Knuuti, J., Lancellotti, P., Leclercq, C., McDonagh, T.A., Piepoli, M.F., Ponikowski, P., Richter, D.J., Roffi, M., Shlyakhto, E., Sousa-Uva, M., Simpson, I.A., Zamorano, J.L., Pagano, D., Freemantle, N., Sousa-Uva, M., Chettibi, M., Sisakian, H., Metzler, B., Ibrahimov, F., Stelmashok, V.I., Postadzhiyan, A., Skoric, B., Eftychiou, C., Kala, P., Terkelsen, C.J., Magdy, A., Eha, J., Niemelä, M., Kedev, S.,

- Motreff, P., Aladashvili, A., Mehilli, J., Kanakakis, I.-G., Becker, D., Gudnason, T., Peace, A., Romeo, F., Bajraktari, G., Kerimkulova, A., Rudzītis, A., Ghazzal, Z., Kibarskis, A., Pereira, B., Xuereb, R.G., Hofma, S.H., Steigen, T.K., Witkowski, A., de Oliveira, E.I., Mot, S., Duplyakov, D., Zavatta, M., Beleslin, B., Kovar, F., Bunc, M., Ojeda, S., Witt, N., Jeger, R., Addad, F., Akdemir, R., Parkhomenko, A., Henderson, R., 2019. 2018 ESC/EACTS Guidelines on myocardial revascularization. *Eur. Heart J.* 40, 87-165.
- Newby, A.C., Zaltsman, A.B., 2000. Molecular mechanisms in intimal hyperplasia. *J. Pathol.* 190, 300-309.
- NICE, N.I. for H. and C.E., 2020. Acute coronary syndromes [F] Evidence review for the clinical and cost-effectiveness of drug-eluting stents NICE guideline NG185 Acute coronary syndromes [WWW Document].
- Nikolić, D.L., Boettiger, A.N., Bar-Sagi, D., Carbeck, J.D., Shvartsman, S.Y., 2006. Role of boundary conditions in an experimental model of epithelial wound healing. *Am. J. Physiol. - Cell Physiol.* 291, 68-75.
- Nolte-'t Hoen, E.N.M., Buschow, S.I., Anderton, S.M., Stoorvogel, W., Wauben, M.H.M., 2009. Activated T cells recruit exosomes secreted by dendritic cells via LFA-1. *Blood* 113, 1977-1981.
- Nomura, S., Tandon, N.N., Nakamura, T., Cone, J., Fukuhara, S., Kambayashi, J., 2001. High-shear-stress-induced activation of platelets and microparticles enhances expression of cell adhesion molecules in THP-1 and endothelial cells. *Atherosclerosis* 158, 277-287.
- O'Brien, J., Hayder, H., Zayed, Y., Peng, C., 2018. Overview of microRNA biogenesis, mechanisms of actions, and circulation. *Front. Endocrinol. (Lausanne)*. 9.
- O'Brien, J., Shi, Y., Fard, A., Bauer, T., Zalewski, A., Mannion, J.D., 1997. Wound healing around and within saphenous vein bypass grafts. *J. Thorac. Cardiovasc. Surg.* 114, 38-45.
- O'Sullivan, J.F., Martin, K., Caplice, N.M., 2011. Microribonucleic Acids for Prevention of Plaque Rupture and In-Stent Restenosis: "A Finger in the Dam." *J. Am. Coll. Cardiol.* 57, 383-389.
- O'Sullivan, J.F., Neylon, A., Fahy, E.F., Yang, P., Mcgorrian, C., Blake, G.J., 2019. MiR-93-5p is a novel predictor of coronary in-stent restenosis. *Heart Asia* 11.
- Oda, A., Taniguchi, T., Yokoyama, M., 2001. Leptin Stimulates Rat Aortic Smooth Muscle Cell Proliferation and Migration. *Kobe J. Med. Sci* 47, 141-150.
- Oggero, S., Austin-Williams, S., Norling, L.V., 2019. The contrasting role of extracellular vesicles in vascular inflammation and tissue repair. *Front. Pharmacol.* 10, 1479.
- Ohri, S.K., Benedetto, U., Luthra, S., Grant, S.W., Goodwin, A.T., Trivedi, U., Kendall, S., Jenkins, D.P., 2022. Coronary artery bypass surgery in the UK, trends in activity and outcomes from a 15-year complete national series. *Eur. J. Cardiothorac. Surg.* 61, 449-456.
- Oliveira, A.C., Bovolenta, L.A., Nachtigall, P.G., Herkenhoff, M.E., Lemke, N., Pinhal, D., 2017. Combining Results from Distinct MicroRNA Target Prediction Tools Enhances the Performance of Analyses. *Front. Genet.* 8.
- Östman, A., Heldin, C.H., 2001. Involvement of platelet-derived growth factor in disease: development of specific antagonists. *Adv. Cancer Res.* 80, 1-38.
- Ostrowski, M., Carmo, N.B., Krumeich, S., Fanget, I., Raposo, G., Savina, A., Moita, C.F., Schauer, K., Hume, A.N., Freitas, R.P., Goud, B., Benaroch, P.,

- Hacohen, N., Fukuda, M., Desnos, C., Seabra, M.C., Darchen, F., Amigorena, S., Moita, L.F., Thery, C., 2010. Rab27a and Rab27b control different steps of the exosome secretion pathway. *Nat. Cell Biol.* 12, 19-30.
- Otsuka, F., Vorpahl, M., Nakano, M., Foerst, J., Newell, J.B., Sakakura, K., Kutys, R., Ladich, E., Finn, A. V., Kolodgie, F.D., Virmani, R., 2014. Pathology of second-generation everolimus-eluting stents versus first-generation sirolimus-and paclitaxel-eluting stents in humans. *Circulation* 129, 211-223.
- Owens, C.D., 2010. Adaptive changes in autogenous vein grafts for arterial reconstruction: Clinical implications. *J. Vasc. Surg.* 51, 736-746.
- Owens, C.D., Wake, N., Jacot, J.G., Gerhard-Herman, M., Gaccione, P., Belkin, M., Creager, M.A., Conte, M.S., 2006. Early biomechanical changes in lower extremity vein grafts-distinct temporal phases of remodeling and wall stiffness. *J. Vasc. Surg.* 44, 740-746.
- Packard, R.R.S., Lichtman, A.H., Libby, P., 2009. Innate and adaptive immunity in atherosclerosis. *Semin. Immunopathol.* 31, 5-22.
- Palma, J., Yaddanapudi, S.C., Pigati, L., Havens, M.A., Jeong, S., Weiner, G.A., Weimer, K.M.E., Stern, B., Hastings, M.L., Duelli, D.M., 2012. MicroRNAs are exported from malignant cells in customized particles. *Nucleic Acids Res.* 40, 9125-9138.
- Pan, B.T., Teng, K., Wu, C., Adam, M., Johnstone, R.M., 1985. Electron microscopic evidence for externalization of the transferrin receptor in vesicular form in sheep reticulocytes. *J. Cell Biol.* 101, 942-948.
- Pan, C.H., Chien, S.C., Chen, C.J., Shih, C.M., Hsieh, M.H., Huang, C.Y., Bi, W.F., Chan, C.S., Kao, Y.T., Hsiao, C.Y., Chiang, S.J., Chiang, K.H., Huang, J.H., Liu, Y.R., Luo, J.D., Huang, H.Y., Wu, C.H., 2021. Circulating level of microRNA-142-5p is a potential biomarker for predicting in-stent restenosis: a case-control study. *BMC Cardiovasc. Disord.* 21, 1-7.
- Pan, Q., Ramakrishnaiah, V., Henry, S., Fouraschen, S., De Ruiter, P.E., Kwekkeboom, J., Tilanus, H.W., Janssen, H.L.A., Van Der Laan, L.J.W., 2012. Hepatic cell-to-cell transmission of small silencing RNA can extend the therapeutic reach of RNA interference (RNAi). *Gut* 61, 1330-1339.
- Pan, Y., Liang, H., Liu, H., Li, D., Chen, X., Li, L., Zhang, C.-Y., Zen, K., 2014. Platelet-Secreted MicroRNA-223 Promotes Endothelial Cell Apoptosis Induced by Advanced Glycation End Products via Targeting the Insulin-like Growth Factor 1 Receptor. *J. Immunol.* 192, 437-446.
- Papakonstantinou, N., Baikoussis, N., Goudevenos, J., Papadopoulos, G., Apostolakis, E., 2016. Novel no touch technique of saphenous vein harvesting: Is great graft patency rate provided? *Ann. Card. Anaesth.* 19, 481-488.
- Parang, P., Arora, R., 2009. Coronary vein graft disease: Pathogenesis and prevention. *Can. J. Cardiol.*
- Park, C.Y., Choi, Y.S., McManus, M.T., 2010. Analysis of microRNA knockouts in mice. *Hum. Mol. Genet.* 19, 169-175.
- Parveen, A., Mustafa, S.H., Yadav, P., Kumar, A., 2019. Applications of Machine Learning in miRNA Discovery and Target Prediction. *Curr. Genomics* 20, 537-544.
- Pashova, A., Work, L.M., Nicklin, S.A., 2020. The role of extracellular vesicles in neointima formation post vascular injury. *Cell. Signal.* 76.
- Paterson, E., Blenkiron, C., Danielson, K., Henry, C., 2022. Recommendations for extracellular vesicle miRNA biomarker research in the endometrial cancer context. *Transl. Oncol.* 23.

- Pathan, M., Fonseka, P., Chitti, S. V., Kang, T., Sanwlani, R., Van Deun, J., Hendrix, A., Mathivanan, S., 2019. Vesiclepedia 2019: a compendium of RNA, proteins, lipids and metabolites in extracellular vesicles. *Nucleic Acids Res.* 47, 516-519.
- Paulsson, Y., Karlsson, C., Heldin, C. -H, Westermark, B., 1993. Density-dependent inhibitory effect of transforming growth factor-beta 1 on human fibroblasts involves the down-regulation of platelet-derived growth factor alpha-receptors. *J. Cell. Physiol.* 157, 97-103.
- Pawson, T., 1995. Protein modules and signalling networks. *Nat.* 1995 3736515 373, 573-580.
- Peng, X., Guo, C., Wu, Y., Ying, M., Chang, R., SONG, L., Zhan, L., Zhan, X., 2021. miR-224-5p regulates the proliferation, migration and invasion of pancreatic mucinous cystadenocarcinoma by targeting PTEN. *Mol. Med. Rep.* 23.
- Peng, Z., Duan, Y., Zhong, S., Chen, J., Li, J., He, Z., 2022. RNA-seq analysis of extracellular vesicles from hyperphosphatemia-stimulated endothelial cells provides insight into the mechanism underlying vascular calcification. *BMC Nephrol.* 23, 1-11.
- Peracchia, F., Ferrari, G., Poggi, A., Rotilio, D., 1991. IL-1 beta-induced expression of PDGF-AA isoform in rabbit articular chondrocytes is modulated by TGF-beta 1. *Exp. Cell Res.* 193, 208-212.
- Peterson, S.M., Liaw, L., Lindner, V., 2016. Ligation of the mouse common carotid artery. *Mouse Model. Vasc. Dis.* 43-68.
- Peterson, S.M., Thompson, J.A., Ufkin, M.L., Sathyanarayana, P., Liaw, L., Congdon, C.B., 2014. Common features of microRNA target prediction tools. *Front. Genet.* 5.
- Piao, X., Zhang, X., Wu, L., Belasco, J.G., 2010. CCR4-NOT deadenylates mRNA associated with RNA-induced silencing complexes in human cells. *Mol. Cell. Biol.* 30, 1486-1494.
- Piccin, A., Murphy, W.G., Smith, O.P., 2007. Circulating microparticles: pathophysiology and clinical implications. *Blood Rev.* 21, 157-171.
- Piccolo, R., Bona, K.H., Efthimiou, O., Varenne, O., Baldo, A., Urban, P., Kaiser, C., Remkes, W., Räber, L., de Belder, A., van't Hof, A.W.J., Stankovic, G., Lemos, P.A., Wilsgaard, T., Reifart, J., Rodriguez, A.E., Ribeiro, E.E., Serruys, P.W.J.C., Abizaid, A., Sabaté, M., Byrne, R.A., de la Torre Hernandez, J.M., Wijns, W., Jüni, P., Windecker, S., Valgimigli, M., 2019. Drug-eluting or bare-metal stents for percutaneous coronary intervention: a systematic review and individual patient data meta-analysis of randomised clinical trials. *Lancet* 393, 2503-2510.
- Pierce, G.F., Mustoe, T.A., Altrock, B.W., Deuel, T.F., Thomason, A., 1991. Role of platelet-derived growth factor in wound healing. *J. Cell. Biochem.* 45, 319-326.
- Pinzón, N., Li, B., Martinez, L., Sergeeva, A., Presumey, J., Apparailly, F., Seitz, H., 2017. microRNA target prediction programs predict many false positives. *Genome Res.* 27, 234-245.
- Plotnikov, A., Zehorai, E., Procaccia, S., Seger, R., 2011. The MAPK cascades: Signaling components, nuclear roles and mechanisms of nuclear translocation. *Biochim. Biophys. Acta - Mol. Cell Res.* 1813, 1619-1633.
- Plotnikova, O., Baranova, A., Skoblov, M., 2019. Comprehensive Analysis of Human microRNA-mRNA Interactome. *Front. Genet.* 10.
- Podemska-Jedrzejczak, Z., Malinska, A., Sujka-Kordowska, P., Nowicki, M., Puslecki, M., Jemielity, M., Perek, B., 2018. Vascular restenosis in coronary

- artery bypass grafting might be associated with VEGF-C/VEGFR-3 signaling pathway. *Heart Vessels* 33, 1106-1120.
- Pogribny, I.P., 2018. MicroRNAs as biomarkers for clinical studies. *Exp. Biol. Med.* 243, 283-290.
- Pomatto, M.A.C., Bussolati, B., D'Antico, S., Ghiotto, S., Tetta, C., Brizzi, M.F., Camussi, G., 2019. Improved Loading of Plasma-Derived Extracellular Vesicles to Encapsulate Antitumor miRNAs. *Mol. Ther. Methods Clin. Dev.* 13.
- Pomatto, M.A.C., Negro, F., Camussi, G., 2022. Optimized Protocol for Plasma-Derived Extracellular Vesicles Loading with Synthetic miRNA Mimic Using Electroporation. *Methods Mol. Biol.* 2504, 219-230.
- Prosser, H.M., Koike-Yusa, H., Cooper, J.D., Law, F.C., Bradley, A., 2011. A resource of vectors and ES cells for targeted deletion of microRNAs in mice. *Nat. Biotechnol.* 29, 840-845.
- Pua, H.H., Happ, H.C., Gray, C.J., Mar, D.J., Chiou, N.T., Hesse, L.E., Ansel, K.M., 2019. Increased Hematopoietic Extracellular RNAs and Vesicles in the Lung during Allergic Airway Responses. *Cell Rep.* 26, 933-944.
- Purushothaman, A., Bandari, S.K., Liu, J., Mobley, J.A., Brown, E.A., Sanderson, R.D., 2016. Fibronectin on the Surface of Myeloma Cell-derived Exosomes Mediates Exosome-Cell Interactions. *J. Biol. Chem.* 291, 1652-1663.
- Qin, B., Xiao, B., Liang, D., Xia, J., Li, Y., Yang, H., 2011. MicroRNAs expression in ox-LDL treated HUVECs: MiR-365 modulates apoptosis and Bcl-2 expression. *Biochem. Biophys. Res. Commun.* 410, 127-133.
- Qu, Q., Bing, W., Meng, X., Xi, J., Bai, X., Liu, Q., Guo, Y., Zhao, X., Bi, Y., 2017. Upregulation of miR-126-3p promotes human saphenous vein endothelial cell proliferation in vitro and prevents vein graft neointimal formation ex vivo and in vivo. *Oncotarget* 8, 106790-106806.
- Quinlan, A.R., Hall, I.M., 2010. BEDTools: A flexible suite of utilities for comparing genomic features. *Bioinformatics* 26, 841-842.
- Raines, E.W., 2004. PDGF and cardiovascular disease. *Cytokine Growth Factor Rev.* 15, 237-254.
- Raitoharju, E., Lyytikäinen, L.P., Levula, M., Oksala, N., Mennander, A., Tarkka, M., Klopp, N., Illig, T., Kähönen, M., Karhunen, P.J., Laaksonen, R., Lehtimäki, T., 2011. MiR-21, miR-210, miR-34a, and miR-146a/b are up-regulated in human atherosclerotic plaques in the Tampere Vascular Study. *Atherosclerosis* 219, 211-217.
- Ramirez, M.I., Amorim, M.G., Gadelha, C., Milic, I., Welsh, J.A., Freitas, V.M., Nawaz, M., Akbar, N., Couch, Y., Makin, L., Cooke, F., Vettore, A.L., Batista, P.X., Freezor, R., Pezuk, J.A., Rosa-Fernandes, L., Carreira, A.C.O., Devitt, A., Jacobs, L., Silva, I.T., Coakley, G., Nunes, D.N., Carter, D., Palmisano, G., Dias-Neto, E., 2018. Technical challenges of working with extracellular vesicles. *Nanoscale* 10, 881-906.
- Ramteke, A., Ting, H., Agarwal, C., Mateen, S., Somasagara, R., Hussain, A., Graner, M., Frederick, B., Agarwal, R., Deep, G., 2015. Exosomes Secreted under Hypoxia Enhance Invasiveness and Stemness of Prostate Cancer Cells by Targeting Adherens Junction Molecules. *Mol. Carcinog.* 54, 554-565.
- Rana, S., Claas, C., Kretz, C.C., Nazarenko, I., Zoeller, M., 2011. Activation-induced internalization differs for the tetraspanins CD9 and Tspan8: Impact on tumor cell motility. *Int. J. Biochem. Cell Biol.* 43, 106-119.
- Rana, S., Valbuena, G.N., Curry, E., Bevan, C.L., Keun, H.C., 2022. MicroRNAs as biomarkers for prostate cancer prognosis: a systematic review and a systematic reanalysis of public data. *Br. J. Cancer* 2022 1263 126, 502-513.

- Rana, S., Yue, S., Stadel, D., Zöller, M., 2012. Toward tailored exosomes: the exosomal tetraspanin web contributes to target cell selection. *Int. J. Biochem. Cell Biol.* 44, 1574-1584.
- Rankin-Turner, S., Vader, P., O'Driscoll, L., Giebel, B., Heaney, L.M., Davies, O.G., 2021. A call for the standardised reporting of factors affecting the exogenous loading of extracellular vesicles with therapeutic cargos. *Adv. Drug Deliv. Rev.* 173, 479-491.
- Rao, M.S., Van Vleet, T.R., Ciurlionis, R., Buck, W.R., Mittelstadt, S.W., Blomme, E.A.G., Liguori, M.J., 2019. Comparison of RNA-Seq and microarray gene expression platforms for the toxicogenomic evaluation of liver from short-term rat toxicity studies. *Front. Genet.* 9.
- Raposo, G., Nijman, H.W., Stoorvogel, W., Leijendekker, R., Harding, C. V., Melief, C.J.M., Geuze, H.J., 1996. B lymphocytes secrete antigen-presenting vesicles. *J. Exp. Med.* 183, 1161-1172.
- Raut, S.K., Singh, G.B., Rastogi, B., Saikia, U.N., Mittal, A., Dogra, N., Singh, S., Prasad, R., Khullar, M., 2016. miR-30c and miR-181a synergistically modulate p53-p21 pathway in diabetes induced cardiac hypertrophy. *Mol. Cell. Biochem.* 417, 191-203.
- Razaviyan, J., Hadavi, R., Tavakoli, R., Kamani, F., Paknejad, M., Mohammadi-Yeganeh, S., 2018. Expression of miRNAs Targeting mTOR and S6K1 Genes of mTOR Signaling Pathway Including miR-96, miR-557, and miR-3182 in Triple-Negative Breast Cancer. *Appl. Biochem. Biotechnol.* 186, 1074-1089.
- Rectenwald, J.E., Minter, R.M., Moldawer, L.L., Abouhamze, Z., La Face, D., Hutchins, E., Huber, T.S., Seeger, J.M., Ozaki, C.K., 2002. Interleukin-10 fails to modulate low shear stress-induced neointimal hyperplasia. *J. Surg. Res.* 102, 110-118.
- Rekker, K., Saare, M., Roost, A.M., Kaart, T., Sõritsa, D., Karro, H., Sõritsa, A., Simón, C., Salumets, A., Peters, M., 2015. Circulating miR-200-family microRNAs have altered plasma levels in patients with endometriosis and vary with blood collection time. *Fertil. Steril.* 104, 938-946.
- Ren, W., Liang, L., Li, Y., Wei, F.Y., Mu, N., Zhang, L., He, W., Cao, Y., Xiong, D., Li, H., 2020. Upregulation of miR-423 improves autologous vein graft restenosis via targeting ADAMTS-7. *Int. J. Mol. Med.* 45, 532-542.
- Ren, X.-S., Tong, Y., Qiu, Y., Ye, C., Wu, N., Xiong, X.-Q., Wang, J.-J., Han, Y., Zhou, Y.-B., Zhang, F., Sun, H.-J., Gao, X.-Y., Chen, Q., Li, Y.-H., Kang, Y.-M., Zhu, G.-Q., 2019. MiR155-5p in adventitial fibroblasts-derived extracellular vesicles inhibits vascular smooth muscle cell proliferation via suppressing angiotensin-converting enzyme expression. *J. Extracell. Vesicles* 9.
- Riahi, R., Yang, Y., Zhang, D.D., Wong, P.K., 2012. Advances in wound-healing assays for probing collective cell migration. *J. Lab. Autom.* 17, 59-65.
- Riazifar, M., Pone, E.J., Lotval, J., Zhao, W., 2017. Stem Cell Extracellular Vesicles: Extended Messages of Regeneration. *Annu. Rev. Pharmacol. Toxicol.* 57, 125-154.
- Riches, A., Campbell, E., Borger, E., Powis, S., 2014. Regulation of exosome release from mammary epithelial and breast cancer cells-A new regulatory pathway. *Eur. J. Cancer* 50, 1025-1034.
- Riolo, G., Cantara, S., Marzocchi, C., Ricci, C., 2021. miRNA Targets: From Prediction Tools to Experimental Validation. *Methods Protoc.* 4, 1-20.
- Robert, A.W., Marcon, B.H., Bez, A., Angulski, B., Martins, S.D.T., Leitolis, A., Stimamiglio, M.A., Senegaglia, A.C., Correa, A., Alves, L.R., 2022. Selective Loading and Variations in the miRNA Profile of Extracellular Vesicles from

- Endothelial-like Cells Cultivated under Normoxia and Hypoxia. *Int. J. Mol. Sci.* 23.
- Robson, M.C., Phillips, L.G., Robson, L.E., Thomason, A., Pierce, G.F., 1992. Platelet-derived growth factor BB for the treatment of chronic pressure ulcers. *Lancet* 339, 23-25.
- Romaine, S.P.R., Tomaszewski, M., Condorelli, G., Samani, N.J., 2015. MicroRNAs in cardiovascular disease: an introduction for clinicians. *Heart* 101, 921-928.
- Romancino, D.P., Paterniti, G., Campos, Y., De Luca, A., Di Felice, V., D'Azzo, A., Bongiovanni, A., 2013. Identification and characterization of the nano-sized vesicles released by muscle cells. *FEBS Lett.* 587, 1379-1384.
- Romero, M.E., Yahagi, K., Kolodgie, F.D., Virmani, R., 2015. Neoatherosclerosis from a pathologist's point of view. *Arterioscler. Thromb. Vasc. Biol.* 35, 43-49.
- Roque, M., Fallon, J.T., Badimon, J.J., Zhang, W.X., Taubman, M.B., Reis, E.D., 2000. Mouse Model of Femoral Artery Denudation Injury Associated With the Rapid Accumulation of Adhesion Molecules on the Luminal Surface and Recruitment of Neutrophils. *Arterioscler. Thromb. Vasc. Biol.* 20, 335-342.
- Ross, R., Glomsett, J., Kariya, B., Harkert, L., 1974. A Platelet-Dependent, Serum Factor That Stimulates the Proliferation of Arterial Smooth Muscle Cells In Vitro 71, 1207-1210.
- Roux, P.P., Blenis, J., 2004. ERK and p38 MAPK-Activated Protein Kinases: a Family of Protein Kinases with Diverse Biological Functions. *Microbiol. Mol. Biol. Rev.* 68, 320-344.
- Rouya, C., Siddiqui, N., Morita, M., Duchaine, T.F., Fabian, M.R., Sonenberg, N., 2014. Human DDX6 effects miRNA-mediated gene silencing via direct binding to CNOT1. *RNA* 20, 1398-1409.
- Roy, N.C., Altermann, E., Park, Z.A., Mcnabb, W.C., 2011. A comparison of analog and Next-Generation transcriptomic tools for mammalian studies. *Brief. Funct. Genomics* 10, 135-150.
- Rubin, P., Williams, J.P., Riggs, P.N., Bartos, S., Sarac, T., Pomerantz, R., Castano, J., Schell, M., Green, R.M., 1998. Cellular and molecular mechanisms of radiation inhibition of restenosis. Part I: Role of the macrophage and platelet-derived growth factor. *Int. J. Radiat. Oncol. Biol. Phys.* 40, 929-941.
- Ruby, J.G., Jan, C.H., Bartel, D.P., 2007. Intronic microRNA precursors that bypass Drosha processing. *Nat.* 2007 4487149 448, 83-86.
- Rupert, D.L.M., Claudio, V., Lässer, C., Bally, M., 2017. Methods for the physical characterization and quantification of extracellular vesicles in biological samples. *Biochim. Biophys. Acta - Gen. Subj.* 1861, 3164-3179.
- Rupp, E., Siegbahn, A., Rönstrand, L., Wernstedt, C., Claesson-Welsh, L., Heldin, C. -H, 1994. A Unique Autophosphorylation Site in the Platelet-Derived Growth Factor α Receptor from a Heterodimeric Receptor Complex. *Eur. J. Biochem.* 225, 29-41.
- Saetrom, P.L., Heale, B.S.E., Snøve, O., Aagaard, L., Alluin, J., Rossi, J.J., 2007. Distance constraints between microRNA target sites dictate efficacy and cooperativity. *Nucleic Acids Res.* 35, 2333-2342.
- Safdar, A., Saleem, A., Tarnopolsky, M.A., 2016. The potential of endurance exercise-derived exosomes to treat metabolic diseases. *Nat. Rev. Endocrinol.* 2016 129 12, 504-517.
- Samano, N., Geijer, H., Liden, M., Fremes, S., Bodin, L., Souza, D., 2015. The no-touch saphenous vein for coronary artery bypass grafting maintains a

- patency, after 16 years, comparable to the left internal thoracic artery: A randomized trial. *J. Thorac. Cardiovasc. Surg.* 150, 880-888.
- Sata, M., Maejima, Y., Adachi, F., Fukino, K., Saiura, A., Sugiura, S., Aoyagi, T., Imai, Y., Kurihara, H., Kimura, K., Omata, M., Makuuchi, M., Hirata, Y., Nagai, R., 2000. A mouse model of vascular injury that induces rapid onset of medial cell apoptosis followed by reproducible neointimal hyperplasia. *J. Mol. Cell. Cardiol.* 32, 2097-2104.
- Sata, M., Tanaka, K., Fukuda, D., 2016. Wire-mediated endovascular injury that induces rapid onset of medial cell apoptosis followed by reproducible neointimal hyperplasia. *Mouse Model. Vasc. Dis.* 3-20.
- Schepers, A., Eefting, D., Bonta, P.I., Grimbergen, J.M., De Vries, M.R., Van Weel, V., De Vries, C.J., Egashira, K., Van Bockel, J.H., Quax, P.H.A., 2006. Anti-MCP-1 Gene Therapy Inhibits Vascular Smooth Muscle Cells Proliferation and Attenuates Vein Graft Thickening Both In Vitro and In Vivo. *Arterioscler. Thromb. Vasc. Biol.* 26, 2063-2069.
- Schlessinger, J., 2000. Cell signaling by receptor tyrosine kinases. *Cell* 103, 211-225.
- Schlessinger, J., 1994. SH2/SH3 signaling proteins. *Curr. Opin. Genet. Dev.* 4, 25-30.
- Schlitt, A., Pruefer, D., Buerke, U., Russ, M., Dahm, M., Oelert, H., Werdan, K., Buerke, M., 2006. Neutrophil adherence to activated saphenous vein and mammary endothelium after graft preparation. *Ann. Thorac. Surg.* 81, 1262-1268.
- Schöllmann, C., Grugel, R., Tatje, D., Hoppe, J., Folkman, J., Marme, D., Weich, H.A., 1992. Basic fibroblast growth factor modulates the mitogenic potency of the platelet-derived growth factor (PDGF) isoforms by specific upregulation of the PDGF alpha receptor in vascular smooth muscle cells. *J. Biol. Chem.* 267, 18032-18039.
- Schwartz, J.T., 2021. Exploring TGF- β superfamily-dependent regulation of smooth muscle cell phenotypes in the context of saphenous vein graft disease. PhD thesis, University of Glasgow.
- Sedding, D.G., Tröbs, M., Reich, F., Walker, G., Fink, L., Haberbosch, W., Rau, W., Tillmanns, H., Preissner, K.T., Bohle, R.M., Langheinrich, A.C., 2009. Cellular Biology 3-Deazaadenosine Prevents Smooth Muscle. *Circ. Res.* 104, 1192-1200.
- Seeliger, C., Karpinski, K., Haug, A.T., Vester, H., Schmitt, A., Bauer, J.S., Van Griensven, M., 2014. Five freely circulating miRNAs and bone tissue miRNAs are associated with osteoporotic fractures. *J. Bone Miner. Res.* 29, 1718-1728.
- Seeger, R., Krebs, E.G., 1995. The MAPK signaling cascade. *FASEB J.* 9, 726-735.
- Selbach, M., Schwanhäusser, B., Thierfelder, N., Fang, Z., Khanin, R., Rajewsky, N., 2008. Widespread changes in protein synthesis induced by microRNAs. *Nature* 455, 58-63.
- Serrano-Pertierra, E., Oliveira-Rodríguez, M., Rivas, M., Oliva, P., Villafani, J., Navarro, A., Blanco-López, M.C., Cernuda-Morollón, E., 2019. Characterization of Plasma-Derived Extracellular Vesicles Isolated by Different Methods: A Comparison Study. *Bioengineering* 6.
- Shi, N., Chen, S.Y., 2014. Mechanisms simultaneously regulate smooth muscle proliferation and differentiation. *J. Biomed. Res.* 28, 40-46.
- Shi, Y., Zhang, Y., Ran, F., Liu, J., Lin, J., Hao, X., Ding, L., Ye, Q., 2020. Let-7a-5p inhibits triple-negative breast tumor growth and metastasis through GLUT12-mediated warburg effect. *Cancer Lett.* 495, 53-65.

- Shim, A.H.R., Liu, H., Focia, P.J., Chen, X., Lin, P.C., He, X., 2010. Structures of a platelet-derived growth factor/propeptide complex and a platelet-derived growth factor/receptor complex. *Proc. Natl. Acad. Sci. U. S. A.* 107, 11307-11312.
- Shirjang, S., Mansoori, B., Asghari, S., Duijf, P.H.G., Mohammadi, A., Gjerstorff, M., Baradaran, B., 2019. MicroRNAs in cancer cell death pathways: Apoptosis and necroptosis. *Free Radic. Biol. Med.* 139, 1-15.
- Shtam, T.A., Kovalev, R.A., Varfolomeeva, E.Y., Makarov, E.M., Kil, Y. V., Filatov, M. V., 2013. Exosomes are natural carriers of exogenous siRNA to human cells in vitro. *Cell Commun. Signal.* 11, 1-10.
- Shtam, T.A., Samsonov, R.B., Volnitskiy, A. V., Kamyshinsky, R.A., Verlov, N.A., Kniazeva, M.S., Korobkina, E.A., Orehov, A.S., Vasiliev, A.L., Konevega, A.L., Malek, A. V., 2018. Isolation of Extracellular Microvesicles from Cell Culture Medium: Comparative Evaluation of Methods. *Biochem. (Moscow), Suppl. Ser. B Biomed. Chem.* 2018 122 12, 167-175.
- Shurtleff, M.J., Yao, J., Qin, Y., Nottingham, R.M., Temoche-Diaz, M.M., Schekman, R., Lambowitz, A.M., 2017. Broad role for YBX1 in defining the small noncoding RNA composition of exosomes. *Proc. Natl. Acad. Sci. U. S. A.* 114, 8987-8995.
- Sigwart, U., Puel, J., Mirkovitch, V., Joffre, F., Kappenberger, L., 1987. Intravascular stents to prevent occlusion and restenosis after transluminal angioplasty. *N. Engl. J. Med.* 316, 701-706.
- Silva, A.K.A., Morille, M., Piffoux, M., Arumugam, S., Mauduit, P., Larghero, J., Bianchi, A., Aubertin, K., Blanc-Brude, O., Noël, D., Velot, E., Ravel, C., Elie-Caille, C., Sebbagh, A., Boulanger, C., Wilhelm, C., Rahmi, G., Raymond-Letron, I., Cherukula, K., Montier, T., Martinaud, C., Bach, J.M., Favre-Bulle, O., Spadavecchia, J., Jorgensen, C., Menasché, P., Aussel, C., Chopineau, J., Mosser, M., Ullah, M., Sailliet, N., Luciani, N., Mathieu, N., Rautou, P.E., Brouard, S., Boireau, W., Jauliac, S., Dedier, M., Trouvin, J.H., Gazeau, F., Trouillas, M., Peltzer, J., Monsel, A., Banzet, S., 2021. Development of extracellular vesicle-based medicinal products: A position paper of the group “Extracellular Vesicle translation to clinical perspectives - EVOLVE France.” *Adv. Drug Deliv. Rev.* 179.
- Simon, F., Oberhuber, A., Schelzig, H., 2015. Advantages and Disadvantages of Different Animal Models for Studying Ischemia/Reperfusion Injury of the Spinal Cord. *Eur. J. Vasc. Endovasc. Surg.* 49, 744-750.
- Sinauridze, E.I., Kireev, D.A., Popenko, N.Y., Pichugin, A. V., Panteleev, M.A., Krymskaya, O. V., Ataulakhanov, F.I., 2007. Platelet microparticle membranes have 50- to 100-fold higher specific procoagulant activity than activated platelets. *Thromb. Haemost.* 97, 425-434.
- Sindermann, J.R., Smith, J., Köbber, C., Plenz, G., Skaletz-Rorowski, A., Solomon, J.L., Fan, L., March, K.L., 2002. Direct evidence for the importance of p130 in injury response and arterial remodeling following carotid artery ligation. *Cardiovasc. Res.* 54, 676-683.
- Singh, R., Pan, S., Mueske, C.S., Witt, T., Kleppe, L.S., Peterson, T.E., Slobodova, A., Chang, J.-Y., Caplice, N.M., Simari, R.D., 2001. Role for Tissue Factor Pathway in Murine Model of Vascular Remodeling. *Circ. Res.* 89, 71-76.
- Skog, J., Würdinger, T., van Rijn, S., Meijer, D.H., Gainche, L., Curry, W.T., Carter, B.S., Krichevsky, A.M., Breakefield, X.O., 2008a. Glioblastoma microvesicles transport RNA and proteins that promote tumour growth and provide diagnostic biomarkers. *Nat. Cell Biol.* 10, 1470-1476.

- Skog, J., Würdinger, T., van Rijn, S., Meijer, D.H., Gainche, L., Curry, W.T., Carter, B.S., Krichevsky, A.M., Breakefield, X.O., 2008b. Glioblastoma microvesicles transport RNA and proteins that promote tumour growth and provide diagnostic biomarkers. *Nat. Cell Biol.* 2008 1012 10, 1470-1476.
- Sohel, M.H., 2016. Extracellular/Circulating MicroRNAs: Release Mechanisms, Functions and Challenges. *Achiev. Life Sci.* 10, 175-186.
- Solo, K., Lavi, S., Kabali, C., Levine, G.N., Kulik, A., John-Baptiste, A.A., Fremes, S.E., Martin, J., Eikelboom, J.W., Ruel, M., Huitema, A.A., Choudhury, T., Bhatt, D.L., Tzemos, N., Mamas, M.A., Bagur, R., 2019. Antithrombotic treatment after coronary artery bypass graft surgery: Systematic review and network meta-analysis. *BMJ* 367.
- Sonenberg, N., Hinnebusch, A.G., 2009. Regulation of Translation Initiation in Eukaryotes: Mechanisms and Biological Targets. *Cell* 136, 731-745.
- Sonkoly, E., Pivarcsi, A., 2009. microRNAs in Inflammation. *Int. Rev. Immunol.* 28, 535-561.
- Soroceanu, L., Kharbanda, S., Chen, R., Soriano, R.H., Aldape, K., Misra, A., Zha, J., Forrest, W.F., Nigro, J.M., Modrusan, Z., Feuerstein, B.G., Phillips, H.S., 2007. Identification of IGF2 signaling through phosphoinositide-3-kinase regulatory subunit 3 as a growth-promoting axis in glioblastoma. *Proc. Natl. Acad. Sci. U. S. A.* 104, 3466-3471.
- Souza, D.S.R., Johansson, B., Bojöö, L., Karlsson, R., Geijer, H., Filbey, D., Bodin, L., Arbeus, M., Dashwood, M.R., 2006. Harvesting the saphenous vein with surrounding tissue for CABG provides long-term graft patency comparable to the left internal thoracic artery: Results of a randomized longitudinal trial. *J. Thorac. Cardiovasc. Surg.* 132, 373-378.
- Squadrito, F., Deodato, B., Bova, A., Marini, H., Saporito, F., Calò, M., Giacca, M., Minutoli, L., Venuti, F.S., Caputi, A.P., Altavilla, D., 2003. Crucial role of nuclear factor-kappaB in neointimal hyperplasia of the mouse carotid artery after interruption of blood flow. *Atherosclerosis* 166, 233-242.
- Stahl, P.D., Raposo, G., 2019. Extracellular Vesicles: Exosomes and Microvesicles, Integrators of Homeostasis. *Physiology (Bethesda)*. 34, 169-177.
- Stark, V.K., Warner, T.F., Hoch, J.R., 1997. An ultrastructural study of progressive intimal hyperplasia in rat vein grafts. *J. Vasc. Surg.* 26, 94-103.
- Stary, H.C., Chandler, A.B., Dinsmore, R.E., Fuster, V., Glagov, S., Insull, W., Rosenfeld, M.E., Schwartz, C.J., Wagner, W.D., Wissler, R.W., 1995. A Definition of Advanced Types of Atherosclerotic Lesions and a Histological Classification of Atherosclerosis. *Arterioscler. Thromb. Vasc. Biol.* 15, 1512-1531.
- Stenvang, J., Kauppinen, S., 2007. MicroRNAs as targets for antisense-based therapeutics. *Expert Opin. Biol. Ther.* 8, 59-81.
- Sterpetti, A. V., Cucina, A., Lepidi, S., Randone, B., Stipa, F., Aromatario, C., Travi, D., D'Angelo, L.S., Cavallaro, A., Stipa, S., 1996a. Progression and regression of myointimal hyperplasia in experimental vein grafts depends on platelet-derived growth factor and basic fibroblastic growth factor production. *J. Vasc. Surg.* 23, 568-575.
- Sterpetti, A. V., Cucina, A., Randone, B., Palumbo, R., Stipa, F., Proietti, P., Saragosa, M.T., Santoro-D'Angelo, L., Cavallaro, A., 1996b. Growth factor production by arterial and vein grafts: Relevance to coronary artery bypass grafting. *Surgery* 120, 460-467.
- Storey, R.F., 2011. Exploring Mechanisms of Graft Occlusion: Toward Improved Outcomes in Coronary Artery Bypass Graft Surgery. *J. Am. Coll. Cardiol.* 57,

1078-1080.

- Stuffers, S., Sem Wegner, C., Stenmark, H., Brech, A., 2009. Multivesicular endosome biogenesis in the absence of ESCRTs. *Traffic* 10, 925-937.
- Su, H., Trombly, M.I., Chen, J., Wang, X., 2009. Essential and overlapping functions for mammalian Argonautes in microRNA silencing. *Genes Dev.* 23, 304-317.
- Sudo, T., Hidaka, H., 1998. Regulation of Calcyclin (S100A6) Binding by Alternative Splicing in the N-terminal Regulatory Domain of Annexin XI Isoforms. *J. Biol. Chem.* 273, 6351-6357.
- Sun, D.X., Liu, Z., Tan, X.D., Cui, D.X., Wang, B.S., Dai, X.W., 2012. Nanoparticle-mediated local delivery of an antisense TGF- β 1 construct inhibits intimal hyperplasia in autogenous vein grafts in rats. *PLoS One* 7.
- Sun, H.J., Wu, Z.Y., Nie, X.W., Bian, J.S., 2020. Role of Endothelial Dysfunction in Cardiovascular Diseases: The Link Between Inflammation and Hydrogen Sulfide. *Front. Pharmacol.* 10.
- Sun, T., Rodriguez, M., Kim, L., 2009. Glycogen synthase kinase 3 in the world of cell migration. *Dev. Growth Differ.* 51, 735-742.
- Sung, B.H., Ketova, T., Hoshino, D., Zijlstra, A., Weaver, A.M., 2015. Directional cell movement through tissues is controlled by exosome secretion. *Nat. Commun.* 6.
- Sverdlov, E.D., 2012. Amedeo Avogadro's cry: What is 1 μ g of exosomes? *BioEssays* 34, 873-875.
- Swartz, D.D., Andreadis, S.T., 2013. Animal models for vascular tissue-engineering. *Curr. Opin. Biotechnol.* 24, 916-925.
- Szabo, G., Momen-Heravi, F., 2017. Extracellular vesicles in liver disease. *Nat. Rev. Gastroenterol. Hepatol.* 14, 455-466.
- Tabak, S., Schreiber-Avissar, S., Beit-Yannai, E., 2018. Extracellular vesicles have variable dose-dependent effects on cultured draining cells in the eye. *J. Cell. Mol. Med.* 22, 1992-2000.
- Takayama, T., Shi, X., Wang, B., Franco, S., Zhou, Y., DiRenzo, D., Kent, A., Hartig, P., Zent, J., Guo, L.W., 2015. A murine model of arterial restenosis: Technical aspects of femoral wire injury. *J. Vis. Exp.* 97.
- Takov, K., Yellon, D.M., Davidson, S.M., 2019. Comparison of small extracellular vesicles isolated from plasma by ultracentrifugation or size-exclusion chromatography: yield, purity and functional potential. *J. Extracell. Vesicles* 8.
- Takov, K., Yellon, D.M., Davidson, S.M., 2017. Confounding factors in vesicle uptake studies using fluorescent lipophilic membrane dyes. *J. Extracell. Vesicles* 6.
- Tan, H., Qi, J., Fan, B.Y., Zhang, J., Su, F.F., Wang, H.T., 2018. MicroRNA-24-3p Attenuates Myocardial Ischemia/Reperfusion Injury by Suppressing RIPK1 Expression in Mice. *Cell. Physiol. Biochem.* 51, 46-62.
- Tan, J., Yang, L., Liu, C., Yan, Z., 2017. MicroRNA-26a targets MAPK6 to inhibit smooth muscle cell proliferation and vein graft neointimal hyperplasia. *Sci. Rep.* 7.
- Taylor, D.D., Shah, S., 2015. Methods of isolating extracellular vesicles impact down-stream analyses of their cargoes. *Methods* 87, 3-10.
- Teng, F., Fussenegger, M., 2021. Shedding Light on Extracellular Vesicle Biogenesis and Bioengineering. *Adv. Sci.* 8.
- Théry, C., Amigorena, S., Raposo, G., Clayton, A., 2006. Isolation and characterization of exosomes from cell culture supernatants and biological fluids, in: *Current Protocols in Cell Biology*. *Curr Protoc Cell Biol*, pp.

3.22.1-3.22.29.

- Théry, C., Witwer, K.W., Aikawa, E., Jose Alcaraz, M., Anderson, J.D., Andriantsitohaina, R., Antoniou, A., Bach, M., Bachurski, D., Baharvand, H., Balaj, L., Baldacchino, S., Bauer, N.N., Baxter, A.A., Bebawy, M., Beckham, C., Bedina Zavec, A., Benmoussa, A., Berardi, A.C., Bergese, P., Bielska, E., Blenkiron, C., Bobis-Wozowicz, S., Boilard, E., Boireau, W., Bongiovanni, A., Borràs, F.E., Bosch, S., Boulanger, C.M., Breakefield, X., Breglio, A.M., Brennan, M., Brigstock, D.R., Brisson, A., Broekman, M.L., Bromberg, J.F., Bryl-Górecka, P., Buch, S., Buck, A.H., Burger, D., Busatto, S., Buschmann, D., Bussolati, B., Buzás, E.I., Bryan Byrd, J., Camussi, G., Carter, D.R., Caruso, S., Chamley, L.W., Chang, Y.-T., Chen, C., Chen, S., Cheng, L., Chin, A.R., Clayton, A., Clerici, S.P., Cocks, A., Cocucci, E., Coffey, R.J., Cordeiro-da-Silva, A., Couch, Y., Coumans, F.A., Coyle, B., Crescitelli, R., Ferreira Criado, M., Das, S., Datta Chaudhuri, A., de Candia, P., De Santana Junior, E.F., De Wever, O., del Portillo, H.A., Demaret, T., Deville, S., Devitt, A., Dhondt, B., Di Vizio, D., Dieterich, L.C., Dolo, V., Paula Dominguez Rubio, A., Dominici, M., Dourado, M.R., Driedonks, T.A., Duarte, F. V., Duncan, H.M., Eichenberger, R.M., Ekström, K., Andaloussi, S. EL, Elie-Caille, C., Erdbrügger, U., Falcón-Pérez, J.M., Fatima, F., Fish, J.E., Flores-Bellver, M., Försonits, A., Frelet-Barrand, A., Fricke, F., Fuhrmann, G., Gabrielsson, S., Gámez-Valero, A., Gardiner, C., Gärtner, K., Gaudin, R., Song Gho, Y., Giebel, B., Gilbert, C., Gimona, M., Giusti, I., Goberdhan, D.C., Görgens, A., Gorski, S.M., Greening, D.W., Christina Gross, J., Gualerzi, A., Gupta, G.N., Gustafson, D., Handberg, A., Haraszti, R.A., Harrison, P., Hegyesi, H., Hendrix, A., Hill, A.F., Hochberg, F.H., Hoffmann, K.F., Holder, B., Holthofer, H., Hosseinkhani, B., Hu, G., Huang, Y., Huber, V., Hunt, S., Gamal-Eldin Ibrahim, A., Ikezu, T., Inal, J.M., Isin, M., Ivanova, A., Jackson, H.K., Jacobsen, S., Jay, S.M., Jayachandran, M., Jenster, G., Jiang, L., Johnson, S.M., Jones, J.C., Jong, A., Jovanovic-Talisman, T., Jung, S., 2018. Minimal information for studies of extracellular vesicles 2018 (MISEV2018): a position statement of the International Society for Extracellular Vesicles and update of the MISEV2014 guidelines. *J. Endocrinol. Invest.* 7.
- Tian, M., Wang, X., Sun, H., Feng, W., Song, Y., Lu, F., Wang, L., Wang, Y., Xu, B., Wang, H., Liu, S., Liu, Z., Chen, Y., Miao, Q., Su, P., Yang, Y., Guo, S., Lu, B., Sun, Z., Liu, K., Zhang, C., Wu, Y., Xu, H., Zhao, W., Han, C., Zhou, X., Wang, E., Huo, X., Hu, S., 2021. No-Touch Versus Conventional Vein Harvesting Techniques at 12 Months After Coronary Artery Bypass Grafting Surgery: Multicenter Randomized, Controlled Trial. *Circulation* 144, 1120-1129.
- Tian, T., Wang, Y., Wang, H., Zhu, Z., Xiao, Z., 2010. Visualizing of the cellular uptake and intracellular trafficking of exosomes by live-cell microscopy. *J. Cell. Biochem.* 111, 488-496.
- Tian, T., Zhu, Y.L., Zhou, Y.Y., Liang, G.F., Wang, Y.Y., Hu, F.H., Xiao, Z.D., 2014a. Exosome uptake through clathrin-mediated endocytosis and macropinocytosis and mediating miR-21 delivery. *J. Biol. Chem.* 289, 22258-22267.
- Tian, T., Zhu, Y.L., Zhou, Y.Y., Liang, G.F., Wang, Y.Y., Hu, F.H., Xiao, Z.D., 2014b. Exosome Uptake through Clathrin-mediated Endocytosis and Macropinocytosis and Mediating miR-21 Delivery. *J. Biol. Chem.* 289.
- Tian, Y., Gong, M., Hu, Y., Liu, H., Zhang, W., Zhang, M., Hu, X., Aubert, D., Zhu, S., Wu, L., Yan, X., 2020. Quality and efficiency assessment of six

- extracellular vesicle isolation methods by nano-flow cytometry. *J. Extracell. Vesicles* 9.
- Tian, Y., Li, S., Song, J., Ji, T., Zhu, M., Anderson, G.J., Wei, J., Nie, G., 2014. A doxorubicin delivery platform using engineered natural membrane vesicle exosomes for targeted tumor therapy. *Biomaterials* 35, 2383-2390.
- Tilford, C.A., Siemers, N.O., 2009. Gene set enrichment analysis. *Methods Mol. Biol.* 563, 99-121.
- Tingstrom, A., Reuter Dahl, C., Lindahl, P., Heldin, C., Rubin, K., Craford's forskningsfond, G., 1992. Expression of platelet-derived growth factor-beta receptors on human fibroblasts. Regulation by Recombinant Platelet-Derived Growth Factor-BB, IL-1, and Tumor Necrosis Factor-d. *J. Immunol.* 148, 546-554.
- Tiwari, N., Meyer-Schaller, N., Arnold, P., Antoniadis, H., Pachkov, M., van Nimwegen, E., Christofori, G., 2013. Klf4 Is a Transcriptional Regulator of Genes Critical for EMT, Including Jnk1 (Mapk8). *PLoS One* 8.
- Tkach, M., Théry, C., 2016. Communication by Extracellular Vesicles: Where We Are and Where We Need to Go. *Cell* 164, 1226-1232.
- Togliatto, G., Dentelli, P., Rosso, A., Lombardo, G., Gili, M., Gallo, S., Gai, C., Solini, A., Camussi, G., Brizzi, M.F., 2018. PDGF-BB carried by endothelial Cell-derived extracellular vesicles reduces vascular smooth muscle cell apoptosis in diabetes. *Diabetes* 67, 704-716.
- Tong, Y., Ye, C., Ren, X.S., Qiu, Y., Zang, Y.H., Xiong, X.Q., Wang, J.J., Chen, Q., Li, Y.H., Kang, Y.M., Zhu, G.Q., 2018. Exosome-mediated transfer of ACE (angiotensin-converting enzyme) from adventitial fibroblasts of spontaneously hypertensive rats promotes vascular smooth muscle cell migration. *Hypertension* 72, 881-888.
- Torella, D., Iaconetti, C., Catalucci, D., Ellison, G.M., Leone, A., Waring, C.D., Bochicchio, A., Vicinanza, C., Aquila, I., Curcio, A., Condorelli, G., Indolfi, C., 2011. MicroRNA-133 Controls Vascular Smooth Muscle Cell Phenotypic Switch In Vitro and Vascular Remodeling In Vivo. *Circ. Res.* 109, 880-893.
- Torres Crigna, A., Fricke, F., Nitschke, K., Worst, T., Erb, U., Karremann, M., Buschmann, D., Elvers-Hornung, S., Tucher, C., Schiller, M., Hausser, I., Gebert, J., Bieback, K., 2021. Inter-Laboratory Comparison of Extracellular Vesicle Isolation Based on Ultracentrifugation. *Res. Artic. Transfus Med Hemother* 48, 48-59.
- Trajkovic, K., Hsu, C., Chiantia, S., Rajendran, L., Wenzel, D., Wieland, F., Schwille, P., Brügger, B., Simons, M., 2008. Ceramide triggers budding of exosome vesicles into multivesicular endosomes. *Science* (80-.). 319, 1244-1247.
- Tsai, S., Hollenbeck, S.T., Ryer, E.J., Edlin, R., Yamanouchi, D., Kundi, R., Wang, C., Liu, B., Kent, K.C., 2009. TGF- β through Smad3 signaling stimulates vascular smooth muscle cell proliferation and neointimal formation. *Am. J. Physiol. - Hear. Circ. Physiol.* 297, 540-549.
- Tsao, C.W., Aday, A.W., Almarzooq, Z.I., Alonso, A., Beaton, A.Z., Bittencourt, M.S., Boehme, A.K., Buxton, A.E., Carson, A.P., Commodore-Mensah, Y., Elkind, M.S.V., Evenson, K.R., Eze-Nliam, C., Ferguson, J.F., Generoso, G., Ho, J.E., Kalani, R., Khan, S.S., Kissela, B.M., Knutson, K.L., Levine, D.A., Lewis, T.T., Liu, J., Loop, M.S., Ma, J., Mussolino, M.E., Navaneethan, S.D., Perak, A.M., Poudel, R., Rezk-Hanna, M., Roth, G.A., Schroeder, E.B., Shah, S.H., Thacker, E.L., Vanwagner, L.B., Virani, S.S., Voecks, J.H., Wang, N.Y., Yaffe, K., Martin, S.S., 2022. Heart Disease and Stroke Statistics-2022 Update: A Report from the American Heart Association. *Circulation* 145,

153-639.

- Tseng, C.-N., Karlof, E., Chang, Y.-T., Lengquist, M., Rotzius, P., Berggren, P.-O., Hedin, U., Eriksson, E.E., 2014. Contribution of endothelial injury and inflammation in early phase to vein graft failure: The causal factors impact on the development of intimal hyperplasia in murine models. *PLoS One* 9.
- Tsounis, D., Deftereos, S., Bouras, G., Giannopoulos, G., Anatoliotakis, N., Raisakis, K., Kossyvakis, C., W. Cleman, M., 2013. High sensitivity troponin in cardiovascular disease. Is there more than a marker of myocardial death? *Curr. Top. Med. Chem.* 13, 201-215.
- Tsui, J.C.S., Souza, D.S.R., Filbey, D., Karlsson, M.G., Dashwood, M.R., 2002. Localization of nitric oxide synthase in saphenous vein grafts harvested with a novel “no-touch” technique: Potential role of nitric oxide contribution to improved early graft patency rates. *J. Vasc. Surg.* 35, 356-362.
- Tyczyński, P., Karcz, M.A., Kalińczuk, Ł., Fronczak, A., Witkowski, A., 2014. Early stent thrombosis. Aetiology, treatment, and prognosis. *Postep. w Kardiol. Interwencyjnej* 10, 221-225.
- Vader, P., Mol, E.A., Pasterkamp, G., Schiffelers, R.M., 2016. Extracellular vesicles for drug delivery. *Adv. Drug Deliv. Rev.* 106, 148-156.
- Vajen, T., Benedikter, B.J., Heinzmann, A.C.A., Vasina, E.M., Henskens, Y., Parsons, M., Maguire, P.B., Stassen, F.R., Heemskerk, J.W.M., Schurgers, L.J., Koenen, R.R., Mathivanan, S., 2017. Platelet extracellular vesicles induce a pro-inflammatory smooth muscle cell phenotype. *J. Extracell. Vesicles* 6.
- Valadi, H., Ekström, K., Bossios, A., Sjöstrand, M., Lee, J.J., Lötvall, J.O., 2007. Exosome-mediated transfer of mRNAs and microRNAs is a novel mechanism of genetic exchange between cells. *Nat. Cell Biol.* 9, 654-659.
- Valencia-Nuñez, D.M., Kreutler, W., Moya-Gonzalez, J., Alados-Arboledas, P., Muñoz-Carvajal, I., Carmona, A., Ramirez-Chamond, R., Carracedo-Añon, J., 2017. Endothelial vascular markers in coronary surgery. *Heart Vessels* 32, 1390-1399.
- Van Horsen, R., Galjart, N., Rens, J.A.P., Eggermont, A.M.M., Ten Hagen, T.L.M., 2006. Differential effects of matrix and growth factors on endothelial and fibroblast motility: Application of a modified cell migration assay. *J. Cell. Biochem.* 99, 1536-1552.
- van Niel, G., Charrin, S., Simoes, S., Romao, M., Rochin, L., Saftig, P., Marks, M.S., Rubinstein, E., Raposo, G., 2011. The tetraspanin CD63 regulates ESCRT-independent and -dependent endosomal sorting during melanogenesis. *Dev. Cell* 21, 708-721.
- van Niel, G., D'Angelo, G., Raposo, G., 2018. Shedding light on the cell biology of extracellular vesicles. *Nat. Rev. Mol. Cell Biol.* 19, 213-228.
- Van Rooij, E., 2011. The Art of MicroRNA Research. *Circ. Res.* 108, 219-234.
- Van Rooij, E., Sutherland, L.B., Thatcher, J.E., DiMaio, J.M., Naseem, R.H., Marshall, W.S., Hill, J.A., Olson, E.N., 2008. Dysregulation of microRNAs after myocardial infarction reveals a role of miR-29 in cardiac fibrosis. *Proc. Natl. Acad. Sci. U. S. A.* 105, 13027-13032.
- Vanhaesebroeck, B., Guillermet-Guibert, J., Graupera, M., Bilanges, B., 2010. The emerging mechanisms of isoform-specific PI3K signalling. *Nat. Rev. Mol. Cell Biol.* 2010 115 11, 329-341.
- Vanhaesebroeck, B., Stephens, L., Hawkins, P., 2012. PI3K signalling: the path to discovery and understanding. *Nat. Rev. Mol. Cell Biol.* 2012 133 13, 195-203.
- Vanhoutte, P.M., 2010. Regeneration of the endothelium in vascular injury. *Cardiovasc. Drugs Ther.* 24, 299-303.

- Varela, N., Lanas, F., Salazar, L.A., Zambrano, T., 2019. The Current State of MicroRNAs as Restenosis Biomarkers. *Front. Genet.* 10.
- Vargas, A., Zhou, S., Éthier-Chiasson, M., Flipo, D., Lafond, J., Gilbert, C., Barbeau, B., 2014. Syncytin proteins incorporated in placenta exosomes are important for cell uptake and show variation in abundance in serum exosomes from patients with preeclampsia. *FASEB J.* 28, 3703-3719.
- Veerman, R.E., Teeuwen, L., Czarnewski, P., Güclüler Akpınar, G., Sandberg, A.S., Cao, X., Pernemalm, M., Orre, L.M., Gabrielsson, S., Eldh, M., 2021. Molecular evaluation of five different isolation methods for extracellular vesicles reveals different clinical applicability and subcellular origin. *J. Extracell. Vesicles* 10.
- Vinik, Y., Ortega, F.G., Mills, G.B., Lu, Y., Jurkowicz, M., Halperin, S., Aharoni, M., Gutman, M., Lev, S., 2020. Proteomic analysis of circulating extracellular vesicles identifies potential markers of breast cancer progression, recurrence, and response. *Sci. Adv.* 6.
- Vinten-Johansen, J., 2004. Involvement of neutrophils in the pathogenesis of lethal myocardial reperfusion injury. *Cardiovasc. Res.* 61, 481-497.
- Vivanco, I., Sawyers, C.L., 2002. The phosphatidylinositol 3-Kinase AKT pathway in human cancer. *Nat. Rev. Cancer* 2, 489-501.
- Vogel, R., Coumans, F.A.W., Maltesen, R.G., Böing, A.N., Bonnington, K.E., Broekman, M.L., Broom, M.F., Buzás, E.I., Christiansen, G., Hajji, N., Kristensen, S.R., Kuehn, M.J., Lund, S.M., Maas, S.L.N., Nieuwland, R., Osteikoetxea, X., Schnoor, R., Scicluna, B.J., Shambrook, M., de Vrij, J., Mann, S.I., Hill, A.F., Pedersen, S., 2016. A standardized method to determine the concentration of extracellular vesicles using tunable resistive pulse sensing. *J. Extracell. Vesicles* 5.
- Von Der Leyen, H.E., Gibbons, G.H., Morishita, R., Lewis, N.P., Zhang, L., Nakajima, M., Kaneda, Y., Cooke, J.P., Dzau, V.J., 1995. Gene therapy inhibiting neointimal vascular lesion: in vivo transfer of endothelial cell nitric oxide synthase gene. *Proc. Natl. Acad. Sci.* 92, 1137-1141.
- Vu, L.T., Gong, J., Pham, T.T., Kim, Y., Le, M.T.N., 2020. microRNA exchange via extracellular vesicles in cancer. *Cell Prolif.* 53.
- Wadey, K., Lopes, J., Bendeck, M., George, S., 2018. Role of smooth muscle cells in coronary artery bypass grafting failure. *Cardiovasc. Res.* 114, 601-610.
- Waghray, S., Williams, C., Coon, J.J., Wickens, M., 2015. Xenopus CAF1 requires NOT1-mediated interaction with 4E-T to repress translation in vivo. *RNA* 21, 1335-1345.
- Wahle, E., Winkler, G.S., 2013. RNA decay machines: Deadenylation by the Ccr4-Not and Pan2-Pan3 complexes. *Biochim. Biophys. Acta - Gene Regul. Mech.* 1829, 561-570.
- Wahlgren, J., Karlson, T.D.L., Brisslert, M., Vaziri Sani, F., Telemo, E., Sunnerhagen, P., Valadi, H., 2012. Plasma exosomes can deliver exogenous short interfering RNA to monocytes and lymphocytes. *Nucleic Acids Res.* 40.
- Wan, S., Cao, H., Zhao, Y., Guo, Y., Li, C., Li, N., Cao, C., Hua, Z., Li, Z., 2020. Differentially Expressed MicroRNAs Associated with Vein Graft Restenosis in Rats. *Cardiovasc. Innov. Appl.* 5, 45-55.
- Wang, B., Zhang, M., Urabe, G., Shirasu, T., Guo, L.-W., Kent, C., 2021. PERK Inhibition Promotes Post-angioplasty Re-endothelialization via Modulating SMC Phenotype Changes. *J. Surg. Res.* 257, 294-305.
- Wang, D., Gao, B., Yue, J., Liu, F., Liu, Y., Fu, W., Si, Y., 2019. Exosomes from mesenchymal stem cells expressing miR-125b inhibit neointimal hyperplasia

- via myosin IE. *J. Cell. Mol. Med.* 23, 1528-1540.
- Wang, F., Zhao, X.Q., Liu, J.N., Wang, Z.H., Wang, X.L., Hou, X.Y., Liu, R., Gao, F., Zhang, M.X., Zhang, Y., Bu, P.L., 2012. Antagonist of microRNA-21 improves balloon injury-induced rat iliac artery remodeling by regulating proliferation and apoptosis of adventitial fibroblasts and myofibroblasts. *J. Cell. Biochem.* 113, 2989-3001.
- Wang, G., Cao, X., Lai, S., Luo, X., Feng, Y., Xia, X., Yen, P.M., Gong, J., Hu, J., 2013a. PI3K stimulates DNA synthesis and cell-cycle progression via its p55PIK regulatory subunit interaction with PCNA. *Mol. Cancer Ther.* 12, 2100-2109.
- Wang, G., Chen, C., Yang, R., Cao, X., Lai, S., Luo, X., Feng, Y., Xia, X., Gong, J., Hu, J., 2013b. p55PIK-PI3K stimulates angiogenesis in colorectal cancer cell by activating NF- κ B pathway. *Angiogenesis* 16, 561-573.
- Wang, G.K., Zhu, J.Q., Zhang, J.T., Li, Q., Li, Y., He, J., Qin, Y.W., Jing, Q., 2010. Circulating microRNA: a novel potential biomarker for early diagnosis of acute myocardial infarction in humans. *Eur. Heart J.* 31, 659-666.
- Wang, H., Chen, C., Ding, K., Zhang, W., Hou, J., 2020. MiR-24-3p as a prognostic indicator for multiple cancers: from a meta-analysis view. *Biosci. Rep.* 40.
- Wang, K., Zhou, X., Zhou, Z., Mal, N., Fan, L., Zhang, M., Lincoff, A.M., Plow, E.F., Topol, E.J., Penn, M.S., 2005. Platelet, not endothelial, P-selectin is required for neointimal formation after vascular injury. *Arterioscler. Thromb. Vasc. Biol.* 25, 1584-1589.
- Wang, S., Aurora, A.B., Johnson, B.A., Qi, X., McAnally, J., Hill, J.A., Richardson, J.A., Bassel-Duby, R., Olson, E.N., 2008. The Endothelial-Specific MicroRNA miR-126 Governs Vascular Integrity and Angiogenesis. *Dev. Cell* 15, 261-271.
- Wang, S., Liu, N., Tang, Q., Sheng, H., Long, S., Wu, W., 2020. MicroRNA-24 in Cancer: A Double Side Medal With Opposite Properties. *Front. Oncol.* 10.
- Wang, X., Chen, Yihuan, Zhao, Z., Meng, Q., Yu, Y., Sun, J., Yang, Z., Chen, Yueqiu, Li, J., Ma, T., Liu, H., Li, Z., Yang, J., Shen, Z., 2018. Engineered Exosomes With Ischemic Myocardium-Targeting Peptide for Targeted Therapy in Myocardial Infarction. *J. Am. Hear. Assoc. Cardiovasc. Cerebrovasc. Dis.* 7.
- Wang, X., Xu, X., Ma, Z., Huo, Y., Xiao, Z., Li, Y., Wang, Y., 2011. Dynamic mechanisms for pre-miRNA binding and export by Exportin-5. *RNA* 17, 1511-1528.
- Wang, Y., Xu, Z., Wang, X., Zheng, J., Peng, L., Zhou, Y., Song, Y., Lu, Z., 2021. Extracellular-vesicle containing miRNA-503-5p released by macrophages contributes to atherosclerosis. *Aging (Albany, NY)*. 13, 12239-12257.
- Wang, Y.S., Wang, H.Y.J., Liao, Y.C., Tsai, P.C., Chen, K.C., Cheng, H.Y., Lin, R.T., Juo, S.H.H., 2012a. MicroRNA-195 regulates vascular smooth muscle cell phenotype and prevents neointimal formation. *Cardiovasc. Res.* 95, 517-526.
- Wang, Y.S., Wang, H.Y.J., Liao, Y.C., Tsai, P.C., Chen, K.C., Cheng, H.Y., Lin, R.T., Juo, S.H.H., 2012b. MicroRNA-195 regulates vascular smooth muscle cell phenotype and prevents neointimal formation. *Cardiovasc. Res.* 95, 517-526.
- Wang, Z., Gerstein, M., Snyder, M., 2009a. RNA-Seq: a revolutionary tool for transcriptomics. *Nat. Rev. Genet.* 10, 57-63.
- Wang, Z., Gerstein, M., Snyder, M., 2009b. RNA-Seq: a revolutionary tool for transcriptomics. *Nat. Rev. Genet.* 2008 101 10, 57-63.

- Wang, Z., Li, X., Shen, J., Tian, D., Ji, Q., Xia, L., Lv, Q., 2018. Plasma microRNAs reflecting cardiac and inflammatory injury in coronary artery bypass grafting surgery. *J. Surg. Res.* 224, 58-63.
- Wang, Z., Zhu, H., Shi, H., Zhao, H., Gao, R., Weng, X., Liu, R., Li, X., Zou, Y., Hu, K., Sun, A., Ge, J., 2019. Exosomes derived from M1 macrophages aggravate neointimal hyperplasia following carotid artery injuries in mice through miR-222/CDKN1B/CDKN1C pathway. *Cell Death Dis.* 10.
- Ward, A.O., Caputo, M., Angelini, G.D., George, S.J., Zakkar, M., 2017. Activation and inflammation of the venous endothelium in vein graft disease. *Atherosclerosis* 265, 266-274.
- Warne, P.H., Viciano, P.R., Downward, J., 1993. Direct interaction of Ras and the amino-terminal region of Raf-1. *Nature* 364, 352-355.
- Watanabe, Y., Yachie, N., Numata, K., Saito, R., Kanai, A., Tomita, M., 2005. Computational analysis of microRNA targets in *Caenorhabditis elegans* 365, 2-10.
- Webber, J., Clayton, A., 2013. How pure are your vesicles? *J. Extracell. Vesicles* 2.
- Weber, J.A., Baxter, D.H., Zhang, S., Huang, D.Y., Huang, K.H., Lee, M.J., Galas, D.J., Wang, K., 2010. The MicroRNA Spectrum in 12 Body Fluids. *Clin. Chem.* 56, 1733-1741.
- Welt, F.G.P., Edelman, E.R., Simon, D.I., Rogers, C., 2000. Neutrophil, Not Macrophage, Infiltration Precedes Neointimal Thickening in Balloon-Injured Arteries. *Arterioscler. Thromb. Vasc. Biol.* 20, 2553-2558.
- Welt, F.G.P., Rogers, C., 2002. Inflammation and restenosis in the stent era. *Arterioscler. Thromb. Vasc. Biol.* 22, 1769-1776.
- Welton, J.L., Webber, J.P., Botos, L.A., Jones, M., Clayton, A., 2015. Ready-made chromatography columns for extracellular vesicle isolation from plasma. *J. Extracell. Vesicles* 4, 1-9.
- Westerband, A., Crouse, D., Richter, L.C., Aguirre, M.L., Wixon, C.C., James, D.C., Mills, J.L., Hunter, G.C., Heimark, R.L., 2001. Vein adaptation to arterialization in an experimental model. *J. Vasc. Surg.* 33, 561-569.
- Whaley, D., Damyar, K., Witek, R.P., Mendoza, A., Alexander, M., Lakey, J.R.T., 2021. Cryopreservation: An Overview of Principles and Cell-Specific Considerations. *Cell Transplant.* 30.
- Wightman, B., Ha, L., Ruvkun, G., 1993. Posttranscriptional Regulation of the Heterochronic Gene *lin-14* by *W-4* Mediates Temporal Pattern Formation in *C. elegans*. *Cell* 75, 855-862.
- Wiklander, O.P.B., Brennan, M., Lötvall, J., Breakefield, X.O., Andaloussi, S.E.L., 2019. Advances in therapeutic applications of extracellular vesicles. *Sci. Transl. Med.* 11.
- Wiklander, O.P.B., Nordin, J.Z., O'Loughlin, A., Gustafsson, Y., Corso, G., Mäger, I., Vader, P., Lee, Y., Sork, H., Seow, Y., Heldring, N., Alvarez-Erviti, L., Edvard Smith, C.I., Le Blanc, K., Macchiarini, P., Jungebluth, P., Wood, M.J.A., El Andaloussi, S., 2015. Extracellular vesicle in vivo biodistribution is determined by cell source, route of administration and targeting. *J. Extracell. vesicles* 4, 1-13.
- Willms, E., Cabañas, C., Mäger, I., Wood, M.J.A., Vader, P., 2018. Extracellular vesicle heterogeneity: Subpopulations, isolation techniques, and diverse functions in cancer progression. *Front. Immunol.* 9.
- Willms, E., Johansson, H.J., Mäger, I., Lee, Y., Blomberg, K.E.M., Sadik, M., Alaarg, A., Smith, C.I.E., Lehtiö, J., El Andaloussi, S., Wood, M.J.A., Vader, P., 2016. Cells release subpopulations of exosomes with distinct molecular

- and biological properties. *Sci. Reports* 2016 6 1, 1-12.
- Windecker, S., Stortecky, S., Stefanini, G.G., DaCosta, B.R., Rutjes, A.W., Di Nisio, M., Siletta, M.G., Maione, A., Alfonso, F., Clemmensen, P.M., Collet, J.P., Cremer, J., Falk, V., Filippatos, G., Hamm, C., Head, S., Kappetein, A.P., Kastrati, A., Knuuti, J., Landmesser, U., Laufer, G., Neumann, F.J., Richter, D., Schauerte, P., Uva, M.S., Taggart, D.P., Torracca, L., Valgimigli, M., Wijns, W., Witkowski, A., Kolh, P., Juni, P., 2014. Revascularisation versus medical treatment in patients with stable coronary artery disease: network meta-analysis. *BMJ* 348.
- Wise, E.S., Brophy, C.M., 2016. The Case for Endothelial Preservation via Pressure-Regulated Distension in the Preparation of Autologous Saphenous Vein Conduits in Cardiac and Peripheral Bypass Operations. *Front. Surg.* 3.
- Witwer, K.W., Buzás, E.I., Bemis, L.T., Bora, A., Lässer, C., Lötvall, J., Nolte-Hoehn, E.N., Piper, M.G., Sivaraman, S., Skog, J., Théry, C., Wauben, M.H., Hochberg, F., 2013. Standardization of sample collection, isolation and analysis methods in extracellular vesicle research. *J. Extracell. Vesicles* 2.
- Wolff, R.A., Malinowski, R.L., Heaton, N.S., Hullett, D.A., Hoch, J.R., 2006. Transforming growth factor- β 1 antisense treatment of rat vein grafts reduces the accumulation of collagen and increases the accumulation of h-caldesmon. *J. Vasc. Surg.* 43, 1028-1036.
- Wong, A.P., Nili, N., Strauss, B.H., 2004. In vitro differences between venous and arterial-derived smooth muscle cells: potential modulatory role of decorin. *Cardiovasc. Res.* 65, 702-710.
- Worringer, K.A., Rand, T.A., Hayashi, Y., Sami, S., Takahashi, K., Tanabe, K., Narita, M., Srivastava, D., Yamanaka, S., 2014. The let-7/LIN-41 Pathway Regulates Reprogramming to Human Induced Pluripotent Stem Cells by Controlling Expression of Pro-differentiation Genes. *Cell Stem Cell* 14, 40-52.
- Wu, J.R., Liou, S.F., Lin, S.W., Chai, C.Y., Dai, Z.K., Liang, J.C., Chen, I.J., Yeh, J.L., 2009. Lercanidipine inhibits vascular smooth muscle cell proliferation and neointimal formation via reducing intracellular reactive oxygen species and inactivating Ras-ERK1/2 signaling. *Pharmacol. Res.* 59, 48-56.
- Wu, L., Zhang, Y., Huang, Z., Gu, H., Zhou, K., Yin, X., Xu, J., 2019. MiR-409-3p inhibits cell proliferation and invasion of osteosarcoma by targeting zinc-finger E-box-binding homeobox-1. *Front. Pharmacol.* 10.
- Wu, S., Huang, S., Ding, J., Zhao, Y., Liang, L., Liu, T., Zhan, R., He, X., 2010. Multiple microRNAs modulate p21Cip1/Waf1 expression by directly targeting its 3' untranslated region. *Oncogene* 29, 2302-2308.
- Wu, W., Wang, C., Zang, H., Qi, L., Azhar, M., Nagarkatti, M., Nagarkatti, P., Cai, G., Weiser-Evans, M.C.M., Cui, T., 2020. Mature vascular smooth muscle cells, but not endothelial cells, serve as the major cellular source of intimal hyperplasia in vein grafts. *Arterioscler. Thromb. Vasc. Biol.* 40, 1870-1890.
- Wu, W., Zhang, W., Choi, M., Zhao, J., Gao, P., Xue, M., Singer, H.A., Jourdeuil, D., Long, X., 2019. Vascular smooth muscle-MAPK14 is required for neointimal hyperplasia by suppressing VSMC differentiation and inducing proliferation and inflammation. *Redox Biol.* 22.
- Xiao, D., Ohlendorf, J., Chen, Y., Taylor, D.D., Rai, S.N., Waigel, S., Zacharias, W., Hao, H., McMasters, K.M., 2012. Identifying mRNA, MicroRNA and Protein Profiles of Melanoma Exosomes. *PLoS One* 7.
- Xie, M., Li, M., Vilborg, A., Lee, N., Shu, M. Di, Yartseva, V., Šestan, N., Steitz,

- J.A., 2013. Mammalian 5'-capped microRNA precursors that generate a single microRNA. *Cell* 155, 1568-1580.
- Xie, Q., Liu, R., Zou, Z., Feng, Y., Huang, Y., Xu, G., Sun, W., Liang, Y., Zhong, W., 2022. MYPT1 inhibits the metastasis of renal clear cell carcinoma via the MAPK8/N-cadherin pathway. *FEBS Open Bio* 11, 2083-2095.
- Xie, Y., Tobin, L.A., Camps, J., Wangsa, D., Yang, J., Rao, M., Witas, E., Awad, K.S., Yoo, N., Ried, T., Kwong, K.F., 2013. MicroRNA-24 regulates XIAP to reduce the apoptosis threshold in cancer cells. *Oncogene* 32, 2442-2451.
- Xin, M., Small, E.M., Sutherland, L.B., Qi, X., McAnally, J., Plato, C.F., Richardson, J.A., Bassel-Duby, R., Olson, E.N., 2009. MicroRNAs miR-143 and miR-145 modulate cytoskeletal dynamics and responsiveness of smooth muscle cells to injury. *Genes Dev.* 23, 2166-2178.
- Xu, J., Li, C.X., Li, Y.S., Lv, J.Y., Ma, Y., Shao, T.T., Xu, L. De, Wang, Y.Y., Du, L., Zhang, Y.P., Jiang, W., Li, C.Q., Xiao, Y., Li, X., 2011. MiRNA-miRNA synergistic network: construction via co-regulating functional modules and disease miRNA topological features. *Nucleic Acids Res.* 39, 825-836.
- Xu, J., Wong, C.-W., 2013. Enrichment Analysis of miRNA Targets. *Methods Mol. Biol.* 936.
- Xu, J., Wong, C., 2008. A computational screen for mouse signaling pathways targeted by microRNA clusters. *RNA* 14.
- Xu, M.Y., Ye, Z.S., Song, X.T., Huang, R.C., 2019. Differences in the cargos and functions of exosomes derived from six cardiac cell types: a systematic review. *Stem Cell Res. Ther.* 10.
- Xu, W., Lucas, A.S., Wang, Z., Liu, Y., 2014. Identifying microRNA targets in different gene regions. *BMC Bioinformatics* 15.
- Xu, W., Yu, M., Qin, J., Luo, Y., Zhong, M., 2020. LACTB Regulates PIK3R3 to Promote Autophagy and Inhibit EMT and Proliferation Through the PI3K/AKT/mTOR Signaling Pathway in Colorectal Cancer. *Cancer Manag. Res.* 12, 5181-5200.
- Xu, Y., Ouyang, L., He, L., Qu, Y., Han, Y., Duan, D., 2020. Inhibition of exosomal miR-24-3p in diabetes restores angiogenesis and facilitates wound repair via targeting PIK3R3. *J. Cell. Mol. Med.* 24, 13789-13803.
- Xue, Q., Yu, C., Wang, Y., Liu, L., Zhang, K., Fang, C., Liu, F., Bian, G., Song, B., Yang, A., Ju, G., Wang, J., 2016. miR-9 and miR-124 synergistically affect regulation of dendritic branching via the AKT/GSK3B pathway by targeting Rap2a. *Sci. Reports* 2016 6, 1-11.
- Yahagi, K., Kolodgie, F.D., Otsuka, F., Finn, A. V., Davis, H.R., Joner, M., Virmani, R., 2016. Pathophysiology of native coronary, vein graft, and in-stent atherosclerosis. *Nat. Rev. Cardiol.* 13, 79-98.
- Yamada, M., Kubo, H., Ota, C., Takahashi, T., Tando, Y., Suzuki, Takaya, Fujino, N., Makiguchi, T., Takagi, K., Suzuki, Takashi, Ichinose, M., 2013. The increase of microRNA-21 during lung fibrosis and its contribution to epithelial-mesenchymal transition in pulmonary epithelial cells. *Respir. Res.* 14, 1-13.
- Yamashita, T., Kawashima, S., Ozaki, M., Rikitake, Y., Hirase, T., Inoue, N., Hirata, K.I., Yokoyama, M., 2001. A calcium channel blocker, benidipine, inhibits intimal thickening in the carotid artery of mice by increasing nitric oxide production. *J. Hypertens.* 19, 451-458.
- Yang, F., Gao, J.Y., Chen, H., Du, Z.H., Zhang, X.Q., Gao, W., 2017. Targeted inhibition of the phosphoinositide 3-kinase impairs cell proliferation, survival, and invasion in colon cancer. *Onco. Targets. Ther.* 10.
- Yang, J., Chen, L., Ding, J., Fan, Z., Li, S., Wu, H., Zhang, J., Yang, C., Wang,

- H., Zeng, P., Yang, Jun, 2016a. MicroRNA-24 inhibits high glucose-induced vascular smooth muscle cell proliferation and migration by targeting HMGB1. *Gene* 586, 268-273.
- Yang, J., Fan, Z., Yang, Jun, Ding, J., Yang, C., Chen, L., 2016b. MicroRNA-24 Attenuates Neointimal Hyperplasia in the Diabetic Rat Carotid Artery Injury Model by Inhibiting Wnt4 Signaling Pathway. *Int. J. Mol. Sci* 17.
- Yang, L., Wei, C., Li, Y., He, X., He, M., 2020. miR-224 is an early-stage biomarker of hepatocellular carcinoma with miR-224 and miR-125b as prognostic biomarkers. *Biomark. Med.* 14, 1485-1500.
- Yang, S., Maurin, T., Robine, N., Rasmussen, K.D., Jeffrey, K.L., Chandwani, R., Papapetrou, E.P., Sadelain, M., O'Carroll, D., Lai, E.C., 2010. Conserved vertebrate mir-451 provides a platform for Dicer-independent, Ago2-mediated microRNA biogenesis. *Proc. Natl. Acad. Sci. U. S. A.* 107, 15163-15168.
- Yang, Z., Xie, J., Zhu, J., Kang, C., Chiang, C., Wang, Xinmei, Wang, Xiaobing, Kuang, T., Chen, F., Chen, Z., Zhang, A., Yu, B., Lee, R.J., Teng, L., Lee, L.J., 2016. Functional exosome-mimic for delivery of siRNA to cancer: in vitro and in vivo evaluation. *J. Control. Release* 243, 160-171.
- Yao, Y., Du, J., Cao, X., Wang, Y., Huang, Y., Hu, S., Zheng, Z., 2014. Plasma Levels of MicroRNA-499 Provide an Early Indication of Perioperative Myocardial Infarction in Coronary Artery Bypass Graft Patients. *PLoS One* 9.
- Yazdani, S.K., Farb, A., Nakano, M., Vorpahl, M., Ladich, E., Finn, A. V., Kolodgie, F.D., Virmani, R., 2012. Pathology of drug-eluting versus bare-metal stents in saphenous vein bypass graft lesions. *JACC Cardiovasc. Interv.* 5, 666-674.
- Ye, Y., Perez-Polo, J.R., Qian, J., Birnbaum, Y., 2011. The role of microRNA in modulating myocardial ischemia-reperfusion injury. *Physiol. Genomics* 43, 534-542.
- Yoon, C., Lu, J., Ryeom, S.W., Simon, M.C., Yoon, S.S., 2021. PIK3R3, part of the regulatory domain of PI3K, is upregulated in sarcoma stem-like cells and promotes invasion, migration, and chemotherapy resistance. *Cell Death Dis.* 2021 128 12, 1-11.
- Yu, H., Clarke, M.C.H., Figg, N., Littlewood, T.D., Bennett, M.R., 2011. Smooth muscle cell apoptosis promotes vessel remodeling and repair via activation of cell migration, proliferation, and collagen synthesis. *Arterioscler. Thromb. Vasc. Biol.* 31, 2402-2409.
- Yuan, A., Farber, E.L., Rapoport, A.L., Tejada, D., Deniskin, R., Akhmedov, N.B., Farber, D.B., 2009. Transfer of MicroRNAs by Embryonic Stem Cell Microvesicles. *PLoS One* 4.
- Yuan, Y., Shen, C., Zhao, S.L., Hu, Y.J., Song, Y., Zhong, Q.J., 2019. MicroRNA-126 affects cell apoptosis, proliferation, cell cycle and modulates VEGF/TGF- β levels in pulmonary artery endothelial cells. *Eur. Rev. Med. Pharmacol. Sci.* 23, 3058-3069.
- Yuana, Y., Sturk, A., Nieuwland, R., 2013. Extracellular vesicles in physiological and pathological conditions. *Blood Rev.* 27, 31-39.
- Zekri, L., Kuzuoğlu-Öztürk, D., Izaurralde, E., 2013. GW182 proteins cause PABP dissociation from silenced miRNA targets in the absence of deadenylation. *EMBO J.* 32, 1052-1065.
- Zeng, Z., Xia, L., Fan, X., Ostriker, A.C., Yarovinsky, T., Su, M., Zhang, Y., Peng, X., Xie, Y., Pi, L., Gu, X., Chung, S.K., Martin, K.A., Liu, R., Hwa, J., Tang, W.H., 2019. Platelet-derived miR-223 promotes a phenotypic switch in arterial injury repair. *J. Clin. Invest.* 129, 1372-1386.

- Zhang, D., Shi, J., Liang, G., Liu, D., Zhang, J., Pan, S., Lu, Y., Wu, Q., Gong, C., Guo, Y., 2022. miR-16-5p Is a Novel Mediator of Venous Smooth Muscle Phenotypic Switching. *J. Cardiovasc. Transl. Res.* 15, 876-889.
- Zhang, G. jun, Zhou, H., Xiao, H. xu, Li, Y., Zhou, T., 2013. Up-regulation of miR-224 promotes cancer cell proliferation and invasion and predicts relapse of colorectal cancer. *Cancer Cell Int.* 13, 1-10.
- Zhang, H., Xue, S., Feng, Y., Shen, J., Zhao, J., 2020. MicroRNA-24-3p inhibition prevents cell growth of vascular smooth muscle cells by targeting Bcl-2-like protein 11. *Exp. Ther. Med.* 19, 2467-2474.
- Zhang, J., Zhou, W., Liu, Y., Liu, T., Li, C., Wang, L., 2018. Oncogenic role of microRNA-532-5p in human colorectal cancer via targeting of the 5'UTR of RUNX3. *Oncol. Lett.* 15, 7215-7220.
- Zhang, L., Huang, J., Yang, N., Greshock, J., Liang, S., Hasegawa, K., Giannakakis, A., Poulos, N., O'Brien-Jenkins, A., Katsaros, D., Butzow, R., Weber, B.L., Coukos, G., 2007. Integrative Genomic Analysis of Phosphatidylinositol 3'-Kinase Family Identifies PIK3R3 as a Potential Therapeutic Target in Epithelial Ovarian Cancer. *Clin. Cancer Res.* 13, 5314-5321.
- Zhang, L., Huang, L.S., Chen, G., Feng, Z.B., 2017. Potential Targets and Clinical Value of MiR-224-5p in Cancers of the Digestive Tract. *Cell. Physiol. Biochem.* 44, 682-700.
- Zhang, L., Peppel, K., Brian, L., Chien, L., Freedman, N.J., 2004. Vein graft neointimal hyperplasia is exacerbated by tumor necrosis factor receptor-1 signaling in graft-intrinsic cells. *Arterioscler. Thromb. Vasc. Biol.* 24, 2277-2283.
- Zhang, W., Bai, X., Zhao, B., Li, Y., Zhang, Y., Li, Z., Wang, X., Luo, L., Han, F., Zhang, J., Han, S., Cai, W., Su, L., Tao, K., Shi, J., Hu, D., 2018. Cell-free therapy based on adipose tissue stem cell-derived exosomes promotes wound healing via the PI3K/Akt signaling pathway. *Exp. Cell Res.* 370, 333-342.
- Zhang, W., Yan, L., Li, Y., Chen, W., Hu, N., Wang, H., Ou, H., 2015. Roles of miRNA-24 in regulating endothelial nitric oxide synthase expression and vascular endothelial cell proliferation. *Mol. Cell. Biochem.* 405, 281-289.
- Zhang, Y., Liu, D., Chen, X., Li, J., Li, L., Bian, Z., Sun, F., Lu, J., Yin, Y., Cai, X., Sun, Q., Wang, K., Ba, Y., Wang, Q., Wang, D., Yang, J., Liu, P., Xu, T., Yan, Q., Zhang, J., Zen, K., Zhang, C.Y., 2010. Secreted Monocytic miR-150 Enhances Targeted Endothelial Cell Migration. *Mol. Cell* 39, 133-144.
- Zhang, Y., Liu, Z., Zhou, M., Liu, C., 2016. MicroRNA-129-5p inhibits vascular smooth muscle cell proliferation by targeting Wnt5a. *Exp. Ther. Med.* 12.
- Zhang, Y., Wu, W., Pan, X., Wang, Y., Wu, C., Lu, L., Yu, X.-Y., Li, Y., 2022. Extracellular vesicles as novel therapeutic targets and diagnosis markers. *Extracell. Vesicle* 1.
- Zhang, Y., Yu, M., Dai, M., Chen, C., Tang, Q., Jing, W., Wang, H., Tian, W., 2017. miR-450a-5p within rat adipose tissue exosome-like vesicles promotes adipogenic differentiation by targeting WISP2. *J. Cell Sci.* 130, 1158-1168.
- Zhang, Y.X., Tang, R.N., Wang, L.T., Liu, B.C., 2021. Role of crosstalk between endothelial cells and smooth muscle cells in vascular calcification in chronic kidney disease. *Cell Prolif.* 54.
- Zhao, F., Cheng, L., Shao, Q., Chen, Z., Lv, X., Li, J., He, L., Sun, Y., Ji, Q., Lu, P., Ji, Y., Ji, J., 2020. Characterization of serum small extracellular vesicles and their small RNA contents across humans, rats, and mice. *Sci. Reports* 2020 101 10, 1-16.

- Zhao, Y., Li, Y., Luo, P., Gao, Y., Yang, J., Lao, K.H., Wang, G., Cockerill, G., Hu, Y., Xu, Q., Li, T., Zeng, L., 2016. XBP1 splicing triggers miR-150 transfer from smooth muscle cells to endothelial cells via extracellular vesicles. *Sci. Reports* 2016 61 6, 1-12.
- Zhou, J., Chen, G.B., Tang, Y.C., Sinha, R.A., Wu, Y., Yap, C.S., Wang, G., Hu, J., Xia, X., Tan, P., Goh, L.K., Yen, P.M., 2012. Genetic and bioinformatic analyses of the expression and function of PI3K regulatory subunit PIK3R3 in an Asian patient gastric cancer library. *BMC Med. Genomics* 5.
- Zhou, J., Wang, K.C., Wu, W., Subramaniam, S., Shyy, J.Y.J., Chiu, J.J., Li, J.Y.S., Chien, S., 2011. MicroRNA-21 targets peroxisome proliferators-activated receptor- α in an autoregulatory loop to modulate flow-induced endothelial inflammation. *Proc. Natl. Acad. Sci. U. S. A.* 108, 10355-10360.
- Zhou, N., Yan, H.L., 2018. MiR-24 promotes the proliferation and apoptosis of lung carcinoma via targeting MAPK7. *Eur. Rev. Med. Pharmacol. Sci.* 22, 6845-6852.
- Zhou, S., Wang, Y., Meng, Y., Xiao, C., Liu, Z., Brohawn, P., Higgs, B.W., Jallal, B., Jia, Q., Qu, B., Huang, X., Tang, Y., Yao, Y., Harley, J.B., Shen, N., 2016. In Vivo Therapeutic Success of MicroRNA-155 Antagomir in a Mouse Model of Lupus Alveolar Hemorrhage. *Arthritis Rheumatol. (Hoboken, N.J.)* 68, 953-964.
- Zhou, S.S., Jin, J.P., Wang, J.Q., Zhang, Z.G., Freedman, J.H., Zheng, Y., Cai, L., 2018. miRNAs in cardiovascular diseases: potential biomarkers, therapeutic targets and challenges. *Acta Pharmacol. Sin.* 2018 397 39, 1073-1084.
- Zhou, Y.F., Yu, Z.X., Wanishswad, C., Shou, M., Epstein, S.E., 1999. The Immediate Early Gene Products of Human Cytomegalovirus Increase Vascular Smooth Muscle Cell Migration, Proliferation, and Expression of PDGF β -Receptor. *Biochem. Biophys. Res. Commun.* 256, 608-613.
- Zhu, X.F., Shan, Z., Ma, J.Y., Wang, M., Zhang, C.X., Liu, R.M., Wu, W. Bin, Shi, Y.W., Li, W., Wang, S.M., 2015. Investigating the Role of the Post-transcriptional Gene Regulator MIR-24-3p in the Proliferation, Migration and Apoptosis of Human Arterial Smooth Muscle Cells in Arteriosclerosis Obliterans. *Cell. Physiol. Biochem.* 36, 1359-1370.
- Zitvogel, L., Regnault, A., Lozier, A., Wolfers, J., Flament, C., Tenza, D., Ricciardi-Castagnoli, P., Raposo, G., Amigorena, S., 1998. Eradication of established murine tumors using a novel cell-free vaccine: dendritic cell-derived exosomes. *Nat. Med.* 4, 594-600.
- Zou, X., Tang, X.Y., Qu, Z.Y., Sun, Z.W., Ji, C.F., Li, Y.J., Guo, S.D., 2022. Targeting the PDGF/PDGFR signaling pathway for cancer therapy: A review. *Int. J. Biol. Macromol.* 202, 539-557.
- Zou, Y., Dietrich, H., Hu, Y., Metzler, B., Wick, G., Xu, Q., 1998. Mouse Model of Venous Bypass Graft Arteriosclerosis. *Am. J. Pathol.* 153, 1301-1310.